

The Design, Synthesis and Optimisation of Phosphoinositide-3-kinase (PI3K) Inhibitors as Potential Anti-inflammatory Agents



Charlotte Hardy

2014

This thesis is the result of the author's original research. It has been composed by the author and has not been previously submitted for examination which has led to the award of a degree.

The copyright of this thesis belongs to GlaxoSmithKline in accordance with the author's contract of employment with GSK under the terms and conditions of the United Kingdom Copyrights Act. Due acknowledgement must always be made of any material contained in, or derived from, this thesis.

Signed:

June 2014

ABSTRACT

Phosphoinositide-3-kinases (PI3Ks) are a family of lipid kinases which control a wide range of intracellular pathways implicated in inflammatory respiratory diseases. In this thesis, the optimisation of two chemical templates, (i) a pyridone series, and (ii) an aminopyrimidine series, is described, with the aim of finding a PI3K γ selective small molecule inhibitor.

Whilst work on the pyridone template did not result in any one compound which met all of the target criteria, progress was made in identifying analogues with significantly improved physicochemical properties. Furthermore, the exploration of this template has led to increased understanding of the PI3K γ active site, which has enabled the design of isoform selective inhibitors such as a key imidate structure.

Work on the aminopyrimidine series focused on improving the physicochemical profile for *i.v.* dosing. A prototype pro-drug was prepared, and profiled in blood stability and DMPK assays. Although its profile was not optimal, these results enabled the design of a second iteration of pro-drugs, with the aim of progressing to *in vivo* target validation studies. Further work on this series delivered significant improvements in the physicochemical properties of the template. Whilst this did not translate into improved cellular activity for this template, the learnings can now be applied to future work on novel cores.

Finally, a programme of fragment-based drug discovery was initiated to identify novel templates as PI3K γ inhibitors. Whilst an initial screen and follow-up chemistry delivered novel inhibitors with interesting profiles, concern over the physicochemical profile of the templates rapidly led to termination of this work. However, the subsequent design and screening of a bespoke fragment set, specifically targeting the identification of saturated or semi-saturated hinge binding fragments, was extremely successful. A variety of hits were identified which provide exciting opportunities for the discovery of PI3K γ inhibitors with the desired balance of biological and physicochemical profiles.

ACKNOWLEDGEMENTS

Firstly, I would like to thank my supervisors Professor William Kerr, Dr Nicole Hamblin and Dr David House for their enthusiasm, advice, and support throughout my PhD.

I am also extremely grateful to Professor Harry Kelly and Professor William Kerr for all their hard work in making the GSK-University of Strathclyde PhD programme a reality.

I would like to thank all my colleagues at GSK, in particular the many PI3K γ programme members past and current, who have played a role in the work described in this thesis. I would also like to thank the current members of the Kerr group who made me feel extremely welcome at Strathclyde.

Finally, the biggest thank you of all to my husband Dan, for his unwavering support and encouragement, whilst I have been busy writing sections of this thesis!

ABBREVIATIONS

AHR	Airway hyperresponsiveness
ALI	Acute lung injury
AMP	Artificial membrane permeability
ARDS	Acute respiratory distress syndrome
ActRIIA	Activin type IIA receptor
ActRIIB	Activin type IIB receptor
ATP	Adenosine triphosphate
BOC	<i>tert</i> -Butyloxycarbonyl
CCL19	Chemokine ligand 19
CCL21	Chemokine ligand 21
CD4⁺	Cluster of differentiation 4 glycoprotein
CD8⁺	Cluster of differentiation 8 glycoprotein
CLND	Chemiluminescent nitrogen detection
CMR	Calculated molar refractivity
COPD	Chronic obstructive pulmonary disease
CXCL12	Chemokine ligand 12
DBU	1,8-Diazabicycloundec-7-ene
DCM	Dichloromethane
DIPEA	Diisopropylethylamine
DMF	<i>N,N</i> -Dimethylformamide
DMSO	Dimethylsulfoxide
dppf	1,1'-Bis(diphenylphosphino)ferrocene
Et	Ethyl
fMLP	Fomyl-methionyl-leucyl-phenylalanine
GSK3	Glycogen synthase kinase 3
HAC	Heavy atom count
HATU	2-(7-Aza-1 <i>H</i> -benzotriazole-1-yl)-1,1,3,3-tetramethyluronium hexafluorophosphate
HBA	Hydrogen bond acceptor
HBD	Hydrogen bond donor
HPLC	High performance liquid chromatography

HRMS	High resolution mass spectrometry
IgE	Immunoglobulin
IL-1β	Interleukin 1-beta
IL-5	Interleukin 5
IL-2	Interleukin 2
IR	Infra-red
<i>i.v.</i>	Intravenous
LCMS	Liquid chromatography mass spectrometry
L.E.	Ligand efficiency
L.L.E.	Lipophilic ligand efficiency
LPS	Lipopolysaccharide
Me	Methyl
MIDA	<i>N</i> -Methyliminodiacetic acid
m.p.	Melting point
MW	Molecular weight
NFκB	Nuclear factor kappa-B
NMR	Nuclear magnetic resonance
PDB	Protein database
PI3K	Phosphoinositide-3-kinase
PI3Kα	Phosphoinositide-3-kinase alpha
PI3Kβ	Phosphoinositide-3-kinase beta
PI3Kγ	Phosphoinositide-3-kinase gamma
PI3Kδ	Phosphoinositide-3-kinase delta
PI3KC2α	Phosphoinositide-3-kinase Class 2 alpha
PI3KC2β	Phosphoinositide-3-kinase Class 2 beta
PI3KC2γ	Phosphoinositide-3-kinase Class 2 gamma
PIP₂	Phosphatidylinositol 4,5-biphosphate
PIP₃	Phosphatidylinositol 3,4,5-triphosphate
ppm	Parts per million
PSA	Polar surface area
PtdIns(4,5)P₂	Phosphatidylinositol 4,5-biphosphate
PtdIns(3,4,5)P₃	Phosphatidylinositol 3,4,5-triphosphate

Pybop	Benzotriazol-1-yl-oxytripyrrolidinophosphonium hexafluorophosphate
ROS	Reactive oxygen species
RSC	Royal Society of Chemistry
RT	Room temperature
Rt	Retention time
RPM	Revolutions per minute
SAR	Structure-activity relationship
SPE	Solid phase extraction
SPhos	2-Dicyclohexylphosphino-2'-6'-dimethoxybiphenyl
TBD	Triazabicyclodecane
TFA	Trifluoroacetic acid
THF	Tetrahydrofuran
TNFα	Tumour necrosis factor alpha
TPPTS	3,3',3''-Phosphinidynetris(benzenesulfonic acid) trisodium salt
VEGF	Vascular endothelial growth factor
Vps34	Vacuolar protein sorting mutagen 34 protein, also known as Phosphoinositide-3-kinase Class 3 (PI3KC3)

CONTENTS

ABSTRACT	3
ACKNOWLEDGEMENTS	4
ABBREVIATIONS	5
CONTENTS	8
1.0 INTRODUCTION	11
1.1 Respiratory Disease	11
1.1.1 Asthma	11
1.1.2 Chronic Obstructive Pulmonary Disease.....	12
1.1.3 Acute Lung Injury	14
1.2 Kinases	15
1.3 Phosphoinositide-3-Kinases	16
1.3.1 PI3K Inhibitors for the Treatment of Respiratory Disease	17
PI3K γ Inhibitors for the Treatment of Asthma	19
PI3K γ Inhibitors for the Treatment of COPD	20
PI3K γ Inhibitors for the Treatment of ALI	21
1.3.2 PI3K Structure	22
1.3.3 Small Molecule PI3K Inhibitors	25
Thiazolidinones	27
2-Aminothiazoles	30
2-Aminoheterocycles	34
Other.....	41
Summary	46
1.3.4 Target Product Profile.....	46
2.0 PYRIDONE SERIES	47
2.1 Historical Data Review	47
2.2 Medicinal Chemistry Strategy and Proposed Work	62
2.3 Investigating R¹	63
2.3.1 Results and Discussion.....	64

Synthesis via Suzuki Coupling	64
Synthesis of Key Intermediate 3-Bromo-5-[4-hydroxy-3-(methoxy)phenyl]-1-methyl-2(1H)-pyridinone	64
Suzuki Coupling of 3-Bromo-5-[4-hydroxy-3-(methoxy)phenyl]-1-methyl-2(1H)-pyridinone	65
MIDA Boronates	70
An Alternative Approach: Synthesis of {5-[3,4-Bis(methoxy)phenyl]-1-methyl-2-oxo-1,2-dihydro-3-pyridinyl} boronic acid	72
Bespoke Heterocycle Synthesis	77
1,3,4-Oxadiazole	78
1,2,4-Oxadiazole	79
Semi-saturated Bicycles	83
2.3.2 Data Analysis	85
Key SAR	88
Summary	95
2.4 Further Exploration of Imidazole 234	96
2.4.1 Results and Discussion	97
2.5 Further Exploration of Semi-Saturated Analogue 201	101
2.5.1 Results and Discussion	101
2.6 Carboxylic Acid Containing Pyridones	104
2.6.1 Increased Lipophilicity	111
2.6.2 Results and Discussion	116
2.6.3 Summary and Future Work	122
2.7 Accessing a New Region of the Protein	123
2.7.1 Results and Discussion	126
2.7.2 Future Work	139
2.8 Conclusions	139
3.0 AMINOPYRIMIDINE SERIES	143
3.1 Change of Indication	143
3.2 Phosphate Pro-drugs	147
3.2.1 Results and Discussion	149

3.2.2	Future Work.....	160
3.3	Removing Aromatic Rings.....	162
3.3.1	Results and Discussion.....	163
3.3.2	Future Work.....	183
3.4	Conclusions.....	184
4.0	FRAGMENT EFFORT.....	186
4.1	Results and Discussion.....	186
4.1.1	Cluster 4.....	189
4.1.2	Cluster 5.....	198
4.2	Conclusions.....	206
4.3	Follow-up Fragment Screen.....	207
4.4	Conclusions and Future Work.....	214
5.0	EXPERIMENTAL.....	216
5.1	General Methods.....	216
5.2	Preparative Procedures.....	220
6.0	REFERENCES.....	341
7.0	GLOSSARY.....	354
8.0	APPENDICES.....	355
	Appendix 1: Sequence Alignments of Human PI3K Isoforms.....	355
	Appendix 2: PI3K Alpha, Beta, Delta and Gamma Assays.....	356
	Appendix 3: CLND Solubility Assay.....	358
	Appendix 4: ChromLogD Assay.....	359
	Appendix 5: PI3K Gamma Dependent CD63 Up-regulation in Activated Basophils Assay.....	359
	Appendix 6: Artificial Membrane Permeability Assay.....	361

1.0 INTRODUCTION

1.1 Respiratory Disease

Respiratory diseases are a major contributor to mortality, hospital admissions and primary care consultation throughout the world.¹ The Respiratory Therapy Area within our laboratories is focused on developing novel treatments for diseases where there is the greatest unmet medical need. In particular, this leads to the targeting of subsets of patients whose disease is not well controlled with current therapies, diseases where current therapies provide only symptomatic treatment, or diseases where no drug therapies are available. Among the main diseases of interest are asthma, chronic obstructive pulmonary disease and acute lung injury.

1.1.1 Asthma

Asthma is a very common disease which results in shortness of breath, wheezing and tightness in the chest. These symptoms are all a result of inflammation, which can result in narrowing of the airways and, sometimes, the production of excess mucus (Figure 1).²

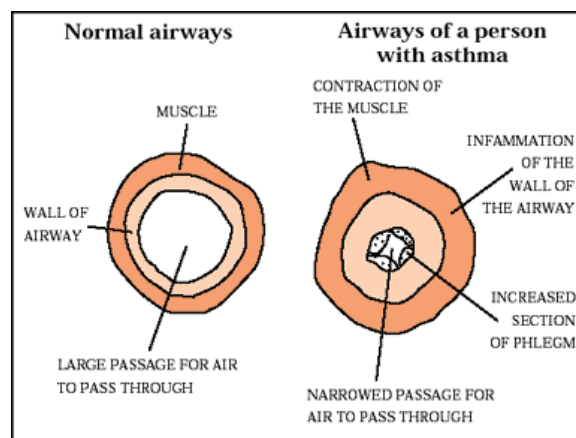


Figure 1: Impact of asthma on the airways²

Asthma often worsens in response to triggers such as allergens (house dust mite, animal fur, pollen), exercise, irritants, or viral infections.³ This worsening of symptoms is commonly called an 'asthma attack' or exacerbation, and the frequency and impact of these attacks can depend on the severity of the disease. Patients are often classified depending on how well their asthma is controlled by medication.^{4,5}

There are currently several well established, treatments for asthma. Inhaled corticosteroids, which target the glucocorticoid receptor, are the most potent anti-inflammatory agents for the treatment of asthma. However there can be significant variability in patient sensitivity.⁶ Inhaled β_2 agonists, which result in bronchodilation, are another common treatment.⁷ Short acting ‘reliever’ treatments have been supplemented with longer acting ‘preventer’ molecules, which are usually dosed in combination with corticosteroids (either separately or as a combination therapy).⁸ Leukotriene antagonists are another option, providing both anti-inflammatory and bronchodilatory effects. Their oral formulation is often more convenient to the patient. However, once again, wide variability in symptom control is observed.⁹

More recently, monoclonal antibody treatments have been developed, targeting specific mediators such as immunoglobulin E (IgE) or interleukins (IL-5 or IL-12), however, these therapies are significantly more expensive and access is limited to the most severe patients only.¹⁰ Finally, antihistamines have a limited role in treating patients whose exacerbations are triggered by allergens, such as pollen or animal fur.¹¹

Alone or in combination, these therapies provide effective control for a large percentage of asthmatics. However, there is still a need for new treatments for those patients whose symptoms are not well controlled and experience severe exacerbations.¹²

1.1.2 Chronic Obstructive Pulmonary Disease

Chronic obstructive pulmonary disease (COPD) is a term used to describe patients who suffer from chronic bronchitis, emphysema, or both. This inflammation of the lung and/or loss of aveolar elasticity leads to symptoms such as cough, phlegm, and shortness of breath (Figure 2).²

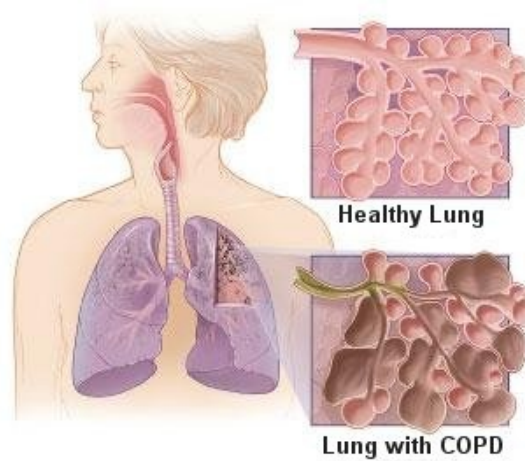


Figure 2: Pictorial representation of a COPD patient's lung¹³

Around 3 million people in the UK have COPD, with an estimated further half a million people remaining undiagnosed.¹⁴ The major cause of COPD is smoking; however a small number of cases may be related to occupational exposure to air pollutants, dust, or chemicals.

The Global Initiative for Chronic Obstructive Pulmonary Disease classifies patients based on the severity of airway obstruction into mild, moderate, severe, or very severe.¹⁵ The most effective treatment for all patients is smoking cessation combined with a suitable exercise programme, however, several drug therapies are also utilised.¹⁶

Similar to asthma, inhaled corticosteroids and bronchodilators (either β_2 agonists or, in this case, also muscarinic antagonists) are the mainstay of treatment and patients are often prescribed combination therapies (Figure 3).^{17,18} Whilst these medicines go some way to treat patient symptoms, there are currently no treatments available that modify the course of the disease. Oxygen therapy and ventilator support are also used to prolong survival, although often do not improve quality of life.

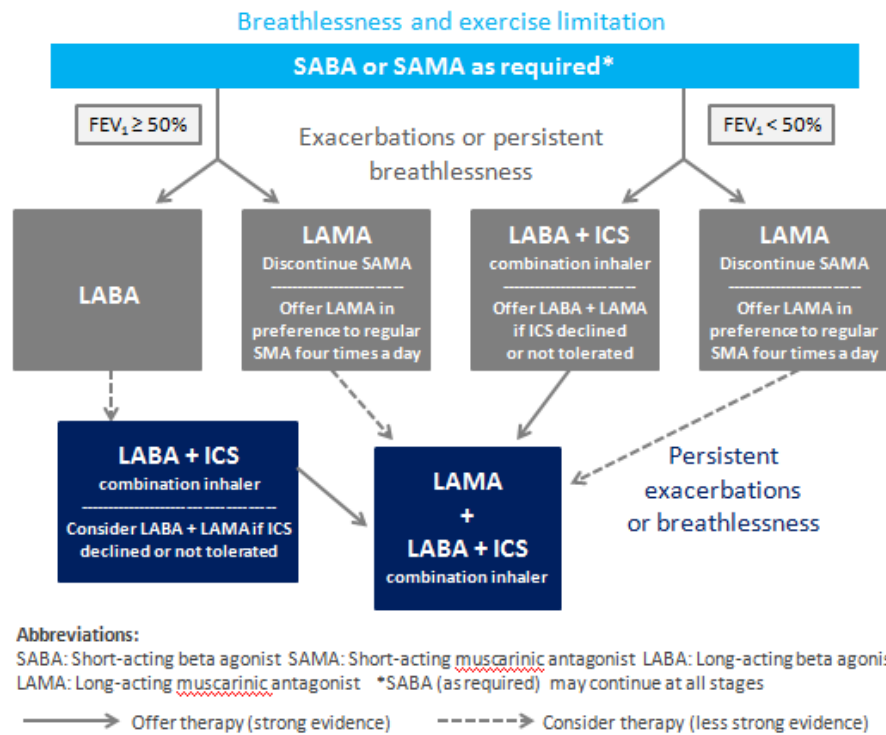


Figure 3: Schematic of COPD treatments¹⁸

1.1.3 Acute Lung Injury

Patients with acute lung injury (ALI) and acute respiratory distress syndrome (ARDS) suffer from hypoxemia, which means a deficiency of oxygen in arterial blood. The difference between ALI and the more severe ARDS is based solely on a calculated index of oxygenation efficiency (Figure 4), where PaO₂ is the partial pressure of oxygen in arterial blood and FiO₂ is the fraction of inspired oxygen.¹⁹

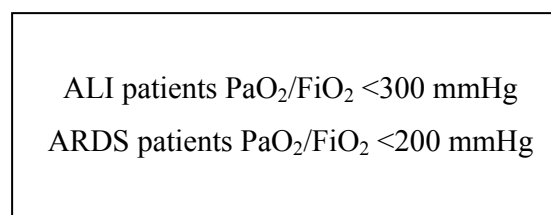


Figure 4: Clinical definitions of ALI and ARDS

ALI can be triggered by direct lung injury e.g. a chest infection or damage resulting from severe trauma, or by indirect lung injury e.g. sepsis or burns.² Around 190,000 people are diagnosed with ALI annually in the US alone and both ALI and ARDS have high mortality rates of 35-40%.¹⁹ Patients with ALI are critically ill and are managed in

Intensive Care Units of hospitals, contributing to the large health-care cost associated with the disease.

There are currently no approved drug therapies for ALI and treatment consists of carefully controlled mechanical ventilation and fluid/nutrition management.²⁰ There is clearly a high unmet need for a therapy that could either prevent high risk patients from developing ALI, or would improve the outcome for patients diagnosed with the disease.

1.2 Kinases

Kinases are a class of intracellular enzymes which catalyse phosphorylation reactions by transferring the terminal phosphate from adenosine triphosphate (ATP) to their substrate (Figure 5).

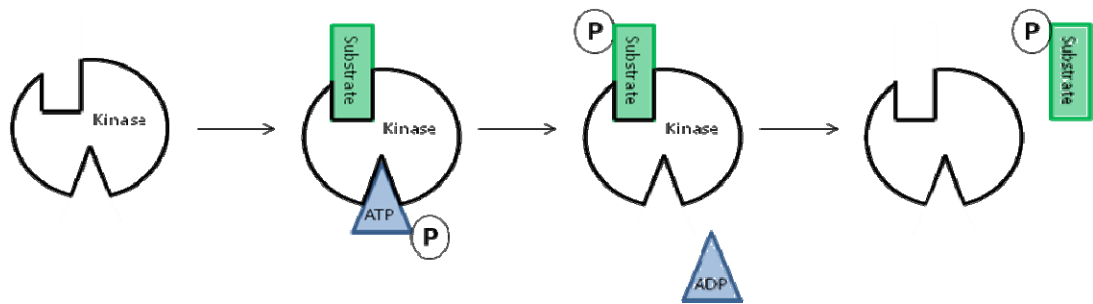


Figure 5: Kinase function

Protein kinases catalyse the phosphorylation of protein substrates (e.g. the serine-threonine kinases, which phosphorylate serine and/or threonine side chains of their substrate protein), whilst lipid kinases phosphorylate lipid substrates. Kinase inhibitors have long been of interest to the pharmaceutical industry for the treatment of a wide range of diseases, as controlling the phosphorylation state of the protein and/or lipid substrates can affect a range of downstream signalling processes.²¹

1.3 Phosphoinositide-3-Kinases

Phosphoinositide-3-kinases are a family of intracellular lipid kinases which play a key role in controlling a wide range of cellular functions, such as cell growth, proliferation, survival and migration.²² They have been divided into three classes based on their mode of regulation, substrate specificity, protein sequence and structure.²²

- Class I: PI3K α , PI3K β , PI3K δ , PI3K γ
- Class II: PI3KC2 α , PI3KC2 β , PI3KC2 γ
- Class III: Vps34

The Class I enzymes, which are the focus of this thesis, catalyse the conversion of phosphatidylinositol 4,5-bisphosphate (also called PIP₂ or PtdIns(4,5)P₂) into secondary messenger phosphatidylinositol 3,4,5-triphosphate (PIP₃ or PtdIns(3,4,5)P₃) *in vivo*²³ (Figure 6). The generation of PIP₃ at the cell surface then provides a docking site for other proteins containing a particular amino acid sequence and structure, called a pleckstrin-homology domain, which ultimately allows control of a wide range of signalling cascades and cellular functions.²⁴

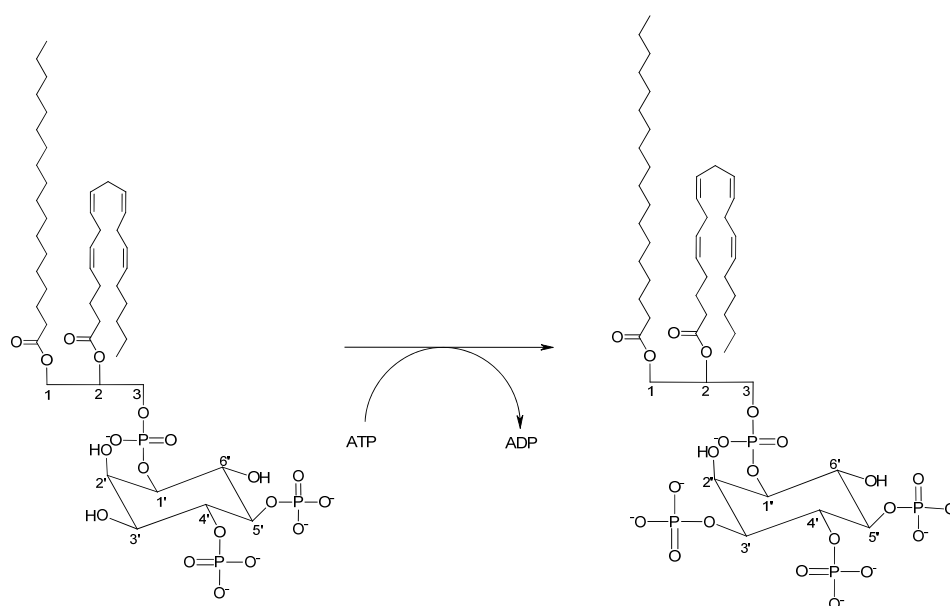


Figure 6: Conversion of PIP₂ to PIP₃

The four Class I proteins are further subdivided by mode of regulation into Class IA (PI3K α , β and δ) and Class IB (PI3K γ) (Figure 7).²⁵ Whilst the Class IA enzymes are

often activated through cell surface expressed receptor tyrosine kinases, the Class IB enzyme is regulated by G-protein coupled receptors. The four isoforms also differ in their expression profiles; whilst PI3K α and β are ubiquitously expressed, PI3K δ and γ are primarily found in leukocytes.²⁶

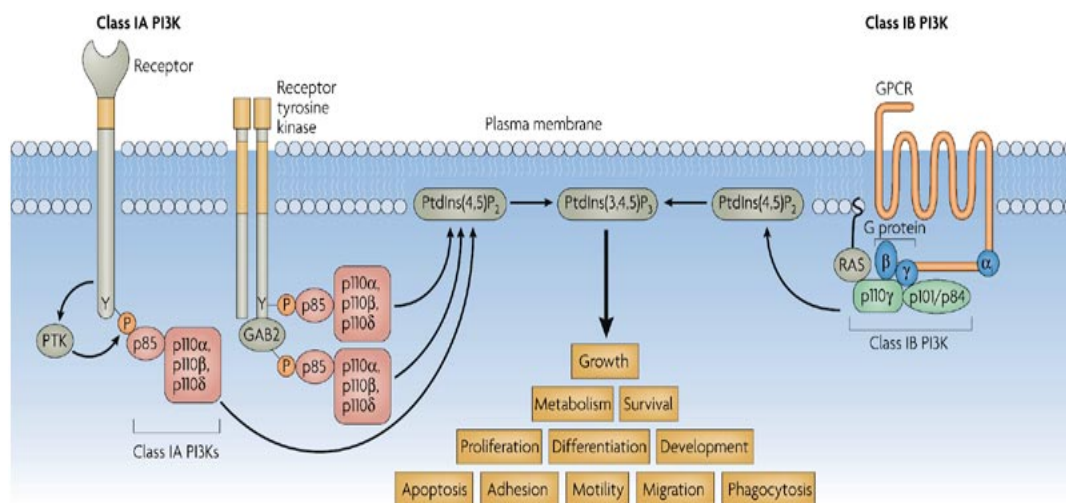


Figure 7: Class I PI3K signalling pathway²⁵

The Class II and III PI3Ks are currently less well understood, but are involved in the generation of different secondary messengers which are believed to control other cell functions.²⁴

1.3.1 PI3K Inhibitors for the Treatment of Respiratory Disease

Although all four Class I PI3K isoforms are responsible for generating the same lipid product, it appears that signalling pathways may be able to differentiate between PIP₃ generated from individual isoforms, by the presence of other adaptor proteins.^{27,28} Many studies have been carried out in attempts to elucidate the role of each isoform *in vivo* and thereby validate each protein as a target for modifying disease. Studies on genetically modified knock-out mice (where the whole gene is deleted) and/or kinase-inactive knock-in mice (where the protein is artificially expressed in a mutated form), in particular, have provided a wealth of information on the physiological function of these enzymes. PI3K α and β knock-out mice are embryonically lethal²⁹⁻³¹ and this, combined with their broad expression pattern, has prohibited interest in small molecule PI3K α or β inhibitors for indications other than oncology, where their role in cell growth and

proliferation is of interest.^{32,33} Mice lacking PI3K δ or γ (expression or function) are viable and survive for a normal life span. However, these mice demonstrate altered physiology when their immune system is challenged.^{34,35} PI3K δ mutant mice demonstrate specific defects in B-cell, T-cell- and mast cell-mediated processes,³⁶⁻³⁸ whilst mice lacking PI3K γ show reduced recruitment of neutrophils and macrophages to sites of inflammation, in addition to effects on T-cells and mast cells.³⁹⁻⁴² Figure 8 summarises the cell types implicated in the function of each isoform, γ and δ .

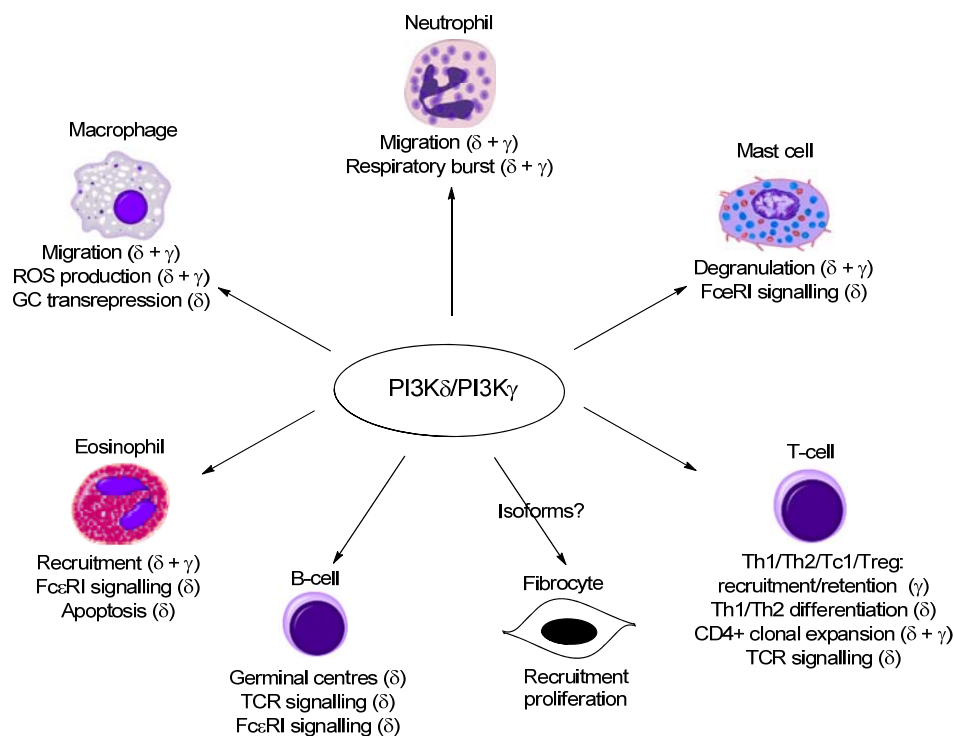


Figure 8: Roles of PI3K δ and PI3K γ signalling in selected cells important in respiratory disease²⁴

The clear role of PI3K δ and γ in cells involved in both the innate and adaptive immune system, coupled with their restricted expression profile, identifies small molecule PI3K δ and γ inhibitors as attractive targets for the treatment of inflammatory respiratory diseases.⁴³ This thesis will describe a programme of research to design and synthesise selective inhibitors of PI3K γ .

PI3K γ Inhibitors for the Treatment of Asthma

Asthma is typically characterised by eosinophilic inflammation of the large airways; however this is a complex inflammatory disease in which many cell types are recruited to, or activated in the lung, including mast cells, neutrophils, T lymphocytes and eosinophils.⁴⁴ Through the study of PI3K γ knockout mice *in vivo* and a range of cellular assays *in vitro*, PI3K γ has been implicated in a range of processes which may impact the disease.

Firstly, PI3K γ deficient mice show reduced chemotaxis of eosinophils to the lung in response to allergen challenge⁴⁵ and reduced chemotaxis of neutrophils to the lung in response to a range of chemokine activators (e.g. fMLP or LPS).⁴⁶ Inhibition of PI3K γ would therefore be expected to result in an anti-inflammatory effect, with not only reduced cell numbers, but also an associated reduction in the release of the pro-inflammatory cytokines which propagate further inflammatory processes.

Secondly, PI3K γ has been associated with airway remodelling, promoting irreversible changes in the airways, such as subepithelial fibrosis and goblet cell hyperplasia, observed in asthma patients.^{47,48} Reduced levels of peribronchial smooth muscle have also been observed in PI3K γ deficient mice, which correlated with a small, but statistically significant, reduction in airway hyperresponsiveness (AHR).⁴⁵

Thirdly, through studies with knockout mice, PI3K γ has been shown to play a role in amplifying mast cell activation, which is an important component of allergic asthma.⁴² Mast cell degranulation occurs in response to antigens, which bind to IgE receptors on the cell surface and leads to the release of a range of mediators and cytokines which further drive the allergic reaction and inflammation.⁴⁹

Finally, it has been proposed that reduced clearance of Th2 cells, due to a defect in apoptotic pathways, may play a role in the development of chronic inflammation in asthma.⁵⁰ Inhibition of PI3K γ has been shown to increase prostaglandin D₂ (PGD₂) induced apoptosis of T lymphocytes⁵¹ and, thereby, may be of benefit in promoting inflammatory resolution.

In summary, the establishment of a small molecule PI3K γ inhibitor for the treatment of asthma would aim to reduce the numbers of inflammatory cells in the lung (by reducing chemotaxis of eosinophils and neutrophils and promoting apoptosis of T cells), reduce mast cell degranulation, and may also have a positive effect on airway remodelling and hyperresponsiveness.

PI3K γ Inhibitors for the Treatment of COPD

In contrast to asthma, inflammation in COPD is thought to be driven largely by neutrophils in the large airways, however the smaller airways and lung parenchyma are populated with predominantly T lymphocytes.⁵² Figure 9 shows the overlap between the two diseases; mucus hypersecretion and oxidative stress are the predominant “COPD-specific” features of the disease.⁵²

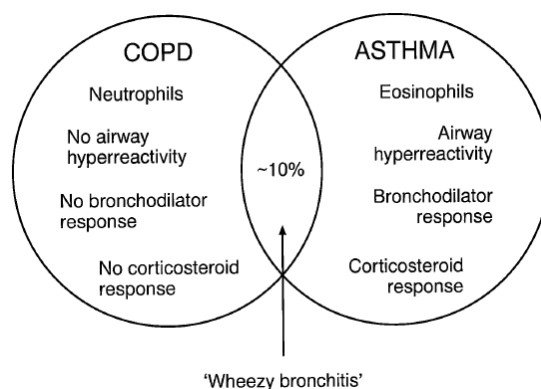


Figure 9: Differences between COPD and asthma; approximately 10% of patients with COPD also have asthma and therefore share pathologic features (“wheezy bronchitis”)⁵²

Whilst there is less direct experimental work establishing PI3K γ as a key driver of COPD pathology, there are several areas where a small molecule PI3K γ inhibitor may be of benefit.²⁴

As previously described, PI3K γ deficient mice show reduced chemotaxis of neutrophils to the lung, in response to a range of chemokine attractants (e.g. fMLP or LPS).⁴⁶ Although it is not yet clear which isoform(s) are critical to the process, PI3K has also been implicated in regulating the numbers of lung macrophages, through recruitment of

monocytes from the peripheral circulation.⁵³ Additionally, there is evidence that PI3K γ plays a role in T cell migration, with knock-out mice displaying decreased chemotaxis of CD4⁺ and CD8⁺ T cells to chemokine attractants (CXCL12, CCL10 and CCL21).⁵⁴

Similar to the rationale in asthma, inhibition of PI3K γ would be expected to have a broad anti-inflammatory effect, reducing cell numbers and the release of pro-inflammatory mediators in the lung.

PI3K γ Inhibitors for the Treatment of ALI

In simplistic terms, the direct or indirect lung injury which causes ALI, results in two main physiological changes in a patient's lung: firstly, an increase in the levels of pro-inflammatory cytokines and, secondly, altered alveolar fluid balance resulting in increased lung permeability and edema.⁵⁵ Through a range of *in vitro* and *in vivo* experiments,⁵⁶ neutrophils have been shown to play an important role in ALI and, as such, an effective treatment would aim to attenuate the cellular pathways in neutrophils, which drive these outcomes.

PI3K γ has been shown to have several important roles in neutrophils (Figure 10). Firstly, through activation of Akt, PI3K γ plays a role in the activation of NF κ B. NF κ B (or nuclear factor kappa-light-chain-enhancer of activated B cells) is a protein complex which, once activated, translocates to the nucleus and is responsible for the upregulation of a battery of genes which produce a range of pro-inflammatory cytokines, such as IL-1 β and TNF α .⁵⁶ Inhibition of PI3K γ has been shown in animal models to reduce the generation of these cytokines in response to stimulation with lipopolysaccharide (LPS).⁵⁷ In the same studies, PI3K γ inhibition also reduced levels of reactive oxygen species (ROS), which through their induction of other inflammatory mediators such as VEGF (vascular endothelial growth factor), have been linked to increased vascular leakage.⁵⁷

Secondly, neutrophil chemotaxis in response to a range of chemokine attractants (e.g. fMLP or LPS), has been shown to be PI3K γ dependent.^{46,58} The number of neutrophils in the lungs of ALI patients has been linked with both disease severity and prognosis,⁵⁹ and so reducing the influx of these cells to the site of injury is expected to be desirable for treatment.

Finally, PI3K γ inhibition has been shown to increase the apoptosis of LPS-induced neutrophils in the pleural cavity of mice *in vivo*.⁶⁰ Modulating the rate of apoptosis provides another mechanism for reducing cell numbers and limiting the release of pro-inflammatory mediators in the lung.

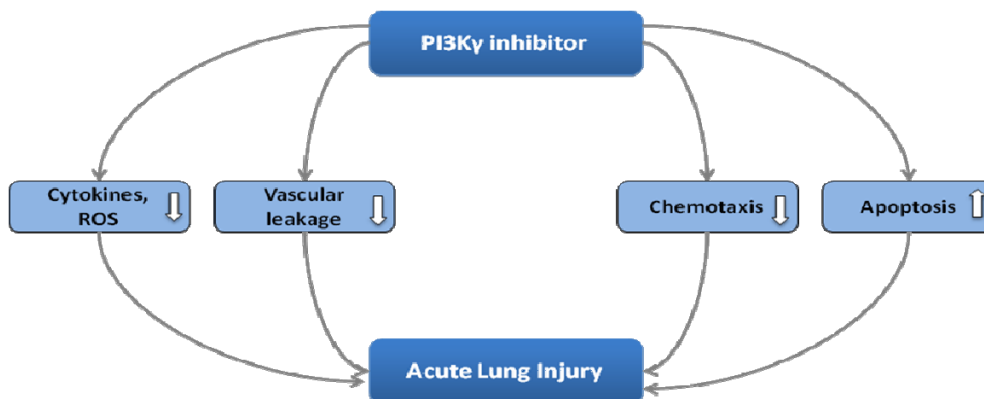


Figure 10: Mechanisms by which PI3K γ inhibition may benefit ALI patients

Targeting a small molecule PI3K γ inhibitor for the treatment of ALI would therefore aim to reduce the production of pro-inflammatory cytokines, increase the apoptosis of cells present in the lungs, and reduce the influx of fresh cells to the site of injury. Furthermore, there is some evidence that inhibition of PI3K γ may lead to reduced vascular permeability.

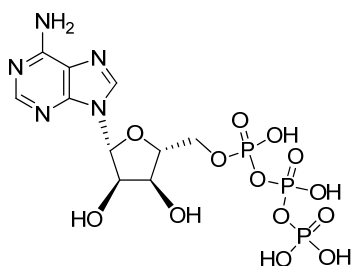
1.3.2 PI3K Structure

The protein sequence is known for all four Class I PI3Ks. They are all heterodimeric, and composed of a p110 (α , β , δ or γ) catalytic subunit and an associated regulatory subunit.⁶¹ The catalytic domain is similar to that of protein kinases, with the ATP-binding pocket located between the *N*- and *C*-lobes of the protein. All known PI3K inhibitors are reported to be ATP-competitive (sometimes referred to as Type I inhibitors) and target the active conformation of the protein.⁶² This increases the challenge for achieving selectivity, as all four isoforms, and indeed the wider kinome, bind the same substrate (ATP).

X-ray crystal structures of ATP bound to porcine PI3K γ are known in the literature⁶² (Figure 11). The adenine is shown to form two hydrogen bonds to valine 882 and

glutamic acid 880 residues in the hinge region of the protein (common to all kinases; shown as dashed yellow lines in Figure 11), with the ribose and phosphate groups occupying other regions of the protein. The porcine and human enzymes have 95.3% overall homology and have no sequence differences in the ATP binding pocket.⁶³

(a)



(b)

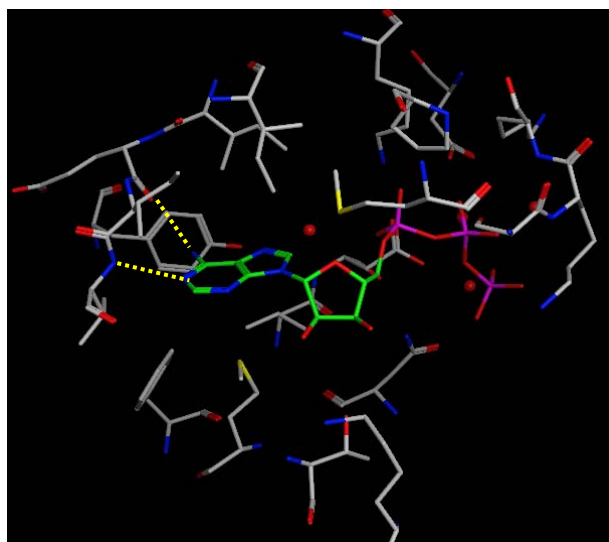
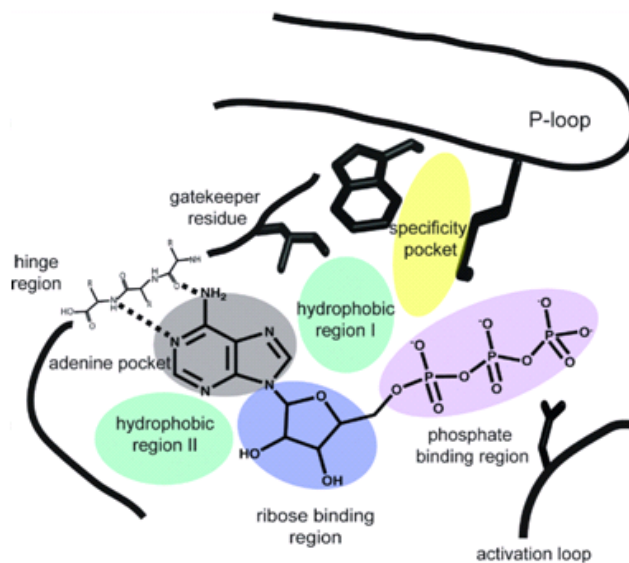


Figure 11: (a) Structure of ATP; (b) X-ray crystal structure of ATP bound to porcine *PI3Kγ*²

Using these and other inhibitor crystal structures, pharmacophore models of the ATP-binding site have been reported.⁶⁴ Figure 12 shows a pharmacophore model alongside the crystal structure shown above, with each region marked.

(a)



(b)

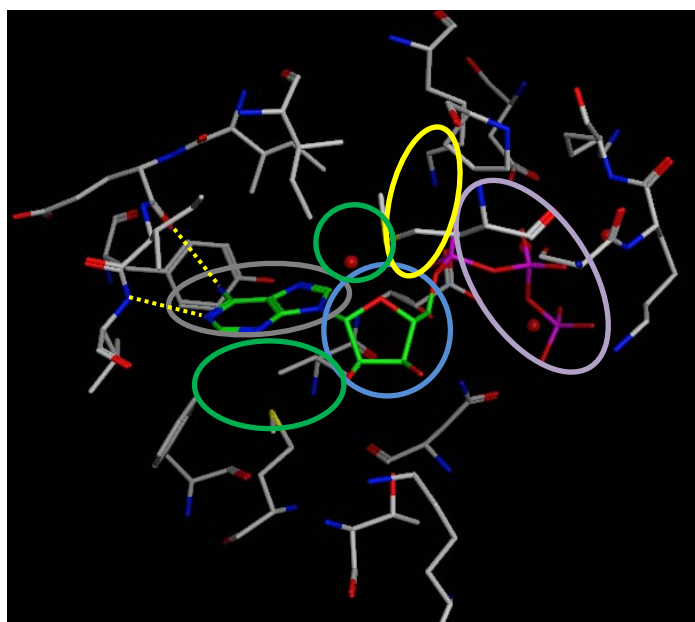


Figure 12: (a) Pharmacophore model of ATP binding site in PI3K;⁶⁴ (b) X-ray crystal structure of ATP in porcine PI3K γ with pharmacophore regions marked⁶³

Inhibitors commonly have a central core which occupies the adenine pocket, forming H-bond interactions with the hinge region of the protein. Substitution off the core then allows access to other nearby regions providing a means to increase affinity (e.g. the hydrophobic or phosphate regions).

The four isoforms of human PI3K have high levels of homology, although there are some differences in the ATP binding site. Figure 13 shows the crystal structure of ATP bound to PI3K γ ⁶³ with key residues which are different in the other isoforms highlighted in yellow (see Appendix 1 for the full protein sequence).

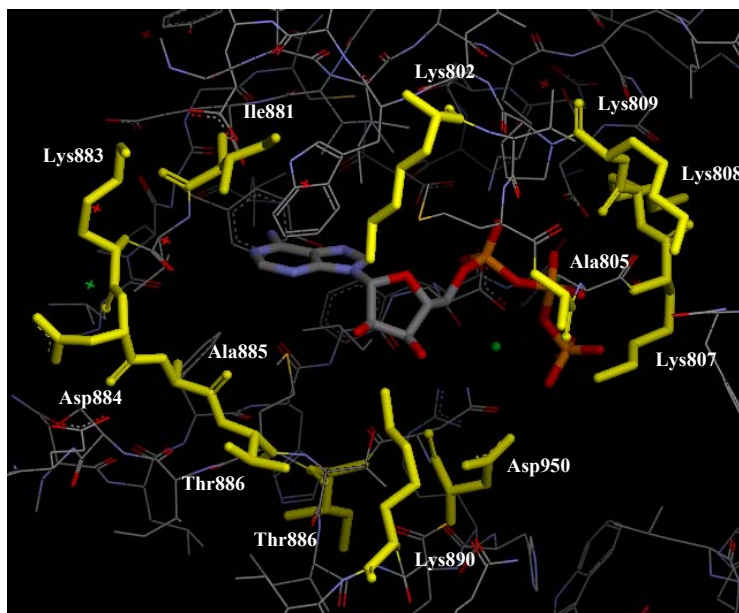


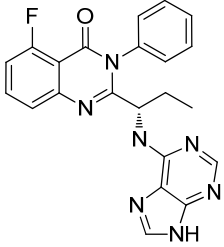
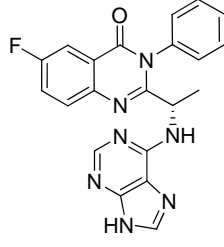
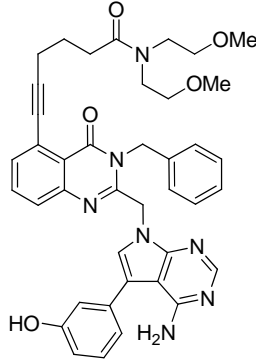
Figure 13: X-ray crystal structure of porcine PI3K γ with residues which differ between human isoforms highlighted

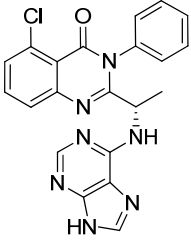
Targeting interactions with one or more of these amino acid residues is one strategy for achieving isoform selective inhibitors; however, some residues show more promise than others. The chain of amino acids in PI3K γ from lysine 883 to threonine 886, for example, can be seen in the ATP crystal structure to all have their side chains pointing away from the ATP binding site, so targeting interactions in this region of the protein is unlikely to deliver isoform selectivity. We must also consider the dynamic nature of proteins, which is not captured by X-ray crystallography. Indeed, protein structure can change significantly on the binding of an inhibitor⁶⁵ and differences in flexibility may provide another opportunity for achieving isoform selectivity.

1.3.3 Small Molecule PI3K Inhibitors

There is a wealth of literature on small molecule PI3K inhibitors, covering a wide range of structural classes with varying isoform selectivity profiles. Table 1 summarises those

PI3K γ selective, PI3K δ selective and PI3K γ/δ dual inhibitors which are currently in clinical trials.⁶⁶⁻⁷¹ It is clear that achieving an appreciably isoform-selective inhibitor is challenging. Indeed, there are no PI3K γ selective inhibitors currently in the clinic and of the PI3K δ inhibitors, only Idelalisib shows >200-fold selectivity against the undesired isoforms.

Cpd. No.	Inhibitor (company)	PI3K pIC ₅₀	Structure	Stage
PI3KδInhibitors				
1	Idelalisib (Gilead Sciences)	δ 8.6 α <6.1 β <6.3 γ <7.0		Phase III
2	GS-9820 (Gilead Sciences)	δ 7.9 α 5.3 β 5.5 γ 5.9		Phase I/II
3	AMG-319 (Amgen)	Unknown	Not published	Phase I
4	TGR-1202 (TG Therapeutics)	δ 6.9	Not published	Phase I
PI3Kδ/γ Dual Inhibitors				
5	Rv1729* (Respivert)	δ 7.9 γ 7.6 α 6.7		Phase I

6	IPI-145 (Infinity Pharmaceuticals)	δ 7.5 γ 7.2 α <6.2 β <6.2		Phase II
---	--	---	--	----------

*Table 1: PI3K γ and δ inhibitors in clinical development; data shown is from literature and not in-house profiling;⁶⁶⁻⁷¹ * indicates the chemical structure has not been published by Respivot, but surmised from published patents*

In addition to those compounds which are known to have reached clinical trials, there are numerous publications describing novel small molecule PI3K inhibitors. The following review summarises those which demonstrate some degree of PI3K γ selectivity (or claim some degree of PI3K γ selectivity, where biological data is not published). All data shown is from literature sources.

Thiazolidinones

Merck Serono,^{68,72} Warner Lambert⁷³ and Applied Research Systems⁷⁴ (now part of Merck Serono) have published on a range of thiazolidinone containing compounds as PI3K γ selective inhibitors (Table 2). Whilst many of these published patents do not contain any biological data for the α , β and δ isoforms, example compounds show good to excellent potency against PI3K γ .

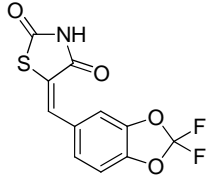
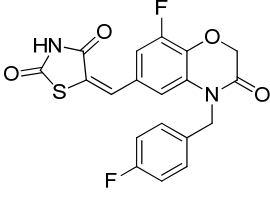
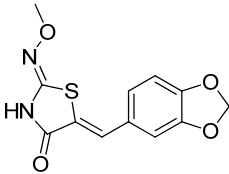
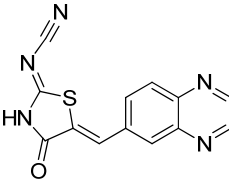
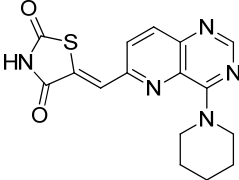
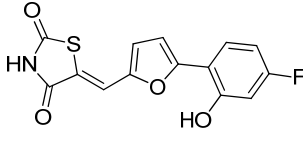
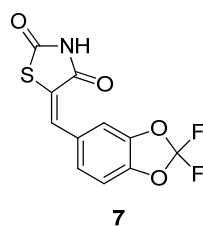
Cpd No.	Source	Structure	PI3K pIC ₅₀	C5a pAkt Macrophage pIC ₅₀
7	Merck-Serono AS-604850		γ 6.6 α 5.4 β <4.7 δ <4.7	-
8	Warner Lambert WO2004/052373 Example 298		γ 9.0	-
9	Merck Serono WO2005/011686 Example 20		γ >6.0	-
10	Merck Serono WO2005/011686 Example 21		γ >6.0	-
11	Applied Research Systems WO2006/024666 Example 1		γ 8.4	>8.0
12	Merck Serono <i>J. Med. Chem.</i> 2006 , 49, 3857		γ 7.5 α 6.0 β 4.7 δ 4.7	6.6

Table 2: Thiazolidinone PI3K γ inhibitors

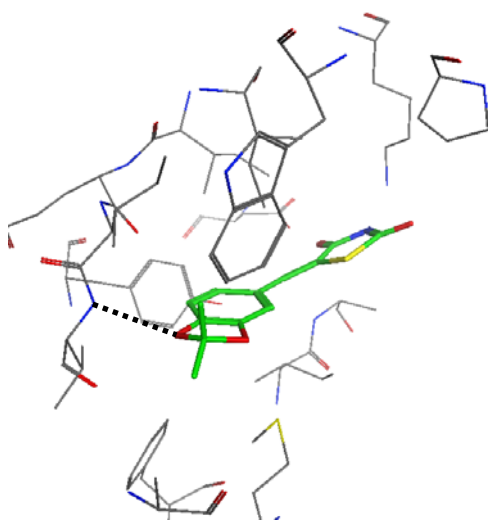
Of particular interest for the programme of work described in this thesis, are compounds **7**⁷⁵ and **12**⁶⁸ which, despite their small size, show ≥ 10 -fold selectivity for the γ isoform. The X-ray crystal structure of **7** bound to PI3K γ has been published⁷⁶ and is shown in Figure 14. The ligand binds to the hinge region of the PI3K γ protein *via* an H-bond interaction between one of the oxygens of the 1,3-benzodioxole and valine 882. The

thiazolidinone group extends into the phosphate pocket, forming a charge-charge interaction between the negatively charged ring nitrogen (at least partially ionised at physiological pH) and lysine 833. These interactions do not readily explain the degree of γ -selectivity however, as the amino acid residues in question are conserved in all four isoforms.⁷⁷ There are also hydrophobic interactions between the ligand and the protein; in particular, the (mostly) planar 1,3-benzodioxole core has good shape complementarity with the adenine pocket, as can be seen in Figure 14c.

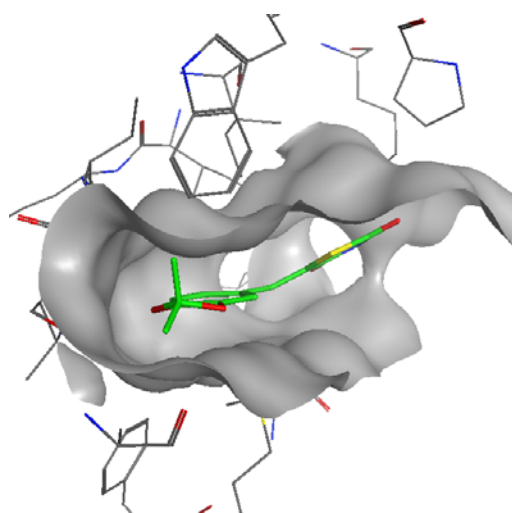
(a)



(b)



(c)



(d)

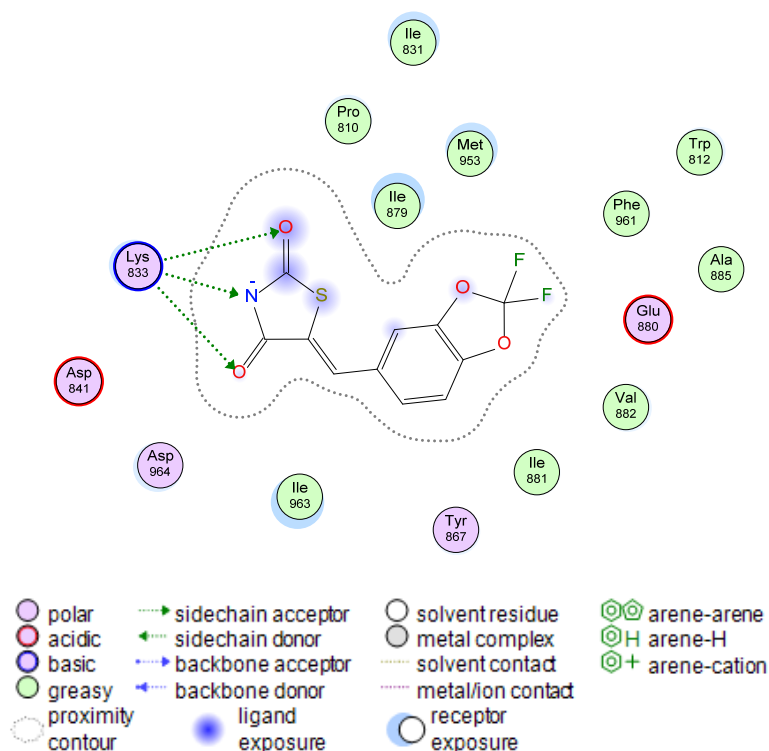


Figure 14: (a) Ligand 7; (b) X-ray crystal structure of 7 bound to PI3Kγ (PDB code 2a4z), H-bond interactions with the hinge shown in black;⁷⁶ (c) X-ray crystal structure of 7 bound to PI3Kγ with surface shown; (d) 2D representation of X-ray crystal structure with key interactions shown

An X-ray crystal structure of compound **12** bound to PI3Kγ is described by Pomel *et al.*⁶⁸ (although no structure has been deposited in the PDB), and reveals similar interactions to compound 7 in the phosphate pocket, but, in this case, the phenol hydroxyl group forms a hinge H-bond interaction with valine 882. Hydrophobic interactions of the phenyl and furan rings with lipophilic residues in the active site are also described.

2-Aminothiazoles

Another scaffold well exemplified amongst PI3Kγ inhibitors is the 2-aminothiazole template (Table 3). Initially reported by Novartis in 2003,⁷⁸ this template has been heavily patented by a range of companies,⁷⁸⁻⁸⁶ though little selectivity data has been reported.

Cpd No.	Source	Structure	PI3K pIC ₅₀	C5a pAkt Macrophage pIC ₅₀
13	Novartis WO2003/072557 Example 156		γ 8.7	-
14	Novartis WO2004/078754 Example 47		No data included	-
15	Novartis WO2005/021519 Example 96		γ 7.4 α 6.0 δ 5.7	-
16	Applied Research Systems WO2005/068444 Example 1		γ 8.0	5.5
17	Applied Research Systems WO2006/125805 Example 8		γ 6.7	-
18	Applied Research Systems WO2006/125805 Example 13		γ 7.9	-
19	Novartis WO2007/068473 Example 27		γ 7.0	-

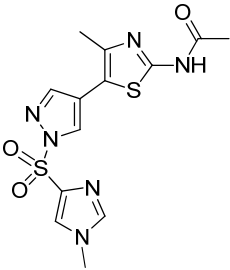
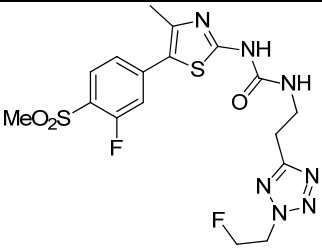
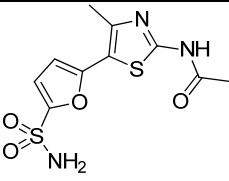
20	Merck Serono WO2007/082956 Example 8		γ 7.0	-
21	Novartis WO2007/134827 Example 7		γ 7.6	-
22	Vertex WO2008/027584 Example 19		γ >7.0	-

Table 3: 2-Aminothiazole PI3K γ inhibitors

An X-ray crystal structure of compound **13** has been published⁸⁷ and reveals an H-bond interaction at the hinge between the aminothiazole NH and valine 882 (Figure 15). A range of further polar interactions are present in the phosphate pocket and the biaryl scaffold makes a good hydrophobic contact with the protein surface in the adenine pocket.

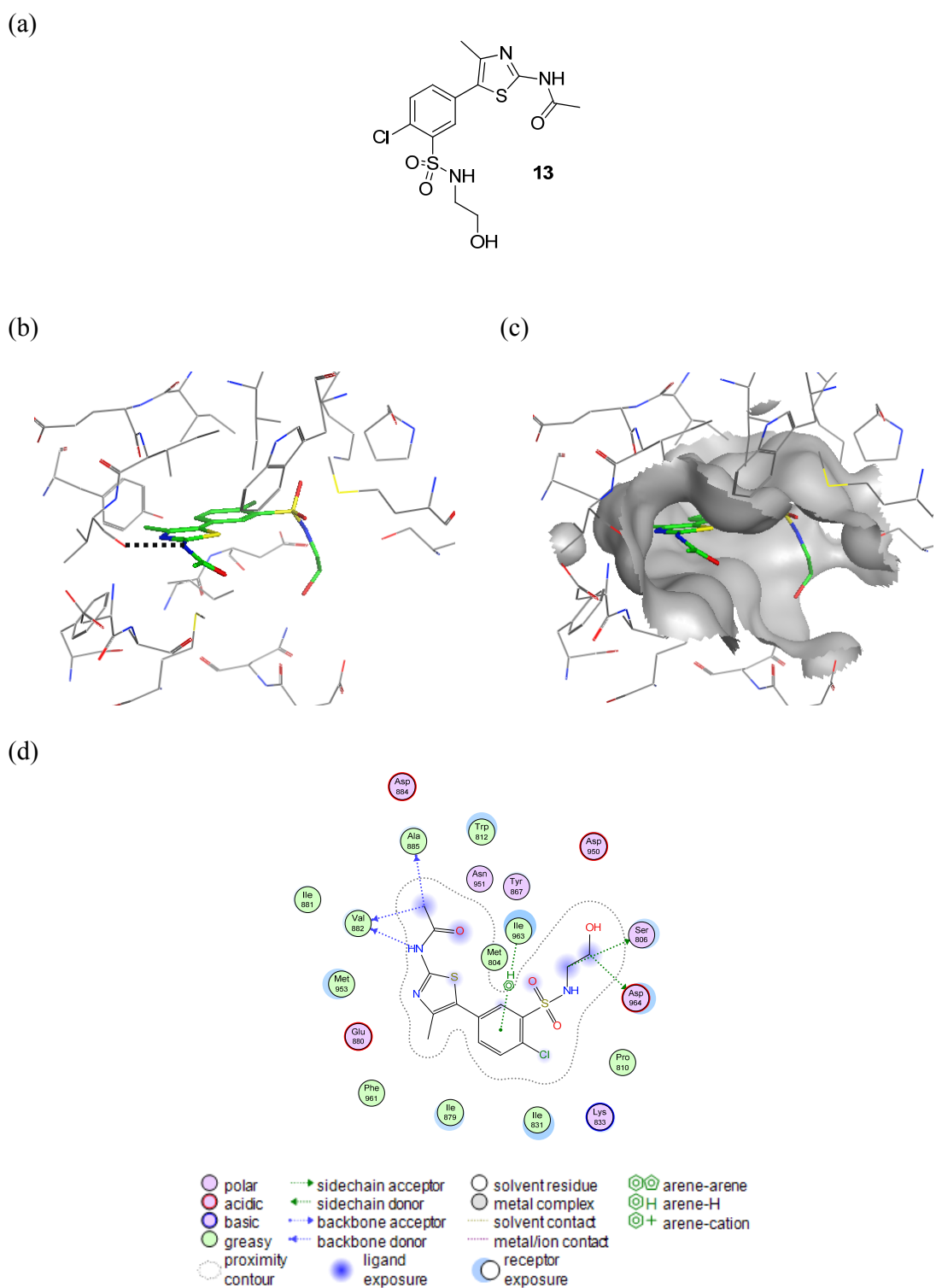


Figure 15: (a) Ligand **13**; (b) X-ray crystal structure of **13** bound to PI3K γ (PDB code 2chz), H-bond interactions with the hinge shown in black; (c) X-ray crystal structure of **13** bound to PI3K γ with surface shown; (d) 2D representation of X-ray crystal structure with key interactions shown

In 2007, Chroma Therapeutics published two patents based on the aminothiazole template,^{88,89} describing the use of lipophilic amino acid ester motifs, to facilitate cell accumulation (Table 4). The amino acid esters are designed to readily cross the cell membrane, but once inside are hydrolysed by intracellular carboxylesterases. Moffat *et al.* propose the resultant acids are then too polar to re-cross the cell membrane, thus providing a mechanism for prolonged and enhanced PI3K inhibitory activity. No isoform selectivity data was provided.

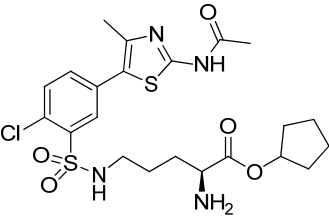
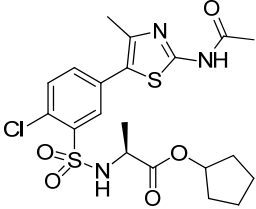
Cpd No.	Source	Structure	PI3K pIC ₅₀	LPS THP-1 cell pIC ₅₀
23	Chroma Therapeutics WO2007/129005 Example 19		$\gamma > 6.0$	5.0-6.0
24	Chroma Therapeutics WO2007/129048 Example 20		$\gamma > 7.0$	<6.0

Table 4: Chroma Therapeutics 2-aminothiazole derivatives

2-Aminoheterocycles

In addition to the aminothiazole template, a range of other 2-aminoheterocycle templates have also been reported. Merck Serono and Vertex have both published on an azabenzothiazole/benzathioazole template (Table 5),⁹⁰⁻⁹² the most recent examples of which show reasonable selectivity profiles with >20-fold against the α , β and δ isoforms.

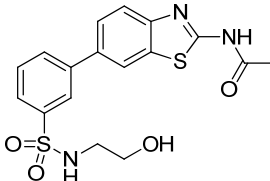
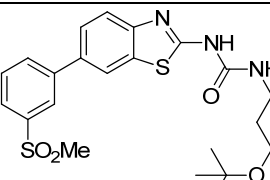
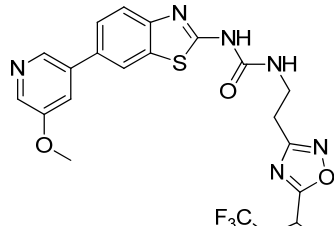
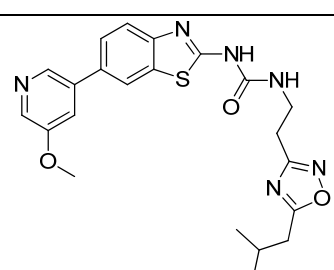
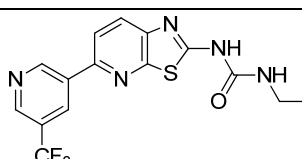
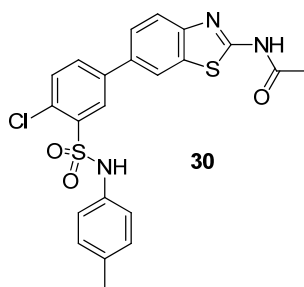
Cpd No.	Source	Structure	PI3K pIC ₅₀	C5a pAkt Macrophage pIC ₅₀
25	Merck Serono WO2009/133127 Example 4		$\gamma > 6.0$ $\alpha > 6.0$ $\beta > 6.0$ $\delta > 6.0$	>5.3
26	Merck Serono WO2009/133127 Example 87		$\gamma > 5.3$ $\alpha < 4.7$ $\beta > 4.7$ $\delta < 4.7$	-
27	Merck Serono WO2010/100144 Example 348		$\gamma > 6.0$ $\alpha < 4.7$ $\beta > 4.7$ $\delta > 4.7$	>6.0
28	Merck Serono WO2010/100144 Example 356		$\gamma > 6.0$ $\alpha < 4.7$ $\beta > 4.7$ $\delta < 4.7$	>6.0
29	Vertex WO2009/129211 Example 13		$\gamma \geq 8.0$	-

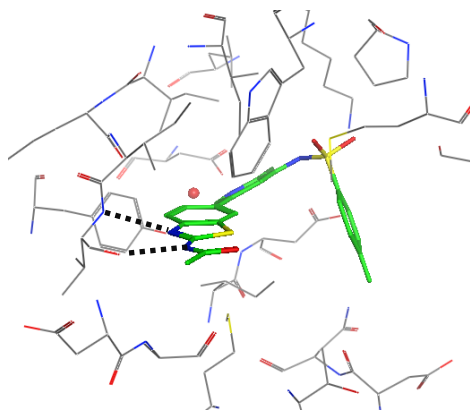
Table 5: Azabenzothiazole/Benzothiazole PI3K γ inhibitors

An X-ray crystal structure of the closely related PI3K α inhibitor **30**, described by Amgen in 2009,⁹³ reveals a similar binding mode to the 2-aminothiazole **13** (Figure 16). In this case, the aminoheterocyclic motif acts as a H-bond donor and acceptor, forming two H-bond interactions with valine 882. The large phenyl sulfonamide extends deep into the phosphate pocket, with an interesting twist between the two rings.

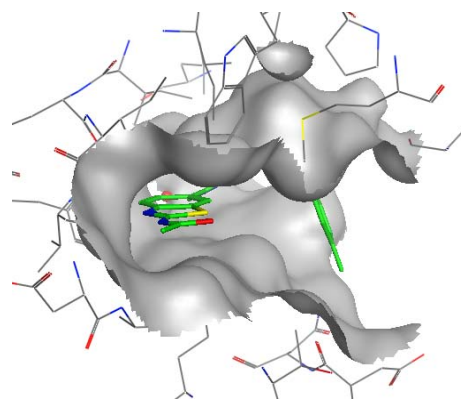
(a)



(b)



(c)



(d)

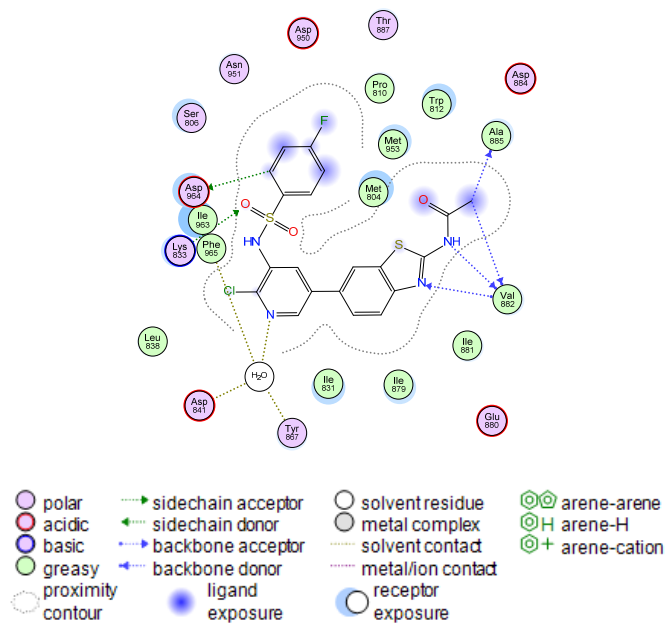


Figure 16: (a) Ligand **30**; (b) X-ray crystal structure of **30** bound to PI3K γ (PDB cde 3qk0), H-bond interactions with the hinge shown in black; (c) X-ray crystal structure of **30** bound to PI3K γ with surface shown; (d) 2D representation of X-ray crystal structure with key interactions shown

A related template has been described by Shionogi^{94,95} and Vertex,⁹⁶ where the phenyl ring of the benzothiazole scaffold has been successfully replaced by a piperidine. Of particular note is Shionogi's compound **32**, which is reported to have at least 100-fold selectivity against the α , β and δ isoforms (Table 6).

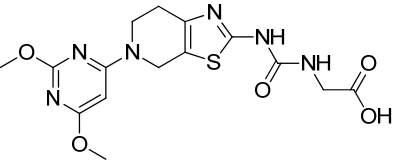
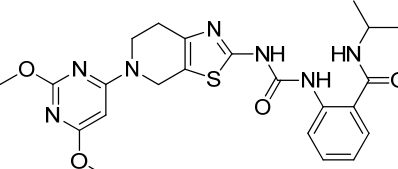
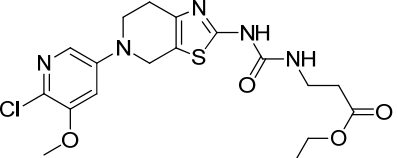
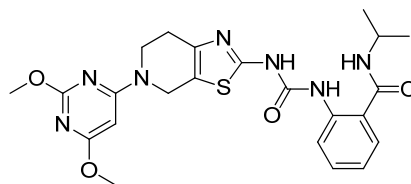
Cpd No.	Source	Structure	PI3K pIC ₅₀
31	Shionogi WO2010/024258 Example 208		γ 7.7
32	Shionogi WO2010/125799 Example 12		γ >7.5 α <5.5 β 5.5-6.5 δ 5.5-6.5
33	Vertex WO2010/096389 Example 52		γ 8.5

Table 6: Thiazolopiperidine PI3K γ inhibitors

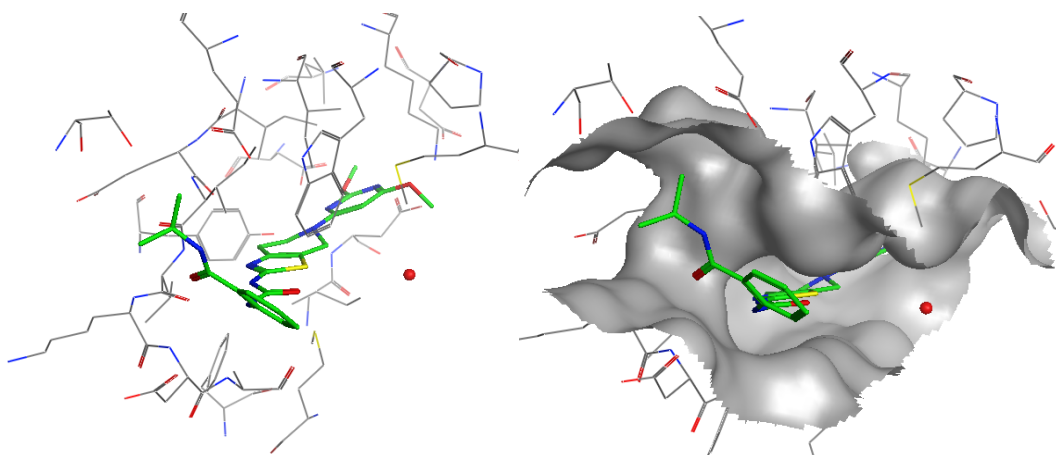
Interestingly, the binding mode of these analogues is similar to the more planar benzothiazole **30**, as confirmed by an proprietary X-ray structure of compound **32**⁹⁷ (Figure 17). The aminothiazole is still forming interactions with the hinge region of the protein, with the dimethoxypyrimidine occupying the phosphate pocket. The urea substituent extends along the hinge towards the solubility pocket, occupying a region of the protein not previously explored by the structures reviewed so far, which may be of significance considering its superior selectivity profile. It should be noted that examples from both the 2-aminothiazole and benzothiazole templates (e.g. compounds **15** and **28**) are also likely to occupy this region of the protein. However, structural information is not yet available for extended analogues from these templates.

(a)



32

(b)



(d)

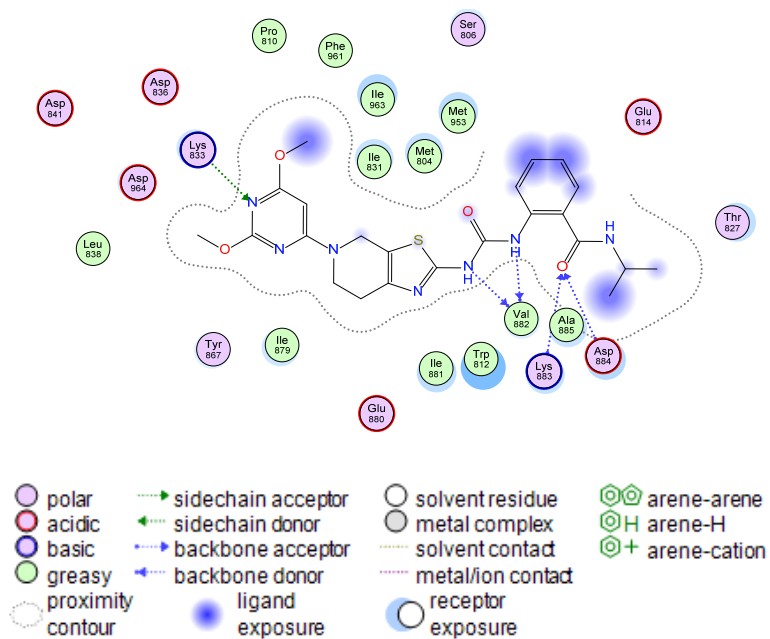


Figure 17: (a) Ligand **32**; (b) X-ray crystal structure of **32** bound to PI3K γ ; (c) X-ray crystal structure of **32** bound to PI3K γ with surface shown; (d) 2D representation of X-ray crystal structure with key interactions shown

Cellzome have authored a range of publications from 2008 onwards, on alternative 6,5-templates,⁹⁸⁻¹⁰³ also claiming selectivity for PI3K γ . Key examples are shown in Table 7, with the most promising compounds, such as **36**, showing >10-fold selectivity over the α , β and δ isoforms.

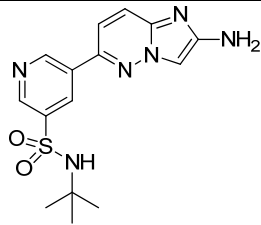
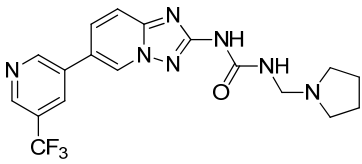
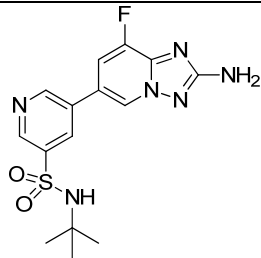
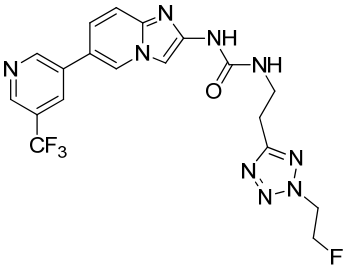
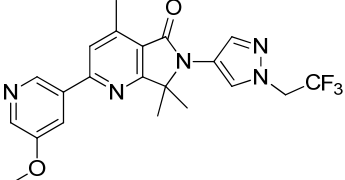
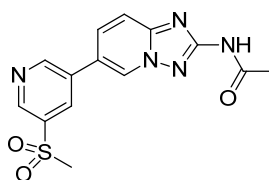
Cpd No.	Source	Structure	PI3K pIC ₅₀
34	Cellzome WO2010/007099 Example 2		$\gamma > 6.7$ $\alpha < 5.0$ β 6.0-7.0 δ 5.0-6.0
35	Cellzome WO2010/092015 Example 9		$\gamma > 7.0$ α 5.0-6.0 $\beta < 5.0$ δ 5.0-6.0
36	Cellzome <i>Nat. Chem. Biol.</i> 2012 , 8, 576		γ 7.6 α 5.6 β 6.7 δ 5.8
37	Novartis WO2009/010530 Example 1-35		Examples with $\gamma \geq 8.0$
38	Vertex WO2011/087776 Example 568		$\gamma > 7.0$

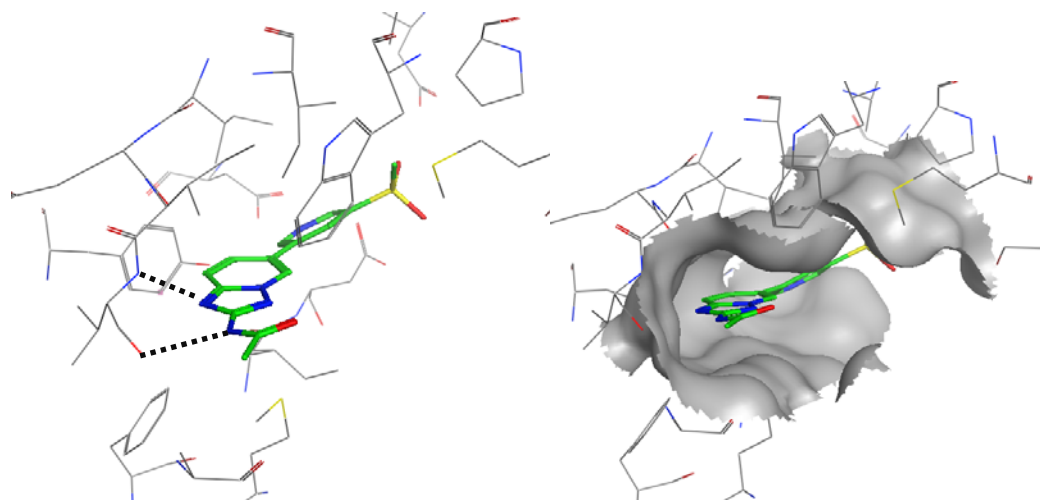
Table 7: Further 2-aminoheterocycle PI3K γ inhibitors

The X-ray crystal structure of analogue **39** was included in their most recent publication¹⁰³ (Figure 18) and confirms these compounds bind in a similar way to benzothiazole **30**, with the pyridine sulfone occupying the phosphate pocket. It is presumed that the longer urea substituents of compounds such as **35**, extend along the hinge like the Shionogi ligand **32**. Further patents from Novartis¹⁰⁴ and Vertex¹⁰⁵ describe some additional 6,5-fused templates. The latter, as exemplified by compound **38**, is an interesting incorporation of saturation into the five-membered ring and perhaps forms its H-bond to the hinge *via* the γ -lactam carbonyl. Indeed, the vector extending towards the solubilising pocket is likely to be altered compared with the 2-aminoheterocyclic scaffolds.

(a)

**39**

(b)



(d)

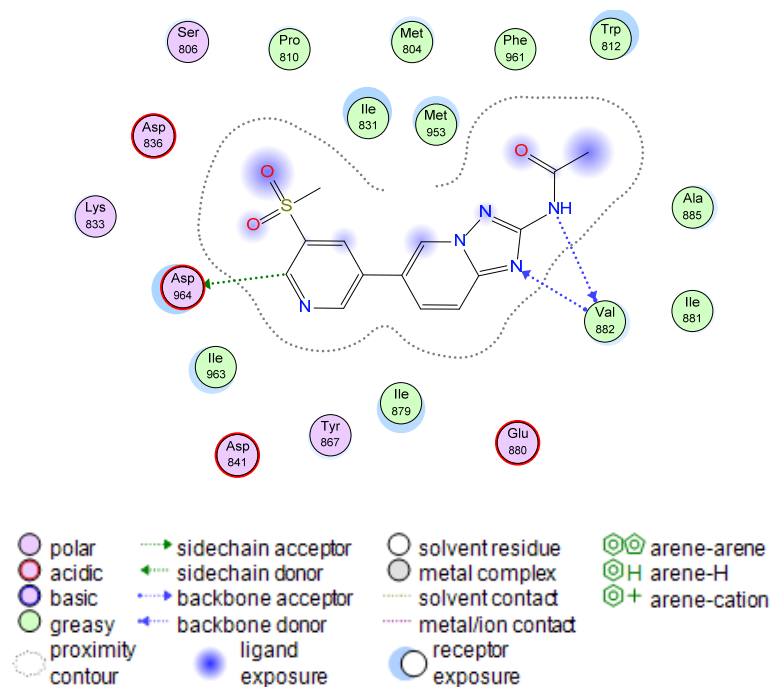
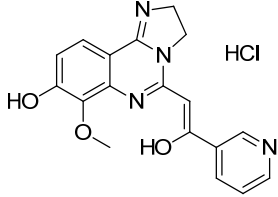
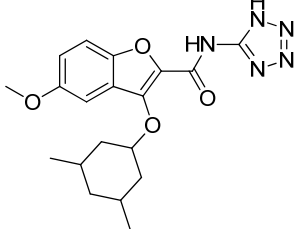
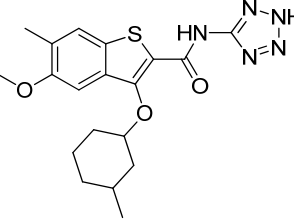
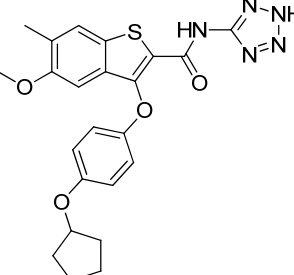
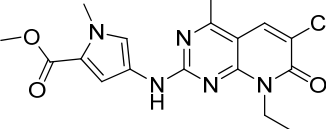
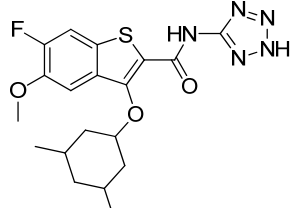
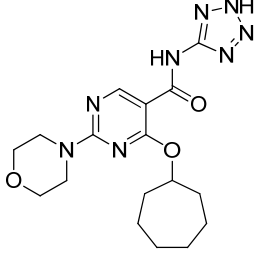
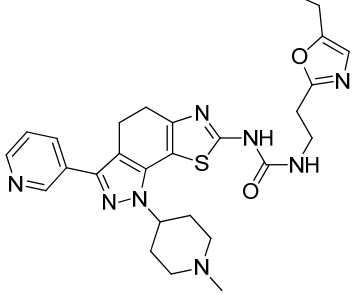
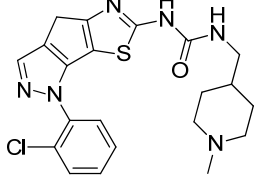
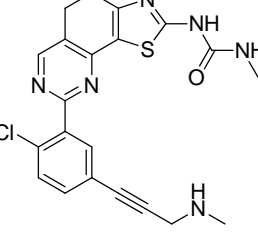
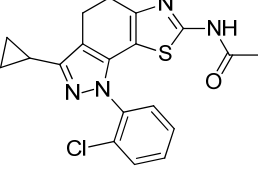
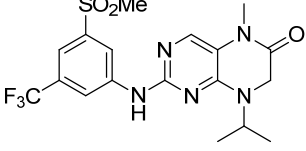
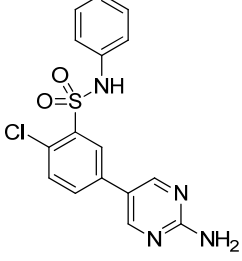


Figure 18: (a) Ligand **39**; (b) X-ray crystal structure of **39** bound to PI3K γ (PDB code 4aof); (c) X-ray crystal structure of **39** bound to PI3K γ with surface shown; (d) 2D representation of X-ray crystal structure with key interactions shown

Other

A diverse range of further chemical templates have been reported in the literature as producing selective PI3K γ inhibitors (Table 8), with varying amounts of biological data to support these claims.¹⁰⁶⁻¹²² The examples shown in Table 8 all show good levels of potency against PI3K γ , although little isoform selectivity data is given.

Cpd No.	Source	Structure	PI3K pIC ₅₀
40	Bayer WO2004/029055 Example 1-4		$\gamma \geq 7.0$ $\beta \geq 6.3$
41	Warner Lambert WO2004/108709 Example 22		γ 7.4
42	Warner Lambert WO2004/108713 Examples 7		γ 8.5
43	Warner Lambert WO2004/108715 Examples B-17		γ 8.4
44	Warner Lambert WO2005/105801 Example 30		γ 8.7
45	Pfizer WO2005/023800 Example 15		Examples with $\gamma \geq 6.7$

46	Pfizer WO2005/042519 Example 1		Examples with $\gamma > 6.7$
47	Boehringer Ingelheim WO2007/115930 Example 94		$\gamma > 6.1$
48	Boehringer Ingelheim WO2007/115931 Example 120		$\gamma > 6.1$
49	Boehringer Ingelheim WO2007/115932 Example 2		$\gamma > 6.1$
50	Boehringer Ingelheim US2009/0093474 Example 1		$\gamma > 6.2$
51	Novartis WO2008/092831 Example 1		$\gamma > 6.1$
52	Novartis WO2009/013348 Example 1-1		$\gamma 8.4$

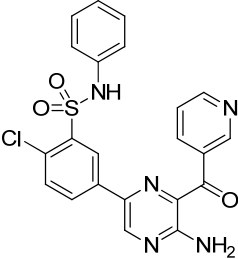
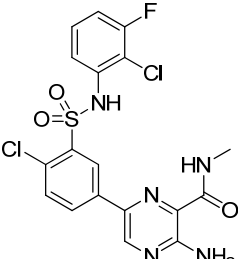
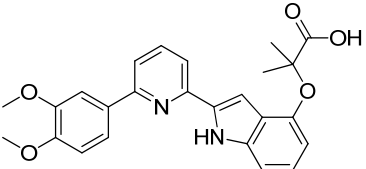
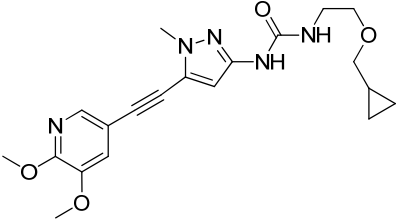
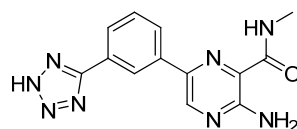
53	Novartis WO2009/115517 Example 13		γ 7.9
54	Exelixis <i>J. Med. Chem.</i> , 2012 , 55, 5467 Example 27		γ 7.7 α 6.0 β 5.4 δ 5.9
55	Shionogi WO2010/061903 Example 248		γ 8.3
56	Vertex WO2011/041634 Example 3		γ >7.0

Table 8: Miscellaneous PI3K inhibitors

The aminopyrazine template, first described by Novartis,^{119,120} has recently been investigated by Exelixis.¹¹⁰ Compound **54** represents the most potent and selective from this series with >50-fold selectivity against the α , β and δ isoforms, however structural information is provided on close analogue **57** (Figure 19). The aminopyrazine binds to the hinge region of the protein with the tetrazole (and presumably the phenyl sulfonamide of **54**) extending into the phosphate pocket. The methyl amide extends towards the solubility pocket, but was shown by Leahy *et al.* not to be critical for isoform selectivity.¹¹⁰

(a)

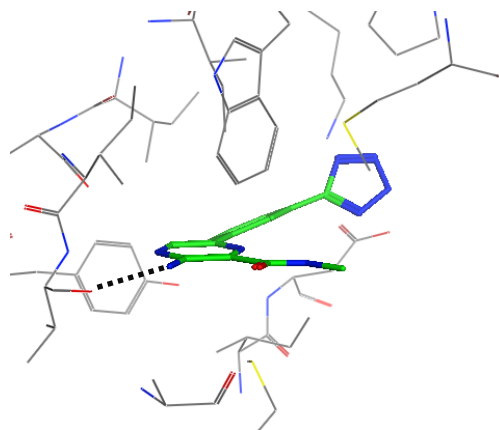


57

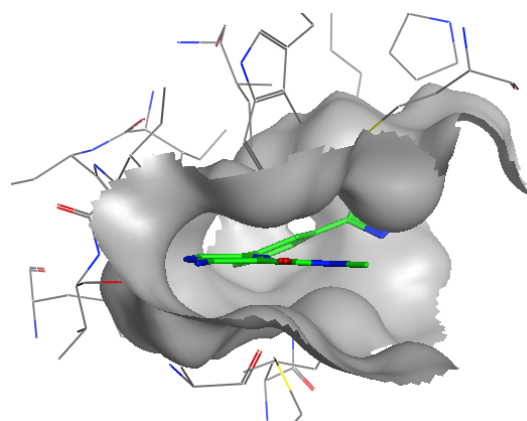
PI3K γ 7.7

α 6.3, β 5.2, δ 5.4

(b)



(c)



(d)

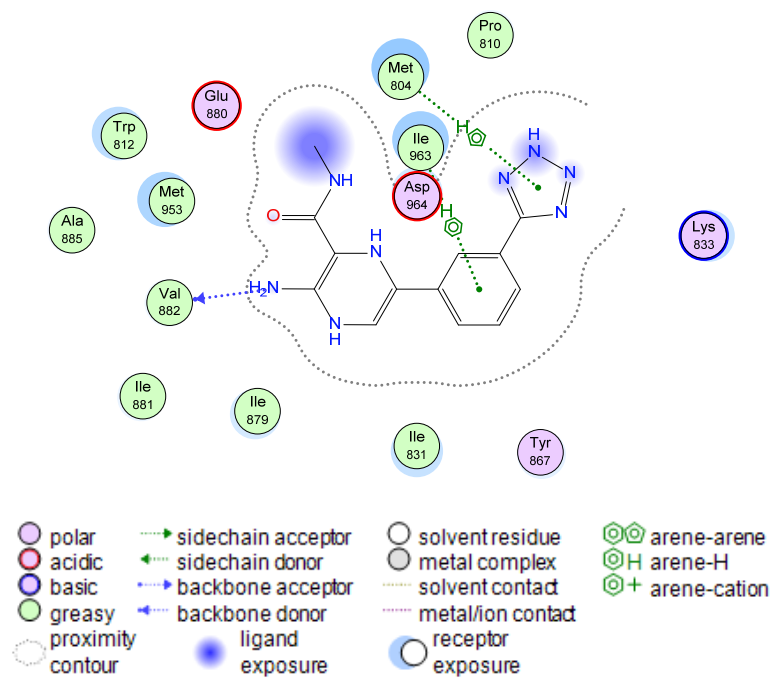


Figure 19: (a) Aminopyrazine 57; (b) and (c) X-ray crystal structure of aminopyrazine 57 bound to PI3K γ (PDB code 4anu), without and with protein surface; (d) 2D representation of X-ray crystal structure with key interactions shown

Summary

In conclusion, a diverse range of chemical templates have been exemplified in the literature as selective PI3K γ inhibitors. Although limited biological data are available in many of these publications, the best examples show \geq 30-fold selectivity against the other Class I PI3K isoforms (e.g. compounds **7**, **12**, **27** and **36**). The significant exception to this is compound **32**, published by Shionogi, which has an impressive selectivity profile (>100 -fold against α , β and δ).

1.3.4 Target Product Profile

Based on the biological rationale presented above and the chemical tractability of this target, a small molecule PI3K γ inhibitor programme was initiated. Whilst further *in vitro* and *in vivo* target validation studies were required to fully define our desired product profile, initial work focused on developing a chemical series suitable for an oral or inhaled treatment of asthma and COPD.

2.0 PYRIDONE SERIES

2.1 Historical Data Review

Several chemical series have previously been investigated as PI3K γ selective inhibitors in our laboratories. One key example was the pyridone template (Figure 20).

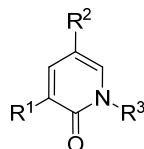
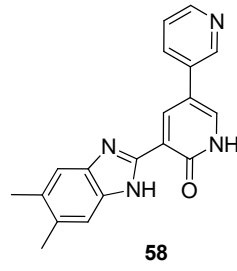


Figure 20: Pyridone template

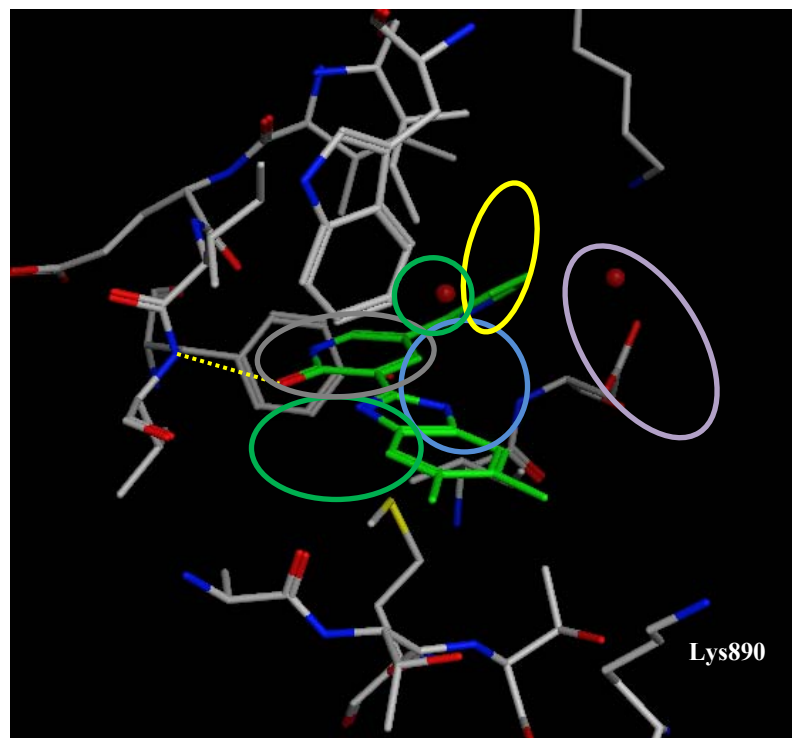
In these previous studies over 300 analogues had been prepared in this series, exploring the R¹, R² and R³ substituents.¹²³ As a whole, the spectrum of prepared molecules showed moderate to promising enzyme potency¹²⁴ (see Appendix 2 for assay protocols), with the most potent analogues achieving a pIC₅₀ >8 against the isolated PI3K γ enzyme.¹²³

The binding mode of these compounds in the PI3K γ protein has been confirmed by X-ray crystallography;¹²⁵ a representative example is shown in Figure 21. As illustrated, the pyridone carbonyl acts as the hinge binder, forming an H-bond with valine 882. The R² group occupies the hydrophobic region I (shown in Figure 12) and the R¹ substituent points towards the sugar pocket.

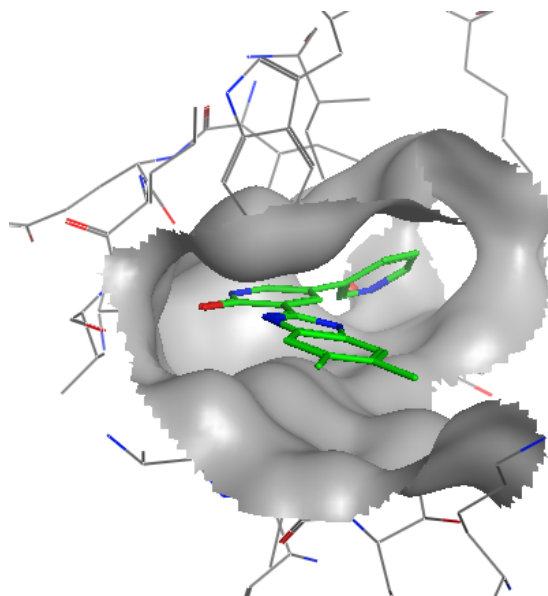
(a)



(b)



(c)



(d)

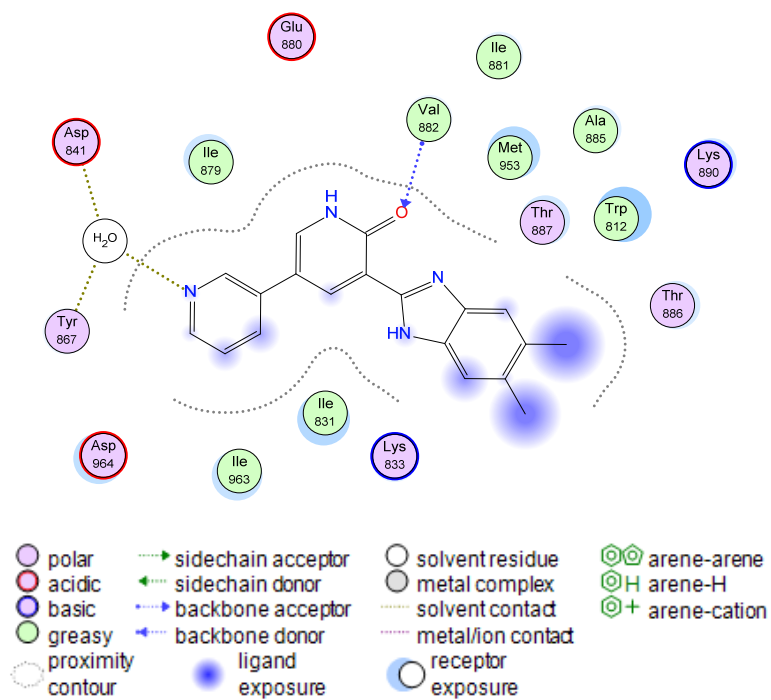


Figure 21: (a) Pyridone ligand **58**; (b) and (c) X-ray crystal structure of a pyridone **58** bound to PI3K γ without and with protein surface; yellow dashed line represents hinge interaction, coloured circles show pharmacophore regions as defined in Figure 12; (d) 2D representation of X-ray crystal structure with key interactions shown

Analysis of the historical data revealed some clear SAR around the pyridone nitrogen substituent (R^3), which can be rationalised by considering the proximity of this component to the protein surface. Whilst compounds where $R^3=H$ were generally more potent against PI3K γ , methylation of this position was beneficial for selectivity against the wider kinome (exemplified by protein kinases ActRIIA and ActRIIB in this case) without major impact on the PI3K γ potency (Table 9).¹²³ Interestingly, this suggests a greater flexibility in this region of the PI3K structure than in protein kinases ActRIIA and ActRIIB.

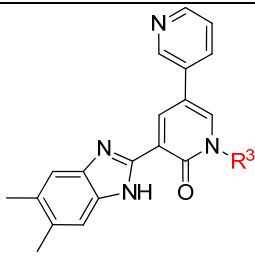
Compound No.		PI3K γ pIC50 [#]	Kinase selectivity [±]
58	H	6.2	ActRIIA 6.9 ActRIIB 6.9
59	Me	5.9	>10-fold vs. 38 kinases
60	Et	<4.5	-

Table 9: SAR of R^3 substituent

[#] Values are mean of ≥ 2 experiments in all tables unless otherwise stated

[±] Potencies against selected protein kinases are displayed; ActRIIA and B are activin receptor kinases

In this specific regard, Xie *et al.* have previously proposed that the flexibility of a key tyrosine residue in this region of PI3K γ (tyrosine 867; conserved in all PI3K isoforms, but not in protein kinases) is responsible for the improved selectivity profile of their *N*-methyl analogue DW12Me against protein kinase GSK3 (Figure 22).¹²⁶

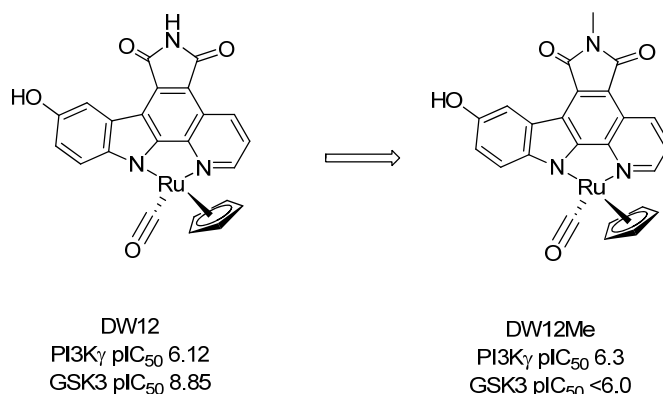


Figure 22: Effect of N-methylation on selectivity against protein kinase¹²⁶

Whilst only one analogue with R³=Et has been prepared previously, this compound showed poor activity against PI3K γ ;¹²³ the increase in steric bulk probably results in a clash with the protein backbone. Due to the significant improvement in selectivity and only moderate drop in PI3K γ potency with R³=Me, this substitution was selected for use in all subsequent compounds made.

Analysis of the SAR relating to the pyridone 3-substituent (R¹) and pyridone 5-substituent (R²) units was more complex. Figure 23 shows a 2D plot of the chemical space covered at these two positions, with the range of R¹ groups exemplified on the y-axis and R² on the x-axis. This graph clearly demonstrates that the majority of compounds were made in 1D arrays, where either R² (most commonly 3,4-dimethoxyphenyl or 3-pyridyl) or R¹ (most commonly 5,6-dimethyl-1*H*-benzimidazole or 5-(4-morpholinyl)-1*H*-benzimidazole) were fixed and the other position varied.

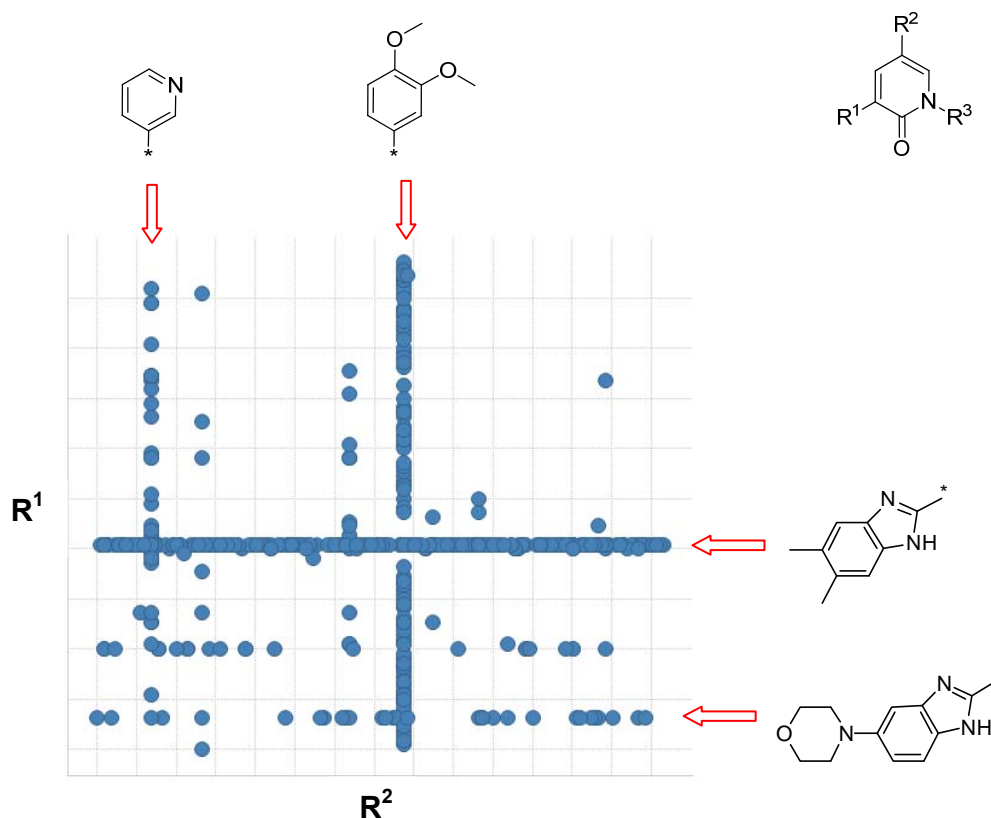


Figure 23: Graphical representation of chemical space covered at the R^1 and R^2 positions

In order to further interrogate the SAR, a Free Wilson analysis¹²⁷ of the data was conducted. Free Wilson is a statistical analysis which compares pairs of compounds to ascertain whether the SAR observed for each substituent of a core template is independent of the other. In due course, it was concluded that the SAR for the two positions of the pyridone template was additive, albeit with the caveat that a fairly high number of substituents were only exemplified once which weakens the statistical significance. Additive SAR not only simplifies interpretation of the data from this series, but also the future medicinal chemistry strategy. Independent optimisation of each position and subsequent combination of the best groups is possible in this situation, reducing the number of analogues requiring synthesis.

At the R^1 position, a range of benzimidazole analogues were made and some key examples with the dimethoxyphenyl R^2 group are shown in Table 10.¹²³

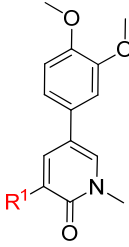
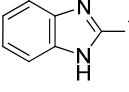
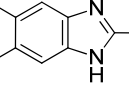
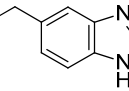
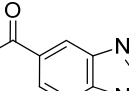
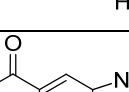
Compound No.		PI3K γ pIC ₅₀	PI3K Isoform pIC ₅₀
61		6.8	α 5.5, β 5.0 ^{*‡} , δ 5.5
62		7.0	α 5.4, β <4.6, δ 6.1 [*]
63		7.1	α 6.3, β 5.2, δ 6.6
64		7.5 [*]	α 6.2 [*] , β <4.6 [*] , δ 5.7 [*]
65		7.1	α 5.4 [±] , β <4.6, δ 5.3 [‡]

Table 10: R¹ Benzimidazole SAR; * indicates n=1 value; [±] indicates one result not included in mean as below the threshold of the assay (i.e. pIC₅₀ <4.6); [‡] indicates two results not included in mean as below the threshold of the assay (i.e. pIC₅₀ <4.6)

Generally, these compounds showed good potency and some selectivity for PI3K γ over the other isoforms. Both small lipophilic and basic benzimidazole substituents are tolerated (**62**, **63**), whilst the addition of a carboxylic acid group gives the best combination of potency and selectivity (**64**, **65**). It is hypothesised that this is due to an H-bond interaction between the carboxylic acid and a lysine residue (lysine 890) in PI3K γ (see Figure 21 for illustration). Lysine 890 is a residue which is not conserved in any of the other isoforms.

In addition to varying the benzimidazole substituent, a few compounds were also made with alternative heterocycles at the R¹ position (Table 11),¹²³ in this case with a 3-methoxy-4-phenol R² group.

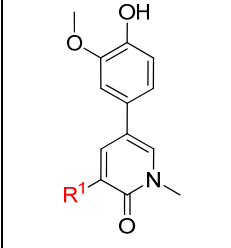
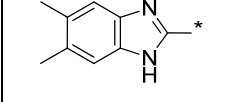
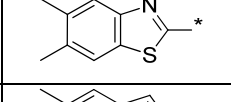
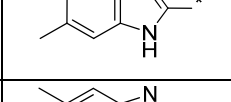
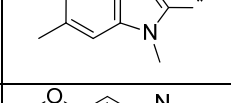
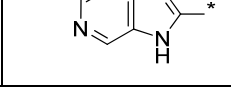
Compound No.		PI3K γ pIC ₅₀	PI3K isoform selectivity
66		7.0	α 5.7 [‡] , β 5.1 [§] , δ 5.7
67		6.4 [*]	α 5.5 [±] , β 5.6 [±] , δ 5.5
68		6.6 [*]	α 5.6, β 5.0, δ 6.2
69		<4.5	α <4.5, β <4.5, δ 4.7 [‡]
70		7.0	α 5.9, β 4.9, δ 6.0

Table 11: SAR of benzimidazole replacements; * indicates $n=1$ data; [±] indicates one result not included in mean as below the threshold of the assay (i.e. $pIC_{50} < 4.6$); [‡] indicates two results not included in mean as below the threshold of the assay (i.e. $pIC_{50} < 4.6$); [§] indicates six results not included in mean as below the threshold of the assay (i.e. $pIC_{50} < 4.6$)

Replacement of the benzimidazole in compound **66** with benzothiazole **67** results in a drop in potency. In the crystal structure shown in Figure 21, the distance from the benzimidazole NH to the nearest acceptor on the protein backbone is within H-bonding range (2.5-3.5 Å),¹²⁸ which could explain the drop in potency for benzothiazole analogue **67** where no H-bond donor is present. For indole **68**, the difference in potency to benzimidazole **66** is much less significant, but the situation is more complicated. Based on its higher pK_a , indole would be predicted to be a weaker H-bond donor than benzimidazole. However, the replacement of nitrogen with carbon in the 3-position could also affect binding due to the removal of an H-bond acceptor functionality.

Another possibility is that the benzimidazole/indole NH could form an intramolecular H-bond with the pyridone carbonyl (Figure 24). An intramolecular H-bond like this would

fix the benzimidazole conformation in a planar arrangement with the pyridone core, which is predicted to be the lowest energy conformation. If this was also the preferred conformation for binding, an increase in potency would result due to the reduced entropy penalty resulting from conformational selection. Again, heterocycles with no, or weaker, H-bonding potential should result in a drop in potency. In relation to this, it is shown in Table 11 that *N*-methylbenzimidazole **69** gives complete loss of activity, which could be due to disruption of the H-bonding interaction (be it intramolecular or with the protein). Alternatively, it may simply be a consequence of poor shape complementarity with the enzyme. Additionally, the methyl group could affect the relative conformation of the two rings, resulting in a greater dihedral angle between the pyridone core and the R¹ substituent, which may be unfavourable for binding.

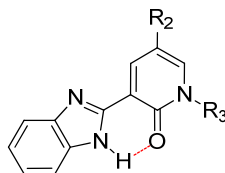


Figure 24: Proposed intramolecular hydrogen bond

Finally, imidazopyridine analogue **70** is well tolerated and will also modify the physicochemical profile relative to benzimidazole, increasing the polar surface area (PSA) and potentially improving solubility.

Investigation of R² was mostly limited to substituted phenyl or pyridyl groups, however, a few other mono- and bicyclic heterocycles had also been prepared and analysed.¹²³ Table 12 shows the optimum substituents as identified by the Free Wilson analysis.¹²⁷ Whilst the pyridine sulfonamides **72** and **73** give good PI3K γ potency, they also increase potency against the other isoforms (α and δ).

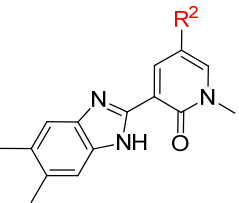
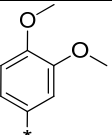
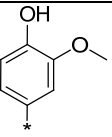
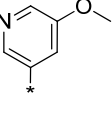
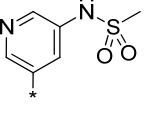
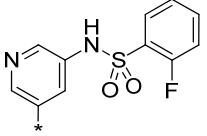
Compound No.		PI3K γ pIC ₅₀	PI3K isoform selectivity
62		7.0	α 5.4, β <4.6, δ 6.1*
66		7.0	α 5.7 [‡] , β <4.9 [‡] , δ 5.7
71		6.0	α <4.6, β <4.6, δ <4.6
72		7.2	α 5.9 [±] , β <5.3, δ 6.0
73		7.7	α 6.2, β <4.6, δ 6.5

Table 12: R² SAR; [±] indicates one result not included in mean as below the threshold of the assay (i.e. pIC₅₀ <4.6) [‡] indicates one result not included in mean as below the threshold of the assay (i.e. pIC₅₀ <4.6)

In summary, these historical data demonstrated that analogues from the pyridone series could achieve good potency against PI3K γ , good wider kinase selectivity, and some selectivity against the other PI3K isoforms.

Aside from the biological data on this series, the physicochemical profiles of the compounds were also analysed. In general, the relevant structures are fairly compliant with Lipinski's "rule of five" for obtaining good permeability and oral absorption.^{129,130}

Lipinski's rule of 5:
 cLogP <5
 MW <500 Da
 Number of hydrogen acceptors <10
 Number of hydrogen bond donors <5

Figure 25a shows that the majority of compounds fall within the desired MW and cLogP range, whilst Figure 25b shows this series has an acceptable HBD/HBA profile.

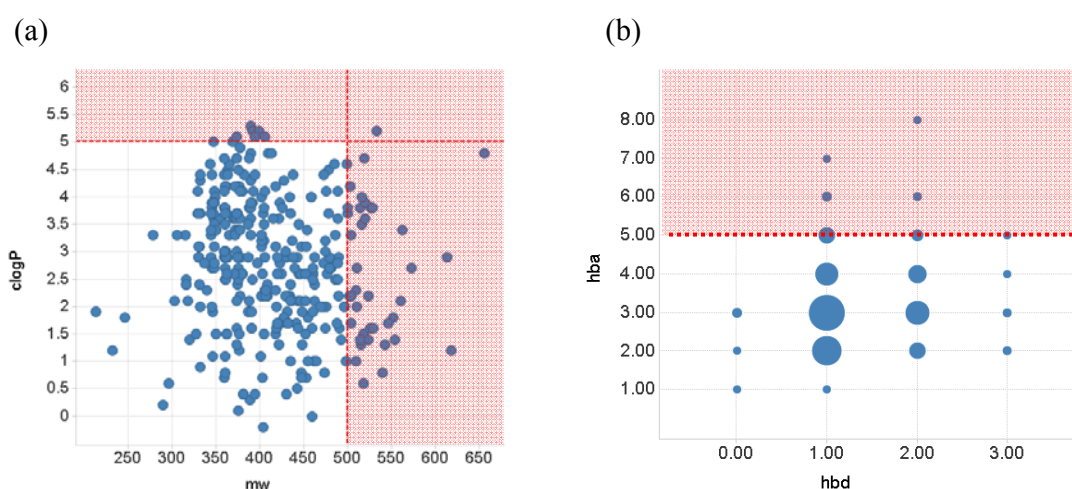
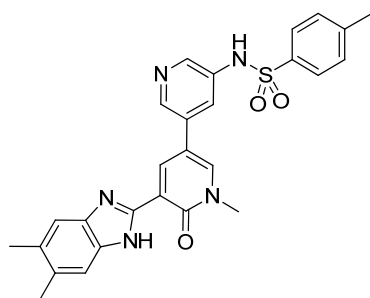


Figure 25: Lipinski cut-offs are marked by red dashed lines; undesirable space shaded red; (a) cLogP vs. MW; (b) Number of hydrogen bond donors vs. acceptors, the size of pie represents number of compounds

However, whilst the majority of compounds obey Lipinski's rules, at such an early stage in a drug discovery programme there is greater interest in compounds with lower molecular weight (~300-400 Da) and lipophilicity (cLogP <3), as optimising potency and selectivity further generally results in increases in these parameters.¹³¹ Consequently, the parameters of ligand efficiency (L.E.) and lipophilic ligand efficiency (L.L.E.) were more strongly considered,¹³²⁻¹³⁴ with a view to obtaining the maximum potency for the size and lipophilicity of the compound.

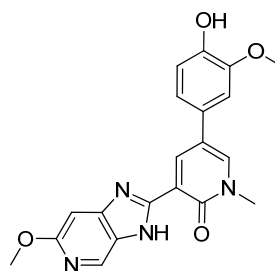
$$\text{L.E.} = (1.37 \times \text{pIC}_{50}) / \text{heavy atom count}$$
$$\text{Astex L.L.E.} = 0.111 + (1.37 \times (\text{pIC}_{50} - \text{clogP}) / \text{heavy atom count})$$

Whilst there was a wide spread of ligand efficiencies for the series as a whole (Figure 26), a significant number of compounds had a reasonable value of L.E. (>0.3). Fewer analogues met the desired range for L.L.E. (also >0.3). Those analogues with particularly good profiles are marked in green and generally contain smaller R¹ and R² substituents. This is clearly exemplified by compound **74**, where the large increase in MW and lipophilicity over compound **70** does not give a significant increase in potency, resulting in poor L.E. and L.L.E.

**74**PI3K γ pIC₅₀ 7.1

MW 500, cLogP 4.7

L.E. 0.27, L.L.E. 0.20

**70**PI3K γ pIC₅₀ 7.0

MW 378, cLogP 2.9

L.E. 0.34, L.L.E. 0.31

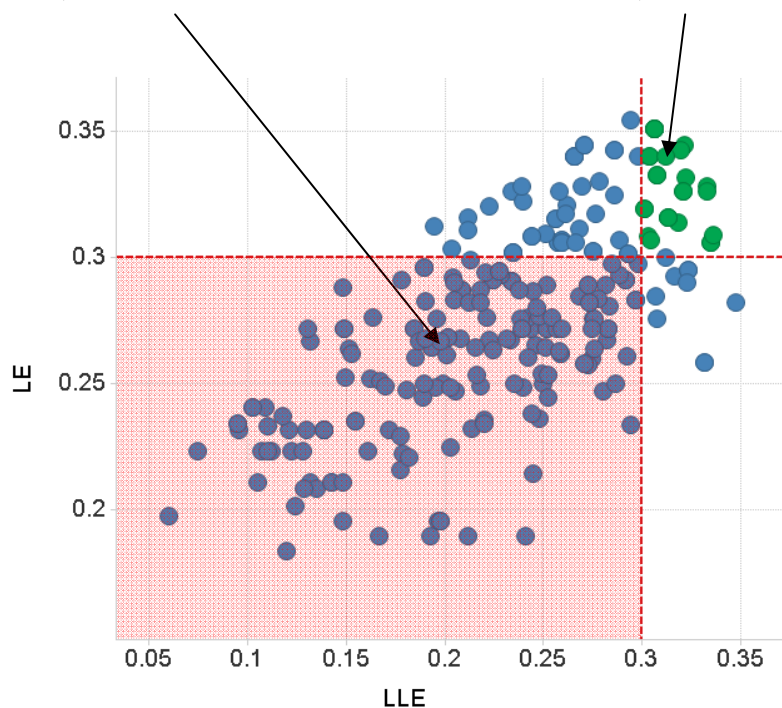


Figure 26: Ligand efficiency vs. lipophilic ligand efficiency; undesirable efficiency space shaded red

Figure 27 shows the total PSA vs. cLogP for the series. There are a range of PSAs and whilst some compounds have high lipophilicities, there are few compounds with a cLogP >3 and PSA <75 (marked in red), which has recently been highlighted as a physicochemical space with higher risk of toxicity-related attrition.^{135,136} There was therefore a drive to avoid this area when targeting any future analogues prepared within this programme.

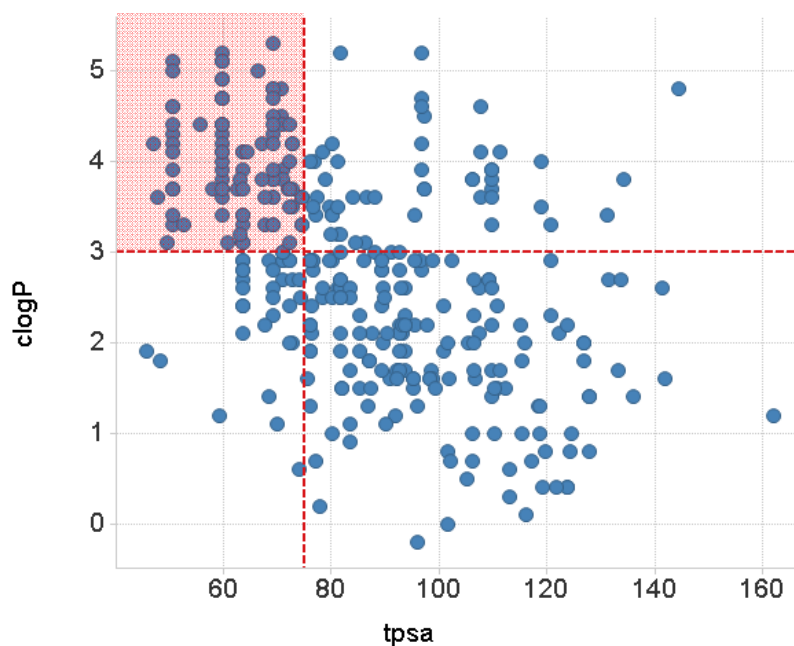


Figure 27: PSA vs. *cLogP*; red boxes indicate compounds with a higher risk of toxicity

Finally, Figure 28 shows measured CLND solubility¹³⁷ (see Appendix 3) vs. measured chromatographic LogD at pH 7.4 (GSK's preferred high throughput measure of lipophilicity, see Glossary and Appendix 4)¹³⁸ for the series, with the high L.E./low molecular weight compounds marked in green. Whilst the series covers a wide range of ChromLogD, with some highly lipophilic compounds, a significant number of analogues fall in the highly desirable range with ChromLogD ≤ 5 . Indeed, the measured ChromLogD range looks more acceptable than *cLogP*, however, this probably reflects the number of analogues with ionisable functionality, which disguises their intrinsic lipophilicity.

Solubility, however, is more of an issue for this series. Although the high throughput CLND measurement will only provide an approximate indication of aqueous solubility, it is more likely to overestimate, than underestimate, a compound's thermodynamic solubility. Whilst there are clearly analogues which have good solubility in this assay, further analysis of the chemical structures indicates that it is only compounds which contain polar or ionisable groups attached to the benzimidazole substituent (i.e. solubilising groups) which have a solubility $>50 \mu\text{M}$. This is an issue which will be

addressed as part of this programme of work; reducing the aromatic ring count¹³⁹ and/or planarity¹⁴⁰ of the compounds are expected to be strategies for achieving this.

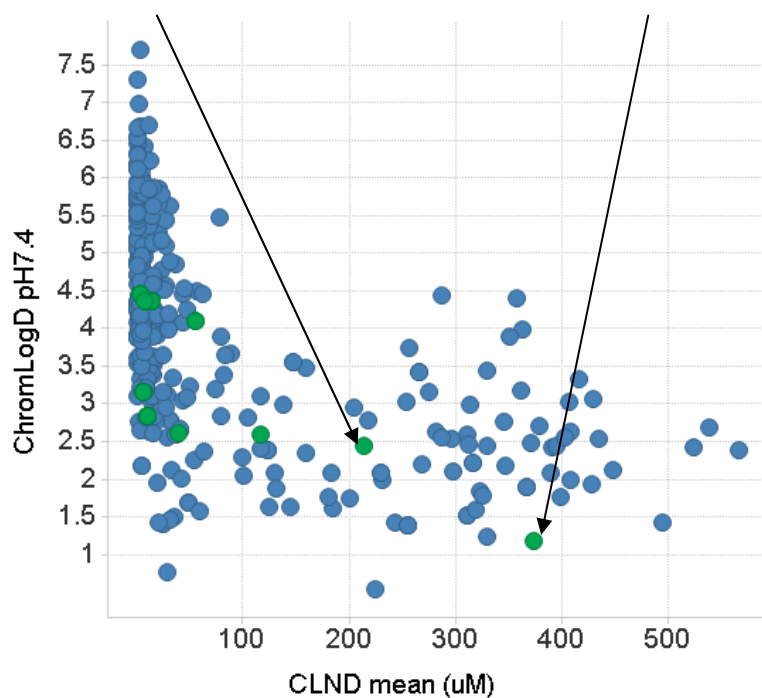
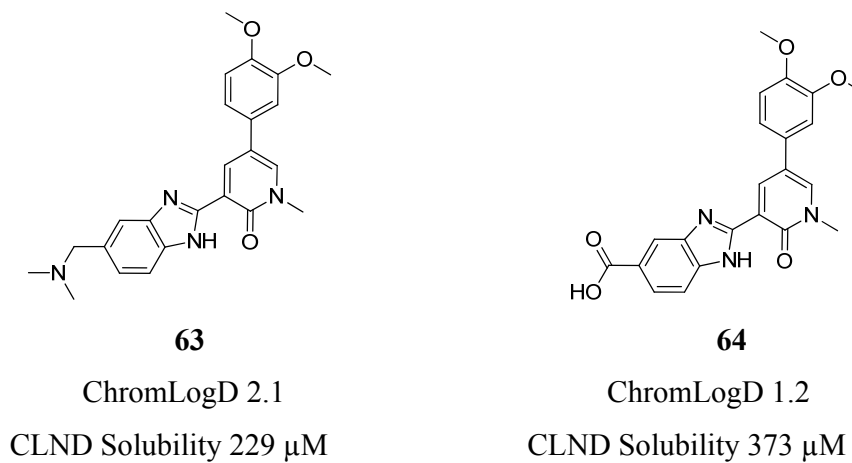


Figure 28: Measured solubility vs. measured ChromLogD; green indicates compounds with high ligand efficiency

2.2 Medicinal Chemistry Strategy and Proposed Work

The initial medicinal chemistry strategy for the pyridones was designed to address key issues with this emerging series. If the approach taken was successful, this would allow progression of this overall programme into full lead optimisation to identify a drug candidate molecule for the treatment of asthma and/or COPD. In addition, the identification of a so-called “tool molecule” which could be profiled within *in vitro* and *in vivo* target validation studies was desired; a tool molecule is used to refer to a compound which has a suitable biological profile to be used to validate the role of a target protein, but may not be of sufficient quality to be developed as a drug. Identifying a tool molecule would enable profiling of the PI3K γ mechanism in a range of *in vitro* and *in vivo* models of asthma and COPD, enabling further definition of our target product profile.

To meet these objectives, the following criteria for the series were defined; a tool molecule would ideally meet all of these.

- PI3K γ pIC₅₀ >7
- Potency in a relevant cellular assay pIC₅₀ >6
- Isoform and wider kinase selectivity >30-fold
- MW <400 Da
- cLogP <4
- Aromatic ring count \leq 3
- CLND solubility >200 μ M

Whilst no specific criteria were set for a suitable pharmacokinetic profile, for the tool molecule a profile consistent with inhaled delivery (i.e. low oral absorption, high clearance) was preferred. Taking into account the profile of the compounds which had already been synthesised in the pyridone series within our laboratories,¹²³ the following key target features were therefore identified:

- Improving isoform selectivity
- Improving solubility

2.3 Investigating R¹

It is common in the early stages of a medicinal chemistry programme to explore each region of a lead molecule to identify what substitution patterns and modifications are tolerated. Although ~300 pyridones had already been synthesised,¹²³ exploration of the R¹ space had been fairly limited, with the majority of compounds containing a benzimidazole unit at this position. Further exploration of this area of the molecule, initially investigating alternative heterocyclic replacements for the benzimidazole was therefore proposed.

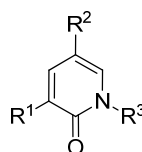


Figure 29: Pyridone template

Considering the key objectives for the series, targets were designed to explore general potency/isoform selectivity and to improve solubility. Alternative mono- and bicyclic heterocycles were selected to establish SAR and identify key binding interactions with the protein. The monoheterocyclic targets were also expected to improve solubility due to the reduced aromatic ring count. Additional analogues with substitution *ortho* to the position of attachment to the pyridone core were included, to investigate whether less planar (and potentially more soluble) analogues would be tolerated.

In order to ensure that a diverse set of heterocycles could be explored by parallel synthesis without bespoke synthesis of each compound, the initial proposed synthetic strategy relied on palladium-catalysed Suzuki couplings to introduce the R¹ group (Figure 30).

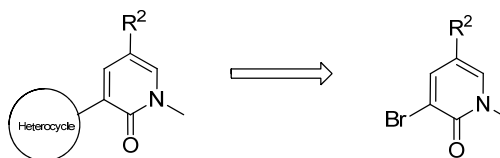
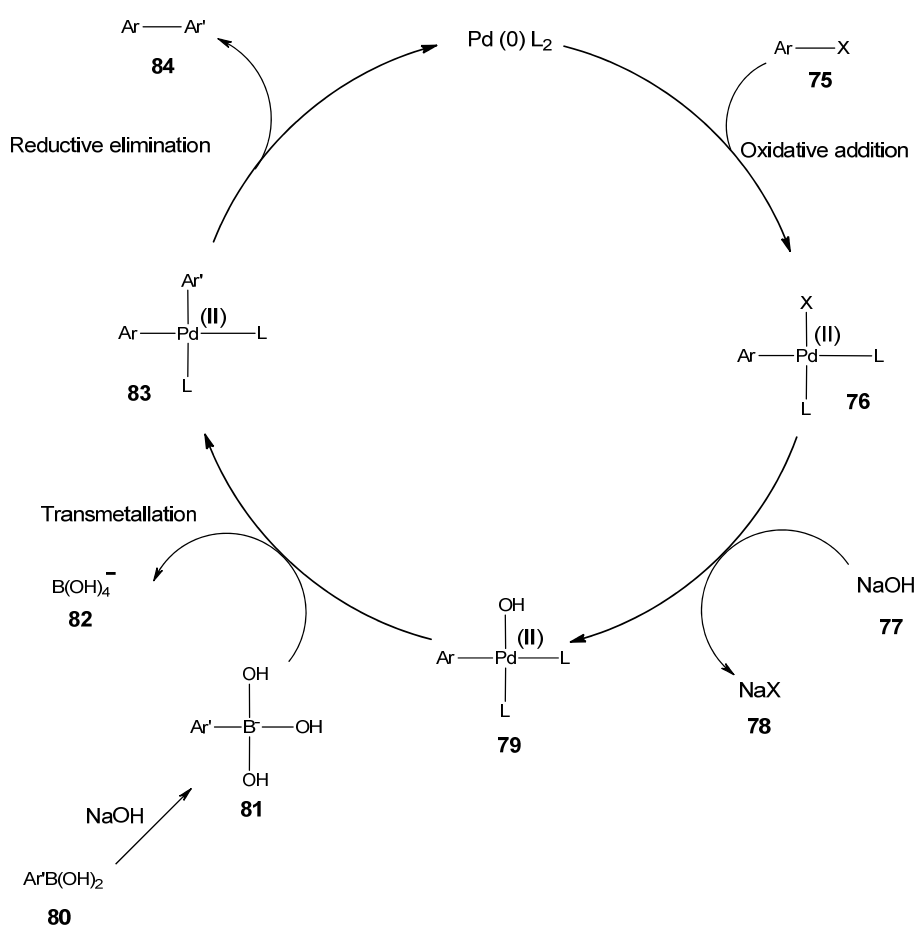


Figure 30: Proposed synthetic strategy towards 3-heterocyclic pyridone targets

2.3.1 Results and Discussion

Synthesis via Suzuki Coupling

The Suzuki reaction^{141,142} is a palladium-catalysed cross-coupling reaction, typically between an aryl boronate and aryl halide (or triflate). The first step is oxidative addition of the aryl halide **75** to give a 4-coordinate Pd(II) complex **76** (Scheme 1). The base can then play a dual role; exchanging with the halide on the palladium and/or activating the aryl boronic acid (or ester) to give the negatively charged arylborate species **81**.¹⁴³ Transmetalation to give a new 4-coordinate Pd(II) complex **83**, followed by reductive elimination, generates the required product **84** and regenerates the Pd(0) catalyst.



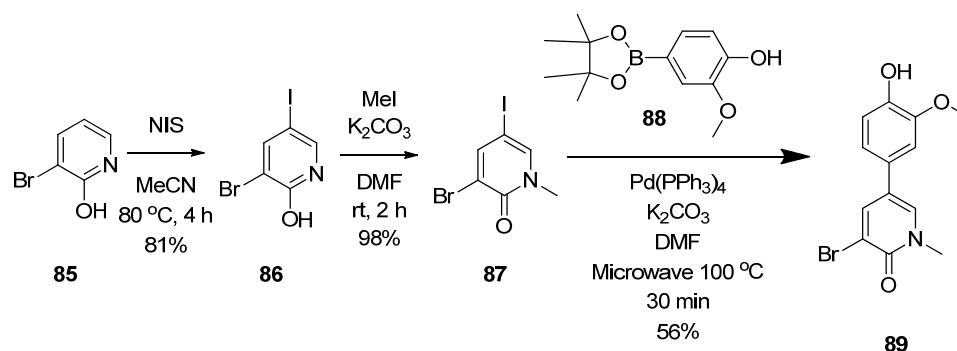
Scheme 1: Mechanism of the Suzuki reaction

Synthesis of Key Intermediate 3-Bromo-5-[4-hydroxy-3-(methoxy)phenyl]-1-methyl-2(1H)-pyridinone

The R² substituent for this work was chosen based on Free-Wilson analysis of potency contributions, ensuring sufficient data on historical analogues containing this motif was

available, to allow interpretation of the data generated on new compounds.¹²³ Accordingly, central to this programme was access to intermediate **89** (Scheme 2), which was readily synthesised from commercially available 3-bromo-2(1*H*)-pyridinone **85**.

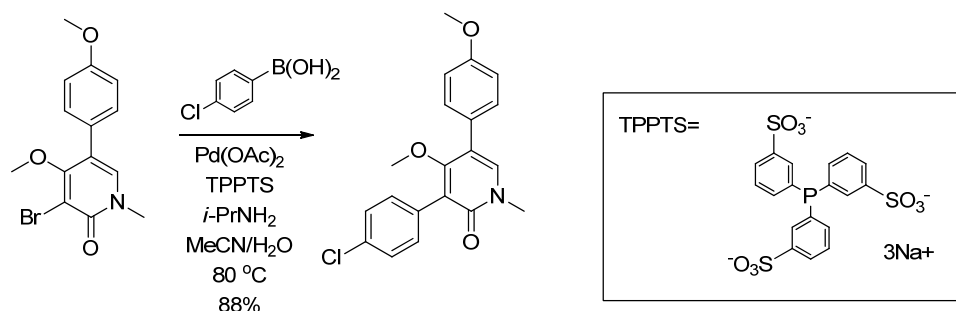
Selective iodination of 2-bromo-2(1*H*)-pyridinone **85** at C-5, previously described by Meana *et al.*,¹⁴⁴ gave 3-bromo-5-iodo-2(1*H*)-pyridinone **86** in excellent yield (Scheme 2). The hydroxyl directing group stabilises the intermediate formed from electrophilic attack at C-5, resulting in the regioselectivity observed. Selective *N*-methylation was achieved, using potassium carbonate and methyl iodide to give pyridone **87**. Subsequent palladium-catalysed Suzuki coupling gave the desired intermediate **89** in 44% overall yield, over 3 steps on multi-gram scale. As predicted, the palladium cross-coupling occurs selectively at C-5 due to the weaker carbon-iodine bond, which is more susceptible to oxidative addition. Whilst none of the C-3 substituted product is observed by LCMS, the isolated yield for this Suzuki reaction is moderate, which may be, in part, a result of some protodeboronation of the starting material **88** within this reaction.



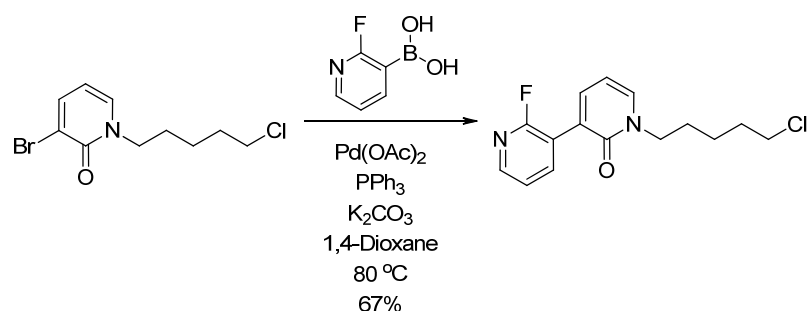
Scheme 2: Synthesis of key intermediate **89**

Suzuki Coupling of 3-Bromo-5-[4-hydroxy-3-(methoxy)phenyl]-1-methyl-2(1*H*)-pyridinone

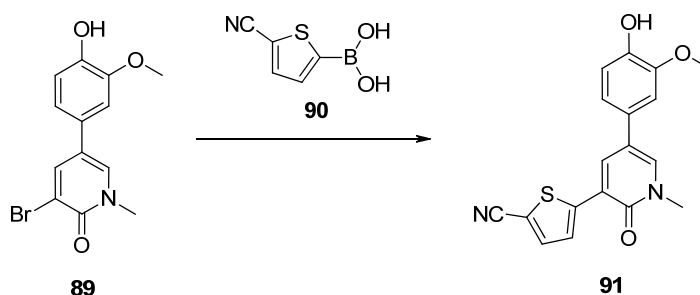
A review of the literature reveals that Suzuki couplings of 3-bromopyridones are not as well precedented as expected. Most examples involve phenyl boronate coupling partners, as exemplified by Corneau *et al.*¹⁴⁵ (Scheme 3). In these cases, typical conversions are high with standard Pd(0) or Pd(II) catalysts.

Scheme 3: Work by Corneaux *et al.*¹⁴⁵

More relevant examples of 2- and 3-substituted heterocyclic coupling partners are less precedented, although good yields have been achieved in some cases, as exemplified by Bertani *et al.*¹⁴⁶ (Scheme 4).

Scheme 4: Work by Bertani *et al.*¹⁴⁶

In order to investigate the Suzuki coupling of our bromopyridone template and optimise conditions, initial work focused on a trial reaction, coupling 3-bromo-5-[4-hydroxy-3-(methoxy)phenyl]-1-methyl-2(1*H*)-pyridinone **89** with a prototypical heterocyclic boronic acid: (5-cyano-2-thienyl)boronic acid **90** (Scheme 5).



Scheme 5: Trial Suzuki reaction (conditions specified in Table 13)

Firstly, conditions similar to those used in the synthesis of the bromo starting material **89** were applied. *Tetrakis*(triphenylphosphine) palladium(0) catalyst and potassium

carbonate base were used, with a switch to 1,4-dioxane as solvent (Table 13, entry 1). Whilst some of the desired coupled material was observed by LCMS, the major product was starting material, which suggested that oxidative addition of the aryl bromide starting material was the problematic step.

Further reactions with *tetrakis*(triphenylphosphine) palladium(0) were conducted, varying both the identity and quantity of base used (entries 2-5), however no improvement on the initial conditions was observed. On changing to a palladium(II) catalyst (palladium acetate) with a phosphine ligand (either SPhos or PPh₃), some desired product and starting material was observed, but, the major product was protodebrominated starting material. This suggests that when oxidative addition was occurring, the transmetallation step was also slow.

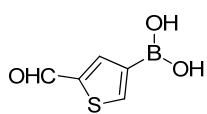
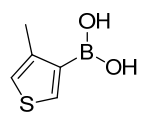
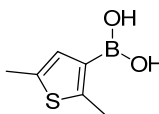
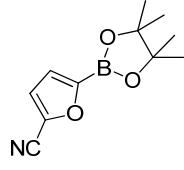
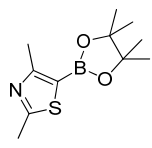
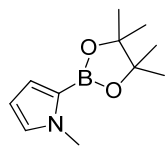
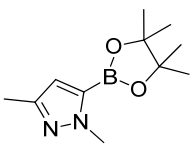
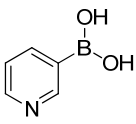
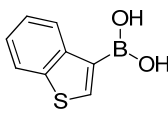
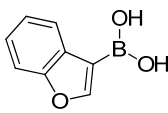
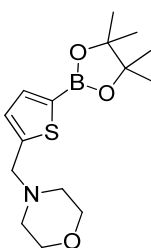
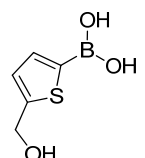
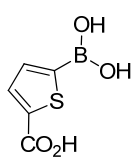
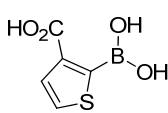
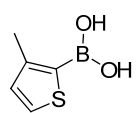
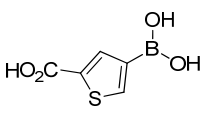
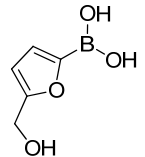
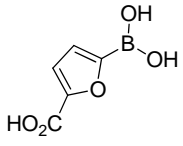
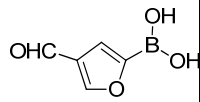
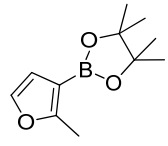
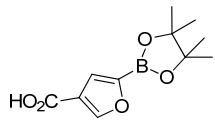
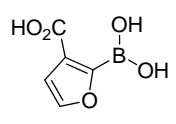
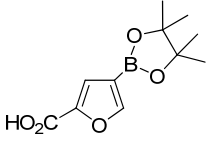
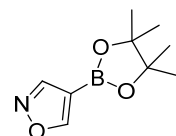
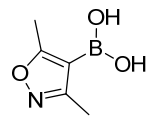
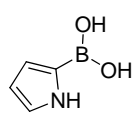
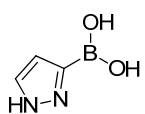
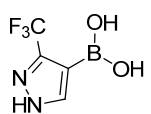
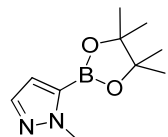
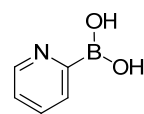
	Catalyst	Base	Ligand	Conditions	% Product [†]	Major Component(s) [‡]
1	Pd(PPh ₃) ₄	K ₂ CO ₃	-	110 °C/10 min/μW	17	Starting material
2	Pd(PPh ₃) ₄	NaHCO ₃	-	110 °C/10 min/μW	10	Starting material
3	Pd(PPh ₃) ₄	NaHCO ₃ [±]	-	110 °C/10 min/μW	12	Starting material
4	Pd(PPh ₃) ₄	Na ₂ CO ₃ [±]	-	110 °C/10 min/μW	4	Starting material
5	Pd(PPh ₃) ₄	NaOH [±]	-	110 °C/10 min/μW	7	Starting material
6	Pd(OAc) ₂	K ₃ PO ₄ [*]	SPhos	100 °C/18 h	14	Dehalogenation + starting material
7	Pd(OAc) ₂	K ₃ CO ₃	PPh ₃	100 °C/18 h	3	Dehalogenation + starting material

Table 13: Reaction screening of Suzuki coupling.

All reactions were carried out in 1,4-dioxane with 1 eq aqueous solution of base unless otherwise stated ([±]2 eq base; ^{*}7.5 eq base)

[†] Percentage product based on UV peak in LCMS; material not isolated

[‡] Major components (other than desired product) were identified by LCMS analysis of crude reaction mixtures.

<p>92</p>  <p>14%</p>	<p>93</p>  <p>4%</p>	<p>94</p>  <p>10%</p>	<p>95</p>  <p>22%</p>	<p>96</p>  <p>6%</p>
<p>97</p>  <p>3%</p>	<p>98</p>  <p>7%</p>	<p>99</p>  <p>13%</p>	<p>100</p>  <p>19%</p>	<p>101</p>  <p>14%</p>
<p>102</p> 	<p>103</p> 	<p>104</p> 	<p>105</p> 	<p>106</p> 
<p>107</p> 	<p>108</p> 	<p>109</p> 	<p>110</p> 	<p>111</p> 
<p>112</p> 	<p>113</p> 	<p>114</p> 	<p>115</p> 	<p>116</p> 
<p>117</p> 	<p>118</p> 	<p>119</p> 	<p>120</p> 	<p>121</p> 

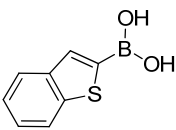
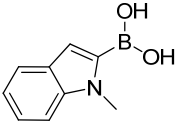
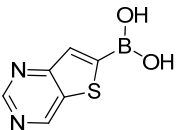
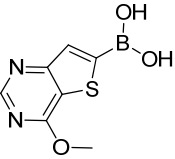
122	123	124	125	
				

Table 14: Heterocyclic boronates used in Suzuki array with CsOAc conditions; isolated yields quoted where reactions were successful

Although a small array of heterocyclic replacements for the benzimidazole unit has been secured, greater diversity at this position was still desirable. More robust coupling partners were therefore considered. In particular, the use of *N*-methyliminodiacetic acid (MIDA) boronates was proposed as a potentially beneficial preparative strategy.

MIDA Boronates

Knapp *et al.* have recently described the use of *N*-methyliminodiacetic acid (MIDA) boronates (Figure 31) for the successful coupling of 2- or 3-heterocyclic boronated partners,¹⁵¹ which are otherwise inherently unstable.

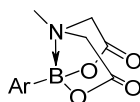
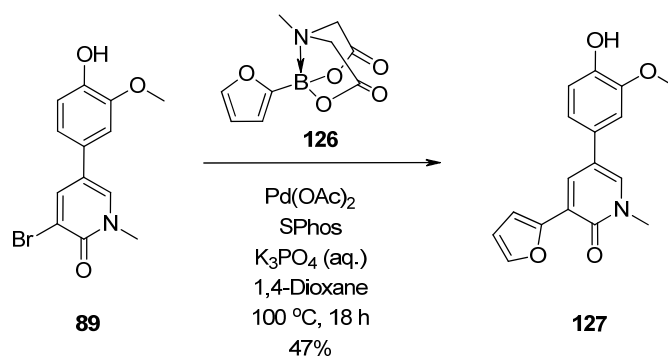


Figure 31: MIDA boronate

The MIDA boronate provides an air-stable surrogate for the unstable boronic acid, which is slowly released *in situ* under the optimised reaction conditions. The reduced potential for decomposition of the boronic acid due to protodeboronation or oxidation, therefore, results in improved yields, relative to using the boronic acid directly. The use of K₃PO₄ in 5:1 dioxane/water is described as being key to this methodology, promoting the slow release of the free boronic acid over a period of ~3 h at 60 °C.

These conditions were adopted and successfully applied to our template as exemplified by the cross-coupling of the furan MIDA boronate, where the desired product **127** was isolated in 47% yield (Scheme 7).



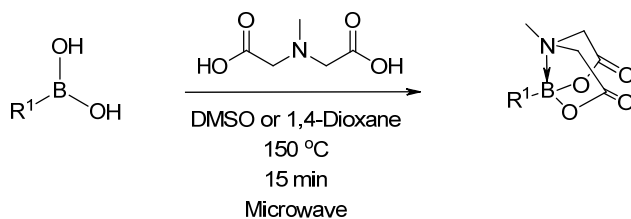
Scheme 7: Application of MIDA boronates to pyridone template

A subsequent array of MIDA boronates was applied with some good levels of success, and certainly with improved yields compared to the boronic acids and esters shown in Table 14. However, this series was limited in diversity and size due to the (lack of) commercial availability of the required monomers (Table 15).

128 26%	129 37%	130 30%	131 34%
132 51%	133 23%	134 16%	

Table 15: MIDA boronates used in array with isolated yields

Whilst the synthesis and isolation of a wider range of MIDA boronates from the corresponding boronic acids was achieved elsewhere in our laboratory¹⁵² (Scheme 8), this approach would be time-consuming on an array format; consequently an alternative synthetic strategy was sought.

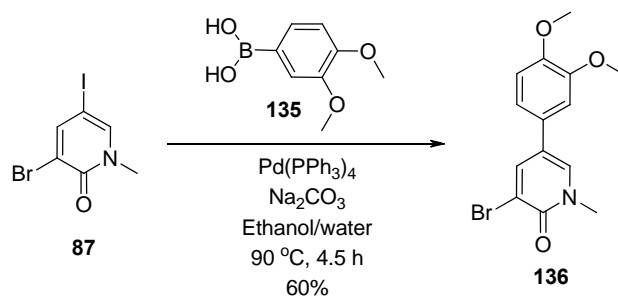


Scheme 8: Synthesis of MIDA boronate

An Alternative Approach: Synthesis of {5-[3,4-Bis(methoxy)phenyl]-1-methyl-2-oxo-1,2-dihydro-3-pyridinyl}boronic acid

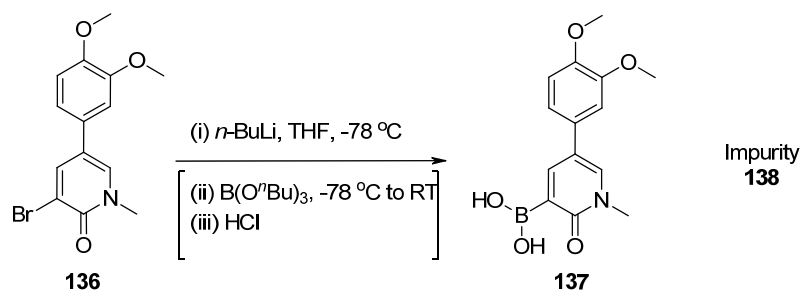
So far, efforts had been concentrated on coupling the 5-bromopyridone core with a range of different boronate species *via* Suzuki coupling. As the major problems encountered with this methodology appeared to be related to the instability of the heterocyclic boronates, the reversal of coupling partners was considered and the synthesis of the boronate of the pyridone core initiated. An alternative R² substituent was selected for this work, which did not contain the potentially problematic acidic phenol functionality. This change in strategy meant that direct comparison with previously synthesised analogues would not be possible. However, with historic data available for the closely related dimethoxyphenyl group (e.g. **61**, Table 12),¹²³ data interpretation of new compounds containing this fragment would be aided.

Key intermediate 5-[3,4-bis(methoxy)phenyl]-3-bromo-1-methyl-2(1*H*)-pyridinone **136** was readily synthesised from the previously described intermediate **87** in 60% yield (Scheme 9).

Scheme 9: Synthesis of key intermediate **136**

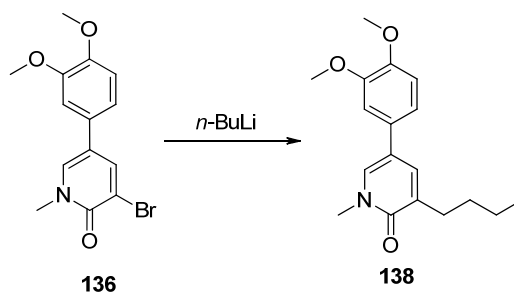
Synthesis of the requisite boronic acid was initially attempted from compound **136**, *via* an approach based on lithiation chemistry (Scheme 10). Pyridone bromide **136** was

treated with *n*-BuLi (1.1 eq), however the lithium/bromine exchange was observed to be very slow; monitoring of the reaction mixture at $-78\text{ }^{\circ}\text{C}$ for 40 min showed little conversion, with the starting bromide being the major component observed.



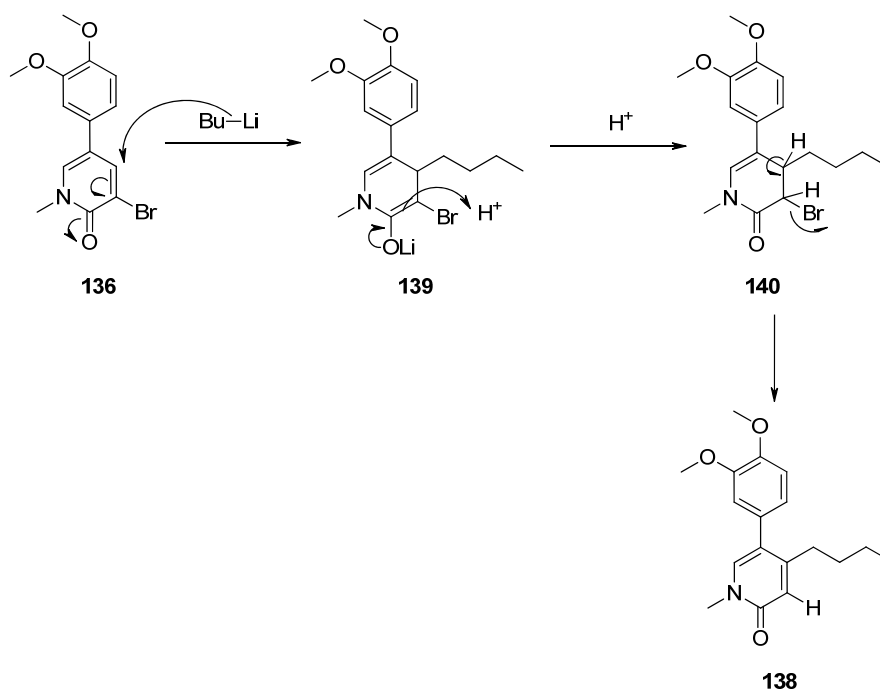
Scheme 10: Lithiation approach to formation of boronic acid on pyridone template

On repeating the reaction with *n*-BuLi (1.5 eq), after 75 min at $-78\text{ }^{\circ}\text{C}$ the starting material was completely consumed, however the major component was not the desired intermediate. LCMS showed a mass ion consistent with dehalogenation and addition of an *n*-butyl group. A product consistent with this analytical data could be formed from simple lithium/bromine exchange, followed by alkylation with the 1-bromobutane formed *in situ* (Scheme 11). However, the very slow lithium/halogen exchange observed in previous reactions does not support this hypothesis.



Scheme 11: Possible identity of impurity 138

Alternatively, 1,4-addition of *n*-BuLi to the pyridone carbonyl, followed by subsequent elimination of hydrogen bromide, would also give a product consistent with the analytical data (Scheme 12). Indeed, literature precedent for such conjugate addition processes with Grignard species on similar pyridones has been established by Follman *et al.*¹⁵³ Unfortunately, without an isolated sample of the impurity it is impossible to state conclusively which of these proposed structures is correct.

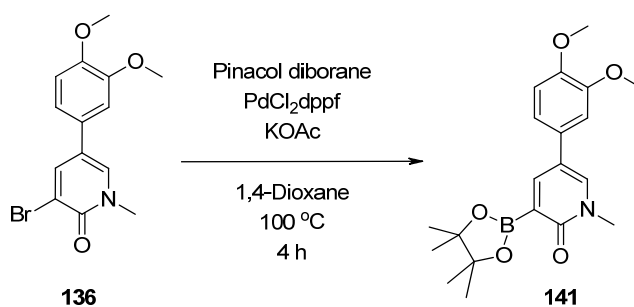


Scheme 12: Alternative proposed structure and formation of impurity **138**

Running the reaction with *n*-BuLi (1.2 eq) gave the best reaction profile by LCMS, with approximately 50% conversion of starting material to lithiated species and only minor impurities observed after 30 min. Interestingly, impurity **138** was not observed, which suggests the equivalents of *n*-BuLi and timecourse were critical.

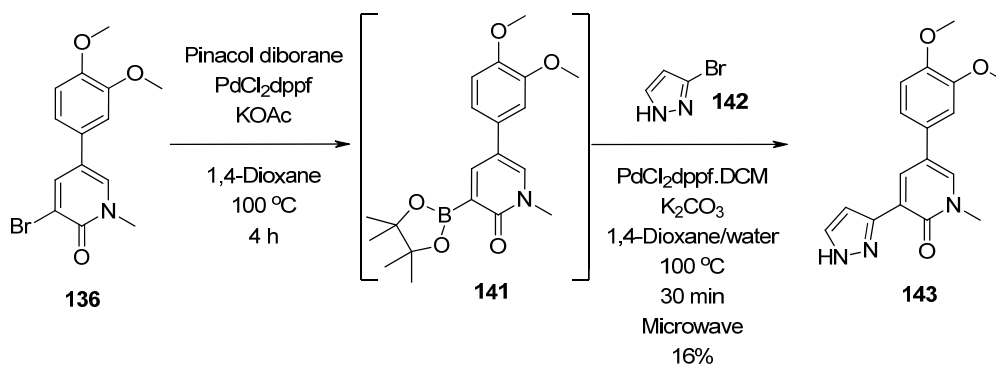
To further improve on this, we investigated the use of the more reactive and more sterically hindered *sec*-BuLi (1.25 eq). On a small scale this successfully gave complete conversion to the lithiated species in only 5 min. A subsequent quench with tributyl borate and an acid work-up, gave crude material consistent with the boronic acid by LCMS. Attempts to repeat this on scale, however, were unsuccessful and lithium/halogen exchange was again observed to be very slow, with the major product being unreacted starting material. To be sure this was not as a result of wet reagents or starting materials, the reaction was repeated with fresh solvents, fresh *sec*-BuLi, and after rigorously re-drying the starting material. However, the same disappointing result was observed.

As lithiation of the pyridone bromide was not reproducible, the synthesis of the desired boronate *via* palladium chemistry was considered.



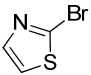
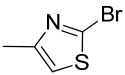
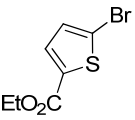
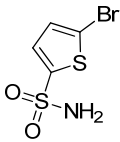
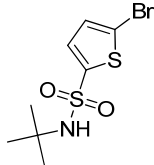
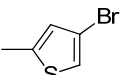
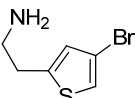
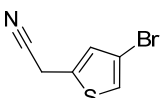
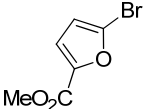
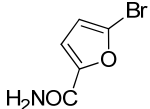
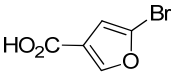
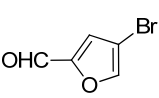
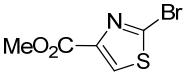
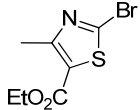
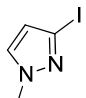
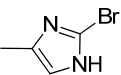
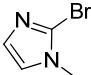
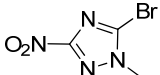
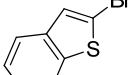
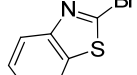
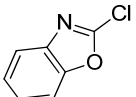
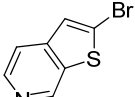
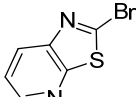
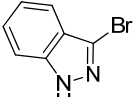
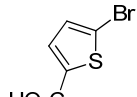
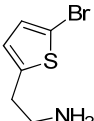
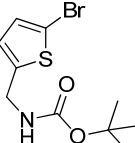
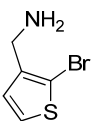
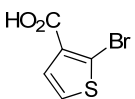
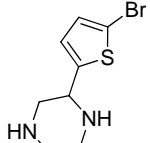
Scheme 13: Formation of boronate on pyridone template

Under typical Miyaura borylation conditions^{154,155} (Scheme 13) clean formation of the boronic ester was observed by LCMS. Attempted purification of this intermediate by column chromatography led to protodeboronation, so the material was used in crude form to assess the subsequent coupling (Scheme 14).



Scheme 14: Trial coupling with heterocyclic halides

The successful coupling and isolation of pyrazole analogue **143**, albeit in low yield, was encouraging, so a trial array of a further six analogues was carried out to ascertain applicability to a wider range of coupling partners. Pleasingly, a high success rate then drove attempts to prepare the full array of compounds shown in Table 16. In time, a large number of the desired analogues, including a range of thiophene, furan, thiazole, imidazole and bicyclic heterocycles were accessed. This methodology also tolerated monomers containing a variety of functional groups (sulfonamides, amines, esters and amides) which had failed in previous arrays (Tables 14 and 15). Analysis of the monomers which failed in this series, once again, did not reveal any trends.

<p>144</p>  <p>19%</p>	<p>145</p>  <p>35%</p>	<p>146</p>  <p>26%</p>	<p>147</p>  <p>20%</p>	<p>148</p>  <p>27%</p>
<p>149</p>  <p>26%</p>	<p>150</p>  <p>11%</p>	<p>151</p>  <p>32%</p>	<p>152</p>  <p>54%</p>	<p>153</p>  <p>13%</p>
<p>154</p>  <p>8%</p>	<p>155</p>  <p>25%</p>	<p>156</p>  <p>37%</p>	<p>157</p>  <p>15%</p>	<p>158</p>  <p>5%</p>
<p>159</p>  <p>7%</p>	<p>160</p>  <p>17%</p>	<p>161</p>  <p>10%</p>	<p>162</p>  <p>28%</p>	<p>163</p>  <p>31%</p>
<p>164</p>  <p>26%</p>	<p>165</p>  <p>25%</p>	<p>166</p>  <p>5%</p>	<p>167</p>  <p>15%</p>	<p>168</p>  <p></p>
<p>169</p> 	<p>170</p> 	<p>171</p> 	<p>172</p> 	<p>173</p> 

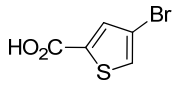
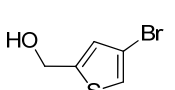
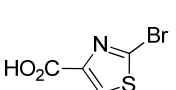
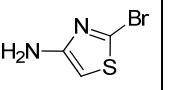
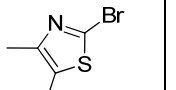
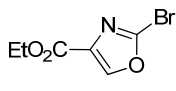
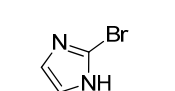
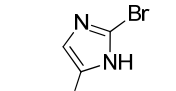
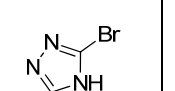
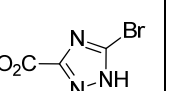
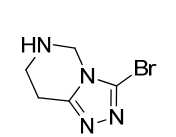
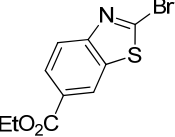
174	175	176	177	178
				
179	180	181	182	183
				
184	185			
				

Table 16: Monomers used for reverse Suzuki couplings; isolated yields quoted where reactions were successful

Bespoke Heterocycle Synthesis

Whilst the Suzuki approach enabled the synthesis of a wide range of heterocycles in array format, there were certain templates which could not be accessed due to the unavailability of the corresponding heterocyclic halides or boronates (Figure 32). The calculated physicochemical profiles of oxadiazole containing compounds were significantly different to the compounds already made (higher PSA, predicted higher solubility), so alternative syntheses were sought to explore this SAR space. A recent analysis, comparing the 1,2,4- and 1,3,4-oxadiazole regioisomers,¹⁵⁶ demonstrated differences in their lipophilicity and solubility profiles, so routes to both isomers were sought.

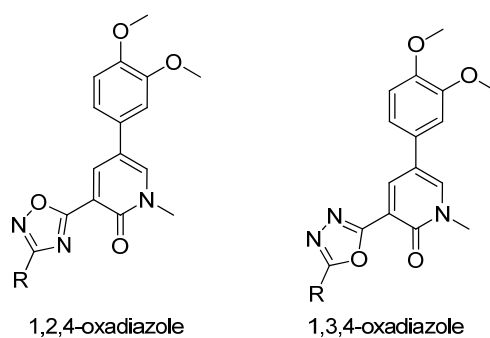
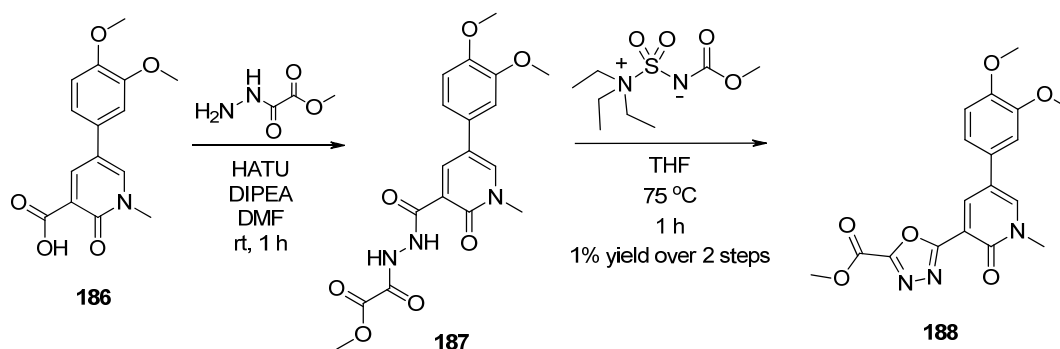


Figure 32: Heterocyclic templates not exemplified via array chemistry

1,3,4-Oxadiazole

A 1,3,4-oxadiazole with an ester at the 2-position was synthesised as shown in Scheme 15. The ester substituent was targeted as it would allow direct comparison of SAR with other heterocycles already synthesised and could also provide a useful group for functionalisation, should this template be of further interest.

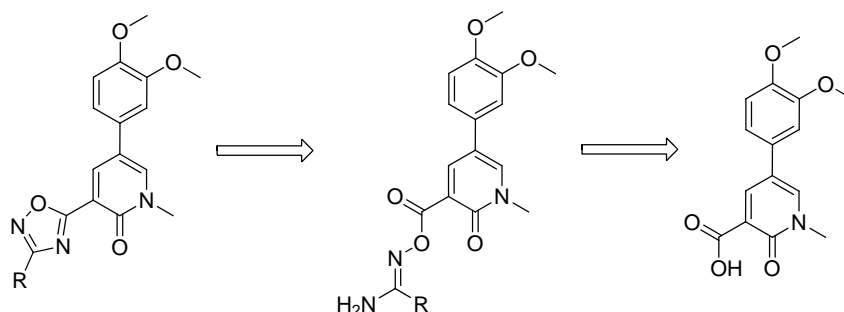
Coupling of the pyridone carboxylic acid **186**¹⁵⁷ with commercially available methyl hydrazinecarboxylate and subsequent cyclisation with Burgess reagent,^{158,159} as preceded by Bethel *et al.*,¹⁶⁰ furnished the desired product **188**. The very low yield reflects the poor solubility of the hydrazide intermediate, which made purification and isolation challenging, coupled with the poor reaction profile of the cyclisation, where a spectrum of by-products was observed by LCMS. However, a sufficient quantity of the desired product was isolated for biological testing, so the route was not optimised further.



Scheme 15: Synthesis of 1,3,4-oxadiazole

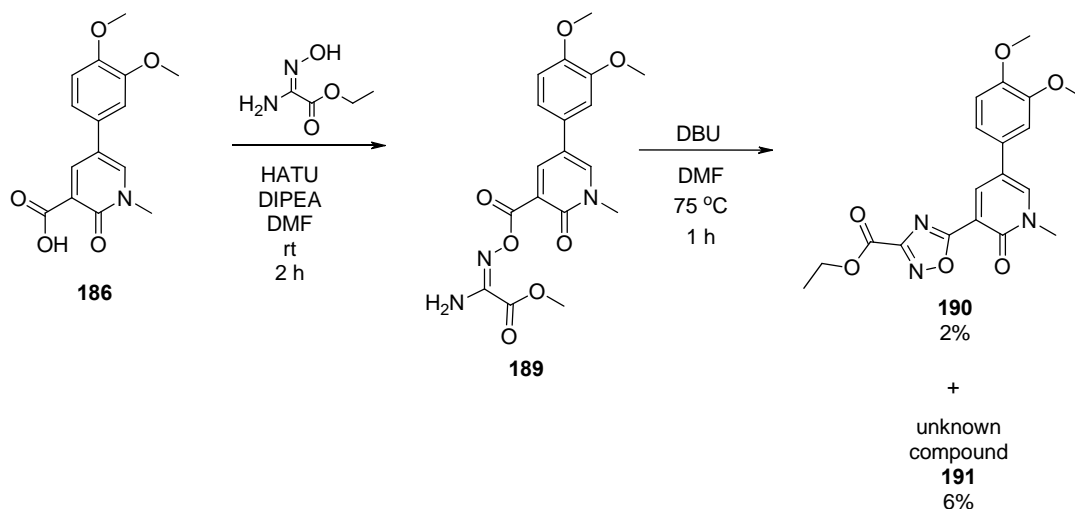
1,2,4-Oxadiazole

The proposed retrosynthetic analysis of the 1,2,4-oxadiazole is shown in Scheme 16. A simple coupling and cyclisation, as described in previous work,¹⁶¹ would give the desired heterocycle. Again, an ester substituent was targeted initially.



Scheme 16: Retrosynthesis of 1,2,4-oxadiazole

The coupling of the pyridone carboxylic acid¹⁵⁷ with a commercially available amidoxime gave the desired intermediate **189**. However, the subsequent cyclisation was problematic (Scheme 17).



Scheme 17: Synthesis of 1,2,4-oxadiazole

Initially, intermediate **189** was not isolated, but DBU was added to the crude reaction and the mixture heated to 75 °C for 1 h. Monitoring by LCMS revealed a minor peak with mass consistent with desired product **190**. However, a major peak for an unknown

by-product **191** was also present. Work-up and purification yielded only a small amount (<10 mg) of each product component.

^1H NMR of by-product **191** (Figure 33) revealed the pyridone core (singlet at 3.79 ppm, two doublets at 8.60 and 8.62 ppm) and dimethoxyphenyl group (two singlets at 3.69 and 3.85 ppm, three signals at 7.04-7.21 ppm) were intact. The only other signal was observed at very low field (12.50 ppm).

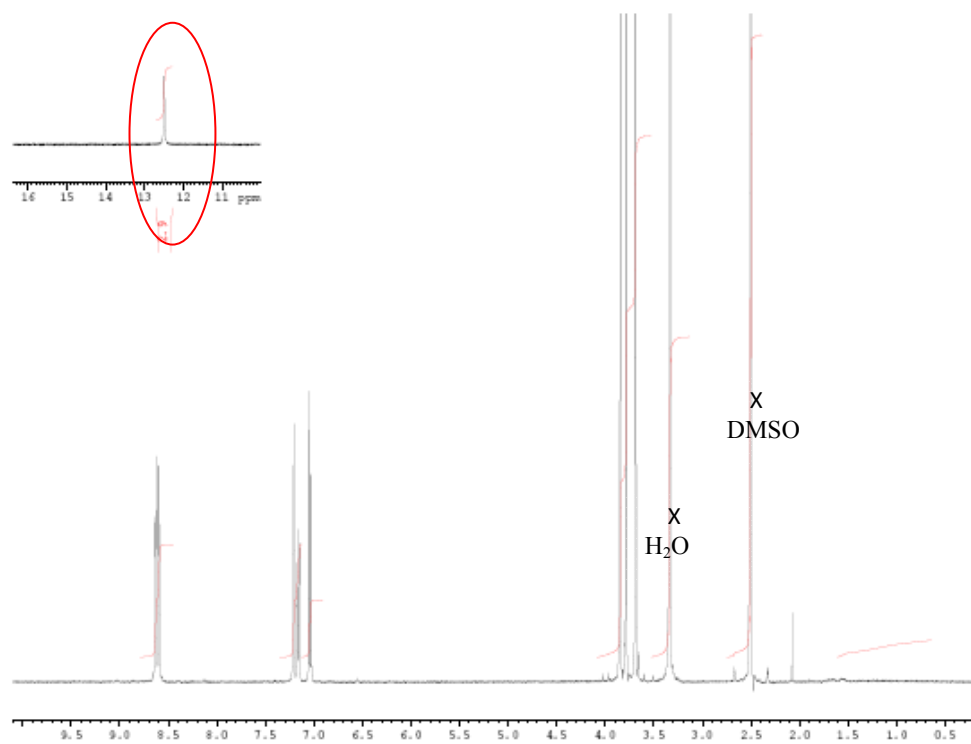


Figure 33: ^1H NMR of **191**

Further analysis of **191** by LCMS and ^{13}C NMR led us to the proposed structure shown in Figure 34 and subsequent IR analysis confirmed this, with a characteristic absorption at $\nu = 2253\text{ cm}^{-1}$ for the nitrile functionality.

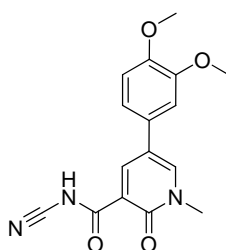
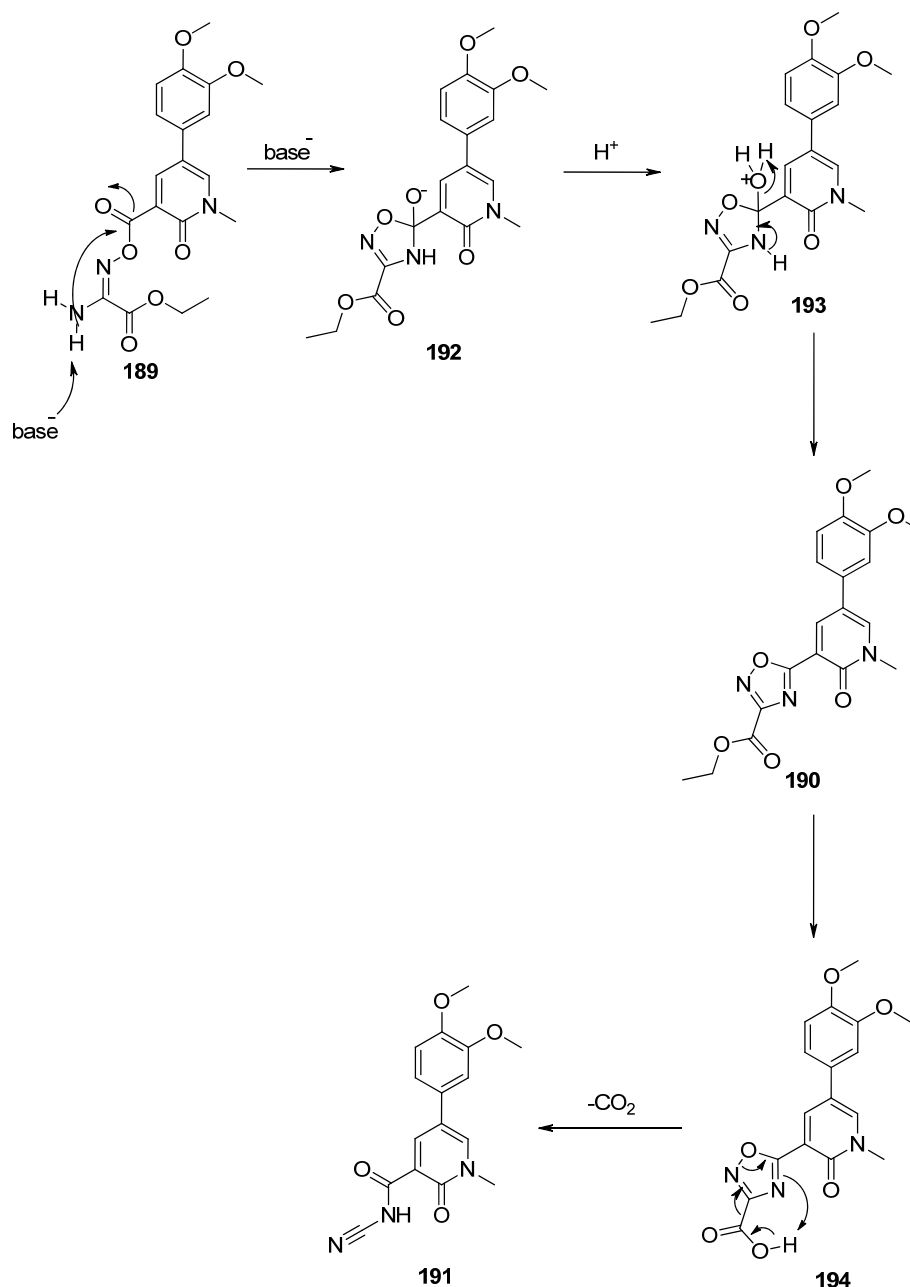


Figure 34: Proposed structure of **191**

A possible mechanism for the formation of this by-product is shown in Scheme 18. If the desired product is formed, then ester hydrolysis, followed by decarboxylation could lead to the proposed compound **191**. Whilst this mechanism portrays the formation of the desired product **190** by acidic workup, this could also occur under basic conditions. Unfortunately, as the ^1H NMR of **190** was inconclusive, the initial formation of this desired product cannot be confirmed.



Scheme 18: Possible mechanism for formation of 191

At this stage it was considered that either the HATU by-products (not removed prior to cyclisation) or water could potentially be interfering within the reaction. The synthesis was therefore repeated: intermediate **189** was isolated and purified to remove the HATU by-products and rigorously dried over P_2O_5 to remove water. The cyclisation was attempted under the same conditions and monitoring by LCMS was encouraging, with the major peak consistent with the desired product. Two different work-up procedures were then trialled. Firstly, the reaction mixture was concentrated directly under high vacuum, prior to purification by mass-directed HPLC (MDAP). However, after purification, analysis revealed the peak consistent with the desired product had been converted to **191**. Alternatively, the reaction mixture was partitioned between ethyl acetate and water and the layers were separated. Analysis of both layers revealed that no peak for the desired product remained. A brief look at alternative cyclisation conditions, e.g. in acidic media, was also unsuccessful.

The apparent greater instability of the ester analogue of the 1,2,4-oxadiazole compared with the 1,3,4-oxadiazole is interesting, however, without isolating pure samples of the esters and carboxylic acids for each isomer (Figure 35) and further investigating their relative stability, it cannot be established whether this is due to a greater susceptibility of the 1,2,4-analogue to ester hydrolysis or a more facile decarboxylation leading to ring opening. Indeed, we must also consider the different reaction conditions used. Whilst ester hydrolysis would not be predicted in either case, the reagents and conditions may be responsible for the different reaction profiles, rather than an inherent difference in stability/reactivity of the two isomers.

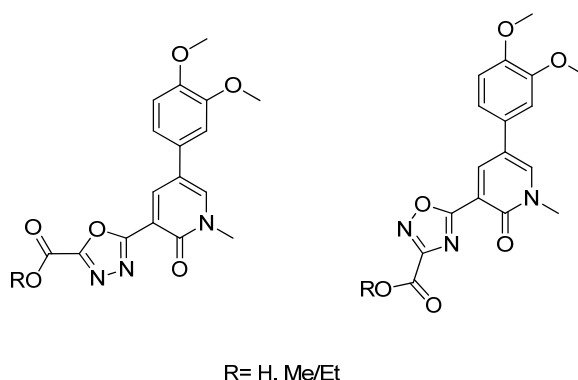
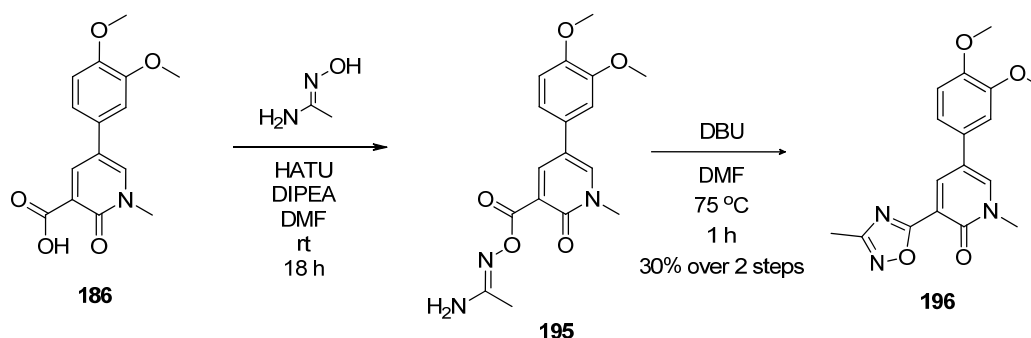


Figure 35: Oxadiazole intermediates

Although we cannot confirm the mechanistic rationale for the formation of **191**, it is clear that the intermediate product, thought to be desired species **190**, is highly unstable under the reaction conditions chosen. As the hydrolysis of the ester substituent would appear to be key to this instability, synthesis of the 3-methyl-1,2,4-oxadiazole was attempted instead (Scheme 19). This would still enable comparison of SAR with other heterocycles previously synthesised and, if selected for progression, alternative chemistries could be sought to functionalise further at the 3-position. The synthesis of the 3-methyl analogue **196** proceeded without difficulty and the desired product was isolated in a 30% yield over 2 steps.



Scheme 19: Synthesis of 3-methyl-1,2,4-oxadiazole

Semi-saturated Bicycles

In addition to bicyclic aromatic heterocycles, the replacement of the benzimidazole with a semi-saturated ring system was also of interest. The reduction in aromatic ring count and reduced planarity of such a system would be expected to improve solubility.

Based on the evidence that a nitrogen atom was tolerated in azabenzimidazole **70** (Table 11), the semi-saturated replacement **197** was proposed (Figure 36), which, if active, would be followed by exploring substitution of the piperidine nitrogen.

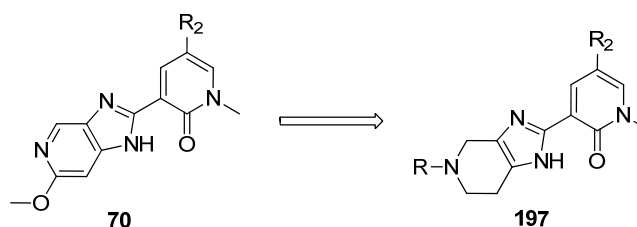
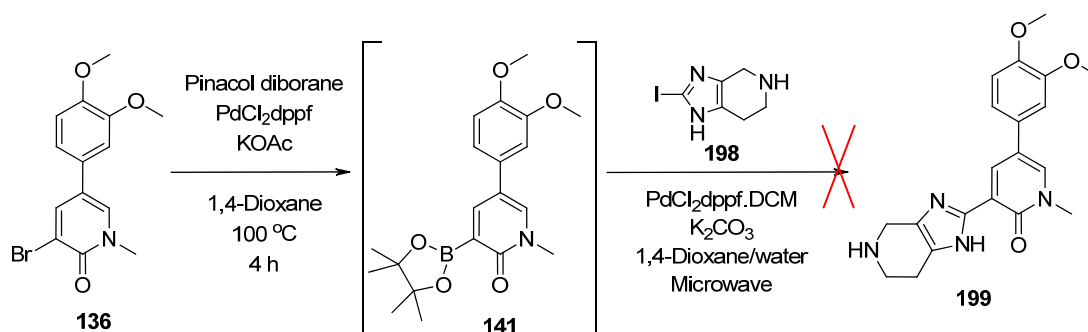


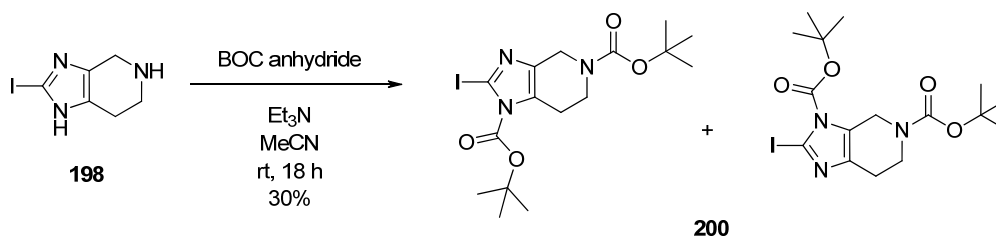
Figure 36: Semi-saturated target

The initial synthetic strategy was to utilise the Suzuki coupling conditions which had already been successfully applied to the pyridone template. Halide coupling partner 2-iodo-4,5,6,7-tetrahydro-1*H*-imidazo[4,5-*c*]pyridine **198** was therefore sourced.¹⁶² Coupling to the pyridone template using the previously optimised conditions was then attempted (Scheme 20). This reaction was initially attempted in the microwave at a range of temperatures (100-150 °C). However, no trace of desired product was observed.



Scheme 20: Coupling of semi-saturated heterocycle

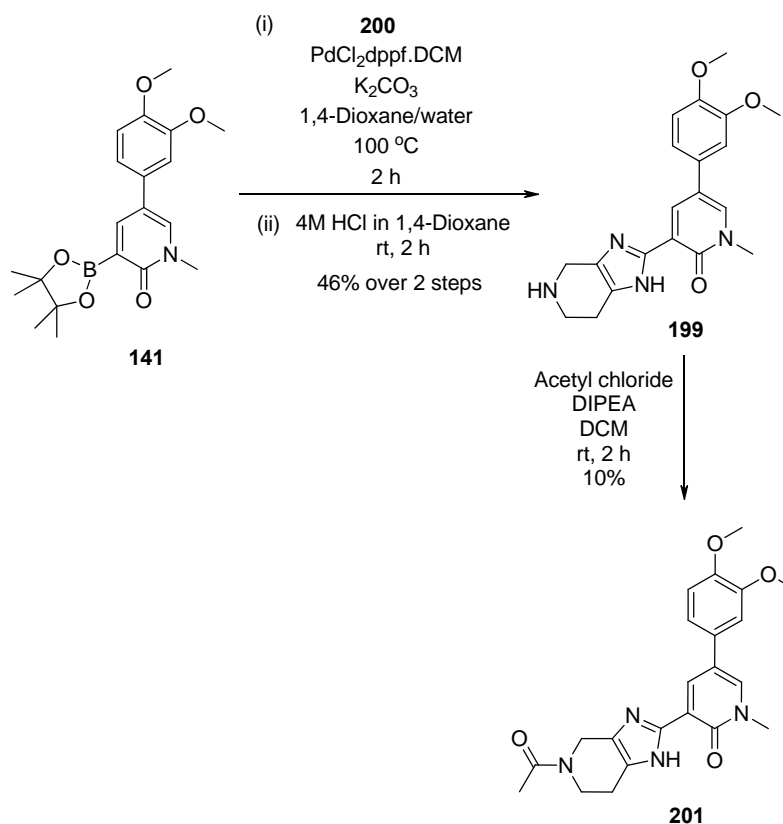
It was then recognised that protecting the amine functionalities could improve the reaction profile, by preventing coordination of the free amine to palladium. The BOC protected material was therefore prepared using standard conditions (Scheme 21); two regioisomers were formed due to tautomerism of the imidazole ring.



Scheme 21: BOC protection

The subsequent coupling of the fully protected material successfully gave the desired product (Scheme 22), although one of the BOC groups was also partially removed during the reaction. The crude mixture was then treated with 4 M HCl in dioxane to give fully deprotected product **199** before isolation. Subsequent acylation with acetyl chloride gave two peaks with the desired mass by LCMS, proposed to be regioisomers as

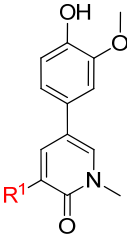
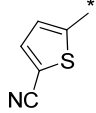
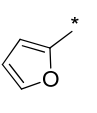
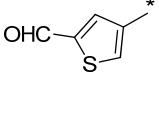
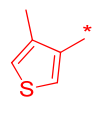
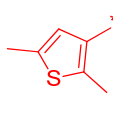
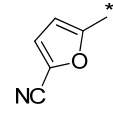
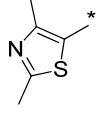
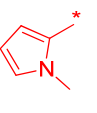
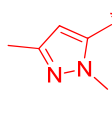
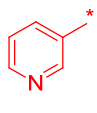
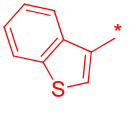
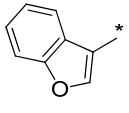
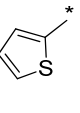
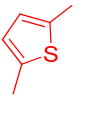
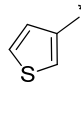
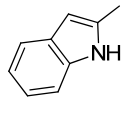
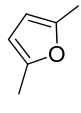
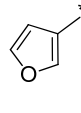
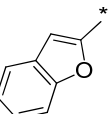
a result of acylation of the imidazole or the piperidine nitrogen. The desired acylpiperidine **201** was isolated by HPLC.



Scheme 22: Synthesis of semi-saturated bicycle

2.3.2 Data Analysis

All of the heterocyclic targets synthesised were profiled in the PI3K assays (Appendix 2) and the PI3K γ data are shown in Table 17. Compounds are coloured by ligand efficiency, calculated using potency (pIC₅₀) against PI3K γ , with actual pIC₅₀ values shown below. Ligand efficiency allows a more balanced and comprehensive comparison of the mono- and bicyclic systems than potency (pIC₅₀) alone, as the larger bicyclic compounds would be expected to gain extra binding interactions.

					
91	127	202	203	204	205
 5.8	 5.0	 6.2	 <4.5	 4.8 ^{*±}	 5.7
206	207	208	209	210	211
 5.4 ^{*±}	 <4.6 [*]	 <4.5	 5.1 [±]	 4.6 [±]	 6.2
212	213	214	215	216	217
 4.9	 4.9	 5.1	 6.5	 5.1	 5.7
218					
 6.2					

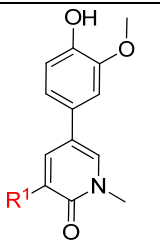
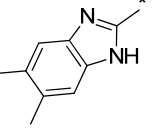
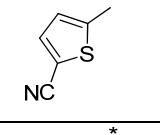
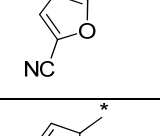
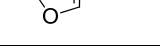
143	188	196	199	201	219
5.6	<4.5	<4.5	5.9	6.8	5.3
220	221	222	223	224	225
5.4	5.4	5.6	5.4 [‡]	4.8 ^{*±}	4.7 [±]
226	227	228	229	230	231
6.1	6.0	5.8	4.9	6.2	5.9 [*]
232	233	234	235	236	237
5.4	4.7 [*]	5.8	<4.5	<4.5	5.8
238	239	240	241	242	
6.3	5.5	6.7	6.2	4.7 ^{*±}	

Table 17: Data on heterocyclic targets. Compounds in red have L.E. <0.3, those in black have L.E. ≥ 0.3; PI3KγpIC₅₀ values are shown below each structure; * indicates n=1 data; ± indicates one value not included in mean as below the threshold of assay (i.e. pIC₅₀ <4.6); ‡ indicates two values not included in mean as below the threshold of the assay (i.e. pIC₅₀ <4.6)

Compounds shown in red have low ligand efficiencies which reflects poor inhibition of PI3K γ for the size of the ligand. Whilst these analogues were not of interest for further progression, analysis of the entire data set revealed some clear SAR.

Key SAR

Comparison of the mono- and bicyclic ring systems revealed that although absolute potency is lost by removing an aromatic ring, the ligand efficiency is retained compared with the benzimidazole. Full data for the best monoheterocyclic analogues are shown in Table 18. The SAR is relatively flat across a range of different scaffolds, with all analogues shown maintaining L.E. above 0.3. Interestingly, the L.L.E. of the monoheterocycles is improved over benzimidazoles **66** and **62**, however this should be interpreted with some caution, as these figures will be influenced by the relative lipophilicity of any pendant groups attached to the rings, which are not directly comparable with the benzimidazoles.

Cpd No.		PI3K γ pIC50	L.E.	L.L.E.	PI3K isoform selectivity	CLND Solubility (μ M)
66		7.0	0.34	0.27	α 5.7 [‡] , β <4.9 [‡] , δ 5.7	14
91		5.8	0.33	0.30	α 5.4, β <4.6, δ 5.6	5
205		5.7	0.33	0.32	α 5.6, β 5.2, δ 5.4	30
217		5.7	0.35	0.32	α 5.2, β <4.6, δ 5.5	16

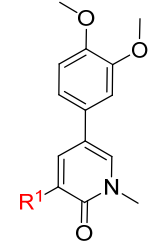
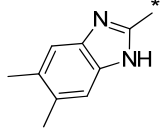
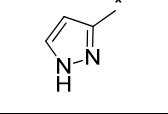
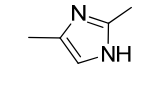
Cpd No.		PI3K γ pIC ₅₀	L.E.	L.L.E.	PI3K isoform selectivity	CLND Solubility (μ M)
62		7.0	0.33	0.24	α 5.4, β <4.6, δ 6.1*	28
143		5.6	0.33	0.32	α 4.7, β 4.4* \ddagger , δ 5.1	258
234		5.8	0.33	0.32	α 4.8* \pm , β <4.6, δ 5.0	294

Table 18: Data on selected monoheterocyclic compounds; * indicates $n=1$ data; \pm indicates one value not included in mean as below the threshold of the assay (i.e. pIC₅₀ <4.6); \ddagger indicates two values not included in mean as below the threshold of the assay (i.e. pIC₅₀ <4.6); \S indicates three values not included in mean as below the threshold of the assay (i.e. pIC₅₀ <4.6)

Unfortunately, none of the monoheterocyclic analogues demonstrated promising isoform selectivity and only the pyrazole **143** and imidazole **234** show improved solubility.

Substitution in the *ortho*-position of the aryl unit attached to the pyridone ring (e.g. **203**, **204**, **206**, **207**, **208**, **235** and **236**, Table 17) was clearly detrimental to potency. It was hypothesized that this was due to a resultant conformational change; substitution at this position will result in an increase in the dihedral angle between the two rings, as exemplified for thiophene series **214**, **203**, and **204** in Table 19.

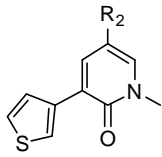
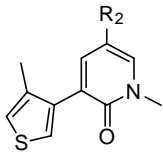
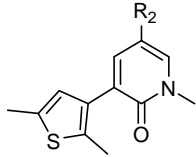
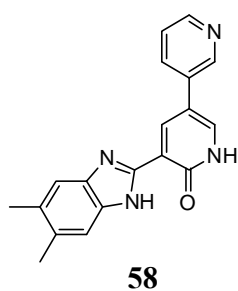
			
	214	203	204
PI3K γ pIC ₅₀	5.1	<4.5	4.8 ^{*±}
Dihedral angle (°)	42	59	63

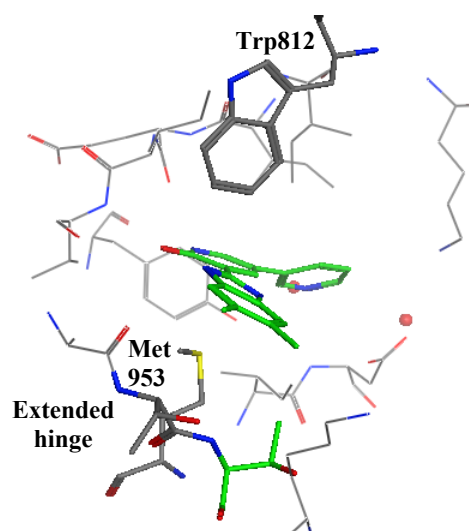
Table 19: Dihedral angles based on Molecular Operating Environment energy minimisations using MMFF94x;¹⁶³ * indicates n=1 data; ± indicates one value not included in mean as below the threshold of assay (i.e. pIC₅₀ < 4.6)

Indeed, closer inspection of the X-ray crystal structure of pyridone **58**^{97,125} supports this hypothesis, with typtophan 812 and part of the extended hinge forming a clamp above and below the plane of the R¹ substituent (Figure 37). Figure 37d, in particular, demonstrates how close the ligand is to the protein surface in this region and, therefore, how rotation of this group, out of plane with the pyridone ring, would not be tolerated. As predicted by the Free Wilson analysis of the historical compounds,¹²³ this trend is observed for analogues with both the dimethoxyphenyl and methoxyphenol R¹ substituents.

(a)



(b)



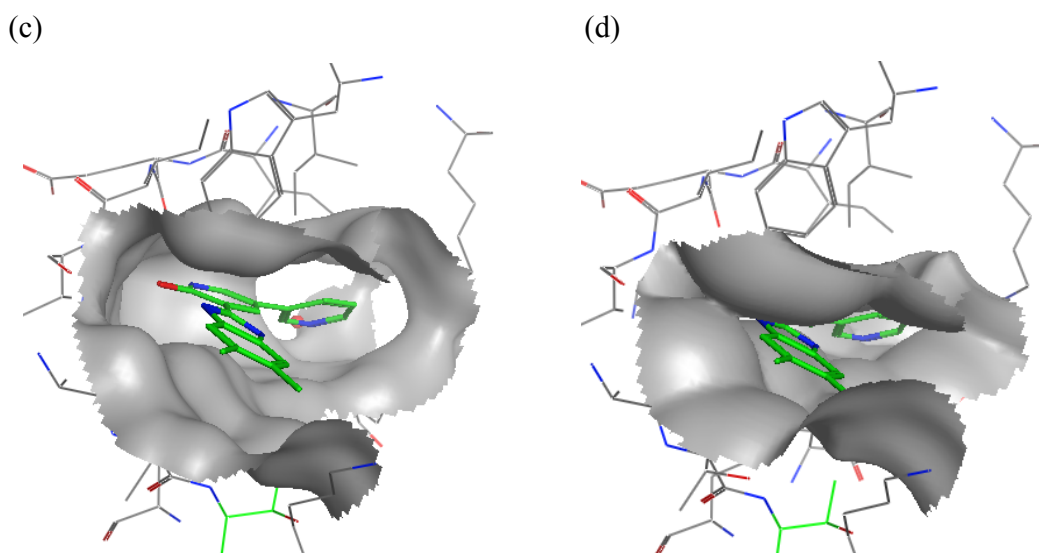


Figure 37: (a) Compound 58; (b) X-ray crystal structure of ligand 58 bound to PI3Kγ with key amino acid residues indicated; (c) X-ray crystal structure of ligand 58 bound to PI3Kγ with protein surface shown; (d) X-ray crystal structure of ligand 58 bound to PI3Kγ with double the Van der Waals protein surface shown i.e. contact between surface and ligand represents good fit

The low potency of the benzoxazole **239** and oxadiazole analogues **188** and **196** is interesting, especially when compared with the benzothiazole **238**, thienylpyridine **240**, and benzofuran **218** (Table 17). One possible explanation for these differences would be to consider the orientation of the heterocycle with respect to the pyridone core. Whilst we have already established that co-planarity of these rings is required for binding to PI3Kγ, *ab initio* torsional energy profiles for representative heterocycles¹⁶⁴ (Figure 38) show that co-planar conformations are favoured in all four cases studied. The benzimidazole (green) shows a strong preference for the co-planar conformation at 0°, due to the formation of an intramolecular hydrogen bond between the benzimidazole NH and the pyridone carbonyl. For the benzothiazole (yellow), a positive interaction between the sulfur and pyridone carbonyl¹⁶⁵ favours the co-planar conformation at 0°, whilst a clash between the sulfur and the proton at the 4-position of the pyridone core, and repulsion between the nitrogen and oxygen lone pairs disfavours the conformation at 180°. The benzofuran (black) shows a similar profile; in this case the steric clash between the proton at the 4-position of the pyridone core and the 3-position of the benzofuran, and the repulsion between the oxygen lone pairs results in a lower energy

for the conformation at 180°. Finally, the benzoxazole (red) shows a very different profile to the other heterocycles; there is a much smaller difference between the two co-planar conformations, so no strong preference for either would be anticipated.

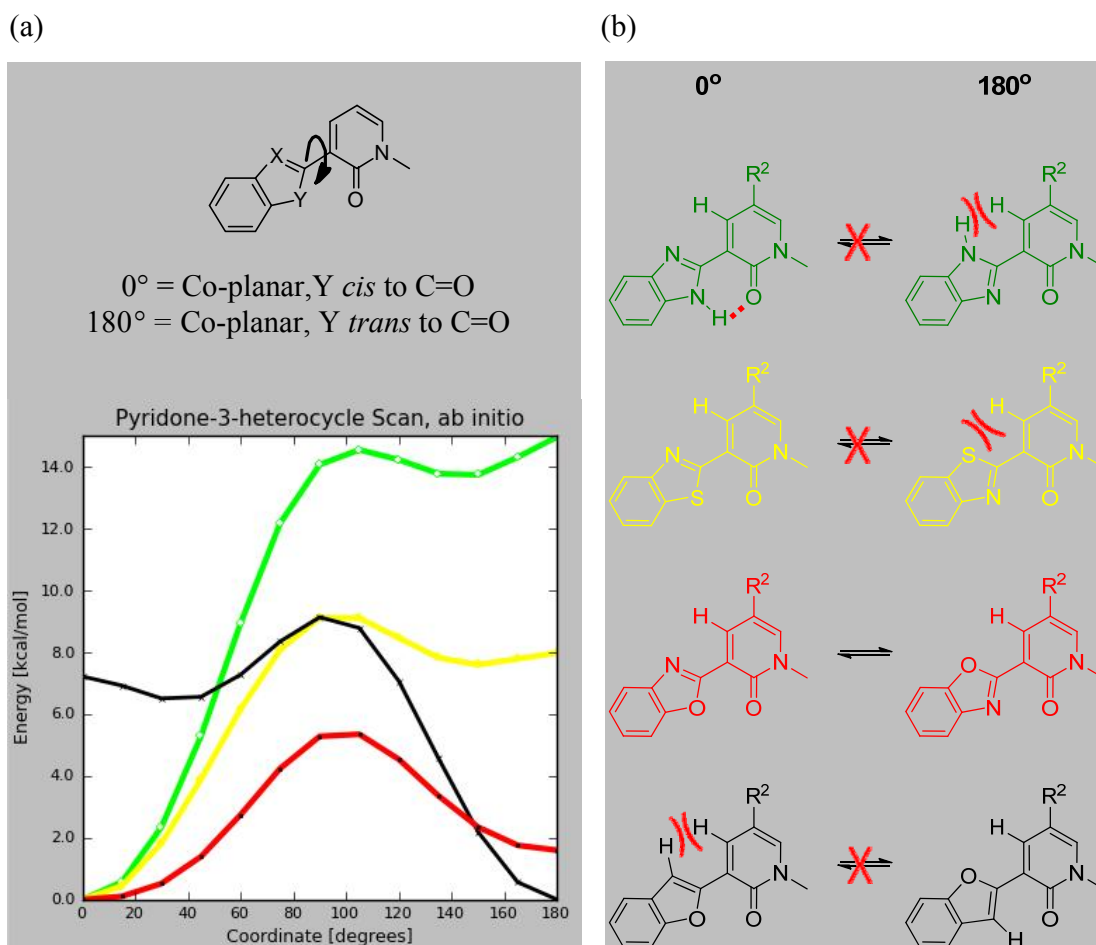


Figure 38: (a) *Ab initio* torsional energy profiles in the gas phase using B3LYP/6-31G** for benzimidazole (green), benzothiazole (yellow), benzoxazole (red) and benzofuran (black); (b) Conformations at 0 and 180° shown in full for each heterocycle

These profiles do not readily explain the observed SAR as they suggest all four heterocycles, including the benzoxazole (and, by analogy, both oxadiazole examples) would be able to adopt a co-planar conformation required for binding to PI3K γ . However, these calculations only provide information on the lowest energy conformation of these molecules in the gas phase and take no account of solvent or protein effects. Indeed, changing the heteroatoms in the 5-membered ring of the heterocycle will result in changes to the orientation and electron density of the fused

benzene ring, which will impact the binding interactions above and below the plane (e.g. with tryptophan 812, as previously shown in Figure 37). Additionally, changes to the heteroatom *cis* to the pyridone carbonyl could impact interactions with nearby residues on the hinge region of the protein (Figure 39). For example, the benzoxazole is the only one of the four which will place a HBA oxygen or nitrogen (with their associated lone pairs) in proximity of the hinge. Finally, the size and directionality of pendant groups on each heterocyclic template must also be taken into account. In reality, it is most likely a complex combination of these factors which leads to the observed SAR.

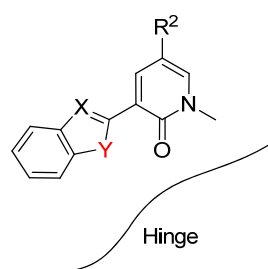
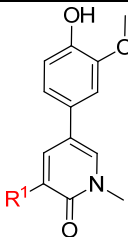
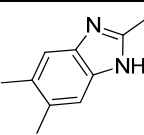
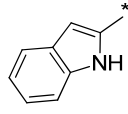
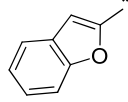


Figure 39: Pictorial representation of pyridone bound to active site, showing proximity to hinge

Full data for the most preferred bicyclic compounds are shown in Table 20, again, referenced against benzimidazoles **62** and **66**.

Cpd. No.		PI3K γ pIC50	L.E.	L.L.E.	PI3K isoform selectivity	CLND Sol. (μ M)
66		7.0	0.34	0.27	α 5.7 [¥] , β 5.1 [§] , δ 5.7	14
215		6.5	0.34	0.28	α 5.6, β <4.6, δ 6.1	7
218		6.2	0.33	0.23	α 5.3 [±] , β <4.6, δ 5.9	3

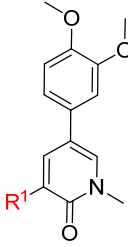
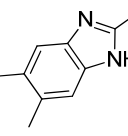
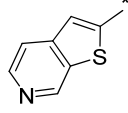
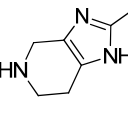
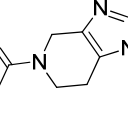
Cpd. No.		PI3K γ pIC ₅₀	L.E.	L.L.E.	PI3K isoform selectivity	CLND Sol. (μ M)
62		7.0	0.33	0.24	α 5.4, β <4.6, δ 6.1*	28
240		6.7	0.34	0.27	α 5.5, β <4.6, δ 5.7 ‡	1
199		5.9	0.30	0.36	α 5.7, β 5.0, δ 6.0	209
201		6.8	0.31	0.42	α 6.0, β 4.9, δ 6.8	378

Table 20: Data on selected bicyclic compounds; * indicates $n=1$ data; ‡ indicates one value not included in mean as below the threshold of assay (i.e. $pIC_{50} < 4.6$); ‡ indicates two values not included in mean as below the threshold of assay (i.e. $pIC_{50} < 4.6$); \S indicates six values not included in mean as below the threshold of assay (i.e. $pIC_{50} < 4.6$)

Indole **215**, benzofuran **218** and thienylpyridine **240** were the most potent unsaturated replacements for the benzimidazole, whilst results for the semi-saturated analogues **199** and **201** were also encouraging. In particular, the acetylated analogue **201** is equipotent with benzimidazole **62** and demonstrates that saturation can be tolerated in this region of the protein, with a significant improvement in solubility. Unfortunately, the selectivity profile for analogue **201** was less promising, as it can be seen that both PI3K α and δ potencies increased relative to unsaturated cores **62** and **240**. Examining the residue differences between the four isoforms in this region of the protein does not readily explain this result, so further iterative design was necessary to fully explore this observation. However, the introduction of saturation/removal of an aromatic ring successfully improved the solubility profile.

Summary

Overall, a wide range of novel PI3K γ inhibitors were synthesised which further expanded our understanding of the R¹ substituent on the pyridone template and the PI3K enzyme structure. The results clearly indicated that planar R¹ groups directly attached to the pyridone were optimal for potency. Saturation was tolerated further out from the core, e.g. semi-saturated analogue **201**, however, this did negatively impact isoform selectivity.

In replacing the benzimidazole, we learnt that the possible H-bond interaction with valine 882 on the protein is not critical for potency as other atoms are tolerated at this position e.g. a sulfur atom in thienylpyridine **240**.

Whilst no major improvements in potency or isoform selectivity were achieved in this work, key exemplars significantly improved the physicochemical profile of the series (Table 21). Imidazole **234** and semi-saturated analogue **201** both successfully reduced the aromatic ring count, reduced lipophilicity, and improved solubility.

In order to regain potency, improve isoform selectivity, and potentially modify the physicochemical properties further (e.g. solubility, PSA), additional optimisation of pendant groups off imidazole **234** and semi-saturated analogues **201** were of interest.

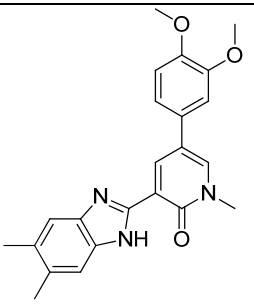
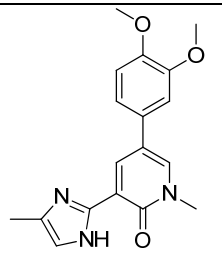
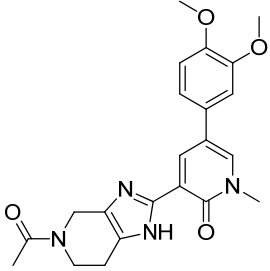
Compound	PI3K γ pIC ₅₀	PI3K isoform selectivity	L.E.	MW	No. aromatic rings	Chrom LogD	CLND sol. (μ M)
 62	7.0	α 5.4 β <4.6 δ 6.1*	0.33	389	4	5.1	28
 234	5.8	α 4.8* \pm β <4.6 δ 5.0	0.33	325	3	2.9	294
 201	6.8	α 6.0 β 4.9 δ 6.8	0.31	408	3	2.0	378

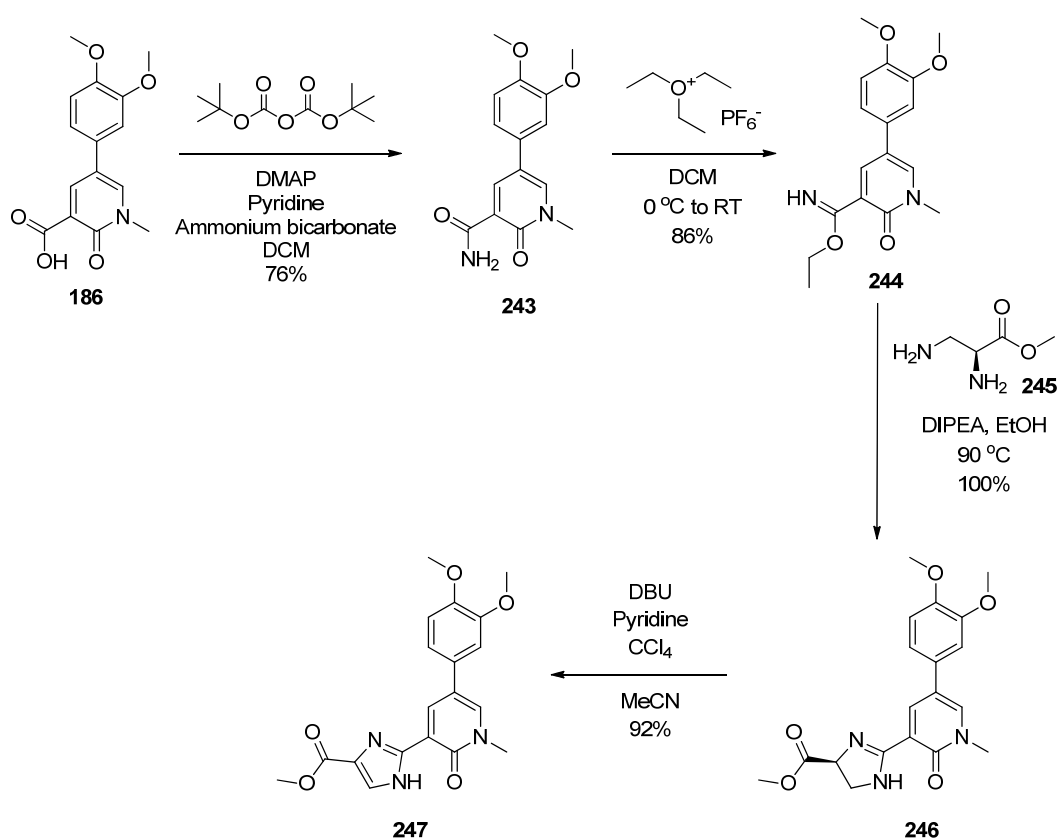
Table 21: Profiles of key compounds; * indicates $n=1$ data; \pm indicates one value not included in mean as below the threshold of assay (i.e. pIC₅₀ < 4.6)

2.4 Further Exploration of Imidazole 234

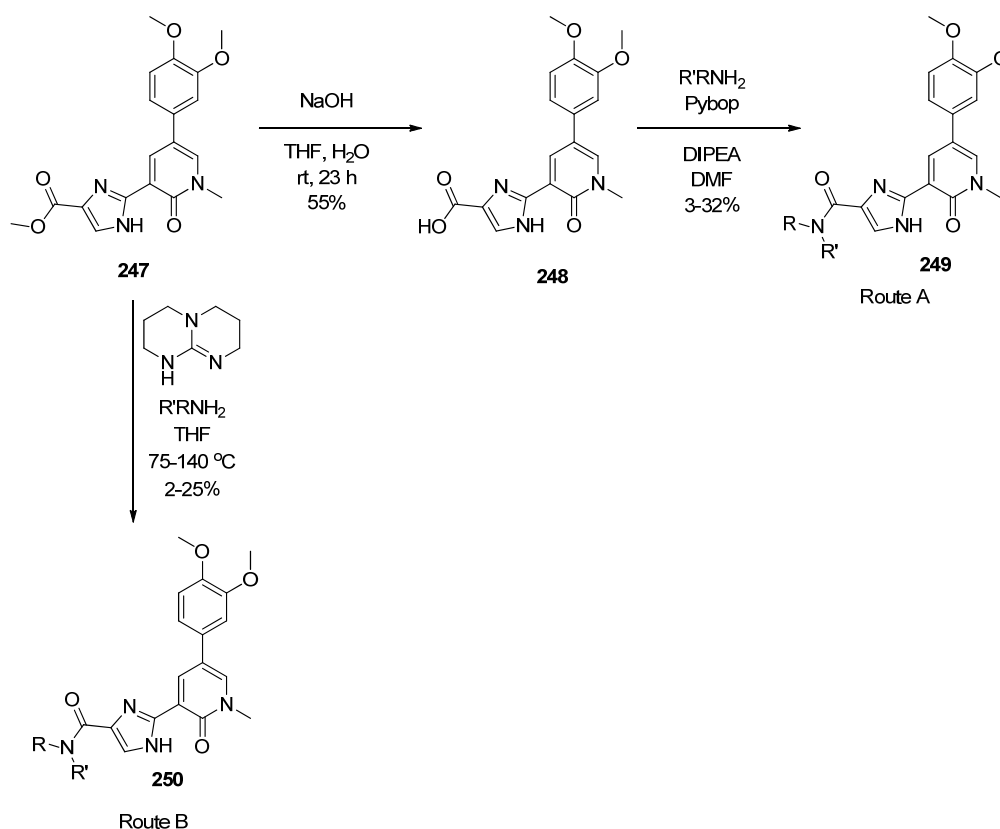
As previously discussed, whilst imidazole **234** did not meet potency criteria, it had good L.E. and a promising selectivity profile relative to PI3K α and β . Perhaps even more importantly, it demonstrated improved solubility over other R¹ groups. We were therefore interested in investigating substitution of the imidazole unit in order to increase potency and selectivity, whilst maintaining the promising solubility profile.

2.4.1 Results and Discussion

Key intermediate **247** (Scheme 23) was accessed elsewhere in our laboratories¹⁶⁶ via a four step synthetic sequence starting from the previously described pyridone carboxylic acid **186**. Formation of imidate **244** was achieved in two steps by synthesis of the primary carboxamide, followed by treatment with Meerwein's salt, in 65% overall yield. Subsequent cyclisation with diamino ester **245** gave the dihydroimidazole **246**. Finally, oxidation¹⁶⁷ yielded the imidazole intermediate **247**, bearing a methyl ester substituent. A methyl ester was chosen to provide a site for subsequent modification of this position. Direct amide formation using triazabicyclodecane (TBD)¹⁶⁸ or ester hydrolysis followed by conventional amide coupling gave access to a range of amide analogues (Scheme 24).



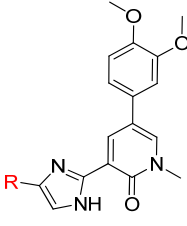
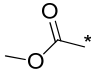
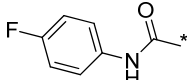
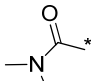
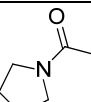
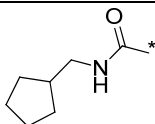
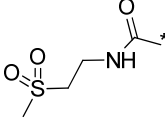
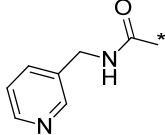
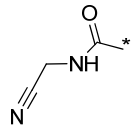
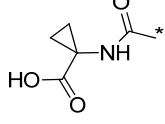
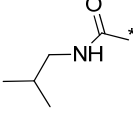
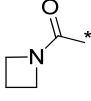
Scheme 23: Synthesis of key intermediate **247**



Scheme 24: Derivatisation of imidazole ester **247**

The amine building blocks were selected to include primary and secondary amines, with a range of alkyl, cycloalkyl and aryl substituents. Monomers with pendant H-bond donor/acceptor groups were also included to probe for polar interactions with the protein.

All of the amides synthesised (and the parent ester **247**) were tolerated (Table 22), with moderate potencies against PI3K γ (pIC₅₀ range 5.7-6.9). Whilst some analogues did not show an increase in potency commensurate with the increase in ligand size or lipophilicity (e.g. compound **250d**, where L.E. and L.L.E. have dropped compared with lead compound **234**), others showed good retention of efficiency (e.g. compounds **249g**, **250a** and **250b**). In general, small alkyl substituents were most favoured for PI3K γ binding efficiency.

Cpd No.		PI3K γ pIC ₅₀	L.E.	L.L.E.	PI3K isoform selectivity	CLND Sol. (μ M)
247		6.0	0.31	0.34	α 5.4, β <4.6, δ 5.3	319
249a		6.6	0.27	0.24	α 4.8, β <4.5, δ 5.9	13
249b		5.8	0.28	0.36	α 5.0, β <4.5, δ 5.5	422
249c		6.1	0.28	0.33	α 5.1, β <4.5, δ 5.7	483
249d		6.6	0.28	0.24	α 5.4, β <4.5, δ 6.1	348
249e		6.7	0.29	0.37	α 5.4, β 4.6 ^{*y} , δ 5.8	402
249f		6.7	0.28	0.30	α 4.8, β 4.8, δ 6.8	419
249g		6.9 [*]	0.33	0.39	α 5.2 [*] , β <4.5 [*] , δ 5.3 [*]	463
249h		6.3	0.27	0.31	α 5.3, β <4.5, δ 5.4	476
249i		6.7	0.31	0.28	α 5.2, β <4.5, δ 5.8	486
250a		6.6	0.30	0.39	α 5.5, β 4.6 ^{*y} , δ 5.5	37

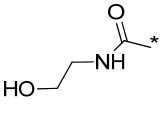
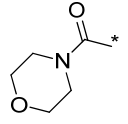
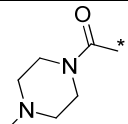
250b		6.6 [‡]	0.31	0.37	α 5.3 [‡] , β 4.5 ^{*§} , δ 5.6 [‡]	1
250c		6.3 [*]	0.28	0.35	α 5.2 [*] , β <4.5 [*] , δ 6.0 [*]	568
250d		5.7	0.24	0.30	α 5.0, β <4.5, δ 5.3	312

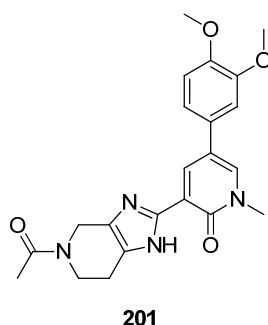
Table 22: Imidazole analogues; * indicates $n=1$ data; [‡] indicates one value not included in mean as below the threshold of the assay (i.e. $pIC_{50} < 4.6$); [‡] indicates two values not included in mean as below the threshold of the assay (i.e. $pIC_{50} < 4.6$); [§] indicated four values not included in the mean as below the threshold of the assay (i.e. $pIC_{50} < 4.6$)

Interestingly, modification of this position in the imidazole unit also influenced the isoform selectivity profile, in particular with respect to PI3K δ . Compounds **249f**, **250c** and **250d** were all equipotent against γ and δ . In contrast, compounds **249g**, **249h**, **249i**, **250a** and **250b** showed ~10-fold or greater selectivity for the γ isoform. The rationale for improved selectivity is not clear as a range of lipophilic and polar substituents show improved profiles. However, small substituents were most beneficial for γ selectivity. Finally, it was pleasing to observe that with the exception of anilide **249a**, acylazetidine **250a** and alcohol **250b**, all compounds maintained or improved the solubility profile of the parent imidazole **234**.

Compound **249g** was arguably the most interesting from this set, with a good L.E. and solubility, coupled with a reasonable selectivity profile. Unfortunately, the PI3K γ potency fell just below our target criteria and, with small substituents showing optimal selectivity profiles, it was not clear how to improve on this. Accordingly, despite significant advances having been made, this area of work was not pursued any further.

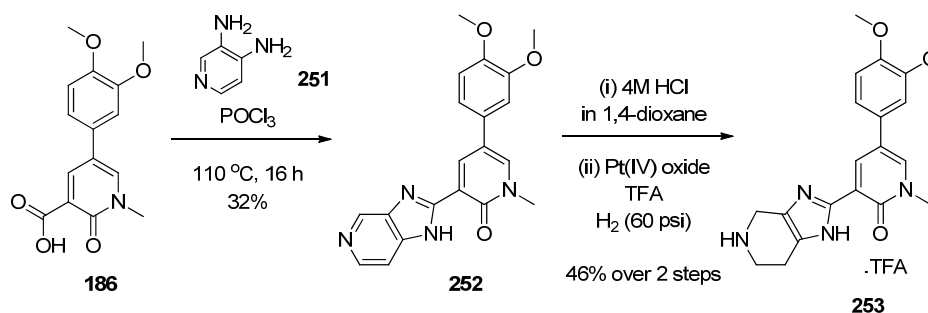
2.5 Further Exploration of Semi-Saturated Analogue 201

Further work on semi-saturated analogue **201** was also of interest, and, in particular, investigation of the *N*-substituent on the piperidine ring.



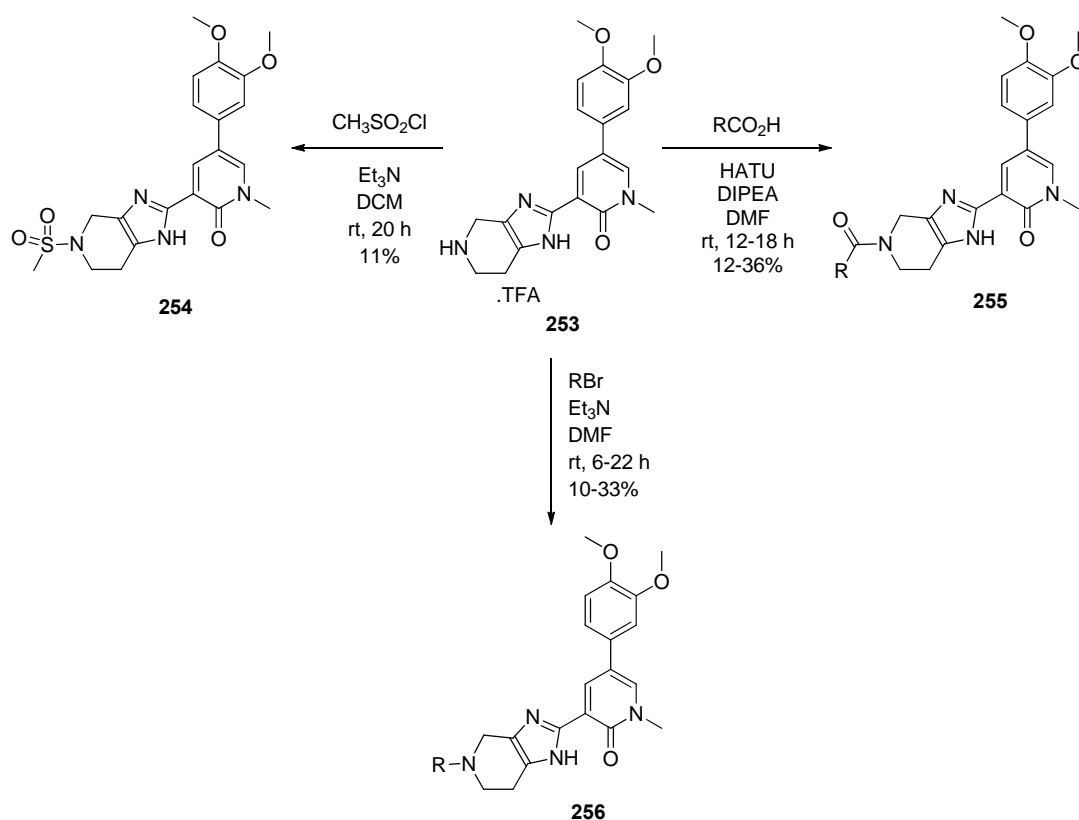
2.5.1 Results and Discussion

Key intermediate **253** was prepared by a 2-step synthesis from starting material **186** (Scheme 25).¹⁶⁹ Phosphorous oxychloride mediated coupling and cyclisation with diamine **251**¹⁷⁰ gave azabenzimidazole **252**. The HCl salt was then prepared in order to facilitate selective reduction of the pyridine ring. However, this subsequently proved to be unnecessary as TFA was required as a solvent in the reduction step to aid solubility of the substrate.



Scheme 25: Synthesis of key intermediate 253

Further derivatisation to explore the pendant substituent was achieved *via* straightforward sulfonylation, acylation, or alkylation chemistry (Scheme 26).



Scheme 26: Derivatisation of semi-saturated template 252

Data for these compounds are shown in Table 23. Unfortunately, no real improvement in PI3K γ potency was observed for any of these analogues and the introduction of lipophilic substituents resulted in an increase in PI3K δ potency; in particular, examples **255c** and **255e** showed ~10-fold selectivity for the δ isoform over the γ isoform.

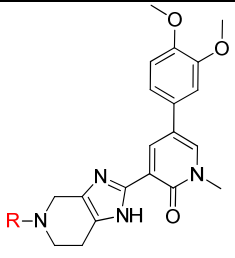
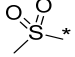
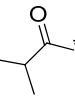
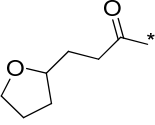
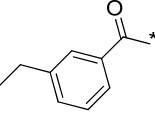
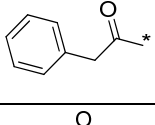
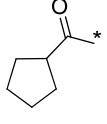
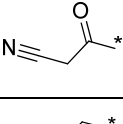
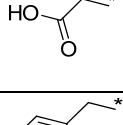
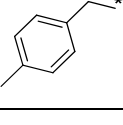
Cpd. No.		PI3K γ pIC ₅₀	L.E.	L.L.E.	PI3K isoform selectivity	CLND Sol. (μ M)
254a		6.8	0.30	0.39	α 6.1, β 5.1, δ 6.4	437
255a		6.6	0.28	0.36	α 6.1, β 4.6 [±] , δ 6.9	402
255b		6.4	0.24	0.31	α 6.1, β 4.6, δ 7.1	383
255c		6.5	0.28	0.22	α 6.0, β 5.1, δ 7.4	20
255d		6.8	0.26	0.28	α 6.6, β 5.3, δ 7.5	92
255e		6.9	0.28	0.33	α 6.5, β 5.0, δ 7.6	432
255f		6.9	0.30	0.41	α 6.3, β 6.0, δ 7.2	446
256a		6.3	0.28	0.43	α 6.0, β 4.6 [±] , δ 5.7	442
256b		6.0	0.24	0.19	α 6.0, β 5.2, δ 6.9	90

Table 23: Data on semi-saturated analogues; * indicates $n=1$ data; [±] indicates one value not included in mean as below the threshold of the assay (i.e. pIC₅₀ < 4.6)

Similar to the imidazole analogues, most of these compounds also show promising solubility profiles. However, the disappointing potency and selectivity over PI3K δ means this area of the programme was not pursued further.

2.6 Carboxylic Acid Containing Pyridones

As previously described, compounds bearing a suitably positioned carboxylic acid moiety within the R¹ group had been shown to confer superior PI3K γ potency and selectivity against the other Class I isoforms (e.g. compound **64**, Table 10). This observation had been investigated elsewhere in our laboratories¹⁷¹ and the SAR had proven to translate well from the benzimidazole series to an amide scaffold at R¹ (compounds **257** and **258**, Table 24). Compound **258** showed a particularly impressive profile, with high potency, >100-fold selectivity over that observed for the α , β and δ isoforms, and excellent ligand efficiency (both L.E. and L.L.E.).

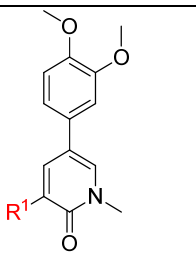
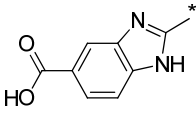
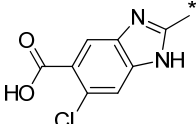
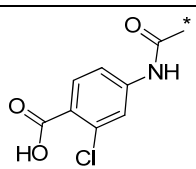
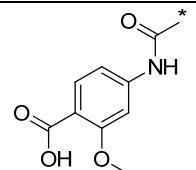
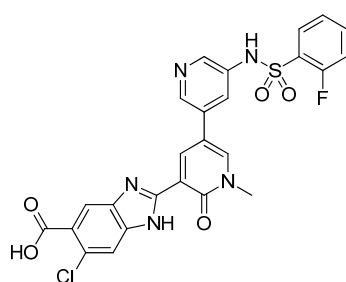
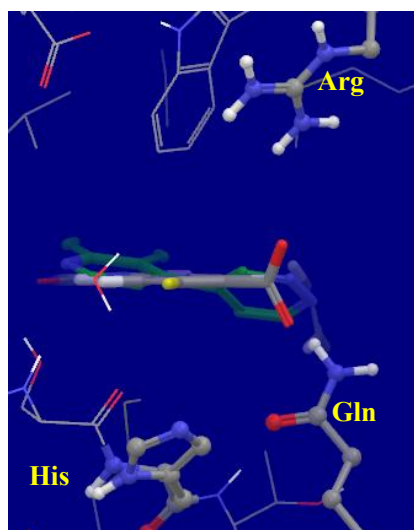
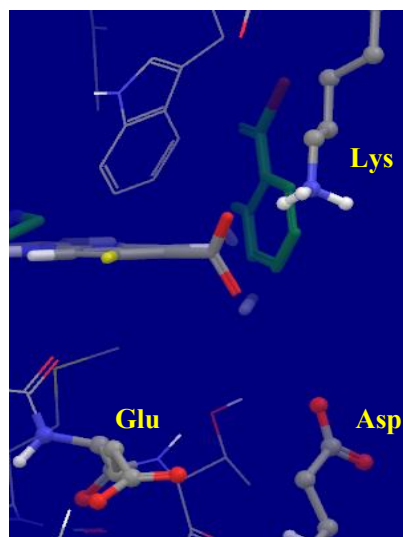
Cpd. No.		PI3K γ pIC ₅₀	L.E.	L.L.E.	PI3K isoform selectivity
64		7.5*	0.34	0.30	α 6.2*, β <4.6*, δ 5.7*
65		7.1	0.31	0.27	α 5.4 [±] , β <4.6, δ 5.3 ^{*‡}
257		7.6	0.34	0.33	α 5.2, β <4.5, δ 5.3
258		7.8	0.33	0.36	α 4.9, β <4.5, δ 5.0

Table 24: Carboxylic acid containing pyridones with good potency and selectivity; * indicates n=1 data; [±] indicates one value not included in mean as below the threshold of the assay (i.e. pIC₅₀ < 4.6); [‡] indicates two values not included in mean as below the threshold of the assay (i.e. pIC₅₀ < 4.6)

Previously (see Section 2.1), we hypothesised that the origin of this selectivity was a charge-charge interaction between the carboxylate anion and lysine 890 in PI3K γ , a residue which is not conserved across the other isoforms. Figure 40 shows the X-ray crystal structure of another historical carboxylic acid-containing pyridone **259** in PI3K γ ¹²³ and computational models of the same ligand in the other three isoforms, focusing on the key residues which surround the carboxylic acid region. Whilst there is a clear rationale for obtaining selectivity over β and δ (due to the unfavourable interactions between the negatively charged carboxylate on the ligand and negatively charged aspartate residues in both proteins), the reason for selectivity over α is less clear.

**259**PI3K γ 8.7* α 6.9*, β <4.6*, δ 6.3***PI3K α (model)****PI3K β (model)**

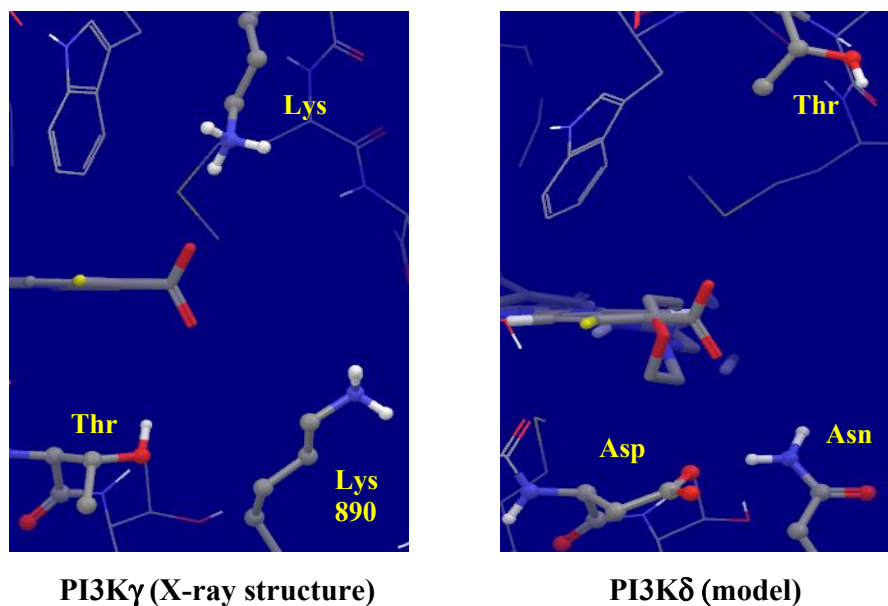
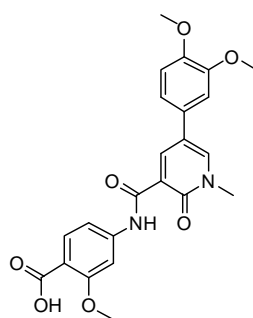


Figure 40: Ligand **259** shown in all four PI3K isoforms with key amino acids labelled;
* indicates $n=1$ data

The successful crystallisation of carboxylic acid containing analogue **258**⁹⁷ in PI3K γ , revealed that an H-bond interaction between the carboxylate anion (which is ionised at physiological pH) and the side chain hydroxyl of threonine 886 may also be important (Figure 41). Although, in theory, this interaction could be maintained in the α isoform (histidine can also act as a H-bond donor), the overall orientation may not efficiently accommodate this interaction.

(a)



258

PI3K γ 7.8

α 4.9, β <4.5, δ 5.0

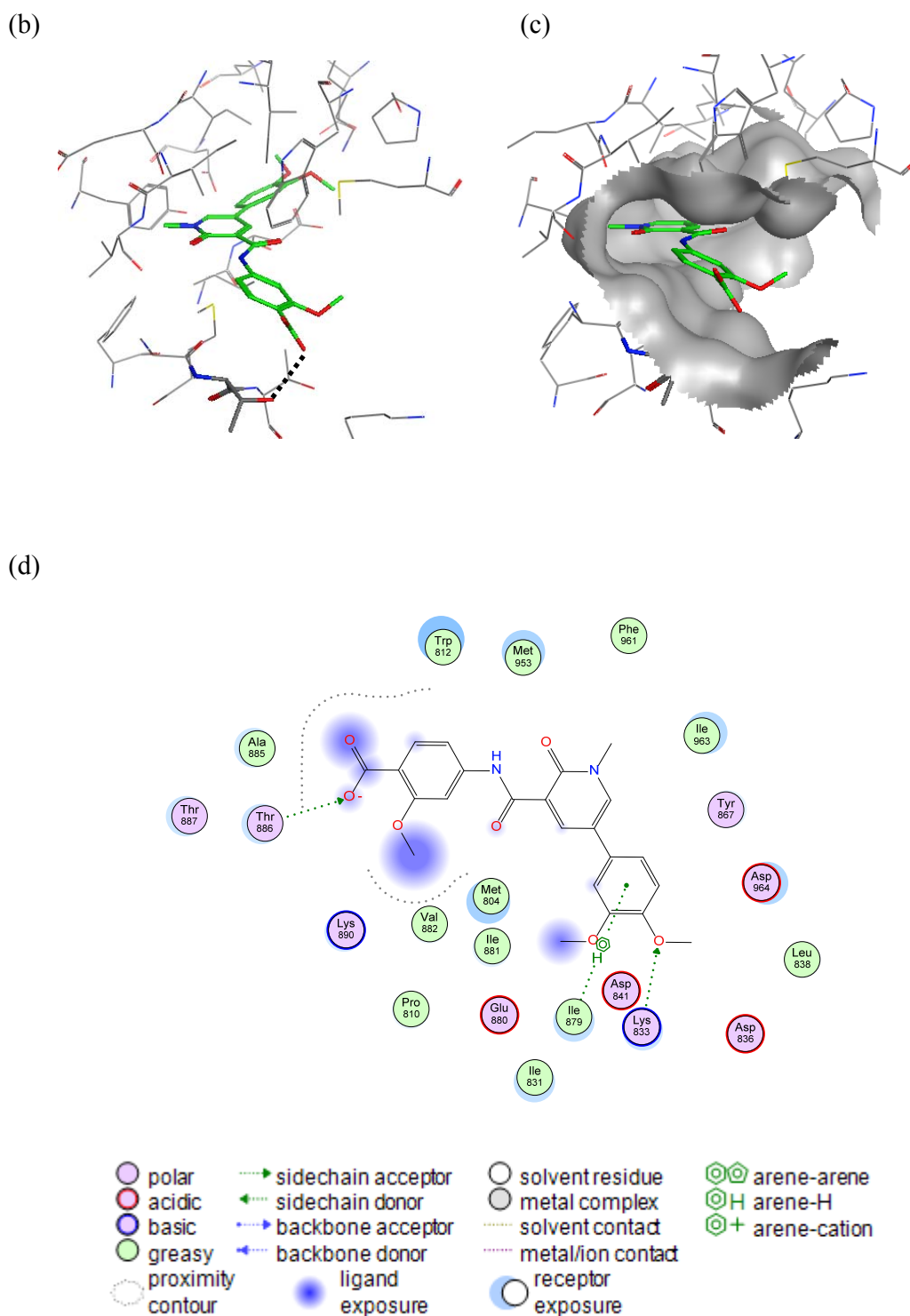


Figure 41: (a) Compound 258; (b) X-ray crystal structure of 258, with key H-bond to threonine 886 marked in black; (c) X-ray crystal structure of 258, with protein surface shown; (d) 2D representation of X-ray crystal structure with key interactions shown

These carboxylic acid containing analogues represented the first compounds from the pyridone template which met our potency and selectivity criteria, so, a subset of these compounds were progressed to a cellular assay to measure PI3K γ inhibition in a system more relevant to an *in vivo* setting. Table 25 shows data for key analogues in a human peripheral blood mononuclear cell (PBMC) assay, which measures inhibition of fMLP stimulated degranulation of basophils (see Appendix 5 for assay protocol).¹²⁴ The compounds showed no, or very low, inhibition in this assay, despite the high potency against the isolated PI3K γ enzyme (7.6-7.8), indicating a drop in potency of >100-fold between the two assay systems.

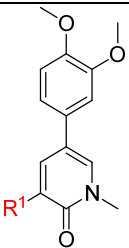
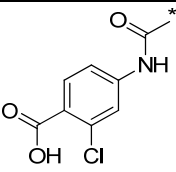
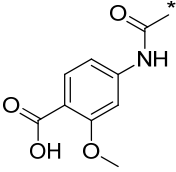
Cpd. No.		PI3K γ pIC ₅₀	L.E.	L.L.E.	fMLP PBMC pIC ₅₀
257		7.6	0.34	0.33	5.4 ^{*‡}
258		7.8	0.33	0.36	<5.0

Table 25: Cell data for carboxylic acid containing analogues; * indicates $n=1$ data; [‡] indicates five values not included in mean as below the threshold of the assay (i.e. $pIC_{50} < 5.0$)

A reduction in potency might be expected on moving from an isolated enzyme assay to a cellular assay for several reasons. Firstly, the cell membrane provides an additional barrier, which must be crossed in order for the inhibitor to reach the intracellular target. Secondly, the ATP concentration within the cell may be higher than in the isolated enzyme assay, which will result in a reduction in the absolute potency of the inhibitor (for an ATP competitive inhibitor).

Of particular concern for the carboxylic acids was their membrane permeability. Figure 42 shows measured lipophilicity (ChromLogD)¹³⁸ plotted against measured permeability in an artificial membrane permeability (AMP) assay¹⁷² (Appendix 6) for the entire set of pyridone compounds which had been synthesised at that time. This permeability assay is used in a similar way to the high throughput CLND solubility assay, providing some indication of the probability a compound has of exhibiting good cell permeability. The graph has a bell-shaped distribution, with the highest permeabilities observed for compounds with ChromLogD values between 3 and 6, which defines the optimum lipophilicity window within this chemical series for good permeability. This distribution is expected, as compounds which are very polar typically have low permeabilities as they cannot pass through the main part of the cell membrane comprising of hydrophobic phospholipid tails. Conversely, compounds with very high lipophilicity are likely to be large in size and unable to pass the polar hydrophilic phospholipid head groups.

The acids (marked in pink) all have low permeability (<50 nm/s) in the AMP assay, which is not unusual for compounds containing this functionality, due to the pK_a of the carboxylate group.¹⁷³ At physiological pH, the negatively charged carboxylate anion will predominate and it is well precedented that ionised species do not readily cross cell membranes *via* passive diffusion.¹⁷⁴

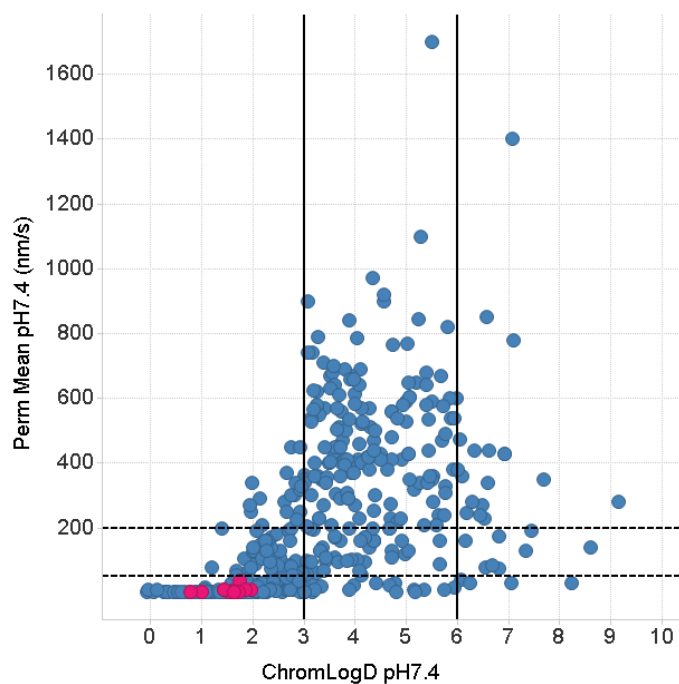


Figure 42: ChromLogD pH 7.4 vs. measured permeability; carboxylic acids marked in pink; vertical lines represent target ChromLogD range for obtaining good permeability; horizontal lines represent cut-offs between low, medium, and high permeability classes

Another physicochemical property which may influence the transport of a drug across a cell membrane is its solubility. Figure 43 shows measured lipophilicity plotted against measured CLND solubility for the entire set of synthesised pyridones. Once again, the carboxylic acid containing analogues are marked in pink and, pleasingly, the majority of these species have high solubilities ($>200 \mu\text{g/mL}$), suggesting this property is unlikely to be limiting cell penetration.

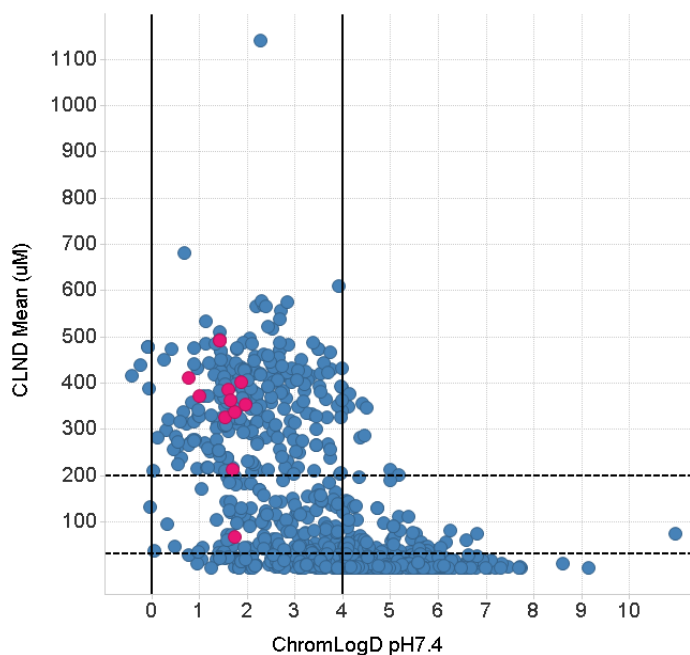


Figure 43: ChromLogD pH 7.4 vs. measured solubility; carboxylic acid containing analogues marked in pink; vertical lines represent target ChromLogD range for obtaining good solubility; horizontal lines represent cut-offs between low, moderate and high solubility classes

Based on all of the above, new carboxylic acid-containing pyridones were therefore designed to improve permeability, whilst maintaining the desirable potency and selectivity profile.

2.6.1 Increased Lipophilicity

The first strategy was to design analogues with increased lipophilicity as a method of increasing permeability; specifically, the incorporation of more lipophilic substituents on the phenyl R² group or replacement of benzimidazole with the more lipophilic benzothiazole was planned (Figure 44). Increasing lipophilicity elsewhere in the molecule may compensate for the highly polar and ionisable carboxylate group. The benzothiazole analogues also remove an H-bond donor from the molecule, which may give additional benefits with respect to permeability.¹⁷⁵

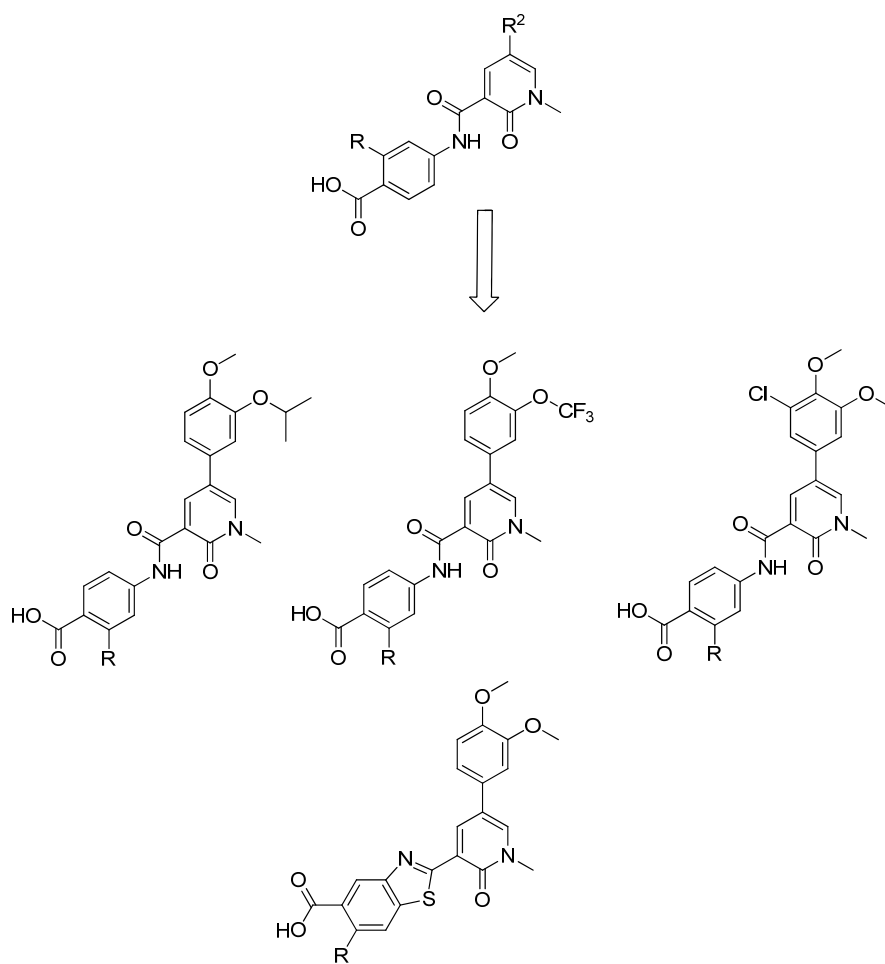


Figure 44: Pyridone analogues targeting increased lipophilicity

The predicted physicochemical properties for these targets (where R=OMe) are shown in Table 26, with compound **258** included for comparison. The calculated ChromLogD¹⁷⁶ for the proposed targets (ChromLogD range 2.8-3.2) are all higher than reference compound **258** (ChromLogD 2.0) and mostly fall within the optimum range for good permeability, as defined in Figure 42. The benzothiazole analogue shows a drop in PSA as a result of the reduction in hydrogen bond donors (HBD), both of which may be beneficial for improving permeability.

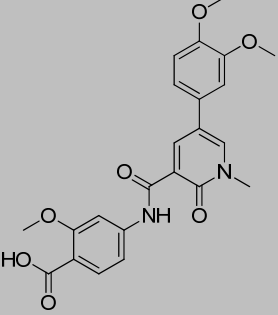
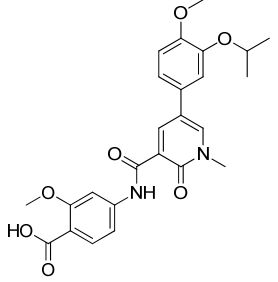
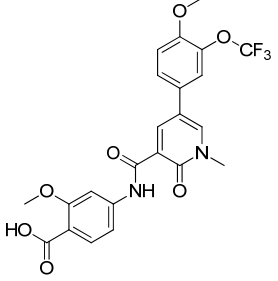
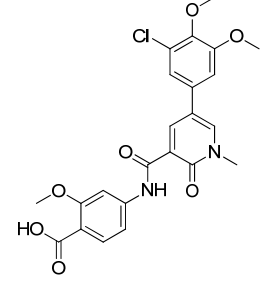
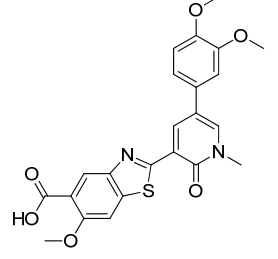
Structure	Calculated ChromLogD	HBA	HBD	PSA	MW
 <p style="text-align: center;">258</p>	2.0	4	1	116	438
	2.8	4	1	116	466
	2.9	4	1	116	492
	3.3	4	1	116	527
	3.2	4	0	100	452

Table 26: Calculated properties for proposed targets

The virtual compounds were also profiled through a proprietary *in silico* permeability model.¹⁷⁷ This model was built using a large data set of measured AMP permeability data on a range of proprietary compounds and uses lipophilicity (specifically ChromLogD) and compound size (calculated molar refractivity or cmr) to predict a compounds' probability of exhibiting good permeability. Figure 45a shows the model validation for the pyridone series; the line represents the cut-off between low probability of good permeability (compounds below the line) and higher probability of good permeability (compounds above the line). The graph is coloured by measured artificial membrane permeability (AMP) class, derived from a high throughput permeability measurement.¹⁷² These classes are defined by the following permeability values in the assay:

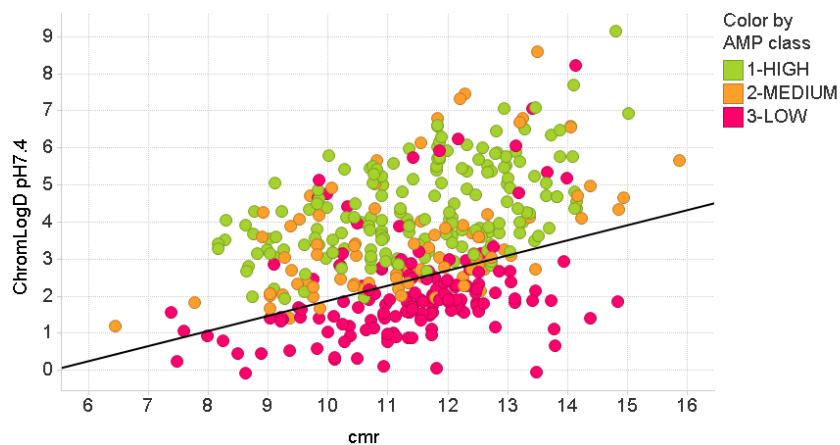
High AMP >200 nm/s

Medium AMP between 50 and 200 nm/s

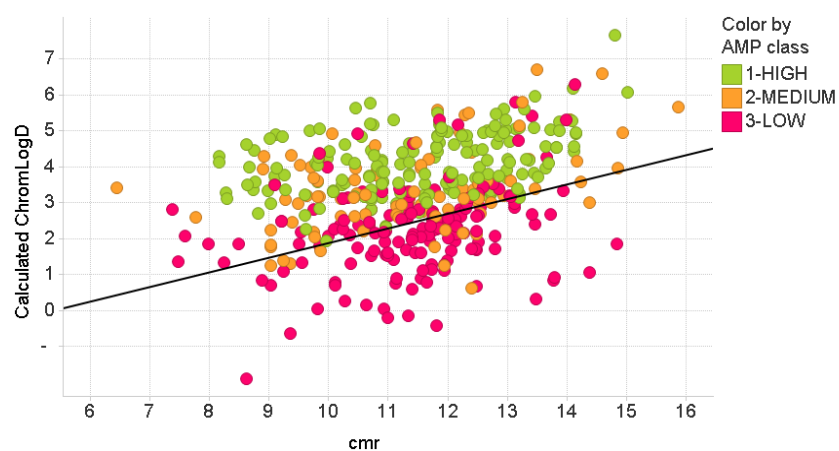
Low AMP <50 nm/s

Whilst Figure 45a shows some compounds which have a medium or low measured permeability in the AMP assay are predicted to be good in this model, importantly no compounds which have a high measured permeability are predicted to be poor. Additionally, the model performs similarly well using a GSK *in silico* prediction of ChromLogD¹⁷⁶ (Figure 45b). This is an ideal situation for an *in silico* tool; the profiling of virtual compounds, can enable a quick and easy decision to reject those compounds which are predicted to have a low chance of success, with high confidence. Figure 45c shows the same model for the carboxylic acid containing pyridones only. Compounds marked in blue are historical analogues and are all predicted to have poor permeability, whilst those shown in pink are the proposed targets, with increased lipophilicity. Pleasingly, these virtual compounds populate a different region of the plot, mostly falling above the permeability cut-off line.

(a)



(b)



(c)

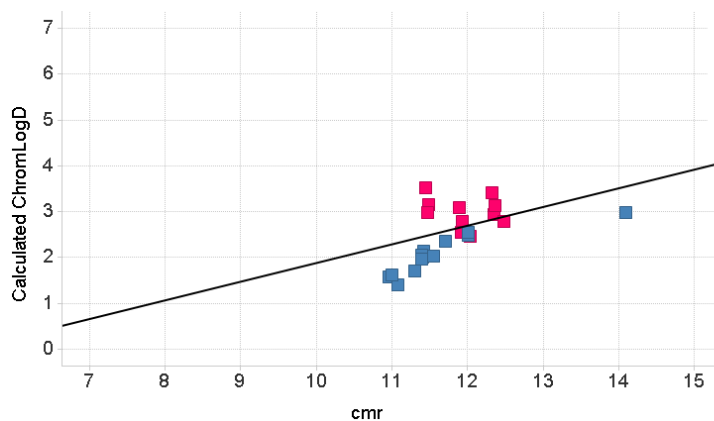
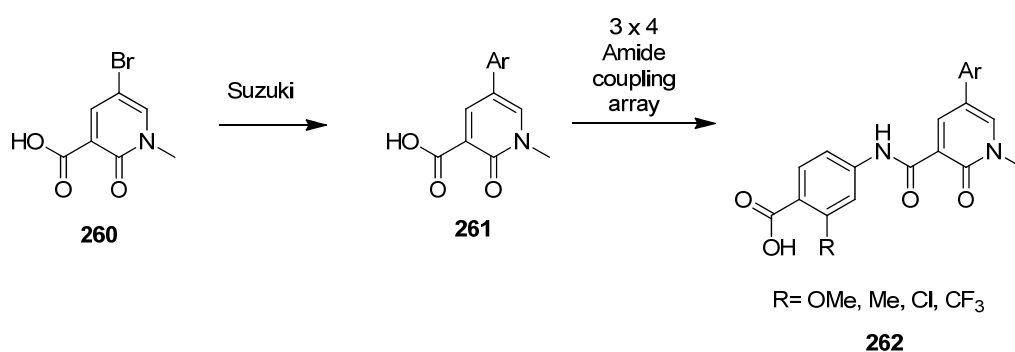


Figure 45: (a) Permeability model using measured ChromLogD for pyridone compounds; (b) Permeability model using calculated ChromLogD for pyridone compounds; (c) Permeability model for acid containing pyridones, virtual compounds shown in pink and previously synthesised compounds shown in blue

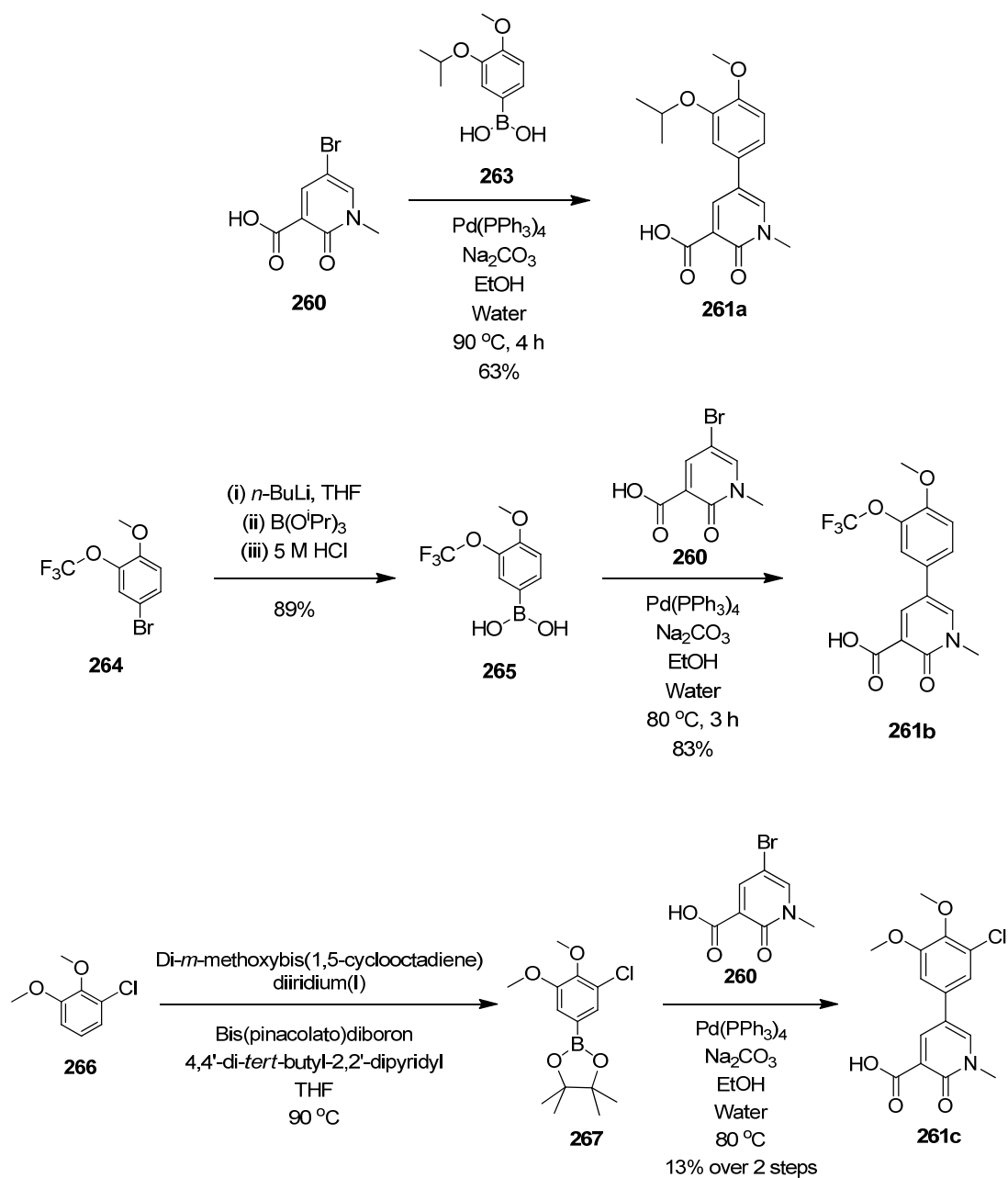
2.6.2 Results and Discussion

The synthesis of the more lipophilic acid containing pyridone amides was attempted *via* key pyridone bromide **260** (Scheme 27).¹⁶⁹ Suzuki coupling with the three required boronic acids would furnish pyridone carboxylate intermediates of type **261**, after which simple amide couplings would give the desired products. Four different anilines were selected for this array, with a range of *ortho*-substituents (Scheme 27). The *ortho*-substituents were selected based on potency at PI3K γ from previous analogues and their impact on the overall lipophilicity of the final compounds.



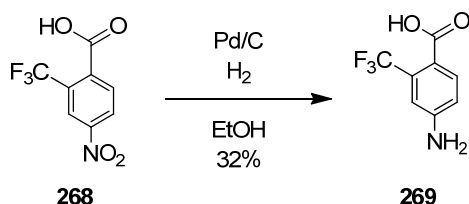
Scheme 27: Route to desired lipophilic pyridone targets

The acid intermediates were synthesised as shown in Scheme 28; in some cases bespoke synthesis of the boronic acid was required. The trifluoromethyl-containing boronic acid **265** was accessed *via* standard lithiation chemistry, previously discussed in Section 2.3.1, whilst the 3-chloro-4,5-dimethoxy analogue **267** was synthesised by C-H activation using iridium-catalysed borylation (Scheme 28).¹⁷⁸ The low overall yield in the latter case was due to incomplete conversion in the borylation step and degradation of the boronate during purification by silica chromatography.



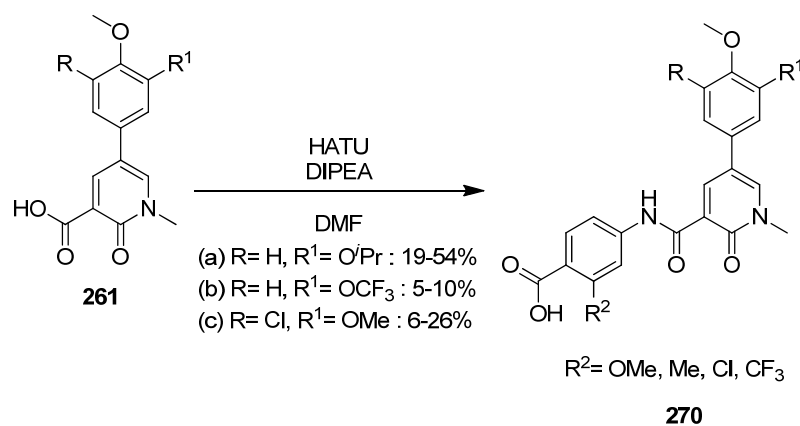
Scheme 28: Synthesis of intermediates for more lipophilic pyridones

One of the desired aniline monomers also required synthesis, *via* simple reduction of the corresponding commercially available nitro compound **268** (Scheme 29). The poor yield reflects difficulties encountered in isolation of compound **269**.



Scheme 29: Synthesis of aniline monomer

Once all of the required monomers had been made, amide coupling furnished the desired products in 5-54% yield (Scheme 30). Notably, the reactions using carboxylic acid **261b** proceeded in particularly low yield; indeed, the synthesis of compound **270** where R=H, R¹=OCF₃, R²=OMe was unsuccessful. This was attributed to the low purity of intermediate **261b** (only 82% by LCMS) which was used in crude form.



Scheme 30: Amide couplings

Data for these compounds are shown in Table 27, and it can be seen that all of the back pocket changes result in a drop in potency compared with the previously described dimethoxyphenyl analogue **258**. However, many analogues still maintain at least 10-fold selectivity for PI3K γ (e.g. **270b**, **270e**).

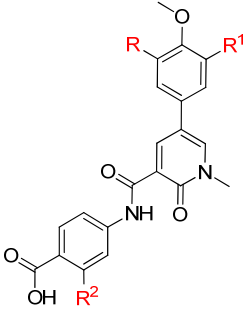
Compound No.				PI3K γ pIC ₅₀	PI3K isoform selectivity
	R	R ¹	R ²		
258	H	OMe	OMe	7.8	α 4.9, β <4.5, δ 5.0
270a	H	O ⁱ Pr	Cl	6.7	α 5.0, β <4.5, δ 5.1
270b			Me	6.5	α 4.6 ^{*‡} , β <4.5, δ 4.7 [±]
270c			OMe	6.7	α 4.7, β <4.5, δ 4.5 ^{*±}
270d			CF ₃	6.7	α 4.8, β <4.5, δ <4.5
270e	H	OCF ₃	Cl	6.8	α 4.9, β 4.5 ^{*±} , δ 5.2
270f			Me	6.6	α 4.6 ^{*±} , β <4.5, δ 4.8
270g			CF ₃	6.8	α 4.6 ^{*±} , β <4.5, δ 4.7
270h	Cl	OMe	Cl	6.0	α 4.6 ^{*±} , β <4.5, δ 5.1 ^{*±}
270i			Me	5.5	α 4.9 ^{*±} , β <4.5, δ 5.4
270j			OMe	5.7	α <4.5, β <4.5, δ 5.1 ^{*‡}
270k			CF ₃	5.8	α <4.5, β <4.5, δ 4.7 ^{*±}

Table 27: Data on analogues targeting increased lipophilicity; * indicates n=1 data; [±] indicates one value not included in mean as below the threshold of the assay (i.e. pIC₅₀ <4.6); [‡] indicates two values not included in the mean as below the threshold of the assay (i.e. pIC₅₀ <4.6); [§] indicates three values not included in the mean as below the threshold of the assay (i.e. pIC₅₀ <4.6)

The most potent examples were progressed to the fMLP PBMC cellular assay and the data are also shown in Table 28. Disappointingly, despite the measured ChromLogD showing a significant increase in lipophilicity, none of these analogues show any improvement in cellular potency compared with analogue **258** and, indeed, the measured AMP permeability data supports this observation, with only compound **270f** achieving a medium permeability classification. Some of the compounds also show disappointing solubility (**270c, f, g, j** and **k**), however many analogues maintain the promising profile previously seen.

One hypothesis for these disappointing cellular data is that carboxylic acid containing compounds have a narrower set of optimal physicochemical property requirements in order to achieve good permeability than compounds which do not contain a functional group which ionises to form an anion. Therefore the ChromLogD range and permeability model cannot be reliably applied to this specific subset of compounds.

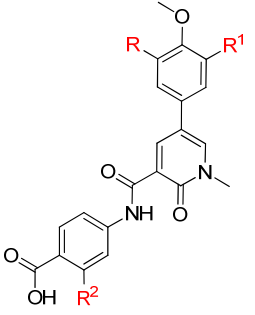
Cpd. No.				PI3K γ pIC ₅₀	fMLP PBMC pIC ₅₀	AMP Perm. (nm/s)	CLND Sol. (μ M)	Chrom LogD pH7.4
	R	R ¹	R ²					
258	H	OMe	OMe	7.8	<5.0	10	492	1.4
270a	H	O ⁱ Pr	Cl	6.7	5.2	6	403	2.4
270b			Me	6.5	5.4	23	371	2.5
270c			OMe	6.7	<5.0	15	46	2.3
270d			CF ₃	6.7	5.5	8	592	2.6
270e	H	OCF ₃	Cl	6.8	5.2 ^{*±}	13	198	2.8
270f			Me	6.6	<5.0	93	29	3.0
270g			CF ₃	6.8	<5.0	15	61	3.1
270h	Cl	OMe	Cl	6.0	5.0	9	187	2.5
270i			Me	5.5	NT	34	403	2.5
270j			OMe	5.7	NT	30	49	2.4
270k			CF ₃	5.8	5.3	7	38	2.7

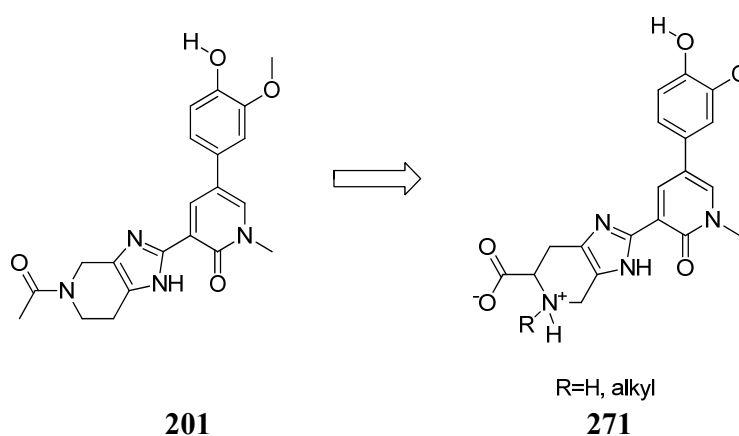
Table 28: Cellular data for new carboxylic acid containing analogues; * indicates $n=1$ data; [±] indicates one value not included in mean as below the threshold of the assay (i.e. $pIC_{50} < 5.0$)

2.6.3 Summary and Future Work

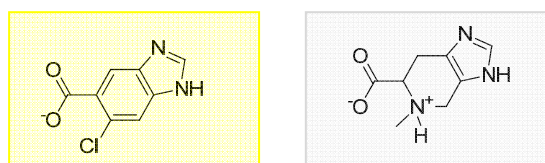
Whilst increasing the lipophilicity of the carboxylic acid containing pyridone compounds did not deliver a significant improvement in their cellular activity, a second strategy for improving permeability would be the introduction of a basic centre to the molecules, to give zwitterionic compounds. Zwitterions are well preceded as having improved permeability over carboxylate anions due to neutralisation of the negative charge on addition of the basic group.¹⁷⁴

Based on semi-saturated analogue **201**, a scaffold previously shown to be well tolerated, compounds of type **271** (Figure 46) are proposed. Whilst the introduction of a stereogenic centre will affect the absolute orientation of the acid group in the enzyme relative to the fully unsaturated benzimidazole analogues, energy minimisations of a representative benzimidazole acid vs. zwitterionic compound are shown to overlay relatively well (Figure 46b).¹⁶³

(a)



(b)



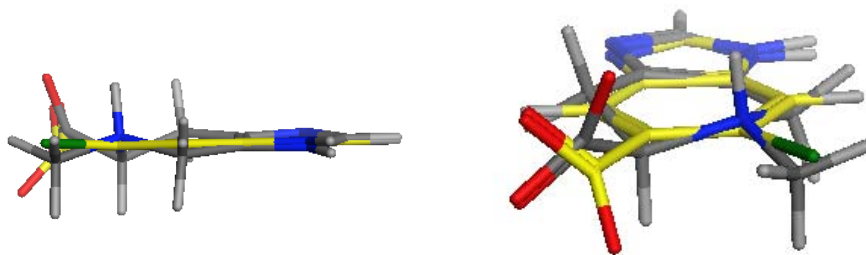


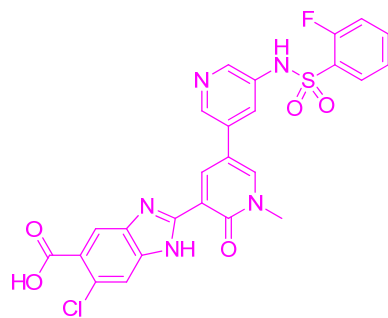
Figure 46: (a) Proposed zwitterionic targets; (b) Overlay of energy minimised substructures of proposed targets using Moe

These compounds could provide an alternative strategy for addressing the cellular activity of the carboxylic acid-containing pyridone compounds, which otherwise display an excellent potency and selectivity profile.

2.7 Accessing a New Region of the Protein

In addition to exploring replacements for the benzimidazole R¹ substituent, the introduction of pendant groups off this ring system was also of interest; in particular, substitution at the 7-position of the benzimidazole. An overlay of the X-ray crystal structures for pyridone benzimidazole **259**⁹⁷ with the literature PI3K γ inhibitor **32**^{94,97} (Figure 48) shows that the PI3K γ protein is flexible in this region, with lysine 883 moving to accommodate the large isopropyl benzamide of compound **32** (Figure 47c clearly shows a large difference in the position of lysine 833). The analogous residues in the other PI3K isoforms (arginine, serine and leucine in α , β and δ respectively)⁷⁷ are not as flexible, possibly a consequence of influence from adjacent amino acids residues (e.g. nearby glutamic acid 798 in α could be forming a strong charge-charge interaction with the arginine, fixing its conformation), therefore this induced fit observed in PI3K γ was hypothesised to be responsible for the excellent isoform selectivity of compound **32**. Exploring this region of space from the pyridone template, was of interest, not only to further investigate protein flexibility, but to identify another moiety (preferably neutral at physiological pH, unlike the carboxylate) for obtaining good isoform selectivity.

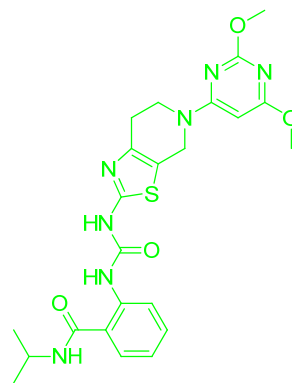
(a)



259

PI3K γ 8.7*

α 6.9*, β <4.6*, δ 6.3*

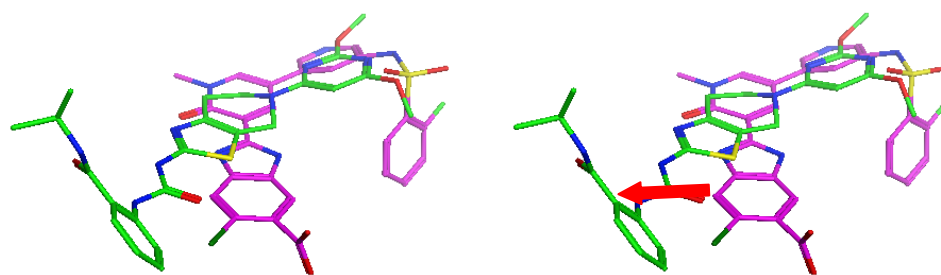


32

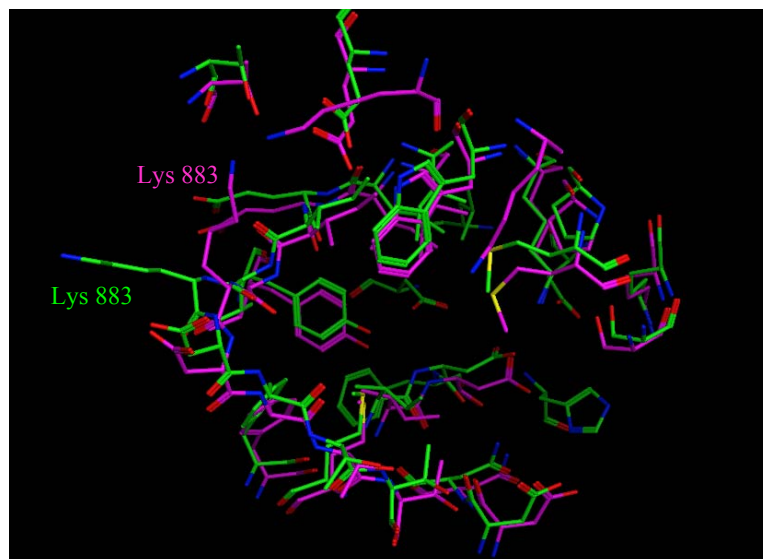
PI3K γ 8.6

α 4.8[‡], β 6.0, δ 5.9

(b)



(c)



(d)

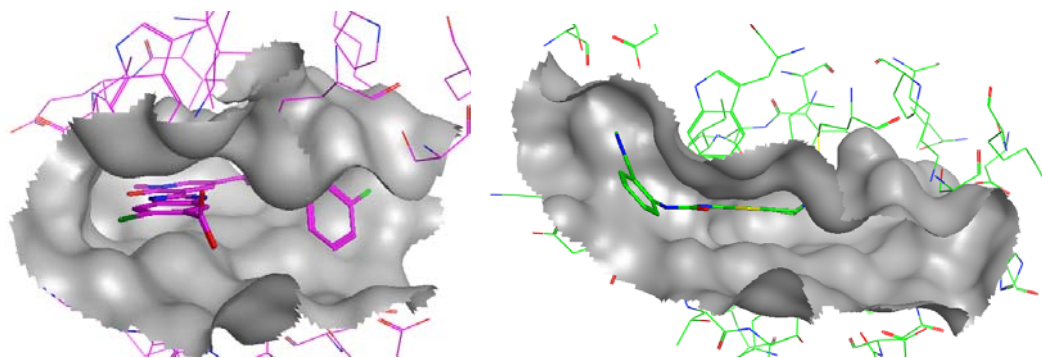


Figure 48: (a) Pyridone benzimidazole **259** and literature compound **32**, with biological data from GSK assays;⁹⁴ (b) Overlay of X-ray crystal structures of pyridone benzimidazole **259** (pink)⁹⁷ and literature compound **32** (green) in PI3K γ (no protein shown for clarity), red arrow indicates vector of growth from pyridone; (c) Overlay of X-ray crystal structures of pyridone benzimidazole **259** (pink) and literature compound **32** (green) in PI3K γ (only protein shown); (d) X-ray crystal structures of each compound with protein surface shown in white; * indicates $n=1$ data; ‡ indicates two values not included in mean as below the threshold of the assay (i.e. $pIC_{50} < 4.6$)

Initial targets were designed using overlays of the X-ray crystal structures for the two templates (Figure 49).

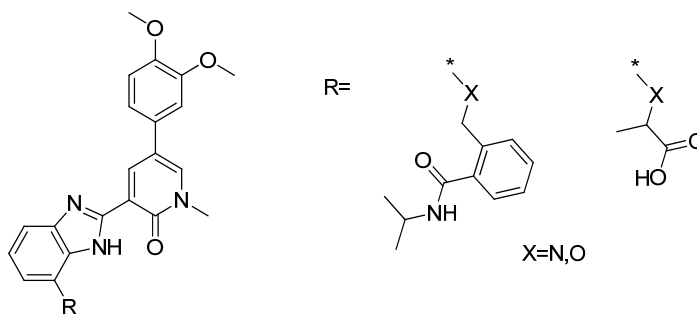
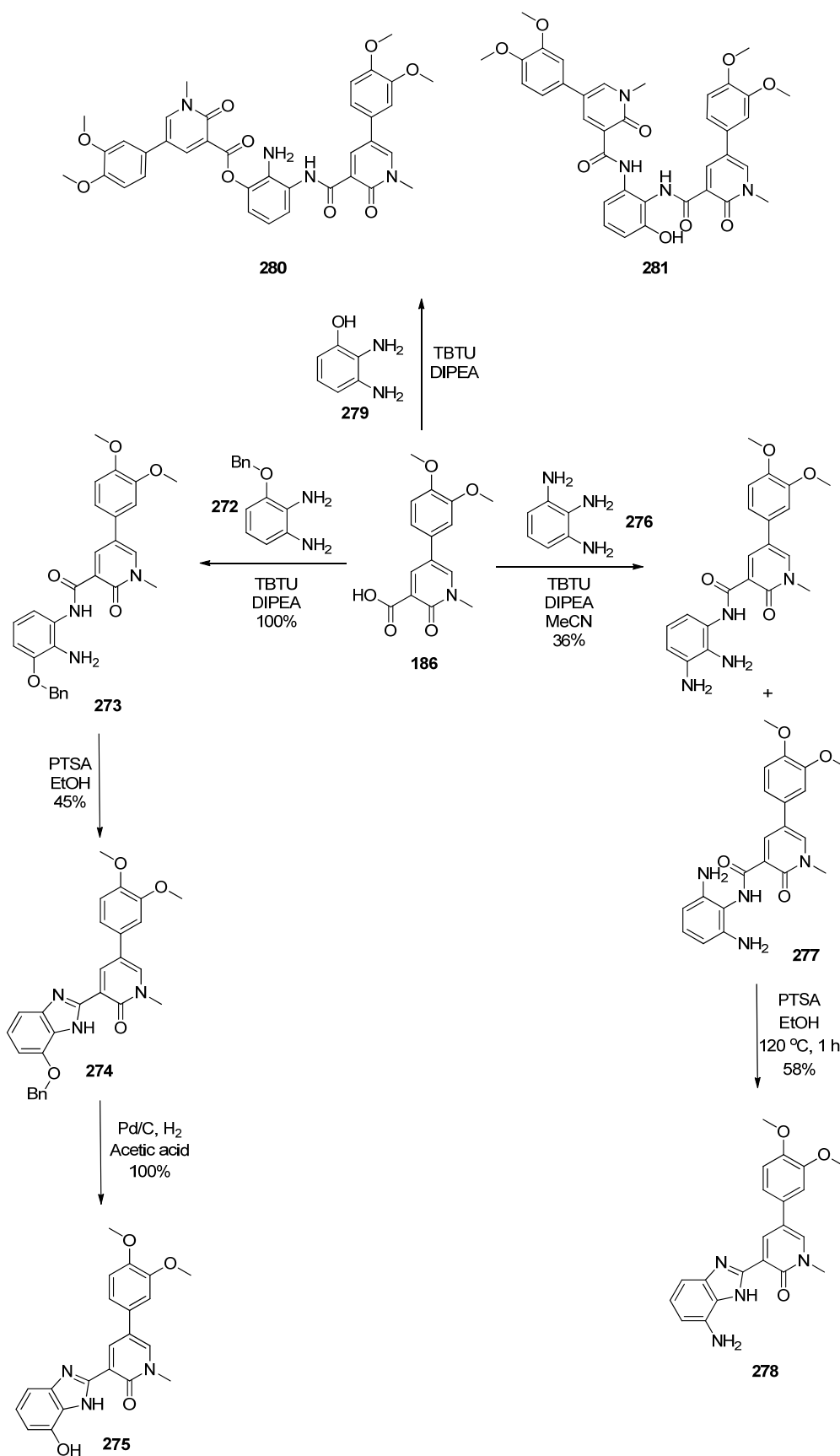


Figure 49: Proposed targets to investigate the induced fit of pyridone inhibitors

2.7.1 Results and Discussion

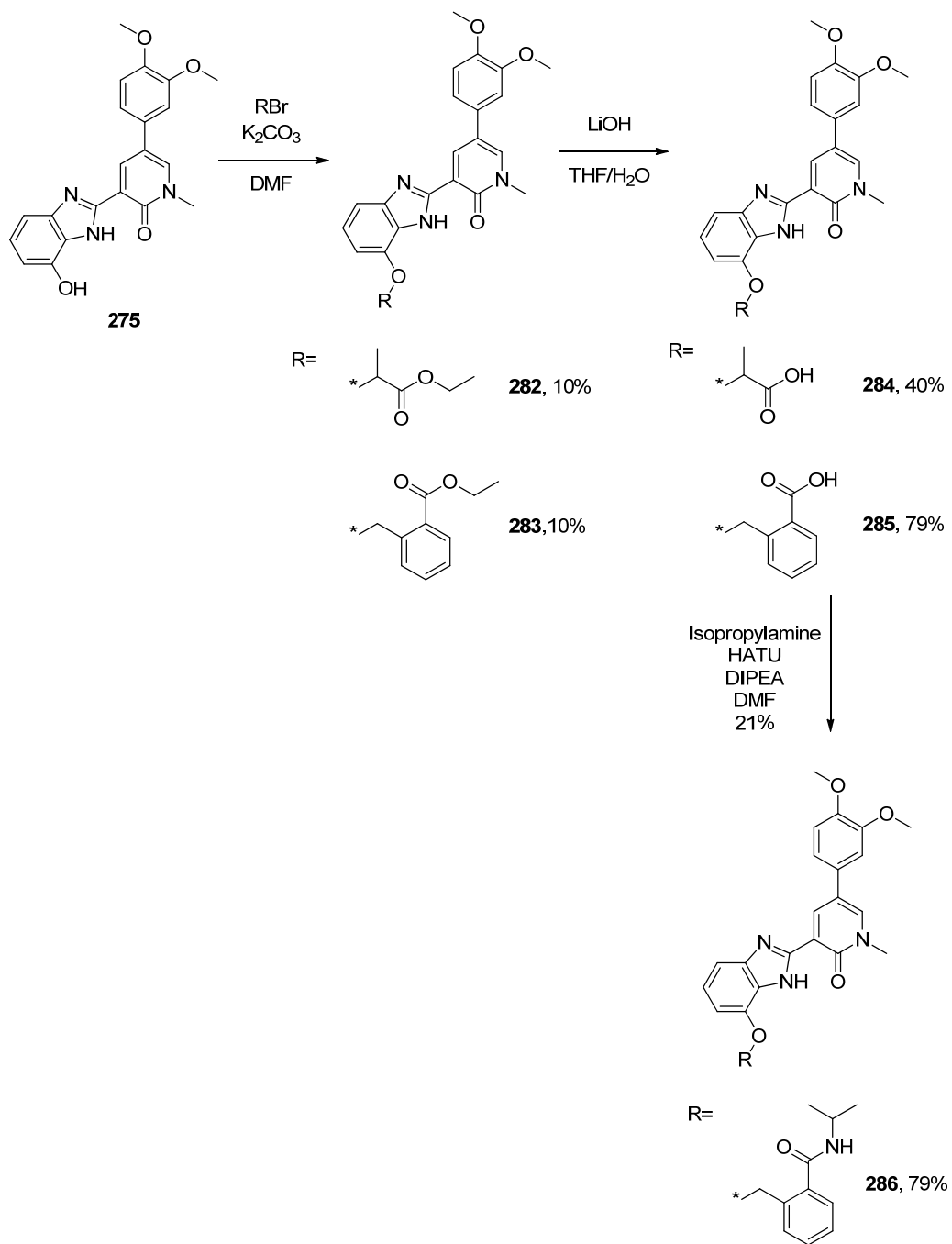
Synthesis of these targets relied on the preparation of key intermediates **275** and **278**, which were accessed in two or three steps from the pyridone carboxylic acid **186** (Scheme 31). Aniline **278** was prepared by an amide coupling and subsequent cyclisation with *p*-toluenesulfonic acid in acceptable yield, given that no purification of the intermediate was undertaken. Phenol **275** was prepared elsewhere in our laboratories.¹⁷⁹ In this case a protecting group was required to prevent by-product formation in the amide coupling step. Although this by-product was not fully characterised, LCMS analysis was consistent with a dimer such as compound **280** or **281**.



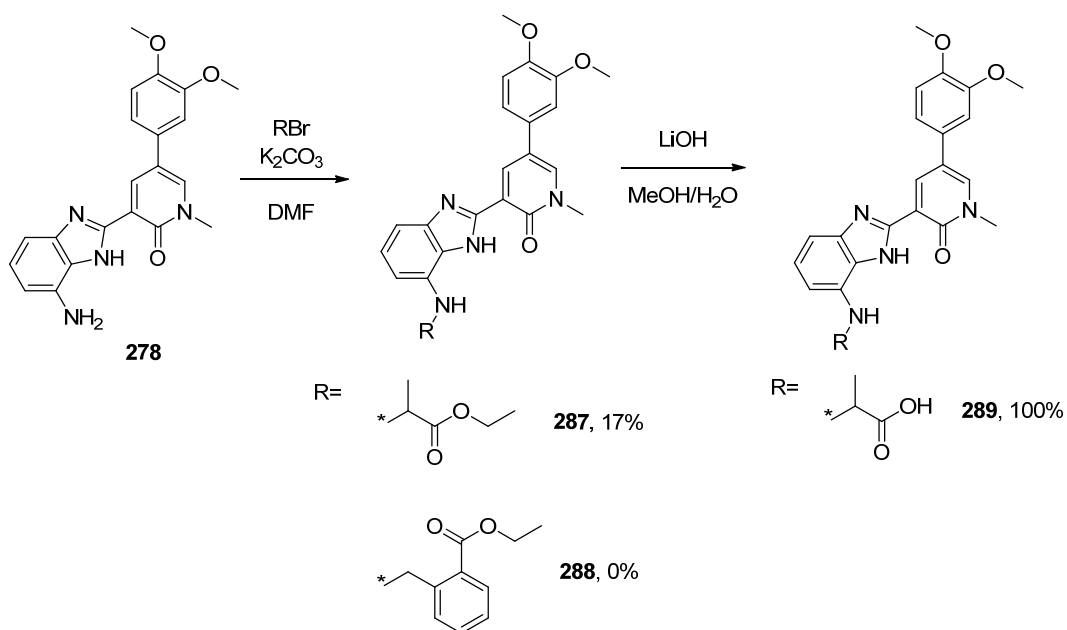
Scheme 31: Synthesis of key intermediates **275** and **278**

Alkylation with the appropriate alkyl halides was subsequently attempted. Again, elsewhere in our laboratories and starting from phenol **275**, all of the desired oxygen-linked products were obtained¹⁷⁹ (albeit in variable yield, Scheme 32).

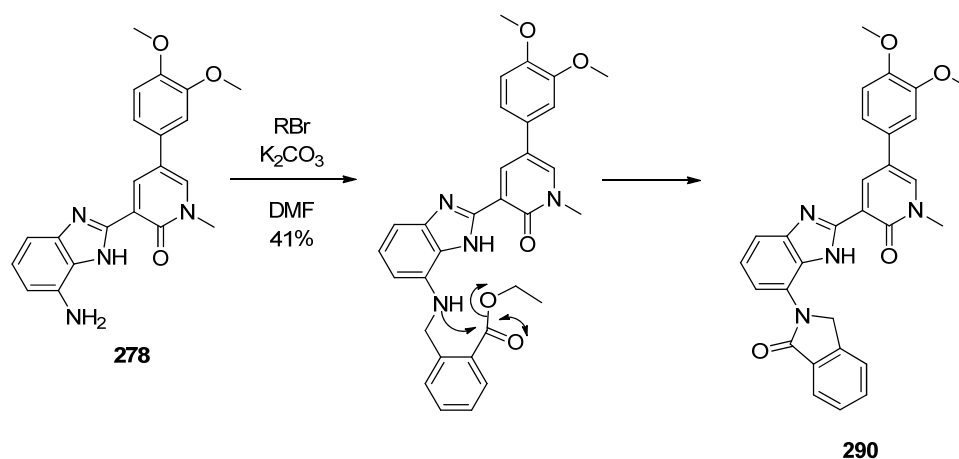
In addition and as part of this programme, the α -methyl acetic acid analogues **287** and **289** were synthesised from aniline **278** (Scheme 33). However, on attempting to alkylate aniline **278** with a benzyl bromide derivative to give **288**, a single peak inconsistent with the desired product was observed by LCMS. Isolation and characterisation of this product revealed the formation of lactam **290** in 41% yield, which had been formed by cyclisation of the desired amine product (Scheme 34).



Scheme 32: Oxygen linked compounds



Scheme 33: Nitrogen linked compounds

Scheme 34: Mechanism for formation of lactam **290**

Biological data for all of these analogues are shown in Table 29. Whilst the three acid analogues **284**, **285**, and **289** have reasonable selectivity profiles, the serendipitously formed lactam **290**, stands out as having a far superior profile, with >100-fold selectivity over all other PI3K isoforms. This may suggest that the more rigid lactam scaffold is required in order to induce movement of lysine 883, as shown with literature compound **32**. Unfortunately, attempts to confirm this hypothesis by obtaining an X-ray crystal structure of ligand **290** bound to PI3K γ failed, probably due to the poor solubility profile of this compound.

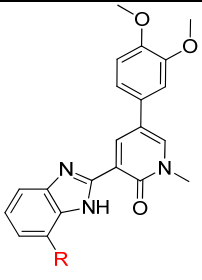
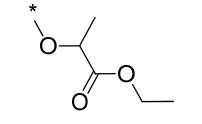
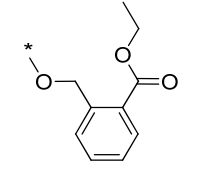
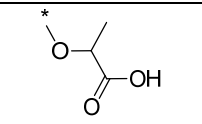
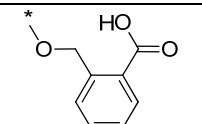
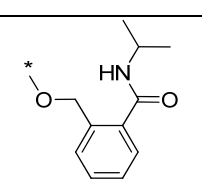
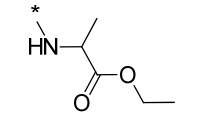
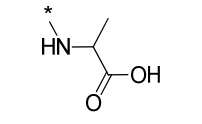
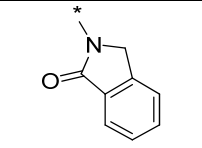
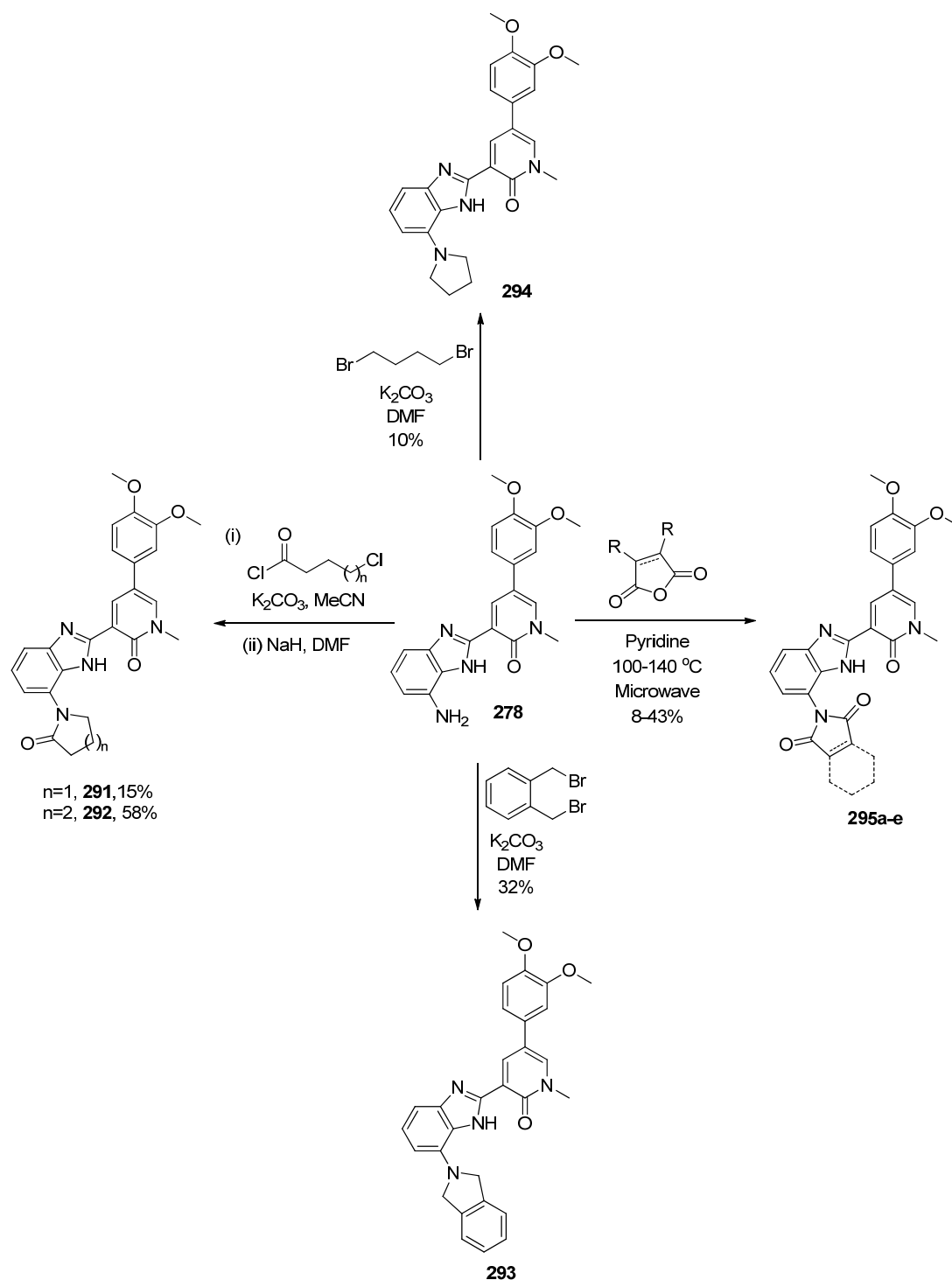
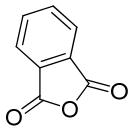
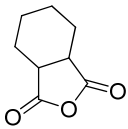
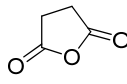
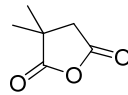
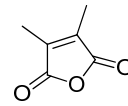
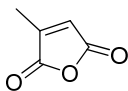
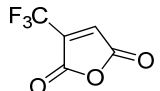
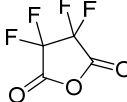
Cpd. No.		PI3K γ pIC ₅₀	L.E.	L.L.E.	PI3K isoform selectivity
282		6.4*	0.25	0.20	α 5.1, β <4.5, δ 5.9
283		5.8	0.20	0.11	α 5.1* \pm , β <4.5, δ 5.5
284		6.6	0.27	0.25	α 5.1, β <4.5, δ 5.1
285		7.3	0.27	0.20	α 6.1, β 4.7, δ 6.4
286		<4.5*	-	-	α 5.5*, β 4.8*, δ 6.4*
287		6.6	0.26	0.21	α 4.9, β <4.5, δ 5.9
289		6.6 \pm	0.27	0.25	α 5.5 \ddagger , β <4.5, δ 5.3 \pm
290		7.4	0.27	0.22	α <4.5, β <4.5, δ 5.2

Table 29: Data on compounds targeting induced fit of protein; * indicates $n=1$ data; \pm indicates one value not included in mean as below the threshold of the assay (i.e. pIC₅₀ <4.6); \ddagger indicates two values not included in mean as below the threshold of the assay (i.e. pIC₅₀ <4.6)

Further analogues were prepared to follow-up on these results, with the aim of identifying the key requirements for selectivity. Synthesis was straightforward and is summarised in Scheme 35 and Table 30.



Scheme 35: Preparation of analogues based on lactam **290**

296  14%	297  21%	298  26%	299  8%	300  43%
301 	302 	303 		

*Table 30: Monomers for synthesis of imides **295a-e**; isolated yields shown where reactions were successful*

Some interesting SAR data were observed and are presented in Table 31. Removal of the fused aryl ring from **290** to give **291** or the 6-membered analogue **292** results in a significant drop in potency, but with ligand efficiency and some selectivity maintained. Indoline **293** and pyrrolidine **294** suggest that removal of the carbonyl is also detrimental. Addition of a second carbonyl to give imides **295a-e** is well tolerated and, once again, the selectivity profiles are promising.

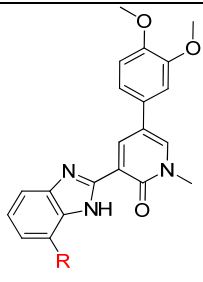
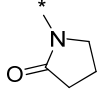
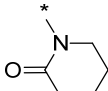
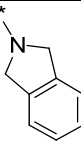
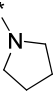
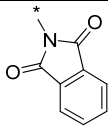
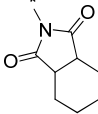
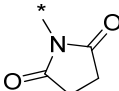
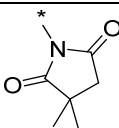
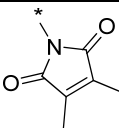
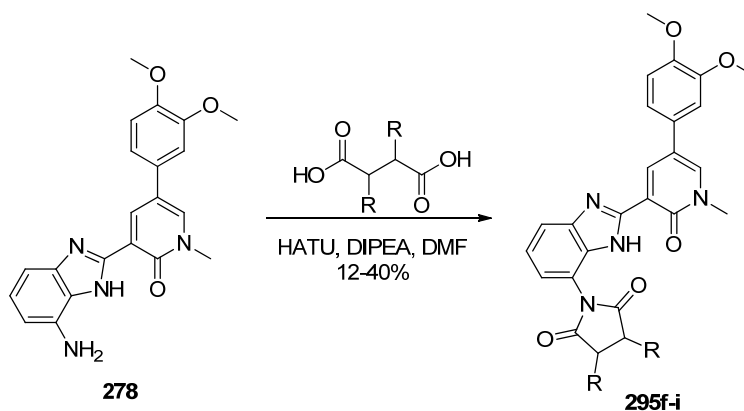
Compound No.		PI3K γ pIC ₅₀	L.E.	L.L.E.	PI3K isoform selectivity
291		6.4	0.27	0.24	α 4.9 [±] , β <4.5, δ 5.3
292		6.2	0.25	0.21	α 4.9, β <4.5, δ 5.1
293		6.0*	0.23	0.16	α 4.5*, β <4.5*, δ 4.9*
294		6.1	0.26	0.20	α 4.7 [±] , β <4.5, δ 5.4
295a		6.9	0.25	0.21	α 5.4, β <4.5, δ 5.2 [±]
295b		6.5	0.23	0.23	α 5.1, β <4.5, δ 5.1*
295c		6.2	0.25	0.29	α 4.8, β <4.5, δ 4.9
295d		6.4	0.24	0.24	α 4.7, β <4.5, δ 5.1*
295e		6.8	0.26	0.22	α <4.5, β <4.5, δ <4.5*

Table 31: Further SAR; * indicates $n=1$ data; [±] indicates one value not included in mean as below the threshold of the assay (i.e. pIC₅₀ <4.6); [±] indicates three values not included in the mean as below the threshold of the assay (i.e. pIC₅₀ <4.6)

Based on these data, another iteration of synthesis was initiated, to further explore substitution of imide **295c**. The use of substituted succinic acid building blocks facilitated this (Scheme 36 and Table 32).¹⁸⁰



Scheme 36: Synthesis of further imides

304 16%	305 12%	306 40%	307 31%	308
309 	310 	311 		

Table 32: Monomers for imide synthesis

Data for these compounds are shown in Table 33. Of particular interest was analogue **295f**, which showed almost a 100-fold increase in potency (and a significant increase in L.E. and L.L.E.) over compound **295c**, with a promising selectivity profile (>100-fold against the β and δ isoforms and ~25-fold against the α isoform). Compound **295f** also demonstrated good solubility in the CLND assay. It was therefore desirable to confirm

the binding mode, to establish whether this compound was indeed accessing the same region of the protein as literature compound **32**.

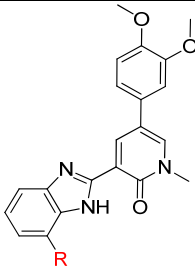
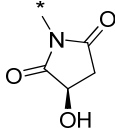
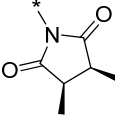
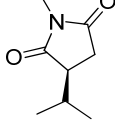
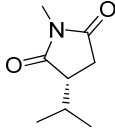
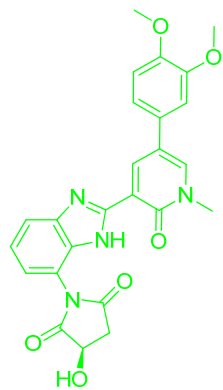
Cpd. No.		PI3K γ pIC ₅₀	L.E.	L.L.E.	PI3K isoform selectivity	CLND Sol. (μ M)
295f		8.0	0.31	0.32	α 6.6, β 5.0 ^{*‡} , δ 5.8	313
295g		6.4	0.24	0.24	α 5.0, β <4.5, δ 4.8	11
295h		6.2	0.23	0.22	α 4.9, β <4.5, δ 5.1	22
295i		6.0	0.22	0.21	α <4.5, β <4.5, δ 4.7	45

Table 33: Data on further imidate analogues; * indicates $n=1$ data; ‡ indicates two values not included in mean as below the threshold of the assay (i.e. pIC₅₀ < 4.6)

Pleasingly, an X-ray crystal structure of compound **295f** bound to PI3K γ was successfully obtained⁹⁷ (Figure 50). The structure revealed that ligand **295f** was in fact accessing a different region of the protein to literature compound **32**, with the hydroxyl substituent forming a through-water H-bond interaction to the NH of a backbone alanine in the P-loop of the protein. This is a region of the protein previously unexplored by the pyridone series, or indeed any of the competitor compounds where binding modes are known, and is therefore of great interest. In particular, the promising selectivity profile of analogue **295f** suggests that interactions in this region of the protein could provide a means of obtaining PI3K γ selectivity, without the need for highly ionized functionality.

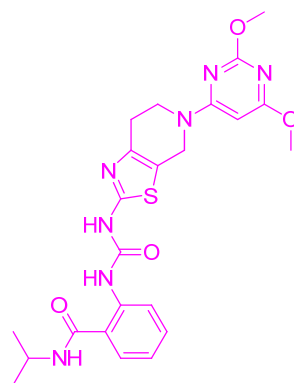
(a)



295f

PI3Kγ 8.0

α 6.6, β 5.0^{*‡}, δ 5.8

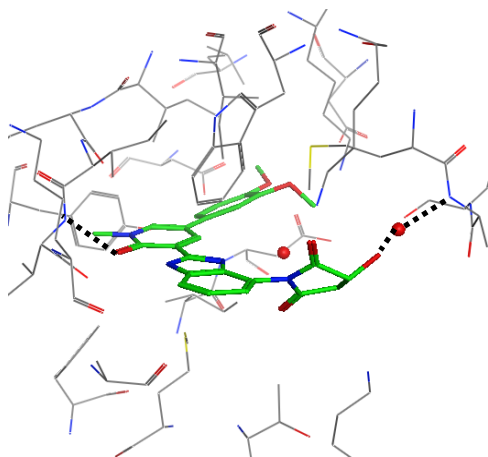


32

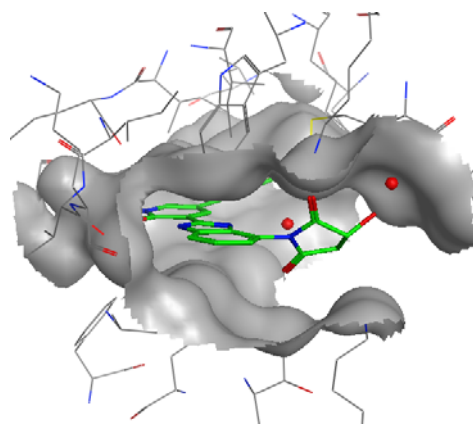
PI3Kγ 8.6

α 4.8[‡], β 6.0, δ 5.9

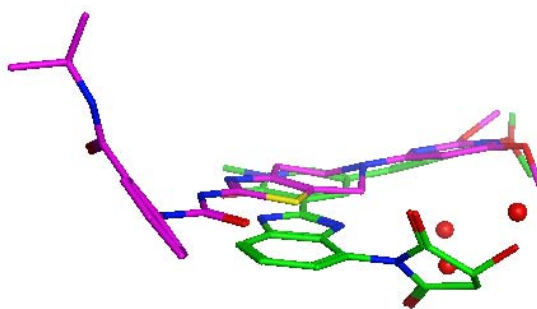
(b)



(c)



(d)



(e)

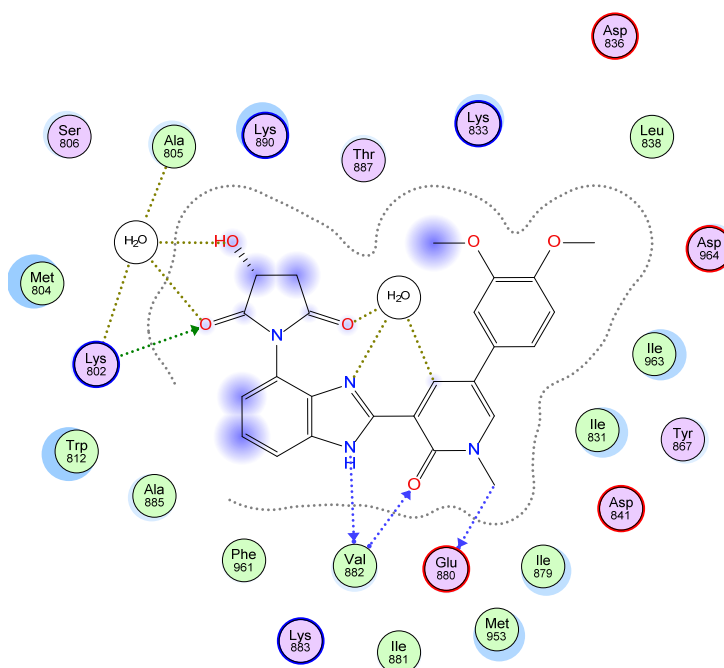


Figure 50: (a) Compound **295f** and **32**; (b) X-ray crystal structure of **295f**, with key H-bonds marked in black; (c) X-ray crystal structure of **295f** with protein surface shown; (d) Overlay of X-ray crystal structure of **295f** with X-ray crystal structure for literature compound **32** (only ligands shown for clarity); (e) 2D representation of X-ray crystal structure of **295f** with key interactions shown; * indicates $n=1$ data; ‡ indicates two values not included in mean as below the threshold of the assay (i.e. $pIC_{50} < 4.6$)

2.7.2 Future Work

Further analogues to follow up on compound **295f** are of great interest. Figure 51 shows some of the compounds considered with the aim of further exploring either water mediated, or direct hydrogen bond interactions with the P-loop.

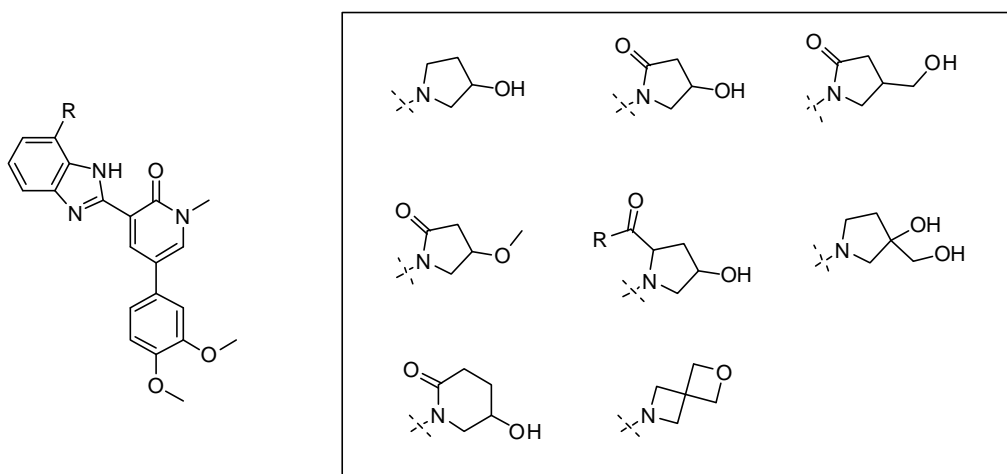


Figure 51: Proposed targets to explore interactions with the P-loop

2.8 Conclusions

Work on the pyridone series has delivered significant improvements in key areas for the template; namely solubility and isoform selectivity.

In exploring the R¹ substituent, the removal or replacement of aromatic rings led to imidazole **234** and semi-saturated analogue **201**, both of which showed significant improvements in solubility over the benzimidazole analogues initially reported. Additionally, this work provided some clear information on the PI3K γ binding site, identifying an area where planarity of the ligand is critical for binding. Unfortunately, further work on these ring systems did not manage to regain sufficient levels of PI3K γ selectivity, and were therefore not progressed further.

Conversely, carboxylic acid-containing derivatives such as compound **258**, showed excellent potency, selectivity, and solubility profiles. An X-ray crystal structure of analogue **258** bound to PI3K γ , identified threonine 886 as a key amino acid residue for achieving excellent isoform selectivity; this is a key interaction not previously explored

in the PI3K γ literature. However, whilst the carboxylic acid functionality was needed for selectivity (and solubility), unfortunately it was detrimental to the compounds' permeability. Modifying the gross physicochemical properties of the molecule have, so far, been unsuccessful in improving the cellular activity of these compounds, however the synthesis of zwitterionic targets are proposed as an alternative strategy to overcome this.

Additional information on obtaining selective PI3K γ inhibitors has been gained from an X-ray crystal structure with competitor ligand **32**, which led to the hypothesis that a movement in the PI3K γ (but not α , β or δ) protein(s) on ligand binding is responsible for its excellent selectivity profile. Attempts to access the same region of the protein from the pyridone template has led to yet further knowledge. The synthesis of ligand series **295** led to the discovery of **295f**, which demonstrated an excellent potency and promising selectivity profile. A subsequent X-ray crystal structure of this ligand, revealed interactions with the P-loop of the protein through which PI3K γ potency and selectivity are gained. Again, this is not an area of the protein which has been well explored based on the structural information available on competitor ligands.

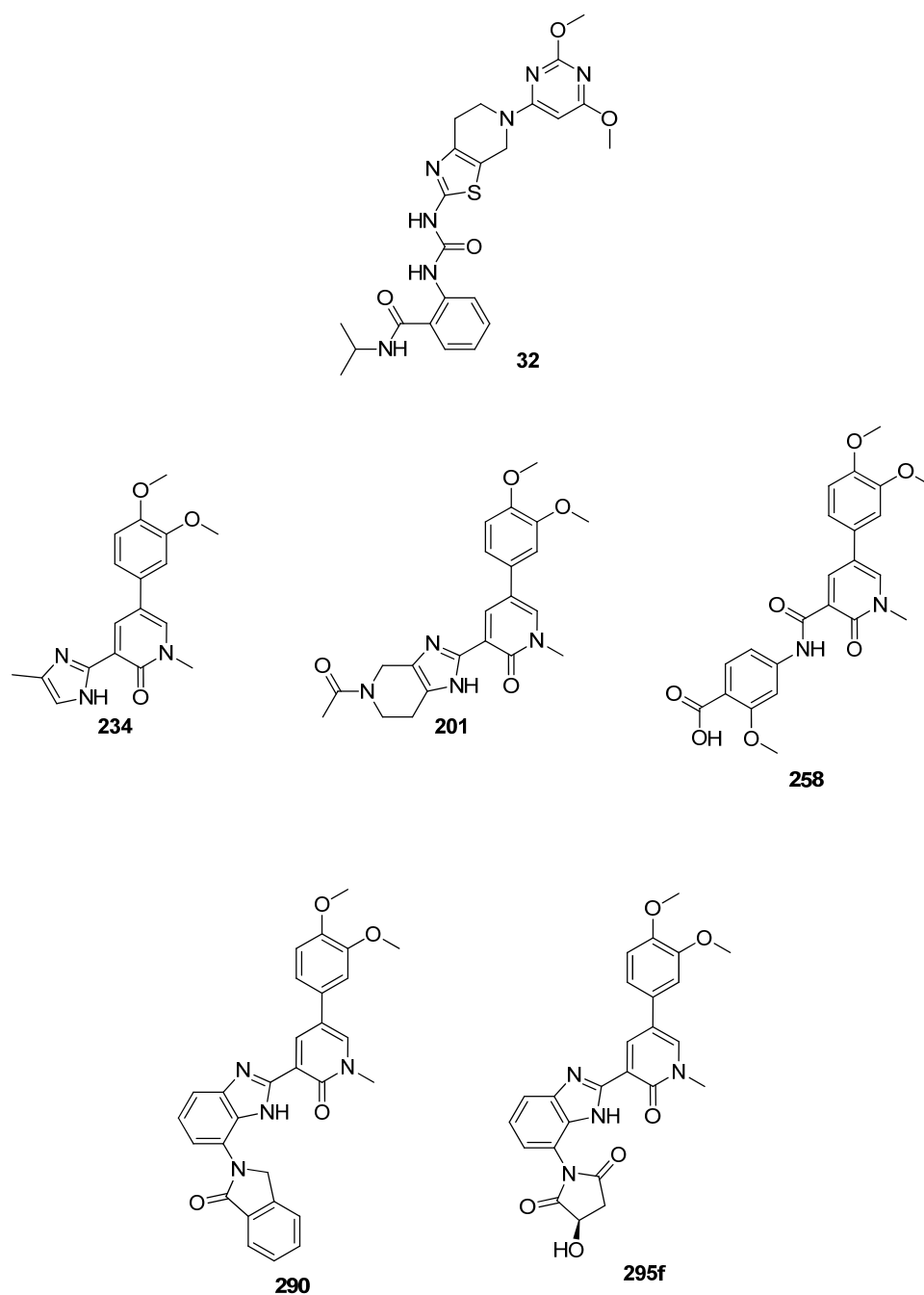


Figure 52: Key pyridone analogues

In summary, the pyridone template provides a very novel chemotype of PI3K γ inhibitor, examples from which can clearly match the best isoform selectivity profiles known in the literature (e.g. compounds **258** and **290** *cf.* competitor ligand **32**). More extensive comparison of (for example) cellular data is unfortunately not possible due to the lack of equivalent data. Whilst significant progress has been made in improving the

physicochemical profile of this template, balancing this with potency and selectivity requirements remains the biggest challenge in delivering a single pyridone with the desired profile.

Arguably more important than the progress in individual compound profiles, is the discovery of interactions at two novel regions of the protein, not previously accessed by known PI3K γ inhibitors. Through the work described in this chapter, these regions are found to be important for obtaining PI3K γ potency and selectivity. Not only can these vectors be exploited in further iterative design of pyridone analogues, but they could also be transferred to alternative chemical series which may provide compounds with a superior overall profile.

3.0 AMINOPYRIMIDINE SERIES

3.1 Change of Indication

As described in Section 2.2, initial medicinal chemistry plans for this programme were designed to identify a tool PI3K γ inhibitor, which could be used in *in vitro* and *in vivo* models to validate the PI3K γ mechanism as a suitable target for the treatment of asthma and/or COPD. As the programme progressed, however, emerging PI3K literature revealed a stronger biological rationale for PI3K γ inhibition in the treatment of acute lung injury (see Section 1.3.1). A simultaneous review of GSK's respiratory portfolio provided additional reasons to move away from targeting the treatment of asthma within this particular programme of work, and ultimately led to a change in focus. Accordingly, the PI3K γ inhibitor program was repositioned for the treatment of acute lung injury.

Due to the severity of the disease, ALI patients are treated in an Intensive Care Unit, where they are mechanically ventilated and closely monitored, usually for a relatively short period of time. As such, it was proposed that an intravenous formulation was optimal for this indication and a new target compound profile was drafted:

- PI3K γ pIC₅₀ >8
- Potency in a relevant cellular assay pIC₅₀ >7
- Isoform and wider kinase selectivity >100-fold
- MW <400 Da
- cLogP <4
- Aromatic ring count \leq 3
- **Aqueous solubility >5 mg/mL**
- Clearance < $\frac{1}{3}$ LBF, ideally < $\frac{1}{4}$ LBF
- Chemically stable in solution
- Stable to sterilisation process (ideally autoclave)

Key changes in the profile on switching to *i.v.* dosing were the high aqueous solubility and stability (to enable storage of the formulated material) and low *in vivo* clearance, as the compound will be dosed directly to the systemic circulation.

At the time of switching focus to an *i.v.* treatment for ALI, the pyridone series had not delivered any molecules which met these potency, selectivity, and cellular activity criteria, so other chemical templates which had been investigated in the historical PI3K γ programme were re-evaluated. The aminopyrimidine/triazine series was of particular interest due to its impressive isoform selectivity profile, as exemplified by compounds **312** and **313** (Table 34).¹²³

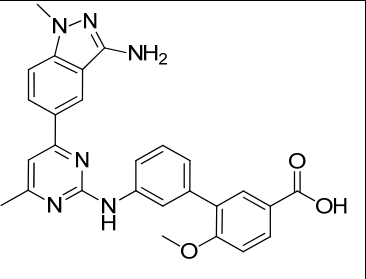
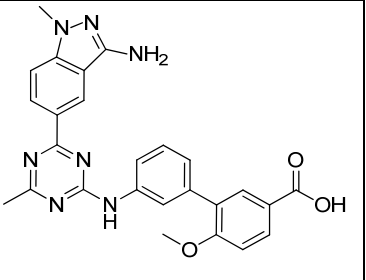
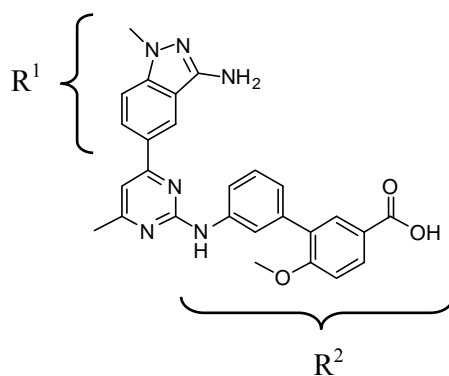
		
Compound no.	312	313
PI3Kγ pIC₅₀	8.8	8.4
L.E. / L.L.E.	0.34 / 0.26	0.32 / 0.27
PI3K isoform selectivity	α 6.6, β 4.6 ^{*‡} , δ 5.8	α 6.0, β <4.6, δ 4.7 [‡]
fMLP PBMC pIC₅₀	5.9 [‡] (n=2)	5.7 [‡] (n=7)
MW	481	482
ChromLogD	2.4	2.1
CLND Solubility μM	134	28
Permeability nm/sec	99	23

Table 34: Key compounds from aminopyrimidine/triazine series; * indicates n=1 data; [‡] indicates one value not included in mean as below the threshold of the assay; [‡] indicates four values not included in mean as below the threshold of the assay

Whilst these compounds have unfavourably high MW and aromatic ring count, the overall lipophilicity and ligand efficiencies are reasonable. Additionally, despite containing a carboxylic acid moiety, examples showed moderate activity in the fMLP PBMC cellular assay.¹²⁴

An X-ray crystal structure of aminopyrimidine **312** in PI3K γ is shown in Figure 53.¹²⁵ The aminopyrimidine core forms two H-bonds to the hinge region of the protein with the aminoindazole R¹ group pointing towards the phosphate pocket and the biphenyl R² group occupying the solubility pocket. Interestingly, the pendant carboxylic acid group on the biphenyl ring system forms an H-bond interaction with alanine 805, the same residue on the P-loop of the protein with which pyridone **295f** forms a water mediated H-bond. This adds weight to the hypothesis that interacting with this region of the protein is a good strategy for achieving PI3K γ selective inhibitors. The aminoindazole group forms both lipophilic and polar interactions in the phosphate pocket, with the NH₂ substituent forming an H-bond interaction with aspartic acid 841.

(a)

PI3K γ 8.8 α 6.6, β 4.6^{*#}, δ 5.8

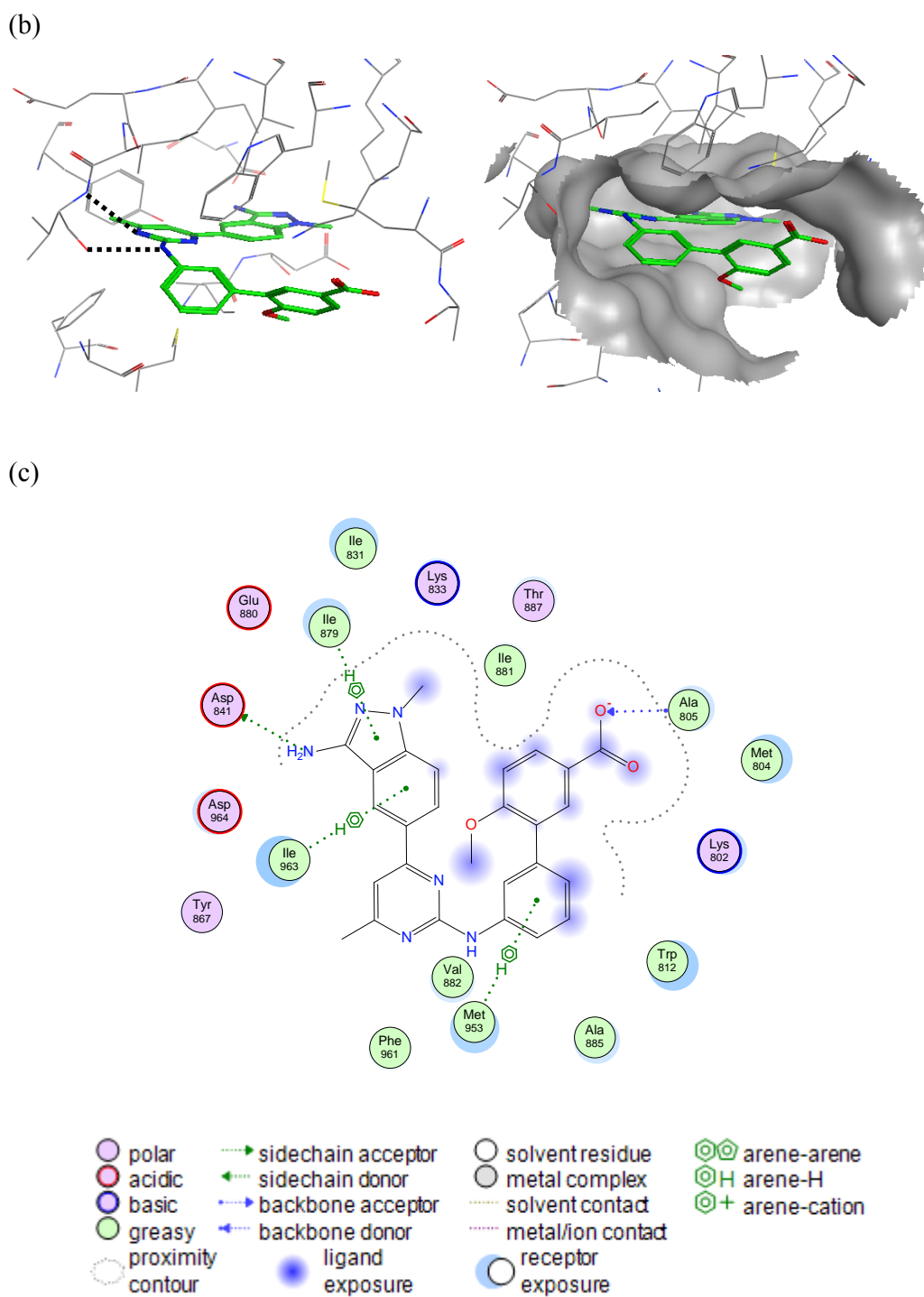


Figure 53: (a) Compound **312**; (b) X-ray crystal structure of aminopyrimidine **312** bound to PI3K γ ¹²⁵ (c) 2D representation of X-ray crystal structure with key interactions shown; * indicates $n=1$ data; † indicates four values not included in mean as below the threshold of the assay (i.e. $pIC_{50} < 4.6$)

The key issue with this series with respect to developing an *i.v.* molecule was the poor solubility. The initial medicinal chemistry strategy was therefore focused on improving solubility, whilst maintaining the desirable potency and selectivity profile. Targets were divided into two main areas:

- (i) Synthesis of phosphate pro-drugs of existing compounds, and
- (ii) Removing and/or replacing aromatic rings

3.2 Phosphate Pro-drugs

Pro-drugs are bioreversible derivatives of drugs, which are designed to release an active parent once converted by enzymatic and/or chemical transformation in the body (Figure 54).

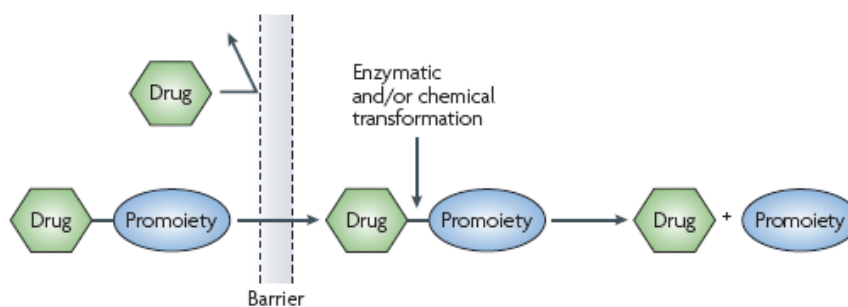


Figure 54: Schematic of pro-drug concept¹⁸¹

There are several reasons why pro-drugs might be employed, but most commonly it is to overcome a limitation of the parent drug, e.g. poor oral absorption, lack of site specificity of drug distribution, poor aqueous solubility, or poor shelf life. The promoiety is designed to alter the overall properties of the molecule in a way that fixes the problem, but must also be safe and, ideally, rapidly cleared once released within the body.¹⁸² Pro-drugs are usually designed by appending the promoiety to an existing functional group in the drug parent; Figure 55 shows common functionalities which have been utilised and some of the types of pro-drugs which are typically synthesised.

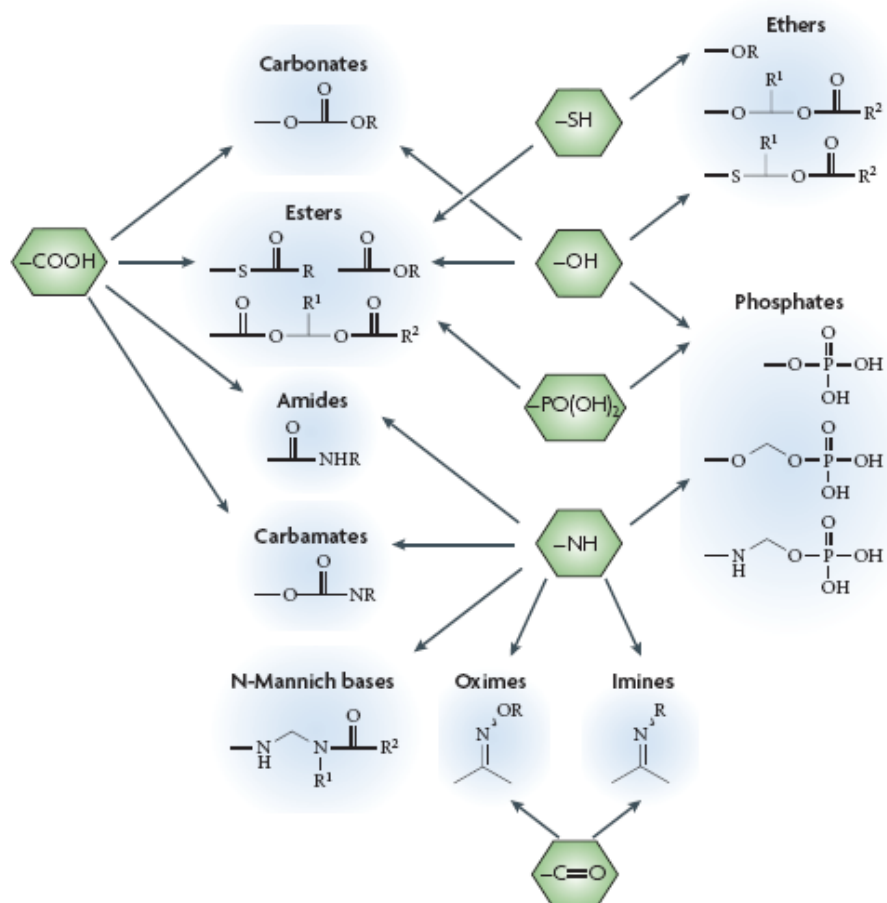


Figure 55: Functional groups amenable to pro-drug design¹⁸¹

As previously discussed, the main limitation of the aminopyrimidine compound **312** was its poor aqueous solubility, which makes it unsuitable for *i.v.* dosing. Inadequate aqueous solubility is a common problem with *i.v.* medications and there are many examples of water-soluble pro-drugs being developed for this route of administration.¹⁸¹ Phosphate monoester pro-drugs are the best exemplified, with several marketed drugs utilising this pro-drug strategy for improving aqueous solubility (Figure 56). Fosphenytoin, for example, has an aqueous solubility of 142 mg/mL (25 °C, pH 9) vs. 20-30 µg/mL (25 °C) for the active parent phenytoin.¹⁸¹ Phosphate monoesters have also demonstrated high chemical stability and have a well understood enzymatic transformation back to the parent molecule, initiated by alkaline phosphatases present in the blood.¹⁸¹ Applying this to our programme of work, it was therefore of interest to consider the synthesis of a phosphate pro-drug of aminopyrimidine **312**.

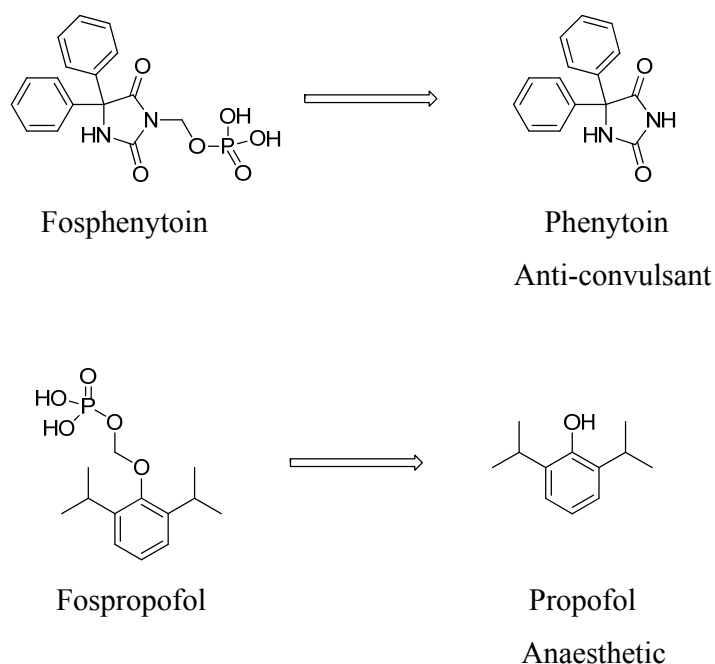


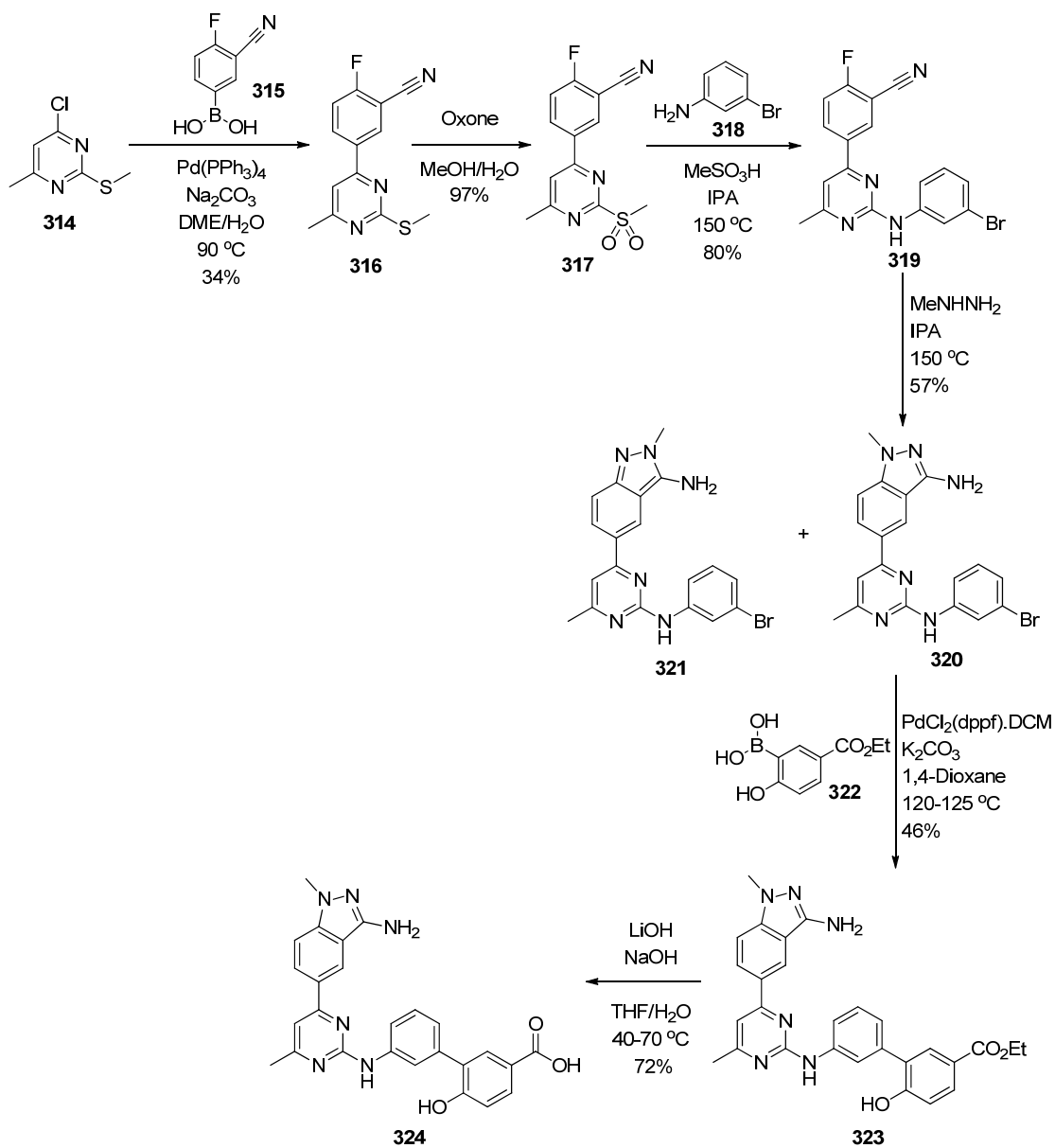
Figure 56: Marketed i.v. drugs which use phosphate monoester pro-drugs to enhance solubility

3.2.1 Results and Discussion

There were several positions in the central molecular framework of compound **312** where a phosphate could be incorporated; however, for synthetic ease the terminal phenyl ring was initially targeted. Methoxy was already known to be a preferred group on this ring (e.g. compounds **312** and **313**), so the phenol analogue **324** was proposed with a view to derivatising to a phosphate pro-drug if the parent hydroxyl group was well tolerated (Scheme 37).

Suzuki coupling of 4-chloro-6-methyl-2-(methylthio)pyrimidine **314** with the commercially-available boronic acid **315** proceeded in moderate yield. Oxidation of the sulfide to the sulfone and subsequent displacement with 3-bromoaniline gave intermediate **319**. The 2-fluorobenzonitrile substituent was then cyclised with methylhydrazine to give the desired aminoindazole **320** in 57% yield. The modest yield reflects, in part, formation of a minor product consistent with the undesired regioisomer **321** (observed by LCMS analysis of the crude reaction mixture). This regioisomer was easily separated from the desired product due to their differing solubility in isopropanol, but was not isolated and fully characterised. A second Suzuki coupling introduced the

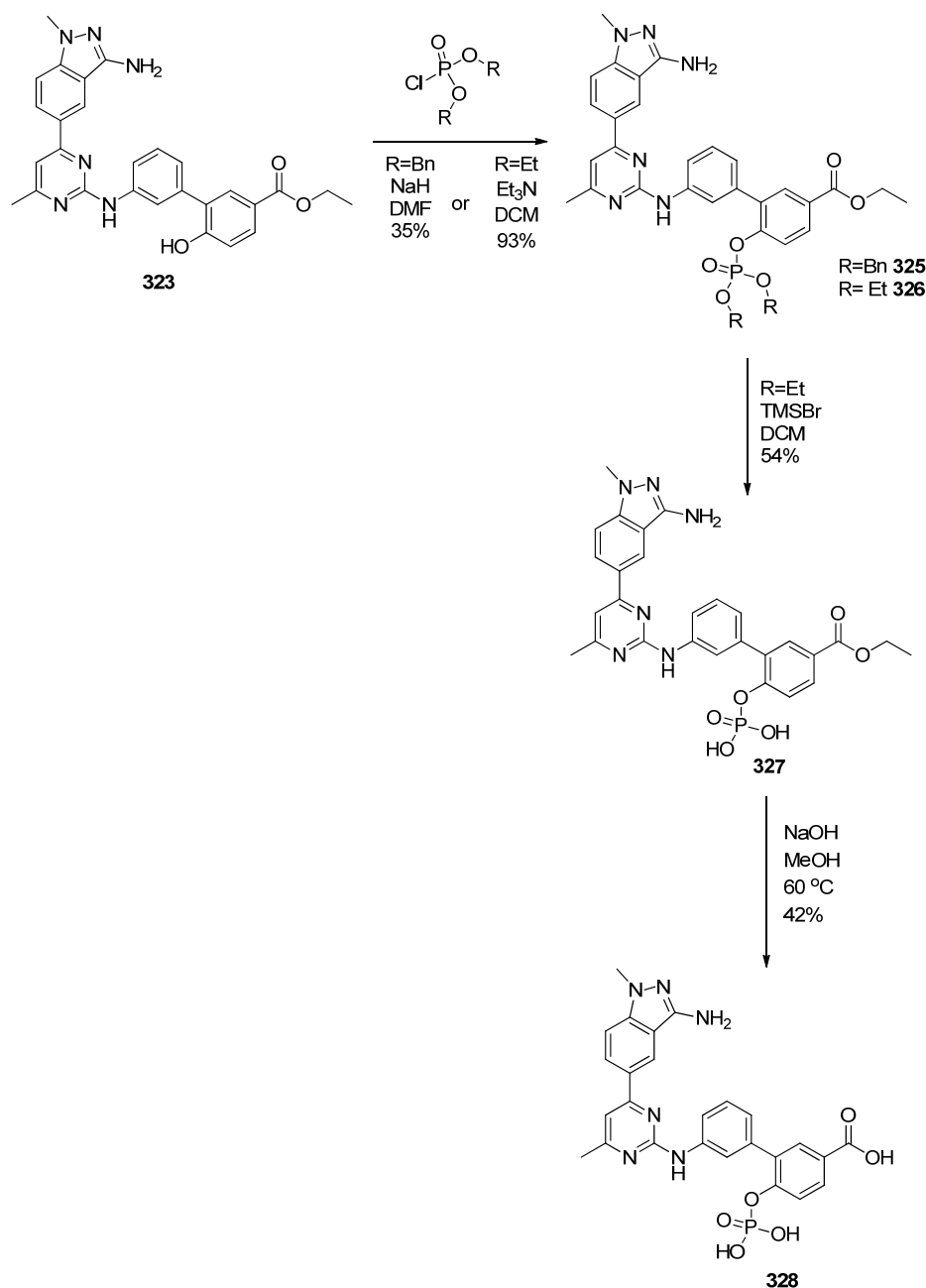
final phenyl ring, followed by a straightforward saponification to give the desired product in 5% yield over 6 steps.



Scheme 37: Synthesis of phenol **324**

The hydroxyl group was shown to be well tolerated (Table 35) so synthesis of the phosphate pro-drug was then attempted starting from previously described ester **323** (Scheme 38). Initial attempts to functionalise the phenol with dibenzyl phosphorochloridate gave the desired intermediate **325** (R=Bn) in moderate yield, however subsequent deprotection of the benzyl groups *via* Pd-mediated hydrogenation

was slow, with only mono-debenzylation being observed by LCMS. Switching to diethyl phosphorochloridate enabled more efficient phosphorylation and, indeed, facile deprotection of intermediate **326** (R=Et) with TMS bromide. Simple saponification gave the desired pro-drug **328** in 21% yield over 3 steps.



7Scheme 38: Synthesis of aminopyrimidine pro-drug **328**

Biological data for the pro-drug is also shown in Table 35; moderate activity against PI3K γ is observed whilst some level of selectivity against the other PI3K isoforms is

also retained. This selectivity profile is theoretically beneficial; if hydrolysis to the parent phenol is not immediate on dosing, restricted off-target activity at the other PI3K isoforms should minimise potential for side effects. However, the physicochemical properties of the pro-drug, in particular its extremely high polar surface area, mean it is unlikely to demonstrate good permeability (due to its highly ionised form at physiological pH), so should never reach the intracellular compartment where the PI3K enzymes are located.

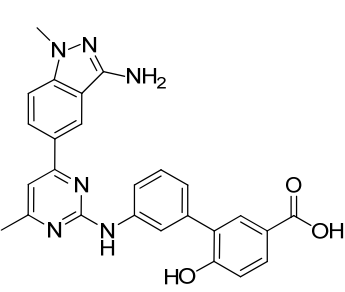
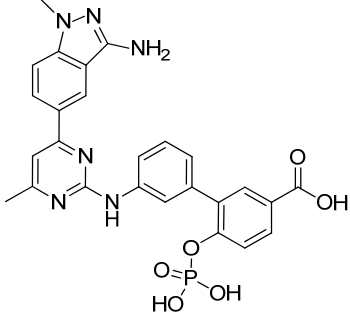
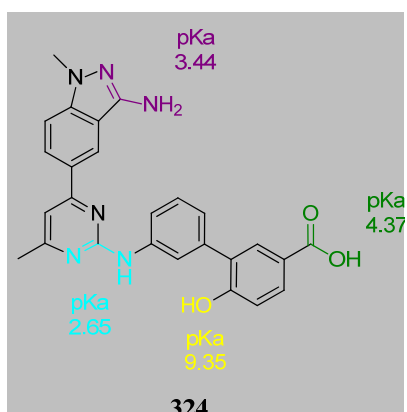
		
Compound No.	324	328
PI3Kγ pIC₅₀	8.4	6.1
L.E.	0.33	0.22
PI3K isoform selectivity	$\alpha < 4.5$, $\beta < 4.5$, $\delta < 4.5$	α 4.8 ^{*‡} , β 4.6 ^{*‡} , δ 5.0
Solubility in saline pH 6.5 (mg/mL)	0.003	0.037
Solubility in saline pH 8 (mg/mL)	0.026	>3.0

Table 35: SAR towards a pro-drug; * indicates n=1 data; ‡ indicates one value not included in mean as below the threshold of the assay (i.e. pIC₅₀ < 4.6); § indicates one value not included in mean as below the threshold of the assay (i.e. pIC₅₀ < 4.6)

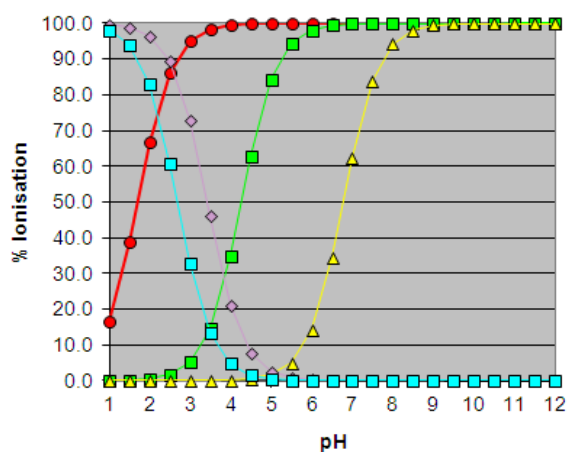
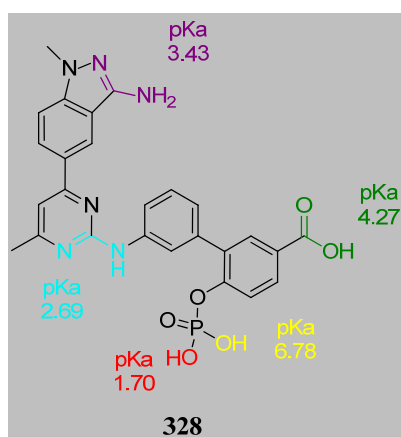
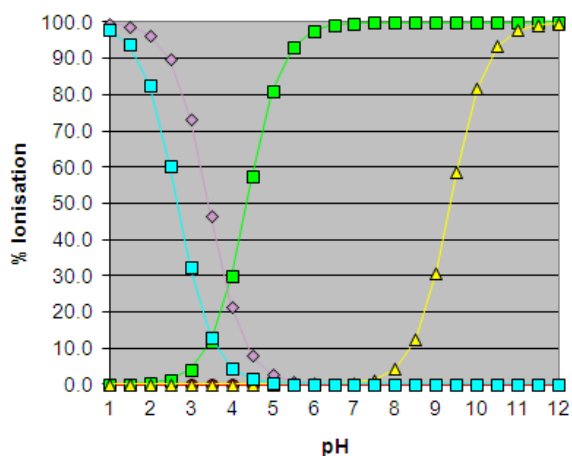
Solubility data¹⁸³ showed a dramatic improvement for pro-drug **328** over parent phenol **324** (Table 35) and, interestingly, a greater solubility at pH 8 than pH 6.5. This pH dependent increase in solubility is also observed for the parent phenol (Table 35), although the difference it not as large. As shown in Figure 57, it is possible to

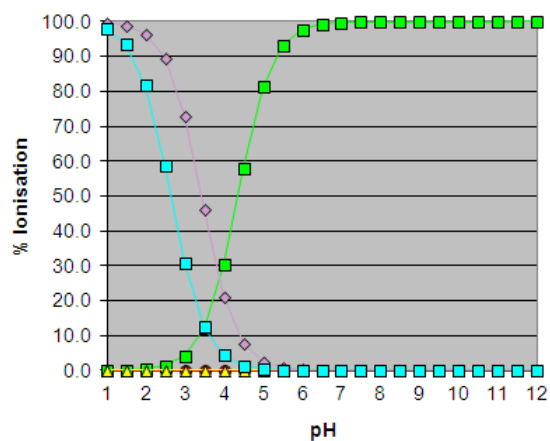
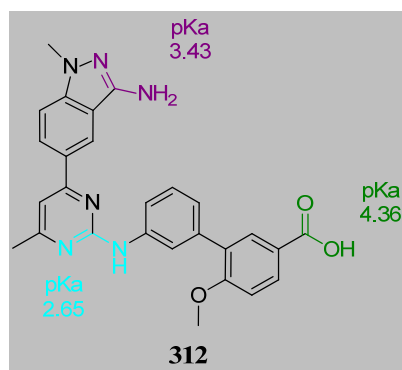
rationalise that this increased solubility at pH 8 is related to an increase in the percentage ionisation of each compound; the predicted pKa for the phenol in parent **324** and the second phosphate pKa in pro-drug **328** both fall near this pH range. This is shown most clearly in Figure 57c; on moving from pH 6.5 to pH 8 an increase in overall charge is predicted for pro-drug **328** and (to a small extent) phenol **324**, which is consistent with the observed solubility profiles. However, this argument that increased ionisation is responsible for the improved solubility at pH 8, does not apply to the methoxy analogue **312**. This compound displays the same pattern of pH dependent solubility, despite no change in overall ionisation state within this pH range (Figure 57c and Table 36).

(a)



(b)





(c)

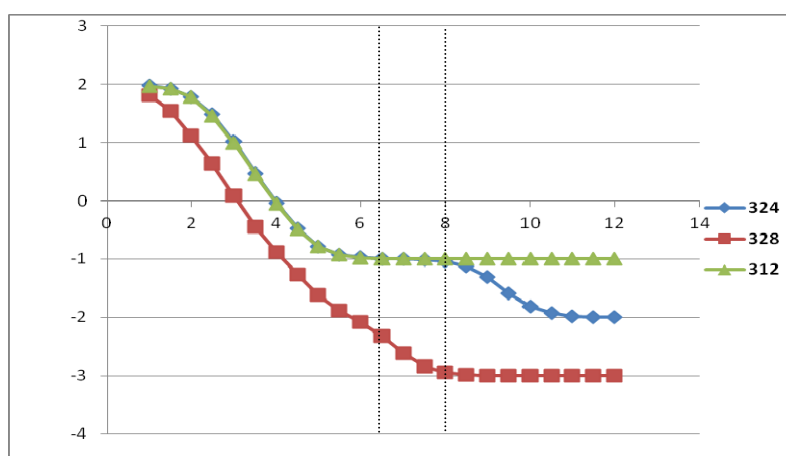


Figure 57: (a) Chemaxon predicted pKa values for compound 324, 328 and 312; (b) Graphs to show ionisation profile for each compound (c) Graph to show overall charge for compounds 324, 328 and 312 at varying pH

Compound No.	312
Solubility in saline pH 7.4 (mg/mL)	0.002
Solubility in saline pH 8 (mg/mL)	0.018
ChromLogD pH 2.0	2.7
ChromLogD pH 7.4	2.4
ChromLogD pH 10.5	1.7

Table 36: Solubility and lipophilicity measurements for compound 312

One hypothesis to explain these results is a possible intramolecular hydrogen bond between the carboxylic acid and aminoindazole functionalities, which means neither centre behaves completely independently of the other. Indeed, an energy minimisation of the anionic form expected to be present at pH 7.4 and the hypothetical zwitterionic form of compound **312** (in the absence of the protein) shows close proximity of the two groups (Figure 58).

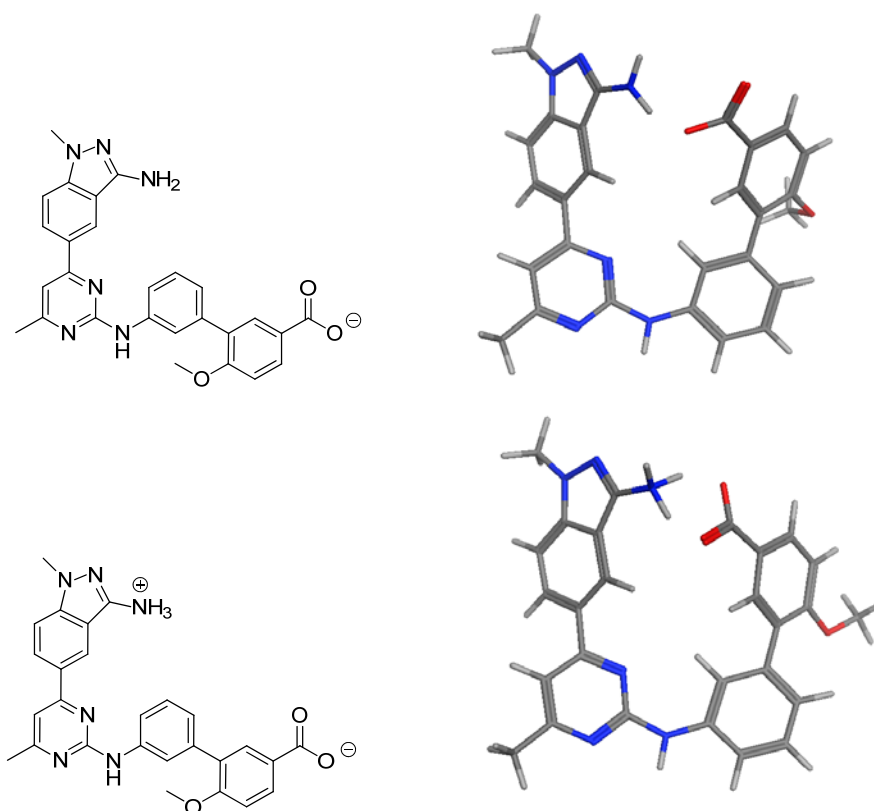


Figure 58: Energy minimisation of the anionic and zwitterionic forms of compound **312**

Interestingly, a pH dependent effect is also observed in the lipophilicity measurements of compound **312**,¹³⁸ with a greater drop in lipophilicity observed between pH 7.4 and pH 10, than between pH 2.0 and 7.4 (Table 36). This is the opposite of what might be expected based solely on the predicted pKa profile, but adds weight to the hypothesis that there may be an intramolecular buffering effect at play.

Initial blood stability data on pro-drug **328** were disappointing (Figure 59).¹⁸⁴ The compound was incubated in rat blood at 37 °C for 2 h, however no conversion to the parent compound was observed.

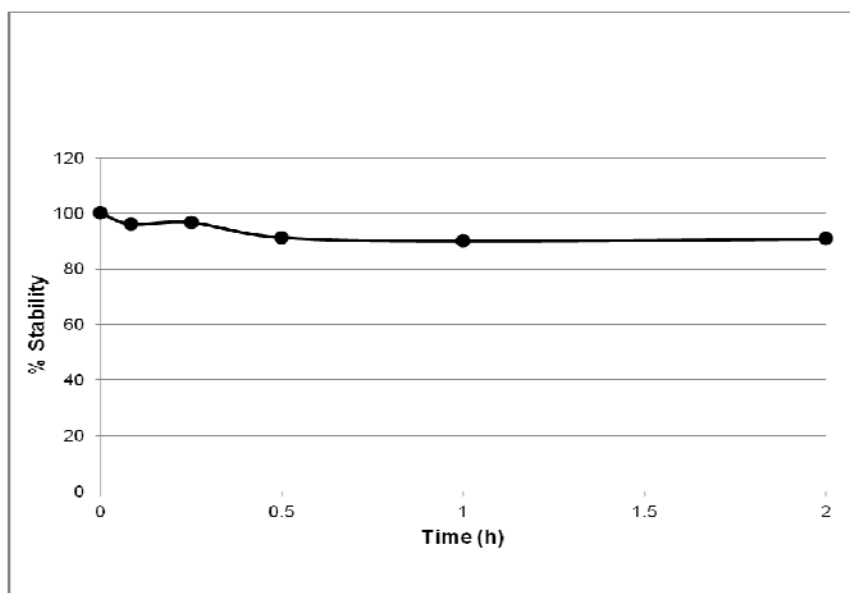


Figure 59: Blood stability data for pro-drug **328**; parent compound **324** remained below the levels of quantification for the entire 2 h period¹⁸⁴

Despite these data, both the parent **324** and pro-drug **328** were progressed to *in vivo* pharmacokinetic studies¹⁸⁵ as additional hydrolysis mechanisms are possible *in vivo* (e.g. by liver enzymes). Both studies were conducted in Wister Han rats, dosing as an *i.v.* infusion at 1 mg/kg for 1 h and blood samples were taken periodically to monitor compound levels.¹⁸⁴

Figure 60 shows the blood concentration profile for parent compound **324**. An apparent steady state concentration of >100 ng/mL was achieved during the initial infusion period and the concentrations rapidly drop to below the level of quantification before the 2 h time point. This profile is consistent with high clearance of the compound from the blood, which has been attributed to the presence of the phenol functionality. *In vivo*, phenols are particularly susceptible to Phase II metabolism, typically *via* glucuronidation,¹⁸⁶ and this is the most likely route of clearance for this molecule.

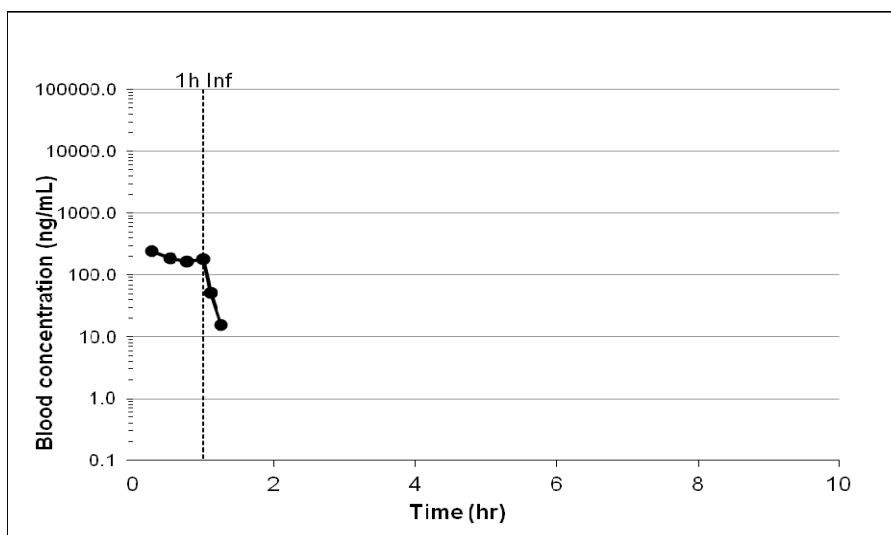


Figure 60: Concentrations of parent **324** after a 1 h infusion of parent **324** at 1 mg/kg to male Wister Han rat¹⁸⁴

The profile obtained after dosing pro-drug **328** is shown in Figure 61. In this case, levels of the prodrug rise more slowly during the infusion period to a peak concentration of 19300 ng/mL, before falling gradually over several hours.

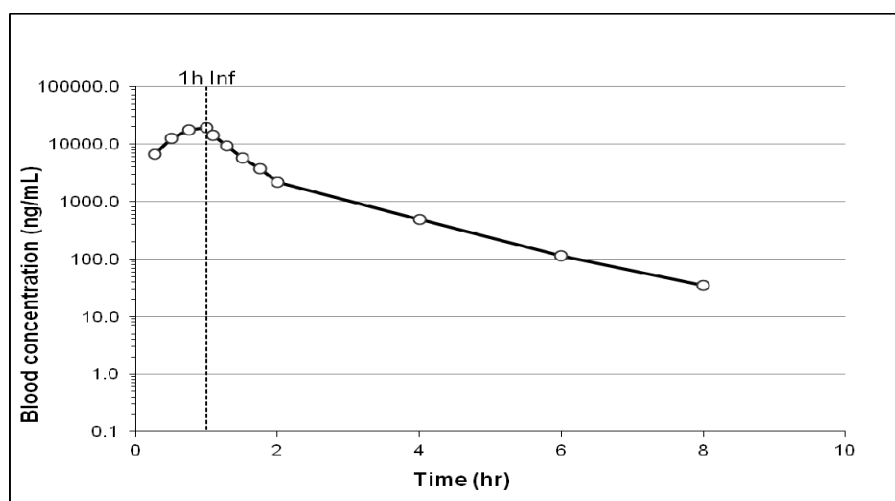


Figure 61: Concentrations of pro-drug **328** after a 1 h infusion of pro-drug **328** at 1 mg/kg to male Wister Han rat¹⁸⁴

The DMPK profiles for these compounds are summarised in Table 37, but unfortunately did not meet our target profile. Ideally, fast hydrolysis of the pro-drug would release

active parent which would have a low clearance, maintaining levels of active drug in the circulation for longer.

Parameter	324	328
CL _b (mL/min/kg)	91 (100% lbf)	0.8 (ca. 1% lbf)
T _{1/2} (h)	0.1	1.0
V _{ss} (L/kg)	0.5	0.04
AUC _{0-inf} (ng.h/mL)	187	21700

Table 37: DMPK summary for parent **324** and pro-drug **328**; rat liver blood flow(lbf) = 85 mL/min/kg¹⁸⁴

In the *i.v.* study of pro-drug **328**, levels of parent **324** were also monitored in the blood samples (Figure 62). The concentration profile achieved for parent **324** on dosing the pro-drug is significantly different to dosing the parent compound directly. In this case, the slow conversion of pro-drug to active parent, results in a modified clearance profile for the parent. Although, in theory, this could be used *in vivo* as a way of maintaining drug levels of the parent **324** over time, there are several issues with this strategy. Firstly, the concentration of pro-drug is significantly higher than parent at all time points, which is the opposite to the ideal profile; selecting a suitable dose, based on the concentration of parent required to achieve efficacy, could lead to very high levels of pro-drug. Secondly, on moving towards dosing in humans, subtle differences in the rate of hydrolysis of the pro-drug could have large effects on the blood concentrations of active parent. Finally, any toxicological studies carried out would be required to prove a sufficient therapeutic window with respect to the high concentration of the pro-drug present, potentially making a clean safety read-out even more challenging.

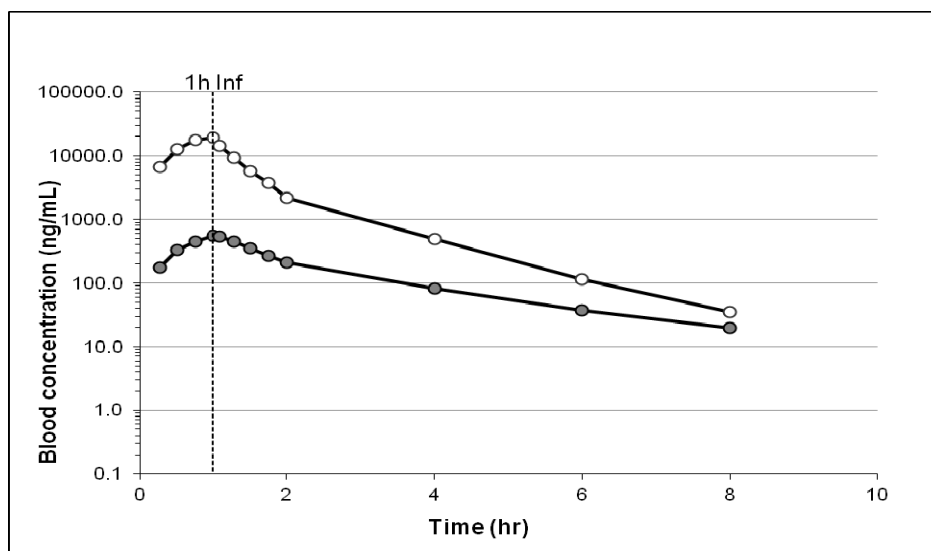


Figure 62: Concentrations of pro-drug **328** (open circles) and parent **324** (filled circles) in blood after a 1 h infusion of pro-drug **328** at 1 mg/kg to make Wister Han rat¹⁸⁴

3.2.2 Future Work

The synthesis of pro-drug **328** confirmed that this strategy could deliver a molecule with aqueous solubility in the desired range, however this particular compound does not have the desired pharmacokinetic profile. In order to address these DMPK issues, the synthesis of alternative pro-drugs are of interest. One hypothesis for the surprising stability of pro-drug **328** is that steric hindrance of the phosphate hampers cleavage by phosphatase enzymes. Introducing a methylene linker between the attachment point on the parent and the phosphate group should increase the susceptibility of the pro-drug to hydrolysis. This particular moiety is well precedented, as shown earlier for Fosphenytoin and Fospropofol.¹⁸¹ Unlike the original pro-drug **328**, cleavage by phosphatase enzymes no longer generates the active parent directly, however the hemiacetal released upon enzymatic cleavage of phosphate is highly unstable and decomposes, releasing formaldehyde as a by-product.

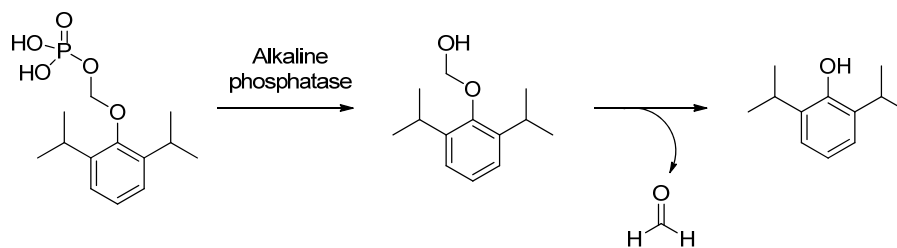
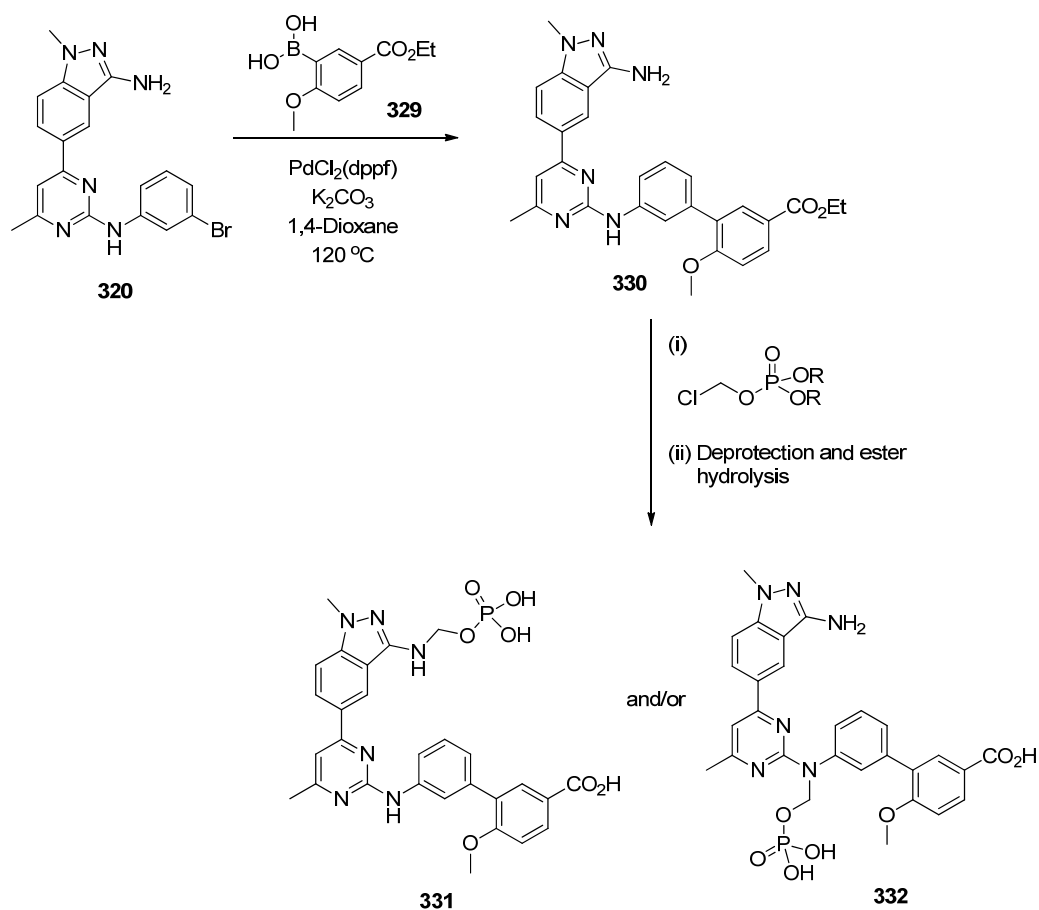
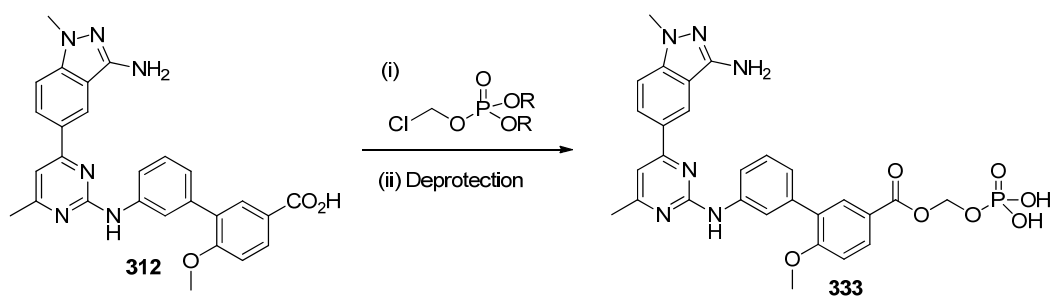


Figure 63: Two stage release of active drug

In addition to altering the promoiety, alternative attachment points for the pro-drug may also be of interest, enabling removal of the phenol functionality thought to be responsible for the high clearance of parent **324**. Pro-drugs **331**, **332** and **333** are all considered targets for future exploration.



Scheme 39: Proposed synthesis of alternative pro-drugs linked via nitrogen



Scheme 40: Proposed synthesis of alternative pro-drug linked via the carboxylic acid

3.3 Removing Aromatic Rings

A longer term goal for the aminopyrimidine/triazine series was to improve the physicochemical properties of the template (i.e. reduce the number of aromatic rings and increase solubility), primarily with the aim of making the series more developable and reducing the risk of compound-related toxicity. Whilst targeting a solubility profile suitable for *i.v.* dosing without the need for a pro-drug would be the ultimate aim, it was considered unlikely that this series in its current form would deliver this goal, given the typical low solubility (<10 $\mu\text{g}/\text{mL}$).

Initial targets were designed to remove or replace one or more aromatic ring(s) from the template, specifically replacing the aminoindazole group with mono- or bicyclic saturated or semi-saturated ring systems. Molecular modelling suggested that it would be beneficial to keep some degree of planarity adjacent to the pyrimidine/triazine core due to proximity to the protein above and below the plane of the ligand (Figure 64b).

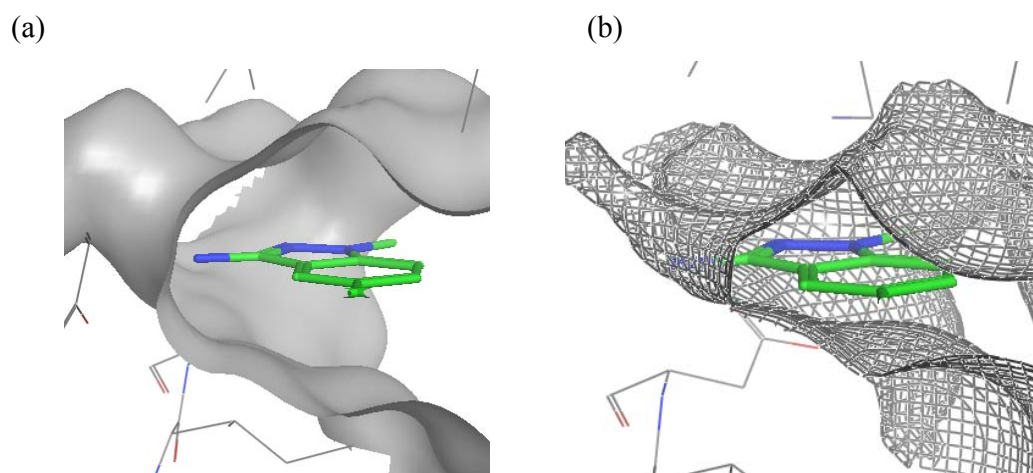


Figure 64: X-ray crystal structure of aminopyrimidine **312**, focusing on phosphate pocket region; (a) view of phosphate pocket with protein surface shown; (b) view of phosphate pocket with double Van der Waals surface shown (contact between mesh surface and ligand indicates good contact)

Installation of a nitrogen atom or an sp^2 hybridised carbon as the linker atom was prioritised based on the overall structural considerations as discussed above (Figure 65).

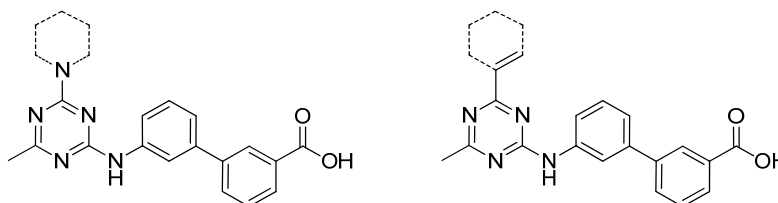


Figure 65: Targets to explore replacement of the aminoindazole substituent

3.3.1 Results and Discussion

In order to access a diverse range of substituents, synthesis of *N*-linked analogues on the triazine template was prioritised. A simplified biphenyl group in the solubility pocket compared with the lead compound **313** was adopted as the required aniline monomer **336** was commercially available. This group had previously demonstrated a reasonable retention of L.E. (albeit with a drop in absolute potency), compared with the methoxy analogue previously described (Table 38).

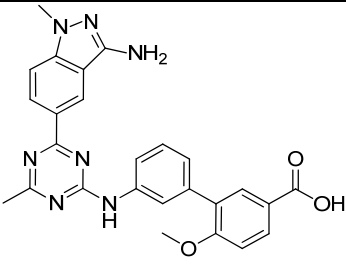
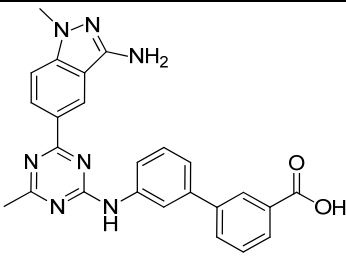
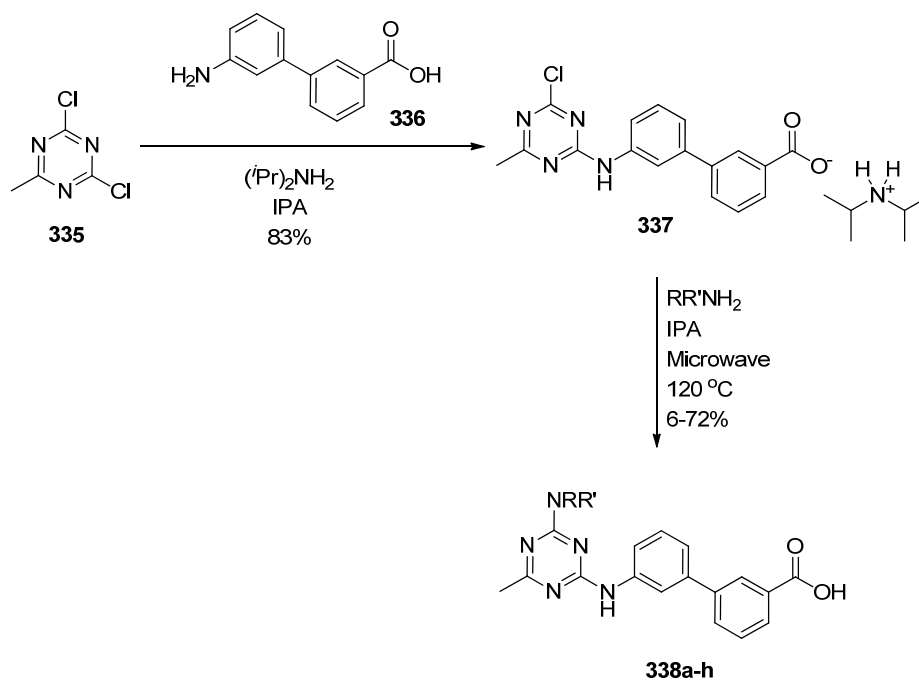
		
Compound no.	313	334
PI3Kγ pIC₅₀	8.4	7.6
L.E.	0.32	0.31
PI3K isoform selectivity	α 6.0, β <4.6, δ 4.7 [±]	α 4.8* [±] , β <4.5, δ 5.3* [±]

Table 38: Data on simplified solubility pocket; * indicates $n=1$ data; [±] indicates one value not included in mean as below the threshold of the assay (i.e. pIC₅₀ <4.5)

The symmetry of the 2,4-dichloro-6-methyl-1,3,5-triazine starting material (which would not be present in the analogous pyrimidine) meant the target compounds could be accessed *via* sequential displacement reactions (Scheme 41). Displacement of the 2,4-dichloro-6-methyl-1,3,5-triazine starting material **335** with 3'-amino-[1,1'-biphenyl]-3-carboxylic acid proceeded in good yield without the need for protection of the carboxylate group. Indeed, the isolation of the diisopropylamine salt of the product was achieved by simple filtration. Subsequent displacement with a range of secondary amines gave target compounds in variable yield (Table 39). Monomers were chosen based on their complementarity with the phosphate pocket and their potential to impart improved solubility on the ligand.

Scheme 41: Synthesis of *N*-linked aminoindazole replacements

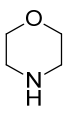
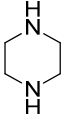
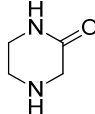
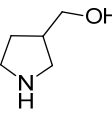
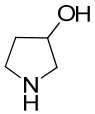
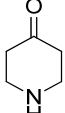
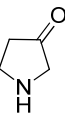
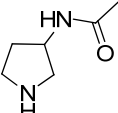
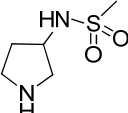
339  61%	340  72%	341  29%	342  29%	343  65%
344  55%	345  6%	346  54%	347  6%	

Table 39: Amine monomers used as aminoindazole replacements; isolated yields shown where reactions were successful

Biological data for these targets are shown in Table 40. Whilst they all show a significant drop in potency from the aminoindazole reference compound **334**, it was pleasing to see that examples such as the piperidin-4-one **338f**, maintained micromolar activity and modest L.E./L.L.E.

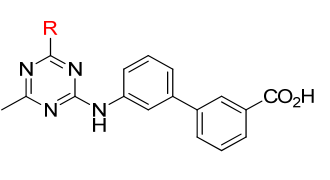
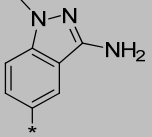
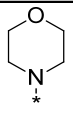
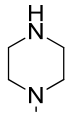
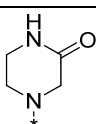
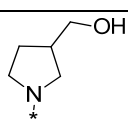
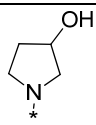
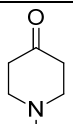
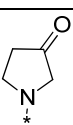
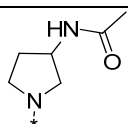
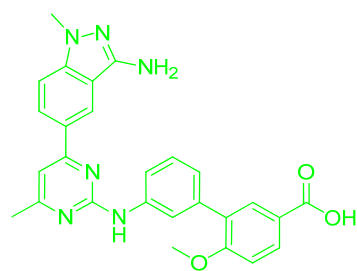
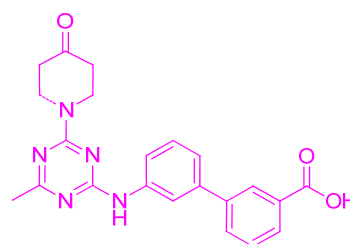
Cpd. No.		PI3K γ pIC ₅₀	L.E.	L.L.E.	PI3K isoform selectivity
334		7.6	0.31	0.23	α 4.8* [±] , β <4.5, δ 5.3* [±]
338a		5.3* [±]	0.25	0.17	α <4.5, β <4.5, δ 4.8* [‡]
338b		<4.5	0.21	–	α <4.5, β <4.5, δ <4.5
338c		6.0	0.27	0.22	α 5.0, β <4.5, δ <4.5
338d		5.7	0.26	0.22	α 4.7* [‡] , β <4.5, δ 5.8* [‡]
338e		5.2	0.25	0.19	α <4.5, β <4.5, δ 5.1* [±]
338f		6.0	0.27	0.21	α <4.5, β <4.5, δ <4.5
338g		5.0	0.24	0.16	α <4.5, β 4.7* [±] , δ <4.5* [±]
338h		5.2* [±]	0.22	0.18	α <4.5, β <4.5, δ 5.0

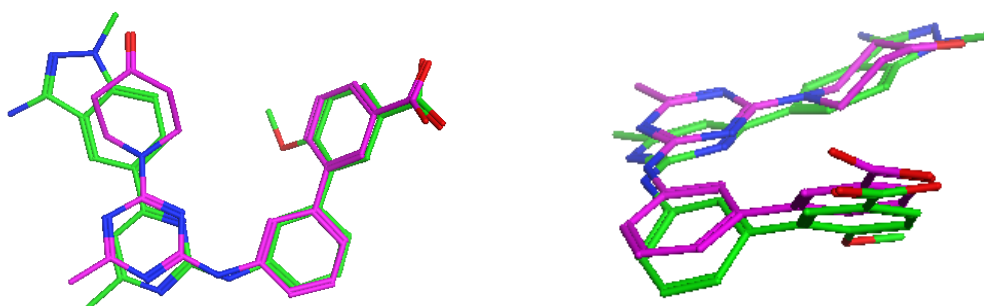
Table 40: Data for aminoindazole replacement; * indicates n=1 data; [±] indicates one value not included in mean as below the threshold of the assay); [‡] indicates two values not included in mean as below the threshold of the assay; [‡] indicates three values not included in mean as below the threshold of the assay

An X-ray crystal structure of piperidin-4-one **338f**⁹⁷ revealed the expected binding mode, with the piperidine-4-one occupying the phosphate pocket. Comparison with the structure of aminoindazole **312** (Figure 66) shows a very similar binding mode, with a slight shift in the core as a result of changes in the phosphate pocket. Interestingly, despite its smaller size, the piperidin-4-one extends almost as far into the phosphate pocket, and has good complementarity with the protein in this region.

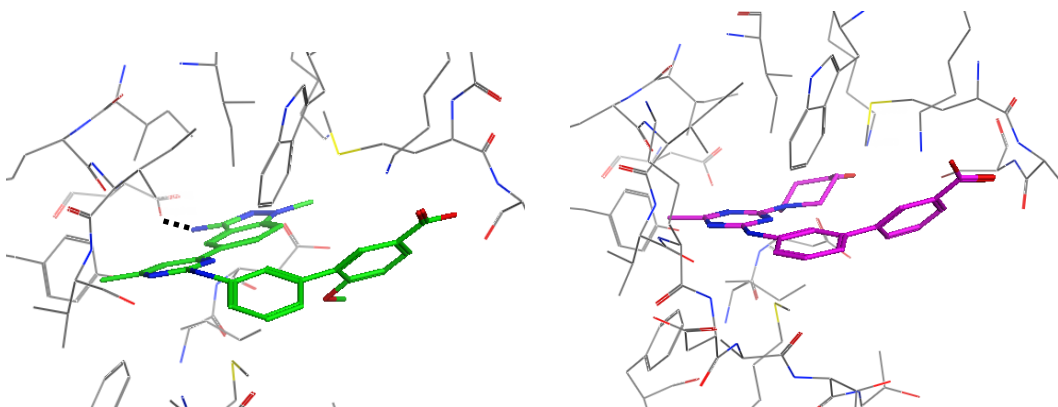
(a)

**312****338f**

(b)



(c)



*Figure 66: Comparison of X-ray crystal structures for aminoindazole aminopyrimidine **312** and piperidin-4-one aminotriazine **338f**; (a) ligands **312** and **338f**; (b) overlay of crystal structure for ligands **312** and **338f** from two angles (no protein shown for clarity); (c) X-ray crystal structure of **312** and **338f** with H-bonding interactions in the back pocket indicated by black lines*

Following on from these promising results, a second iteration array was designed, in order to further investigate phosphate pocket binding interactions. The amine monomer selection is shown in Table 41. The monomer set was selected to further explore 6-membered piperidine and piperazine analogues, but also incorporated a range of spirocyclic and semi-saturated bicyclic systems to investigate re-growing the smaller saturated compounds, such as **338f** from the first array. Synthesis proceeded from key intermediate **337**, using the same methodology as shown in Scheme 41. For monomers **348**, **349** and **350**, the BOC protecting group was removed after purification of the displacement reaction, by treatment with trifluoroacetic acid.

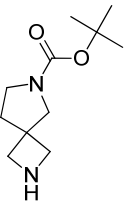
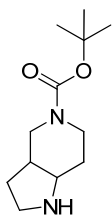
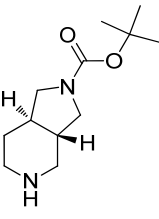
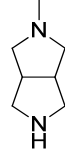
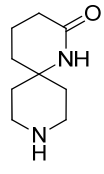
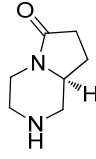
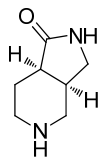

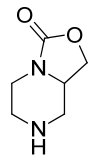
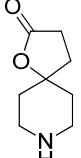
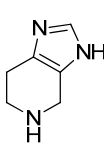
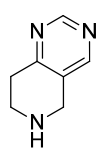
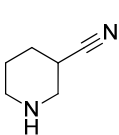
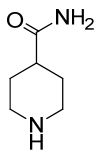
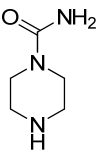
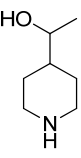
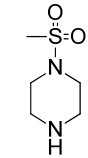
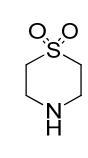
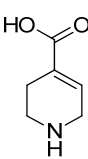
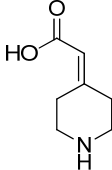
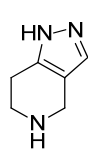
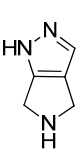
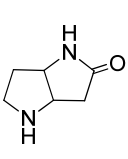
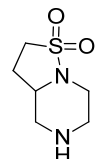
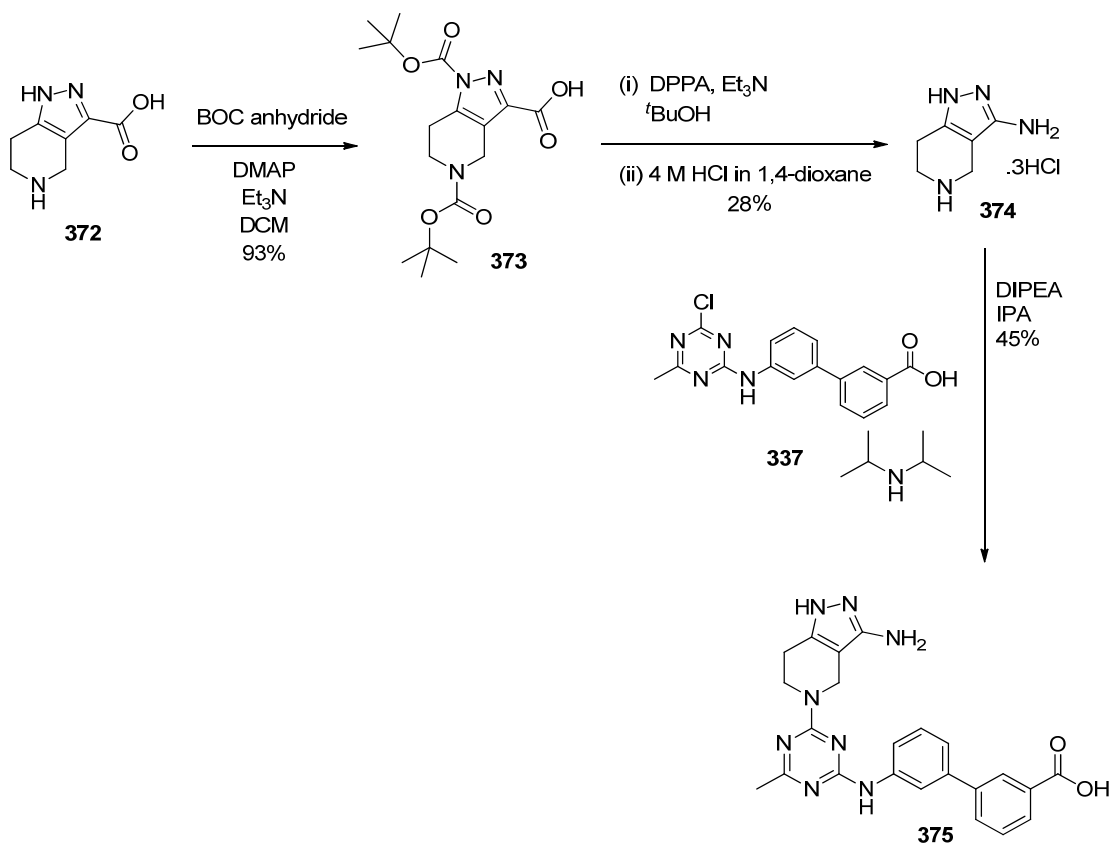
<p>348</p>  <p>67%*</p>	<p>349</p>  <p>62%*</p>	<p>350</p>  <p>86%*</p>	<p>351</p>  <p>31%</p>	<p>352</p>  <p>14%</p>	<p>353</p>  <p>49%</p>
<p>354</p>  <p>37%</p>	<p>355</p>  <p>3%</p>	<p>356</p>  <p>34%</p>	<p>357</p>  <p>51%</p>	<p>358</p>  <p>66%</p>	<p>359</p>  <p>42%</p>
<p>360</p>  <p>47%</p>	<p>361</p>  <p>46%</p>	<p>362</p>  <p>44%</p>	<p>363</p>  <p>57%</p>	<p>364</p>  <p>34%</p>	<p>365</p>  <p>7%</p>
<p>366</p>  <p>45%</p>	<p>367</p>  <p>54%</p>	<p>368</p>  <p>58%</p>	<p>369</p>  <p>20%</p>	<p>370</p> 	<p>371</p> 

Table 41: Amine monomers for second iteration array; isolated yields shown for successful reactions; * indicates yield is over 2 steps (amine displacement and protecting group removal)

Additionally, bespoke synthesis of non-commercially available amine **374** was also attempted (Scheme 42). This monomer was designed based on the aminoindazole group present in compounds **312** and **313**, with the aim of regaining the H-bond interaction with aspartic acid **841** previously described, whilst improving the physicochemical profile of the compound. 4,5,6,7-Tetrahydro-1*H*-pyrazolo[4,3-*c*]pyridine-3-carboxylic was bis-BOC-protected to give intermediate **373**. A subsequent Curtius rearrangement

in *tert*-butanol initially gave the *tert*-butyl carbamate, which was deprotected *in situ* to give the desired monomer **374**. Finally, coupling with aminopyrimidine **337** gave the desired final compound **375**.



Scheme 42: Bespoke synthesis of alternative back pocket group

Data for all of the analogues synthesised are shown in Table 42. Compounds are coloured by L.E., with those showing the best L.E. (≥ 0.24) in black. All of the spirocyclic amines and many of the fully saturated fused bicyclic systems have poor activity; this is likely to be due to their high degree of 3-D character, which is not well tolerated in this region of the protein. Interestingly, several of the semi-saturated bicycles showed good levels of potency such as compounds **387**, **396**, and **397**. The bespoke analogue **375** did not show any increase in potency over closely related analogue **396**. This implies that the pendant NH₂ group is not correctly orientated to form the desired H-bond interaction with aspartic acid 841. In addition to the semi-saturated analogues, carboxylic acid containing analogues **394** and **395** also show good levels of potency and high L.E.s.

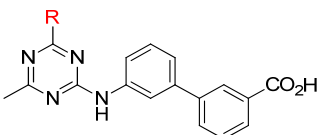

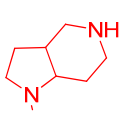
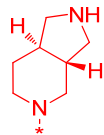
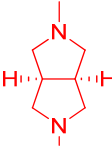
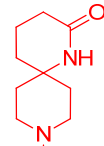
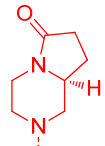
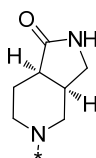

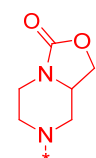

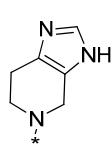
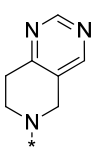
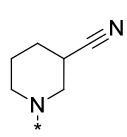
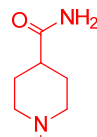
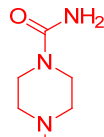
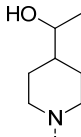
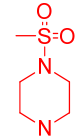
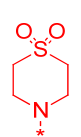
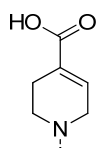
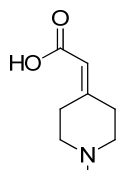
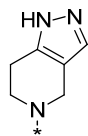
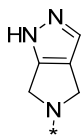
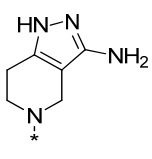
					
376  4.6 ^{*±}	377  4.6 [*]	378  <4.5	379  <4.5	380  <4.5	381  4.8 ^{*±}
382  5.8	383  <4.5	384  5.6	385  5.4	386  5.5	387  6.1
388  5.4	389  5.3	390  5.6	391  5.8	392  5.3	393  5.2
394  5.9	395  6.4	396  6.3	397  6.6	375  6.0	

Table 42: Data on amine back pockets on aminopyrimidine series. Compounds in red have L.E. <0.24, those in black have L.E. ≥ 0.24; * indicates n=1 data; ± indicates one value not included in mean as below the threshold of the assay

Table 43 shows a broader data set for a selection of the most potent and ligand efficient analogues. Whilst the L.E. has significantly dropped, in most cases, compared with the aminoindazole reference compound **334**, encouragingly the saturated and semi-saturated

compounds do maintain L.L.E. and isoform selectivity. Pleasingly, all of these compounds also show an increase in CLND solubility and a decrease in lipophilicity (measured ChromLogD).

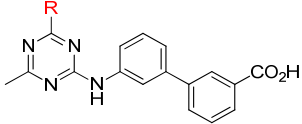
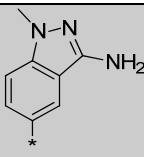
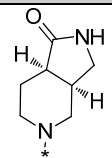
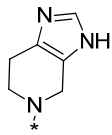
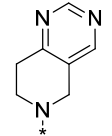
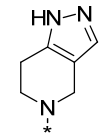
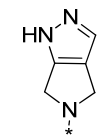
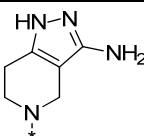
							
Cpd. No.	R	PI3K γ pIC ₅₀	L.E.	L.L.E.	PI3K isoform sel.	CLND Sol μ M	ChromLogD pH 7.4
334		7.6	0.31	0.23	α 4.8 ^{*\pm} β <4.5 δ 5.3 ^{*\pm}	237	2.3
382		5.8	0.24	0.22	α <4.5 β <4.5 δ <4.5	490	1.4
386		5.5	0.24	0.20	α <4.5 β <4.5 δ <4.5	360	1.6
387		6.1	0.24	0.21	α <4.5 β <4.5 δ <4.5	502	1.8
396		6.3	0.27	0.22	α 4.5 ^{*\pm} β <4.5 δ <4.5	395	1.8
397		6.6	0.29	0.25	α 5.6 ^{*\ddagger} β <4.5 δ 4.5 ^{*\ddagger}	306	1.6
375		6.0	0.25	0.22	α 4.7 β <4.5 δ 5.0	312	1.2

Table 43: Data on most promising aminoindazole replacements; * indicates $n=1$ data; ^{\pm} indicates one value not included in mean as below the threshold of the assay (i.e. $pIC_{50} < 4.5$); ^{\ddagger} indicates two values not included in mean as below the threshold of the assay (i.e. $pIC_{50} < 4.5$)

Whilst none of these initial compounds met the potency criteria for further progression within our wider programme, they provided evidence that removal or replacement of aromaticity in this template could successfully improve the physicochemical properties without detriment to the selectivity profile. In an attempt to increase potency, whilst maintaining the preferential physicochemical properties, the best analogues were synthesised with the biraryl solubility pocket found in lead compounds **312** and **313** (Figure 67). The addition of the methoxy substituent in the terminal phenyl ring was expected to give ~10-fold increase in PI3K γ potency (Table 38), which would give compounds with sufficient potency to profile further in the fMLP PBMC assay.

The same synthetic strategy was employed as for the previous arrays, however this time the biphenyl carboxylic acid monomer **398** required bespoke synthesis elsewhere within our laboratories.¹⁸⁷

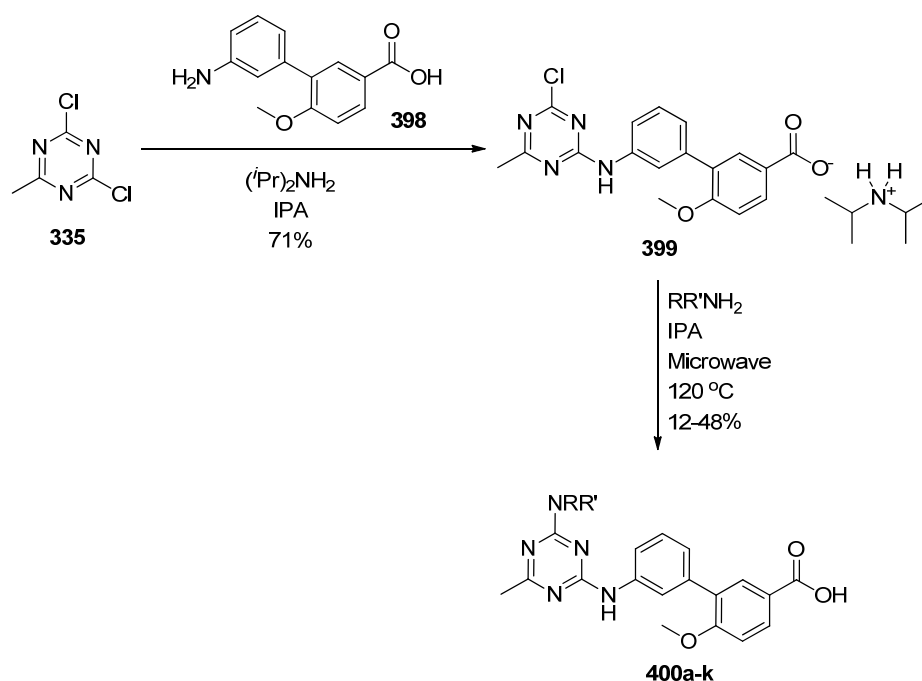
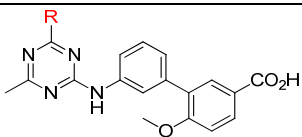
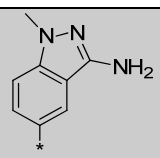
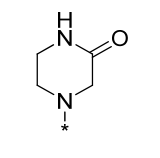
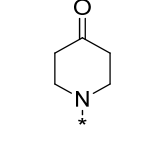
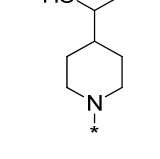
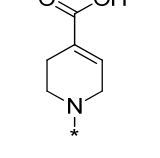
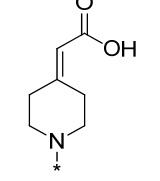


Figure 67: Synthesis of best saturated/semi-saturated back pockets with alternative biaryl solubility pocket

Biological data for this second set of compounds is shown in Table 44; in accordance with our predictions, the introduction of the methoxy substituent increased PI3K γ potency in nearly all cases. Of particular interest are analogues **400b** and **400k** as

these show the best potency and efficiency, whilst maintaining the promising CLND solubilities. These analogues were now of sufficient potency to profile in the cellular fMLP PBMC assay (Table 45), however, disappointingly, neither compound showed activity across the concentration range tested.

							
Cpd. No.	R	PI3K γ pIC ₅₀	L.E.	L.L.E.	PI3K isoform sel.	CLND Sol μ M	ChromLogD pH 7.4
313		8.4	0.32	0.27	α 6.0 β <4.6 δ 4.7 \pm	28	2.1
400a		6.8	0.29	0.27	α 4.9 \ddagger β <4.6 δ <4.6	323	1.2
400b		7.0	0.30	0.26	α <4.6 β <4.6 δ <4.6	289	1.9
400c		6.6	0.27	0.23	α <4.5 β <4.5 δ <4.5	349	2.2
400d		6.8	0.27	0.25	α 5.0 β <4.5 δ <4.5 \ddagger	72	0.7
400e		7.1	0.28	0.23	α 5.0 β <4.5 δ <4.5	339	0.9

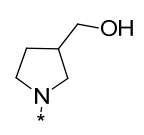
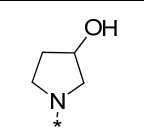
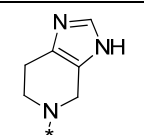
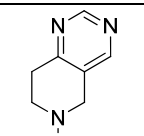
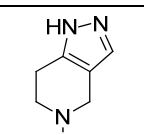
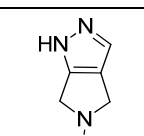
400f		6.2	0.27	0.25	α 4.7 ^{*‡} β <4.6 δ <4.6	351	1.5
400g		5.9 [±]	0.26	0.24	α <4.6 β <4.6 δ 4.7 ^{*‡}	288	1.4
400h		5.8 [*]	0.23	0.22	α <4.5 β <4.5 δ 4.7 ^{*‡}	184	1.6
400i		6.7	0.26	0.25	α <4.5 β <4.5 δ <4.5	242	1.8
400j		6.9	0.28	0.25	α <4.5 β <4.5 δ <4.5	295	1.8
400k		7.2	0.30	0.28	α 4.9 ^{*‡} β <4.5 δ <4.5	285	1.6

Table 44: Data on compounds **400a-e**; * indicates $n=1$ data; [±] indicates one value not included in mean as below the threshold of the assay (i.e. $pIC_{50} < 4.6$); [‡] indicates two values not included in mean as below the threshold of the assay (i.e. $pIC_{50} < 4.6$); [‡] indicates five values not included in mean as below the threshold of the assay (i.e. $pIC_{50} < 4.6$);

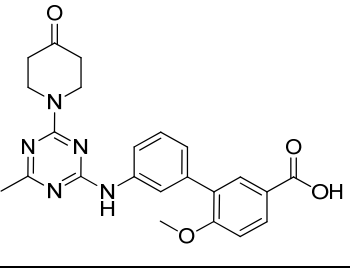
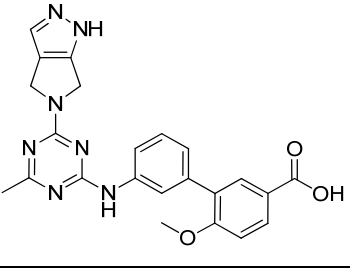
		
Compound no.	400b	400k
PI3Kγ pIC₅₀	7.0	7.2
fMLP PBMC pIC₅₀	<5.1	<5.0

Table 45: fMLP PBMC data on key compounds

At this time, only a few compounds from the aminopyrimidine series had shown robust activity in the fMLP PBMC assay so a data review was conducted to ascertain if there were any trends in physicochemical properties which could help in the design of further compounds with good activity.

Figure 68 is a plot of all the fMLP PBMC data collected on compounds from the aminopyrimidine series. Each discrete column on the x-axis represents a different compound, with potency in the fMLP PBMC cellular assay shown on the y-axis. Where compounds have been tested on more than one occasion (two replicates are collected as default, but larger n numbers are often sought in cellular assays where variability is commonly higher than for primary assays), multiple entries appear in each column. It can clearly be seen that some compounds demonstrated very large variability between test occasions, whilst others showed more consistent data. The compounds were therefore classified into three categories; those showing robust, reproducible activity (defined as pIC₅₀ \geq 5.4), those showing no activity (i.e. consistently returning a pIC₅₀ < 5) and those showing weak and/or variable activity. Further data analysis could therefore consider not only the mean pIC₅₀ value, but also the variability of data, allowing more meaningful conclusions to be drawn.

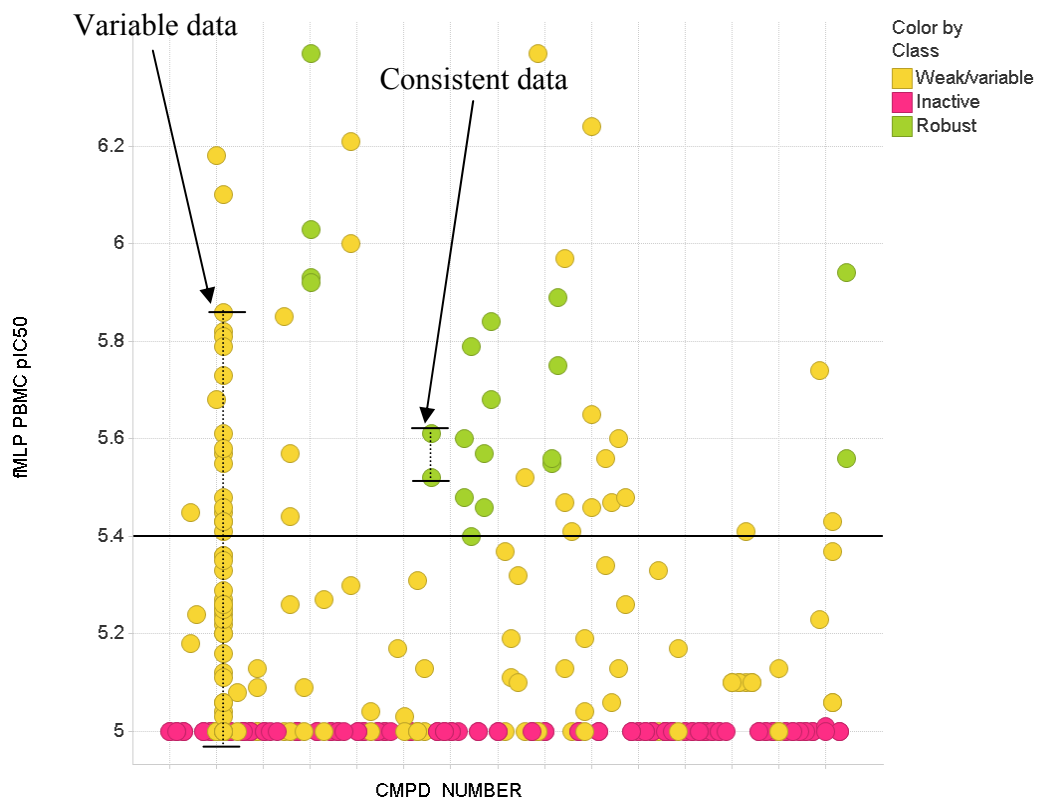


Figure 68: fMLP PBMC data for the aminopyrimidine series; coloured by activity class as shown in graph legend

Two of the most common drivers for activity in cellular systems are good compound solubility and permeability, so these parameters were investigated for correlations with the fMLP PBMC data. Figure 69a is a plot of solubility forecast indicator vs. fMLP PBMC potency, with compounds coloured as per the classification of activity in the fMLP PBMC assay described above. Solubility forecast indicator (SFI) is a GSK-developed prediction of solubility derived from the *in silico* (or measured) lipophilicity of a compound (usually ChromLogD) and the number of aromatic rings it contains.^{139,188}

$$\text{SFI} = \text{ChromLogD}_{7,4} + \text{number of aromatic rings}$$

Analysis of the GSK compound collection has shown an SFI < 7 to be indicative of good measured CLND solubility and, indeed, an SFI < 6 is preferred for a candidate quality molecule. No evidence of a correlation of robust activity in the cellular assay could be found with SFI; in fact, the majority of the robustly active compounds have high SFIs,

above the desirable range. Measured CLND solubility data was also analysed (Figure 69b), but again no correlation with mean fMLP PMBC potency, or activity class is observed.

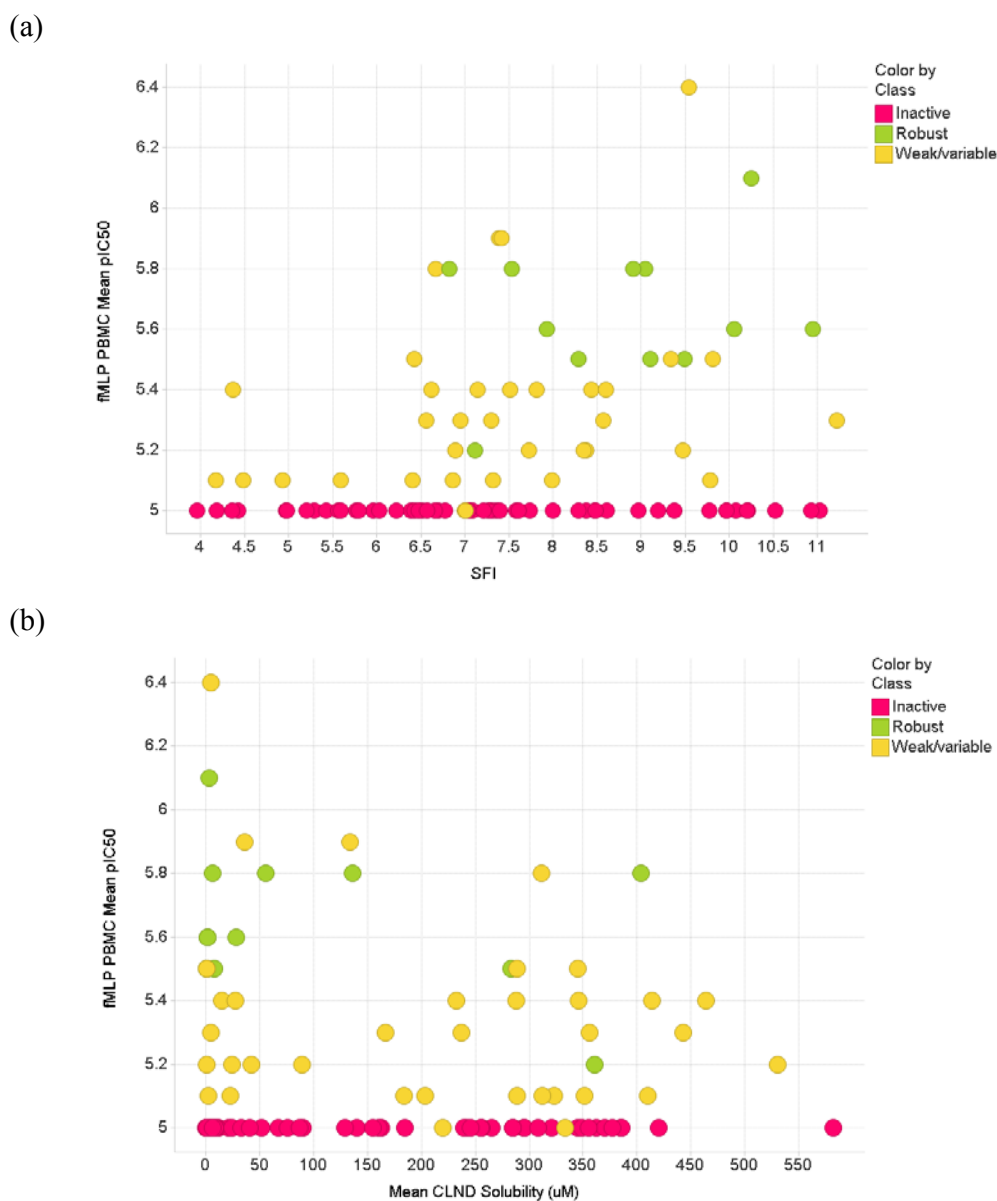
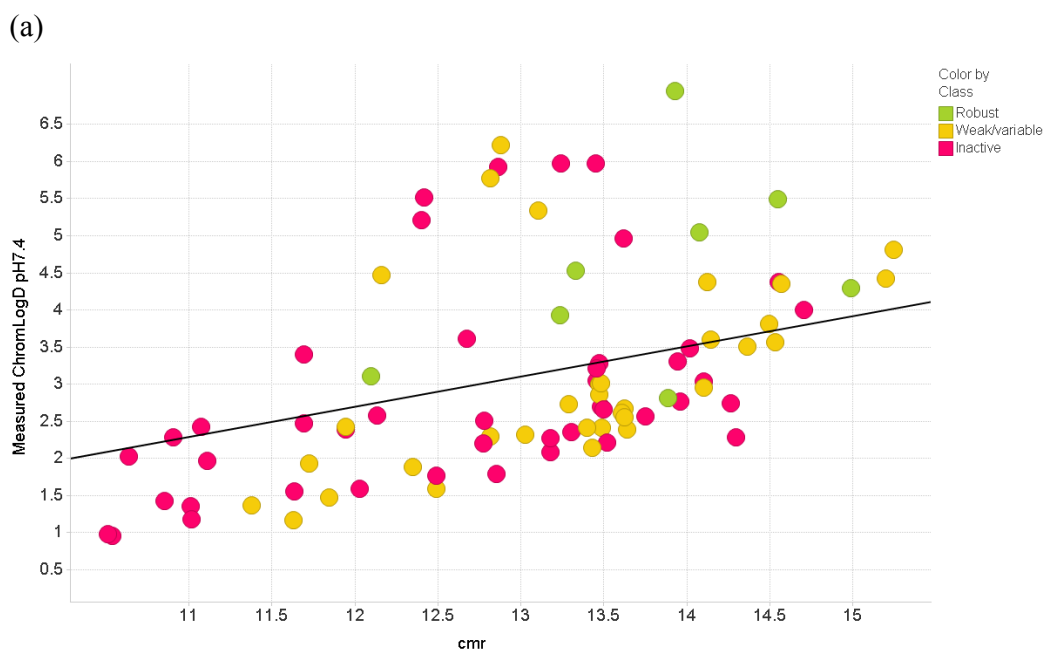


Figure 69: Solubility profiles of aminopyrimidine compounds; (a) SFI vs fMLP PBMC potency; (b) measured CLND solubility vs. fMLP PBMC potency; compounds are coloured in both plots by activity classification using raw (not meaned) data from the cellular assay.

Permeability of the compounds was predicted using the GSK *in silico* permeability model described in Section 2.6.1. Figure 70a shows the permeability plot of cmr vs. ChromLogD at pH 7.4; compounds below the line are predicted to have poor permeability and those above are predicted to have a higher chance of achieving good permeability. Whilst this analysis is not clear cut, all but one of the compounds with robust activity in the fMLP PBMC assay fall above the line: the area predicted to have a higher probability of good permeability. The model does not however differentiate between the inactive and weakly/variably active compounds. In order to investigate this potential correlation with permeability further, measured permeability data (from the artificial membrane permeability assay, see Section 2.6.1) was adopted (Figure 70b). In this case, no correlations were observed.



(b)

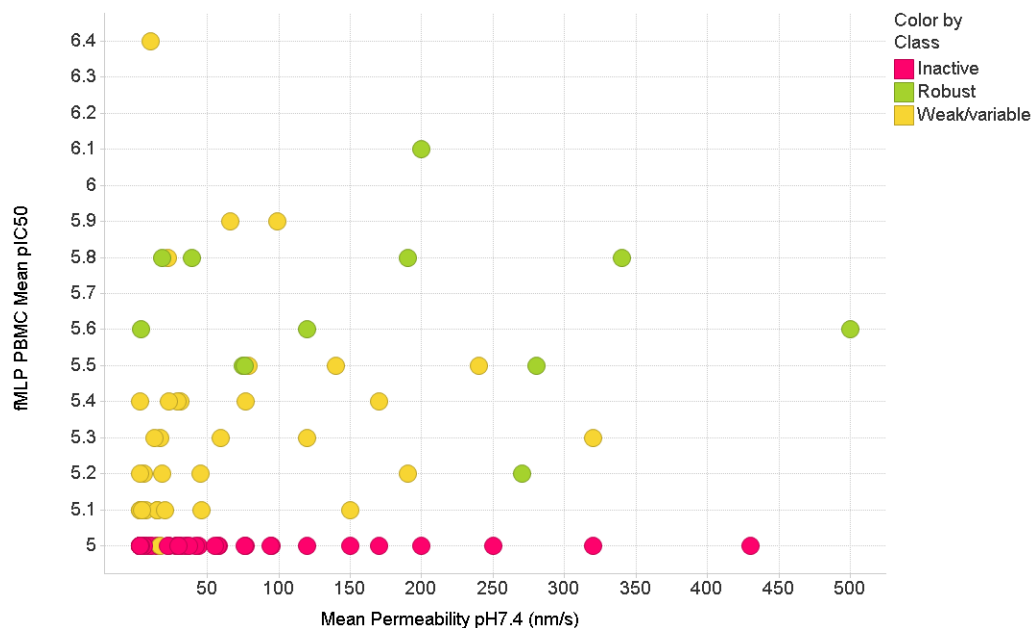


Figure 70: Plots to investigate the effect of compound permeability on cellular activity of aminopyrimidine compounds; (a) GSK *in silico* permeability model; (b) AMP measured permeability data

The lack of correlation of with any single parameter such as solubility and permeability should not be entirely surprising; cellular systems are inherently complex and activity will be influenced by protein binding, cellular compartmentalisation, efflux, and other transport mechanisms. Typically a set of “rules” would need to be established empirically to explain cellular SAR in any given series. In some cases single parameters may be found to dominate SAR relationships; often they do not.

Although the measured permeability data for these compounds did not show any correlations, of particular concern for achieving good cellular activity was the presence of a carboxylic acid group. As previously described for the pyridone template in Section 2.6, the presence of a carboxylate can lead to poor permeability (due to high ionisation of the compound at physiological pH), but can also result in high plasma protein binding, which reduces the level of free compound available to pass into the cell. Initial fMLP PBMC data on analogues **312** and **313** had been encouraging (Table 34), however, the generation of additional data replicates on different test occasions, revealed that, both of

these compounds showed very high variability in this assay, often returning potency values below the threshold of the assay (i.e. $pIC_{50} < 5$).

With the carboxylic acid moiety being such a key feature of the series, the impact of ionisation state on cellular activity was looked at more closely for the entire data set. Figure 71 shows a plot of predicted pK_a vs. mean fMLP PBMC potency, again coloured by the reproducibility of the data. It is quite striking that all of the compounds containing an acidic centre with a $pK_a \sim 4$ (i.e. those containing a carboxylic acid moiety or acid isostere) do not show robust activity in this assay.

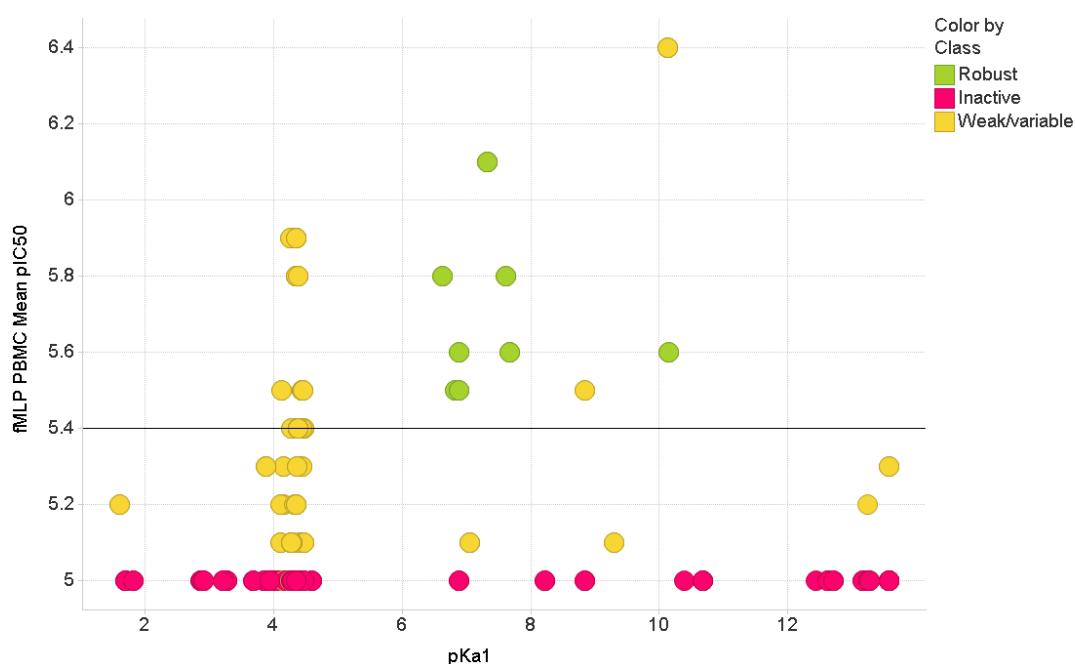


Figure 71: Predicted Chemaxon pK_a (of most acidic centre) vs. fMLP PBMC potency; coloured by activity classification using raw (not meaned) data from the cellular assay

Indeed, the measured AMP data for only those compounds containing a carboxylic acid group are shown in Figure 72 and there are no compounds with good permeability (>200 nm/s). In this subset of compounds, low to moderate permeability is correlating with poor or variable activity in the fMLP cellular assay.

Factors governing cellular activity are likely to vary with different subsets of compounds; in this case the presence of ionisable functionality dominates, which is highly plausible given this functional group will have a very large impact on the physicochemical properties of the compounds.

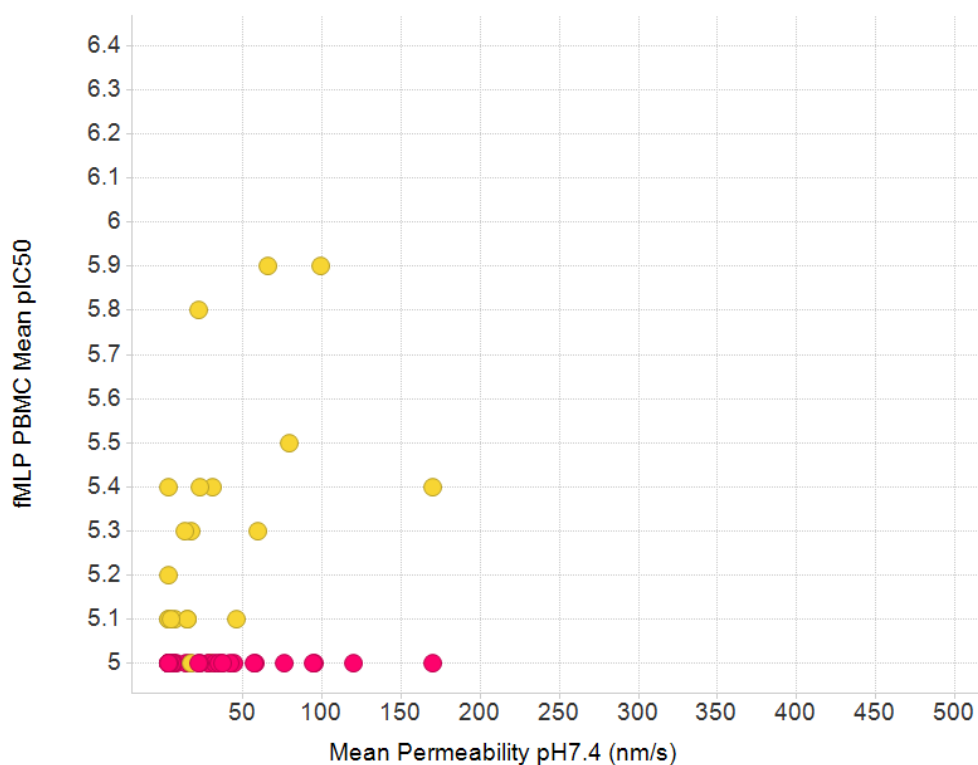


Figure 72: Plot to show correlation of measured AMP permeability with fMLP activity for only carboxylic acid containing analogues

3.3.2 Future Work

The lack of robust activity from any compounds containing a carboxylic acid moiety, along with previous experience from the pyridone template, led to the decision to terminate work on this subset of carboxylic acid containing aminopyrimidine compounds. X-ray crystallography (Figure 53) and previous SAR had shown the carboxylate was important for obtaining the impressive selectivity profile achieved with this series, so future work will focus on establishing whether this group could be replaced by an alternative functionality, which could maintain the selectivity profile, whilst altering the physicochemical profile of the compounds sufficiently to achieve good cellular activity (Figure 73).

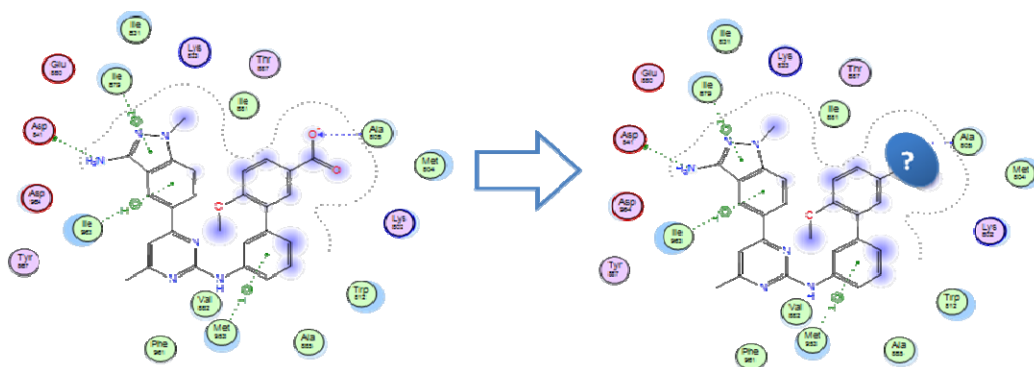


Figure 73: Pictorial representation of proposed future work on the aminopyrimidine series

3.4 Conclusions

Work on the aminopyrimidine series has been focused on improving the physicochemical properties of the series and, in particular, solubility. The design and synthesis of prototype pro-drug **328**, has successfully demonstrated that this approach can deliver the solubility profile required for an *i.v.* formulation. Whilst this particular compound did not meet our blood stability and DMPK criteria, alternative pro-drugs could be designed to achieve the desired profile.

Further work on this template was focused on improving the inherent physicochemical properties of the series and has delivered compounds with improved profiles in this regard. Key compounds with the best PI3K γ potency were further profiled in the fMLP PBMC assay but, unfortunately, showed disappointing cellular activity. A more general review of cellular data from this series revealed that, similar to the pyridone series, carboxylic acid containing analogues showed poor or variable activity in this assay, which may be attributed to their high polarity and low permeability. A clear decision was made to move away from carboxylic acids; future work will focus on the identification of alternative functionalities which maintain the productive ligand-protein interactions (and associated selectivity profile) whilst improving the physicochemical profile.

Similar to the pyridone series, the aminopyrimidine template provides a novel chemotype of PI3K γ inhibitor which matches the best known selectivity profile

described in the PI3K literature. Although our efforts on this template have not delivered a molecule which meets our target profile for further progression, we have made significant progress in other respects. Firstly, we have successfully validated the concept of a pro-drug approach for achieving the high solubility required for intravenous dosing. Secondly, we have further extended our knowledge of the PI3K γ protein especially with regard to the phosphate pocket. All of the competitor compounds, where structural data is available, place an aromatic or completely planar aliphatic group in this region (see Section 1.3.3). Our work on the aminopyrimidine series has shown that saturated or semi-saturated groups with a high ratio of sp^3 to sp^2 centres can be tolerated, which provides a useful means for improving the solubility of this, or any other template explored. The value of these learnings are reflected in an examination of competitor structures (and, indeed, many of our own inhibitors): physicochemical properties are a shortcoming of PI3K γ inhibitors, with structures characterised by highly planar, highly aromatic features.

The knowledge that physicochemical properties can be enhanced by targeting ligand binding features in the phosphate pocket, complements nicely the learnings from the pyridone template, which were primarily built on improving the selectivity profile through interactions in the solubility pocket/P-loop. Together, these data provide us with critical information to aid the design of future PI3K γ selective inhibitors.

4.0 FRAGMENT BASED DRUG DISCOVERY

Both the pyridone and aminopyrimidine series described in the preceding chapters had their origins in legacy PI3K γ programmes conducted elsewhere in our laboratories. These compounds were already highly optimised, with physicochemical properties at the limit (or, in some cases, above) the desirable cut-offs for “drug-like” space. As part of this programme, efforts were concentrated on selectively improving the physicochemical properties of these series. In due course, the approach in this area was re-tuned in favour of a fragment-based drug discovery approach.

Fragment-based drug discovery is founded on the principle of identifying small, ligand efficient molecules (fragments) with known binding modes at a given target.^{189,190} Careful analysis of X-ray crystallography data is then used to prioritise templates which have clear vectors to access additional ligand-protein interactions. Through a process of iterative, structure-based design, these fragments are gradually grown into lead molecules, which may then progress onto full lead optimisation. Typically, fragment-based drug discovery relies on the synthesis of low numbers of compounds which probe key regions of the binding site.^{191,192} Close attention is paid to ligand efficiency measurements throughout the process, in order to ensure the final molecules have the desired balance between potency and physicochemical properties (such as lipophilicity). Our aim was, therefore, to use fragment-based drug design, to help identify some novel chemotypes of PI3K γ inhibitors with improved physicochemical profiles with respect to the pyridone/aminopyrimidine series and competitor molecules from the literature.

4.1 Results and Discussion

The proprietary fragment collection (known within GSK as FBDD1) is a set of approximately 1000 compounds which have desirable lead-like properties and good developability characteristics; in particular, low MW, few aromatic rings, and low lipophilicity, as well as good chemical tractability and stability (Figure 74).

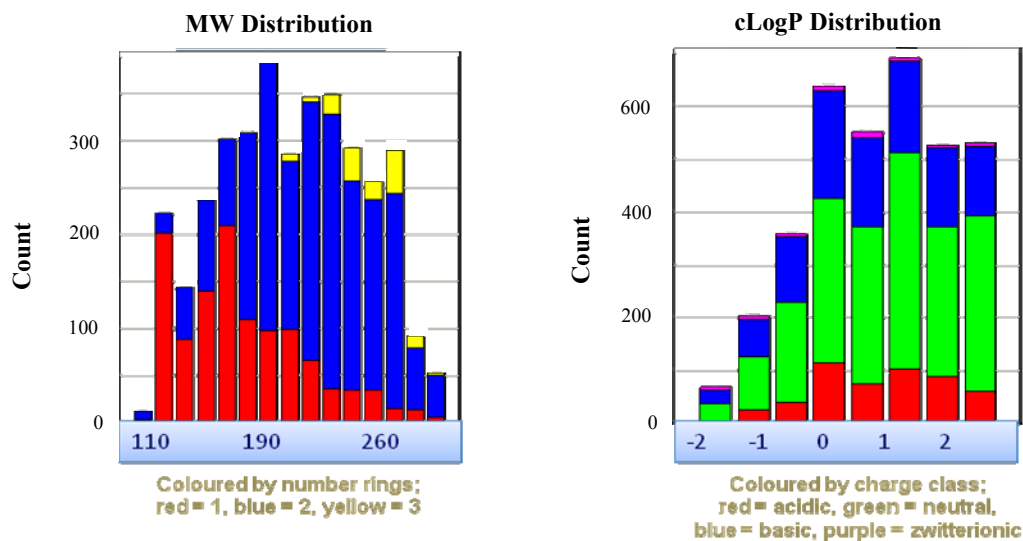


Figure 74: Physicochemical properties of FBDD1; (a) Histogram of MW, coloured to indicate the number of aromatic rings; (b) Histogram of cLogP, coloured to indicate charge class¹⁹³

This set of compounds is screened (biochemically and/or biophysically) against a particular target to identify new starting points for fragment-based design, in a similar way to the more traditional high-throughput screening (HTS), which has been used to identify starting points for classical lead optimisation. FBDD1 was therefore screened biochemically against PI3K γ and δ . Due to the small molecule size and low complexity of these fragments, the biochemical screening was conducted using a higher maximum concentration than in the standard assay described thusfar, giving a lower assay limit of pIC₅₀ ~2.8.¹²⁴ The data generated were used to select compounds which showed statistically significant selectivity for PI3K γ over δ (>0.4 log unit difference in pIC₅₀) and these hits were progressed to biophysical screening to confirm activity. Although the selectivity profile of a compound can change as it is grown (as demonstrated by the pyridone template), it was hypothesised that a template which displayed inherent selectivity for PI3K γ from the outset may facilitate the discovery of a highly selective pre-candidate molecule.

Biochemical screening of FBDD1 identified 28 hits with the target selectivity profile. These 28 hits were subsequently progressed to a saturation transfer difference (STD)

NMR biophysical assay.¹⁹⁴ Use of this technique can give additional evidence of a binding interaction between a ligand and its target by following changes in the NMR (Figure 75). The assay was run in the presence and absence of ATP in an attempt to establish whether the ligands are ATP-competitive, i.e. binding to the same site as ATP in the protein.

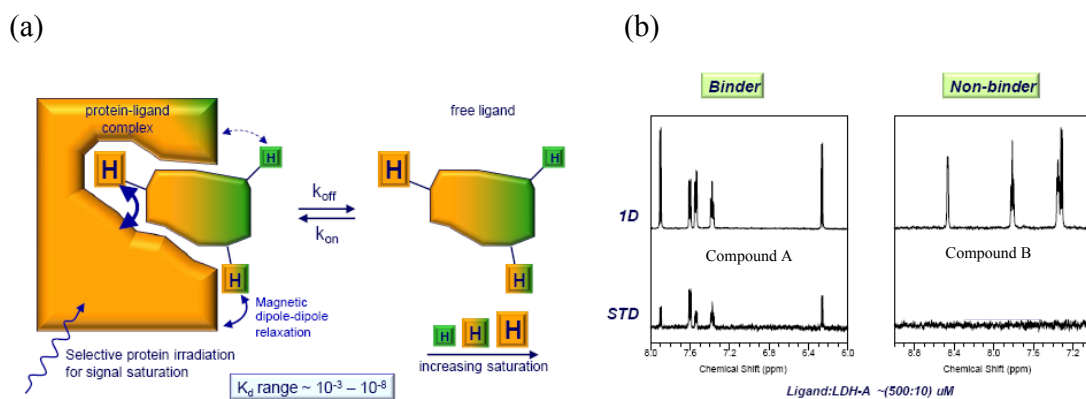


Figure 75: (a) Schematic representation of STD NMR assay illustrating the intermolecular saturation transfer from the protein to the bound ligand; (b) ^1H NMR and STD spectra of two compounds demonstrating the profile expected for a binder and non-binder.¹⁹³

Of the 28 PI3K γ selective hits from the biochemical assay, only one showed no binding in the NMR assay. All of the 27 NMR binders were shown to be ATP competitive. This set of 27 hits underwent crystallisation trials in an attempt to establish precise details of binding by X-ray crystallography. The compounds were prioritised by L.E. and chemical diversity, and 17 crystal structures of varying quality (2.3 to 3.5 Å resolution) were successfully obtained.⁹⁷ Perhaps unsurprisingly for a kinase target, all of the ligands were observed to bind to the hinge region of the protein; this is a highly conserved binding interaction amongst ATP-competitive kinase inhibitors, and provides a critical contribution to the ligand's binding affinity. However, there was diversity in the range of chemical functionalities forming the hinge interaction, as well as in relation to shape and space-filling achieved by the fragments.

The 17 crystal structures gave rise to 8 ligand clusters. The clusters were developed subjectively based on their binding modes and vectors available for substitution;

different fragments within a cluster would be anticipated to access similar regions of the protein as they are grown (Figure 76). Caution is always necessary when growing fragment structures as binding modes can often change when substituents are added. This can lead to confounding SAR and is best managed by solving crystal structures for multiple analogues throughout the process. The independent programme of work described here will focus on the exploration of Clusters 4 and 5a, which were selected for initial work based on PI3K γ potency, selectivity, L.E. (full biological data not shown), and chemical tractability.

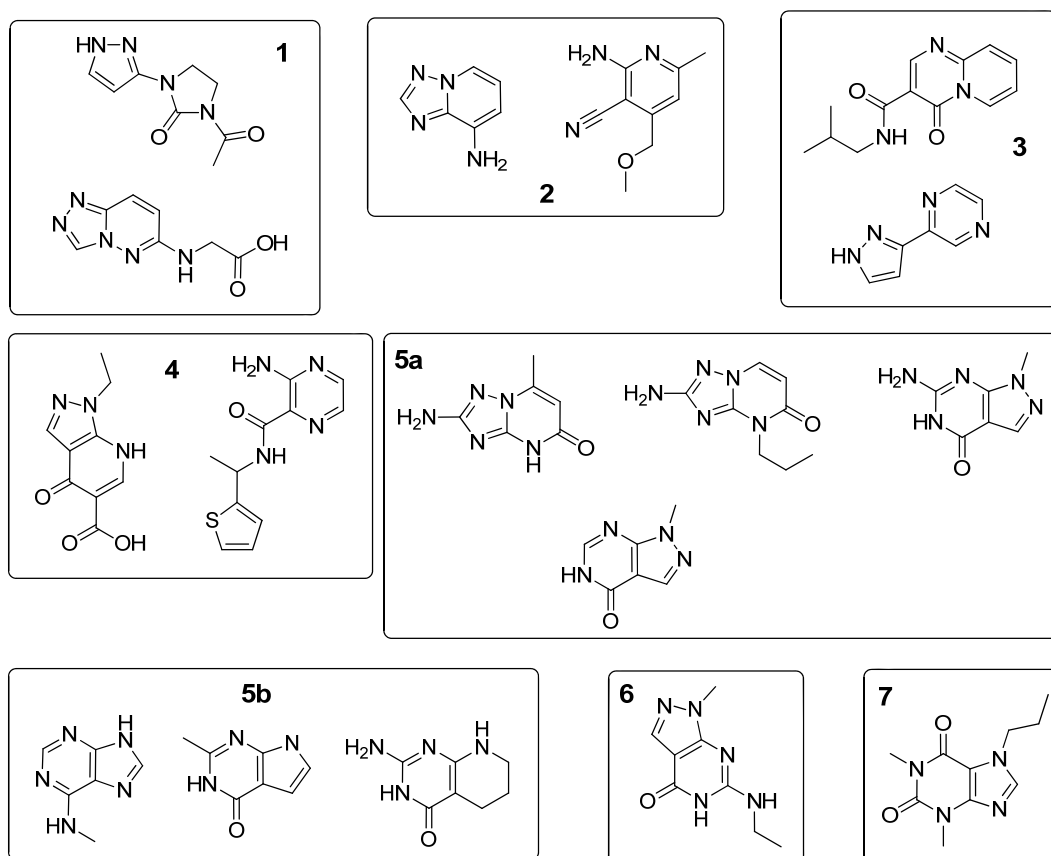


Figure 76: Structures and clusters of fragment hits for which X-ray crystal structures were successfully obtained

4.1.1 Cluster 4

Cluster 4 contained two compounds **401** and **402**, which showed differing selectivities for PI3K γ (Table 46, the H-bonding hinge interactions are indicated by red arrows). In addition to these two compounds, a further fragment **403**, for which X-ray

crystallography failed, would be expected to belong to this cluster due to its close structural similarity to **402**. Interestingly, this fragment showed a significant increase in potency and L.E. over **402**, although these data must be interpreted cautiously without structural confirmation of the binding mode.

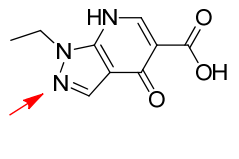
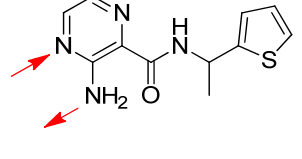
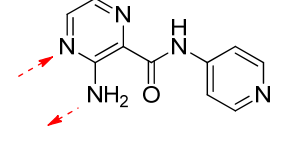
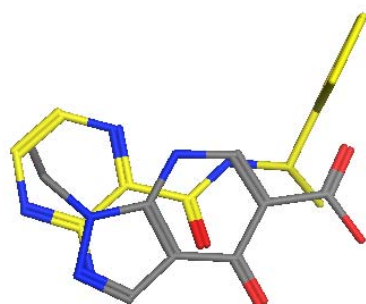
			
	401	402	403
PI3Kγ/δ pIC₅₀	4.2 / 3.6	4.1 / 4.0*	5.2 / 5.1
L.E.	0.38	0.33	0.45
L.L.E.	0.50	0.29	0.51

Table 46: Fragments in Cluster 4; H-bonding indicated by red arrows (from donor to acceptor); * indicates $n=1$ data

Figure 77 shows X-ray crystal structures for Cluster 4.⁹⁷ Whilst the two templates bind in a very different manner, the thiophene and carboxylic acid groups extend along a similar vector, to a region of the protein which has not previously been explored in other PI3K γ inhibitor chemotypes.

(a)



(b)

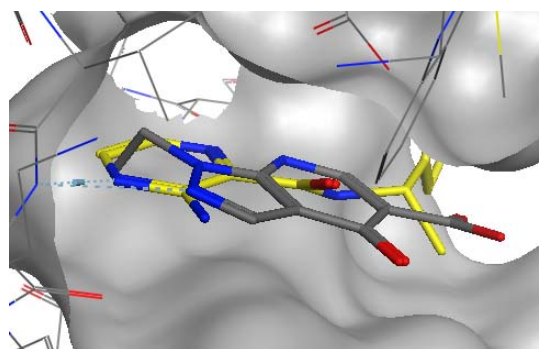


Figure 77: Cluster 4; (a) X-ray crystal structures of **401** (grey) and **402** (yellow) from Cluster 4 in PI3K γ active site (no protein shown for clarity); (b) X-ray crystal structures of ligands from Cluster 4 rotated 90°, with protein and partial surface shown.

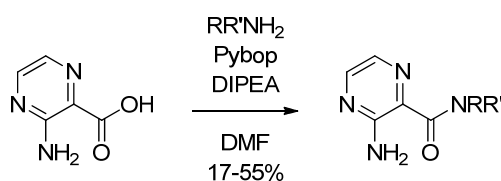
The interesting SAR of analogues **402** and **403**, combined with the lower aromatic ring count of the hinge binding motif, led us to prioritise investigation of the aminopyrazine template over pyrazolopyridone **401**. Aminopyrazines have been described in the literature as PI3K γ inhibitors (see Section 1.3.5), although the chemotypes recently described by Excelixis had not been divulged when work on this cluster was initiated.¹¹⁰ Early attempts to build SAR for this template were based on two arrays (Figure 78).



Figure 78: Arrays to follow up on Cluster 4

Array 1 was designed to investigate the amide substituent more thoroughly, following up on the significant difference in potency and selectivity of **402** and **403**; Array 2 would investigate other 6-membered heteroaromatic cores as alternatives to the pyrazine unit. These array compounds were expected not only to offer different potency and L.E. profiles, but also to provide novel vectors for growing the fragment in the direction of the phosphate pocket.

In the first array, a range of primary and secondary aliphatic and aromatic amines were introduced *via* amide coupling with the commercially available pyrazine carboxylic acid (Scheme 43 and Table 47).



Scheme 43: Synthesis of Array

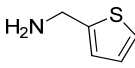
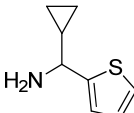
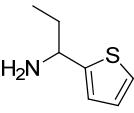
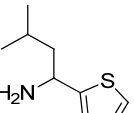
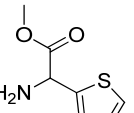
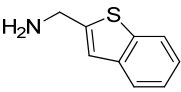
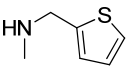
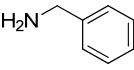
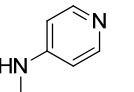
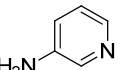
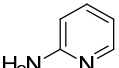
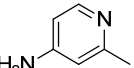
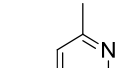
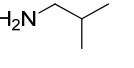
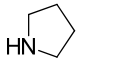
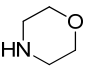
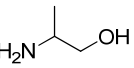
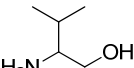
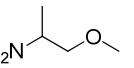
<p>404</p>  <p>32%</p>	<p>405</p>  <p>54%</p>	<p>406</p>  <p>52%</p>	<p>407</p>  <p>54%</p>	<p>408</p>  <p>55%</p>
<p>409</p>  <p>37%</p>	<p>410</p>  <p>53%</p>	<p>411</p>  <p>45%</p>	<p>412</p>  <p>26%</p>	<p>413</p>  <p>40%</p>
<p>414</p>  <p>19%</p>	<p>415</p>  <p>26%</p>	<p>416</p>  <p>28%</p>	<p>417</p>  <p>17%</p>	<p>418</p>  <p>41%</p>
<p>419</p>  <p>35%</p>	<p>420</p>  <p>39%</p>	<p>421</p>  <p>48%</p>	<p>422</p>  <p>41%</p>	

Table 47: Amine monomers used for amide array; isolated yields quoted where reactions were successful

Disappointingly, none of the compounds demonstrated improved L.E. / L.L.E. profiles over the pyridine analogue **403**, for which crystallography had failed (Figure 79).

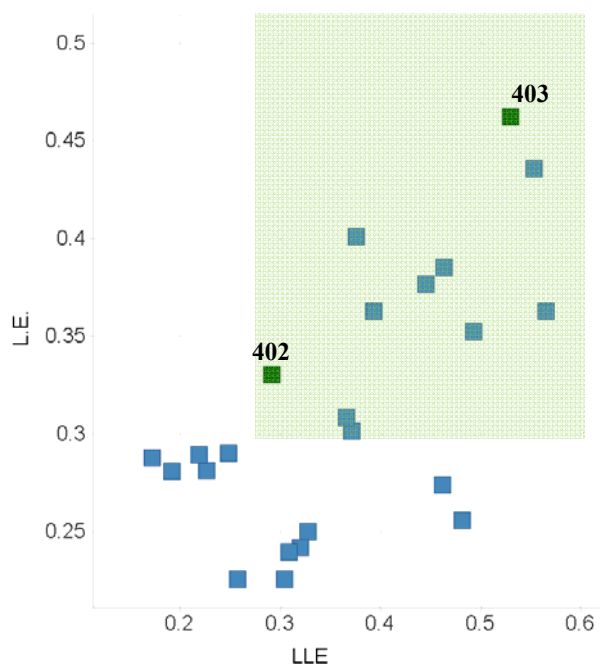


Figure 79: Data generated from Array 1

However, some useful SAR was observed; Table 48 summarises the key results and includes analogue **428**, which was identified by sub-structure searching of the GSK compound database. Small alkyl analogues **427** and **428**, show promising L.E. / L.L.E. profiles and suggest it may be possible to move away from aromatic/heteroaromatic amide substituents. Compounds **425** and **426** demonstrate that tertiary amides are not well tolerated. Although X-ray crystallography of **402** does not indicate that the amide NH is involved in any specific H-bonding interactions, substitution at this position would be predicted to push the amide substituent out of plane with the pyrazine ring, which may not be favourable for ligand binding.

Finally, analogues **423** and **424** demonstrate that increasing steric bulk of the substituent α to the amide is also unfavourable; the potency does not increase commensurately with the MW added and, as a result, both L.E. and L.L.E. drop.

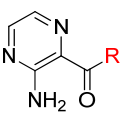
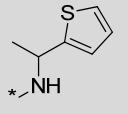
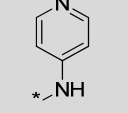
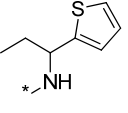
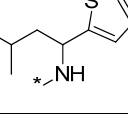
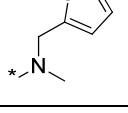
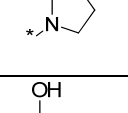
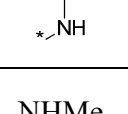
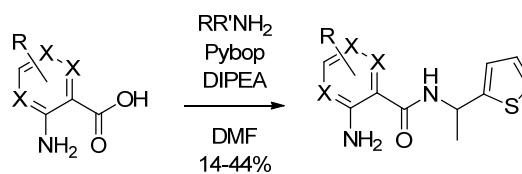
Compound No.		PI3K γ/δ pIC ₅₀	L.E.	L.L.E.
402		4.1 / 4.0*	0.33	0.29
403		5.2 / 5.1	0.45	0.51
423		3.8 / 3.8	0.29	0.22
424		4.2 / 3.9 [±]	0.29	0.17
425		<2.8 / 3.1 [±]	-	-
426		<2.8 / <2.8	-	-
427		3.6 / 3.2	0.35	0.49
428	NHMe	3.5 / 3.5	0.44	0.55

Table 48: SAR from Array 1; * indicates $n=1$ data; [±] indicates one value not included in mean as below the threshold of the assay (i.e. $pIC_{50} < 2.8$)

In the second array, a range of commercially available carboxylic acids were coupled with 1-(thiophen-2-yl)ethanamine (Scheme 44 and Table 49).



Scheme 44: Synthesis of Array 2

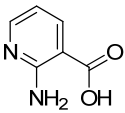
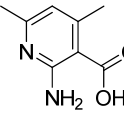
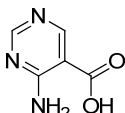
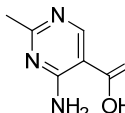
429	430	431	432
			
34%	15%	36%	14%

Table 49: Carboxylic acid monomers for Array 2; isolated yields quoted where reactions were successful

The biological data for Array 2 are shown in Table 50. Unfortunately, none of the alternative cores match the profile of pyrazine **403** in terms of potency and selectivity. Whilst examination of the crystal structure of **403** does not provide a strong rationale for these results, all of the template changes could affect the orientation of the amide substituent, due to changes in the 4-position of the central core, *ortho* to the amide substituent.

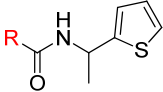
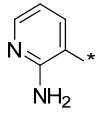
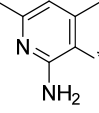
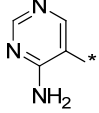
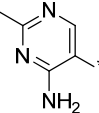
Compound No.		PI3K γ/δ pIC ₅₀	L.E.	L.L.E.
433		3.2 / 3.2	0.26	0.18
434		<2.8* / 3.0*	-	-
435		3.0 / 2.8 [±]	0.24	0.20
436		<2.8* / <2.8*	-	-

Table 50: SAR from Array 2; * indicates $n=1$ data; [±] indicates one value not included in mean as below the threshold of the assay (i.e. pIC₅₀ < 2.8)

Alongside these arrays, sub-structure searching of the GSK compound collection identified some further analogues for screening, which provided additional data (Table

51). Compound **438**, is in fact exemplified in a Novartis patent¹⁹⁵ and had previously been synthesised elsewhere in our laboratories.¹⁹⁶

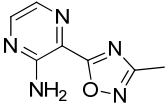
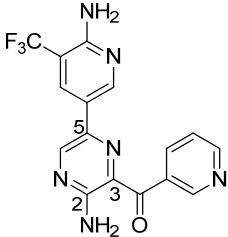
Compound No.	Structure	PI3K γ/δ pIC ₅₀	L.E.	L.L.E.
437		3.4 [‡] / 4.2 [‡]	0.36	0.50
438		7.0 / 6.3	0.37	0.38

Table 51: Biological data from compounds identified by SSS of the GSK compound collection for Cluster 4; [‡] indicates two values not included in mean as below the threshold of the assay run at standard concentration range (i.e. pIC₅₀ < 4.6)

Compound **437** demonstrated that a heterocycle is well tolerated as a replacement for the amide linker, whilst the larger analogue **438** showed a significant increase in potency with reasonable retention of L.E. / L.L.E. with respect to the hit compounds. In this compound, the amide is replaced with a ketone at the 2-position and there is an additional aromatic substituent at the 5-position. The presence of the 6-aminopyridine moiety provides an alternative hinge binding motif, so the binding mode of this compound could not automatically be assumed to be analogous to lead compound **402**. However, overlay of the crystal structure of **402** with that of pyridone analogue **258** does suggest that growing the 5-position vector (as shown by the red arrow in Figure 80) may enable access to the phosphate pocket, occupied by the dimethoxy phenyl group in the pyridone structure shown and, presumably, the 6-aminopyridine unit within compound **438**.

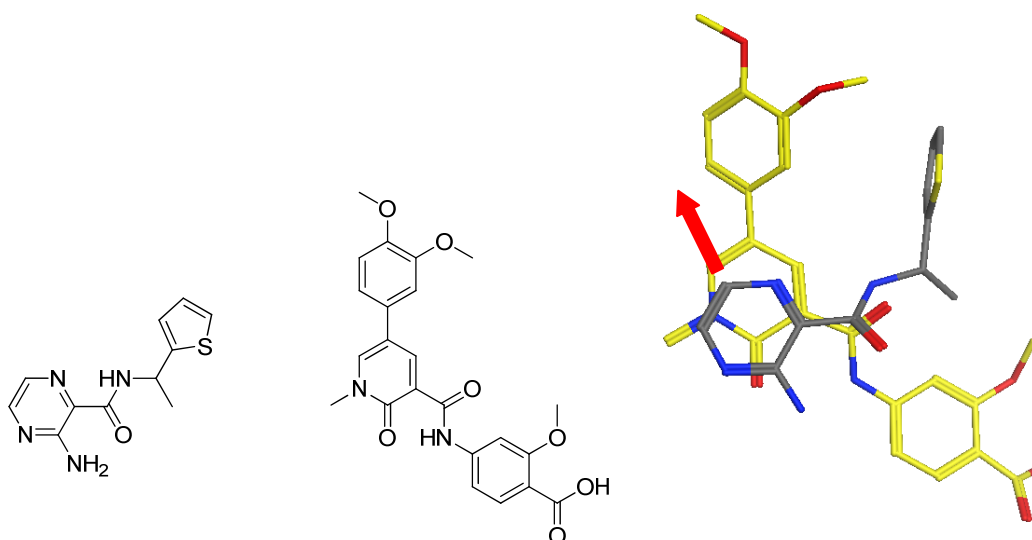


Figure 80: Overlay of X-ray crystal structure of aminopyrazine **402** (grey) and pyridone **258** (yellow)

Indeed, an X-ray crystal structure for **438** was obtained,⁹⁷ which confirmed a similar binding mode to hit **402**, with the aminopyrazine acting as the hinge-binding motif and the aminopyridine ring occupying the phosphate pocket (Figure 81). The absolute orientation of the core has rotated slightly compared with **402**, to accommodate the additional aromatic ring.

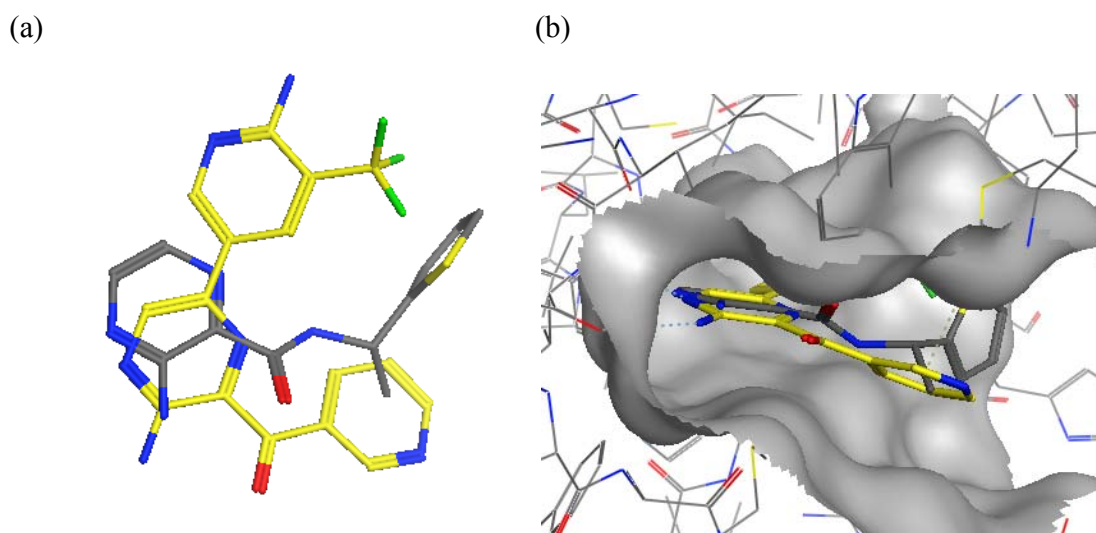


Figure 81: (a) X-ray crystal structures of ligands **402** (grey) and **438** (yellow) in PI3K γ active site (no protein shown for clarity); (b) X-ray crystal structures of ligands **402** and **438** rotated 90°, with protein and partial surface shown.

The recent publication from Excelixis¹¹⁰ added additional weight to this hypothesis, with a similar binding mode described for their closely related aminopyrazine **57** (Figure 82). It also suggested that growing the aromatic ring further into the phosphate pocket may provide a method for obtaining additional PI3K γ potency and selectivity.

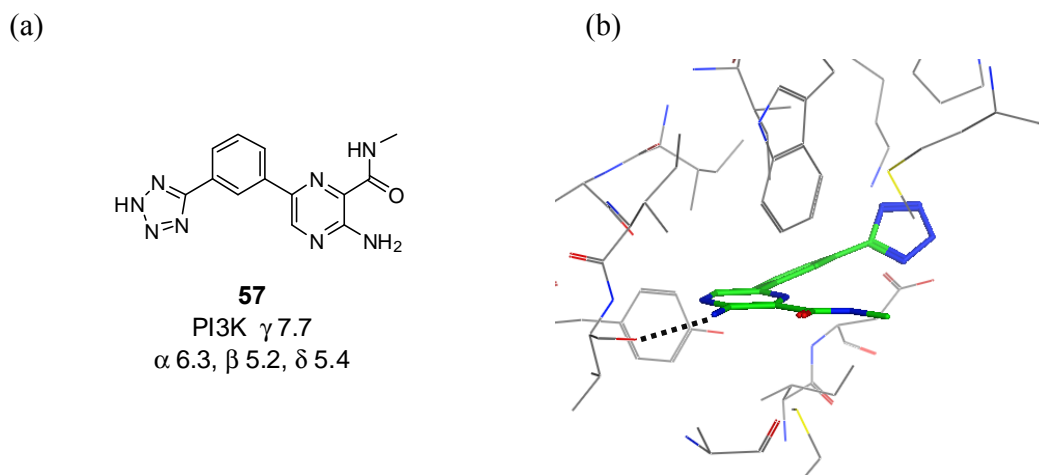


Figure 82: (a) Aminopyrazine **57**; (b) and (c) X-ray crystal structure of aminopyrazine **57** bound to PI3K γ (PDB code 4anu), without protein surface

Whilst further targets were considered for this template, concerns around the physicochemical properties and intellectual property led to a deprioritisation compared with other templates identified from the fragment screening.

4.1.2 Cluster 5

Cluster 5, contained a large number of structures (Table 52), and was therefore subjectively sub-divided into Cluster 5a and 5b, based on small differences in the orientation of the ligands.

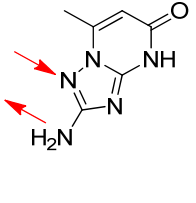
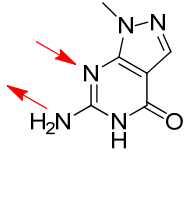
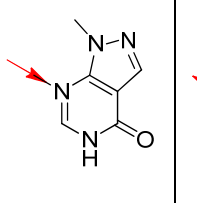
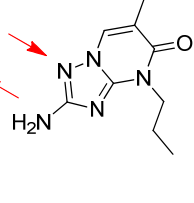
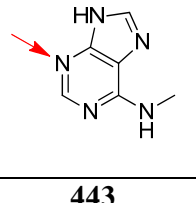
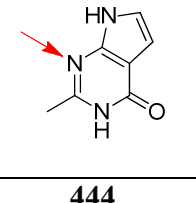
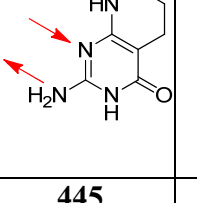
Cluster 5a				
	439	440	441	442
PI3K γ/δ pIC ₅₀	3.8 / <2.8*	3.4* [±] / 3.0*	3.5 / 3.0* [±]	3.5 / <2.8
L.E.	0.43	0.39	0.44	0.32
L.L.E.	0.70	0.65	0.69	0.44
Cluster 5b				
	443	444	445	
PI3K γ/δ pIC ₅₀	3.7 / <2.8*	3.1 / <2.8*	3.6 / 2.9	
L.E.	0.46	0.39	0.41	
L.L.E.	0.48	0.49	0.55	

Table 52: Fragments in Cluster 5a and 5b; H-bonding indicated by red arrows (from donor to acceptor); * indicates $n=1$ data; [±] indicates one value not included in mean as below the threshold of the assay (i.e. pIC₅₀ < 2.8)

Figure 83, shows X-ray crystal structures for Clusters 5a and 5b.⁹⁷ All of the ligands clearly occupy a similar region of space to the adenine of ATP, but the methyl substituents present on the compounds within Cluster 5a (shown with red circles in Figure 83) result in a slight shift of the core away from the hinge relative to the compounds in Cluster 5b. As a consequence of this shift, the vectors available for substitution in the direction of the phosphate pocket also differ (see red arrows in Figure 83). Whilst all four compounds in Cluster 5a have a very similar vector available for substitution, those in Cluster 5b are more diverse.

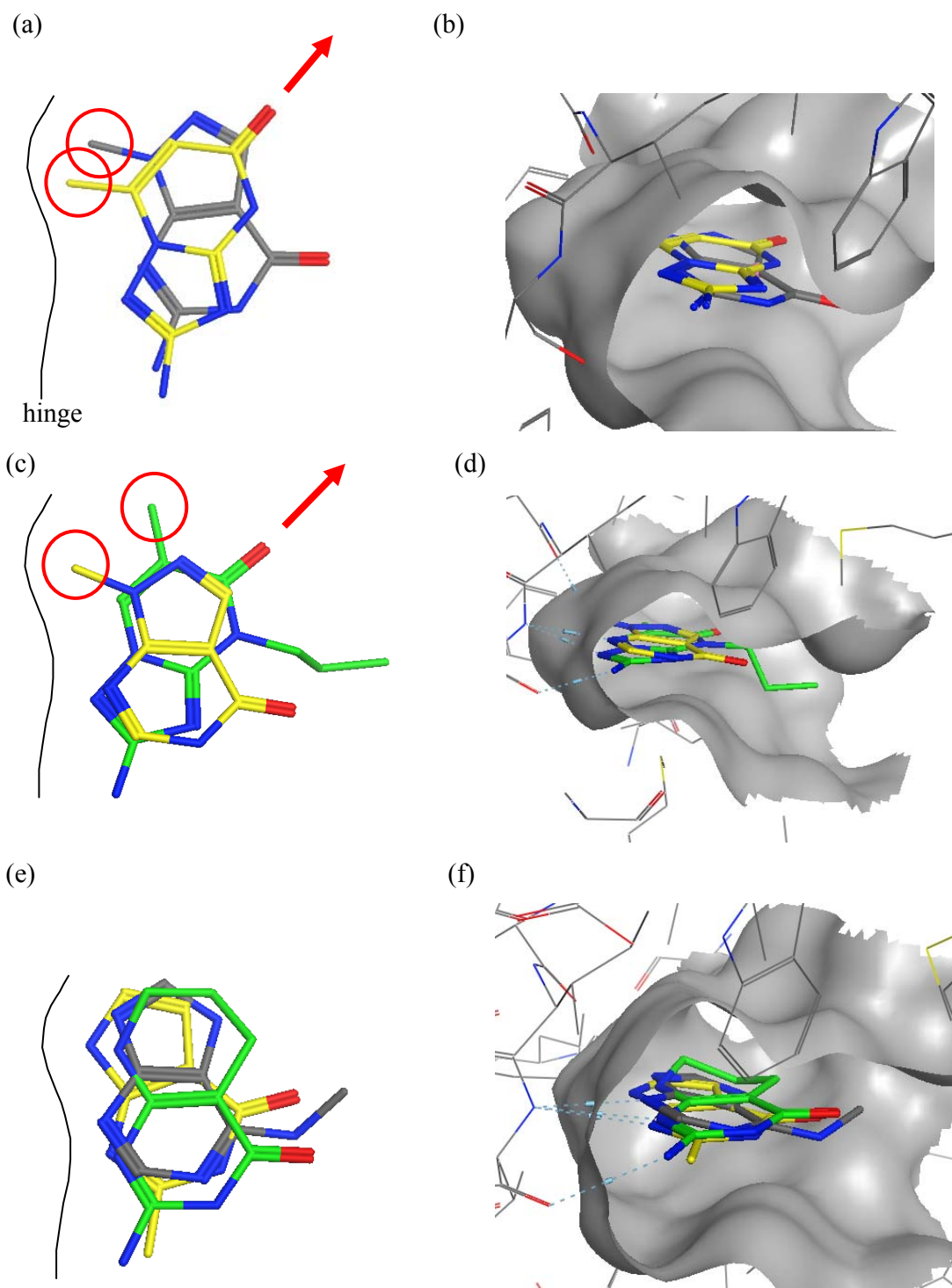


Figure 83: Cluster 5; (a) X-ray crystal structures of ligands **439** (yellow) and **440** (grey) from Cluster 5a in PI3K active site (only a pictorial representation of hinge shown for clarity); (b) X-ray crystal structures of ligands **439** and **440** from Cluster 5a rotated 90°, with protein and partial surface shown; (c) X-ray crystal structures of ligands **441** (yellow), **442** (green) from Cluster 5a in PI3K active site (only a pictorial

representation of the hinges shown for clarity); (d) X-ray crystal structures of ligands **441** and **442** from Cluster 5a rotated 90°, with protein and partial surface shown; (e) X-ray crystal structures of ligands **443** (grey), **444** (yellow) and **445** (green) from Cluster 5b in PI3K γ active site (only a pictorial representation of the hinge shown for clarity); (f) X-ray crystal structures of ligands **443**, **444** and **445** from Cluster 5b rotated 90°, with protein and partial surface shown

Of particular interest from this set were compound **439** from Cluster 5a for its impressive L.E. / L.L.E. profile and compound **445** from Cluster 5b, which demonstrates that saturation can be tolerated in this region.

An overlay of fragment **439** with pyridone **258**⁹⁷ (Figure 84) revealed that the 7-methyl substituent of the triazolopyrimidinone template occupies a similar region of space to the *N*-methyl of the pyridone series, which would be predicted to confer good selectivity over the wider protein kinases for this template. Whilst there is not a direct overlay for the vectors of the 3- and 5-substituents on the pyridone template, it is clear that substitution at the 5-position of the triazolopyrimidinone could enable additional binding interactions to be gained, as this should allow access to the phosphate pocket.

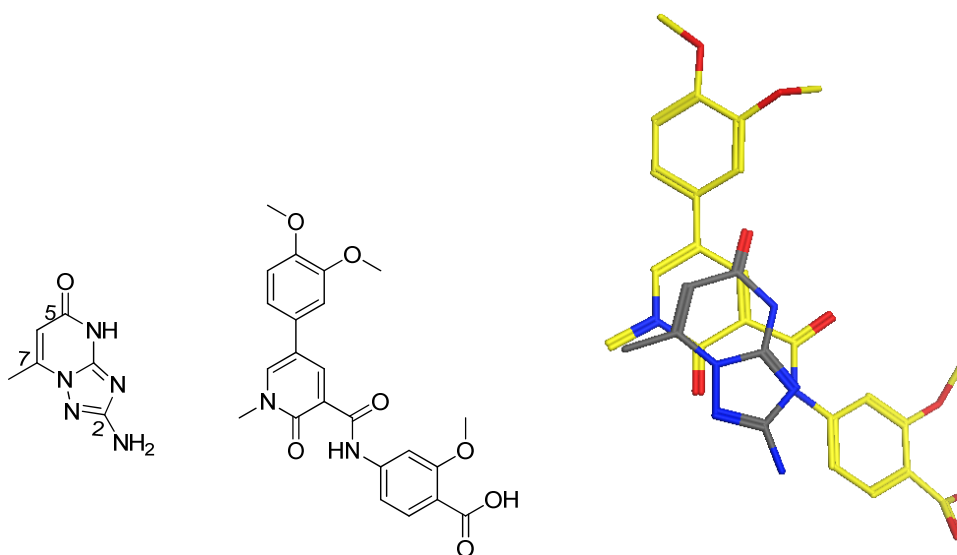


Figure 84: Overlay of X-ray crystal structure of triazolopyrimidinone **439** (grey) and pyridone **258** (yellow)

Based on this observation, initial targets were designed to investigate growth of this fragment towards the phosphate pocket (Figure 85). Direct attachment of an aryl or heteroaryl group would mimic the types of aryl phosphate group preceded in the pyridone series, albeit positioned slightly differently in the protein. The introduction of an *O*- or *N*-linker would probe new chemotypes and may also improve physicochemical properties, and particularly solubility due to a reduction in planarity.

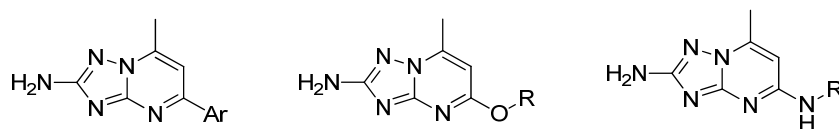
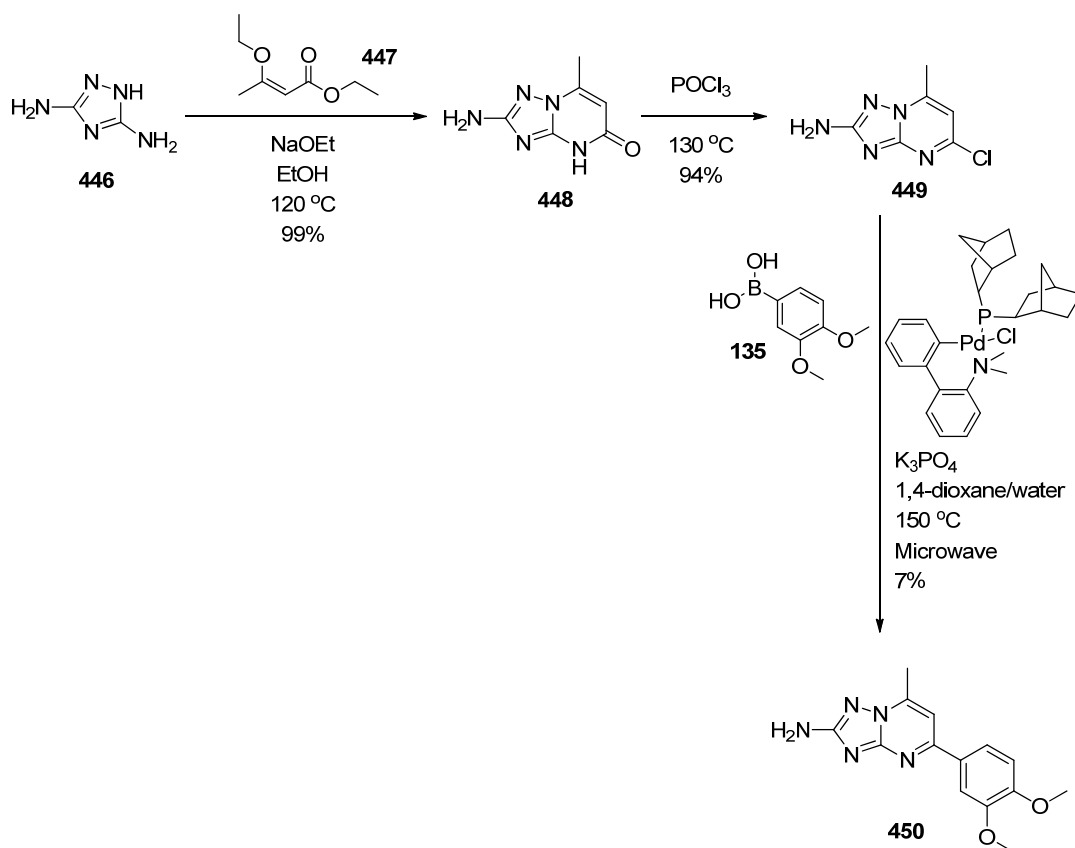


Figure 85: Proposed targets to investigate growing the triazolopyrimidinone fragment

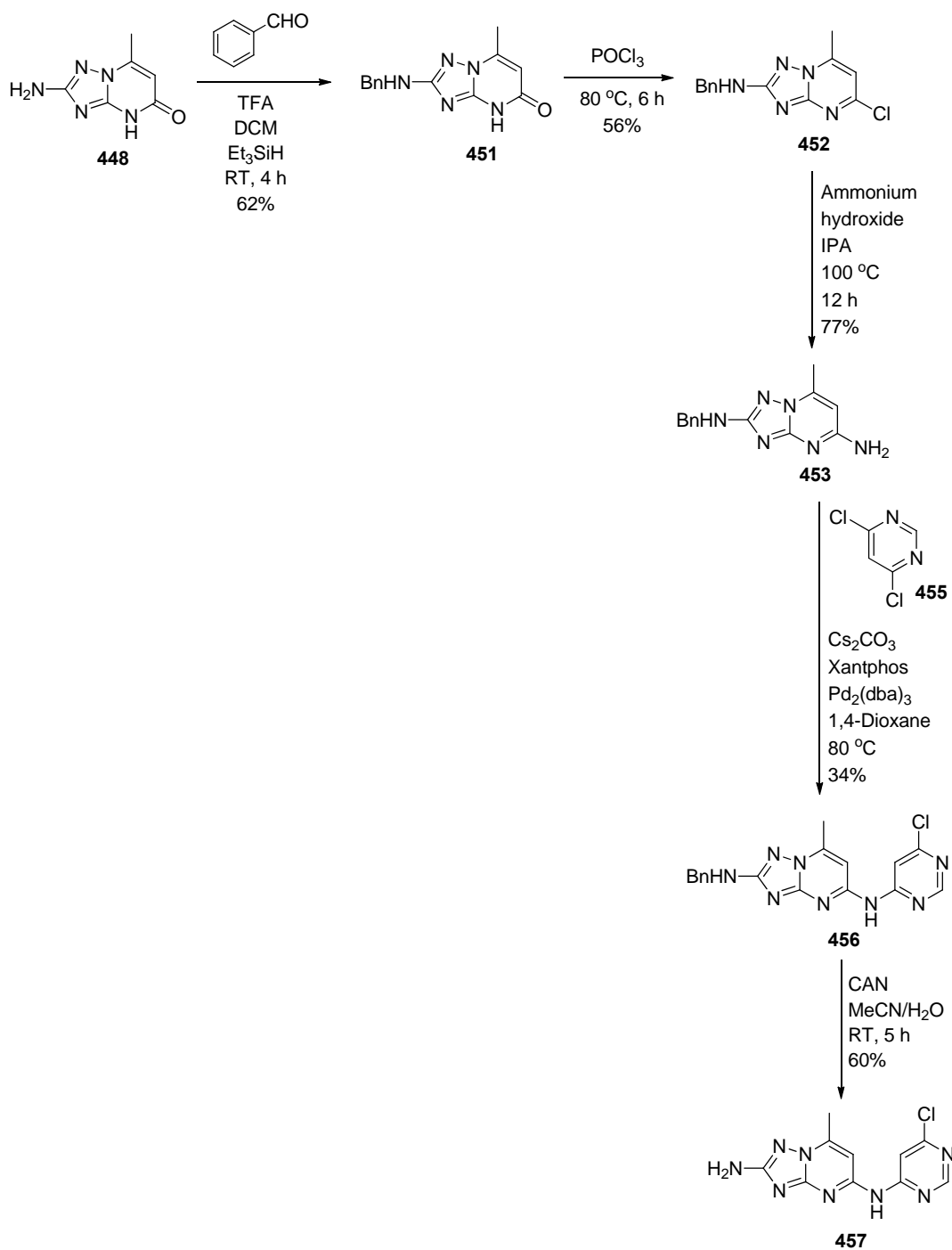
439

The first example was synthesised as shown in Scheme 45. The triazolopyrimidinone intermediate **448** was accessed in one step from commercially available triazole **446** and ethyl 3-ethoxybut-2-enoate **447**, following a procedure described by Williams *et al.* in 1961.¹⁹⁷ Literature precedent for the formation of this ring system is sparse, however this methodology furnished the desired product in good yield. The regiochemistry was confirmed by ¹⁵N NMR spectroscopy, with a key HMBC correlation between the bridgehead nitrogen and the methyl group protons. Subsequent chlorination of the pyrimidinone, followed by Suzuki coupling with the commercially available boronic acid, gave the desired product **450**. Although the yield for the Suzuki reaction was poor, sufficient material was isolated for biological testing, so the chemistry was not further optimised at this stage. The dimethoxyphenyl boronic acid was chosen to allow comparison with the pyridone series.

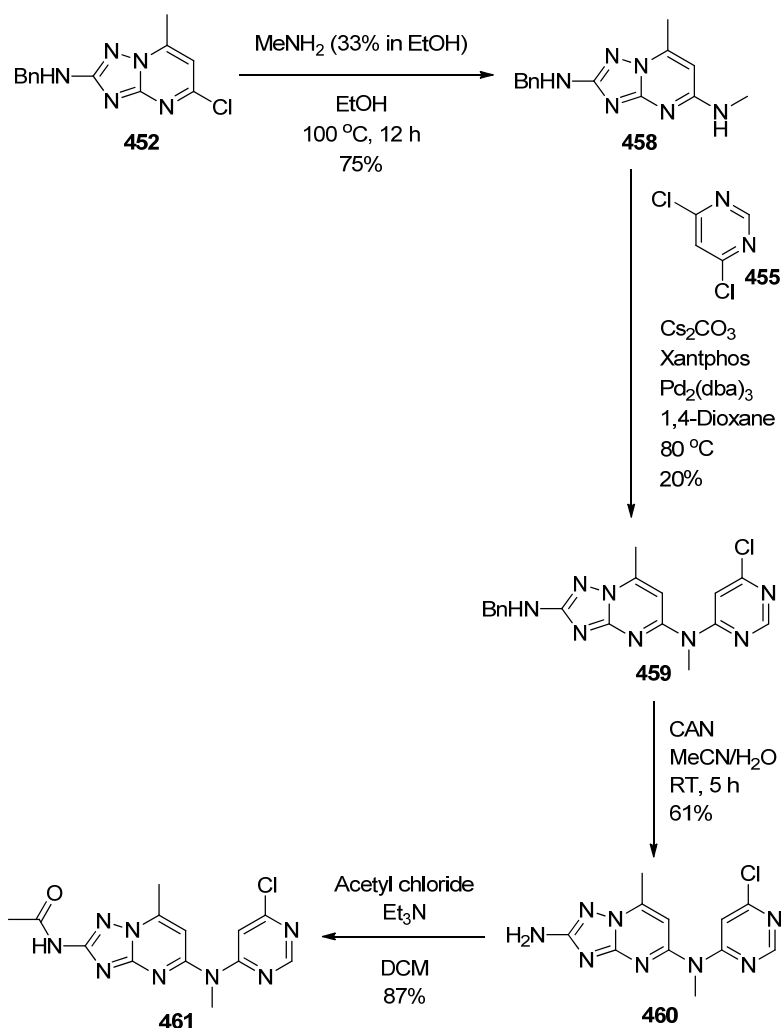


Scheme 45: Synthesis of triazolopyrimidine analogue

Additional *N*-linked targets were outsourced,¹⁶⁹ as shown in Scheme 46 and Scheme 47. The common intermediate **448** was benzyl protected then chlorinated as before. Nucleophilic aromatic substitution (S_NAr) with the relevant amines, gave intermediates **453** and **458** in good yield, which were further functionalised by Buchwald coupling. The dichloropyrimidine motif was chosen based on SAR from another PI3K γ inhibitor template not described in this thesis. Finally, benzyl deprotection and, where appropriate, acetylation gave the target compounds **457**, **460** and **461**.



Scheme 46: Synthesis of N-linked analogues



Scheme 47: Synthesis of further *N*-linked targets

Biological data for all of the triazolopyrimidine targets are shown in Table 53. The dimethoxyphenyl analogue **450** shows an excellent improvement in potency over the hit fragment **439**, with very good L.E. and L.L.E., although no significant selectivity over the δ isoform is observed. Conversely, data on the *N*-linked examples **457**, **460** and **461** are disappointing, with no activity observed at the concentrations screened.

Whilst analogue **450** provided evidence that this template could be grown in a ligand efficient manner, there remained some concerns around the differentiation of the physicochemical profile of this template, from those previously described in Chapters 2 & 3. In particular the presence of three aromatic rings, in an arrangement that leads to a

completely planar molecule, was particularly undesirable. As such work on this template was deprioritised.

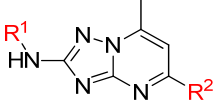
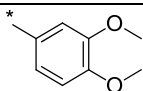
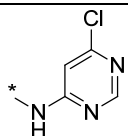
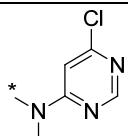
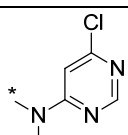
Compound No.			PI3K γ / δ pIC50	L.E.	L.L.E.
	R ¹	R ²			
439	H	O	3.8 / <2.8	0.43	0.70
450	H		6.5* / 5.8	0.42	0.43
457	H		<4.5* / <4.5*	-	-
460	H		<4.5* / <4.5*	-	-
461	Ac		<4.5* / <4.5*	-	-

Table 53: Data on novel triazolopyrimidine analogues; * indicates n=1 data

4.2 Conclusions

Fragment screening of FBDD1 identified a range of novel chemotypes as PI3K γ inhibitors. Initial work on exemplars from Clusters 4 and 5a rapidly led to the deprioritisation of these templates, but there was also a broader concern over the diversity of chemotypes which had been identified as hits. The key aim of this initiative was to identify some novel PI3K γ inhibitor classes with differentiated physicochemical profiles with respect to those previously investigated. Whilst all of the hits were low MW and low lipophilicity (a pre-requisite of all molecules within FBDD1), the majority contained two (often fused) aromatic rings. Whilst this is not unacceptable for a lead compound which is close to delivering the desired biological profile, at such an early

stage in the discovery process, and with such a large increase in potency still required, this led to concern over the predicted profile of more highly elaborated molecules. Those fragments which did not fall into this category (e.g. aminothiazole in Cluster 5a) had other issues, such as novelty.

With this lack of diversity in mind, the methods used to select fragments for screening and progression were re-evaluated. In particular, the use of PI3K γ/δ selectivity in the biochemical assay as a filter for progression to the biophysical screen significantly biased the chemotypes exemplified. Secondly, there was concern over whether FBDD1 contained sufficient representation of the chemotypes which were of particular interest. Consideration was therefore given to the design of a second fragment screen which could address these issues.

4.3 Follow-up Fragment Screen

Of particular interest for a second fragment screen, was the identification of aliphatic hinge binders, which are well precendented in the PI3K literature (Figure 86). A small, ligand efficient, non-aromatic hinge-binding fragment would be expected to deliver fully grown ligands with improved physicochemical properties to those proprietary compounds described in Chapters 2 and 3. These types of hinge binder would also be expected to provide good selectivity over the wider protein kinome, where saturated hinge binders are not well exemplified.

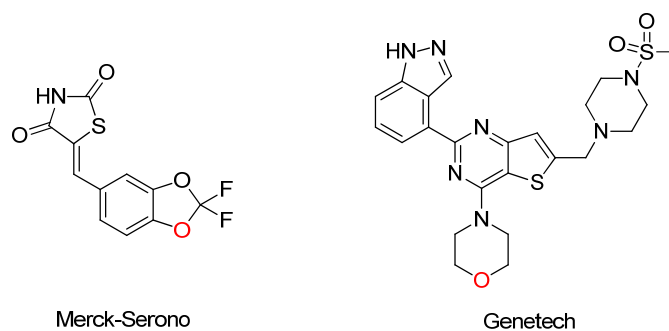


Figure 86: Literature examples of saturated hinge binders in PI3K inhibitors; atoms in red are H-bond acceptors which interact with the hinge

Analysis of FBDD1 revealed that whilst fragments containing saturated H-bond acceptor groups were exemplified, only 14% of the set were aliphatic compounds and there was also a large percentage of undesirable chemotypes (e.g. 30% of the molecules contained ≥ 2 aromatic rings). The design of a bespoke fragment set, specifically targeting saturated or semi-saturated lipid kinase hinge binders was therefore proposed.

Whilst saturated rings containing ether oxygens are the most common aliphatic hinge binder exemplified in the PI3K literature, in designing a bespoke fragment set consideration was also given to other, more novel, saturated hinge binders (Figure 87).

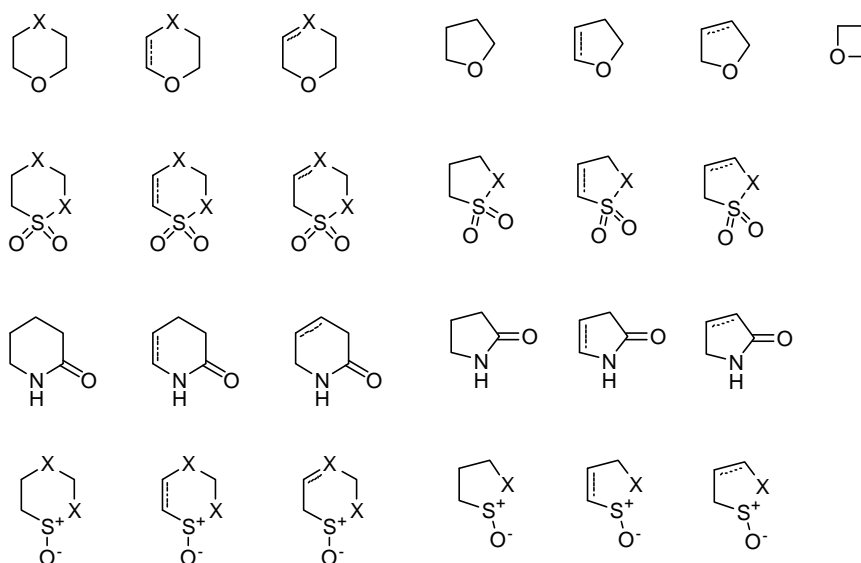


Figure 87: Chemotypes of interest containing aliphatic H-bond acceptor functionality

In order to identify fragments of interest from the GSK compound collection, a SMARTS query was written¹⁹⁸ to identify only compounds which contained an aliphatic H-bond acceptor group of the type shown in Figure 87. This query was used to search the GSK compound collection, with the following additional filters then applied:

- Solid sample availability > 30 mg (to enable creation of a DMSO solution at sufficient concentration for screening)
- Aromatic rings ≤ 2
- Heavy atom count 8-18
- cLogP ≤ 2

- GSK reactivity filters (designed to remove compounds with reactive functionality e.g. isocyanate)

This process identified approximately 5000 compounds with the desired profile, which then required further filtering to give a suitable number for screening. In order to identify the best method to do this, a random test set of 460 compounds were taken forward to the high concentration biochemical and STD NMR biophysical assays (as described for the first fragment effort). By collecting data on a representative subset, it was envisaged that information relating to hit rates from the assays and X-ray crystallography could be used to further optimise this process for the larger set. Hits from either screening assay were progressed to X-ray crystallography and from 67 compounds, 14 X-ray crystal structures of varying resolution (2.3 to 3 Å) were obtained.¹⁹⁹

Analysing the successful structures and associated biochemical/biophysical data identified several learnings which could be applied to the wider compound set:²⁰⁰

- Further filtering of the compound set based on chemical structure was necessary, as some undesirable structures were still present despite original refinement based on physicochemical parameters
- None of the hit compounds containing 2 aromatic rings were considered of interest, so this filter was reduced to ≤ 1 aromatic ring for the wider set
- Very few of the compounds with 0 aromatic rings showed activity in the biochemical assay at the concentrations tested, possibly due to their lower MW. However from the hits from the STD NMR assay (16 compounds with 0 aromatic rings), 3 X-ray crystal structures were successfully obtained. For compounds with 0 aromatic rings, only biophysical screening data would be decision making for progression to X-ray crystallography for the larger set
- For compounds which did contain aromatic rings, activity in both the biochemical and biophysical assays correlated with success in crystallography

The approximately 4500 remaining compounds from the original search were filtered further to remove any compounds containing 2 aromatic rings. The surviving compounds were then clustered based on a Tanimoto similarity method and each cluster

sent *via* an electronic survey¹⁹⁸ to a group of 7 chemists for review. These chemists were asked to comment on the structure of each molecule in very simple terms (like, dislike, neutral) and the opinions were combined to rank the most promising fragments from each cluster. This process identified a further 1060 compounds (600 with 0 aromatic rings and 460 with 1 aromatic rings) for screening. The biochemical and biophysical screening was carried out, applying the learnings from the test set, and 62 compounds were selected for progression to X-ray crystallography (21 compounds with 1 aromatic ring which were active in both the biochemical and biophysical assay and 41 compounds with 0 aromatic rings which were active in the biophysical assay). Crystal structures of 10 compounds were successfully obtained¹⁹⁹ giving an overall total of 24 compounds with known binding modes from this second effort (Figure 88).

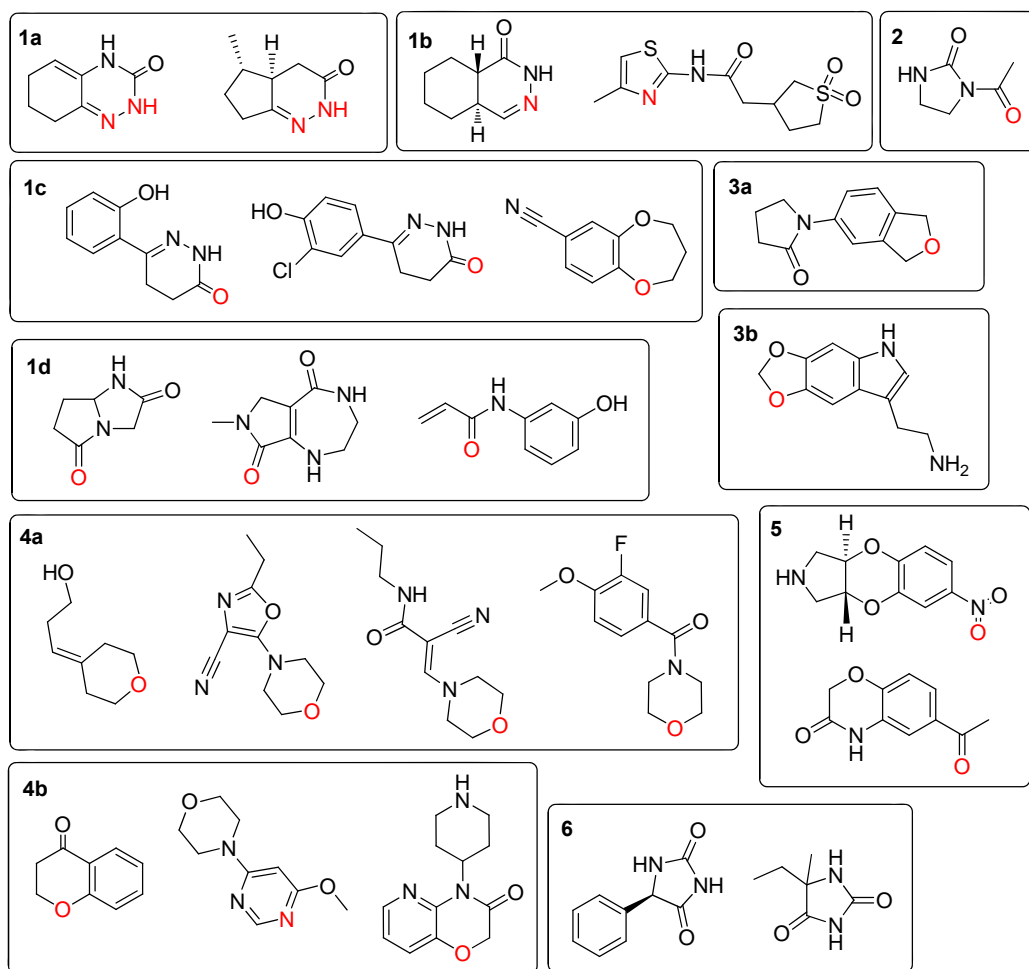


Figure 88: Structures of fragment hits for which X-ray crystal structures were successfully obtained; for those binding in the ATP site the hinge binding atom is marked in red

These 24 compounds were then clustered in a similar fashion to the original fragment effort, based on the binding site and vectors available for growth.²⁰¹ The compounds contained in clusters 1-5 all bind in the ATP site, whilst the two ligands in cluster 6 bind in different regions of the protein. A range of different hinge binding groups were identified (see Figure 88, atoms marked in red) and whilst ethers were the most common H-bond acceptor, other functionalities were also identified e.g. carbonyls. One compound in cluster 5 even has a nitro group forming the hinge interaction; whilst this is interesting as a novel hinge binding motif, it is not generally progressable in a drug molecule due to the toxicology associated with this functionality.

Comparison of the hit structures with those from the previous fragment screening effort shows marked differentiation; designing and screening a bespoke set successfully delivered small, saturated and semi-saturated hinge binders as tractable starting points for fragment-based drug discovery of a PI3K γ inhibitor. Of particular interest were the hits which introduce non-planar functionality at the hinge region (for example compounds **462**, **463** and **464** shown in Figure 89).

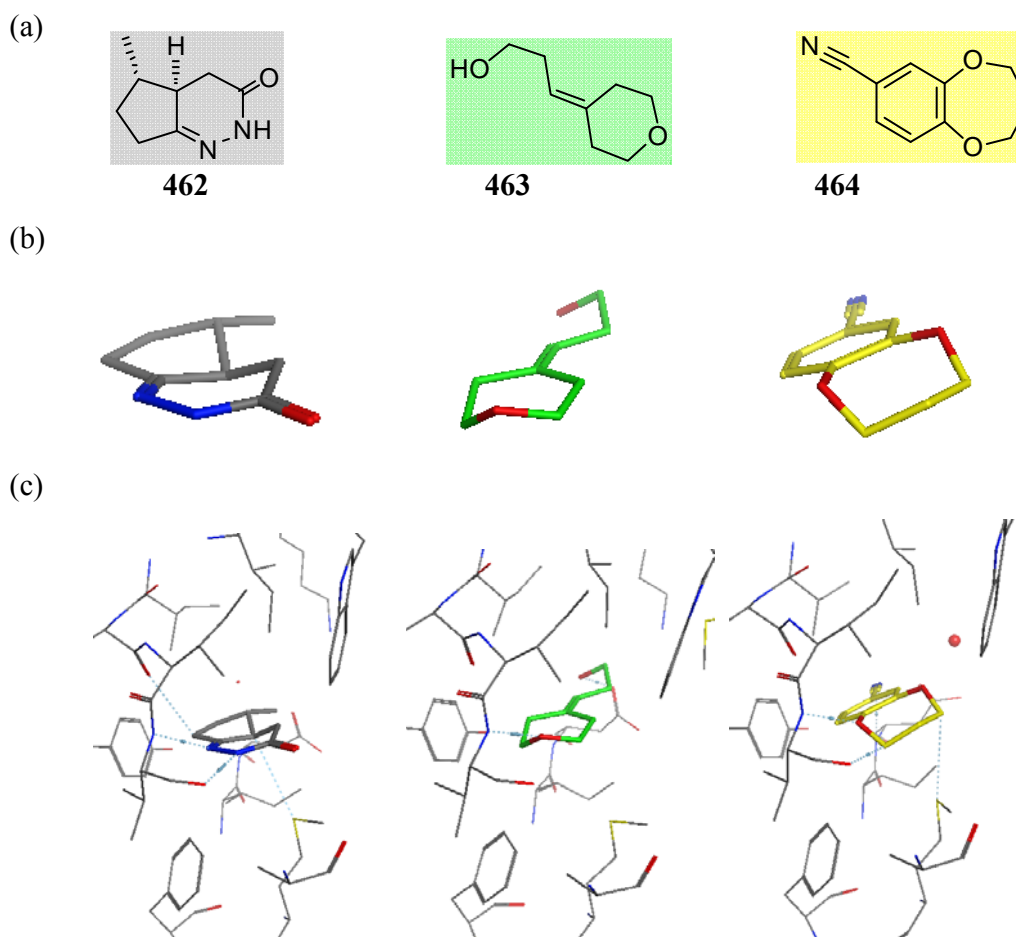


Figure 89: (a) Example non-planar hits; (b) X-ray structures of example hits (no protein shown for clarity)¹⁹⁹; (c) X-ray crystal structures of example non-planar hits

To understand whether this success was driven by the design of a bespoke fragment set, or the altered screening process compared with the first effort, the composition of the screening sets were analysed (Figure 90).

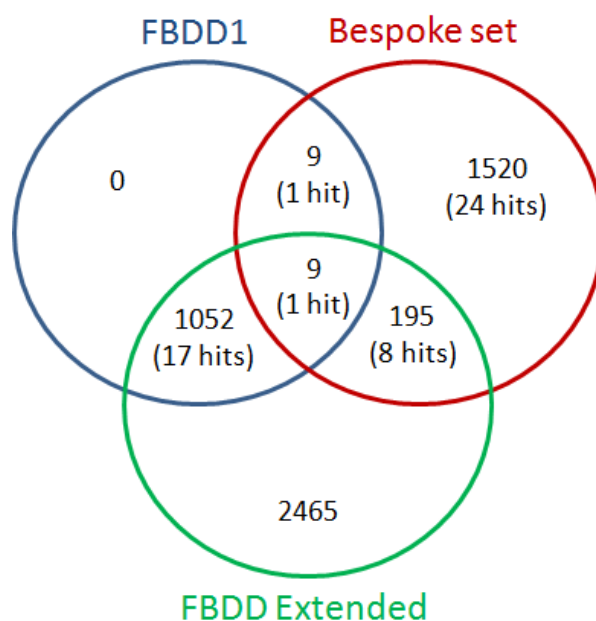


Figure 90: Analysis of compound numbers in each screening set and overlap between sets; bracketed numbers show hits (i.e. compounds identified by screening for which an X-ray crystal structures were successfully obtained)

The overlap between FBDD1 and the bespoke set was small, which was reflected in only 1 hit compound being identified by both fragment screening efforts. Even if FBDD1 had been screened biophysically in its entirety in the first effort, the majority of the hits from the second screen would still not have been identified, as they were not present in the FBDD1 collection. It is however possible, that different hits (still with desirable physicochemical profiles) may have been found. Based on the learnings from this second screen, selecting compounds for progression based on their biochemical selectivity profile alone (as occurred in the first fragment effort), is likely to have removed many compounds with no aromatic rings, which do not show robust activity in this assay.

Comparison of the bespoke set with a second extended GSK fragment set (FBDD Extended) is also shown (Figure 90); FBDD Extended is a larger fragment set containing an additional 1412 compounds to FBDD1. This set is often mined after an initial fragment screen against FBDD1 is run. The overlap between FBDD Extended and the bespoke set is larger than for FBDD1, although still low; an additional 7 of the hits from the bespoke set would have been identified by screening FBDD Extended. This leaves a

total of 16 novel fragments identified from the bespoke set. Without re-screening the remainder of FBDD1 in the biophysical assay it is hard to draw firm conclusions, but the high percentage of hits from this second screen which are only present in the bespoke set (67 %), suggests the custom design of a fragment set, specifically targeting chemotypes of interest for this biological target, played a significant role in the successful outcome of this screen.

Another contrast between the outputs from the two fragment screens is the identification of non-ATP site binders from the second initiative. In addition to the 2 compounds in cluster 6 which bind solely away from the ATP site, there were also a further 4 fragments which bound in additional sites to the ATP binding site. This may reflect the complementarity of other binding sites with the non-planar chemotypes exemplified in the second screen, or may simply reflect the greater absolute number of hits from the second screen giving a greater chance of identifying non-ATP binders (24 vs. 14 X-ray crystal structures obtained). Either way, prosecution of a non-ATP competitive ligand would first rely on proving that binding at an alternative site still led to functional inhibition of the enzyme.

4.4 Conclusions and Future Work

The design and screening of a bespoke lipid kinase hinge binder fragment set has successfully identified a variety of saturated and semi-saturated fragments as starting points for the discovery of a PI3K γ selective inhibitor. Both the custom selection of compounds for screening and the careful interpretation of the biochemical and biophysical data have delivered a significantly different output from initial attempts at a fragment-based approach for this programme. These new hits provide exciting starting points for the discovery of PI3K γ inhibitors with improved physicochemical properties over those previously reported.

Future work in this area will be initially based around sub-structure searching each of the hits to confirm activity and investigate the effect of small structural changes. Subsequent prioritisation of clusters based on prior knowledge, biochemical

activity/ligand efficiencies and chemical tractabilities will then be required to select the preferred templates for active chemistry.

5.0 EXPERIMENTAL

5.1 General Methods

All solvents were of analytical grade, purchased from Sigma-Aldrich in anhydrous form.

Unless otherwise stated, reagents were purchased from regular suppliers such as Sigma-Aldrich and Fluorochem and used without further purification.

Microwave reactions were carried out in a Biotage Initiator set to high absorption, using the conditions stated in each full experimental.

Melting points were determined on a Stuart SMP40 melting point apparatus. Values are quoted to the nearest degree Celsius.

Infrared spectra were recorded on a Perkin Elmer Spectrum One Fourier Transform spectrometer, with samples as solids. Only selected absorptions are reported and quoted in reciprocal centimetres (cm^{-1}).

¹H NMR were recorded on a Bruker AVI (400 MHz), Bruker Nano (400 MHz) or Bruker AVII+ (600 MHz) spectrometer. Chemical shifts (δ_{H}) are quoted in ppm relative to tetramethylsilane and are internally referenced to the residual solvent peak. Coupling constants (J) are given in Hz to the nearest 0.05 Hz (although are only accurate to +/- 0.5 Hz). The following abbreviations are used: s, singlet; d, doublet; t, triplet; q, quartet; dd, doublet doublet; m, multiplet; and br., broad.

¹³C NMR were recorded on a Bruker AVI (400 MHz) or Bruker AVII+ (600 MHz) spectrometer. Chemical shifts (δ_{C}) are quoted in ppm referenced relative to the residual solvent peak.

³¹P NMR were recorded on a Bruker Nano (400 MHz). Chemical shifts (δ_{P}) are quoted in ppm and are nominally referenced relative to phosphoric acid.

^{15}N NMR were recorded on a Bruker AVII+ (600 MHz) spectrometer. Chemical shifts (δ_{N} , measured from the HMBC) are quoted in ppm and are nominally referenced relative to liquid ammonia.

LCMS Method A: The HPLC analysis was conducted on an Acquity UPLC BEH C₁₈ column (1.7 μm , 2.1 mm x 50 mm) at 40 °C.

Solvent A = 0.1% v/v Formic Acid in water

Solvent B = 0.1% v/v Formic acid in acetonitrile

The gradient employed was:

Time (min)	Flow Rate (ml/min)	% A	% B
0	1	97	3
1.5	1	0	100
1.9	1	0	100
2	1	97	3

The UV detection was based on an averaged signal from wavelength of 210 nm to 350 nm and mass spectra were recorded on a mass spectrometer using alternate-scan positive and negative mode electrospray ionization.

LCMS Method B: The HPLC analysis was conducted on a Sunfire C18 column (30 mm, 4.6 mm x 3.5 μm packing diameter) at 30 °C.

Solvent A = 0.1% v/v solution of Formic Acid in Water.

Solvent B = 0.1% v/v solution of Formic Acid in Acetonitrile.

The gradient employed was:

Time (min)	Flow Rate (ml/min)	% A	% B
0	3	97	3
0.1	3	97	3
4.2	3	0	100
4.8	3	0	100
4.9	3	97	3
5.0	3	97	3

The UV detection was based on an averaged signal from wavelength of 210 nm to 350 nm and mass spectra were recorded on a mass spectrometer using alternate-scan positive and negative mode electrospray ionization.

LCMS Method C: The HPLC analysis was conducted on an Acquity UPLC BEH C₁₈ column (1.7 μm, 2.1 mm x 50 mm) at 40 °C.

Solvent A = 0.1% v/v Trifluoroacetic acid in water

Solvent B = 0.1% v/v Trifluoroacetic acid in acetonitrile

The gradient employed was:

Time (min)	Flow Rate (ml/min)	% A	% B
0	1	97	3
1.5	1	0	100
1.9	1	0	100
2	1	97	3

The UV detection was based on an averaged signal from wavelength of 210 nm to 350 nm and mass spectra were recorded on a mass spectrometer using alternate-scan positive and negative mode electrospray ionization.

LCMS Method D: The HPLC analysis was conducted on an Acquity UPLC BEH C₁₈ column (1.7 μm, 2.1 mm x 50 mm) at 40 °C.

Solvent A = 10 mM Ammonium Bicarbonate in water adjusted to pH 10 with Ammonia solution

Solvent B = Acetonitrile

The gradient employed was:

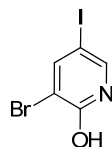
Time (min)	Flow Rate (ml/min)	% A	% B
0	1	93	1
1.5	1	3	97
1.9	1	3	97
2	1	0	100

The UV detection was based on an averaged signal from wavelength of 210 nm to 350 nm and mass spectra were recorded on a mass spectrometer using alternate-scan positive and negative mode electrospray ionization.

High resolution mass spectra were recorded using a Micromass Q-ToF Ultima hybrid quadrupole time-of-flight mass spectrometer equipped with a Z-spray (ESI) interface, over a mass range of 100 – 1100 Da, with a scan time of 0.9 s and an interscan delay of 0.1 s. Reserpine was used as the external mass calibrant ($[M+H]^+ = 609.2812$ Da). The Q-ToF Ultima mass spectrometer was operated in W reflectron mode to give a resolution (FWHM) of 16000-20000. Ionisation was achieved with a spray voltage of 3.2 kV, a cone voltage of 100 V, with cone and desolvation gas flows of 10-20 and 600 L/h, respectively. The source block and desolvation temperatures were maintained at 120 °C and 250 °C, respectively. The elemental composition was calculated using MassLynx v4.1 for the $[M+H]^+$. Mass errors were all <5 ppm.

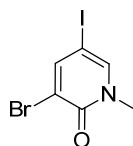
5.2 Preparative Procedures

3-Bromo-5-iodo-2(1H)-pyridinone **86**¹⁴⁴



3-Bromo-2(1H)-pyridinone **85** (5.0 g, 29 mmol) and *N*-iodosuccinimide (6.47 g, 284 mmol) were dissolved in acetonitrile (100 mL) and heated to 80 °C for 4 h. The reaction mixture was allowed to cool to RT and left standing overnight. The cream precipitate was filtered, washed with acetonitrile then dried under vacuum at 50 °C for 18 h to give the title compound (7.08 g, 82%) as a beige solid; m.p. 237-240 °C (lit., 243-244 °C); ¹⁴⁴1H NMR (400 MHz, DMSO-*d*₆) δ ppm 7.72 (d, *J*=2.3 Hz, 1 H), 8.09 (d, *J*=2.3 Hz, 1 H), 12.31 (br. s, 1 H); LCMS (Method A): MH⁺ 300/302, Rt 0.67 min, 93% by UV.

3-Bromo-5-iodo-1-methyl-2(1H)-pyridinone **87**

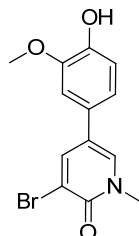


3-Bromo-5-iodo-2(1H)-pyridinone **86** (5.57 g, 18.6 mmol) and potassium carbonate (5.13 g, 37.1 mmol) were suspended in *N,N*-dimethylformamide (35 mL) and stirred at RT for 15 min. Methyl iodide (1.23 mL, 20.4 mmol) in *N,N*-dimethylformamide (35 mL) was added dropwise over ~10 min (exotherm), then the reaction was left stirring at RT for 2 h. The reaction mixture was quenched by the addition of aqueous NaOH (2 N, 40 mL) then extracted with ethyl acetate (40 mL). A solid formed between the layers which was filtered and dried in a vacuum oven at 50 °C overnight.

The remaining layers were separated and the aqueous phase extracted with further ethyl acetate (40 mL). The combined organic extracts were dried over anhydrous sodium sulfate, filtered, concentrated *in vacuo*, and combined with the previous material to give the title compound (5.71 g, 98%) as a cream solid; m.p. 207-208 °C; ¹H NMR (400 MHz, DMSO-*d*₆) δ ppm 3.46 (s, 3 H), 8.09 (d, *J*=2.3 Hz, 1 H), 8.11 (d, *J*=2.3 Hz,

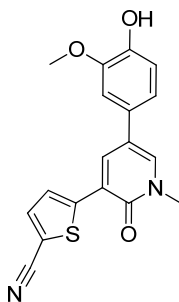
1 H); ^{13}C NMR (100 MHz, DMSO- d_6) δ ppm 38.7, 63.5, 115.8, 144.7, 148.3, 157.6; LCMS (Method A): $\text{MH}^+ = 314/316$, Rt 0.75 min, 89% by UV.

3-Bromo-5-(4-hydroxy-3-methoxyphenyl)-1-methylpyridin-2(1H)-one **89**



2-(Methoxy)-4-(4,4,5,5-tetramethyl-1,3,2-dioxaborolan-2-yl)phenol **88** (Sigma-Aldrich, 2.57 g, 10.3 mmol), 3-bromo-5-iodo-1-methyl-2(1H)-pyridinone **87** (3.22 g, 10.3 mmol) and $\text{Pd}(\text{Ph}_3\text{P})_4$ (1.19 g, 1.03 mmol) were suspended in *N,N*-dimethylformamide (15 mL) and aqueous potassium carbonate (2 M, 10.3 ml, 20.5 mmol) added. The reaction mixture was heated under microwave irradiation to 100 °C for 30 min, then concentrated *in vacuo* to give a brown solid (13 g). The solid was loaded in DMSO onto a C_{18} SPE cartridge (20 g) and eluted with acetonitrile (3 column volumes). The eluent was concentrated *in vacuo* and the residue purified by reverse phase column chromatography using a gradient of 5-55%, 0.1% HCOOH in acetonitrile / 0.1% HCOOH in water. The appropriate fractions were combined and concentrated *in vacuo* to give the title compound (1.80 g, 57%) as a brown solid; $\nu_{\text{max}}/\text{cm}^{-1}$ (solid) 3088 (OH), 1649 (C=O); ^1H NMR (400 MHz, DMSO- d_6) δ ppm 3.57 (s, 3 H), 3.84 (s, 3 H), 6.79 (d, $J=8.1$ Hz, 1 H), 6.98 (dd, $J=8.2, 2.1$ Hz, 1 H), 7.12 (d, $J=2.3$ Hz, 1 H), 8.11 (d, $J=2.5$ Hz, 1 H), 8.28 (d, $J=2.5$ Hz, 1 H), 9.10 (s, 1 H); ^{13}C NMR (100 MHz, DMSO- d_6) δ ppm 38.4, 55.8, 109.9, 114.6, 115.8, 118.0, 118.6, 126.2, 136.0, 140.7, 146.0, 148.0, 157.3; LCMS (Method A): $\text{MH}^+ 310/312$, Rt 0.70 min, 100% by UV; HRMS exact mass calculated for $[\text{M}+\text{H}]^+$ ($\text{C}_{13}\text{H}_{13}^{79}\text{BrNO}_3$) requires m/z 310.0079, found 310.0083.

5-{5-[4-Hydroxy-3-(methoxy)phenyl]-1-methyl-2-oxo-1,2-dihydro-3-pyridinyl}-2-thiophenecarbonitrile **91**

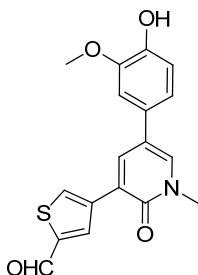


Typical Procedure A:

3-Bromo-5-[4-hydroxy-3-(methoxy)phenyl]-1-methyl-2(1*H*)-pyridinone **89** (31 mg, 0.10 mmol), (5-cyano-2-thienyl)boronic acid **90** (Anichem, 23 mg, 0.15 mmol), PdCl₂(dppf) (3.0 mg, 4.1 μmol) and cesium acetate (48 mg, 0.25 mmol) were combined in tetrahydrofuran (1 mL). The resultant solution was heated under microwave irradiation at 100°C for 30 min. Additional (5-cyano-2-thienyl)boronic acid **90** (23 mg, 0.15 mmol), PdCl₂(dppf) (3.0 mg, 4.1 μmol) and cesium acetate (48 mg, 0.25 mmol) were added and the reaction mixture heated under microwave irradiation at 100 °C for a further 20 min. The reaction mixture was loaded directly onto a C₁₈ SPE cartridge (500 mg) which had been preconditioned with 0.1% TFA/acetonitrile. The column was eluted with 0.1% TFA/acetonitrile (2 column volumes) and the eluent concentrated. The residue was purified by Mass Directed AutoPrep on a Sunfire C18 column using acetonitrile/water with a formic acid modifier. The desired fractions were concentrated to give the title compound (11.2 mg, 30%) as a white solid; m.p. 239-242 °C; $\nu_{\max}/\text{cm}^{-1}$ (solid) 3341 (OH), 2206 (CN), 1640 (C=O); ¹H NMR (400 MHz, DMSO-*d*₆) δ ppm 3.69 (s, 3 H), 3.87 (s, 3 H), 6.85 (d, *J*=8.1 Hz, 1 H), 7.13 (dd, *J*=8.1, 1.5 Hz, 1 H), 7.23 (d, *J*=1.5 Hz, 1 H), 7.95 (d, *J*=4.0 Hz, 1 H), 8.12 (d, *J*=4.3 Hz, 1 H), 8.25 (d, *J*=2.0 Hz, 1 H), 8.64 (d, *J*=2.0 Hz, 1 H), 9.15 (br. s, 1 H); ¹³C NMR (100 MHz, DMSO-*d*₆) δ 37.9, 55.9, 91.1, 107.9, 110.4, 115.8, 118.6, 119.3, 120.5, 124.4, 126.7, 134.3, 136.8, 137.3, 144.3, 146.3, 148.0, 158.5; LCMS (Method A): MH⁺ 339, Rt 0.91 min, 100% by UV; HRMS exact mass calculated for [M+H]⁺ (C₁₈H₁₅N₂O₃S) requires *m/z* 339.0803, found 339.0800.

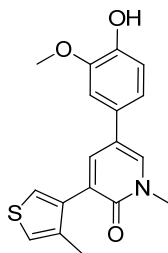
The following experiments were performed using Typical Procedure A, the data are reported as (a) boronate (supplier, g, mmol) x 2; (b) product (mg, % yield).

4-{5-[4-Hydroxy-3-(methoxy)phenyl]-1-methyl-2-oxo-1,2-dihydro-3-pyridinyl}-2-thiophenecarbaldehyde 202



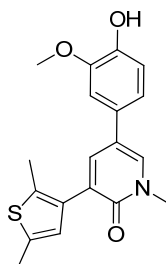
(a) (5-Formyl-3-thienyl)boronic acid **92**, Frontier Scientific Europe, 23 mg, 0.15 mmol; (b) 5.4 mg, 14%; $^1\text{H NMR}$ (600 MHz, $\text{DMSO-}d_6$) δ ppm 3.62 (s, 3 H), 3.87 (s, 3 H), 6.84 (d, $J=7.9$ Hz, 1 H), 7.09 (dd, $J=8.3$, 1.9 Hz, 1 H), 7.21 (d, $J=1.5$ Hz, 1 H), 8.11 (d, $J=2.3$ Hz, 1 H), 8.27 (d, $J=2.6$ Hz, 1 H), 8.7-8.77 (m, 1 H), 8.88-8.90 (m, 1 H), 9.10 (br. s, 1 H), 9.99 (s, 1 H); LCMS (Method A): MH^+ 342, Rt 0.82 min, 99% by UV.

5-[4-Hydroxy-3-(methoxy)phenyl]-1-methyl-3-(4-methyl-3-thienyl)-2(1H)-pyridinone 203



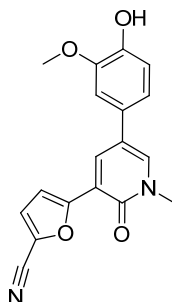
(a) (4-Methyl-3-thienyl)boronic acid **93**, Sigma-Aldrich, 21 mg, 0.15 mmol; (b) 1.3 mg, 4%; $^1\text{H NMR}$ (600 MHz, $\text{DMSO-}d_6$) δ ppm 2.15 (s, 3 H), 3.56 (s, 3 H), 3.83 (s, 3 H), 6.80 (d, $J=8.3$ Hz, 1 H), 6.99 (dd, $J=8.3$, 1.9 Hz, 1 H), 7.13 (d, $J=1.5$ Hz, 1 H), 7.17 (d, $J=3.0$ Hz, 1 H), 7.50 (d, $J=3.2$ Hz, 1 H), 7.73 (d, $J=2.4$ Hz, 1 H), 8.05 (d, $J=2.4$ Hz, 1 H), 9.11 (br. s, 1 H); LCMS (Method A): MH^+ 328, Rt 0.88 min, 99% by UV.

5-[4-Hydroxy-3-(methoxy)phenyl]-3-(2,5-dimethyl-3-thienyl)-1-methyl-2(1H)-pyridinone 204



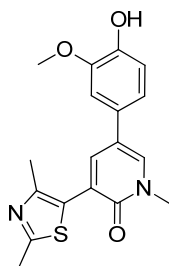
(a) (2,5-Dimethyl-3-thienyl)boronic acid **94**, Borochem, 23 mg, 0.15 mmol; (b) 3.7 mg, 10%; ^1H NMR (600 MHz, $\text{DMSO-}d_6$) δ ppm 2.29 (s, 3 H), 2.37 (s, 3 H), 3.55 (s, 3 H), 3.83 (s, 3 H), 6.78 (s, 1 H), 6.80 (d, $J=8.3$ Hz, 1 H), 6.98 (dd, $J=7.9, 1.5$ Hz, 1 H), 7.12 (d, $J=1.5$ Hz, 1 H), 7.67 (d, $J=2.6$ Hz, 1 H), 8.01 (d, $J=2.3$ Hz, 1 H), 9.04 (br. s, 1 H); LCMS (Method A): MH^+ 341, Rt 0.96 min, 100% by UV.

5-{1,2-Dihydro-5-[4-hydroxy-3-(methoxy)phenyl]-1-methyl-2-oxo-3-pyridinyl}-2-furancarbonitrile 205



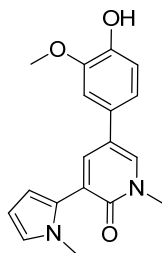
(a) 5-(4,4,5,5-Tetramethyl-1,3,2-dioxaborolan-2-yl)-2-furancarbonitrile **95**, Boropharm, 33 mg, 0.15 mmol; (b) 8.0 mg, 22%; ^1H NMR (600 MHz, $\text{DMSO-}d_6$) δ ppm 3.63 (s, 3 H), 3.86 (s, 3 H), 6.84 (d, $J=8.3$ Hz, 1 H), 7.05 (d, $J=7.9$ Hz, 1 H), 7.19 (br. s, 1 H), 7.44 (d, $J=2.6$ Hz, 1 H), 7.70 (d, $J=2.6$ Hz, 1 H), 8.22 (br. s, 1 H), 8.25 (br. s, 1 H), 9.13 (br. s, 1 H); LCMS (Method A): MH^+ 355, Rt 0.87 min, 100% by UV.

5-[4-Hydroxy-3-(methoxy)phenyl]-1-methyl-{3-(2,4-dimethyl-1,3-thiazol-5-yl)}-2(1H)-pyridinone 206



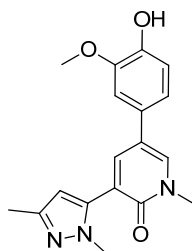
(a) 2,4-Dimethyl-5-(4,4,5,5-tetramethyl-1,3,2-dioxaborolan-2-yl)-1,3-thiazole **96**, Maybridge, 36 mg, 0.15 mmol; (b) 2.3 mg, 6%; $^1\text{H NMR}$ (600 MHz, $\text{DMSO-}d_6$) δ ppm 2.44 (s, 3 H), 2.60 (s, 3 H), 3.59 (s, 3 H), 3.84 (s, 3 H), 6.82 (d, $J=7.9$ Hz, 1 H), 6.99 (dd, $J=7.9, 1.9$ Hz, 1 H), 7.13 (d, $J=1.9$ Hz, 1 H), 7.92 (d, $J=2.3$ Hz, 1 H), 8.07 (d, $J=2.3$ Hz, 1 H), 9.15 (br. s, 1 H); LCMS (Method A): MH^+ 343, Rt 0.64 min, 100% by UV.

5-[4-Hydroxy-3-(methoxy)phenyl]-1-methyl-3-(1-methyl-1H-pyrrol-2-yl)-2(1H)-pyridinone 207



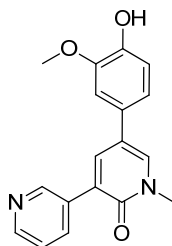
(a) 1-Methyl-2-(4,4,5,5-tetramethyl-1,3,2-dioxaborolan-2-yl)-1H-pyrrole **97**, Combi-blocks, 31 mg, 0.15 mmol; (b) 1 mg, 3%; $^1\text{H NMR}$ (600 MHz, $\text{DMSO-}d_6$) δ ppm 3.53 (s, 3 H), 3.57 (s, 3 H), 3.83 (s, 3 H), 5.75 (s, 1 H), 6.01 (t, $J=2.6$ Hz, 1 H), 6.12-6.13 (m, 1 H), 6.80 (br. s, 1 H), 6.80-6.82 (m, 1 H), 6.97-7.00 (m, 1 H), 7.13 (br. s, 1 H), 7.70 (d, $J=2.3$ Hz, 1 H), 8.04 (d, $J=2.3$ Hz, 1 H); LCMS (Method A): MH^+ 311, Rt 0.79 min, 100% by UV.

5-[4-Hydroxy-3-(methoxy)phenyl]-1-methyl-3-(1,3-dimethyl-1*H*-pyrazol-5-yl)-2(1*H*)-pyridinone 208



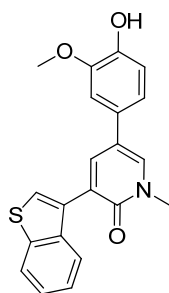
(a) 1,3-Dimethyl-5-(4,4,5,5-tetramethyl-1,3,2-dioxaborolan-2-yl)-1*H*-pyrazole **98**, Chemical Block Ltd, 33 mg, 0.15 mmol; (b) 2.6 mg, 7%; ¹H NMR (600 MHz, DMSO-*d*₆) δ ppm 2.15 (s, 3 H), 3.58 (s, 3 H), 3.64 (s, 3 H), 3.83 (s, 3 H), 6.13 (s, 1 H), 6.81 (d, *J*=8.3 Hz, 1 H), 7.00 (dd, *J*=8.3, 1.9 Hz, 1 H), 7.14 (d, *J*=1.9 Hz, 1 H), 7.83 (d, *J*=2.6 Hz, 1 H), 8.15 (d, *J*=2.6 Hz, 1 H), 8.37 (br. s, 1H); LCMS (Method A): MH⁺ 326, Rt 0.68 min, 90% by UV.

5-[4-Hydroxy-3-(methoxy)phenyl]-1-methyl-3,3'-bipyridin-2(1*H*)-one 209



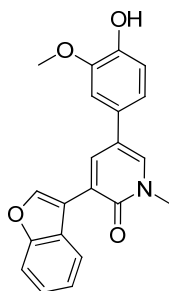
(a) 3-Pyridinylboronic acid **99**, Sigma-Aldrich, 18 mg, 0.15 mmol; (b) 4.6 mg, 13%; ¹H NMR (600 MHz, DMSO-*d*₆) δ ppm 3.60 (s, 3 H), 3.85 (s, 3 H), 6.82 (d, *J*=7.9 Hz, 1 H), 7.07 (dd, *J*=8.3, 1.9 Hz, 1 H), 7.20 (d, *J*=1.9 Hz, 1 H), 7.43 (dd, *J*=7.9, 4.9 Hz, 1 H), 8.03 (d, *J*=2.6 Hz, 1 H), 8.11 (d, *J*=2.3 Hz, 1 H), 8.18-8.21 (m, 1 H), 8.51-8.53 (m, 1 H), 8.95-8.97 (m, 1 H), 9.07 (br. s, 1 H); LCMS (Method A): MH⁺ 309, Rt 0.48 min, 100% by UV.

3-(1-Benzothien-3-yl)-5-[4-hydroxy-3-(methoxy)phenyl]-1-methyl-2(1*H*)-pyridinone 210

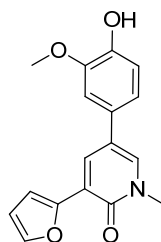


(a) 1-Benzothien-3-ylboronic acid **100**, Sigma-Aldrich, 27 mg, 0.15 mmol; (b) 7.5 mg, 19%; ¹H NMR (600 MHz, DMSO-*d*₆) δ ppm 3.62 (s, 3 H), 3.83 (s, 3 H), 6.82, (d, *J*=8.3 Hz, 1 H), 7.03 (dd, *J*=8.3, 1.5 Hz, 1 H), 7.17 (d, *J*=1.5 Hz, 1 H), 7.36-7.41 (m, 2 H), 7.68-7.71 (m, 1 H), 7.90 (s, 1 H), 7.94 (d, *J*=2.3 Hz, 1 H), 8.01-8.04 (m, 1 H), 8.13 (d, *J*=2.3 Hz, 1 H), 9.07 (br. s, 1 H); LCMS (Method A): MH⁺ 364, Rt 0.99 min, 100% by UV.

3-(1-Benzofuran-3-yl)-5-[4-hydroxy-3-(methoxy)phenyl]-1-methyl-2(1*H*)-pyridinone 211

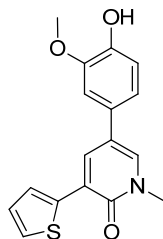


(a) 1-Benzofuran-3-ylboronic acid **101**, AKos Building Blocks, 24 mg, 0.15 mmol; (b) 5.5 mg, 14%; ¹H NMR (600 MHz, DMSO-*d*₆) δ ppm 3.65 (s, 3 H), 3.87 (s, 3 H), 6.87 (d, *J*=7.9 Hz, 1 H), 7.08 (dd, *J*=7.9, 1.9 Hz, 1 H), 7.20 (d, *J*=1.9 Hz, 1 H), 7.36 (t, *J*=7.55 Hz, 1 H), 7.39 (t, *J*=7.2 Hz, 1 H), 7.67 (d, *J*=7.9 Hz, 1 H), 7.95 (d, *J*=7.6 Hz, 1 H), 8.09 (d, *J*=2.3 Hz, 1 H), 8.21 (d, *J*=2.3 Hz, 1 H), 8.70 (s, 1 H), 9.09 (br. s, 1 H); LCMS (Method A): MH⁺ 348, Rt 0.99 min, 100% by UV.

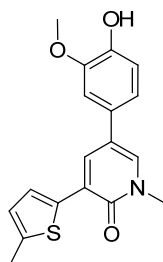
3-(2-Furanyl)-5-[4-hydroxy-3-(methoxy)phenyl]-1-methyl-2(1H)-pyridinone 127*Typical Procedure B:*

3-Bromo-5-[4-hydroxy-3-(methoxy)phenyl]-1-methyl-2(1H)-pyridinone **89** (31 mg, 0.10 mmol), 2-(2-furanyl)-6-methyldihydro-4H-1,3,6,2-dioxaborocine-4,8(5H)-dione **126** (Peakdale Molecular, 27.0 mg, 0.120 mmol), SPhos (4.1 mg, 10.0 μmol) and palladium(II) acetate (1.1 mg, 5.0 μmol) were suspended in 1,4-dioxane (1.25 mL) and aqueous potassium phosphate tribasic (3 M, 0.25 mL, 0.75 mmol) added. The reaction mixture was heated at 100 °C for 18 h, then loaded directly onto a C₁₈ SPE cartridge (500 mg) which had been preconditioned with acetonitrile + 0.1% TFA. The column was eluted with 0.1% TFA/acetonitrile (2 column volumes) and the eluent concentrated. The resultant solid was dissolved in 1:1 MeOH:DMSO (1 mL) and purified by Mass Directed AutoPrep on a Sunfire C₁₈ column using acetonitrile/water with a formic acid modifier. The solvent was concentrated *in vacuo* to give the title compound (14.0 mg, 47%) as a yellow solid; m.p. 205-206 °C; $\nu_{\text{max}}/\text{cm}^{-1}$ (solid) 3541 (OH), 1654 (C=O); ¹H NMR (400 MHz, DMSO-*d*₆) δ ppm 3.61 (s, 3 H), 3.86 (s, 3 H), 6.61 (dd, *J*=3.3, 1.8 Hz, 1 H), 6.84 (d, *J*=8.3 Hz, 1 H), 7.00 (dd, *J*=8.1, 2.0 Hz, 1 H), 7.15 (d, *J*=2.0 Hz, 1 H), 7.30 (d, *J*=3.3 Hz, 1 H), 7.76-7.77 (m, 1 H), 8.04 (d, *J*=2.5 Hz, 1 H), 8.08 (d, *J*=2.5 Hz, 1 H), 9.07 (br. s, 1 H); ¹³C NMR (100 MHz, CDCl₃) δ ppm 38.3, 56.1, 108.8, 111.4, 112.2, 114.9, 119.3, 119.6 (2C), 120.4, 121.2, 132.2, 132.8, 142.0 (2C), 145.3, 149.4; LCMS (Method A): MH⁺ 298, Rt 0.85 min, 100% by UV; HRMS exact mass calculated for [M+H]⁺ (C₁₇H₁₆NO₄) requires *m/z* 298.1079, found 298.1073.

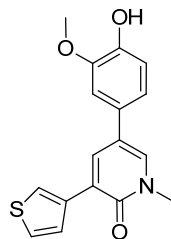
The following experiments were performed using Typical Procedure B, the data are reported as (a) boronate (supplier, g, mmol); (b) product (mg, % yield).

5-[4-Hydroxy-3-(methoxy)phenyl]-1-methyl-3-(2-thienyl)-2(1H)-pyridinone 212

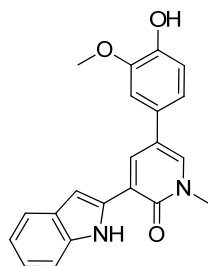
(a) 6-Methyl-2-(2-thienyl)dihydro-4H-1,3,6,2-dioxazaborocine-4,8(5H)-dione **128**, Peakdale Molecular, 29 mg, 0.12 mmol; (b) 9.1 mg, 26%; ^1H NMR (600 MHz, DMSO- d_6) δ ppm 3.63 (s, 3 H), 3.87 (s, 3 H), 6.84 (d, $J=7.9$ Hz, 1 H), 7.08 (dd, $J=7.9$, 1.9 Hz, 1 H), 7.13 (dd, $J=5.3$, 3.8 Hz, 1 H), 7.20 (d, $J=1.9$ Hz, 1 H), 7.54 (d, $J=5.2$ Hz, 1 H), 7.92 (d, $J=3.0$ Hz, 1 H), 8.05 (d, $J=1.9$ Hz, 1 H), 8.33 (d, $J=1.9$ Hz, 1 H), 9.12 (br. s, 1 H); LCMS (Method A): MH^+ 314, Rt 0.89 min, 99% by UV.

5-[4-Hydroxy-3-(methoxy)phenyl]-1-methyl-3-(5-methyl-2-thienyl)-2(1H)-pyridinone 213

(a) 6-Methyl-2-(5-methyl-2-thienyl)dihydro-4H-1,3,6,2-dioxazaborocine-4,8(5H)-dione **129**, Peakdale Molecular, 30 mg, 0.12 mmol; (b) 13.6 mg, 37%; ^1H NMR (600 MHz, DMSO- d_6) δ ppm 2.46 (s, 3 H), 3.61 (s, 3 H), 3.86 (s, 3 H), 6.81 (d, $J=3.0$ Hz, 1 H), 6.83 (d, $J=7.9$ Hz, 1 H), 7.06 (dd, $J=7.9$, 1.9 Hz, 1 H), 7.18 (d, $J=1.9$ Hz, 1 H), 7.71 (d, $J=3.4$ Hz, 1 H), 8.00 (d, $J=2.3$ Hz, 1 H), 8.21 (d, $J=2.6$ Hz, 1 H), 9.09 (br. s, 1 H); LCMS (Method A): MH^+ 328, Rt 0.96 min, 100% by UV.

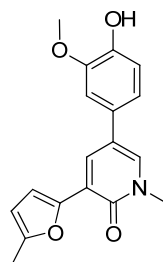
5-[4-Hydroxy-3-(methoxy)phenyl]-1-methyl-3-(3-thienyl)-2(1H)-pyridinone 214

(a) 6-Methyl-2-(3-thienyl)dihydro-4H-1,3,6,2-dioxazaborocine-4,8(5H)-dione **130**, Peakdale Molecular, 29 mg, 0.12 mmol; (b) 10.6 mg, 30%; ^1H NMR (600 MHz, DMSO- d_6) δ ppm 3.61 (s, 3 H), 3.86 (s, 3 H), 6.83 (d, $J=8.3$ Hz, 1 H), 7.07 (dd, $J=8.3$, 1.9 Hz, 1 H), 7.18 (d, $J=1.9$ Hz, 1 H), 7.57 (dd, $J=4.9$, 3.0 Hz, 1 H), 7.82 (d, $J=4.9$ Hz, 1 H), 8.03 (d, $J=2.3$ Hz, 1 H), 8.15 (d, $J=2.3$ Hz, 1 H), 8.41 (d, $J=2.6$ Hz, 1 H), 9.09 (br. s, 1 H); LCMS (Method A): MH^+ 314, Rt 0.88 min, 99% by UV.

5-[4-Hydroxy-3-(methoxy)phenyl]-3-(1H-indol-2-yl)-1-methyl-2(1H)-pyridinone 215

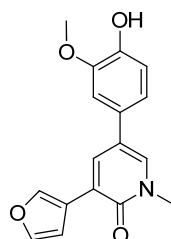
(a) 2-(1H-Indol-2-yl)-6-methyldihydro-4H-1,3,6,2-dioxazaborocine-4,8(5H)-dione **131**, Peakdale Molecular, 45 mg, 0.12 mmol; (b) 17.4 mg, 34% as a cream solid; m.p. 226-228 °C; $\nu_{\text{max}}/\text{cm}^{-1}$ (solid) 3372 (OH), 1645 (C=O); ^1H NMR (600 MHz, DMSO- d_6) δ ppm 3.66 (s, 3 H), 3.89 (s, 3 H), 6.87 (d, $J=7.9$ Hz, 1 H), 6.99 (t, $J=7.2$ Hz, 1 H), 7.09 (t, $J=7.4$ Hz, 1 H), 7.13 (dd, $J=7.9$, 1.5 Hz, 1 H), 7.23 (d, $J=1.5$ Hz, 1 H), 7.40 (s, 1 H), 7.48 (d, $J=8.3$ Hz, 1 H), 7.54 (d, $J=7.6$ Hz, 1 H), 8.10 (d, $J=1.9$ Hz, 1 H), 8.38 (d, $J=2.3$ Hz, 1 H), 9.10 (br. s, 1 H), 11.54 (br. s, 1 H); ^{13}C NMR (100 MHz, DMSO- d_6) δ ppm 37.7, 55.9, 101.8, 110.1, 111.3, 115.8, 118.3, 118.6, 119.1, 120.0, 120.2, 121.6, 127.4, 128.1, 133.1, 134.1, 134.7, 136.3, 146.0, 148.0, 159.1; LCMS (Method A): MH^+ 347, Rt 1.04 min, 100% by UV; HRMS exact mass calculated for $[\text{M}+\text{H}]^+$ ($\text{C}_{21}\text{H}_{19}\text{N}_2\text{O}_3$) requires m/z 347.1396, found 347.1396.

5-[4-Hydroxy-3-(methoxy)phenyl]-1-methyl-3-(5-methyl-2-furanyl)-2(1H)-pyridinone 216



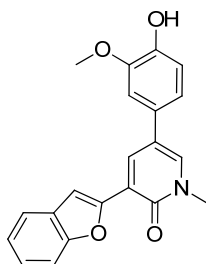
(a) 6-Methyl-2-(5-methyl-2-furanyl)dihydro-4*H*-1,3,6,2-dioxaborocine-4,8(5*H*)-dione **132**, Peakdale Molecular, 28 mg, 0.12 mmol; (b) 17.6 mg, 51%; ¹H NMR (600 MHz, DMSO-*d*₆) δ ppm 2.36 (s, 3 H), 3.60 (s, 3 H), 3.85 (s, 3 H), 6.21 (d, *J*=2.3 Hz, 1 H), 6.84 (d, *J*=7.9 Hz, 1 H), 6.99 (dd, *J*=7.9, 1.5 Hz, 1 H), 7.13 (d, *J*=1.9 Hz, 1 H), 7.19 (d, *J*=3.0 Hz, 1 H), 7.97-7.99 (m, 2 H), 9.11 (br. s, 1 H); LCMS (Method A): MH⁺ 312, Rt 0.91 min, 97% by UV.

3-(3-Furanyl)-5-[4-hydroxy-3-(methoxy)phenyl]-1-methyl-2(1H)-pyridinone 217



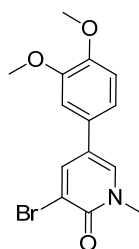
(a) 2-(3-Furanyl)-6-methyldihydro-4*H*-1,3,6,2-dioxaborocine-4,8(5*H*)-dione **133**, Peakdale Molecular, 27 mg, 0.12 mmol; (b) 7.6 mg, 23%; ¹H NMR (600 MHz, DMSO-*d*₆) δ ppm 3.61 (s, 3 H), 3.87 (s, 3 H), 6.83 (d, *J*=8.3 Hz, 1 H), 7.07 (dd, *J*=7.9, 1.9 Hz, 1 H), 7.18 (d, *J*=1.9 Hz, 1 H), 7.24-7.26 (m, 1 H), 7.72-7.73 (m, 1 H), 8.00 (d, *J*=2.3 Hz, 1 H), 8.09 (d, *J*=2.3 Hz, 1 H), 8.52 (br. s, 1 H), 9.11 (br. s, 1 H); LCMS (Method A): MH⁺ 298, Rt 0.83 min, 100% by UV.

3-(1-Benzofuran-2-yl)-5-[4-hydroxy-3-(methoxy)phenyl]-1-methyl-2(1H)-pyridinone 218



(a) 2-(1-Benzofuran-2-yl)-6-methyldihydro-4*H*-1,3,6,2-dioxaborocine-4,8(5*H*)-dione **134**, Sigma-Aldrich, 33 mg, 0.12 mmol; (b) 6.0 mg, 16%; ¹H NMR (600 MHz, DMSO-*d*₆) δ ppm 3.66 (s, 3 H), 3.88 (s, 3 H), 6.88 (d, *J*=7.9 Hz, 1 H), 7.05 (dd, *J*=7.9, 1.9 Hz, 1 H), 7.19-7.20 (m, 1 H), 7.25 (t, *J*=7.6 Hz, 1 H), 7.33 (t, *J*=7.9 Hz, 1 H), 7.62 (d, *J*=8.3 Hz, 1 H), 7.70 (d, *J*=7.6 Hz, 1 H), 7.79 (s, 1 H), 8.17 (d, *J*=1.9 Hz, 1 H), 8.32 (d, *J*=2.3 Hz, 1 H), 9.18 (br. s, 1 H); LCMS (Method A): MH⁺ 348, Rt 1.06 min, 100% by UV.

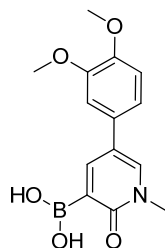
3-Bromo-5-[3,4-bis(methoxy)phenyl]-1-methyl-2(1H)-pyridinone 136



Ethanol (48 mL) and water (16 mL) were de-gassed via a stream of nitrogen for 5 min, then Na₂CO₃ (3.39 g, 32.0 mmol), [3,4-bis(methoxy)phenyl]boronic acid **135** (Sigma-Aldrich, 2.91 g, 16.0 mmol), 3-bromo-5-iodo-1-methyl-2(1*H*)-pyridinone **87** (5.02 g, 16.0 mmol) and Pd(Ph₃P)₄ (0.56 g, 0.48 mmol) were added. The mixture was de-gassed for a further 2 min and heated to 90 °C for 4.5 h, then allowed to cool to RT overnight. The mixture was partitioned between ethyl acetate (250 mL) and water (200 mL) and vigorously stirred for 20 min. The mixture was separated and the aqueous phase extracted with further ethyl acetate (100 mL). The combined organic extracts were washed with water (100 mL) and brine (100 mL) then dried over anhydrous sodium sulfate and concentrated *in vacuo*. The resulting solid was purified by column chromatography (silica) eluting with 0-100% ethyl acetate in cyclohexane. The appropriate fractions were concentrated *in vacuo* to provide the title compound (3.1 g,

60%) as a pale yellow solid; m.p. 159-165 °C; $\nu_{\max}/\text{cm}^{-1}$ (solid) 1648 (C=O); ^1H NMR (400 MHz, $\text{DMSO-}d_6$) δ ppm 3.58 (s, 3 H), 3.77 (s, 3 H), 3.83 (s, 3 H), 6.98 (d, $J=8.3$ Hz, 1 H), 7.11 (dd, $J=8.1, 2.0$ Hz, 1 H), 7.16 (d, $J=2.3$ Hz, 1 H), 8.16 (d, $J=2.5$ Hz, 1 H), 8.32 (d, $J=2.5$ Hz, 1 H); ^{13}C NMR (100 MHz, $\text{DMSO-}d_6$) δ ppm 38.4, 55.6, 55.7, 109.5, 112.1, 114.7, 117.7, 118.2, 127.6, 136.4, 140.7, 148.2, 149.1, 157.4; LCMS (Method B): MH^+ 324/326, Rt 2.14 min; HRMS exact mass calculated for $[\text{M}+\text{H}]^+$ ($\text{C}_{14}\text{H}_{15}\text{BrNO}_3$) requires m/z 324.0235, found 324.0236.

Attempted formation of {5-[3,4-bis(methoxy)phenyl]-1-methyl-2-oxo-1,2-dihydro-3-pyridinyl}boronic acid **137**



Method A:

n-Butyllithium (420 μL , 0.68 mmol, 1.6 M solution in hexanes) was added dropwise to a suspension of 5-[3,4-bis(methoxy)phenyl]-3-bromo-1-methyl-2(1*H*)-pyridinone **136** (200 mg, 0.617 mmol) in anhydrous tetrahydrofuran (3 mL) at -78 °C. The mixture was stirred at -78 °C for 40 min. An aliquot was quenched with methanol and LCMS showed a major peak was consistent with unreacted starting material. LCMS (Method A): MH^+ 324-326, Rt = 0.82 min.

Method B:

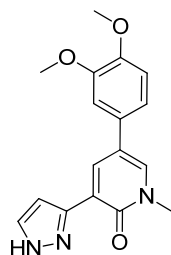
To a suspension of 5-[3,4-bis(methoxy)phenyl]-3-bromo-1-methyl-2(1*H*)-pyridinone **136** (100 mg, 0.308 mmol) in anhydrous tetrahydrofuran (5 mL) at -78 °C was added *n*-butyllithium (290 μL , 0.46 mmol, 1.6 M solution in hexanes) dropwise. The mixture was stirred at -78 °C for 75 min. An aliquot was quenched with methanol and LCMS showed a major peak consistent with undesired product 5-[3,4-bis(methoxy)phenyl]-4-butyl-1-methyl-2(1*H*)-pyridinone, **138**. LCMS (Method A): MH^+ 302, Rt = 0.99 min.

Method C:

n-Butyllithium (230 μ L, 0.37 mmol, 1.6 M solution in hexanes) was added dropwise to a suspension of 5-[3,4-bis(methoxy)phenyl]-3-bromo-1-methyl-2(1*H*)-pyridinone **136** (100 mg, 0.308 mmol) in anhydrous tetrahydrofuran (5 mL) at -78 $^{\circ}$ C. The mixture was stirred at -78 $^{\circ}$ C for 30 min. An aliquot was quenched with methanol and LCMS showed a major peak consistent with protonated material resultant from lithium/halogen exchange. LCMS (Method A): MH^+ 246, R_t = 0.67 min.

Method D:

sec-Butyllithium (275 μ L, 0.386 mmol, 1.4 M solution in cyclohexane) was added dropwise to a suspension of 5-[3,4-bis(methoxy)phenyl]-3-bromo-1-methyl-2(1*H*)-pyridinone **136** (100 mg, 0.308 mmol) in anhydrous tetrahydrofuran (5 mL) at -78 $^{\circ}$ C. The mixture was stirred at -78 $^{\circ}$ C for 5 min, an aliquot was quenched with methanol and LCMS showed a major peak consistent with the protonated material resultant from successful lithium/halogen exchange. Tributyl borate (0.10 mL, 0.37 mmol) was added and the reaction mixture stirred at -78 $^{\circ}$ C for 30 min. LCMS showed a major peak which was consistent with the desired product. The reaction mixture was allowed to warm to RT over 2 h, then quenched with 10% 2M HCl in water (2 mL). After vigorously stirring for 10 min, the reaction was diluted with water (10 mL) and ethyl acetate (10 mL). The layers were separated and the aqueous phase washed with further ethyl acetate (10 mL). The combined organics were dried over anhydrous sodium sulfate and concentrated *in vacuo* to give the title compound (117 mg, 131%); LCMS (Method A): MH^+ 290, R_t 0.69 min.

5-[3,4-Bis(methoxy)phenyl]-1-methyl-3-(1*H*-pyrazol-3-yl)-2(1*H*)-pyridinone 143*Typical Procedure C:*

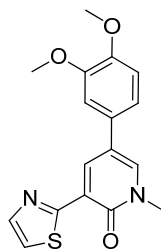
5-[3,4-Bis(methoxy)phenyl]-3-bromo-1-methyl-2(1*H*)-pyridinone **136** (3.05 g, 9.41 mmol), PdCl₂(dppf) (0.69 g, 0.94 mmol), 4,4,4',4',5,5,5',5'-octamethyl-2,2'-bi-1,3,2-

dioxaborolane (3.58 g, 14.1 mmol) and potassium acetate (1.11 g, 11.3 mmol) were suspended in anhydrous 1,4-dioxane (50 mL) and heated to 100 °C for 4 h. The crude reaction mixture was filtered through Celite, washed with DCM, and the filtrate concentrated *in vacuo* to give an impure mixture containing the desired boronic ester **141**, 7.74 g as a brown viscous liquid; LCMS (Method A): MH⁺ 290, Rt 0.69 min, 78% by UV.

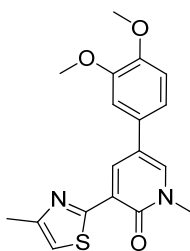
Boronic ester **141** was not stable to purification so was used in crude form:

5-[3,4-Bis(methoxy)phenyl]-1-methyl-3-(4,4,5,5-tetramethyl-1,3,2-dioxaborolan-2-yl)-2(1*H*)-pyridinone **141** (100 mg, ~0.1 mmol based on 100% yield), 3-bromo-1*H*-pyrazole **142** (Allichem LLC, 29 mg, 0.20 mmol), PdCl₂(dppf).DCM (8.2 mg, 10 μmol) and K₂CO₃ (42 mg, 0.30 mmol) were suspended in 1,4-dioxane (0.8 mL) and water (0.2 mL). The reaction vessel was sealed and heated under microwave irradiation to 100 °C for 15 min. Additional 3-bromo-1*H*-pyrazole **142** (29 mg, 0.20 mmol) was added and the reaction mixture heated to 100 °C for a further 15 min. The crude reaction mixture was loaded onto a C₁₈ SPE (pre-conditioned with 0.1% TFA/acetonitrile) and eluted with 0.1% TFA/acetonitrile. The filtrate was concentrated to give a brown solid (160 mg), which was dissolved in 1:1 MeOH:DMSO (2 mL) and purified by Mass Directed AutoPrep on Sunfire C₁₈ column using acetonitrile/water with formic acid modifier. The appropriate fractions were concentrated *in vacuo* to give the title compound (4.9 mg, 16%) as a brown solid; ¹H NMR (400 MHz, CDCl₃) δ ppm 3.77 (s, 3 H), 3.94 (s, 3 H), 3.97 (s, 3 H), 6.72 (d, *J*=1.3 Hz, 1 H), 6.93 (d, *J*=2.0 Hz, 1 H), 6.96 (d, *J*=8.3 Hz, 1 H), 6.97 (s, 1 H), 7.00 (dd, *J*=8.3, 2.0 Hz, 1 H), 7.50 (d, *J*=2.5 Hz, 1 H), 7.65 (d, *J*=1.8 Hz, 1 H), 8.04 (d, *J*=2.5 Hz, 1 H); LCMS (Method A): MH⁺ 312, Rt 0.74 min, 93% by UV.

The following experiments were performed using Typical Procedure C, the data are reported as (a) bromide (supplier, g, mmol) x 2; (b) product (mg, % yield).

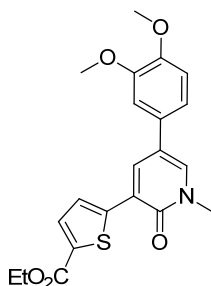
5-[3,4-Bis(methoxy)phenyl]-1-methyl-3-(1,3-thiazol-2-yl)-2(1H)-pyridinone 219

(a) 2-Bromo-1,3-thiazole **144**, Sigma-Aldrich, 33 mg, 0.20 mmol; (b) 7 mg, 19%; ¹H NMR (400 MHz, CDCl₃) δ ppm 3.71 (s, 3 H), 3.79 (s, 3 H), 3.86 (s, 3 H), 7.04 (d, *J*=8.3 Hz, 1 H), 7.17 (dd, *J*=8.3, 2.3 Hz, 1 H), 7.21 (d, *J*=2.0 Hz, 1 H), 7.77 (d, *J*=3.3 Hz, 1 H), 7.98 (d, *J*=3.3 Hz, 1 H), 8.36 (d, *J*=2.8 Hz, 1 H), 8.77 (d, *J*=2.9 Hz, 1 H); LCMS (Method A): MH⁺ 329, Rt 0.85 min, 100% by UV.

5-[3,4-Bis(methoxy)phenyl]-1-methyl-3-(4-methyl-1,3-thiazol-2-yl)-2(1H)-pyridinone 220

(a) 2-Bromo-4-methyl-1,3-thiazole **145**, Anichem, 36 mg, 0.20 mmol; (b) 13.4 mg, 35%; ¹H NMR (400 MHz, CDCl₃) δ ppm 2.44 (s, 3 H), 3.69 (s, 3 H), 3.79 (s, 3 H), 3.85 (s, 3 H), 7.04 (d, *J*=8.0 Hz, 1 H), 7.14 (d, *J*=8.0 Hz, 1 H), 7.19-7.21 (m, 1 H), 7.30 (s, 1 H), 8.30-8.32 (m, 1 H) 8.67-8.69 (m, 1 H); LCMS (Method A): MH⁺ 343, Rt 0.89 min, 100% by UV.

1,2-Dihydro-ethyl-5-{5-[3,4-bis(methoxy)phenyl]-1-methyl-2-oxo-3-pyridinyl}-2-thiophenecarboxylate 221



Typical Procedure D:

5-[3,4-Bis(methoxy)phenyl]-3-bromo-1-methyl-2(1*H*)-pyridinone **136** (3.05 g, 9.41 mmol), PdCl₂(dppf) (0.69 g, 0.94 mmol), 4,4,4',4',5,5,5',5'-octamethyl-2,2'-bi-1,3,2-dioxaborolane (3.58 g, 14.1 mmol) and potassium acetate (1.11 g, 11.3 mmol) were suspended in anhydrous 1,4-dioxane (50 mL) and heated to 100 °C for 4 h. The crude reaction mixture was filtered through Celite, washed with DCM and the filtrate concentrated *in vacuo* to give an impure mixture containing the desired boronic ester **141**, 7.74 g as a brown viscous liquid; LCMS (Method A): MH⁺ 290, Rt 0.69 min, 78% by UV.

Product **141** was not stable to purification so was used in crude form:

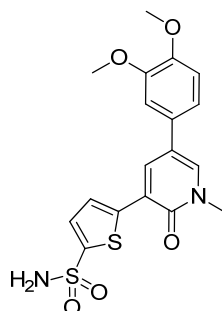
5-[3,4-Bis(methoxy)phenyl]-1-methyl-3-(4,4,5,5-tetramethyl-1,3,2-dioxaborolan-2-yl)-2(1*H*)-pyridinone **141** (100 mg, ~0.1 mmol based on 100% yield), ethyl 5-bromo-2-thiophenecarboxylate **146** (Avocado Research Chemicals, 47 mg, 0.20 mmol), PdCl₂(dppf).DCM (8.2 mg, 10 μmol) and K₂CO₃ (42 mg, 0.30 mmol) were suspended in 1,4-dioxane (0.8 mL) and water (0.2 mL). The reaction vessel was sealed and heated under microwave irradiation to 100 °C for 20 min.

The crude reaction mixture was loaded onto a C₁₈ SPE (pre-conditioned with 0.1% TFA/acetonitrile) and eluted with 0.1% TFA/acetonitrile. The filtrate was concentrated to give a solid, which was dissolved in 1:1 MeOH:DMSO (1 mL) and purified by Mass Directed AutoPrep on Sunfire C₁₈ column using acetonitrile/water with formic acid modifier. The appropriate fractions were concentrated *in vacuo* to give the title compound (11.6 mg, 26%); ¹H NMR (400 MHz, CDCl₃) δ ppm 1.31 (t, *J*=7.0 Hz, 3 H), 3.67 (s, 3 H), 3.79 (s, 3 H), 3.87 (s, 3 H), 4.28 (q, *J*=6.8 Hz, 2 H), 7.02 (d, *J*=8.3 Hz, 1 H), 7.24 (d, *J*=8.3 Hz, 1 H), 7.25-7.27 (m, 1 H), 7.77 (d, *J*=3.8 Hz, 1 H), 8.01 (d,

$J=3.4$ Hz, 1 H), 8.21-8.24 (m, 1 H), 8.54-8.57 (m, 1 H); LCMS (Method A): MH^+ 400, Rt 1.07 min, 100% by UV.

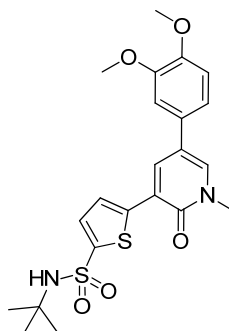
The following experiments were performed using Typical Procedure D, the data are reported as (a) bromide (supplier, g, mmol); (b) product (mg, % yield).

5-{5-1,2-Dihydro-[3,4-bis(methoxy)phenyl]-1-methyl-2-oxo-3-pyridinyl}-2-thiophenesulfonamide 222

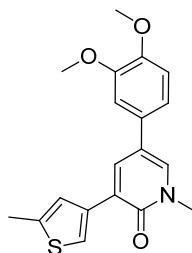


(a) 5-Bromo-2-thiophenesulfonamide **147**, Maybridge, 48 mg, 0.20 mmol; (b) 8.9 mg, 20%; 1H NMR (400 MHz, $CDCl_3$) δ ppm 3.67 (s, 3 H), 3.79 (s, 3 H), 3.87 (s, 3 H), 7.03 (d, $J=8.3$ Hz, 1 H), 7.24 (d, $J=8.0$ Hz, 1 H), 7.26-7.28 (m, 1 H), 7.54 (d, $J=3.8$ Hz, 1 H), 7.58-7.62 (br. s, 2 H), 7.95 (d, $J=3.8$ Hz, 1 H), 8.20-8.23 (m, 1 H), 8.55 (s, 1 H); LCMS (Method A): MH^+ 407, Rt 0.80 min, 100% by UV.

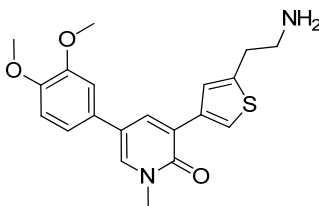
5-{5-1,2-Dihydro-[3,4-bis(methoxy)phenyl]-1-methyl-2-oxo-3-pyridinyl}-N-(1,1-dimethylethyl)-2-thiophenesulfonamide 223



(a) 5-Bromo-*N*-(1,1-dimethylethyl)-2-thiophenesulfonamide **148**, Fluorochem, 60 mg, 0.20 mmol; (b) 13.6 mg, 27%; 1H NMR (400 MHz, $CDCl_3$) δ ppm 1.16 (s, 9 H), 3.67 (s, 3 H), 3.79 (s, 3 H), 3.86 (s, 3 H), 7.03 (d, $J=8.3$ Hz, 1 H), 7.24 (d, $J=8.0$ Hz, 1 H), 7.25-7.27 (m, 1 H), 7.55 (d, $J=4.2$ Hz, 1 H), 7.65 (s, 1 H), 7.94 (d, $J=3.8$ Hz, 1 H), 8.21-8.24 (m, 1 H), 8.53-8.57 (m, 1 H); LCMS (Method A): MH^+ 463, Rt 1.04 min, 100% by UV.

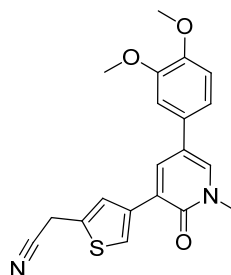
5-[3,4-Bis(methoxy)phenyl]-1-methyl-3-(5-methyl-3-thienyl)-2(1H)-pyridinone 224

(a) 4-Bromo-2-methylthiophene **149**, Fluorochem, 35 mg, 0.20 mmol; (b) 10 mg, 26%; ¹H NMR (400 MHz, CDCl₃) δ ppm 2.48 (s, 3 H), 3.60 (s, 3 H), 3.78 (s, 3 H), 3.85 (s, 3 H), 7.00 (d, *J*=8.3 Hz, 1 H), 7.16-7.19 (m, 1 H), 7.19-7.21 (m, 1 H), 7.49-7.51 (m, 1 H) 8.04-8.06 (m, 1 H), 8.10 (d, *J*=2.6 Hz, 1 H) 8.16-8.17 (br. s, 1 H); LCMS (Method A): MH⁺ 342, Rt 1.06 min, 100% by UV.

3-[5-(2-Aminoethyl)-3-thienyl]-5-[3,4-bis(methoxy)phenyl]-1-methyl-2(1H)-pyridinone 225

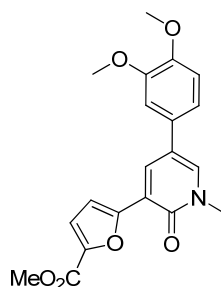
(a) 2-(4-Bromo-2-thienyl)ethanamine **150**, J&W Pharmalab LLC, 41 mg, 0.20 mmol; (b) 4.5 mg, 11%; ¹H NMR (400 MHz, CDCl₃) δ ppm 3.05-3.09 (m, 2H), 3.16-3.17 (m, 2H), 3.60 (s, 3 H), 3.78 (s, 3 H), 3.85 (s, 3 H), 7.01 (d, *J*=8.3 Hz, 1 H), 7.18 (dd, *J*=8.3, 1.9 Hz, 1 H), 7.20 (d, *J*=1.5 Hz, 1 H), 7.63-7.65 (m, 1 H), 8.07 (d, *J*=2.3 Hz, 1 H), 8.15 (d, *J*=2.3 Hz, 1 H), 8.27 (s, 1 H), 8.39-8.41 (br. s, 2 H); LCMS (Method A): MH⁺ 371, Rt 0.62 min, 100% by UV.

(4-{5-1,2-Dihydro-[3,4-bis(methoxy)phenyl]-1-methyl-2-oxo-3-pyridinyl}-2-thienyl)acetonitrile 226



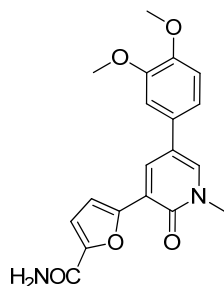
(a) (4-Bromo-2-thienyl)acetonitrile **151**, Matrix Scientific, 40 mg, 0.20 mmol; (b) 12.9 mg, 32%; ^1H NMR (400 MHz, CDCl_3) δ ppm 3.60 (s, 3 H), 3.77 (s, 3 H), 3.85 (s, 3 H), 4.0-4.30 (br. s, 2 H), 7.01 (d, $J=8.0$ Hz, 1 H), 7.18 (dd, $J=8.3, 1.9$ Hz, 1 H), 7.20 (d, $J=1.5$ Hz, 1 H), 7.76-7.78 (m, 1 H), 8.08 (d, $J=2.3$ Hz, 1 H), 8.13 (d, $J=2.3$ Hz, 1 H), 8.30-8.31 (m, 1 H); LCMS (Method A): MH^+ 367, Rt 0.92 min, 100% by UV.

Methyl 5-{5-[3,4-bis(methoxy)phenyl]-1-methyl-2-oxo-1,2-dihydro-3-pyridinyl}-2-furancarboxylate 227



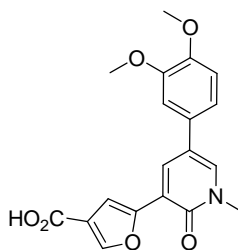
(a) Methyl 5-bromo-2-furancarboxylate **152**, Avocado Research Chemicals, 41 mg, 0.20 mmol; (b) 22 mg, 54% as a pale brown solid; 202-204 $^\circ\text{C}$; $\nu_{\text{max}}/\text{cm}^{-1}$ (solid) 1719 (C=O, ester), 1663 (C=O, pyridone); ^1H NMR (400 MHz, CDCl_3) δ ppm 3.63 (s, 3 H), 3.79 (s, 3 H), 3.84 (s, 3 H), 3.85 (s, 3 H), 7.04 (d, $J=8.3$ Hz, 1 H), 7.12 (d, $J=8.0$ Hz, 1 H), 7.18-7.19 (m, 1 H), 7.41-7.43 (m, 2 H), 8.16 (d, $J=1.9$ Hz, 1 H), 8.21-8.22 (m, 1 H); ^{13}C NMR (100 MHz, DMSO-d_6) δ 37.7, 51.8, 55.6, 55.7, 109.8, 112.0, 112.3, 118.0, 118.1, 119.1 (2C), 128.6, 133.3, 137.4, 142.4, 148.3, 149.1, 153.0, 157.7, 158.3; LCMS (Method A): MH^+ 370, Rt 0.9 min, 100% by UV; HRMS exact mass calculated for $[\text{M}+\text{H}]^+$ ($\text{C}_{20}\text{H}_{20}\text{NO}_6$) requires m/z 370.1291, found 370.1283.

5-{5-[3,4-Bis(methoxy)phenyl]-1-methyl-2-oxo-1,2-dihydro-3-pyridinyl}-2-furancarboxamide 228



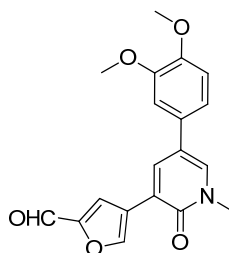
(a) 5-Bromo-2-furancarboxamide **153**, Chembridge, 38 mg, 0.20 mmol; (b) 5.1 mg, 13%; $^1\text{H NMR}$ (400 MHz, CDCl_3) δ ppm 3.63 (s, 3 H), 3.79 (s, 3 H), 3.86 (s, 3 H), 7.03 (d, $J=8.7$ Hz, 1 H) 7.13 (d, $J=3.4$ Hz, 1 H), 7.20-7.23 (m, 2 H), 7.36 (d, $J=3.0$ Hz, 1 H), 7.52 (br. s, 1 H), 8.15 (br. s, 1 H), 8.16-8.18 (m, 1 H), 8.53-8.56 (m, 1 H); LCMS (Method A): MH^+ 354, Rt 0.71min, 100% by UV.

5-{5-1,2-Dihydro-[3,4-bis(methoxy)phenyl]-1-methyl-2-oxo-3-pyridinyl}-3-furancarboxylic acid 229



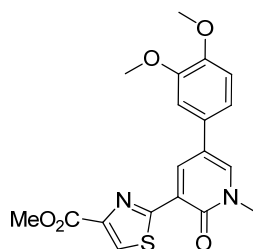
(a) 5-Bromo-3-furancarboxylic acid **154**, Frontier Scientific, 38 mg, 0.20 mmol; (b) 3.1 mg, 8%; $^1\text{H NMR}$ (400 MHz, CDCl_3) δ ppm 3.63 (s, 3 H), 3.70 (br. s, 1 H), 3.78 (s, 3 H), 3.84 (s, 3 H), 7.01 (d, $J=8.0$ Hz, 1 H), 7.13 (d, $J=8.0$ Hz, 1 H), 7.17-7.20 (m, 1 H), 7.46-7.49 (m, 1 H), 8.11-8.14 (m, 2 H), 8.22-8.25 (m, 1 H); LCMS (Method A): MH^+ 356, Rt 0.80 min, 100% by UV.

4-{5-1,2-Dihydro-[3,4-bis(methoxy)phenyl]-1-methyl-2-oxo-3-pyridinyl}-2-furancarbaldehyde 230



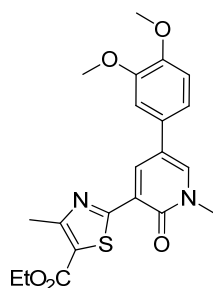
(a) 4-Bromo-2-furancarbaldehyde **155**, Sigma-Aldrich, 35 mg, 0.20 mmol; (b) 9.5 mg, 25%; ^1H NMR (400 MHz, CDCl_3) δ ppm 3.63 (s, 3 H), 3.78 (s, 3 H), 3.86 (s, 3 H), 7.01-7.03 (m, 1 H), 7.22-7.23 (m, 1 H), 7.23-7.24 (m, 1 H), 8.14 (d, $J=2.3$ Hz, 1 H), 8.31 (d, $J=1.9$ Hz, 1 H), 8.33-8.35 (m, 1 H), 8.86-8.87 (m, 1 H), 9.68 (s, 1 H); LCMS (Method A): MH^+ 340, Rt 0.85 min, 100% by UV.

Methyl 2-{5-1,2-dihydro-[3,4-bis(methoxy)phenyl]-1-methyl-2-oxo-3-pyridinyl}-1,3-thiazole-4-carboxylate 231



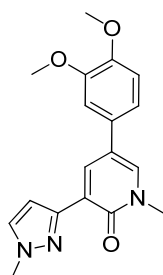
(a) Methyl 2-bromo-1,3-thiazole-4-carboxylate **156**, Synchem, 44 mg, 0.20 mmol; 15.8 mg, 37%; ^1H NMR (400 MHz, CDCl_3) δ ppm 3.71 (s, 3 H), 3.79 (s, 3 H), 3.86 (s, 3 H), 3.86 (s, 3 H), 7.05 (d, $J=8.3$ Hz, 1 H), 7.15 (d, $J=7.9$ Hz, 1 H), 7.21-7.22 (m, 1 H), 8.37-8.39 (m, 1 H), 8.53 (s, 1 H), 8.70 (d, $J=2.3$ Hz, 1 H); LCMS (Method A): MH^+ 387, Rt 0.87 min, 100% by UV.

Ethyl 2-{5-1,2-dihydro-[3,4-bis(methoxy)phenyl]-1-methyl-2-oxo-3-pyridinyl}-4-methyl-1,3-thiazole-5-carboxylate 232



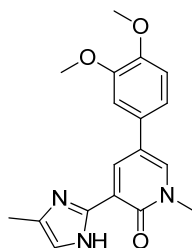
(a) Ethyl 2-bromo-4-methyl-1,3-thiazole-5-carboxylate **157**, Acros Organics, 50 mg, 0.20 mmol; (b) 7.1 mg, 15%; ^1H NMR (400 MHz, CDCl_3) δ ppm 1.31 (t, $J=7.2$ Hz, 3 H), 2.69 (s, 3 H), 3.71 (s, 3 H), 3.79 (s, 3 H), 3.86 (s, 3 H), 4.28 (q, $J=7.2$ Hz, 2 H), 7.04 (d, $J=7.9$ Hz, 1 H), 7.15 (d, $J=7.9$ Hz, 1 H), 7.20-7.22 (m, 1 H), 8.41-8.44 (m, 1 H), 8.73-8.76 (m, 1 H); LCMS (Method A): MH^+ 415, Rt 1.12 min, 100% by UV.

5-[3,4-Bis(methoxy)phenyl]-1-methyl-3-(1-methyl-1H-pyrazol-3-yl)-2(1H)-pyridinone 233



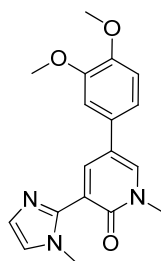
(a) 3-Iodo-1-methyl-1H-pyrazole **158**, Maybridge, 42 mg, 0.20 mmol; (b) 1.9 mg, 5%; ^1H NMR (400 MHz, CDCl_3) δ ppm 3.59 (s, 3 H), 3.78 (s, 3 H), 3.84 (s, 3 H), 3.89 (s, 3 H), 7.00 (d, $J=8.3$, 1 H), 7.08-7.08 (m, 1 H), 7.08-7.10 (m, 1 H), 7.15 (d, $J=1.9$ Hz, 1 H), 7.69 (d, $J=1.9$ Hz, 1 H), 8.08 (d, $J=2.6$ Hz, 1 H), 8.32 (d, $J=2.6$ Hz, 1 H); LCMS (Method A): MH^+ 326, Rt 0.75 min, 100% by UV.

5-[3,4-Bis(methoxy)phenyl]-1-methyl-3-(4-methyl-1*H*-imidazol-2-yl)-2(1*H*)-pyridinone 234



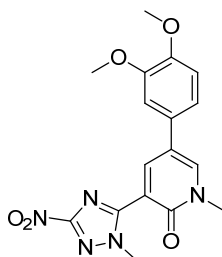
(a) 2-Bromo-4-methyl-1*H*-imidazole **159**, Maybridge, 32 mg, 0.20 mmol; (b) 2.5 mg, 7%; ¹H NMR (400 MHz, CDCl₃) δ ppm 2.20 (s, 3 H), 3.66 (s, 3 H), 3.78 (s, 3 H), 3.85 (s, 3 H), 6.83 (br. s, 1 H), 7.03 (d, *J*=8.7 Hz, 1 H), 7.14 (d, *J*=8.0 Hz, 1 H), 7.17-7.19 (m, 1 H), 8.14-8.18 (m, 1 H), 8.27-8.31 (m, 1 H), 8.48-8.52 (m, 1 H); LCMS (Method A): MH⁺ 326, Rt 0.58 min, 100% by UV.

5-[3,4-Bis(methoxy)phenyl]-1-methyl-3-(1-methyl-1*H*-imidazol-2-yl)-2(1*H*)-pyridinone 235



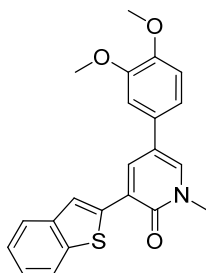
(a) 2-Bromo-1-methyl-1*H*-imidazole **160**, Sigma-Aldrich, 32 mg, 0.20 mmol; (b) 6.1 mg, 17%; ¹H NMR (400 MHz, CDCl₃) δ ppm 3.57 (s, 3 H), 3.61 (s, 3 H), 3.77 (s, 3 H), 3.83 (s, 3 H), 6.94-6.95 (m, 1 H), 7.00 (d, *J*=8.3 Hz, 1 H), 7.12 (dd, *J*=8.3, 1.9 Hz, 1 H), 7.17 (d, *J*=1.5 Hz, 1 H), 7.23-7.25 (m, 1 H), 7.95 (d, *J*=2.3 Hz, 1 H), 8.25 (d, *J*=2.6 Hz, 1 H); LCMS (Method A): MH⁺ 326, Rt 0.49 min, 100% by UV.

5-[3,4-Bis(methoxy)phenyl]-1-methyl-3-(1-methyl-3-nitro-1*H*-1,2,4-triazol-5-yl)-2(1*H*)-pyridinone 236

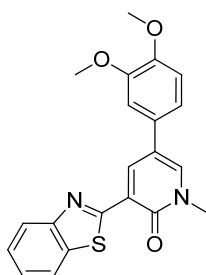


(a) 5-Bromo-1-methyl-3-nitro-1*H*-1,2,4-triazole **161**, ZereneX Molecular Limited, 41 mg, 0.20 mmol; (b) 4.3 mg, 10%; ¹H NMR (400 MHz, CDCl₃) δ ppm 3.65 (s, 3 H), 3.78 (s, 3 H), 3.83 (s, 3 H), 3.94 (s, 3 H), 7.02 (d, *J*=8.3 Hz, 1 H), 7.16 (dd, *J*=8.3, 2.3 Hz, 1 H), 7.20 (d, *J*=1.9 Hz, 1 H), 8.25 (d, *J*=2.3 Hz, 1 H), 8.46 (d, *J*=2.6 Hz, 1 H); LCMS (Method A): MH⁺ 372, Rt 0.80 min, 100% by UV.

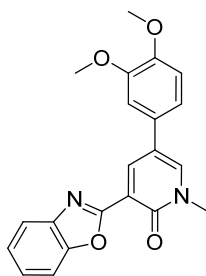
3-(1-Benzothien-2-yl)-5-[3,4-bis(methoxy)phenyl]-1-methyl-2(1*H*)-pyridinone 237



(a) 2-Bromo-1-benzothiophene **162**, Maybridge, 43 mg, 0.20 mmol; (b) 11.9 mg, 28%; ¹H NMR (400 MHz, CDCl₃) δ ppm 3.67 (s, 3 H), 3.80 (s, 3 H), 3.88 (s, 3 H), 7.04 (d, *J*=7.9, 1 H), 7.24 (dd, *J*=7.9, 1.9 Hz, 1 H), 7.26-7.27 (m, 1 H), 7.33 (t, *J*=7.2 Hz, 1 H), 7.37 (t, *J*=7.2 Hz, 1 H), 7.84 (d, *J*=7.6 Hz, 1 H), 7.95 (d, *J*=7.9 Hz, 1 H), 8.20 (d, *J*=1.9 Hz, 1 H), 8.29 (s, 1 H), 8.48 (d, *J*=2.3 Hz, 1 H); LCMS (Method A): MH⁺ 378, Rt 1.16 min, 100% by UV.

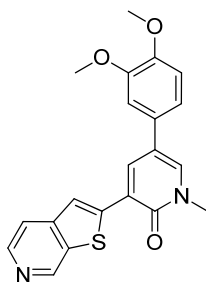
3-(1,3-Benzothiazol-2-yl)-5-[3,4-bis(methoxy)phenyl]-1-methyl-2(1H)-pyridinone**238**

(a) 2-Bromo-1,3-benzothiazole **163**, Sigma-Aldrich, 43 mg, 0.20 mmol; (b) 12.9 mg, 31%; ^1H NMR (400 MHz, CDCl_3) δ ppm 3.73 (s, 3 H), 3.80 (s, 3 H), 3.87 (s, 3 H), 7.07 (d, $J=8.3$ Hz, 1 H), 7.20 (dd, $J=8.7, 1.5$ Hz 1 H), 7.25-7.27 (m, 1 H), 7.42 (t, $J=7.2$ Hz, 1 H), 7.53 (t, $J=7.9$ Hz, 1 H), 8.05 (d, $J=7.9$ Hz, 1 H), 8.14 (d, $J=7.6$ Hz, 1 H), 8.45-8.47 (m, 1 H), 8.93 (d, $J=2.3$ Hz, 1 H); LCMS (Method A): MH^+ 379, Rt 1.08 min, 100% by UV.

3-(1,3-Benzoxazol-2-yl)-5-[3,4-bis(methoxy)phenyl]-1-methyl-2(1H)-pyridinone 239

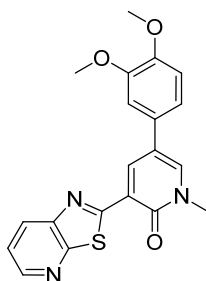
(a) 2-Chloro-1,3-benzoxazole **164**, Sigma-Aldrich, 31 mg, 0.20 mmol; (b) 10.6 mg, 26%; ^1H NMR (400 MHz, CDCl_3) δ ppm 3.65 (s, 3 H), 3.79 (s, 3 H), 3.85 (s, 3 H), 7.03 (d, $J=8.3$ Hz, 1 H), 7.17 (d, $J=7.9$ Hz, 1 H), 7.21-7.24 (m, 1 H), 7.38-7.44 (m, 2 H), 7.76 (d, $J=7.2$ Hz, 1 H), 7.80 (d, $J=7.2$ Hz, 1 H), 8.42-8.45 (m, 1 H), 8.58-8.61 (m, 1 H); LCMS (Method A): MH^+ 363, Rt 0.92 min, 100% by UV

5-[3,4-Bis(methoxy)phenyl]-1-methyl-3-thieno[2,3-*c*]pyridin-2-yl-2(1*H*)-pyridinone 240

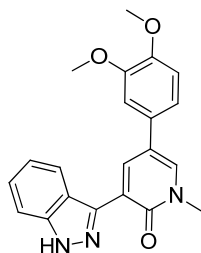


(a) 2-Bromothieno[2,3-*c*]pyridine **165**, Frontier Scientific, 43 mg, 0.20 mmol; (b) 10.4 mg, 25%; m.p. 210-214 °C; $\nu_{\max}/\text{cm}^{-1}$ (solid) 1646 (C=O); ^1H NMR (400 MHz, CDCl_3) δ ppm 3.70 (s, 3 H), 3.80 (s, 3 H), 3.88 (s, 3 H), 7.05 (d, $J=8.3$ Hz, 1 H), 7.25-7.27 (m, 1 H), 7.28-7.30 (m, 1 H), 7.92-7.96 (m, 1 H), 8.34 (d, $J=1.9$ Hz, 1 H), 8.44 (s, 1 H), 8.48 (d, $J=5.7$ Hz, 1 H), 8.71-8.73 (m, 1 H), 9.35-9.38 (m, 1 H); ^{13}C NMR (100 MHz, DMSO-d_6) δ 38.1, 55.6, 55.8, 109.9, 112.2, 117.6, 118.2, 118.7, 119.3, 120.6, 128.2, 136.3, 136.9, 138.6, 139.3, 142.2, 145.2, 148.4, 149.2 (2C), 158.9; LCMS (Method A): MH^+ 379, Rt 0.66 min, 100% by UV; HRMS exact mass calculated for $[\text{M}+\text{H}]^+$ ($\text{C}_{21}\text{H}_{19}\text{N}_2\text{O}_3\text{S}$) requires m/z 379.1116, found 379.1119.

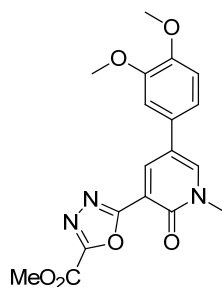
5-[3,4-Bis(methoxy)phenyl]-1-methyl-3-[[1,3]thiazolo[5,4-*b*]pyridin-2-yl]-2(1*H*)-pyridinone 241



(a) 2-Bromo[1,3]thiazolo[5,4-*b*]pyridine **166**, Peakdale Molecular, 43 mg, 0.20 mmol; (b) 2.2 mg, 5%; ^1H NMR (400 MHz, CDCl_3) δ ppm 3.73 (s, 3 H), 3.80 (s, 3 H), 3.87 (s, 3 H), 7.06 (d, $J=7.9$ Hz, 1 H), 7.19 (d, $J=7.6$ Hz, 1 H), 7.23-7.26 (m, 1 H), 7.55-7.59 (m, 1 H), 8.40 (d, $J=8.3$ Hz, 1 H), 8.48-8.51 (m, 1 H), 8.59-8.62 (m, 1 H), 8.89-8.92 (m, 1 H); LCMS (Method A): MH^+ 380, Rt 0.93 min, 100% by UV.

5-[3,4-Bis(methoxy)phenyl]-3-(1*H*-indazol-3-yl)-1-methyl-2(1*H*)-pyridinone 242

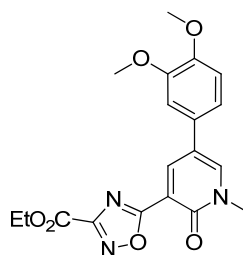
(a) 3-Bromo-1*H*-indazole **167**, Allichem LLC, 39 mg, 0.20 mmol; (b) 6 mg, 15%; ¹H NMR (400 MHz, CDCl₃) δ ppm 3.65 (s, 3 H), 3.78 (s, 3 H), 3.84 (s, 3 H), 7.01 (d, *J*=8.1 Hz, 1 H), 7.09 (t, *J*=7.2 Hz, 1 H), 7.14 (d, *J*=7.9 Hz, 1 H), 7.19 (br. s, 1 H), 7.34 (t, *J*=7.2 Hz, 1 H), 7.54 (d, *J*=8.3 Hz, 1 H), 7.94 (d, *J*=8.3 Hz, 1 H), 8.13 (br. s, 1 H), 8.19-8.21 (m, 1 H), 8.53 (br. s, 1 H); LCMS (Method A): MH⁺ 392, Rt 0.89 min, 100% by UV.

Methyl 5-{5-[3,4-bis(methoxy)phenyl]-1-methyl-2-oxo-1,2-dihydro-3-pyridinyl}-1,3,4-oxadiazole-2-carboxylate 188

1,2-Dihydro-5-[3,4-bis(methoxy)phenyl]-1-methyl-2-oxo-3-pyridinecarboxylic acid¹⁵⁷ **186** (500 mg, 1.73 mmol), HATU (657 mg, 1.73 mmol) and *N,N*-diisopropylethylamine (600 μL, 3.46 mmol) were suspended in *N,N*-dimethylformamide and stirred at RT for 10 min. Methyl hydrazine(oxo)acetate (Chembridge, 204 mg, 1.73 mmol) was added and the reaction mixture stirred at RT for a further 1 h. The solvent was removed *in vacuo* and the residue purified by column chromatography on a Si cartridge (70 g), eluting with 0-100% ethyl acetate/cyclohexane followed by 0-20% methanol/ethyl acetate. The required fractions were combined and concentrated and the residue partitioned between ethyl acetate and saturated aqueous NaHCO₃ solution. The layers were separated and the aqueous phase was extracted with further ethyl acetate (3 x 5 mL). The combined organic fractions were dried over anhydrous sodium sulfate and concentrated *in vacuo* to give a yellow solid, 275 mg.

The solid was dried in a desiccator over P₂O₅, then dissolved in anhydrous tetrahydrofuran (5 mL). Burgess reagent (618 mg, 2.59 mmol) was added and the reaction mixture heated to 75 °C for 1 h. After cooling, the solvent was removed *in vacuo* and the residue purified by column chromatography on a Si cartridge (50 g), eluting with 0-100% ethyl acetate/cyclohexane followed by 0-20% methanol/ethyl acetate. The required fractions were combined and concentrated *in vacuo* to give a yellow solid (249 mg), which was further purified by Mass Directed AutoPrep on a Sunfire C₁₈ column using acetonitrile/water with a formic acid modifier. The desired fractions were concentrated to give the title compound (6.2 mg, 1%); ¹H NMR (400 MHz, DMSO-*d*₆) δ ppm 3.77 (s, 3 H), 3.94 (s, 3 H), 3.97 (s, 3 H), 4.09 (s, 3 H), 6.92-6.95 (m, 1 H), 6.95-6.97 (m, 1 H), 7.00 (dd, *J*=8.3, 2.0 Hz, 1 H), 7.77 (d, *J*=2.8 Hz, 1 H), 8.61 (d, *J*=2.8 Hz, 1 H); LCMS (Method B): MH⁺ 372, Rt 0.75 min.

Attempted formations of ethyl 5-{5-[3,4-bis(methoxy)phenyl]-1-methyl-2-oxo-1,2-dihydro-3-pyridinyl}-1,2,4-oxadiazole-3-carboxylate 190

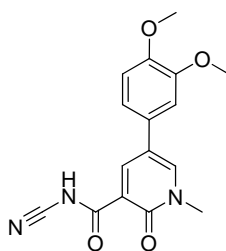


Method E:

1,2-Dihydro-5-[3,4-bis(methoxy)phenyl]-1-methyl-2-oxo-3-pyridinecarboxylic acid¹⁵⁷ **186** (100 mg, 0.346 mmol), HATU (131 mg, 0.346 mmol) and *N,N*-diisopropylethylamine (121 μL, 0.691 mmol) were suspended in *N,N*-dimethylformamide (3 mL) and stirred at RT for 20 min. Ethyl (2*Z*)-(hydroxyamino)(imino)ethanoate (Sigma-Aldrich, 46 mg, 0.35 mmol) was added and the reaction mixture stirred at RT for a further 2 h. DBU (260 μL, 1.73 mmol) was added and the reaction mixture heated to 75 °C for 1 h. After cooling to RT, the reaction mixture was acidified with 2 N aqueous HCl and diluted with water (4 mL) then ethyl acetate (4 mL). The layers were separated and the organic phase concentrated to give a crude solid which was purified by column chromatography on a Si cartridge (20 g), eluting with 0-100% ethyl acetate/cyclohexane then 0-20% methanol/ethyl acetate. The appropriate fractions were combined and concentrated *in vacuo* to give two products:

(i) An impure yellow solid (30 mg) which was further purified by Mass Directed Autoprep on a Sunfire C₁₈ column using acetonitrile/water with a formic acid modifier. The required fractions were concentrated to give the title compound (3 mg, 2%); ¹H NMR and LCMS were not conclusive, and insufficient material was obtained to confirm the structure.

(ii)



N-Cyano-1,2-dihydro-5-[3,4-bis(methoxy)phenyl]-1-methyl-2-oxo-3-pyridinecarboxamide, **191** (7 mg, 6%) as a yellow solid; $\nu_{\max}/\text{cm}^{-1}$ (solid) 2253 (CN), 1692 (C=O), 1638 (C=O); ¹H NMR (600 MHz, DMSO-*d*₆) δ ppm 3.69 (s, 3 H), 3.79 (s, 3 H), 3.85 (s, 3 H), 7.04 (d, *J*=8.4 Hz, 1 H), 7.16 (dd, *J*=8.1, 1.8 Hz, 1 H), 7.21 (d, *J*=2.2 Hz, 1 H), 8.60 (d, *J*=2.6 Hz, 1 H), 8.62 (d, *J*=2.6 Hz, 1 H), 12.50 (s, 1 H); ¹³C NMR (150 MHz, DMSO-*d*₆) δ ppm 38.2, 55.6, 55.7, 108.1, 109.6, 112.2, 115.6, 118.1, 119.4, 127.2, 142.8, 143.8, 148.6, 149.2, 160.6, 164.1; LCMS (Method B): MH⁺ 314, Rt 0.81 min; HRMS exact mass calculated for [M+H]⁺ (C₁₆H₁₆N₃O₄) requires *m/z* 314.1141, found 314.1136. Insufficient material remained after biological testing to obtain a melting point.

Method F:

1,2-Dihydro-5-[3,4-bis(methoxy)phenyl]-1-methyl-2-oxo-3-pyridinecarboxylic acid **186** (100 mg, 0.346 mmol), HATU (131 mg, 0.346 mmol) and *N,N*-diisopropylethylamine (120 μ L, 0.691 mmol) were suspended in *N,N*-dimethylformamide (3 mL) and stirred at RT for 20 min. Ethyl (2*Z*)-(hydroxyamino)(imino)ethanoate (46 mg, 0.35 mmol) was added and the reaction mixture stirred at RT for a further 2 h. The solvent was removed *in vacuo* and the residue purified by column chromatography on a Si cartridge (10 g), eluting with 0-100% ethyl acetate/cyclohexane then 0-20% methanol/ethyl acetate. The appropriate fractions were combined and concentrated *in vacuo* to give the desired intermediate (140 mg) as a yellow gum.

The gum was dried in a dessicator over P₂O₅ overnight, then dissolved in *N,N*-dimethylformamide (2 mL) and DBU (260 μL, 1.73 mmol) was added and the reaction mixture heated to 75 °C for 1 h. LCMS showed major peaks consistent with desired product and **190**. After cooling to RT, the reaction mixture was concentrated and the crude residue purified by Mass Directed Autoprep on a Sunfire C₁₈ column using acetonitrile/water with a formic acid modifier. No product was collected and analysis of the LCMS trace showed a single peak MH⁺ 314, Rt 7.75 min eluted which was consistent with *N*-cyano-1,2-dihydro-5-[3,4-bis(methoxy)phenyl]-1-methyl-2-oxo-3-pyridinecarboxamide, **191**.

Method G:

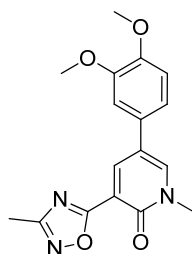
1,2-Dihydro-5-[3,4-bis(methoxy)phenyl]-1-methyl-2-oxo-3-pyridinecarboxylic acid **186** (300 mg, 10.4 mmol), HATU (394 mg, 1.04 mmol) and *N,N*-diisopropylethylamine (360 μL, 2.07 mmol) were suspended in *N,N*-dimethylformamide (6 mL) and stirred at RT for 20 min. Ethyl (2*Z*)-(hydroxyamino)(imino)ethanoate (137 mg, 1.04 mmol) was added and the reaction mixture stirred at RT for a further 2 h. The solvent was removed *in vacuo* and the residue purified by column chromatography on a Si cartridge (50 g), eluting with 0-100% ethyl acetate/cyclohexane then 0-20% methanol/ethyl acetate. The appropriate fractions were combined and concentrated *in vacuo* to give the desired intermediate (128 mg) as a yellow gum.

(a) The yellow gum (73 mg) was dried in a dessicator over P₂O₅ overnight, then dissolved in *N,N*-dimethylformamide (1 mL) and DBU (140 μL, 0.900 mmol) added. The reaction mixture was heated to 75 °C for 1 h. LCMS showed major peaks consistent with desired product and structure **190**. The reaction mixture was diluted with ethyl acetate (3 mL) and water (3 mL). The layers were separated and analysed by LCMS. Neither contained a peak consistent with desired product; the major peak in each case was consistent with *N*-cyano-1,2-dihydro-5-[3,4-bis(methoxy)phenyl]-1-methyl-2-oxo-3-pyridinecarboxamide, **191**.

(b) The yellow gum (55 mg) was dissolved in anhydrous 1,4-dioxane and 4 M HCl in 1,4-dioxane (4 drops) was added. The reaction vessel was sealed and heated in a Biotage

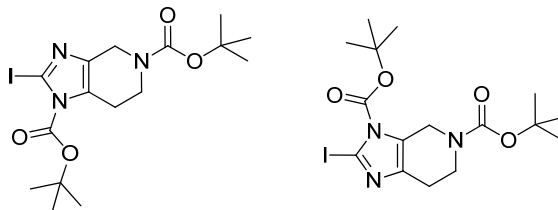
microwave to 100 °C for 10 min. LCMS showed major peak was consistent with starting material.

5-[3,4-Bis(methoxy)phenyl]-1-methyl-3-(3-methyl-1,2,4-oxadiazol-5-yl)-2(1H)-pyridinone 196



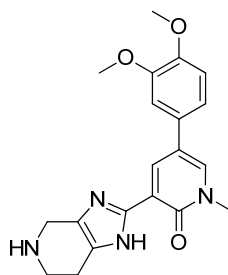
1,2-Dihydro-5-[3,4-bis(methoxy)phenyl]-1-methyl-2-oxo-3-pyridinecarboxylic acid **186** (150 mg, 0.519 mmol), HATU (198 mg, 0.519 mmol) and *N,N*-diisopropylethylamine (0.181 mL, 1.04 mmol) were suspended in *N,N*-dimethylformamide (2 mL) and stirred at RT for 20 min. (*E*)-*N*-Hydroethanimidamide (ABCR-Gelest, 38 mg, 0.52 mmol) was added and the reaction mixture stirred at RT for 18 h. DBU (390 μ L, 2.59 mmol) was added and the reaction mixture heated to 75 °C for 1 h. The reaction mixture was concentrated *in vacuo* and the residue purified by Mass Directed AutoPrep on a Sunfire C₁₈ column using acetonitrile/water with a formic acid modifier. The desired fractions were concentrated to give the title compound (50 mg, 30%) as a yellow solid; m.p. 191-199 °C; $\nu_{\max}/\text{cm}^{-1}$ (solid) 1670 (C=O); ¹H NMR (400 MHz, DMSO-*d*₆) δ ppm 2.41 (s, 3 H), 3.64 (s, 3 H), 3.79 (s, 3 H), 3.85 (s, 3 H), 7.03 (d, *J*=8.3 Hz, 1 H), 7.15 (dd, *J*=8.3, 2.0 Hz, 1 H), 7.19-7.22 (m, 1 H), 8.49 (d, *J*=2.5 Hz, 1 H), 8.55 (d, *J*=2.5 Hz, 1 H); ¹³C NMR (100 MHz, DMSO-*d*₆) δ ppm 11.1, 37.9, 55.6, 55.7, 109.5, 112.2, 112.8, 117.6, 117.8, 127.7, 141.7, 142.4, 148.4, 149.2, 157.2, 166.7, 173.6; LCMS (Method B): MH⁺ 328, Rt 1.88 min; HRMS exact mass calculated for [M+H]⁺ (C₁₇H₁₈N₃O₄) requires *m/z* 328.1297, found 328.1298.

Bis(1,1-dimethylethyl) 6,7-dihydro-2-iodo-1*H*-imidazo[4,5-*c*]pyridine-1,5(4*H*)-dicarboxylate / bis(1,1-dimethylethyl) 6,7-dihydro-2-iodo-3*H*-imidazo[4,5-*c*]pyridine-3,5(4*H*)-dicarboxylate **200**



4,5,6,7-Tetrahydro-2-iodo-1*H*-imidazo[4,5-*c*]pyridine hydrochloride¹⁶² **198** (500 mg, 1.55 mmol), di-*tert*-butyl dicarbonate (847 mg, 3.88 mmol) and triethylamine (1.1 mL, 7.8 mmol) were suspended in acetonitrile (10 mL) and stirred at RT for 18 h. The solvent was removed *in vacuo* and the residue purified by column chromatography on a Si cartridge (20 g), eluting with 0-100% ethyl acetate/cyclohexane. The appropriate fractions were combined and concentrated to give the desired product as a mixture of two regioisomers (207 mg, 30%); ¹H NMR (400 MHz, CDCl₃) δ ppm 1.47 (s, 9 H), 1.49 (s, 9 H), 1.65 (s, 9 H), 1.66 (s, 9 H), 2.62-2.70 (m, 2 H), 2.84-2.94 (m, 2 H), 3.60-3.72 (m, 4 H), 4.40-4.44 (m, 2 H), 4.57-4.67 (m, 2 H) (NMR reported for both regioisomers i.e. double the number of protons); LCMS (Method A): MH⁺ 450, Rt 1.21 min and 1.24 min.

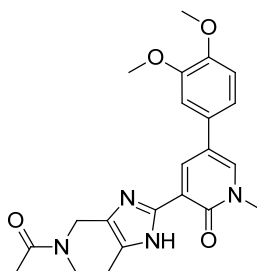
5-[3,4-Bis(methoxy)phenyl]-1-methyl-3-(4,5,6,7-tetrahydro-1*H*-imidazo[4,5-*c*]pyridin-2-yl)-2(1*H*)-pyridinone **199**



5-[3,4-Bis(methoxy)phenyl]-1-methyl-3-(4,4,5,5-tetramethyl-1,3,2-dioxaborolan-2-yl)-2(1*H*)-pyridinone **141** (200 mg, ~0.20 mmol), bis(1,1-dimethylethyl) 6,7-dihydro-2-iodo-1*H*-imidazo[4,5-*c*]pyridine-1,5(4*H*)-dicarboxylate / bis(1,1-dimethylethyl) 6,7-dihydro-2-iodo-3*H*-imidazo[4,5-*c*]pyridine-3,5(4*H*)-dicarboxylate **200** (151 mg, 0.336 mmol), potassium carbonate (93 mg, 0.67 mmol) and PdCl₂(dppf).DCM (19 mg, 0.020 mmol) were suspended in 1,4-dioxane (2 mL) and water (0.5 mL). The reaction vessel was sealed and heated in Biotage microwave to 100 °C for 2 h. HCl in 1,4-

dioxane (4 M, 2 mL) was added and the crude reaction mixture stirred at RT for 2 h. The crude reaction mixture was loaded directly onto a C₁₈ SPE cartridge (2 g) (pre-conditioned with 0.1% TFA/MeCN) and eluted with 0.1% TFA/MeCN then methanol. The methanol fractions were concentrated afford a dark yellow solid (141 mg) which was purified by Mass Directed AutoPrep on Sunfire C₁₈ column using acetonitrile/water with a formic acid modifier. The required fractions were combined and the solvent was evaporated *in vacuo* to give the required product (34 mg, 46%); ¹H NMR (400 MHz, DMSO-*d*₆) δ ppm 3.03-3.07 (m, 2 H), 3.40-3.53 (m, 2 H), 3.77 (s, 3 H), 3.93 (s, 3 H), 3.98 (s, 3 H), 4.27 (s, 2 H), 6.93 (d, *J*=8.3 Hz, 1 H), 7.00-7.03 (m, 1 H), 7.05 (d, *J*=8.6 Hz, 1 H), 7.55-7.59 (m, 1 H), 8.19-8.26 (m, 2 H), 8.66-8.69 (m, 1 H); LCMS (Method B): MH⁺ 367, Rt 0.91 min.

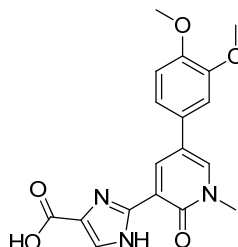
3-(5-Acetyl-4,5,6,7-tetrahydro-1*H*-imidazo[4,5-*c*]pyridin-2-yl)-5-[3,4-bis(methoxy)phenyl]-1-methyl-2(1*H*)-pyridinone 201



5-[3,4-Bis(methoxy)phenyl]-1-methyl-3-(4,5,6,7-tetrahydro-1*H*-imidazo[4,5-*c*]pyridin-2-yl)-2(1*H*)-pyridinone **199** (34 mg, 0.083 mmol) was suspended in dichloromethane (2 mL). *N,N*-Diisopropylethylamine (29 μL, 0.17 mmol) and acetyl chloride (6 μL, 0.08 mmol) were then added. The reaction mixture was stirred at RT for 2 h. The solvent was removed *in vacuo* and the residue purified by HPLC eluting with 35-50% MeOH/10 mM aqueous ammonium bicarbonate adjusted to pH10 with ammonia solution to give the desired product (9 mg, 10%) as a yellow solid; $\nu_{\max}/\text{cm}^{-1}$ (solid) 1669 (C=O), 1658 (C=O); Mixture of tautomers (~1.4:1); some signals duplicated in NMR ¹H NMR (400 MHz, CDCl₃) δ ppm 2.19 and 2.21 (s, 3 H), 2.78 and 2.83 (t, *J*=5.4 Hz, 2 H), 3.757 and 3.762 (s, 3 H), 3.93 (s, 3 H), 3.94-3.98 (m, 2 H), 3.96 (s, 3 H), 4.60 and 4.74 (s, 2 H), 6.92 (d, *J*=8.3 Hz, 1 H), 6.99 (m, 1 H), 7.05 (dd, *J*=8.3, 2.0 Hz, 1 H), 7.51 and 7.52 (d, *J*=2.5 Hz, 1 H), 8.63 and 8.67 (d, *J*=2.3 Hz, 1 H), 11.94 (br. s, 1 H); LCMS (Method B): MH⁺ 409, Rt 0.57 min; HRMS exact mass calculated for [M+H]⁺

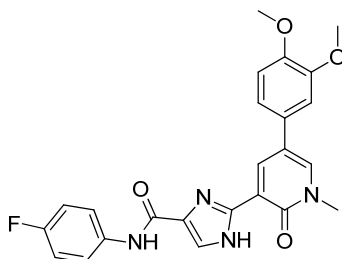
(C₂₂H₂₅N₄O₄) requires *m/z* 409.1876, found 409.1861. Insufficient material remained after biological testing to obtain a ¹³C NMR and melting point.

2-(5-(3,4-Dimethoxyphenyl)-1-methyl-2-oxo-1,2-dihydropyridin-3-yl)-1*H*-imidazole-4-carboxylic acid 248



Ethyl 2-(5-(3,4-dimethoxyphenyl)-1-methyl-2-oxo-1,2-dihydropyridin-3-yl)-1*H*-imidazole-4-carboxylate **247** (1.0 g, 2.6 mmol) was dissolved in tetrahydrofuran (20 mL) and aqueous sodium hydroxide (0.05 M, 5.20 mL, 0.26 mmol) was added slowly. The reaction mixture was stirred at RT for 18 h, after which time additional aqueous sodium hydroxide (0.05 M, 5.20 mL, 0.26 mmol) was added. After stirring for an additional 5 h, the reaction mixture was neutralised by the addition of 2 M aqueous hydrochloric acid. The volatile organic solvents were removed *in vacuo* and the remaining aqueous diluted to ~750 mL with water. The solution was passed through a pre-conditioned Oasis SPE cartridge (1 g), washing with additional water. The cartridge was then eluted with methanol (50 mL) and the solvent removed *in vacuo*. The residue was purified by column chromatography (silica) eluting with 0-10% methanol in dichloromethane. The appropriate fractions were concentrated *in vacuo* to give the title compound (927 mg, 55%). ¹H NMR (400 MHz, DMSO-*d*₆) δ ppm 3.69 (s, 3 H), 3.79 (s, 3 H), 3.86 (s, 3 H), 7.04 (d, *J*=8.3 Hz, 1 H), 7.15 (dd, *J*=8.3, 2.0 Hz, 1 H), 7.20 (d, *J*=1.8 Hz, 1 H), 7.48 (br. s, 1 H), 8.25 (d, *J*=2.8 Hz, 1 H), 8.30-8.32 (br. s, 1 H), 8.57 (d, *J*=2.5 Hz, 1 H), 12.20 (br. s, 1 H); LCMS (Method A): MH⁺ 356, Rt 0.57 min, 99% by UV.

2-(5-(3,4-Dimethoxyphenyl)-1-methyl-2-oxo-1,2-dihydropyridin-3-yl)-N-(4-fluorophenyl)-1H-imidazole-4-carboxamide 249a

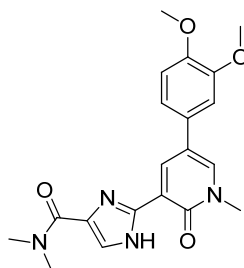


Typical Procedure E:

2-(5-(3,4-Dimethoxyphenyl)-1-methyl-2-oxo-1,2-dihydropyridin-3-yl)-1H-imidazole-4-carboxylic acid **248** (36 mg, 0.10 mmol), 4-fluoroaniline (Sigma-Aldrich, 12 mg, 0.11 mmol), PyBOP (52 mg, 0.10 mmol) and DIPEA (35 μ L, 0.20 mmol) were combined in *N,N*-dimethylformamide (0.4 mL) and stirred at RT for 22 h. DMSO (0.5 mL) was added and the sample purified by Mass Directed AutoPrep on Atlantis column using acetonitrile/water with a formic acid modifier. The appropriate fractions were concentrated *in vacuo* to give the title compound (9.2 mg, 18%). ^1H NMR (600 MHz, DMSO- d_6) δ ppm 3.70 (s, 3 H), 3.80 (s, 3 H), 3.88 (s, 3 H), 7.07 (d, $J=8.3$ Hz, 1 H), 7.15-7.22 (m, 3 H), 7.23-7.25 (m, 1 H), 7.75 (s, 1 H), 7.86-7.89 (m, 2 H), 8.29 (d, $J=2.3$ Hz, 1 H), 8.79 (d, $J=2.3$ Hz, 1 H), 9.93 (br. s, 1 H), 12.65 (br. s, 1 H); LCMS (Method A): MH^+ 449, Rt 0.99 min, 99% by UV.

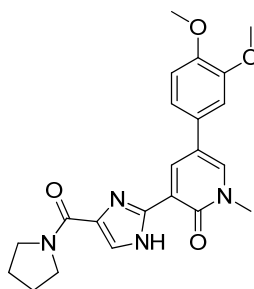
The following experiments were performed using Typical Procedure E, the data are reported as (a) amine (supplier, g, mmol); (b) product (mg, % yield).

2-(5-(3,4-Dimethoxyphenyl)-1-methyl-2-oxo-1,2-dihydropyridin-3-yl)-*N,N*-dimethyl-1*H*-imidazole-4-carboxamide 249b



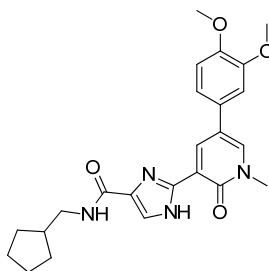
(a) *N,N*-Dimethylamine, Sigma-Aldrich, 5.0 mg, 0.11 mmol; (b) 15 mg, 32% as a yellow solid; m.p. 146-152 °C; $\nu_{\max}/\text{cm}^{-1}$ (solid) 1650 and 1590 (C=O); ^1H NMR (600 MHz, $\text{DMSO-}d_6$) δ ppm 3.17 (s, 6 H), 3.69 (s, 3 H), 3.79 (s, 3 H), 3.85 (s, 3 H), 7.05 (d, $J=8.3$ Hz, 1 H), 7.14 (dd, $J=8.3, 1.89$ Hz, 1 H), 7.19 (d, $J=1.9$ Hz, 1 H), 7.59 (s, 1 H), 8.28 (d, $J=1.9$ Hz, 1 H), 8.57-8.59 (m, 1 H), 12.79 (br. s, 1 H); ^{13}C NMR (101 MHz, $\text{DMSO-}d_6$) δ ppm 38.2, 56.1 (2C), 56.2 (2C), 110.0, 112.6, 117.9, 118.4 (2C), 119.3, 128.3, 128.8 (2C), 135.4, 137.4, 138.0, 148.8, 149.6, 159.8 nb. formic acid carbon not observed; LCMS (Method A): MH^+ 383, Rt 0.65 min, 100% by UV; HRMS exact mass calculated for $[\text{M}+\text{H}]^+$ ($\text{C}_{20}\text{H}_{23}\text{N}_4\text{O}_4$) requires m/z 383.1714, found 383.1714.

5-(3,4-Dimethoxyphenyl)-1-methyl-3-(4-(pyrrolidine-1-carbonyl)-1*H*-imidazol-2-yl)pyridin-2(1*H*)-one 249c



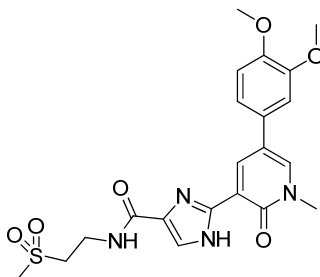
(a) Pyrrolidine, Sigma-Aldrich, 8.0 mg, 0.11 mmol; (b) 14 mg, 27%; ^1H NMR (600 MHz, $\text{DMSO-}d_6$) δ ppm 1.82 (t, $J=6.8$ Hz, 2 H), 1.88-1.97 (m, 2 H), 3.48 (t, $J=6.8$ Hz, 2 H), 3.69 (s, 3 H), 3.79 (s, 3 H), 3.85 (s, 3 H), 4.06-4.20 (m, 2 H), 7.04 (d, $J=8.3$ Hz, 1 H), 7.13 (dd, $J=8.3, 1.9$ Hz, 1 H), 7.19 (d, $J=1.9$ Hz, 1 H), 7.59 (s, 1 H), 8.25-8.27 (m, 1 H), 8.57-8.59 (m, 1 H), 12.57 (br. s, 1 H); LCMS (Method A): MH^+ 409, Rt 0.72 min, 100% by UV.

***N*-(Cyclopentylmethyl)-2-(5-(3,4-dimethoxyphenyl)-1-methyl-2-oxo-1,2-dihydropyridin-3-yl)-1*H*-imidazole-4-carboxamide 249d**



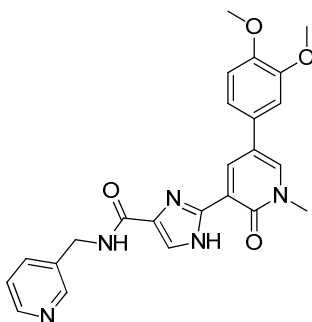
(a) Cyclopentylmethanamine, Fluorochem Ltd., 11 mg, 0.11 mmol; (b) 13 mg, 27%; ¹H NMR (600 MHz, DMSO-*d*₆) δ ppm 1.16-1.29 (m, 2 H), 1.43-1.51 (m, 2 H), 1.53-1.59 (m, 2 H), 1.60-1.67 (m, 2 H), 2.08-2.19 (m, 1 H), 3.13-3.19 (m, 2 H), 3.68 (s, 3 H), 3.79 (s, 3 H), 3.85 (s, 3 H), 7.04 (d, *J*=8.3 Hz, 1 H), 7.12-7.15 (m, 1 H), 7.19-7.21 (m, 1 H), 7.56 (d, *J*=1.9 Hz, 1 H), 8.03-8.07 (m, 1 H), 8.25 (d, *J*=2.3 Hz, 1 H), 8.65 (d, *J*=2.3 Hz, 1 H), 12.52 (s, 1 H); LCMS (Method A): MH⁺ 437, Rt 0.97 min, 100% by UV.

2-(5-(3,4-Dimethoxyphenyl)-1-methyl-2-oxo-1,2-dihydropyridin-3-yl)-*N*-(2-(methylsulfonyl)ethyl)-1*H*-imidazole-4-carboxamide 249e



(a) 2-(Methylsulfonyl)ethanamine, Enamine, 14 mg, 0.11 mmol; (b) 11.1 mg, 22%; ¹H NMR (600 MHz, DMSO-*d*₆) δ ppm 3.03 (s, 3 H), 3.34-3.42 (m, 2 H), 3.68 (s, 3 H), 3.68-3.73 (m, 2 H), 3.79 (s, 3 H), 3.86 (s, 3 H), 7.05 (d, *J*=7.9 Hz, 1 H), 7.11-7.14 (m, 1 H), 7.18-7.20 (m, 1 H), 7.59-7.61 (m, 1 H), 8.25 (d, *J*=2.3 Hz, 1 H), 8.31-8.34 (m, 1 H), 8.62 (d, *J*=2.3 Hz, 1 H), 12.56 (br. s, 1 H); LCMS (Method A): MH⁺ 461, Rt 0.69 min, 96% by UV.

2-(5-(3,4-Dimethoxyphenyl)-1-methyl-2-oxo-1,2-dihydropyridin-3-yl)-N-(pyridin-3-ylmethyl)-1H-imidazole-4-carboxamide 249f

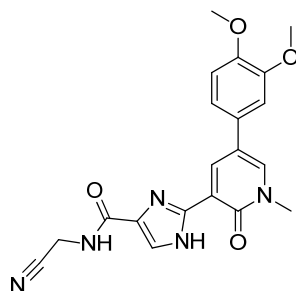


Typical Procedure F:

2-(5-(3,4-Dimethoxyphenyl)-1-methyl-2-oxo-1,2-dihydropyridin-3-yl)-1H-imidazole-4-carboxylic acid **248** (36 mg, 0.10 mmol), pyridin-3-ylmethanamine (Sigma-Aldrich, 12 mg, 0.11 mmol), PyBOP (52 mg, 0.10 mmol) and DIPEA (35 μ L, 0.20 mmol) were combined in *N,N*-dimethylformamide (0.4 mL) and stirred at RT for 22 h. DMSO (0.5 mL) was added and the sample purified by Mass Directed AutoPrep on Atlantis column using acetonitrile/water with a formic acid modifier. The appropriate fractions were concentrated *in vacuo*, then further purified by Mass Directed AutoPrep on Xbridge column using acetonitrile/water with an ammonium bicarbonate modifier purified to give the title compound (2.4 mg, 4%). ^1H NMR (600 MHz, DMSO- d_6) δ ppm 3.68 (s, 3 H), 3.78 (s, 3 H), 3.85 (s, 3 H), 4.47 (d, $J=5.7$ Hz, 2 H), 7.00-7.07 (m, 1 H), 7.12 (d, $J=7.9$ Hz, 1 H), 7.15-7.21 (m, 1 H), 7.31-7.38 (m, 1 H), 7.61 (s, 1 H), 7.69-7.75 (m, 1 H), 8.26 (br. s, 1 H), 8.42-8.48 (m, 1 H), 8.52-8.58 (m, 1 H), 8.64 (br. s, 1 H), 8.74 (t, $J=5.9$ Hz, 1 H), 12.56 (br. s, 1 H); LCMS (Method A): MH^+ 446, R_t 0.56 min, 100% by UV.

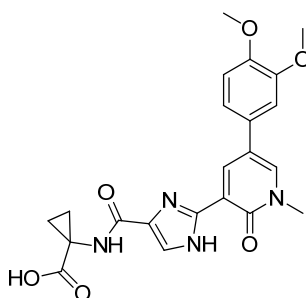
The following experiments were performed using Typical Procedure F, the data are reported as (a) amine (supplier, g, mmol); (b) product (mg, % yield).

***N*-(Cyanomethyl)-2-(5-(3,4-dimethoxyphenyl)-1-methyl-2-oxo-1,2-dihydropyridin-3-yl)-1*H*-imidazole-4-carboxamide 249g**



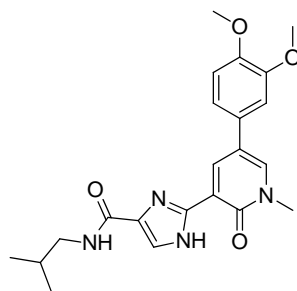
(a) 2-Aminoacetonitrile, Sigma-Aldrich, 6.0 mg, 0.11 mmol; (b) 1.2 mg, 3%; ¹H NMR (600 MHz, DMSO- *d*₆) δ ppm 3.69 (s, 3 H), 3.80 (s, 3 H), 4.86 (s, 3 H), 4.26 (d, *J*=5.7 Hz, 2 H), 7.06 (d, *J*=8.3 Hz, 1 H), 7.14 (d, *J*=8.3 Hz, 1 H), 7.21 (s, 1 H), 7.67 (s, 1 H), 8.28 (s, 1 H), 8.62-8.68 (m, 1 H), 8.76 (t, *J*=5.5 Hz, 1 H), 12.63 (br. s, 1H); LCMS (Method A): MH⁺ 394, Rt 0.72 min, 100% by UV.

1-(2-(5-(3,4-Dimethoxyphenyl)-1-methyl-2-oxo-1,2-dihydropyridin-3-yl)-1*H*-imidazole-4-carboxamido)cyclopropanecarboxylic acid 249h



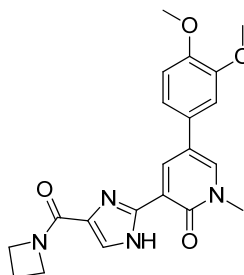
(a) 1-Aminocyclopropanecarboxylic acid, Acros Organics, 11 mg, 0.11 mmol; (b) 2 mg, 3%; ¹H NMR (600 MHz, DMSO- *d*₆) δ ppm 1.15-1.17 (m, 2 H), 1.25-1.31 (m, 2 H), 3.65 (s, 3 H), 3.76 (s, 3 H), 3.84 (s, 3 H), 7.05 (d, *J*=8.3 Hz, 1 H), 7.12-7.19 (m, 1 H), 7.21 (s, 1 H), 7.54 (s, 1 H), 8.26 (br. s, 1 H), 8.44-8.50 (m, 1 H), 8.65 (br. s, 1 H), 12.51 (br. s, 1H), nb. the carboxylic acid proton was thought to coincide with the water peak; LCMS (Method A): MH⁺ 439, Rt 0.70 min, 94% by UV.

2-(5-(3,4-Dimethoxyphenyl)-1-methyl-2-oxo-1,2-dihydropyridin-3-yl)-*N*-isobutyl-1*H*-imidazole-4-carboxamide 249i



(a) 2-Methylpropan-1-amine, Sigma-Aldrich, 8.0 mg, 0.11 mmol; (b) 3 mg, 6%; ¹H NMR (600 MHz, DMSO- *d*₆) δ ppm 0.87 (d, *J*=6.4 Hz, 6 H), 1.80-1.86 (m, 1 H), 3.07 (t, *J*=6.6 Hz, 2 H), 3.69 (s, 3 H), 3.79 (s, 3 H), 3.85 (s, 3 H), 7.04 (d, *J*=8.3 Hz, 1 H), 7.14 (d, *J*=8.3 Hz, 1 H), 7.20 (s, 1 H), 7.56 (br. s, 1 H), 8.03 (br. s, 1 H), 8.26 (br. s, 1 H), 8.64 (br. s, 1 H), 12.50 (br. s, 1 H) ; LCMS (Method A): MH⁺ 411, Rt 0.87 min, 100% by UV.

3-(4-(Azetidine-1-carbonyl)-1*H*-imidazol-2-yl)-5-(3,4-dimethoxyphenyl)-1-methylpyridin-2(1*H*)-one 250a



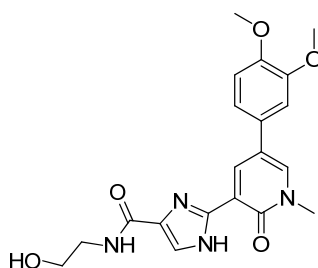
Typical Procedure G:

Ethyl 2-(5-(3,4-dimethoxyphenyl)-1-methyl-2-oxo-1,2-dihydropyridin-3-yl)-1*H*-imidazole-4-carboxylate **247**¹⁶⁶ (38 mg, 0.1 mmol), azetidine (Sigma-Aldrich, 11 mg, 0.20 mmol) and TBD (4 mg, 0.3 mmol) were combined in tetrahydrofuran (0.5 mL). The reaction was heated under microwave irradiation to 140 °C for 1 h. The solvent was removed and the residue dissolved in DMSO (0.5 mL) and purified by Mass Directed AutoPrep on Xbridge column using acetonitrile/water with an ammonium bicarbonate modifier. The appropriate fractions were concentrated *in vacuo* to give the title compound as a cream solid (11 mg, 25%); m.p. 230-232 °C; $\nu_{\max}/\text{cm}^{-1}$ (solid) 1651 and 1590 (C=O); ¹H NMR (400 MHz, DMSO-*d*₆) δ ppm 2.21-2.31 (m, 2 H), 3.68 (s, 3 H), 3.79 (s, 3 H), 3.85 (s, 3 H), 3.94-4.04 (m, 2 H), 4.57-4.66 (m, 2 H), 7.05 (d, *J*=8.3 Hz,

1 H), 7.12 (dd, $J=8.3, 1.8$ Hz, 1 H), 7.18 (d, $J=1.8$ Hz, 1 H), 7.55 (s, 1 H), 8.23 (d, $J=2.5$ Hz, 1 H), 8.52 (d, $J=2.5$ Hz, 1 H), 12.51 (br. s, 1 H); ^{13}C NMR (101 MHz, DMSO- d_6) δ ppm 16.0, 37.5, 55.6 (2C), 55.7 (2C), 109.9, 112.4, 117.8, 118.7, 120.9, 124.0, 128.5, 134.5, 136.2, 136.9, 142.4, 148.3, 149.2, 159.3, 162.4; LCMS (Method A): MH^+ 395, Rt 0.67 min, 98% by UV; HRMS exact mass calculated for $[\text{M}+\text{H}]^+$ ($\text{C}_{21}\text{H}_{23}\text{N}_4\text{O}_4$) requires m/z 395.1714, found 395.1718.

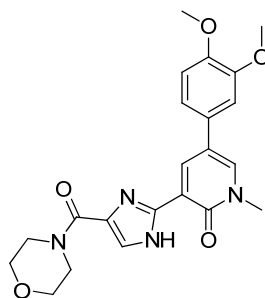
The following experiments were performed using Typical Procedure G, the data are reported as (a) amine (supplier, g, mmol); (b) product (mg, % yield).

2-(5-(3,4-Dimethoxyphenyl)-1-methyl-2-oxo-1,2-dihydropyridin-3-yl)-N-(2-hydroxyethyl)-1H-imidazole-4-carboxamide 250b



(a) Ethanolamine, Sigma-Aldrich, 12 mg, 0.20 mmol; (b) 7 mg, 17%; ^1H NMR (400 MHz, DMSO- d_6) δ ppm 3.31-3.38 (m, 2 H) 3.47-3.55 (m, 2 H), 3.69 (s, 3 H), 3.80 (s, 3 H), 3.86 (s, 3 H), 4.75 (br. s, 1 H), 7.05 (d, $J=8.3$ Hz, 1 H), 7.15 (dd, $J=8.3, 2.0$ Hz, 1 H), 7.20 (d, $J=2.0$ Hz, 1 H), 7.58 (s, 1 H), 7.96 (br. s, 1 H), 8.25 (d, $J=2.8$ Hz, 1 H), 8.62 (d, $J=2.5$ Hz, 1 H), 12.40 (br. s, 1 H); LCMS (Method A): MH^+ 499, Rt 0.60 min, 100% by UV.

5-(3,4-Dimethoxyphenyl)-1-methyl-3-(4-(morpholine-4-carbonyl)-1*H*-imidazol-2-yl)pyridin-2(1*H*)-one 250c

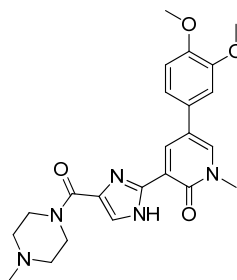


Typical Procedure H:

Ethyl 2-(5-(3,4-dimethoxyphenyl)-1-methyl-2-oxo-1,2-dihydropyridin-3-yl)-1*H*-imidazole-4-carboxylate **247**¹⁶⁶ (38 mg, 0.10 mmol), morpholine (Sigma-Aldrich, 13 mg, 0.15 mmol) and TBD (4 mg, 0.3 mmol) were combined in tetrahydrofuran (1 mL). The reaction was heated to 75 °C for 18 h. The solution was transferred to a microwave vial and heated under microwave irradiation to 140 °C for 1.5 h. The solvent was removed and the residue dissolved in DMSO (0.5 mL) and purified by Mass Directed AutoPrep on Xbridge column using acetonitrile/water with an ammonium bicarbonate modifier. The appropriate fractions were concentrated *in vacuo* to give the title compound (1 mg, 2%). ¹H NMR (400 MHz, DMSO-*d*₆) δ ppm 3.62-3.66 (m, 4 H), 3.69 (s, 3 H), 3.79 (s, 3 H), 3.85 (s, 3 H), 7.05 (d, *J*=8.3 Hz, 1 H), 7.14 (dd, *J*=8.3, 1.8 Hz, 1 H), 7.19 (d, *J*=1.8 Hz, 1 H), 7.58 (s, 1 H), 8.23-8.26 (m, 1 H), 8.50-8.53 (m, 1 H), 12.44 (br. s, 1 H), nb. four morpholine protons appear at the same shift as the water peak at 3.29 ppm; LCMS (Method A): MH⁺ 425, Rt 0.67 min, 100% by UV.

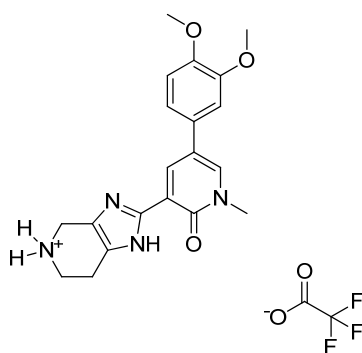
The following experiments were performed using Typical Procedure H, the data are reported as (a) amine (supplier, g, mmol); (b) product (mg, % yield).

5-(3,4-Dimethoxyphenyl)-1-methyl-3-(4-(4-methylpiperazine-1-carbonyl)-1H-imidazol-2-yl)pyridin-2(1H)-one 250d



(a) 1-Methylpiperazine, Sigma-Aldrich, 15 mg, 0.15 mmol; (b) 2.4 mg, 5%; ^1H NMR (400 MHz, $\text{DMSO-}d_6$) δ ppm 2.19 (s, 3 H), 2.31-2.40 (m, 4 H), 3.12-3.21 (m, 4 H), 3.69 (s, 3 H), 3.79 (s, 3 H), 3.85 (s, 3 H), 7.05 (d, $J=8.3$ Hz, 1 H), 7.13 (dd, $J=8.3, 2.0$ Hz, 1 H), 7.18 (d, $J=1.8$ Hz, 1 H), 7.55 (s, 1 H), 8.23-8.26 (m, 1 H), 8.49-8.52 (m, 1 H), 12.43 (br. s, 1 H); LCMS (Method A): MH^+ 438, R_t 0.54 min, 99% by UV.

2-(5-(3,4-Dimethoxyphenyl)-1-methyl-2-oxo-1,2-dihydropyridin-3-yl)-4,5,6,7-tetrahydro-1H-imidazo[4,5-c]pyridin-5-ium 2,2,2-trifluoroacetate 253



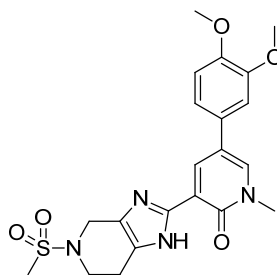
5-(3,4-Dimethoxyphenyl)-1-methyl-2-oxo-1,2-dihydropyridine-3-carboxylic acid **186** (5.0 g, 17 mmol) and 3,4-diaminopyridine **251** (Sigma-Aldrich, 3.0 g, 28 mmol) were mixed and added portionwise to phosphorous oxychloride (20 mL). The reaction mixture was heated to reflux for 16 h and then the excess phosphorous oxychloride removed *in vacuo*. The crude residue was suspended in ice water and basified with 0.88 aqueous ammonia to \sim pH 8. The aqueous phase was then extracted with 10% methanol/dichloromethane, the layers separated and the organic washed with water and brine. The organic layer was then dried over anhydrous sodium sulfate, filtered and concentrated *in vacuo* to give a crude residue which was purified by column chromatography (silica), eluting with 0-10% methanol/dichloromethane. The appropriate fractions were concentrated *in vacuo* to give 5-(3,4-dimethoxyphenyl)-3-

(1*H*-imidazo[4,5-*c*]pyridin-2-yl)-1-methylpyridin-2(1*H*)-one **252** (2 g, 32%) as a yellow solid.

5-(3,4-Dimethoxyphenyl)-3-(1*H*-imidazo[4,5-*c*]pyridin-2-yl)-1-methylpyridin-2(1*H*)-one **252** (2.0 g, 5.5 mmol) was suspended in 4 M hydrochloric acid in 1,4-dioxane (40 mL) at 0 °C. The reaction mixture was warmed to RT and stirred for 3 h. The solvent was removed *in vacuo* and the crude residue washed with diethyl ether and dried in a vacuum oven at 40 °C for 1 h to give 5-(3,4-dimethoxyphenyl)-3-(1*H*-imidazo[4,5-*c*]pyridin-2-yl)-1-methylpyridin-2(1*H*)-one hydrochloride (2 g, 91%) as a red solid.

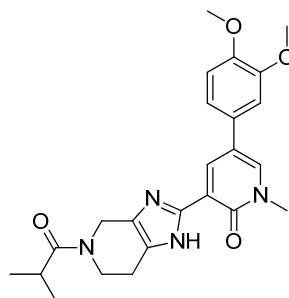
Platinum oxide (1.06 g, 4.67 mmol) was added to 5-(3,4-dimethoxyphenyl)-3-(1*H*-imidazo[4,5-*c*]pyridin-2-yl)-1-methylpyridin-2(1*H*)-one hydrochloride (3.29 g, 8.27 mmol) in trifluoroacetic acid (60 mL). The reaction mixture was stirred under an atmosphere of hydrogen at 60 psi for 24 h. The crude reaction mixture was filtered through Celite and the filtrate concentrated *in vacuo* to give the crude residue which was purified by reverse phase HPLC. The appropriate fractions were combined and concentrated *in vacuo* to give the title compound (2 g, 50%) as a yellow solid; ¹H NMR (400 MHz, DMSO-*d*₆) δ ppm 2.93-3.01 (m, 2 H), 3.43-3.51 (m, 2 H), 3.71 (s, 3 H), 3.80 (s, 3 H), 3.86 (s, 3 H), 4.25-4.32 (m, 2 H), 7.06 (d, *J*=8.6 Hz, 1 H), 7.17 (dd, *J*=8.3, 2.3 Hz, 1 H), 7.22 (d, *J*=2.0 Hz, 1 H), 8.41 (d, *J*=2.3 Hz, 1 H), 8.63 (d, *J*=2.5 Hz, 1 H), 9.19-9.25 (m, 2 H), nb. not all exchangeable protons were observed; LCMS (Method D): MH⁺ 367, Rt 1.28 min, 100% by UV.

5-(3,4-Dimethoxyphenyl)-1-methyl-3-(5-(methylsulfonyl)-4,5,6,7-tetrahydro-1H-imidazo[4,5-c]pyridin-2-yl)pyridin-2(1H)-one 254a



5-(3,4-Dimethoxyphenyl)-1-methyl-3-(4,5,6,7-tetrahydro-1H-imidazo[4,5-c]pyridin-2-yl)pyridin-2(1H)-one 2,2,2-trifluoroacetate **253** (50 mg, 0.10 mmol) was suspended in dichloromethane (2 mL) and triethylamine (29 μ L, 0.21 mmol). Methanesulfonyl chloride (Sigma-Aldrich, 8.1 μ L, 0.10 mmol) was added and the reaction mixture stirred at RT for 2 h. Additional methanesulfonyl chloride (8.1 μ L, 0.10 mmol) was added and the reaction mixture stirred at RT for a further 18 h. The reaction was diluted with methanol and the solvent removed *in vacuo*. The residue was dissolved in 1:1 MeOH:DMSO (2 mL) and purified by Mass Directed AutoPrep on Sunfire C₁₈ column using acetonitrile/water with a formic acid modifier. The appropriate fractions were concentrated *in vacuo* to give the title compound (5 mg, 11%). ¹H NMR (400 MHz, CDCl₃-*d*) δ ppm 2.86 (s, 3 H), 2.86-2.91 (m, 2 H), 3.70 (t, *J*=5.7 Hz, 1 H), 3.75 (s, 3 H), 3.86-3.90 (m, 1 H), 3.92 (s, 3 H), 3.95 (s, 3 H), 4.49 (s, 2 H), 6.92 (d, *J*=8.3 Hz, 1 H), 6.99 (d, *J*=1.8 Hz, 1 H), 7.04 (dd, *J*=8.3, 2.0 Hz, 1 H), 7.52 (d, *J*=2.5 Hz, 1 H), 8.65 (br. s, 1 H), 11.99 (br. s, 1 H); LCMS (Method A): MH⁺ 445, Rt 0.61 min, 98% by UV.

5-(3,4-Dimethoxyphenyl)-3-(5-isobutyramide-4,5,6,7-tetrahydro-1H-imidazo[4,5-c]pyridin-2-yl)-1-methylpyridin-2(1H)-one 255a

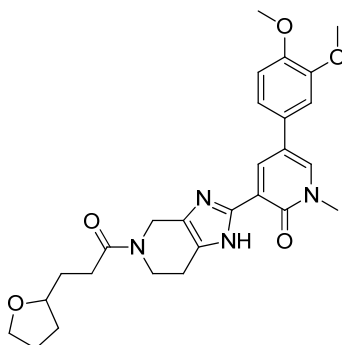


Typical Procedure I:

Isobutyric acid (Sigma-Aldrich, 18 mg, 0.20 mmol), HATU (76 mg, 0.20 mmol) and DIPEA (52 μ L, 0.30 mmol) were combined in *N,N*-dimethylformamide (0.25 mL) and stirred at RT for 10 min. A solution of 5-(3,4-dimethoxyphenyl)-1-methyl-3-(4,5,6,7-tetrahydro-1H-imidazo[4,5-c]pyridin-2-yl)pyridin-2(1H)-one 2,2,2-trifluoroacetate **253** (48 mg, 0.10 mmol) in *N,N*-dimethylformamide (0.25 mL) was added and the reaction mixture stirred at RT for 18 h. The solvent was removed and the residue dissolved in DMSO (0.6 mL) and purified by Mass Directed AutoPrep on Xbridge column using acetonitrile/water with an ammonium bicarbonate modifier. The appropriate fractions were concentrated *in vacuo* to give the title compound as a clear gum (16 mg, 33%); $\nu_{\max}/\text{cm}^{-1}$ (methanol) 1644 and 1641 (C=O); $^1\text{H NMR}$ (600 MHz, DMSO- d_6) δ ppm 1.03 (d, $J=6.4$ Hz, 6 H), 2.66 (br. s, 1 H), 2.76 (br. s, 1 H), 2.98 (spt, $J=6.4$ Hz, 1 H), 3.68 (s, 3 H), 3.74-3.78 (m, 2 H), 3.78 (s, 3 H), 3.85 (s, 3 H), 4.44-4.55 (m, 1 H), 4.55-4.68 (m, 1 H), 7.02 (d, $J=8.3$ Hz, 1 H), 7.11-7.14 (m, 1 H), 7.17 (s, 1 H), 8.14-8.17 (m, 1 H), 8.48 (d, $J=1.9$ Hz, 1 H), 12.16 (br. s, 1 H); $^{13}\text{C NMR}$ (101 MHz, DMSO- d_6) δ ppm 19.3, 19.6, 29.3, 37.5 (2C), 55.6 (2C), 55.6 (2C), 109.5, 112.3 (2C), 117.8, 118.7, 128.6, 132.9, 135.6, 141.3, 148.3 (2C), 149.2 (2C), 159.2, 175.1; LCMS (Method A): MH^+ 437, R_t 0.66 min, 100% by UV; HRMS exact mass calculated for $[\text{M}+\text{H}]^+$ ($\text{C}_{24}\text{H}_{29}\text{N}_4\text{O}_4$) requires m/z 437.2183, found 437.2191.

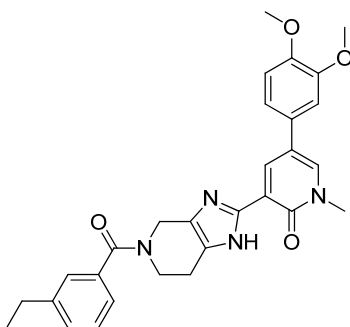
The following experiments were performed using Typical Procedure I, the data are reported as (a) amine (supplier, g, mmol); (b) product (mg, % yield).

5-(3,4-Dimethoxyphenyl)-1-methyl-3-(5-(3-(tetrahydrofuran-2-yl)propanoyl)-4,5,6,7-tetrahydro-1H-imidazo[4,5-c]pyridin-2-yl)pyridin-2(1H)-one 255b



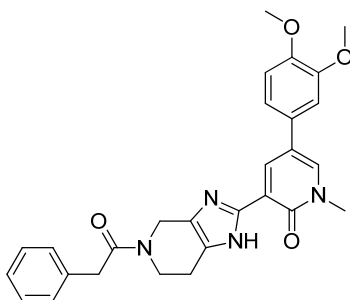
(a) 3-(Tetrahydrofuran-2-yl)propanoic acid, Enamine, 29 mg, 0.20 mmol; (b) 17 mg, 12%; ^1H NMR (600 MHz, $\text{DMSO-}d_6$) δ ppm 1.33-1.45 (m, 1 H), 1.61-1.72 (m, 2 H), 1.72-1.83 (m, 2 H), 1.85-1.98 (m, 1 H), 2.40-2.47 (m, 2 H), 2.60-2.70 (m, 1 H), 2.72-2.79 (m, 1 H), 3.49-3.60 (m, 2 H), 3.67 (s, 3 H), 3.69-3.76 (m, 3 H), 3.78 (s, 3 H), 3.85 (s, 3 H), 4.44-4.51 (m, 1 H), 4.53-4.61 (m, 1 H), 7.01-7.04 (m, 1 H), 7.10-7.15 (m, 1 H), 7.16-7.18 (m, 1 H), 8.14-8.18 (m, 1 H), 8.47-8.50 (m, 1 H), 12.15-12.18 (m, 1 H); LCMS (Method A): MH^+ 493, Rt 0.68 min, 100% by UV.

5-(3,4-Dimethoxyphenyl)-3-(5-(3-ethylbenzoyl)-4,5,6,7-tetrahydro-1H-imidazo[4,5-c]pyridin-2-yl)-1-methylpyridin-2(1H)-one 255c



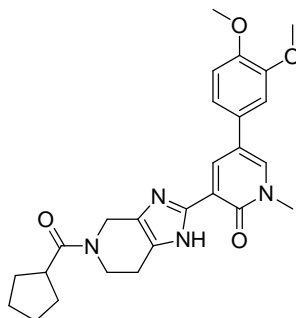
(a) 3-Ethylbenzoic acid, ABCR-Gelest UK Ltd., 30 mg, 0.20 mmol; (b) 19 mg, 35%; ^1H NMR (400 MHz, $\text{DMSO-}d_6$) δ ppm 1.16-1.25 (m, 3 H), 2.66 (q, $J=7.3$ Hz, 3 H), 2.72-2.82 (m, 1 H), 3.60 (br. s, 1 H), 3.67 (s, 3 H), 3.79 (s, 3 H), 3.85 (s, 3 H), 3.96 (br. s, 1 H), 4.35-4.76 (m, 2 H), 7.03 (d, $J=8.6$ Hz, 1 H), 7.13 (dd, $J=8.3, 1.8$ Hz, 1 H), 7.17 (br. s, 1 H), 7.24 (d, $J=7.3$ Hz, 1 H), 7.27 (s, 1 H), 7.30-7.41 (m, 2 H), 8.14 (br. s, 1 H), 8.49 (br. s, 1 H), 12.18 (br. s, 1 H); LCMS (Method A): MH^+ 499, Rt 0.82 min, 98% by UV.

5-(3,4-Dimethoxyphenyl)-1-methyl-3-(5-(2-phenylacetyl)-4,5,6,7-tetrahydro-1H-imidazo[4,5-c]pyridin-2-yl)pyridin-2(1H)-one 255d



(a) Phenylacetic acid, Sigma-Aldrich, 27 mg, 0.20 mmol; (b) 20 mg, 36%; ^1H NMR (600 MHz, DMSO- d_6) δ ppm 2.56-2.60 (m, 1 H), 2.66-2.71 (m, 1 H), 3.66 (s, 3 H), 3.73-3.77 (m, 2 H), 3.78 (s, 3 H), 3.83 (s, 2 H), 3.84 (s, 3 H), 4.47-4.55 (m, 1 H), 4.56-4.65 (m, 1 H), 6.99-7.04 (m, 1 H), 7.10-7.15 (m, 1 H), 7.15-7.19 (m, 1 H), 7.19-7.25 (m, 2 H), 7.25-7.33 (m, 3 H), 8.13-8.17 (m, 1 H), 8.45-8.49 (m, 1 H), 12.12-12.22 (m, 1 H); LCMS (Method A): MH^+ 485, Rt 0.74 min, 99% by UV.

3-(5-(Cyclopentanecarbonyl)-4,5,6,7-tetrahydro-1H-imidazo[4,5-c]pyridin-2-yl)-5-(3,4-dimethoxyphenyl)-1-methylpyridin-2(1H)-one 255e



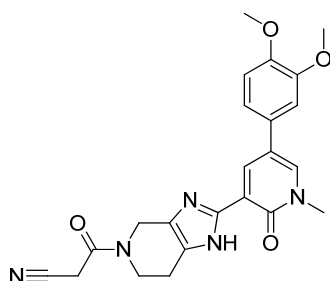
Typical Procedure J:

Cyclopentanecarboxylic acid (15 mg, 0.20 mmol), HATU (76 mg, 0.20 mmol) and DIPEA (52 μL , 0.30 mmol) were combined in *N,N*-dimethylformamide (0.5 mL). A solution of 5-(3,4-dimethoxyphenyl)-1-methyl-3-(4,5,6,7-tetrahydro-1H-imidazo[4,5-c]pyridin-2-yl)pyridin-2(1H)-one 2,2,2-trifluoroacetate **253** (48 mg, 0.10 mmol) in *N,N*-dimethylformamide (0.5 mL) was added and the reaction mixture stirred at RT for 12 h. The crude reaction mixture was loaded onto a pre-conditioned silica SPE (1 g) and eluted with 10% methanol/ethyl acetate. The solvent was removed and the residue dissolved in DMSO (0.5 mL) and purified by Mass Directed AutoPrep on Sunfire C18 column using acetonitrile/water with a formic acid modifier. The appropriate fractions

were concentrated *in vacuo* to give the title compound (17 mg, 30%). ^1H NMR (600 MHz, $\text{DMSO-}d_6$) δ ppm 1.48-1.72 (m, 6 H), 1.75-1.85 (m, 2 H), 2.58-2.66 (m, 1 H), 2.71 (br. s, 1 H), 3.03-3.12 (m, 1 H), 3.47-3.62 (m, 2 H), 3.67 (s, 3 H), 3.78 (s, 3 H), 3.85 (s, 3 H), 4.48-4.64 (m, 2 H), 7.03 (d, $J=7.9$ Hz, 1 H), 7.13 (d, $J=6.8$ Hz, 1 H), 7.17 (s, 1 H), 8.16 (br. s, 1 H), 8.47 (br. s, 1 H), 12.15 (br. s, 1 H); LCMS (Method A): MH^+ 463, Rt 0.75 min, 100% by UV.

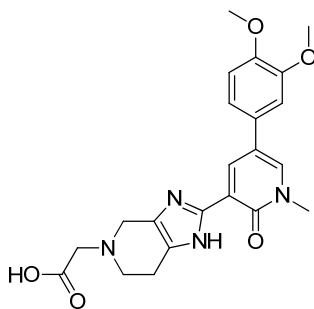
The following experiments were performed using Typical Procedure J, the data are reported as (a) amine (supplier, g, mmol); (b) product (mg, % yield).

3-(2-(5-(3,4-Dimethoxyphenyl)-1-methyl-2-oxo-1,2-dihydropyridin-3-yl)-6,7-dihydro-1H-imidazo[4,5-c]pyridin-5(4H)-yl)-3-oxopropanenitrile 255f



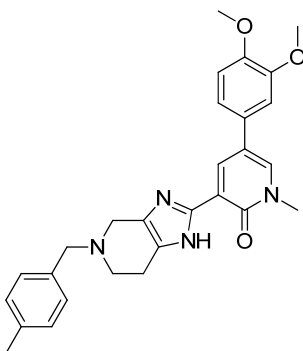
(a) Cyanoacetic acid, Sigma-Aldrich, 17 mg, 0.20 mmol; (b) 15 mg, 35%; ^1H NMR (400 MHz, $\text{DMSO-}d_6$) δ ppm 2.66-2.74 (m, 1 H), 2.76-2.84 (m, 1 H), 3.17 (s, 2 H), 3.64 (br. s, 2 H), 3.67 (s, 3 H), 3.79 (s, 3 H), 3.85 (s, 3 H), 4.41-4.62 (m, 2 H), 7.03 (d, $J=8.3$ Hz, 1 H), 7.10-7.14 (m, 1 H), 7.15-7.18 (m, 1 H), 8.14-8.17 (m, 1 H), 8.48 (d, $J=2.5$ Hz, 1 H), 12.18 (br. s, 1 H); LCMS (Method A): MH^+ 434, Rt 0.55 min, 100% by UV.

2-(2-(5-(3,4-Dimethoxyphenyl)-1-methyl-2-oxo-1,2-dihydropyridin-3-yl)-6,7-dihydro-1H-imidazo[4,5-c]pyridin-5(4H)-yl)acetic acid 256a



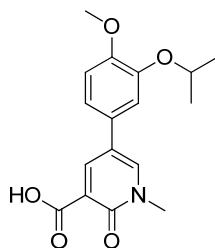
5-(3,4-Dimethoxyphenyl)-1-methyl-3-(4,5,6,7-tetrahydro-1H-imidazo[4,5-c]pyridin-2-yl)pyridin-2(1H)-one 2,2,2-trifluoroacetate **253** (50 mg, 0.10 mmol) and 2-bromoacetic acid (Sigma-Aldrich, 15 mg, 0.10 mmol) were suspended in *N,N*-dimethylformamide (2 mL) and triethylamine (29 μ L, 0.21 mmol) was added. The reaction mixture was stirred at RT for 18 h. Additional 2-bromoacetic acid (7.5 mg, 0.052 mmol) was added and the reaction stirred at RT for a further 4 h. The reaction was diluted with methanol and the solvent removed *in vacuo*. The residue was dissolved in 1:1 MeOH:DMSO (1 mL) and purified by Mass Directed AutoPrep on Xbridge column using acetonitrile/water with an ammonium bicarbonate modifier. The appropriate fractions were concentrated *in vacuo* to give the title compound (4.5 mg, 10%). ^1H NMR (400 MHz, Methanol- d_4) δ ppm 2.65 (s, 2 H), 3.09 (m, 2 H), 3.63 (m, 2 H), 3.74 (s, 3 H), 3.77 (s, 2 H), 3.87 (s, 3 H), 3.92 (s, 3 H), 4.38 (br. s, 1 H), 7.02 (d, $J=8.3$ Hz, 1 H), 7.15 (dd, $J=8.3, 2.3$ Hz, 1 H), 7.19 (d, $J=2.0$ Hz, 1 H), 8.02 (d, $J=2.5$ Hz, 1 H), 8.62 (d, $J=2.5$ Hz, 1 H) (nb. exchangeable NH proton not seen); LCMS (Method A): MH^+ 425, Rt 0.48 min, 100% by UV.

5-(3,4-Dimethoxyphenyl)-1-methyl-3-(5-(4-methylbenzyl)-4,5,6,7-tetrahydro-1H-imidazo[4,5-c]pyridin-2-yl)pyridin-2(1H)-one 256b



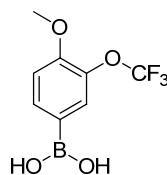
5-(3,4-Dimethoxyphenyl)-1-methyl-3-(4,5,6,7-tetrahydro-1H-imidazo[4,5-c]pyridin-2-yl)pyridin-2(1H)-one 2,2,2-trifluoroacetate **253** (50 mg, 0.10 mmol) was dissolved in *N,N*-dimethylformamide (2 mL) and triethylamine (29 μ L, 0.21 mmol). 1-(Bromomethyl)-4-methylbenzene (19 mg, 0.10 mmol) was added and the reaction mixture stirred at RT for 4 h. Additional 1-(bromomethyl)-4-methylbenzene (19 mg, 0.10 mmol) was added and the reaction stirred at RT for a further 2 h. The mixture was diluted with methanol then concentrated *in vacuo*. The residue was dissolved in 1:1 MeOH: DMSO (1 mL) and purified by Mass Directed AutoPrep on Xbridge column using acetonitrile/water with an ammonium bicarbonate modifier. The appropriate fractions were concentrated *in vacuo* to give the title compound (16 mg, 33%); m.p. 150-152°C; ^1H NMR (400 MHz, DMSO- d_6) δ ppm 2.13-2.27 (m, 2 H), 2.29 (s, 3 H), 2.63-2.73 (m, 1 H), 2.78 (t, $J=5.5$ Hz, 1 H), 3.41-3.63 (m, 2 H), 3.66 (s, 5 H), 3.80 (s, 3 H), 3.85 (s, 3 H), 7.01 (d, $J=8.3$ Hz, 1 H), 7.05-7.09 (m, 1 H), 7.12 (d, $J=8.1$ Hz, 2 H), 7.13-7.15 (m, 1 H), 7.22 (d, $J=8.1$ Hz, 2 H), 7.93 (d, $J=2.8$ Hz, 1 H), 8.40-8.44 (m, 1 H), 11.76 (br. s, 1 H); LCMS (Method A): MH^+ 471, R_t 0.69 min, 95% by UV.

5-(3-Isopropoxy-4-methoxyphenyl)-1-methyl-2-oxo-1,2-dihydropyridine-3-carboxylic acid 261a



5-Bromo-1-methyl-2-oxo-1,2-dihydropyridine-3-carboxylic acid **260**¹⁶⁹ (1.11 g, 4.76 mmol), (3-isopropoxy-4-methoxyphenyl)boronic acid **263** (Combi-blocks, 1.0 g, 4.8 mmol), *tetrakis*(triphenylphosphine) palladium(0) (165 mg, 0.143 mmol) and sodium carbonate (1.01 g, 9.52 mmol) were suspended in ethanol (15 mL) and water (5 mL) and the reaction mixture heated to 90 °C for 4 h. The solvent was removed *in vacuo* and the residue partitioned between ethyl acetate (30 mL) and 2 M aqueous sodium hydroxide (50 mL). The layers were separated and the aqueous phase acidified to ~pH 3 with 2 M aqueous hydrochloric acid. The resultant yellow precipitate was filtered and dried in a vacuum oven at 40 °C overnight to give the title compound (950 mg, 63%). ¹H NMR (400 MHz, DMSO-*d*₆) δ ppm 1.28 (d, *J*=6.0 Hz, 6 H), 3.74 (s, 3 H), 3.79 (s, 3 H), 4.66-4.73 (m, 1 H), 7.06 (d, *J*=8.6 Hz, 1 H), 7.19 (dd, *J*=8.3, 2.0 Hz, 1 H), 7.24 (d, *J*=2.0 Hz, 1 H), 8.58 (q, *J*=2.8 Hz, 2 H), 14.75 (br. s, 1 H); LCMS (Method A): MH⁺ 318, Rt 0.90 min, 94% by UV.

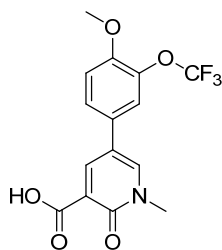
(4-Methoxy-3-(trifluoromethoxy)phenyl)boronic acid 265



4-Bromo-1-methoxy-2-(trifluoromethoxy)benzene **264** (Manchester Organics, 555 mg, 2.05 mmol) was added dropwise to a solution of *n*-butyllithium (1.6 M in hexanes, 1.4 mL, 2.3 mmol) in anhydrous tetrahydrofuran (4 mL) at -78 °C. The reaction mixture was stirred at -78 °C for 20 min, after which time triisopropyl borate (Sigma-Aldrich, 543 μL, 2.36 mmol) was added in one charge. The reaction mixture was stirred to -78 °C for 20 min, then additional triisopropyl borate (236 μL, 1.02 mmol) was added. After stirring at -78 °C for a further 10 min, the reaction was quenched by the addition of 5 M hydrochloric acid (12 mL, 61 mmol) and allowed to warm to RT. The reaction was

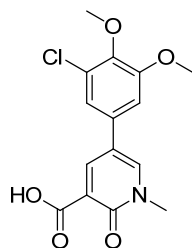
stirred for 10 min, then diluted with water and extracted with ethyl acetate (2 x 50 mL). The layers were separated and the combined organic extracts were washed with brine then concentrated *in vacuo* to give the title compound as a brown gum (430 mg, 89%). ¹H NMR (400 MHz, DMSO-*d*₆) δ ppm 3.86 (s, 3 H), 7.20 (d, *J*=8.3 Hz, 1 H), 7.64-7.72 (m, 1 H), 7.73-7.83 (m, 1 H), 8.07 (s, 2 H); LCMS (Method A): (M-H)⁻ 235, Rt 0.83 min, 95% by UV.

5-(4-Methoxy-3-(trifluoromethoxy)phenyl)-1-methyl-2-oxo-1,2-dihydropyridine-3-carboxylic acid 261b



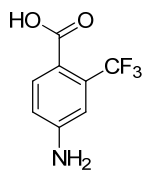
5-Bromo-1-methyl-2-oxo-1,2-dihydropyridine-3-carboxylic acid **260**¹⁶⁹ (310 mg, 1.34 mmol), (4-methoxy-3-(trifluoromethoxy)phenyl)boronic acid **265** (350 mg, 1.48 mmol), *tetrakis*(triphenylphosphine) palladium(0) (51 mg, 0.044 mmol) and sodium carbonate (314 mg, 2.97 mmol) were combined in ethanol (10 mL) and water (2 mL) and the reaction mixture heated to 80 °C for 3 h. The reaction mixture was diluted with 2 M aqueous sodium hydroxide solution (100 mL), filtered and extracted with ethyl acetate (2 x 100 mL). The layers were separated and the aqueous phase acidified to ~pH 1 with 5 M aqueous hydrochloric acid solution and extracted with ethyl acetate (2 x 100 mL). The two organic layers were combined with the solid from the filtration and concentrated *in vacuo* to give the title compound as a grey solid (424 mg, 83%). Material was used in crude form in next step. LCMS (Method A): (M-H)⁻ 344, Rt 0.98 min, 82% by UV.

5-(3-Chloro-4,5-dimethoxyphenyl)-1-methyl-2-oxo-1,2-dihydropyridine-3-carboxylic acid 261c

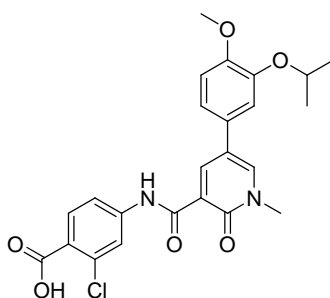


1-Chloro-2,3-dimethoxybenzene **266** (ABCR, 900 mg, 5.21 mmol), bis(pinacolato)diboron (1.32 g, 5.21 mmol), (1,5-cyclooctadiene)(methoxy)iridium (I) dimer (90 mg, 0.14 mmol) and 4,4'-di-tert-butyl-2,2'-dipyridyl (28 mg, 0.10 mmol) were combined. The flask was purged with nitrogen, then vacuum three times before the addition of anhydrous tetrahydrofuran (18 mL). The reaction mixture was heated to 90 °C for 14 h. The solvent was removed *in vacuo* and the residue purified by column chromatography (silica) eluting with 0-100% ethyl acetate in cyclohexane. The appropriate fractions were concentrated *in vacuo* to give a yellow solid (1.9 g).

The yellow solid (1.9 g, assumed to be 5.2 mmol i.e. 100% yield), 5-Bromo-1-methyl-2-oxo-1,2-dihydropyridine-3-carboxylic acid **260**¹⁶⁹ (1.21 g, 5.21 mmol), *tetrakis*(triphenylphosphine) palladium (0) (181 mg, 0.156 mmol) and sodium carbonate (1.11 g, 10.4 mmol) were suspended in ethanol (15 mL) and water (2 mL) and heated under nitrogen to 80 °C for 3 h. The solvent was removed *in vacuo* and the residue partitioned between 2 M aqueous sodium hydroxide solution (50 mL) and ethyl acetate (50 mL). The two layers were filtered then separated and the aqueous acidified to ~pH 3 with 5 M aqueous hydrochloric acid. The resultant precipitate was filtered and dried in a vacuum oven at 50 °C overnight to give a cream solid (826 mg) which was purified by reverse phase column chromatography, eluting with 0-20% acetonitrile/water with an ammonium bicarbonate modifier. The appropriate fractions were concentrated *in vacuo* to give the title compound (221 mg, 13%) as a white solid. ¹H MMR (400 MHz, DMSO-*d*₆) δ ppm 3.61 (s, 3 H), 3.77 (s, 3 H), 3.93 (s, 3 H), 7.22 (d, *J*=1.8 Hz, 1 H), 7.27 (d, *J*=1.8 Hz, 1 H), 8.25 (br. s, 1 H), 8.36 (br. s, 1 H), nb. the carboxylic acid proton was thought to be concealed by water signal; LCMS (Method A): MH⁺ 324/326, Rt 0.92 min, 98% by UV.

4-Amino-2-(trifluoromethyl)benzoic acid 269

4-Nitro-2-(trifluoromethyl)benzoic acid **268** (Apollo, 3.0 g, 13 mmol) was dissolved in ethanol (50 mL) and added to a flask containing 10% palladium on carbon (300 mg, 2.82 mmol). The mixture was reacted under an atmosphere of hydrogen at RT for 18 h. The mixture was filtered through Celite, washing with ethanol and the solvent removed *in vacuo*. The residue was re-dissolved in ethanol (50 mL) and added to a flask containing 10% palladium on carbon (300 mg, 2.82 mmol). The mixture was further reacted under an atmosphere of hydrogen at RT for 5 h. The mixture was filtered through Celite, washing with ethanol and the solvent concentrated *in vacuo* to give an orange solid (1.3 g). The solid was purified by column chromatography (silica) eluting with 0-100% ethyl acetate in cyclohexane. The appropriate fractions were concentrated *in vacuo* to give the title compound (840 mg, 32%). ¹H NMR (400 MHz, DMSO-*d*₆) δ ppm 6.17 (s, 2 H), 6.73 (dd, *J*=8.6, 2.3 Hz, 1 H), 6.96 (d, *J*=2.3 Hz, 1 H), 7.67 (d, *J*=8.6 Hz, 1 H), 12.47 (br. s, 1 H); LCMS (Method A): MH⁺ 322/324, Rt 0.60 min, 89% by UV.

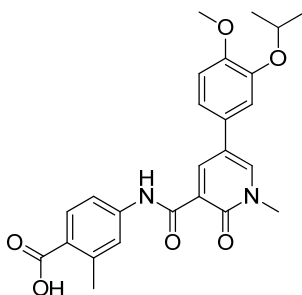
2-Chloro-4-(5-(3-isopropoxy-4-methoxyphenyl)-1-methyl-2-oxo-1,2-dihydropyridine-3-carboxamido)benzoic acid 270a*Typical Procedure K:*

5-(3-Isopropoxy-4-methoxyphenyl)-1-methyl-2-oxo-1,2-dihydropyridine-3-carboxylic acid, **261a** (32 mg, 0.10 mmol), HATU (38 mg, 0.10 mmol) and DIPEA (35 μL, 0.20 mmol) were combined in *N,N*-dimethylformamide (0.4 mL) and left to stand at RT for 10 min. 4-Amino-2-chlorobenzoic acid (Sigma-Aldrich, 17 mg, 0.10 mmol) was added and the reaction left standing at RT for 18 h. The crude reaction mixture was

purified directly by Mass Directed AutoPrep on Sunfire C18 column using acetonitrile/water with a formic acid modifier. The appropriate fractions were concentrated *in vacuo* to give the title compound (26 mg, 50%). $^1\text{H NMR}$ (400 MHz, $\text{DMSO-}d_6$) δ ppm 1.28 (d, $J=6.0$ Hz, 6 H), 3.69 (s, 3 H), 3.78 (s, 3 H), 4.63-4.70 (m, 1 H), 7.03 (d, $J=8.3$ Hz, 1 H), 7.13 (dd, $J=8.3, 1.8$ Hz, 1 H), 7.19 (d, $J=1.8$ Hz, 1 H), 7.55 (dd, $J=8.6, 1.8$ Hz, 1 H), 7.85 (d, $J=8.6$ Hz, 1 H), 8.07 (d, $J=1.8$ Hz, 1 H), 8.47 (d, $J=2.8$ Hz, 1 H), 8.61 (d, $J=2.8$ Hz, 1 H), 12.47 (s, 1 H), nb. the carboxylic acid proton thought to be under the water signal; LCMS (Method A): MH^+ 471/473, Rt 1.06 min, 100% by UV.

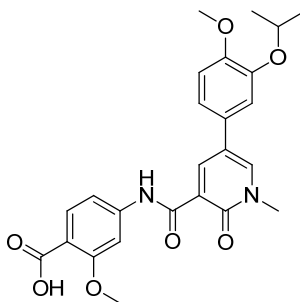
The following experiments were performed using Typical Procedure K, the data are reported as (a) amine (supplier, g, mmol); (b) product (mg, % yield).

4-(5-(3-Isopropoxy-4-methoxyphenyl)-1-methyl-2-oxo-1,2-dihydropyridine-3-carboxamido)-2-methylbenzoic acid 270b



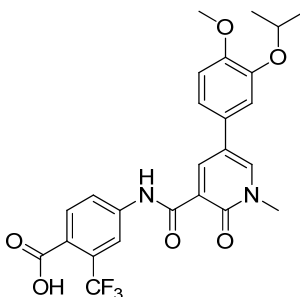
(a) 4-Amino-2-methylbenzoic acid, Sigma-Aldrich, 15 mg, 0.20 mmol; (b) 23 mg, 45%; $^1\text{H NMR}$ (400 MHz, $\text{DMSO-}d_6$) δ ppm 1.28 (d, $J=6.0$ Hz, 6 H), 2.53 (s, 3 H), 3.70 (s, 3 H), 3.78 (s, 3 H), 4.63-4.70 (m, 1 H), 7.04 (d, $J=8.6$ Hz, 1 H), 7.13 (dd, $J=8.6, 2.3$ Hz, 1 H), 7.19 (d, $J=2.0$ Hz, 1 H), 7.56 (d, $J=1.8$ Hz, 1 H), 7.67 (dd, $J=8.6, 2.0$ Hz, 1 H), 7.87 (d, $J=8.6$ Hz, 1 H), 8.46 (d, $J=2.8$ Hz, 1 H), 8.63 (d, $J=2.8$ Hz, 1 H), 12.36 (s, 1 H), nb. the carboxylic acid proton thought to be under the water peak; LCMS (Method A): MH^+ 451, Rt 1.05 min, 89% by UV.

4-(5-(3-Isopropoxy-4-methoxyphenyl)-1-methyl-2-oxo-1,2-dihydropyridine-3-carboxamido)-2-methoxybenzoic acid 270c



(a) 4-Amino-2-methoxybenzoic acid, Sigma-Aldrich, 17 mg, 0.20 mmol; (b) 10 mg, 19%; ^1H NMR (400 MHz, $\text{DMSO-}d_6$) δ ppm 1.29 (d, $J=6.0$ Hz, 6 H), 3.72 (s, 3 H), 3.79 (s, 3 H), 3.84 (s, 3 H), 4.63-4.73 (m, 1 H), 7.06 (d, $J=8.3$ Hz, 1 H), 7.17 (dd, $J=8.3$, 2.0 Hz, 1 H), 7.22 (d, $J=2.0$ Hz, 1 H), 7.26 (dd, $J=8.6$, 1.8 Hz, 1 H), 7.63 (d, $J=1.8$ Hz, 1 H), 7.72 (d, $J=8.6$ Hz, 1 H), 8.50 (d, $J=2.8$ Hz, 1 H), 8.68 (d, $J=2.8$ Hz, 1 H), 12.44 (s, 1 H), nb. the carboxylic acid proton was thought to be under the water peak; LCMS (Method A): MH^+ 467, Rt 1.01 min, 100% by UV.

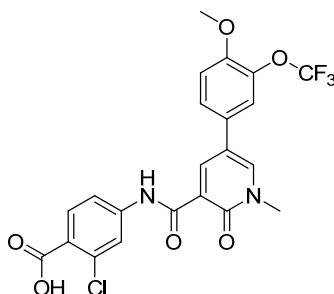
4-(5-(3-Isopropoxy-4-methoxyphenyl)-1-methyl-2-oxo-1,2-dihydropyridine-3-carboxamido)-2-(trifluoromethyl)benzoic acid 270d



(a) 4-Amino-2-(trifluoromethyl)benzoic acid **269**, 21 mg, 0.20 mmol; (b) 30 mg, 54% as a cream solid; m.p. 226-227 °C; $\nu_{\text{max}}/\text{cm}^{-1}$ (solid) 1696 (C=O), 1686 (C=O) and 1636 (C=O); ^1H NMR (400 MHz, $\text{DMSO-}d_6$) δ ppm 1.28 (d, $J=6.0$ Hz, 6 H), 3.69 (s, 3 H), 3.78 (s, 3 H), 4.61-4.71 (m, 1 H), 7.02 (d, $J=8.6$ Hz, 1 H), 7.12 (dd, $J=8.3$, 2.3 Hz, 1 H), 7.19 (d, $J=2.0$ Hz, 1 H), 7.87 (s, 2 H), 8.34 (s, 1 H), 8.47 (d, $J=2.8$ Hz, 1 H), 8.63 (d, $J=2.8$ Hz, 1 H), 12.56 (s, 1 H), nb. the carboxylic acid proton was thought to be concealed under the water peak; ^{13}C NMR (101 MHz, $\text{DMSO-}d_6$) δ ppm 21.9 (2C), 38.1, 55.6, 70.6, 112.9, 113.4, 118.2, 118.5, 119.2, 122.4, 125.4, 127.6, 131.8, 140.8, 141.9,

147.1, 149.9, 161.0, 162.21, 166.8 nb. four carbons not observed due to low signal/noise; LCMS (Method A): MH^+ 505, Rt 1.10 min, 100% by UV; HRMS exact mass calculated for $[M+H]^+$ ($C_{25}H_{24}N_2O_6$) requires m/z 505.1581, found 505.1566.

2-Chloro-4-(5-(4-methoxy-3-(trifluoromethoxy)phenyl)-1-methyl-2-oxo-1,2-dihydropyridine-3-carboxamido)benzoic acid 270e

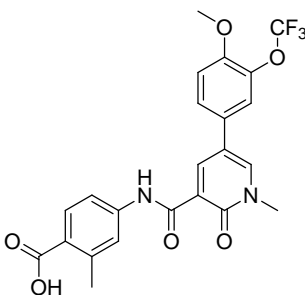


Typical Procedure L:

5-(4-Methoxy-3-(trifluoromethoxy)phenyl)-1-methyl-2-oxo-1,2-dihydropyridine-3-carboxylic acid, **261b** (51 mg, 0.15 mmol), HATU (57 mg, 0.15 mmol) and DIPEA (79 μ L, 0.45 mmol) were combined in *N,N*-dimethylformamide (0.5 mL) and left to stand at RT for 10 min. 4-Amino-2-chlorobenzoic acid (Sigma-Aldrich, 26 mg, 0.15 mmol) was added and the reaction left standing at RT for 18 h. The solvent was removed and the crude residue dissolved in DMSO (0.5 mL) and purified by Mass Directed AutoPrep on Sunfire C_{18} column using acetonitrile/water with a formic acid modifier. The appropriate fractions were concentrated *in vacuo* to give the title compound (4.1 mg, 5%). 1H NMR (600 MHz, $DMSO-d_6$) δ ppm 3.70 (s, 3 H), 3.90 (s, 3 H), 7.34 (d, $J=8.7$ Hz, 1 H), 7.56 (d, $J=8.7$ Hz, 1 H), 7.65 (d, $J=1.9$ Hz, 1 H), 7.67 (s, 1 H), 7.83 (d, $J=8.7$ Hz, 1 H), 8.07 (s, 1 H), 8.60 (d, $J=2.6$ Hz, 1 H), 8.65 (d, $J=2.6$ Hz, 1 H), 12.42 (s, 1 H), nb. the carboxylic acid proton was thought to be under the water signal; LCMS (Method A): MH^+ 497/499, Rt 1.10 min, 100% by UV.

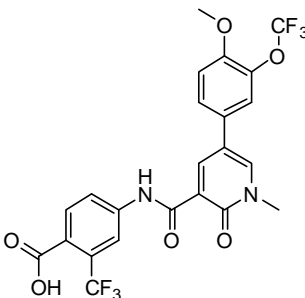
The following experiments were performed using Typical Procedure L, the data are reported as (a) amine (supplier, g, mmol); (b) product (mg, % yield).

4-(5-(4-Methoxy-3-(trifluoromethoxy)phenyl)-1-methyl-2-oxo-1,2-dihydropyridine-3-carboxamido)-2-methylbenzoic acid 270f



(a) 4-Amino-2-methylbenzoic acid, Sigma-Aldrich, 23 mg, 0.15 mmol; (b) 5.3 mg, 7%; ^1H NMR (600 MHz, $\text{DMSO-}d_6$) δ ppm 2.53 (s, 3 H), 3.70 (s, 3 H), 3.90 (s, 3 H), 7.35 (d, $J=9.1$ Hz, 1 H), 7.57 (s, 1 H), 7.63-7.70 (m, 1 H), 7.67 (s, 1 H), 7.86 (d, $J=8.3$ Hz, 1 H), 8.58 (d, $J=2.6$ Hz, 1 H), 8.66 (d, $J=2.6$ Hz, 2 H), 12.32 (s, 1 H), nb. the carboxylic acid proton was thought to be under the water peak; LCMS (Method A): MH^+ 477, Rt 1.09 min, 98% by UV.

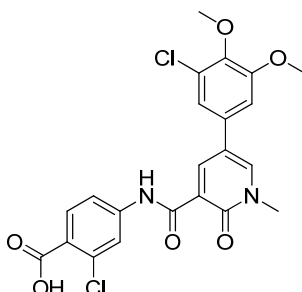
4-(5-(4-Methoxy-3-(trifluoromethoxy)phenyl)-1-methyl-2-oxo-1,2-dihydropyridine-3-carboxamido)-2-(trifluoromethyl)benzoic acid 270g



(a) 4-Amino-2-(trifluoromethyl)benzoic acid **269**, 31 mg, 0.15 mmol; (b) 8.5 mg, 10% as a brown gum; $\nu_{\text{max}}/\text{cm}^{-1}$ (solid) 1717, 1689 and 1638 C=O); ^1H NMR (600 MHz, $\text{DMSO-}d_6$) δ ppm 3.70 (s, 3 H), 3.89 (s, 3 H), 7.33 (d, $J=8.3$ Hz, 1 H), 7.64 (d, $J=2.3$ Hz, 1 H), 7.66 (br. s, 1 H), 7.83-7.89 (m, 2 H), 8.35 (s, 1 H), 8.59 (d, $J=2.6$ Hz, 1 H), 8.66-8.68 (m, 1 H), 12.50 (s, 1 H), nb. the carboxylic acid proton was thought to be under the water peak; ^{13}C NMR (101 MHz, $\text{DMSO-}d_6$) δ ppm 38.2, 56.3, 114.4 (2C) 117.1 (q, $J=5.5$ Hz), 117.5, 118.4, 120.3 (q, $J=258.0$ Hz), 120.4, 123.4 (q, $J=273.7$ Hz), 122.4, 123.2 (q, $J=26.8$ Hz), 126.0, 128.0, 131.7, 137.2 (q, $J=1.8$ Hz), 140.5 (q, $J=3.7$ Hz), 141.8, 142.5, 151.1, 161.1, 162.1, 167.0; LCMS (Method A): $(\text{M-H})^-$ 529, Rt 1.14 min, 100% by UV; HRMS exact mass calculated for $[\text{M}+\text{H}]^+$ ($\text{C}_{23}\text{H}_{17}\text{F}_6\text{N}_2\text{O}_6$) requires m/z

531.0985, found 531.0990. Insufficient material remained after biological testing to obtain a melting point.

2-Chloro-4-(5-(3-chloro-4,5-dimethoxyphenyl)-1-methyl-2-oxo-1,2-dihydropyridine-3-carboxamido)benzoic acid 270h

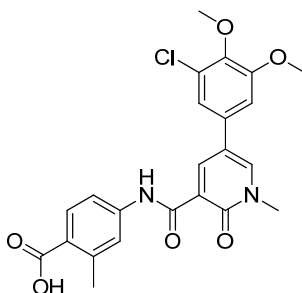


Typical Procedure M:

5-(3-Chloro-4,5-dimethoxyphenyl)-1-methyl-2-oxo-1,2-dihydropyridine-3-carboxylic acid, **261c** (36 mg, 0.11 mmol), HATU (42 mg, 0.11 mmol) and DIPEA (74 μ L, 0.22 mmol) were combined in *N,N*-dimethylformamide (0.5 mL) and left to stand at RT for 10 min. 4-Amino-2-chlorobenzoic acid (Sigma-Aldrich, 19 mg, 0.11 mmol) was added and the reaction was left to stand at RT for 18 h. The solvent was removed and the crude residue dissolved in DMSO (0.5 mL) and purified by Mass Directed AutoPrep on an Atlantis column using acetonitrile/water with a formic acid modifier. The appropriate fractions were concentrated *in vacuo* to give the title compound as a white solid (9.9 mg, 17%); m.p. 168-172 $^{\circ}$ C; $\nu_{\max}/\text{cm}^{-1}$ (solid) 1686, 1636 (C=O); ^1H NMR (600 MHz, DMSO- d_6) δ ppm 3.69 (s, 3 H), 3.77 (s, 3 H), 3.92 (s, 3 H), 7.22-7.26 (m, 1 H), 7.28-7.32 (m, 1 H), 7.51-7.56 (m, 1 H), 7.82 (d, $J=8.3$ Hz, 1 H), 8.04-8.08 (m, 1 H), 8.58-8.61 (m, 1 H), 8.64-8.67 (m, 1 H), 12.36 (s, 1 H), nb. the carboxylic acid proton was thought to be under the water peak; ^{13}C NMR (101 MHz, DMSO- d_6) δ ppm 38.2, 56.3, 60.3, 109.5, 117.7, 117.7, 118.4, 118.5, 120.7, 127.5, 131.9 (2C), 132.2, 132.9, 141.4, 141.9, 142.8, 144.1, 153.9, 161.2, 161.8, 166.0; LCMS (Method A): MH^+ 477/479, Rt 1.08 min, 100% by UV; HRMS exact mass calculated for $[\text{M}+\text{H}]^+$ ($\text{C}_{22}\text{H}_{19}\text{Cl}_2\text{N}_2\text{O}_6$) requires m/z 477.0615, found 477.0623.

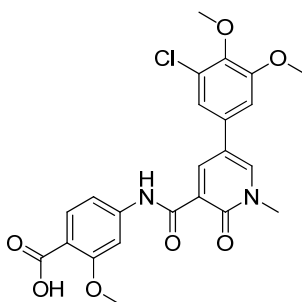
The following experiments were performed using Typical Procedure M, the data are reported as (a) amine (supplier, g, mmol); (b) product (mg, % yield).

4-(5-(3-Chloro-4,5-dimethoxyphenyl)-1-methyl-2-oxo-1,2-dihydropyridine-3-carboxamido)-2-methylbenzoic acid 270i



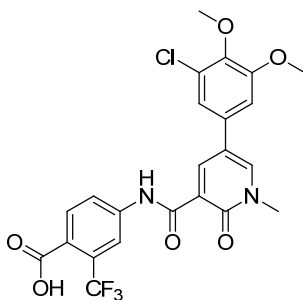
(a) 4-Amino-2-methylbenzoic acid, Sigma-Aldrich, 17 mg, 0.11 mmol; (b) 3.4 mg, 6%; $^1\text{H NMR}$ (600 MHz, $\text{DMSO-}d_6$) δ ppm 2.52 (s, 3 H), 3.71 (s, 3 H), 3.78 (s, 3 H), 3.93 (s, 3 H), 7.25-7.28 (m, 1 H), 7.30-7.32 (m, 1 H), 7.52-7.55 (m, 1 H), 7.62-7.66 (m, 1 H), 7.80-7.83 (m, 1 H), 8.59-8.62 (m, 1 H), 8.68-8.70 (m, 1 H), 12.25 (s, 1 H), nb. the carboxylic acid proton was thought to be under the water peak; LCMS (Method A): M^+ 457/459, Rt 1.07 min, 84% by UV.

4-(5-(3-Chloro-4,5-dimethoxyphenyl)-1-methyl-2-oxo-1,2-dihydropyridine-3-carboxamido)-2-methoxybenzoic acid 270j



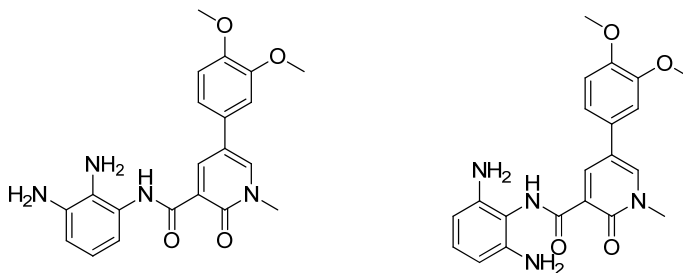
(a) 4-Amino-2-methoxybenzoic acid, Sigma-Aldrich, 18 mg, 0.11 mmol; (b) 7.4 mg, 13%; $^1\text{H NMR}$ (400 MHz, $\text{DMSO-}d_6$) δ ppm 3.71 (s, 3 H), 3.78 (s, 3 H), 3.82 (s, 3 H), 3.94 (s, 3 H), 7.23 (d, $J=8.6$ Hz, 1 H), 7.26-7.29 (m, 1 H), 7.32 (d, $J=1.8$ Hz, 1 H), 7.59-7.62 (m, 1 H), 7.66 (d, $J=8.6$ Hz, 1 H), 8.61 (d, $J=2.3$ Hz, 1 H), 8.71 (d, $J=2.5$ Hz, 1 H), 12.30 (s, 1 H), nb. the carboxylic acid proton was thought to be under the water peak; LCMS (Method A): MH^+ 473, Rt 1.07 min, 93% by UV.

4-(5-(3-Chloro-4,5-dimethoxyphenyl)-1-methyl-2-oxo-1,2-dihydropyridine-3-carboxamido)-2-(trifluoromethyl)benzoic acid 270k



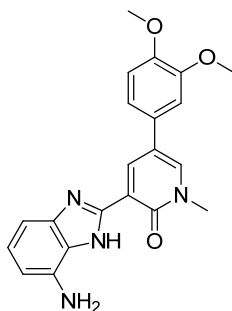
(a) 4-Amino-2-(trifluoromethyl)benzoic acid **357**, 23 mg, 0.11 mmol; (b) 16.5 mg, 26%; ¹H NMR (600 MHz, DMSO-*d*₆) δ ppm 3.71 (s, 3 H), 3.77 (s, 3 H), 3.93 (s, 3 H), 7.25-7.27 (m, 1 H), 7.30-7.32 (m, 1 H), 7.85 (d, *J*=8.1 Hz, 1 H), 7.87 (d, *J*=8.1 Hz, 1H), 8.37 (s, 1 H), 8.60-8.63 (m, 1 H), 8.68-8.71 (m, 1 H), 12.47 (s, 1 H), nb. the carboxylic acid proton was thought to be under the water peak; LCMS (Method A): MH⁺ 511, Rt 1.12 min, 100% by UV.

***N*-(2,3-Diaminophenyl)-5-(3,4-dimethoxyphenyl)-1-methyl-2-oxo-1,2-dihydropyridine-3-carboxamide compound with *N*-(2,6-diaminophenyl)-5-(3,4-dimethoxyphenyl)-1-methyl-2-oxo-1,2-dihydropyridine-3-carboxamide 277**



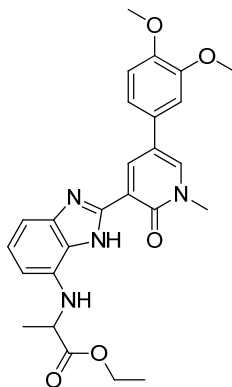
5-(3,4-Dimethoxyphenyl)-1-methyl-2-oxo-1,2-dihydropyridine-3-carboxylic acid **186** (590 mg, 2.04 mmol), TBTU (720 mg, 2.24 mmol) and DIPEA (2.1 mL, 12 mmol) were combined in acetonitrile (20 mL) and stirred at RT for 30 min. Benzene-1,2,3-triamine (Princeton Biomolecular Research, 400 mg, 2.04 mmol) was added and the reaction stirred at RT for 72 h. The reaction mixture was diluted with water and ethyl acetate. The layers were separated and the organic layer washed with brine, dried and concentrated *in vacuo* to give the title compounds (850 mg, 36%), a mixture of two isomers. The material was used in crude form in the next reaction. LCMS (Method A): MH⁺ 395, Rt 0.62 & 0.67 min, 56% by UV.

3-(4-Amino-1*H*-benzo[*d*]imidazol-2-yl)-5-(3,4-dimethoxyphenyl)-1-methylpyridin-2(1*H*)-one 278



N-(2,3-Diaminophenyl)-5-(4-methoxy-3-(trifluoromethoxy)phenyl)-1-methyl-2-oxo-1,2-dihydropyridine-3-carboxamide compound/*N*-(2,6-diaminophenyl)-5-(4-methoxy-3-(trifluoromethoxy)phenyl)-1-methyl-2-oxo-1,2-dihydropyridine-3-carboxamide **277** (850 mg, 0.780 mmol) and 4-methylbenzenesulfonic acid hydrate (295 mg, 1.55 mmol) were combined in ethanol (10 mL) and heated under microwave irradiation to 120 °C for 1 h. The reaction mixture was diluted with ethanol and filtered, washing with further ethanol. The solid was dried in a vacuum oven at 40 °C for 5 h to give the title compound (170 mg, 58%). The material was used in crude form in the next reaction. LCMS (Method A): MH^+ 377, *Rt* 0.64 min, 71% by UV.

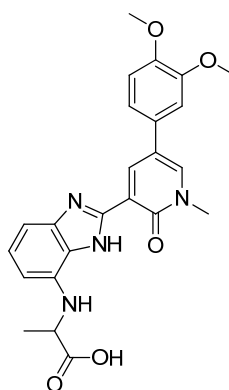
Ethyl 2(*RS*)-((2-(5-(3,4-dimethoxyphenyl)-1-methyl-2-oxo-1,2-dihydropyridin-3-yl)-1*H*-benzo[*d*]imidazol-7-yl)amino)propanoate 287



3-(4-Amino-1*H*-benzo[*d*]imidazol-2-yl)-5-(3,4-dimethoxyphenyl)-1-methylpyridin-2(1*H*)-one **278** (285 mg, 0.760 mmol) and potassium carbonate (157 mg, 1.14 mmol) were suspended in *N,N*-dimethylformamide (4 mL) and ethyl 2-bromopropanoate (Sigma-Aldrich, 118 μ L, 0.910 mmol) was added in one charge. The reaction mixture was stirred at RT for 3 days after which time additional 2-bromopropanoate (118 μ L, 0.910 mmol) was added. After stirring the reaction mixture at RT for 5 h additional

potassium carbonate (157 mg, 1.14 mmol) was added and the reaction left stirring at RT for a further 18 h. The reaction mixture was diluted with water (100 mL) and dichloromethane (100 mL). The layers were separated and the aqueous phase extracted with further dichloromethane (2 x 100 mL). The combined organics were washed with saturated aqueous sodium bicarbonate solution (2 x 50 mL) then concentrated *in vacuo*. The residue was purified by column chromatography (silica), eluting with 0-100% ethyl acetate in dichloromethane. The appropriate fractions were concentrated *in vacuo* to give the title compound (60 mg, 17%) as a yellow solid. ¹H NMR (400 MHz, DMSO-*d*₆) Mixture of tautomers (~1:2 ratio) δ ppm 1.14 (major) and 1.17 (minor) (t, *J*=7.2 Hz, 3 H), 1.49 (minor) and 1.51 (major) (d, *J*=2.8 Hz, 3 H), 3.73 (major) and 3.75 (minor) (s, 3 H), 3.81 (minor) and 3.82 (major) (s, 3 H), 3.88 (minor) and 3.89 (major) (s, 3 H), 4.02-4.20 (major and minor) (m, 2 H), 4.43-4.51 (major and minor) (m, 1 H), 5.65 (major) and 5.68 (minor) (br. s, 1 H), 6.05-6.25 (minor) and 6.12-6.16 (major) (m, 1 H), 6.90-6.97 (major and minor) (m, 2 H), 7.05-7.07 (minor) and 7.07-7.09 (major) (m, 1 H), 7.18-7.20 (major) and 7.21-7.22 (minor) (m, 1 H), 7.23-7.24 (minor) and 7.25-7.26 (major) (m, 1 H), 8.31-8.33 (major) and 8.33-8.34 (minor) (m, 1 H), 8.81-8.82 (minor) and 8.85-8.86 (major) (m, 1 H), 12.41 (major) and 12.52 (minor) (br. s, 1 H); LCMS (Method A): MH⁺ 477, Rt 0.90 min, 95% by UV.

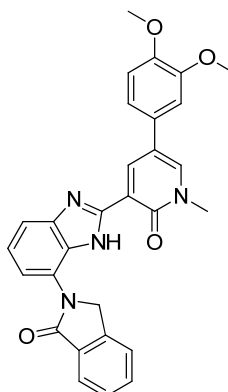
2(*RS*)-((2-(5-(3,4-Dimethoxyphenyl)-1-methyl-2-oxo-1,2-dihydropyridin-3-yl)-1*H*-benzo[*d*]imidazol-7-yl)amino)propanoic acid 289



Lithium hydroxide (9 mg, 0.35 mmol) was added to a suspension of ethyl 2-((2-(5-(3,4-dimethoxyphenyl)-1-methyl-2-oxo-1,2-dihydropyridin-3-yl)-1*H*-benzo[*d*]imidazol-7-yl)amino)propanoate **287** (55 mg, 0.12 mmol) in methanol (2 ml) and water (0.2 mL). The reaction mixture was stirred at RT for 18 h. The solvent was removed and the residue partitioned between 2 M aqueous sodium hydroxide solution and ethyl acetate.

The organic phase was washed with further 2 M aqueous sodium hydroxide solution and the combined organics were acidified to ~pH 5 using 5 M aqueous hydrochloric acid solution. This aqueous phase was extracted with dichloromethane (3 times) and the combined organic extracts dried (hydrophobic frit) and concentrated *in vacuo* to give the title compound (55 mg, 100%) as a brown solid. ¹H NMR (400 MHz, Methanol-*d*₄) Mixture of tautomers (~1:2 ratio) δ ppm 1.91 (major and minor) (s, 3 H), 3.73 (major) and 3.75 (minor) (s, 3 H), 3.81 (major and minor) (s, 3 H), 3.88 (major and minor) (s, 3 H), 4.33-4.37 (major and minor) (m, 1 H), 6.14-6.19 (major and minor) (m, 1 H), 6.21-6.25 (major and minor) (m, 1 H), 6.93-6.96 (major and minor) (m, 2 H), 7.05-7.07 (minor) and 7.07-7.09 (major) (m, 1 H), 7.19-7.22 (major and minor) (m, 1 H), 7.23-7.24 (minor) and 7.24-7.25 (major) (m, 1 H), 8.31-8.33 (major) and 8.33-8.34 (minor) (m, 1 H), 8.81 (minor) and 8.85 (minor) (d, *J*=2.5 Hz, 1 H), 12.42 (major) and 12.52 (minor) (br. s, 1 H), nb. the carboxylic acid proton was thought to be under the water peak; LCMS (Method A): MH⁺ 449, Rt 0.72 min, 98% by UV.

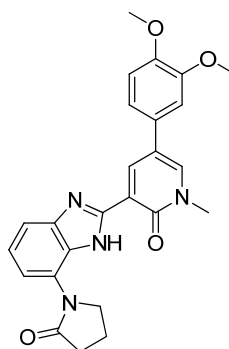
2-(2-(5-(3,4-Dimethoxyphenyl)-1-methyl-2-oxo-1,2-dihydropyridin-3-yl)-1H-benzo[d]imidazol-7-yl)isoindolin-1-one 290



To a suspension of 3-(4-amino-1H-benzo[d]imidazol-2-yl)-5-(3,4-dimethoxyphenyl)-1-methylpyridin-2(1H)-one **278** (170 mg, 0.450 mmol) and potassium carbonate (94 mg, 0.68 mmol) in *N,N*-dimethylformamide (3 mL) was added ethyl 2-(bromomethyl)benzoate (Apollo, 130 mg, 0.54 mmol). The reaction mixture was stirred at RT for 18 h. The reaction mixture was diluted with water (10 mL) and dichloromethane (10 mL), the layers separated and the aqueous extracted with further dichloromethane (10 mL). The combined organic layers were concentrated and the residue dissolved in 1:1 MeOH:DMSO (4 mL) and purified by Mass Directed AutoPrep on Sunfire C₁₈ column using acetonitrile/water with a formic acid modifier. The

appropriate fractions were concentrated *in vacuo* to give the title compound (90 mg, 41%) as a yellow solid. ^1H NMR (600 MHz, $\text{DMSO-}d_6$) Mixture of tautomers (~5:4 ratio) δ ppm 3.74 (minor) and 3.75 (major) (s, 3 H), 3.79 (major) and 3.81 (minor) (s, 3 H), 3.85 (major) and 3.89 (minor) (s, 3 H), 5.21 (minor) and 5.60 (major) (s, 2 H), 7.04 (major) and 7.07 (minor) (d, $J=8.4$ Hz, 1 H), 7.18-7.23 (major) and 7.23-7.27 (minor) (m, 2 H), 7.31-7.34 (minor and major overlapping) (m, 2 H), 7.56-7.65 (minor) and 7.67-7.76 (major) (m, 4 H), 7.84 (major) and 7.94 (minor) (d, $J=7.7$ Hz, 1 H), 8.38 (major) and 8.40 (minor) (d, $J=2.6$ Hz, 1 H), 8.88 (major) and 8.90 (minor) (d, $J=2.6$ Hz, 1 H), 12.77 (minor) and 12.84 (major) (s, 1 H); LCMS (Method A): MH^+ 493, R_t 0.92 min, 98% by UV.

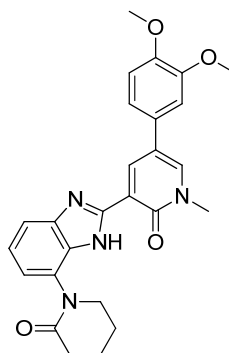
5-(3,4-Dimethoxyphenyl)-1-methyl-3-(7-(2-oxopyrrolidin-1-yl)-1H-benzo[d]imidazol-2-yl)pyridin-2(1H)-one 291



To a suspension of 3-(4-amino-1H-benzo[d]imidazol-2-yl)-5-(3,4-dimethoxyphenyl)-1-methylpyridin-2(1H)-one **278** (75 mg, 0.20 mmol) and potassium carbonate (83 mg, 0.60 mmol) in acetonitrile (2 mL) was added 4-chlorobutanoyl chloride (ABCR, 27 μL , 0.24 mmol) and the reaction mixture was stirred at RT for 2 h. The solvent was removed *in vacuo* and the residue dissolved in *N,N*-dimethylformamide (2 mL). Sodium hydride (60% dispersion in mineral oil, 16 mg, 0.40 mmol) was added and the reaction mixture stirred at RT for 2 h then diluted with water (10 mL) and dichloromethane (10 mL). The layers were separated and the aqueous phase extracted with further dichloromethane (10 mL). The combined organics were concentrated *in vacuo* and the residue triturated with diethyl ether and methanol. The resultant precipitate was filtered and dried to give the title compound (13 mg, 15%) as a dark brown solid. ^1H NMR (400 MHz, $\text{DMSO-}d_6$) Mixture of tautomers (~5:3 ratio) δ ppm 2.11-2.26 (major and minor) (m, 3 H), 2.64 (major and minor) (t, $J=7.9$ Hz, 1 H), 3.73 (major) and 3.74 (minor) (s, 3 H), 3.81 (major

and minor) (s, 3 H), 3.87 (minor) and 3.88 (major) (s, 3 H), 3.99 (major and minor) (t, $J=7.1$ Hz, 1 H), 4.33 (major and minor) (t, $J=6.9$ Hz, 1 H), 7.01-7.40 (major and minor) (m, 5 H), 7.52-7.59 (major and minor) (m, 1 H), 8.36 (minor) and 8.39 (major) (d, $J=2.8$ Hz, 1 H), 8.83 (minor) and 8.87 (major) (d, $J=2.5$ Hz, 1 H), 12.49 (major) and 12.73 (minor) (s, 1 H); LCMS (Method A): MH^+ 445, Rt 0.75 min, 97% by UV.

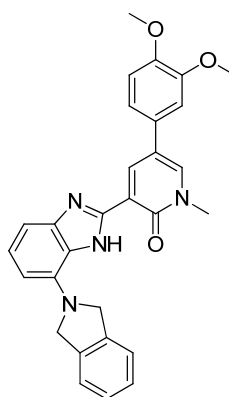
5-(3,4-Dimethoxyphenyl)-1-methyl-3-(7-(2-oxopiperidin-1-yl)-1H-benzo[d]imidazol-2-yl)pyridin-2(1H)-one 292



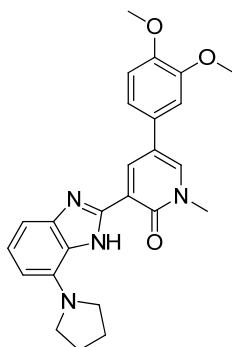
To a suspension of 3-(4-amino-1H-benzo[d]imidazol-2-yl)-5-(3,4-dimethoxyphenyl)-1-methylpyridin-2(1H)-one **278** (100 mg, 0.160 mmol) and potassium carbonate (66 mg, 0.48 mmol) in acetonitrile (2 mL) was added 5-bromopentanoyl chloride (Sigma-Aldrich, 21 μ L, 0.16 mmol) and the reaction mixture was stirred at RT for 2 h. The solvent was removed *in vacuo* and the residue dissolved in *N,N*-dimethylformamide (2 mL). Sodium hydride (60% dispersion in mineral oil, 13 mg, 0.32 mmol) was added and the reaction mixture stirred at RT for 18 h then diluted with water (5 mL) and dichloromethane (5 mL). The layers were separated and the aqueous phase extracted with further dichloromethane (2 x 5 mL). The combined organic extracts were concentrated *in vacuo* and the residue dissolved in 1:1 MeOH:DMSO (1 mL) and purified by Mass Directed AutoPrep on Sunfire C_{18} column using acetonitrile/water with a formic acid modifier. The appropriate fractions were concentrated *in vacuo* to give the title compound (42 mg, 58%) as a yellow solid; m.p. 219-222 $^{\circ}C$; ν_{max}/cm^{-1} (solid) 1649, 1585 (C=O); 1H NMR (400 MHz, DMSO- d_6) Mixture of tautomers (~1.2:1 ratio) δ ppm 1.91-1.99 (major and minor) (m, 4 H), 2.43-2.48 (major and minor) (m, 1 H), 2.52-2.58 (major and minor) (m, 1 H), 3.74 (major and minor) (s, 3 H), 3.75-3.85 (major and minor) (m, 2 H), 3.81 (major and minor) (s, 3 H), 3.87 (major) and 3.88 (minor) (s, 3 H), 7.00-7.27 (major and minor) (m, 5 H), 7.57-7.63 (major and minor) (m, 1 H), 8.37

(major) and 8.40 (minor) (d, $J=2.5$ Hz, 1 H), 8.82 (major) and 8.86 (minor) (d, $J=2.5$ Hz, 1 H), 11.98 (minor) and 12.72 (major) (s, 1 H); ^{13}C NMR (101 MHz, $\text{DMSO-}d_6$) Mixture of tautomers so double the number of peaks δ ppm 21.3, 21.6, 23.5, 23.6, 33.1, 33.1, 38.2, 38.5, 51.2, 51.3, 56.1, 56.1, 56.1, 56.2, 110.0, 110.1, 111.7 (2C), 112.7, 112.8, 117.1, 117.3, 117.8, 118.4, 118.5, 119.3, 119.6, 121.3, 122.3, 122.6, 128.6, 128.8, 129.3, 129.5, 133.6, 136.3, 137.6, 137.9, 139.1, 139.3, 139.4, 144.6, 148.5, 148.8, 148.9, 149.1, 149.6, 149.7, 160.0, 160.3, 169.2, 169.3; LCMS (Method A): MH^+ 459, Rt 0.74 min, 100% by UV; HRMS exact mass calculated for $[\text{M}+\text{H}]^+$ ($\text{C}_{26}\text{H}_{27}\text{N}_4\text{O}_4$) requires m/z 459.2027, found 459.2034.

5-(3,4-Dimethoxyphenyl)-3-(7-(isoindolin-2-yl)-1H-benzo[d]imidazol-2-yl)-1-methylpyridin-2(1H)-one 293

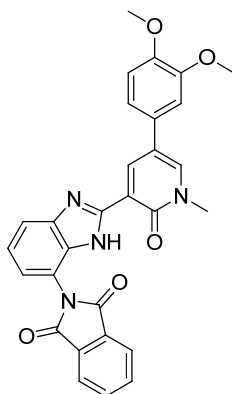


To a suspension of 3-(4-amino-1H-benzo[d]imidazol-2-yl)-5-(3,4-dimethoxyphenyl)-1-methylpyridin-2(1H)-one **278** (50 mg, 0.080 mmol) and potassium carbonate (33 mg, 0.24 mmol) in *N,N*-dimethylformamide (2 mL) was added 1,2-bis(bromomethyl)benzene (Fluka, 25 mg, 0.10 mmol) and the reaction mixture was stirred at RT for 3 days. The reaction mixture was diluted with water (5 mL) and dichloromethane (5 mL), the layers separated and the aqueous extracted with further dichloromethane (2 x 5 mL). The combined organics were concentrated and the residue triturated with ethanol. The resultant precipitate was filtered and dried to give the title compound (12 mg, 32%) as an orange solid. ^1H NMR (400 MHz, $\text{DMSO-}d_6$) δ ppm 3.74 (s, 3 H), 3.82 (s, 3 H), 3.91 (s, 3 H), 5.12 (br. s, 4 H), 6.31-6.33 (m, 1 H), 7.04-7.06 (m, 2 H), 7.09-7.12 (m, 1 H), 7.22-7.28 (m, 2 H), 7.30-7.33 (m, 2 H), 7.44-7.47 (m, 2 H), 8.33 (d, $J=2.8$ Hz, 1 H), 8.88 (d, $J=2.8$ Hz, 1 H), 12.43 (s, 1 H); LCMS (Method A): MH^+ 479, Rt 1.13 min, 100% by UV.

5-(3,4-Dimethoxyphenyl)-1-methyl-3-(7-(pyrrolidin-1-yl)-1H-benzo[d]imidazol-2-yl)pyridin-2(1H)-one 294

To a suspension of 3-(4-amino-1H-benzo[d]imidazol-2-yl)-5-(3,4-dimethoxyphenyl)-1-methylpyridin-2(1H)-one **278** (100 mg, 0.160 mmol) and potassium carbonate (66 mg, 0.48 mmol) in *N,N*-dimethylformamide (3 mL) was added 1,4-dibromobutane (Sigma-Aldrich, 19 μ L, 0.16 mmol). The reaction mixture was stirred at RT for 3 days then additional 1,4-dibromobutane (19 μ L, 0.16 mmol) added. After stirring for a further 2 h the reaction mixture was diluted with water (5 mL) and dichloromethane (5 mL). The layers were separated and the aqueous phase extracted with further dichloromethane (2 x 5 mL). The combined organic extracts were concentrated and the residue dissolved in DMSO (1 mL) and purified by Mass Directed AutoPrep on Xbridge column using acetonitrile/water with an ammonium bicarbonate modifier. The appropriate fractions were concentrated *in vacuo* to give the title compound (7 mg, 10%) as a yellow solid. ^1H NMR (400 MHz, DMSO- d_6) δ ppm 1.93-1.98 (m, 4 H), 3.71-3.74 (m, 4 H), 3.72 (s, 3H), 3.81 (s, 3 H), 3.86 (s, 3 H), 6.14-6.22 (m, 1 H), 6.94-6.96 (m, 2 H), 7.07-7.10 (m, 1 H), 7.14-7.17 (m, 1 H), 7.20-7.22 (m, 1 H), 8.28-8.29 (m, 1 H), 8.74 (d, $J=2.8$ Hz, 1 H), 12.32 (s, 1 H); LCMS (Method A): MH^+ 431, Rt 0.94 min, 80% by UV.

2-(2-(5-(3,4-Dimethoxyphenyl)-1-methyl-2-oxo-1,2-dihydropyridin-3-yl)-1H-benzo[d]imidazol-7-yl)isoindoline-1,3-dione **295a**

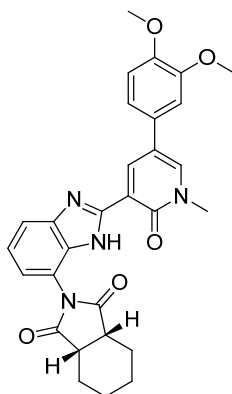


Typical Procedure N:

3-(4-Amino-1H-benzo[d]imidazol-2-yl)-5-(3,4-dimethoxyphenyl)-1-methylpyridin-2(1H)-one **278** (56 mg, 0.15 mmol) and isobenzofuran-1,3-dione **296** (Sigma-Aldrich, 22 mg, 0.15 mmol) were suspended in pyridine (0.5 mL) and heated under microwave irradiation to 100 °C for 30 min. After cooling the reaction mixture, the solvent was removed and the residue dissolved in DMSO (1 mL) and purified by Mass Directed AutoPrep on Xbridge column using acetonitrile/water with an ammonium bicarbonate modifier. The appropriate fractions were concentrated *in vacuo* then re-purified by Mass Directed AutoPrep on Sunfire C₁₈ column using acetonitrile/water with a formic acid modifier. The appropriate fractions were concentrated *in vacuo* to give the title compound (12 mg, 14%). ¹H NMR (600 MHz, DMSO-*d*₆) Mixture of tautomers (~1:1 ratio); NMR reported for both tautomers so double the number of protons reported δ ppm 3.67 (s, 3 H), 3.71 (s, 3 H), 3.73 (s, 3 H), 3.77 (s, 3 H), 3.80 (s, 3 H), 3.87 (s, 3 H), 6.95-6.98 (m, 1 H), 7.04-7.08 (m, 2 H), 7.13-7.15 (m, 1 H), 7.18-7.21 (m, 1 H), 7.23-7.26 (m, 2 H), 7.26-7.27 (m, 1 H), 7.33 (q, *J*=7.6 Hz, 2 H), 7.78 (d, *J*=7.9 Hz, 1 H), 7.84 (d, *J*=7.9 Hz, 1 H), 7.92-7.97 (m, 4 H), 7.99-8.04 (m, 4 H), 8.33-8.35 (m, 1 H), 8.36-8.38 (m, 1 H), 8.63-8.65 (m, 1 H), 8.84-8.86 (m, 1 H), 12.65-12.68 (m, 1 H), 12.90-13.00 (m, 1 H); LCMS (Method A): MH⁺ 507, Rt 0.93 min, 100% by UV.

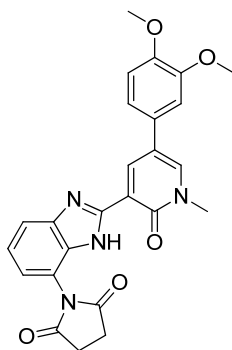
The following experiments were performed using Typical Procedure N, the data are reported as (a) amine (supplier, g, mmol); (b) product (mg, % yield).

(3aR,7aS)-2-(2-(5-(3,4-Dimethoxyphenyl)-1-methyl-2-oxo-1,2-dihydropyridin-3-yl)-1H-benzo[d]imidazol-7-yl)hexahydro-1H-isoindole-1,3(2H)-dione 295b



(a) (3aR, 7aS)-Hexahydroisobenzofuran-1,3-dione **297**, Sigma-Aldrich, 23 mg, 0.15 mmol; (b) 18 mg, 21%; ^1H NMR (400 MHz, $\text{DMSO-}d_6$) Mixture of tautomers (~1:1 ratio); NMR reported for both tautomers so double the number of protons reported δ ppm 1.39-1.66 (m, 8 H), 1.79-1.95 (m, 4 H), 1.98-2.07 (m, 2 H), 3.72-3.76 (m, 6 H), 3.80 (s, 6 H), 3.83-3.89 (m, 6 H), 7.06 (s, 8 H), 7.15-7.24 (m, 2 H), 7.23-7.34 (m, 3 H), 7.72-7.81 (m, 3 H), 8.35-8.42 (m, 3 H), 8.72-8.78 (m, 2 H), 8.86 (d, $J=2.5$ Hz, 1 H), 12.33-12.37 (m, 1 H), 12.73-12.81 (m, 1 H); LCMS (Method A): MH^+ 513, Rt 0.95 min, 100% by UV.

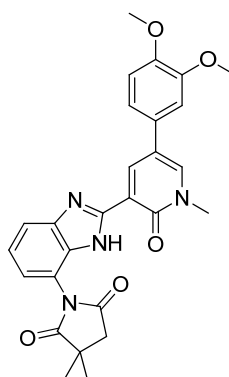
1-(2-(5-(3,4-Dimethoxyphenyl)-1-methyl-2-oxo-1,2-dihydropyridin-3-yl)-1H-benzo[d]imidazol-7-yl)pyrrolidine-2,5-dione 295c



3-(4-Amino-1H-benzo[d]imidazol-2-yl)-5-(3,4-dimethoxyphenyl)-1-methylpyridin-2(1H)-one **278** (75 mg, 0.20 mmol) and dihydrofuran-2,5-dione **298** (Sigma-Aldrich, 20 mg, 0.20 mmol) were suspended in pyridine (1 mL) and heated under microwave irradiation to 110 °C for 30 min. Additional pyridine (0.5 mL) was added and the reaction mixture heated under microwave irradiation at 120 °C for min, 130 °C for 30 min and finally 140 °C for 20 min. After cooling the reaction mixture, the solvent

was removed and the residue dissolved in DMSO (1 mL) and purified by Mass Directed AutoPrep on Sunfire C₁₈ column using acetonitrile/water with a formic acid modifier. The appropriate fractions were concentrated *in vacuo* to give the title compound (20 mg, 26%). ¹H NMR (400 MHz, DMSO-*d*₆) Mixture of tautomers (~1:1 ratio); NMR reported for both tautomers so double the number of protons reported δ ppm 2.49-2.52 (m, 4 H), 2.84-2.91 (m, 4 H), 3.73 (s, 6 H), 3.80 (s, 6 H), 3.87 (s, 6 H), 7.01-7.11 (m, 4 H), 7.12-7.33 (m, 6 H), 7.68-7.84 (m, 2 H), 8.32-8.42 (m, 2 H), 8.66-8.88 (m, 2 H), 12.28-12.43 (m, 1 H), 12.80-12.90 (m, 1 H); LCMS (Method A): MH⁺ 459, Rt 0.72 min, 100% by UV.

1-(2-(5-(3,4-Dimethoxyphenyl)-1-methyl-2-oxo-1,2-dihydropyridin-3-yl)-1H-benzo[d]imidazol-7-yl)-3,3-dimethylpyrrolidine-2,5-dione 295d



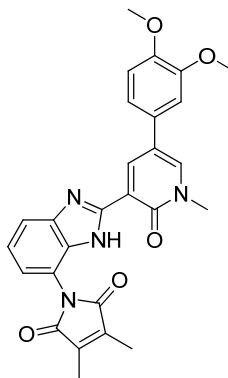
Typical Procedure O:

3-(4-Amino-1H-benzo[d]imidazol-2-yl)-5-(3,4-dimethoxyphenyl)-1-methylpyridin-2(1H)-one **278** (56 mg, 0.15 mmol) and 3,3-dimethyldihydrofuran-2,5-dione **299** (Sigma-Aldrich, 19 mg, 0.15 mmol) were suspended in pyridine (0.5 mL) and heated under microwave irradiation to 100 °C for 30 min. After cooling the reaction mixture, the solvent was removed and the residue dissolved in DMSO (1 mL) and purified by Mass Directed AutoPrep on Sunfire C₁₈ column using acetonitrile/water with a formic acid modifier. The appropriate fractions were concentrated *in vacuo* to give the title compound (6.5 mg, 8%). Mixture of tautomers (~1:1 ratio); NMR reported for both tautomers so double the number of protons reported ¹H NMR (600 MHz, DMSO-*d*₆) δ ppm 1.37 (s, 3H), 1.39 (s, 3 H), 1.49 (s, 6 H), 2.77 (m, 2 H), 2.84 (m, 2 H), 3.73 (s, 6 H), 3.79 (s, 3 H), 3.80 (s, 3 H), 3.84 (s, 3 H), 3.88 (s, 3 H), 7.03-7.11 (m, 4 H), 7.13-7.17 (m, 2 H), 7.19-7.21 (m, 2 H), 7.27 (t, *J*=7.7 Hz, 1 H), 7.31 (t, *J*=7.9 Hz, 1 H), 7.75 (d, *J*=8.3 Hz, 1 H), 7.78 (d, *J*=8.3 Hz, 1 H), 8.38-8.41 (m, 2 H), 8.80 (d, *J*=2.6 Hz, 1 H), 8.86 (d,

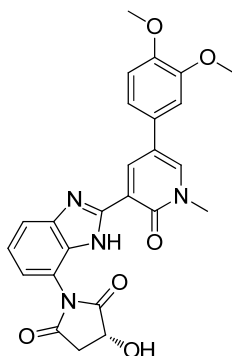
$J=2.3$ Hz, 1 H), 12.35 (br. s, 1 H), 12.85 (br. s, 1 H); LCMS (Method A): MH^+ 487, Rt 0.87 min, 93% by UV.

The following experiments were performed using Typical Procedure O, the data are reported as (a) amine (supplier, g, mmol); (b) product (mg, % yield).

1-(2-(5-(3,4-Dimethoxyphenyl)-1-methyl-2-oxo-1,2-dihydropyridin-3-yl)-1H-benzo[d]imidazol-7-yl)-3,4-dimethyl-1H-pyrrole-2,5-dione 295e



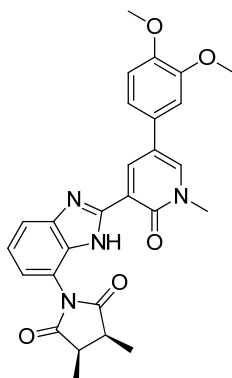
(a) 3,4-Dimethylfuran-2,5-dione **300**, Sigma-Aldrich, 15 mg, 0.15 mmol; (b) 35 mg, 43% as a cream solid; m.p. 263-256 °C; $\nu_{\max}/\text{cm}^{-1}$ (solid) 1708, 1652 (C=O); ^1H NMR (600 MHz, $\text{DMSO-}d_6$) Mixture of tautomers (~1:1 ratio); NMR reported for both tautomers so double the number of protons reported δ ppm 2.02-2.03 (m, 6 H), 2.04-2.05 (m, 6 H), 3.71 (s, 3 H), 3.72 (s, 3 H), 3.78 (s, 3 H), 3.80 (s, 3 H), 3.84 (s, 3 H), 3.87 (s, 3 H), 7.02-7.10 (m, 4 H), 7.11-7.15 (m, 2 H), 7.19-7.21 (m, 1 H), 7.21-7.22 (m, 1 H), 7.25-7.28 (m, 1 H), 7.28-7.31 (m, 1 H), 7.71-7.73 (m, 1 H), 7.77-7.79 (m, 1 H), 8.35 (d, $J=2.6$ Hz, 1 H), 8.39 (d, $J=2.6$ Hz, 1 H), 8.69 (d, $J=2.6$ Hz, 1 H), 8.84 (d, $J=2.6$ Hz, 1 H), 12.43-12.44 (m, 1 H), 12.85-12.96 (m, 1 H); ^{13}C NMR (101 MHz, $\text{DMSO-}d_6$) δ ppm 8.7, 8.8, 37.7, 55.6, 55.6, 109.8, 112.3, 116.7, 117.0, 117.1, 118.2, 118.2, 118.8, 118.9, 121.7, 128.3, 135.5, 137.3 (2C), 139.1, 140.1, 148.4, 149.1, 149.2, 159.5, 170.5, 170.9; LCMS (Method A): MH^+ 485, Rt 0.91 min, 100% by UV; HRMS exact mass calculated for $[M+H]^+$ ($\text{C}_{27}\text{H}_{25}\text{N}_4\text{O}_5$) requires m/z 485.1820, found 485.1823.

(R)-1-(2-(5-(3,4-dimethoxyphenyl)-1-methyl-2-oxo-1,2-dihydropyridin-3-yl)-1H-benzo[d]imidazol-7-yl)-3-hydroxypyrrolidine-2,5-dione 295f*Typical Procedure P:*

A solution of HATU (42 mg, 0.11 mmol) in *N,N*-dimethylformamide (0.1 mL) was added to (*R*)-2-hydroxysuccinic acid **304** (Sigma-Aldrich, 15 mg, 0.11 mmol) followed by DIPEA (35 μ L, 0.20 mmol). The reaction mixture was stirred at RT for 5 min, then 3-(4-amino-1*H*-benzo[*d*]imidazol-2-yl)-5-(3,4-dimethoxyphenyl)-1-methylpyridin-2(1*H*)-one **278** (38 mg, 0.10 mmol) was added as a solution in *N,N*-dimethylformamide (0.2 mL). The mixture was shaken then left standing at RT for 18 h. Additional HATU (42 mg, 0.22 mmol) in *N,N*-dimethylformamide (0.2 mL) and DIPEA (35 μ L, 0.20 mmol) were added, the reactions shaken and left standing at RT for 18 h. The solvent was removed *in vacuo* and the residue dissolved in DMSO (1 mL) and purified by Mass Directed AutoPrep on Xbridge column using acetonitrile/water with an ammonium bicarbonate modifier. The appropriate fractions were concentrated *in vacuo* to give the title compound (8.3 mg, 16%). ¹H NMR (600 MHz, DMSO-*d*₆) δ ppm 2.90-3.07 (m, 2 H), 3.74 (s, 3 H), 3.80 (s, 3 H), 3.88 (s, 3 H), 5.93-6.02 (m, 1 H), 6.28 (d, *J*=13.2 Hz, 1 H), 7.05-7.09 (m, 1 H), 7.12-7.17 (m, 1 H), 7.21 (d, *J*=8.7 Hz, 1 H), 7.25 (d, *J*=1.5 Hz, 1 H), 7.39-7.42 (m, 1 H), 8.36-8.41 (m, 2 H), 8.88 (br. s, 1 H), 12.68-12.86 (m, 1 H); LCMS (Method A): MH⁺ 487, Rt 0.69 min, 89% by UV.

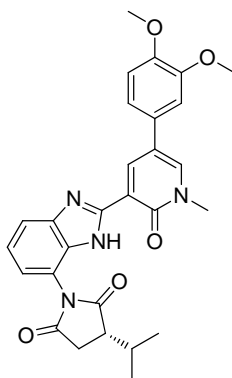
The following experiments were performed using Typical Procedure P, the data are reported as (a) amine (supplier, g, mmol); (b) product (mg, % yield).

(3*R*,4*S*)-1-(2-(5-(3,4-dimethoxyphenyl)-1-methyl-2-oxo-1,2-dihydropyridin-3-yl)-1*H*-benzo[*d*]imidazol-7-yl)-3,4-dimethylpyrrolidine-2,5-dione 295g



(a) (2*R*,3*S*)-2,3-Dimethylsuccinic acid **305**, ABCR, 16 mg, 0.11 mmol; (b) 6.6 mg, 12%; ¹H NMR (600 MHz, DMSO-*d*₆) δ ppm 1.25-1.29 (m, 3 H), 1.29-1.33 (m, 3 H), 3.73 & 3.75 (s, 3 H), 3.79 & 3.80 (s, 3 H), 3.84-3.86 (m, 2 H), 3.88 (s, 3 H), 7.02-7.13 (m, 1 H), 7.13-7.23 (m, 1 H), 7.24-7.32 (m, 2 H), 7.72-7.79 (m, 1 H), 8.36-8.43 (m, 1 H), 8.75-8.80 (m, 1 H), 8.85-8.89 (m, 1 H), 12.80 - 12.90 (m, 1 H), n.b. tautomers seen clearly on some peaks, but not well resolved on others; LCMS (Method A): MH⁺ 487, Rt 0.85 min, 95% by UV.

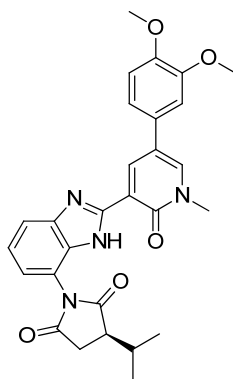
(3*S*)-1-(2-(5-(3,4-Dimethoxyphenyl)-1-methyl-2-oxo-1,2-dihydropyridin-3-yl)-1*H*-benzo[*d*]imidazol-7-yl)-3-isopropylpyrrolidine-2,5-dione 295h



(a) (*S*)-2-Isopropylsuccinic acid **306**, GSK Compound Collection, 18 mg, 0.11 mmol; (b) 22 mg, 40%; ¹H NMR (400 MHz, DMSO-*d*₆) Mixture of tautomers (~1:1 ratio); NMR reported for both tautomers so double the number of protons δ ppm 0.98-1.08 (m, 6 H), 1.08-1.23 (m, 6 H), 2.20-2.36 (m, 2 H), 2.67-2.81 (m, 2 H), 2.89-3.01 (m, 2 H), 3.03-3.15 (m, 2 H), 3.69-3.75 (m, 6 H), 3.80 (s, 6 H), 3.84-3.89 (m, 6 H), 6.99-7.11 (m, 6 H),

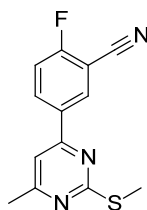
7.15-7.22 (m, 2 H), 7.23-7.33 (m, 2 H), 7.73-7.79 (m, 2 H), 8.34-8.41 (m, 2 H), 8.70-8.89 (m, 2 H), 12.79 (s, 2 H); LCMS (Method A): MH^+ 501, Rt 0.93 min, 98% by UV.

(3R)-1-(2-(5-(3,4-Dimethoxyphenyl)-1-methyl-2-oxo-1,2-dihydropyridin-3-yl)-1H-benzo[d]imidazol-7-yl)-3-isopropylpyrrolidine-2,5-dione 295i



(a) (*R*)-2-Isopropylsuccinic acid **307**, GSK Compound Collection, 18 mg, 0.11 mmol;
 (b) 17 mg, 31%; 1H NMR (600 MHz, $DMSO-d_6$) Mixture of tautomers (~1:1 ratio);
 NMR reported for both tautomers so double the number of protons reported δ ppm 0.93-1.07 (m, 6 H), 1.08-1.22 (m, 6 H), 2.24-2.36 (m, 2 H), 2.68-2.78 (m, 2 H), 2.91-2.99 (m, 2 H), 3.03-3.12 (m, 2 H), 3.73 (s, 6 H), 3.80 (s, 6 H), 3.86 (s, 6 H), 7.02-7.10 (m, 6 H), 7.16-7.23 (m, 2 H), 7.24-7.32 (m, 2 H), 7.73-7.80 (m, 2 H), 8.36-8.43 (m, 2 H), 8.71-8.75 (m, 2 H), 12.78-12.90 (m, 2 H); LCMS (Method A): MH^+ 501, Rt 0.93 min, 93% by UV.

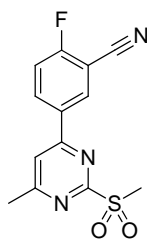
2-Fluoro-5-(6-methyl-2-(methylthio)pyrimidin-4-yl)benzonitrile 316



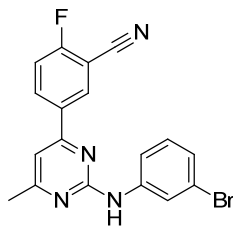
3-(Cyano-4-fluorophenyl)boronic acid **315** (Asymchem, 5.05 g, 30.6 mmol), 4-chloro-6-methyl-2-(methylthio)pyrimidine **314** (Fluorochem, 5.09 g, 29.1 mmol), $Pd(PPh_3)_4$ (Sigma-Aldrich, 337 mg, 0.291 mmol) and sodium carbonate (Fisher, 4.63 g, 43.7 mmol) were suspended in 1,2-dimethoxyethane (100 mL) and water (10 mL). The reaction mixture was heated to 90 °C under nitrogen for 2 h. Additional 1,2-dimethoxyethane (20 mL) and water (2 mL) were added and the reaction mixture heated

for a further 48 h. Additional Pd(PPh₃)₄ (Sigma-Aldrich, 337 mg, 0.291 mmol) was added and the mixture heated for a further 4 h, then diluted with water (500 mL) and methyl *tert*-butyl ether (500 mL). The organic layer was concentrated *in vacuo* to give a crude residue which was recrystallised twice from hot isopropanol to give the title compound (2.6 g, 34%) as an off-white solid. ¹H NMR (400 MHz, DMSO-*d*₆) δ ppm 3.29 (s, 6 H), 7.71 (t, *J*=9.1 Hz, 1 H), 7.81 (s, 1 H), 8.59 (ddd, *J*=8.9, 5.3, 2.4 Hz, 1 H), 8.72 (dd, *J*=6.3, 2.3 Hz, 1 H); LCMS (Method A): MH⁺ 260, Rt 1.15 min, 88% by UV.

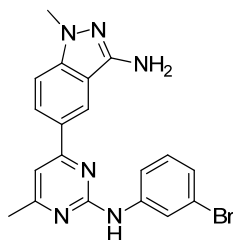
2-Fluoro-5-(6-methyl-2-(methylsulfonyl)pyrimidin-4-yl)benzonitrile 317



2-Fluoro-5-(methyl-2-(methylthio)pyrimidin-4-yl)benzonitrile **316** (2.29 g, 8.83 mmol) and Oxone™ (Sigma-Aldrich, 10.9 g, 17.7 mmol) were suspended in methanol (20 mL) and water (2 mL). The reaction mixture was stirred at RT for 30 min then additional methanol (20 mL) added. The reaction mixture was stirred at RT overnight then the solvent removed *in vacuo*. The crude residue obtained was partitioned between ethyl acetate (100 mL) and water (100 mL). The layers were separated and the organic phase dried over anhydrous magnesium sulfate, filtered and concentrated *in vacuo* to give the title compound (2.50 g, 97%) as a yellow solid. ¹H NMR (400 MHz, DMSO-*d*₆) δ ppm 3.30 (s, 3 H), 3.50 (s, 3 H), 7.78 (t, *J*=9.1 Hz, 1 H), 8.43 (s, 1 H), 8.68 (ddd, *J*=9.1, 5.3, 2.5 Hz, 1 H), 8.85 (dd, *J*=6.2, 2.4 Hz, 1 H); LCMS (Method A): MH⁺ 290, Rt 0.83 min, 75% by UV.

5-(2-((3-Bromophenyl)amino)-6-methylpyrimidin-4-yl)-2-fluorobenzonitrile 319

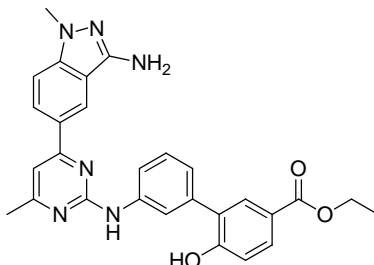
2-Fluoro-5-(6-methyl-3-(methylsulfonyl)pyrimidin-4-yl)benzonitrile **317** (1.25 g, 4.29 mmol), 3-bromoaniline **318** (Sigma-Aldrich, 2.80 mL, 25.7 mmol) and methanesulfonic acid (Acros, 836 μ L, 12.9 mmol) were suspended in isopropanol (15 mL) and heated under microwave irradiation to 150 °C for 1 h. The crude reaction mixture was partitioned between methyl *tert*-butyl ether (200 mL) and saturated aqueous sodium bicarbonate solution (200 mL). The layers were separated and the organic washed with 2 M aqueous hydrochloric acid (200 mL). The layers were separated and the organic layer dried over anhydrous magnesium sulfate, filtered and concentrated *in vacuo* to give the title compound (1.31 g, 80%) as a green solid. ^1H NMR (400 MHz, DMSO- d_6) δ ppm 3.36 (s, 3 H), 7.14 (dq, $J=7.8, 1.0$ Hz, 1 H), 7.27 (t, $J=8.1$ Hz, 1 H), 7.53 (s, 1 H), 7.75 (d, $J=8.8$ Hz, 2 H), 8.23 (t, $J=2.0$ Hz, 1 H), 8.54 (ddd, $J=8.8, 5.3, 2.3$ Hz, 1 H), 8.67 (dd, $J=6.3, 2.3$ Hz, 1 H), 9.91 (s, 1 H); LCMS (Method A): MH^+ 383/385, Rt 1.38 min, 79% by UV.

5-(2-((3-Bromophenyl)amino)-6-methylpyrimidin-4-yl)-1-methyl-1H-indazol-3-amine 320

5-(2-((3-Bromophenyl)amino)-6-(methylpyrimidin-4-yl)-2-fluorobenzonitrile **319** (1.20 g, 3.12 mmol) was dissolved in isopropanol (17 ml) and methylhydrazine (Sigma-Aldrich, 663 mg, 14.4 mmol) added. The reaction mixture was heated under microwave irradiation to 150 °C for 30 min. The yellow precipitate which had formed was filtered off, washed with isopropanol and dried in a vacuum oven at 40 °C for 30 min to give the title compound (728 mg, 57%) as a yellow solid. ^1H NMR (400 MHz, DMSO- d_6) δ ppm 3.30 (s, 3 H), 3.78 (s, 3 H), 5.52-5.63 (m, 1 H), 7.09-7.13 (m, 1 H), 7.27 (t, $J=8.1$ Hz,

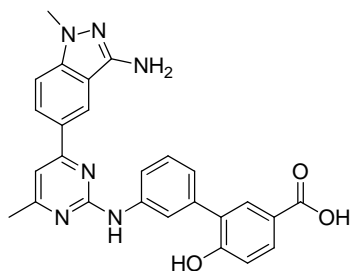
1 H), 7.28-7.30 (m, 2 H), 7.46 (d, $J=8.8$ Hz, 1 H), 7.82-7.85 (m, 1 H), 8.14 (dd, $J=8.8$, 1.5 Hz, 1 H), 8.30 (t, $J=1.8$ Hz, 1 H), 8.55-8.56 (m, 1 H), 9.74 (br. s, 1 H); LCMS (Method A): MH^+ 411/413, Rt 1.94 min, 99% by UV.

Ethyl 3'-((4-(3-amino-1-methyl-1H-indazol-5-yl)-6-methylpyrimidin-2-yl)amino)-6-hydroxy-[1,1'-biphenyl]-3-carboxylate 323



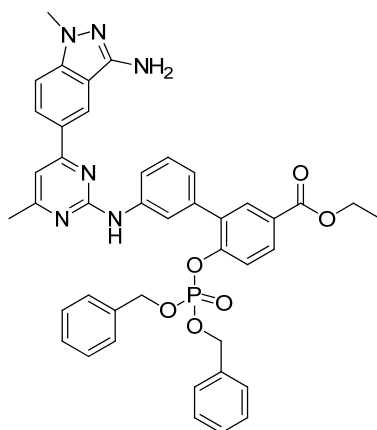
5-(2-((3-Bromophenyl)amino)-6-methylpyrimidin-4-yl)-1-methyl-1H-indazol-3-amine **320** (195 g, 0.476 mmol), (5-(ethoxycarbonyl)-2-hydroxyphenyl)boronic acid **322** (100 mg, 0.476 mmol) and $PdCl_2(dppf).CH_2Cl_2$ (19 mg, 0.024 mmol) were suspended in 1,4-dioxane (4 mL) and 2 M aqueous potassium carbonate solution (714 μ L, 1.43 mmol). The reaction mixture was heated under microwave irradiation to 120 °C for 20 min then 125 °C for 1 h 40 min. The crude mixture was loaded directly onto a pre-conditioned SCX ion exchange cartridge (10 g) and washed with methanol. The column was then eluted with 10% ammonia/methanol and the solvent concentrated *in vacuo* to give a brown solid, which was further purified by column chromatography (aminopropyl column), eluting with 0-100% ethyl acetate/cyclohexane followed by 0-20% methanol. The appropriate fractions were concentrated *in vacuo* to provide the title compound (108 mg, 46%). 1H NMR (400 MHz, $DMSO-d_6$) δ ppm 1.27 (t, $J=7.1$ Hz, 3 H), 3.29 (s, 3 H), 3.76 (s, 3 H), 4.26 (q, $J=7.1$ Hz, 2 H), 5.54-5.62 (m, 2 H), 7.06 (d, $J=8.6$ Hz, 1 H), 7.14 (d, $J=7.6$ Hz, 1 H), 7.24 (s, 1 H), 7.33-7.39 (m, 2 H), 7.82 (dd, $J=8.6$, 2.0 Hz, 1 H), 7.86-7.90 (m, 1 H), 7.91 (d, $J=2.0$ Hz, 1 H), 8.10-8.13 (m, 1 H), 8.14-8.18 (m, 1 H), 8.53-8.56 (m, 1 H), 9.55 (s, 1 H), 10.42-10.49 (m, 1 H); LCMS (Method A): MH^+ 495, Rt 1.02 min, 99% by UV.

3'-((4-(3-Amino-1-methyl-1*H*-indazol-5-yl)-6-methylpyrimidin-2-yl)amino)-6-hydroxy-[1,1'-biphenyl]-3-carboxylic acid **324**



Ethyl 3'-((4-(3-amino-1-methyl-1*H*-indazol-5-yl)-6-methylpyrimidin-2-yl)amino)-6-hydroxy-[1,1'-biphenyl]-3-carboxylate **323** (103 mg, 0.208 mmol) and lithium hydroxide (10 mg, 0.42 mmol) were suspended in tetrahydrofuran (3 mL) and water (3 mL) and stirred at RT for 18 h. 2 M aqueous sodium hydroxide (2 mL) was added and the reaction mixture was stirred at RT for 18 h, at 40 °C for 5 h, then at 70 °C for 4 h. After cooling, the reaction mixture was acidified with 2 M aqueous hydrochloric acid to ~pH 1. The resultant precipitate was filtered and dried in a vacuum oven at 40 °C overnight to give the title compound (70 mg, 72%) as a dark orange solid. ¹H NMR (400 MHz, DMSO-*d*₆) δ ppm 2.45 (s, 3 H), 3.82 (s, 3 H), 4.30 (br. s, 3 H), 7.06 (d, *J*=8.3 Hz, 1 H), 7.19 (d, *J*=7.6 Hz, 1 H), 7.28 (s, 1 H), 7.38 (t, *J*=7.9 Hz, 1 H), 7.46 (d, *J*=9.1 Hz, 1 H), 7.80 (dd, *J*=8.4, 2.1 Hz, 1 H), 7.86-7.90 (m, 1 H), 7.91 (d, *J*=2.0 Hz, 1 H), 8.05 (s, 1 H), 8.20 (dd, *J*=8.8, 1.5 Hz, 1 H), 8.61 (s, 1 H), 9.68 (s, 1 H), 10.32-10.45 (m, 1 H); LCMS (Method A): MH⁺ 467, Rt 0.78 min, 99% by UV.

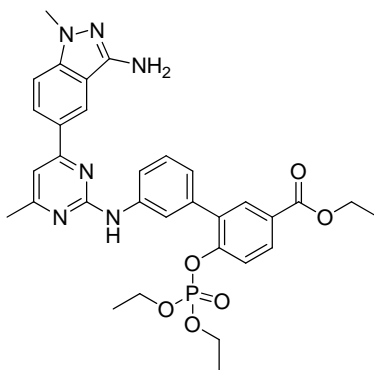
Ethyl 3'-((4-(3-amino-1-methyl-1*H*-indazol-5-yl)-6-methylpyrimidin-2-yl)amino)-6-((bis(benzyloxy)phosphoryl)oxy)-[1,1'-biphenyl]-3-carboxylate **325**



Ethyl 3'-((4-(3-amino-1-methyl-1*H*-indazol-5-yl)-6-methylpyrimidin-2-yl)amino)-6-hydroxy-[1,1'-biphenyl]-3-carboxylate **323** (377 mg, 0.760 mmol) was suspended in

N,N-dimethylformamide (8 mL) and sodium hydride (46 mg, 1.1 mmol) added. The reaction mixture was stirred at RT for 2 h, before dibenzyl phosphorochloridate (Toronto Research Chemicals, 10% w/v solution in benzene, 2.7 mL, 0.92 mmol) was added and the reaction was stirred at RT overnight. The crude reaction mixture was partitioned between water (10 mL) and dichloromethane (10 mL). The layers were separated and the aqueous phase was re-extracted with dichloromethane (15 mL). The combined organics extracts were washed with saturated aqueous lithium chloride (10 mL), separated and concentrated *in vacuo* to give a crude residue which was purified by Mass Directed AutoPrep on a Sunfire C₁₈ column using acetonitrile/water with a formic acid modifier. The solvent was concentrated *in vacuo* to give the title compound (200 mg, 35%) as a dark orange gum. ¹H NMR (400 MHz, CDCl₃) δ ppm 1.36 (t, *J*=7.1 Hz, 3 H), 2.46 (s, 3 H), 3.85 (s, 3 H), 4.36 (q, *J*=7.1 Hz, 2 H), 4.78-4.91 (m, 4 H), 7.04-7.06 (m, 2 H), 7.09-7.15 (m, 4 H), 7.20-7.23 (m, 4 H), 7.35-7.40 (m, 1 H), 7.49-7.53 (m, 1 H), 7.60-7.64 (m, 1 H), 7.98-8.04 (m, 3 H), 8.09 (s, 2 H), 8.13-8.15 (m, 1 H), 8.19-8.22 (m, 1 H), 8.30-8.32 (m, 1 H), nb. three exchangeable NH's were not seen in chloroform; LCMS (Method A): MH⁺ 755, Rt 1.33 min, 92% by UV

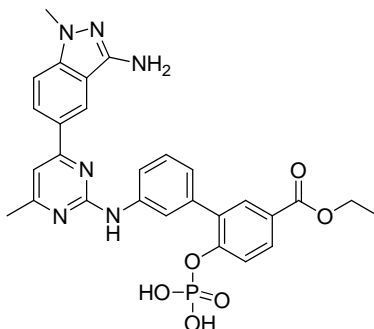
Ethyl 3'-((4-(3-amino-1-methyl-1*H*-indazol-5-yl)-6-methylpyrimidin-2-yl)amino)-6-((diethoxyphosphoryl)oxy)-[1,1'-biphenyl]-3-carboxylate 326



Ethyl 3'-((4-(3-amino-1-methyl-1*H*-indazol-5-yl)-6-methylpyrimidin-2-yl)amino)-6-hydroxy-[1,1'-biphenyl]-3-carboxylate **323** (465 mg, 0.940 mmol) was suspended in dichloromethane (10 mL) and triethylamine (197 μL, 1.41 mmol) and diethyl phosphorochloridate (Sigma-Aldrich, 163 μL, 1.13 mmol) were added. The reaction mixture was stirred at RT for 20 h. The suspension was filtered and the filtrate partitioned between dichloromethane (20 mL) and water (20 mL). The layers were separated, the organic extracts were dried over anhydrous sodium sulfate, filtered and

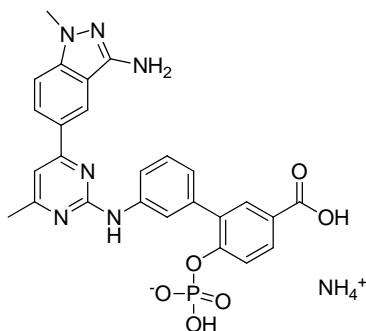
concentrated *in vacuo* to give the title compound (549 mg, 93%) as a yellow solid; LCMS (Method D): MH^+ 631, Rt 1.24 min, 70% by UV.

Ethyl 3'-((4-(3-amino-1-methyl-1*H*-indazol-5-yl)-6-methylpyrimidin-2-yl)amino)-6-(phosphonoxy)-[1,1'-biphenyl]-3-carboxylate 327



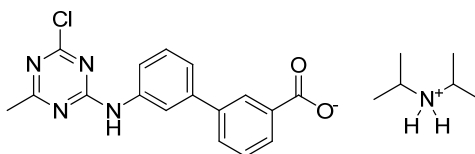
Ethyl 3'-((4-(3-amino-1-methyl-1*H*-indazol-5-yl)-6-methylpyrimidin-2-yl)amino)-6-((diethoxyphosphoryl)oxy)-[1,1'-biphenyl]-3-carboxylate **326** (500 mg, 0.79 mmol) was suspended in dichloromethane (5 mL). Trimethylsilyl bromide (Sigma-Aldrich, 1.54 mL, 11.9 mmol) was added and the reaction mixture stirred at RT for 20 h. Water (10 mL) was added and the resultant precipitate filtered and dried under reduced pressure to give an orange solid (455 mg) which was purified by column chromatography on a C_{18} cartridge (100 g), eluting with 0-60% acetonitrile/water with an ammonium bicarbonate modifier. The required fractions were combined and concentrated to give the title compound (245 mg, 54%) as a yellow solid; 1H NMR (400 MHz, $DMSO-d_6$) δ ppm 1.28 (t, $J=7.0$ Hz, 3 H), 2.44 (s, 3 H), 3.78 (s, 3 H), 4.30 (q, $J=7.0$ Hz, 2 H), 7.17-7.21 (m, 1 H), 7.26 (s, 1 H), 7.40 (s, 2 H), 7.66-7.70 (m, 1 H), 7.96-8.01 (m, 4 H), 8.13-8.17 (m, 1 H), 8.56 (s, 1 H), 9.60 (s, 1 H), nb. the NH_2 and OH exchangeable protons were not observed; LCMS (Method D): MH^+ 575, Rt 0.68 min, 100% by UV.

Ammonium 3'-((4-(3-amino-1-methyl-1*H*-indazol-5-yl)-6-methylpyrimidin-2-yl)amino)-6-(phosphonooxy)-[1,1'-biphenyl]-3-carboxylate 328



Ethyl 3'-((4-(3-amino-1-methyl-1*H*-indazol-5-yl)-6-methylpyrimidin-2-yl)amino)-6-(phosphonooxy)-[1,1'-biphenyl]-3-carboxylate **327** (243 mg, 0.420 mmol) was dissolved in methanol (5 mL) and aqueous sodium hydroxide (2 M, 1 mL) was added. The reaction mixture was stirred at RT for 20 h, then additional aqueous sodium hydroxide (2 M, 1 mL) was added. After stirring at RT for a further 24 h, the reaction mixture was heated to 60 °C for 3 h. The solvent was removed *in vacuo* and the residue triturated with hot isopropanol. After cooling, the precipitate was filtered off and dried under vacuum at 40 °C to give a yellow solid, which was purified by column chromatography on a C₁₈ cartridge, eluting with 5-60% acetonitrile/water with an ammonium bicarbonate modifier. The required fractions were combined and concentrated *in vacuo* to give the title compound (100 mg, 42%) as a pale yellow solid; ¹H NMR (400 MHz, DMSO-*d*₆) δ ppm 2.39 (s, 3 H), 3.72 (s, 3 H), 7.21-7.22 (m, 1 H), 7.24 (s, 1 H), 7.34-7.39 (m, 2 H), 7.68 (d, *J*=8.8 Hz, 1 H), 7.80 (dd, *J*=8.8, 2.3 Hz, 1 H), 7.90 (s, 3 H), 8.11-8.15 (m, 1 H), 8.47 (br. s, 1 H), nb. none of the exchangeable protons were observed; ³¹P NMR (162 MHz, DMSO-*d*₆) δ ppm -4.95; LCMS (Method D): MH⁺ 547, Rt 0.47 min, 100% by UV.

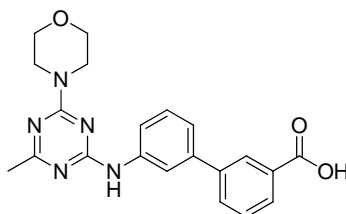
Diisopropylammonium 3'-((4-chloro-6-methyl-1,3,5-triazin-2-yl)amino)-[1,1'-biphenyl]-3-carboxylate 337



2,4-Dichloro-6-methyl-1,3,5-triazine **335** (Chembridge, 769 mg, 4.69 mmol) and 3'-amino-[1,1'-biphenyl]-3-carboxylic acid **336** (VitasM Laboratories, 1.0 g, 4.7 mmol)

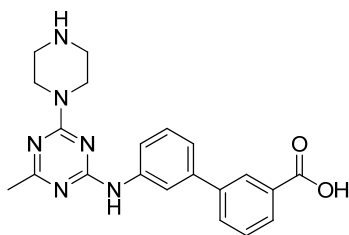
were suspended in isopropanol (10 mL) and *N,N*-diisopropylamine (Sigma-Aldrich, 2.5 mL, 17 mmol) added. The reaction mixture was stirred at RT for 2 h 30 min, then left standing at RT for 48 h. The mixture was diluted with isopropanol (20 mL) and the precipitate filtered, washed with further isopropanol and dried in a vacuum oven at 70 °C overnight to give the title compound (1.71 g, 83%) as a white solid. ¹H NMR (400 MHz, DMSO-*d*₆) δ ppm 1.15 (d, *J*=6.3 Hz, 12 H), 2.43 (s, 3 H), 3.10-3.22 (m, 2 H), 7.38-7.52 (m, 4 H), 7.69 (d, *J*=7.6 Hz, 2 H), 7.90 (d, *J*=7.6 Hz, 1 H), 8.18 (br. s, 1 H), 10.64-10.77 (m, 1 H), nb. two exchangeable protons not observed; LCMS (Method A): MH⁺ 341, Rt 0.99 min, 92% by UV.

3'-((4-Methyl-6-morpholino-1,3,5-triazin-2-yl)amino)-[1,1'-biphenyl]-3-carboxylic acid 338a



Diisopropylammonium 3'-((4-chloro-6-methyl-1,3,5-triazin-2-yl)amino)-[1,1'-biphenyl]-3-carboxylic acid **337** (34 mg, 0.077 mmol) was suspended in isopropanol (0.5 mL) and morpholine **339** (Sigma-Aldrich, 30 μL, 0.34 mmol) was added. The reaction mixture was heated under microwave irradiation to 120 °C for 10 min. The solvent was evaporated *in vacuo* and the crude residue purified by Mass Directed AutoPrep on a Sunfire C₁₈ column using acetonitrile/water with a formic acid modifier. The appropriate fractions were partitioned between dilute aqueous hydrochloric acid and dichloromethane. The layers were separated and the aqueous phase re-extracted with dichloromethane. The combined organic layers were dried over anhydrous magnesium sulfate, filtered and concentrated *in vacuo* to give the title compound (18 mg, 61%) as a white solid; ¹H NMR (400 MHz, DMSO-*d*₆) δ ppm 2.29 (s, 3 H), 3.63-3.69 (m, 4 H), 3.77-3.83 (m, 4 H), 3.91 (br. s, 1 H), 7.33-7.39 (m, 1 H), 7.43 (dd, *J*=8.8, 8.1 Hz, 1 H), 7.61 (t, *J*=7.8 Hz, 2 H), 7.88 (d, *J*=8.1 Hz, 1 H), 7.94 (d, *J*=7.8 Hz, 1 H), 8.18 (s, 1 H), 8.22 (s, 1 H), 9.87-9.95 (m, 1 H); LCMS (Method A): MH⁺ 392, Rt 0.86 min, 100% by UV.

3'-((4-Methyl-6-(piperazin-1-yl)-1,3,5-triazin-2-yl)amino)-[1,1'-biphenyl]-3-carboxylic acid 338b

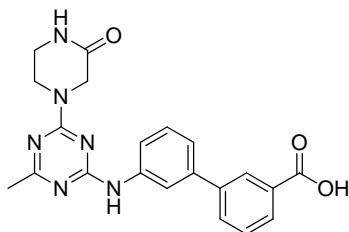


Typical Procedure Q:

Diisopropylammonium 3'-((4-chloro-6-methyl-1,3,5-triazin-2-yl)amino)-[1,1'-biphenyl]-3-carboxylic acid **337** (44 mg, 0.10 mmol) was suspended in isopropanol (2 mL) and piperidine **340** (Sigma-Aldrich, 39 mg, 0.45 mmol) added. The reaction mixture was heated under microwave irradiation to 120 °C for 10 min. The solvent was removed *in vacuo* and the crude residue purified by Mass Directed AutoPrep on a Sunfire C₁₈ column using acetonitrile/water with a trifluoroacetic acid modifier. The appropriate fractions were combined and concentrated *in vacuo* to give the title compound (31 mg, 72 %). ¹H NMR (400 MHz, DMSO-*d*₆) δ ppm 2.29 (s, 3 H), 3.16-3.26 (m, 4 H), 3.96-4.02 (m, 4 H), 4.29 (br. s, 1 H), 7.32-7.36 (m, 1 H), 7.43 (t, *J*=7.8 Hz, 1 H), 7.61 (t, *J*=7.7 Hz, 1 H), 7.70 (d, *J*=7.8 Hz, 1 H), 7.88 (d, *J*=8.1 Hz, 1 H), 7.96 (d, *J*=7.8 Hz, 1 H), 8.14 (s, 1 H), 8.19 (s, 1 H), 8.92 (br. s, 1 H), 9.84 (br. s, 1 H); LCMS (Method A): MH⁺ 391, Rt 0.66 min, 100% by UV.

The following experiments were performed using Typical Procedure Q, the data are reported as (a) amine (supplier, g, mmol); (b) product (mg, % yield).

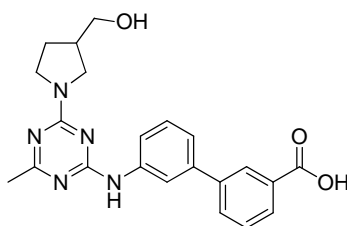
3'-((4-Methyl-6-(3-oxopiperazin-1-yl)-1,3,5-triazin-2-yl)amino)-[1,1'-biphenyl]-3-carboxylic acid 338c



(a) Piperazin-2-one **341**, ABCR, 45 mg, 0.45 mmol; (b) 13 mg, 29% as a white solid; m.p. 228-237 °C; $\nu_{\max}/\text{cm}^{-1}$ (solid) 2892 (OH), 1678 (C=O); ¹H NMR (400 MHz, DMSO-*d*₆) δ ppm 2.27 (s, 3 H), 3.23-3.33 (m, 2 H), 3.51 (br. s, 1 H), 3.89-4.00 (m, 4 H),

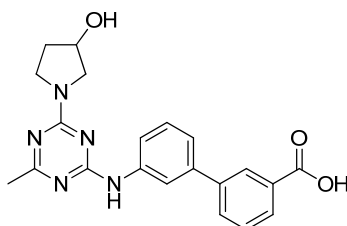
4.25 (s, 1 H), 7.29-7.36 (m, 1 H), 7.40 (t, $J=7.8$ Hz, 1 H), 7.51-7.59 (m, 1 H), 7.59-7.68 (m, 1 H), 7.77-7.84 (m, 1 H), 7.93 (d, $J=7.6$ Hz, 1 H), 8.11 (br. s, 1 H), 8.21 (s, 1 H), 9.76 (br. s, 1 H); ^{13}C NMR (101 MHz, $\text{DMSO-}d_6$) δ ppm 25.2, 46.9 (2C), 54.8, 118.9, 119.1, 120.4, 127.2, 128.2, 129.2 (2C), 129.6, 129.7, 140.3 (3C), 163.7 (2C), 167.9, 174.8, 174.8; LCMS (Method A): MH^+ 405, Rt 0.74 min, 100% by UV; HRMS exact mass calculated for $[\text{M}+\text{H}]^+$ ($\text{C}_{21}\text{H}_{21}\text{N}_6\text{O}_3$) requires m/z 405.1670, found 405.1663.

(3RS)-3'-((4-(3-(Hydroxymethyl)pyrrolidin-1-yl)-6-methyl-1,3,5-triazin-2-yl)amino)-[1,1'-biphenyl]-3-carboxylic acid 338d



(a) (3RS)-Pyrrolidin-3-yl methanol **342**, ABCR, 46 mg, 0.45 mmol; (b) 13 mg, 29%; ^1H NMR (400 MHz, $\text{DMSO-}d_6$) δ ppm 1.69-1.82 (m, 1 H), 1.97-2.08 (m, 1 H), 2.28 (s, 3 H), 2.43 (s, 1 H), 3.32-3.40 (m, 1 H), 3.39-3.51 (m, 2 H), 3.51-3.60 (m, 1 H), 3.64-3.75 (m, 2 H), 4.12 (br. s, 2 H), 7.30-7.35 (m, 1 H), 7.40 (t, $J=7.8$ Hz, 1 H), 7.59 (t, $J=7.7$ Hz, 1 H), 7.69 (d, $J=7.8$ Hz, 1 H), 7.88 (d, $J=8.3$ Hz, 1 H), 7.94 (d, $J=7.8$ Hz, 1 H), 8.23 (s, 1 H), 8.36 (br. s, 1 H), 9.48 (br. s, 1 H); LCMS (Method A): MH^+ 406, Rt 0.72 min, 84% by UV.

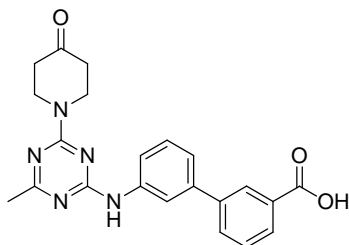
(3RS)-3'-((4-(3-Hydroxypyrrolidin-1-yl)-6-methyl-1,3,5-triazin-2-yl)amino)-[1,1'-biphenyl]-3-carboxylic acid 338e



(3RS)-Pyrrolidin-3-ol **343**, Anichem, 39 mg, 0.45 mmol; (b) 28 mg, 65%; ^1H NMR (400 MHz, $\text{DMSO-}d_6$) δ ppm 1.82-2.04 (m, 2 H), 2.24 (s, 3 H), 3.45-3.74 (m, 4 H), 4.36 (d, $J=12.3$ Hz, 1 H), 7.25-7.33 (m, 1 H), 7.33-7.42 (m, 1 H), 7.52-7.60 (m, 1 H), 7.61-7.68 (m, 1H), 7.80-7.88 (m, 1 H), 7.89-7.97 (m, 1 H), 8.24 (d, $J=12.6$ Hz, , 1 H), 8.42-

8.52 (m, 1 H), 9.56-9.68 (m, 1 H) nb. two exchangeable protons not observed; LCMS (Method C): MH^+ 392, Rt 0.73 min, 98% by UV.

3'-((4-Methyl-6-(4-oxopiperidin-1-yl)-1,3,5-triazin-2-yl)amino)-[1,1'-biphenyl]-3-carboxylic acid 338f

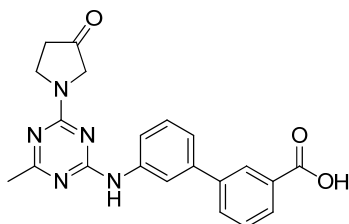


Typical Procedure R:

Diisopropylammonium 3'-((4-chloro-6-methyl-1,3,5-triazin-2-yl)amino)-[1,1'-biphenyl]-3-carboxylic acid **337** (22 mg, 0.050 mmol) was suspended in isopropanol and piperidin-4-one **344** (Apollo Scientific, 27 mg, 0.20 mmol) added. The reaction mixture was heated under microwave irradiation to 120 °C for 10 min. The solvent was removed *in vacuo* and the crude residue purified by Mass Directed AutoPrep on a Sunfire C₁₈ column using acetonitrile/water with a trifluoroacetic acid modifier. The appropriate fractions were combined and concentrated *in vacuo* to give the title compound as a cream solid (12 mg, 55 %); m.p. 237-242 °C; ν_{max}/cm^{-1} (solid) 2891 (OH), 1729 (C=O, ketone), 1679 (C=O carboxylic acid); ¹H NMR (400 MHz, DMSO-*d*₆) δ ppm 2.29 (s, 3 H), 3.35-3.56 (m, 5 H), 4.09 (t, *J*=6.2 Hz, 4 H), 7.33 (d, *J*=7.8 Hz, 1 H), 7.42 (t, *J*=7.8 Hz, 1 H), 7.57-7.66 (m, 2 H), 7.88 (d, *J*=8.1 Hz, 1 H), 7.95 (d, *J*=7.8 Hz, 1 H), 8.19 (s, 1 H), 8.30 (br. s, 1 H), 9.81 (br. s, 1 H); ¹³C NMR (151 MHz, DMSO-*d*₆) δ ppm 25.0, 40.1 (2C), 41.6 (2C), 117.9, 119.2, 120.6, 127.1, 128.3, 129.3 (2C), 130.9, 131.5, 139.6, 140.3, 140.7, 163.6, 164.1, 167.1, 174.5, 207.5; LCMS (Method C): MH^+ 404, Rt 0.76 min, 99% by UV; HRMS exact mass calculated for $[M+H]^+$ (C₂₂H₂₂N₅O₃) requires *m/z* 404.1717, found 404.1711.

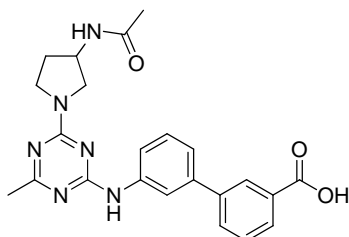
The following experiments were performed using Typical Procedure R, the data are reported as (a) amine (supplier, g, mmol); (b) product (mg, % yield).

3'-((4-Methyl-6-(3-oxopyrrolidin-1-yl)-1,3,5-triazin-2-yl)amino)-[1,1'-biphenyl]-3-carboxylic acid 338g



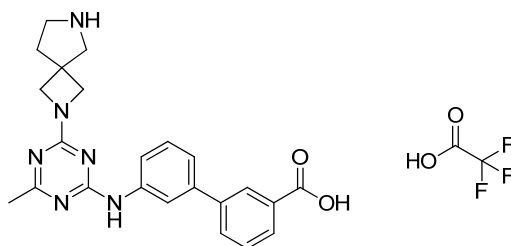
(a) Pyrrolidin-3-one **345**, Anichem, 24 mg, 0.20 mmol; (b) 1.3 mg, 6%; ¹H NMR (400 MHz, DMSO-*d*₆) δ ppm 2.27 (s, 3 H), 2.60-2.77 (m, 2 H), 3.33 (br. s, 1 H), 3.85-3.99 (m, 3 H), 3.99-4.08 (m, 1 H), 7.27 (br. s, 1 H), 7.36-7.43 (m, 1 H), 7.52 (t, *J*=7.6 Hz, 1 H), 7.61-7.68 (m, 1 H), 7.72-7.82 (m, 1 H), 7.91 (d, *J*=7.1 Hz, 1 H), 8.17-8.27 (m, 1 H), 8.37 (s, 1 H), 9.77 (br. s, 1 H); LCMS (Method A): MH⁺ 390, Rt 0.82 min, 100% by UV.

(3RS)-3'-((4-(3-Acetamidopyrrolidin-1-yl)-6-methyl-1,3,5-triazin-2-yl)amino)-[1,1'-biphenyl]-3-carboxylic acid 338h



(a) (3RS)-*N*-(Pyrrolidin-3-yl)acetamide **346**, ABCR, 26 mg, 0.20 mmol; (b) 13 mg, 54%; ¹H NMR (400 MHz, DMSO-*d*₆) δ ppm 1.87 (s, 3 H), 1.87-1.94 (m, 1 H), 2.17-2.24 (m, 1 H), 2.26 (s, 3 H), 3.21 (br. s, 1 H), 3.49-3.64 (m, 2 H), 3.70-3.85 (m, 2 H), 4.28-4.35 (m, 1 H), 7.26-7.32 (m, 1 H), 7.35 (dd, *J*=8.3, 7.3 Hz, 1 H), 7.46 (t, *J*=7.6 Hz, 1 H), 7.61 (d, *J*=8.1 Hz, 1 H), 7.73 (d, *J*=7.8 Hz, 1 H), 7.91 (d, *J*=7.6 Hz, 1 H), 8.27 (s, 1 H), 8.33-8.36 (m, 1 H), 8.40 (s, 1 H), 9.01 (br. s, 1 H); LCMS (Method A): MH⁺ 433, Rt 0.71 min, 100% by UV.

3'-((4-Methyl-6-(2,6-diazaspiro[3.4]octan-2-yl)-1,3,5-triazin-2-yl)amino)-[1,1'-biphenyl]-3-carboxylic acid 2,2,2-trifluoroacetate 376

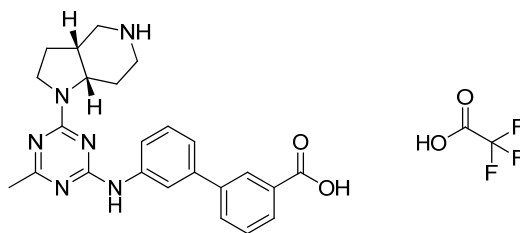


Typical Procedure S:

Diisopropylammonium 3'-((4-chloro-6-methyl-1,3,5-triazin-2-yl)amino)-[1,1'-biphenyl]-3-carboxylic acid **337** (20 mg, 0.14 mmol) and *tert*-butyl 2,6-diazaspiro[3.4]octane-6-carboxylate **348** (Synthonix Inc., 34 mg, 0.16 mmol) were combined in isopropanol (2 mL) and the reaction mixture heated under microwave irradiation to 120 °C for 30 min. The solvent was removed *in vacuo* and the residue dissolved in DMSO and purified by Mass Directed AutoPrep on a Sunfire C₁₈ column using acetonitrile/water with a trifluoroacetic acid modifier. The appropriate fractions were combined, concentrated *in vacuo* and dissolved in dichloromethane (200 μL) and trifluoroacetic acid (200 μL). The reaction mixture was stirred at RT for 2 h, the concentrated *in vacuo* to give the title compound (56 mg, 67%); ¹H NMR (400 MHz, DMSO-*d*₆) δ ppm 2.16-2.27 (m, 2 H), 2.28 (s, 3 H), 3.21-3.32 (m, 2 H), 3.47-3.49 (m, 2 H), 4.07-4.30 (m, 4 H), 7.35-7.44 (m, 2 H), 7.61 (t, *J*=7.7 Hz, 2 H), 7.92 (d, *J*=7.8 Hz, 1 H), 7.96 (d, *J*=7.6 Hz, 1 H), 8.23 (s, 1 H), 8.42 (s, 1 H), 8.92 (br. s, 1 H), 9.17 (br. s, 1 H), 10.21 (br. s, 1 H); LCMS (Method A): MH⁺ 417, Rt 0.63 min, 96% by UV.

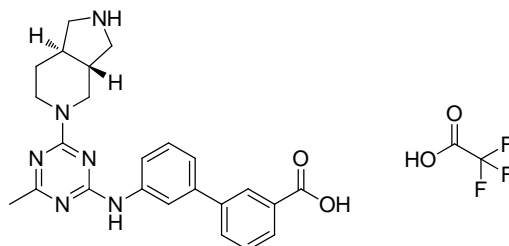
The following experiments were performed using Typical Procedure S, the data are reported as (a) amine (supplier, g, mmol); (b) product (mg, % yield).

3'-((4-Methyl-6-((3aR, 7aS) octahydro-1H-pyrrolo[3,2-c]pyridin-1-yl)-1,3,5-triazin-2-yl)amino)-[1,1'-biphenyl]-3-carboxylic acid 2,2,2-trifluoroacetate 377

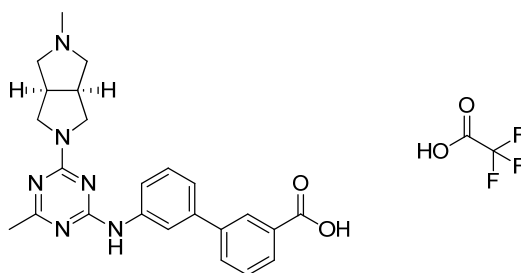


(a) (3a*S*, 7a*R*)-*Tert*-butyl hexahydro-1*H*-pyrrolo[3,2-*c*]pyridine-5(6*H*)-carboxylate **349**, WuXi, 36 mg, 0.16 mmol; (b) 52 mg, 62%; ¹H NMR (400 MHz, DMSO-*d*₆) δ ppm 1.55-1.71 (m, 1 H), 1.89-2.07 (m, 1 H), 2.11-2.28 (m, 2 H), 2.30 (s, 3 H), 2.90-3.05 (m, 1 H), 3.17-3.27 (m, 1 H), 3.32 (d, *J*=10.6 Hz, 1 H), 3.48-3.59 (m, 1 H), 3.60-3.78 (m, 2 H), 4.20-4.41 (m, 2 H), 7.32-7.49 (m, 2 H), 7.56-7.69 (m, 2 H), 7.90 (d, *J*=7.1 Hz, 1 H), 7.92-7.99 (m, 1 H), 8.21 (s, 1 H), 8.32-8.40 (m, 1 H), 8.46-8.59 (m, 1 H), 8.83-9.01 (m, 1 H), 10.31 (br. s, 1 H); LCMS (Method A): MH⁺ 431, Rt 0.59 min, 97% by UV.

3'-((4-((3aR,7aR)-Hexahydro-1H-pyrrolo[3,4-c]pyridin-5(6H)-yl)-6-methyl-1,3,5-triazin-2-yl)amino)-[1,1'-biphenyl]-3-carboxylic acid 2,2,2-trifluoroacetate 378



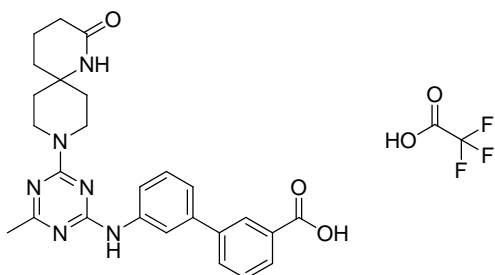
(a) (3a*S*,7a*R*)-*Tert*-butyl hexahydro-1*H*-pyrrolo[3,4-*c*]pyridine-2(3*H*)-carboxylate **350**, Enamine, 36 mg, 0.16 mmol; (b) 73 mg, 86%; ¹H NMR (400 MHz, DMSO-*d*₆) δ ppm 1.30-1.43 (m, 1 H), 1.66-1.76 (m, 1 H), 1.81-1.90 (m, 1 H), 1.99 (dd, *J*=12.6, 2.5 Hz, 1 H), 2.29 (s, 3 H), 2.73-2.93 (m, 4 H), 3.40 (dd, *J*=10.8, 7.3 Hz, 1 H), 3.49 (dd, *J*=10.7, 6.9 Hz, 1 H), 4.93 (d, *J*=13.3 Hz, 1 H), 5.06 (dd, *J*=12.6, 3.5 Hz, 1 H), 7.31-7.34 (m, 1 H), 7.41 (t, *J*=7.8 Hz, 1 H), 7.58 (t, *J*=7.7 Hz, 1 H), 7.66 (d, *J*=8.1 Hz, 1 H), 7.85 (d, *J*=7.8 Hz, 1 H), 7.95 (d, *J*=7.8 Hz, 1 H), 8.19 (s, 1 H), 8.22 (s, 1 H), 8.89 (br. s, 1 H), 9.29 (br. s, 1 H), 10.60 (br. s, 1 H); LCMS (Method A): MH⁺ 431, Rt 0.65 min, 99% by UV.

(3a*S*, 6a*S*)-3'-((4-Methyl-6-(5-methylhexahydropyrrolo[3,4-*c*]pyrrol-2(1*H*)-yl)-1,3,5-triazin-2-yl)amino)-[1,1'-biphenyl]-3-carboxylic acid 2,2,2-trifluoroacetate 379*Typical Procedure T:*

Diisopropylammonium 3'-((4-chloro-6-methyl-1,3,5-triazin-2-yl)amino)-[1,1'-biphenyl]-3-carboxylic acid **337** (20 mg, 0.14 mmol) (3a*S*, 6a*S*)-2-methyloctahydropyrrolo[3,4-*c*]pyrrole hydrochloride **351** (J&W Pharmalab, 32 mg, 0.16 mmol) were combined in isopropanol (2 mL) and the reaction mixture heated under microwave irradiation to 120 °C for 30 min. The solvent was removed *in vacuo* and the residue dissolved in DMSO and purified by Mass Directed AutoPrep on a Sunfire C₁₈ column using acetonitrile/water with a trifluoroacetic acid modifier. The appropriate fractions were combined and concentrated *in vacuo* to give the title compound (26 mg, 31 %). ¹H NMR (400 MHz, DMSO-*d*₆) δ ppm 2.29 (s, 3 H), 2.88 (s, 3 H), 3.22-3.31 (m, 4 H), 3.57-3.66 (m, 2 H), 3.72-3.84 (m, 4 H), 7.31-7.35 (m, 1 H), 7.37-7.43 (m, 1 H), 7.58 (t, *J*=7.7 Hz, 1 H), 7.68 (d, *J*=8.1 Hz, 1 H), 7.88 (d, *J*=8.1 Hz, 1 H), 7.95 (d, *J*=7.8 Hz, 1 H), 8.24 (s, 1 H), 8.31 (s, 1 H), 9.25 (br. s, 1 H), 10.05 (br. s, 1 H); LCMS (Method A): MH⁺ 431, Rt 0.62 min, 98% by UV.

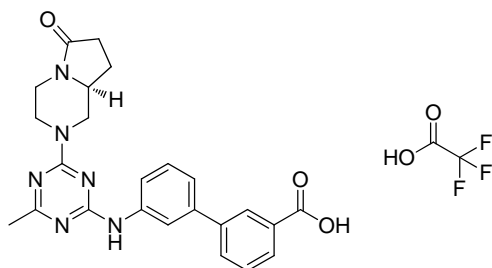
The following experiments were performed using Typical Procedure T, the data are reported as (a) amine (supplier, g, mmol); (b) product (mg, % yield).

3'-((4-Methyl-6-(2-oxo-1,9-diazaspiro[5.5]undecan-9-yl)-1,3,5-triazin-2-yl)amino)-[1,1'-biphenyl]-3-carboxylic acid 2,2,2-trifluoroacetate 380



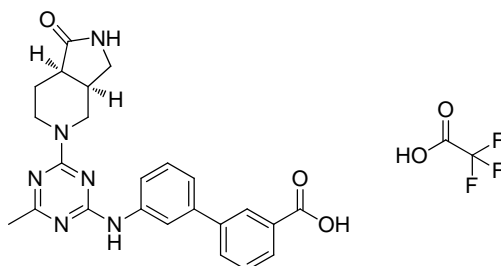
(a) 1,9-Diazaspiro[5.5]undecan-2-one hydrochloride **352**, ABCR, 33 mg, 0.16 mmol; (b) 13 mg, 14%; ^1H NMR (600 MHz, DMSO- d_6) δ ppm 1.58-1.67 (m, 4 H), 1.68-1.75 (m, 6 H), 2.13 (t, $J=6.0$ Hz, 2 H), 2.27 (s, 3 H), 3.48 (br. s, 2 H), 4.17 (d, $J=13.6$ Hz, 2 H), 7.34 (d, $J=7.6$ Hz, 1 H), 7.42 (t, $J=7.9$ Hz, 1 H), 7.54 (s, 1 H), 7.61 (t, $J=7.6$ Hz, 1 H), 7.87 (d, $J=7.9$ Hz, 1 H), 7.95 (d, $J=7.9$ Hz, 1 H), 8.18 (s, 1 H), 8.24 (s, 1 H), 9.87 (br. s, 1 H); LCMS (Method A): MH^+ 473, Rt 0.77 min, 98% by UV.

(8a*S*)-3'-((4-Methyl-6-(6-oxohexahydropyrrolo[1,2-*a*]pyrazin-2(1*H*)-yl)-1,3,5-triazin-2-yl)amino)-[1,1'-biphenyl]-3-carboxylic acid 2,2,2-trifluoroacetate 381



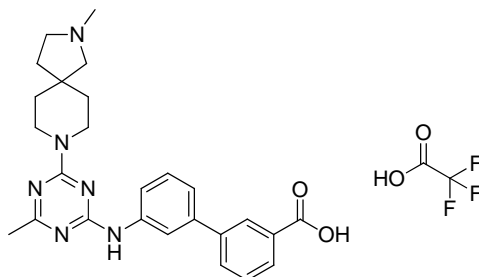
(a) (8a*S*)-Hexahydropyrrolo[1,2-*a*]pyrazin-6(2*H*)-one : (2*S*)-2-acetoxy-2-phenylacetate (1:1) **353**, GSK Compound Collection, 53 mg, 0.16 mmol; (b) 43 mg, 49%; ^1H NMR (400 MHz, DMSO- d_6) δ ppm 1.52-1.69 (m, 1 H), 2.07-2.18 (m, 1 H), 2.24-2.34 (m, 1 H), 2.30 (s, 3 H), 2.71 (dd, $J=12.7, 11.0$ Hz, 1 H), 2.78-2.95 (m, 3 H), 3.55-3.61 (m, 1 H), 3.93 (d, $J=12.8$ Hz, 1 H), 4.70-4.76 (m, 1 H), 4.79-4.86 (m, 1 H), 5.77 (br. s, 1 H), 7.29 (d, $J=7.8$ Hz, 1 H), 7.31-7.44 (m, 3 H), 7.44-7.51 (m, 1 H), 7.55-7.62 (m, 2 H), 8.12 (s, 1 H), 9.15 (br. s, 1 H); LCMS (Method A): MH^+ 459, Rt 0.77 min, 88% by UV.

3'-((4-Methyl-6-((3a*S*,7a*R*)-1-oxohexahydro-1*H*-pyrrolo[3,4-*c*]pyridin-5(6*H*)-yl)-1,3,5-triazin-2-yl)amino)-[1,1'-biphenyl]-3-carboxylic acid 2,2,2-trifluoroacetate 382



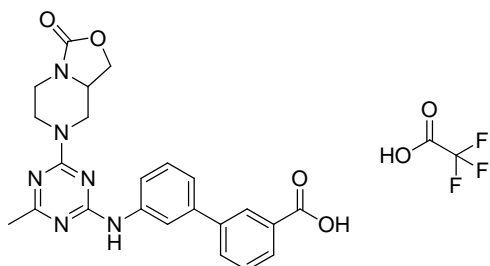
(a) ((3a*R*,7a*R*)-Octahydro-1*H*-pyrrolo[3,4-*c*]pyridin-1-one **354**, GSK Compound Collection, 22 mg, 0.16 mmol; (b) 32 mg, 37%; ¹H NMR (600 MHz, DMSO-*d*₆) δ ppm 1.72-1.82 (m, 1 H), 1.83-1.89 (m, 1 H), 2.29 (s, 3 H), 2.54 (s, 1 H), 2.60-2.66 (m, 1 H), 2.83-2.89 (m, 1 H), 3.13-3.20 (m, 1 H), 3.23 (d, *J*=8.7 Hz, 1 H), 3.29-3.36 (m, 1 H), 3.73 (br. s, 1 H), 4.01-4.12 (m, 1 H), 4.09-4.11 (m, 1 H), 4.19-4.33 (m, 1 H), 7.35 - 7.39 (m, 1 H), 7.44 (t, *J*=7.7 Hz, 1 H), 7.61 (t, *J*=7.6 Hz, 1 H), 7.66 (br. s, 1 H), 7.89 (d, *J*=7.9 Hz, 1 H), 7.96 (d, *J*=7.6 Hz, 1 H), 8.19 (s, 1 H), 8.25 (br. s, 1 H), 10.04 (br. s, 1 H); LCMS (Method A): MH⁺ 445, Rt 0.70 min, 98% by UV.

3'-((4-Methyl-6-(2-methyl-2,8-diazaspiro[4.5]decan-8-yl)-1,3,5-triazin-2-yl)amino)-[1,1'-biphenyl]-3-carboxylic acid 2,2,2-trifluoroacetate 383



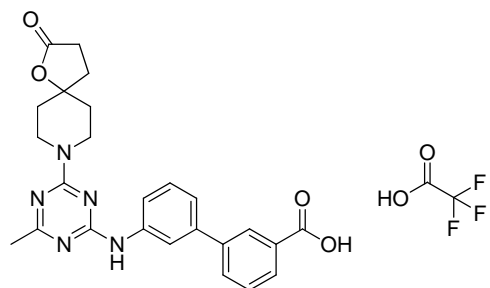
(a) 2-Methyl-2,8-diazaspiro[4.5]decan-8-yl hydrochloride **355**, Chembridge, 36 mg, 0.16 mmol; (b) 3 mg, 3%; ¹H NMR (400 MHz, DMSO-*d*₆) δ ppm 1.55-1.70 (m, 4 H), 1.83-1.93 (m, 1 H), 2.00-2.10 (m, 1 H), 2.26 (s, 3 H), 2.86 (d, *J*=4.0 Hz, 3 H), 2.89 (d, *J*=3.5 Hz, 2 H), 3.49-3.58 (m, 1 H), 3.59-3.67 (m, 1 H), 3.67-3.78 (m, 2 H), 3.83-3.96 (m, 2 H), 4.34 (br. s, 1 H), 7.30-7.36 (m, 1 H), 7.41 (t, *J*=7.8 Hz, 1 H), 7.56-7.61 (m, 1 H), 7.62 (t, *J*=7.7 Hz, 1 H), 7.89 (d, *J*=8.1 Hz, 1 H), 7.96 (d, *J*=7.8 Hz, 1 H), 8.20 (s, 1 H), 8.28 (s, 1 H), 9.85 (br. s, 1 H); LCMS (Method A): MH⁺ 459, Rt 0.69 min, 100% by UV.

(8aRS)-3'-((4-Methyl-6-(3-oxotetrahydro-1H-oxazolo[3,4-a]pyrazin-7(3H)-yl)-1,3,5-triazin-2-yl)amino)-[1,1'-biphenyl]-3-carboxylic acid 2,2,2-trifluoroacetate 384



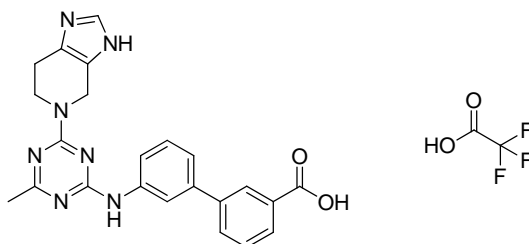
(a) (8aRS)-Tetrahydro-1H-oxazolo[3,4-a]pyrazin-3(5H)-one hydrochloride **356**, Fluorochem, 29 mg, 0.16 mmol; (b) 30 mg, 34%; ¹H NMR (400 MHz, DMSO-*d*₆) δ ppm 2.26 (s, 3 H), 2.46 (s, 1 H), 2.86 (dd, *J*=12.8, 10.8 Hz, 1 H), 2.99 (ddd, *J*=14.6, 12.7, 3.4 Hz, 2 H), 3.64-3.70 (m, 1 H), 3.79-3.87 (m, 1 H), 3.94 (dd, *J*=8.8, 5.8 Hz, 1 H), 4.35 (t, *J*=8.4 Hz, 1 H), 4.69 (d, *J*=11.3 Hz, 1 H), 4.78-4.84 (m, 1 H), 7.27-7.31 (m, 1 H), 7.37 (dd, *J*=8.3, 7.6 Hz, 1 H), 7.55 (dd, *J*=8.6, 7.8 Hz, 1 H), 7.63 (dd, *J*=8.1, 1.0 Hz, 1 H), 7.82 (d, *J*=8.3 Hz, 1 H), 7.92 (d, *J*=7.6 Hz, 1 H), 8.13 (t, *J*=1.9 Hz, 1 H), 8.19 (s, 1 H), 9.19 (br. s, 1 H); LCMS (Method A): MH⁺ 447, Rt 0.87 min, 99% by UV.

3'-((4-Methyl-6-(2-oxo-1-oxa-8-azaspiro[4.5]decan-8-yl)-1,3,5-triazin-2-yl)amino)-[1,1'-biphenyl]-3-carboxylic acid 2,2,2-trifluoroacetate 385



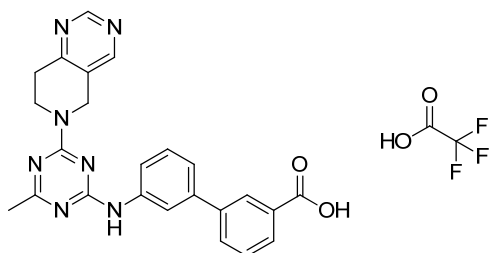
(a) 1-Oxa-8-azaspiro[4.5]decan-2-one hydrochloride **357**, Apollo Scientific, 30 mg, 0.16 mmol; (b) 46 mg, 51%; ¹H NMR (600 MHz, DMSO-*d*₆) δ ppm 1.78-1.81 (m, 2 H), 1.81-1.87 (m, 2 H), 2.04-2.09 (m, 2 H), 2.28 (s, 3 H), 2.63 (t, *J*=8.1 Hz, 2 H), 3.42-3.62 (m, 3 H), 4.18 (d, *J*=13.2 Hz, 2 H), 7.34 (d, *J*=7.6 Hz, 1 H), 7.42 (t, *J*=7.9 Hz, 1 H), 7.62 (t, *J*=7.7 Hz, 2 H), 7.88 (d, *J*=7.9 Hz, 1 H), 7.95 (d, *J*=7.9 Hz, 1 H), 8.19 (s, 1 H), 8.26 (s, 1 H), 9.86 (br. s, 1 H); LCMS (Method A): MH⁺ 460, Rt 0.83 min, 94% by UV.

3'-((4-(6,7-Dihydro-3*H*-imidazo[4,5-*c*]pyridin-5(4*H*)-yl)-6-methyl-1,3,5-triazin-2-yl)amino)-[1,1'-biphenyl]-3-carboxylic acid 2,2,2-trifluoroacetate 386



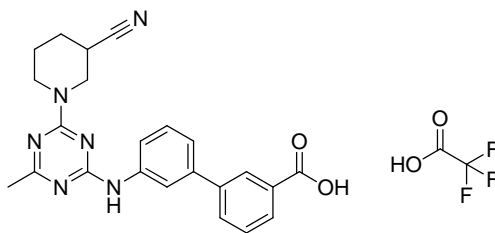
(a) 4,5,6,7-Tetrahydro-3*H*-imidazo[4,5-*c*]pyridine hydrochloride **358**, Apin Chemicals Ltd, 25 mg, 0.16 mmol; (b) 56 mg, 66%; ¹H NMR (400 MHz, DMSO-*d*₆) δ ppm 2.32 (s, 3 H), 2.82 (t, *J*=5.7 Hz, 2 H), 4.20 (t, *J*=5.8 Hz, 2 H), 4.94 (s, 2 H), 7.32-7.37 (m, 1 H), 7.43 (t, *J*=7.8 Hz, 1 H), 7.59 (t, *J*=7.7 Hz, 1 H), 7.75 (d, *J*=8.1 Hz, 1 H), 7.88 (d, *J*=7.8 Hz, 1 H), 7.96 (d, *J*=7.8 Hz, 1 H), 8.12 (s, 1 H), 8.25 (s, 1 H), 8.70 (s, 1 H), 9.30 (br. s, 1 H), 11.11 (br. s, 1 H) nb. carboxylic acid proton not seen; LCMS (Method A): MH⁺ 428, Rt 0.65 min, 98% by UV.

3'-((4-(7,8-Dihydropyrido[4,3-*d*]pyrimidin-6(5*H*)-yl)-6-methyl-1,3,5-triazin-2-yl)amino)-[1,1'-biphenyl]-3-carboxylic acid 2,2,2-trifluoroacetate 387



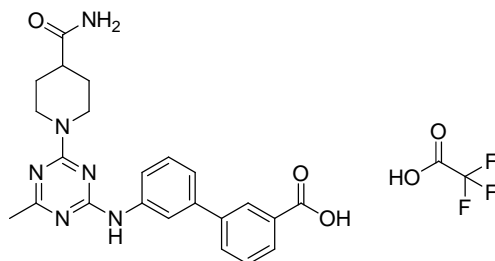
(a) 5,6,7,8-Tetrahydropyrido[4,3-*d*]pyrimidine hydrochloride **359**, Active Scientific, 26 mg, 0.16 mmol; (b) 37 mg, 42%; ¹H NMR (400 MHz, DMSO-*d*₆) δ ppm 2.33 (s, 3 H), 3.00 (t, *J*=6.0 Hz, 2 H), 4.17 (t, *J*=6.0 Hz, 2 H), 4.99 (s, 2 H), 7.34 (d, *J*=7.6 Hz, 1 H), 7.43 (t, *J*=7.6 Hz, 1 H), 7.60 (t, *J*=7.8 Hz, 1 H), 7.70 (d, *J*=8.1 Hz, 1 H), 7.89 (d, *J*=7.8 Hz, 1 H), 7.97 (d, *J*=7.8 Hz, 1 H), 8.23 (s, 1 H), 8.26 (s, 1 H), 8.56 (s, 1 H), 8.93 (s, 1 H), 9.29 (br. s, 1 H), nb. the carboxylic acid proton was not observed; LCMS (Method A): MH⁺ 440, Rt 0.81 min, 97% by UV.

(3*RS*)-3'-((4-(3-Cyanopiperidin-1-yl)-6-methyl-1,3,5-triazin-2-yl)amino)-[1,1'-biphenyl]-3-carboxylic acid 2,2,2-trifluoroacetate 388



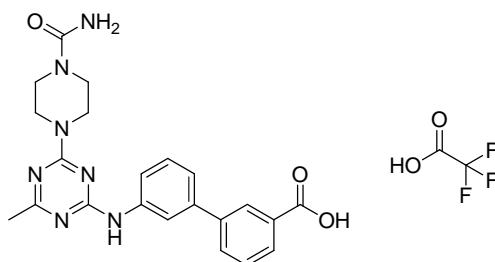
(a) (3*RS*)-Piperidine-3-carbonitrile **360**, ABCR, 17 mg, 0.16 mmol; (b) 39 mg, 47%; ¹H NMR (500 MHz, DMSO-*d*₆) δ ppm 1.57-1.68 (m, 2 H), 1.89-1.99 (m, 2 H), 2.30 (s, 3 H), 3.10-3.21 (m, 1 H), 3.52-3.71 (m, 1 H), 3.85-4.00 (m, 1 H), 4.02-4.13 (m, 1 H), 4.18-4.28 (m, 1 H), 7.33-7.38 (m, 1 H), 7.43 (t, *J*=7.8 Hz, 1 H), 7.59-7.64 (m, 2 H), 7.88 (d, *J*=7.4 Hz, 1 H), 7.95 (d, *J*=7.7 Hz, 1 H), 8.21 (s, 1 H), 8.23-8.27 (m, 1 H), 10.10 (br. s, 1 H) nb. carboxylic acid proton not seen; LCMS (Method A): MH⁺ 415, Rt 0.92 min, 99% by UV.

3'-((4-(4-Carbamoylpiperidin-1-yl)-6-methyl-1,3,5-triazin-2-yl)amino)-[1,1'-biphenyl]-3-carboxylic acid 2,2,2-trifluoroacetate 389



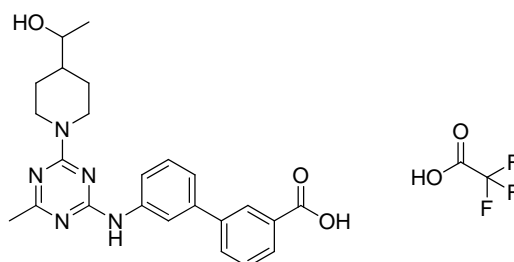
(a) Piperidine-4-carboxamide **361**, Sigma-Aldrich, 20 mg, 0.16 mmol; (b) 39 mg, 46%; ¹H NMR (600 MHz, DMSO-*d*₆) δ ppm 1.47 (br. s, 2 H), 1.79 (d, *J*=11.0 Hz, 2 H), 2.26 (s, 3 H), 2.37-2.44 (m, 1 H), 2.98 (br. s, 2 H), 3.48 (br. s, 1 H), 4.63-4.71 (m, 2 H), 6.80 (br. s, 1 H), 7.27 (br. s, 1 H), 7.33 (d, *J*=7.6 Hz, 1 H), 7.42 (t, *J*=7.9 Hz, 1 H), 7.58-7.62 (m, 1 H), 7.62-7.64 (m, 1 H), 7.88 (d, *J*=7.9 Hz, 1 H), 7.95 (d, *J*=7.9 Hz, 1 H), 8.20 (s, 1 H), 8.26 (br. s, 1 H), 9.81 (br. s, 1 H); LCMS (Method A): MH⁺ 433, Rt 0.68 min, 100% by UV.

3'-((4-(4-Carbamoylpiperazin-1-yl)-6-methyl-1,3,5-triazin-2-yl)amino)-[1,1'-biphenyl]-3-carboxylic acid 2,2,2-trifluoroacetate 390



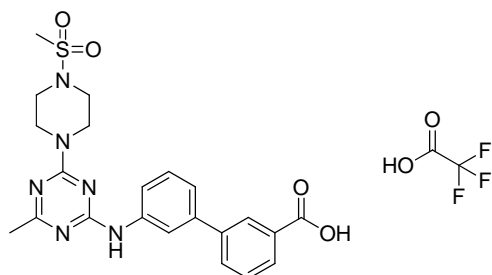
(a) Piperazine-1-carboxamide hydrochloride **362**, Fluorochem, 26 mg, 0.16 mmol; (b) 38 mg, 44%; ^1H NMR (600 MHz, $\text{DMSO-}d_6$) δ ppm 2.30 (s, 3 H), 3.37-3.41 (m, 4 H), 3.76-3.81 (m, 4 H), 3.86-4.01 (m, 1 H), 5.75 (s, 2 H), 7.36-7.39 (m, 1 H), 7.44 (t, $J=7.7$ Hz, 1 H), 7.63 (t, $J=7.9$ Hz, 1 H), 7.66 (d, $J=6.8$ Hz, 1 H), 7.90 (d, $J=7.9$ Hz, 1 H), 7.96 (d, $J=7.6$ Hz, 1 H), 8.19 (s, 1 H), 8.21 (s, 1 H), 9.96 (br. s, 1 H); LCMS (Method A): MH^+ 434, Rt 0.72 min, 97% by UV.

(1RS)-3'-((4-(4-(1-Hydroxyethyl)piperidin-1-yl)-6-methyl-1,3,5-triazin-2-yl)amino)-[1,1'-biphenyl]-3-carboxylic acid 2,2,2-trifluoroacetate 391



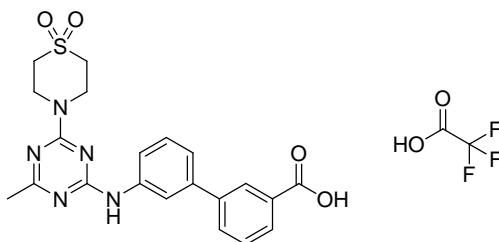
(a) (1RS)-1-(Piperidin-4-yl)ethanol, Maybridge Chemicals **363**, 20 mg, 0.16 mmol; (b) 49 mg, 57%; ^1H NMR (600 MHz, $\text{DMSO-}d_6$) δ ppm 1.03 (d, $J=6.0$ Hz, 3 H), 1.09-1.24 (m, 2 H), 1.46-1.52 (m, 1 H), 1.60-1.68 (m, 1 H), 1.82-1.89 (m, 1 H), 2.29 (s, 3 H), 2.85-2.96 (m, 2 H), 3.38 (d, $J=2.6$ Hz, 1 H), 3.94 (br. s, 2 H), 4.73 (d, $J=11.7$ Hz, 2 H), 7.36-7.41 (m, 1 H), 7.44 (t, $J=7.7$ Hz, 1 H), 7.57-7.59 (m, 1 H), 7.61 (t, $J=7.7$ Hz, 1 H), 7.88 (d, $J=7.9$ Hz, 1 H), 7.95 (d, $J=7.6$ Hz, 1 H), 8.20 (s, 1 H), 8.24 (br. s, 1 H), 10.09 (br. s, 1 H); LCMS (Method A): MH^+ 434, Rt 0.78 min, 92% by UV.

3'-((4-Methyl-6-(4-(methylsulfonyl)piperazin-1-yl)-1,3,5-triazin-2-yl)amino)-[1,1'-biphenyl]-3-carboxylic acid 2,2,2-trifluoroacetate 392



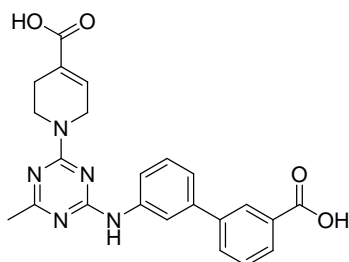
(a) 1-(Methylsulfonyl)piperazine hydrochloride **364**, ABCR, 31 mg, 0.16 mmol; (b) 30 mg, 34%; ^1H NMR (600 MHz, $\text{DMSO-}d_6$) δ ppm 2.27 (s, 3 H), 2.89 (s, 3 H), 3.16-3.20 (m, 4 H), 3.34 (br. s, 1 H), 3.89-3.94 (m, 4 H), 7.31-7.35 (m, 1 H), 7.42 (t, $J=8.3$ Hz, 1 H), 7.61 (t, $J=7.9$ Hz, 1 H), 7.65-7.68 (m, 1 H), 7.89 (d, $J=8.3$ Hz, 1 H), 7.95 (d, $J=8.3$ Hz, 1 H), 8.20 (s, 1 H), 8.22 (s, 1 H), 9.81 (br. s, 1 H); LCMS (Method A): MH^+ 469, Rt 0.86 min, 97% by UV.

3'-((4-(1,1-Dioxidothiomorpholino)-6-methyl-1,3,5-triazin-2-yl)amino)-[1,1'-biphenyl]-3-carboxylic acid 2,2,2-trifluoroacetate 393



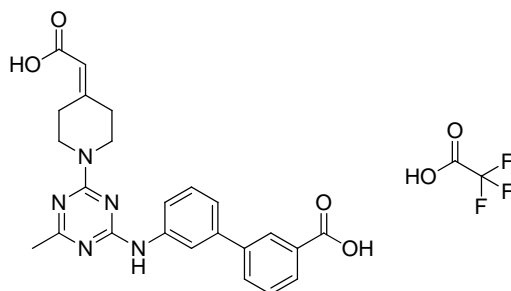
(a) Thiomorpholine 1,1-dioxide **365**, Anichem, 21 mg, 0.16 mmol; (b) 6 mg, 7%; ^1H NMR (600 MHz, $\text{DMSO-}d_6$) δ ppm 2.29 (s, 3 H), 3.34 (br. s, 4 H), 4.23-4.27 (m, 4 H), 7.32-7.35 (m, 1 H), 7.40-7.44 (m, 1 H), 7.63 (t, $J=7.9$ Hz, 2 H), 7.88 (d, $J=7.2$ Hz, 1 H), 7.95 (d, $J=7.6$ Hz, 1 H), 8.15-8.19 (m, 2 H), 9.89 (br. s, 1 H) nb. carboxylic acid proton not seen; LCMS (Method A): MH^+ 440, Rt 0.87 min, 98% by UV.

1-(4-((3'-Carboxy-[1,1'-biphenyl]-3-yl)amino)-6-methyl-1,3,5-triazin-2-yl)-1,2,3,6-tetrahydropyridine-4-carboxylic acid 394



Diisopropylammonium 3'-((4-chloro-6-methyl-1,3,5-triazin-2-yl)amino)-[1,1'-biphenyl]-3-carboxylic acid **337** (51 mg, 0.15 mmol), 1,2,3,6-tetrahydropyridine-4-carboxylic acid hydrochloride **366** (Sigma-Aldrich, 27 mg, 0.17 mmol) and *N,N*-diisopropylethylamine (100 μ L, 0.60 mmol) were combined in isopropanol and the reaction mixture heated under microwave irradiation to 120 $^{\circ}$ C for 30 min. The solvent was removed *in vacuo* and the residue dissolved in DMSO and purified by Mass Directed AutoPrep on a Sunfire C₁₈ column using acetonitrile/water with a trifluoroacetic acid modifier. The appropriate fractions were combined and concentrated *in vacuo* to give the title compound (33 mg, 45%). ¹H NMR (400 MHz, DMSO-*d*₆) δ ppm 2.27 (s, 3 H), 2.31-2.39 (m, 2 H), 3.89-3.96 (m, 2 H), 4.37-4.47 (m, 2 H), 6.92 (br. s, 1 H), 7.31-7.36 (m, 1 H), 7.42 (t, *J*=7.9 Hz, 1 H), 7.61 (t, *J*=7.8 Hz, 1 H), 7.65-7.71 (m, 1 H), 7.90 (d, *J*=7.8 Hz, 1 H), 7.96 (d, *J*=7.8 Hz, 1 H), 8.22 (s, 1 H), 8.29 (br. s, 1 H), 9.79 (br. s, 1 H) nb. carboxylic acid protons not seen; LCMS (Method A): MH⁺ 432, Rt 0.81 min, 100% by UV.

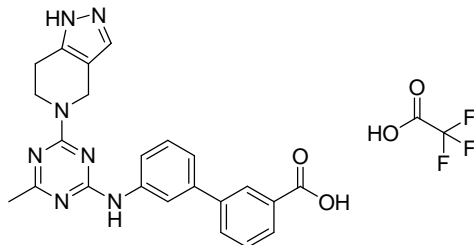
3'-((4-(4-(Carboxymethylene)piperidin-1-yl)-6-methyl-1,3,5-triazin-2-yl)amino)-[1,1'-biphenyl]-3-carboxylic acid 2,2,2-trifluoroacetate 395



Diisopropylammonium 3'-((4-(4-(Carboxymethylene)piperidin-1-yl)-6-methyl-1,3,5-triazin-2-yl)amino)-[1,1'-biphenyl]-3-carboxylic acid **337** (25 mg, 0.18 mmol), 2-(piperidin-4-ylidene)acetic acid **367** (Aurora Building Blocks, 25 mg, 0.18 mmol) and *N,N*-diisopropylethylamine (100 μ L,

0.57 mmol) were combined in isopropanol (2 mL) and the reaction mixture heated under microwave irradiation to 120 °C for 30 min. The solvent was removed *in vacuo* and the residue dissolved in DMSO and purified by Mass Directed AutoPrep on a Sunfire C18 column using acetonitrile/water with a trifluoroacetic acid modifier. The appropriate fractions were combined and concentrated *in vacuo* to give the title compound (51 mg, 54%); m.p. 237-242 °C; $\nu_{\max}/\text{cm}^{-1}$ (solid) 2880 (OH), 1671 (C=O); ^1H NMR (400 MHz, DMSO- d_6) δ ppm 2.30 (s, 3 H), 2.34-2.42 (m, 2 H), 2.90-2.98 (m, 2 H), 3.89 (dt, $J=11.1$, 5.6 Hz, 4 H), 5.75 (s, 1 H), 7.33-7.39 (m, 1 H), 7.44 (dd, $J=8.8$, 8.1 Hz, 1 H), 7.62 (t, $J=7.8$ Hz, 1 H), 7.66-7.70 (m, 1 H), 7.89 (d, $J=7.8$ Hz, 1 H), 7.95 (d, $J=7.6$ Hz, 1 H), 8.20 (s, 1 H), 8.23-8.29 (m, 1 H), 9.91 (br. s, 1 H) nb. carboxylic acid protons not seen; ^{13}C NMR (126 MHz, DMSO- d_6) δ ppm 24.5, 28.8, 35.0, 43.1, 44.1, 115.5 (q, $J=294.1$ Hz, TFA) 115.9, 118.3, 119.5, 121.0, 127.2, 128.4, 129.4, 129.4 (2C), 130.8, 131.0, 131.5, 139.6, 139.8, 140.6, 156.9, 158.5 (q, $J=36.1$ Hz, TFA), 162.9, 167.2 (2C); LCMS (Method A): MH^+ 446, Rt 0.81 min, 100% by UV; HRMS exact mass calculated for $[\text{M}+\text{H}]^+$ ($\text{C}_{24}\text{H}_{24}\text{N}_5\text{O}_4$) requires m/z 446.1823, found 446.1824.

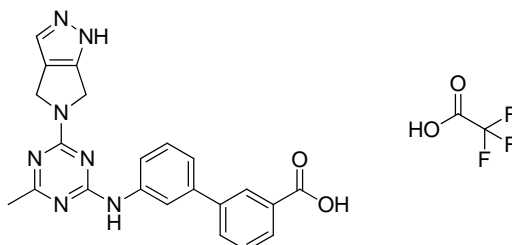
3'-((4-(6,7-Dihydro-1H-pyrazolo[4,3-c]pyridin-5(4H)-yl)-6-methyl-1,3,5-triazin-2-yl)amino)-[1,1'-biphenyl]-3-carboxylic acid 2,2,2-trifluoroacetate 396



Diisopropylammonium 3'-((4-chloro-6-methyl-1,3,5-triazin-2-yl)amino)-[1,1'-biphenyl]-3-carboxylic acid **337** (40 mg, 0.10 mmol), 4,5,6,7-tetrahydro-1H-pyrazolo[4,3-*c*]pyridine **368** (Chembridge, 17 mg, 0.14 mmol) and *N,N*-diisopropylethylamine (100 μL , 0.57 mmol) were combined in isopropanol (2 mL) and the reaction mixture heated under microwave irradiation to 100 °C for 45 min. The solvent was removed *in vacuo* and the residue dissolved in DMSO and purified by Mass Directed AutoPrep on a Sunfire C₁₈ column using acetonitrile/water with a trifluoroacetic acid modifier. The appropriate fractions were combined and concentrated *in vacuo* to give the title compound (58 mg, 58%). ^1H NMR (400 MHz, DMSO- d_6) δ ppm 2.32 (br. s, 3 H), 2.77 (t, $J=5.5$ Hz, 2 H), 4.13 (t, $J=5.6$ Hz, 2 H), 4.85 (s, 2 H), 7.36-7.42 (m, 1 H), 7.46 (t,

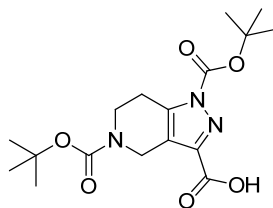
$J=7.5$ Hz, 1 H), 7.51-7.56 (m, 1 H), 7.63 (t, $J=7.7$ Hz, 2 H), 7.90 (d, $J=8.0$ Hz, 1 H), 7.97 (s, 1 H), 8.23 (s, 1 H), 8.26-8.31 (m, 1 H), 9.21 (br. s, 1 H), 10.18 (br. s, 1 H) nb. carboxylic acid not seen; LCMS (Method A): MH^+ 427, Rt 0.76 min, 95% by UV.

3'-((4-Methyl-6-(pyrrolo[3,4-c]pyrazol-5(1*H*,4*H*,6*H*)-yl)-1,3,5-triazin-2-yl)amino)-[1,1'-biphenyl]-3-carboxylic acid 2,2,2-trifluoroacetate **397**



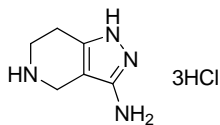
Diisopropylammonium 3'-((4-chloro-6-methyl-1,3,5-triazin-2-yl)amino)-[1,1'-biphenyl]-3-carboxylic acid **337** (40 mg, 0.10 mmol), 1,4,5,6-tetrahydropyrrolo[3,4-c]pyrazole hydrochloride **369** (D-L Chiral Chemicals LLC), 25 mg, 0.14 mmol) and *N,N*-diisopropylethylamine (100 μ L, 0.57 mmol) were combined in isopropanol (2 mL) and the reaction mixture heated under microwave irradiation to 120 $^{\circ}$ C for 45 min. The solvent was removed *in vacuo* and the residue dissolved in DMSO and purified by Mass Directed AutoPrep on a Sunfire C_{18} column using acetonitrile/water with a trifluoroacetic acid modifier. The appropriate fractions were combined and concentrated *in vacuo* to give the title compound (48 mg, 20%); m.p. 177-181 $^{\circ}$ C; ν_{max}/cm^{-1} (solid) 1677 (C=O); 1H NMR (400 MHz, DMSO- d_6) δ ppm 2.33 (s, 3 H), 4.64-4.71 (m, 4 H), 6.18 (br. s, 1 H), 7.34 (d, $J=7.8$ Hz, 1 H), 7.40-7.45 (m, 1 H), 7.48 (s, 1 H), 7.60 (t, $J=7.8$ Hz, 1 H), 7.77 (d, $J=7.6$ Hz, 1 H), 7.90 (d, $J=7.6$ Hz, 1 H), 7.96 (d, $J=7.6$ Hz, 1 H), 8.27 (s, 1 H), 8.32 (br. s, 1 H) 9.22 (br. s, 1 H) nb. carboxylic acid proton not seen; ^{13}C NMR (151 MHz, DMSO- d_6) δ 24.5, 45.7, 45.9, 115.6 (q, $J=291.9$ Hz, TFA), 117.1, 117.3, 120.7, 127.2, 127.2, 128.3, 129.3, 129.3, 130.8, 130.9, 131.5, 131.5, 139.5, 139.6, 140.1, 140.5, 140.6, 158.2 (q, $J=37.6$ Hz, TFA), 167.07, 167.13; LCMS (Method A): MH^+ 413, Rt 0.77 min, 96% by UV; HRMS exact mass calculated for $[M+H]^+$ ($C_{22}H_{20}N_7O_2$) requires m/z 414.1673, found 414.1669.

1,5-Bis(*tert*-butoxycarbonyl)-4,5,6,7-tetrahydro-1*H*-pyrazolo[4,3-*c*]pyridine-3-carboxylic acid **373**



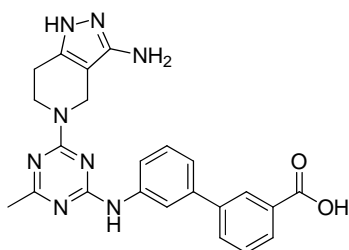
To a stirred solution of 4,5,6,7-tetrahydro-1*H*-pyrazolo[4,3-*c*]pyridine-3-carboxylic acid hydrochloride **372** (Fluorochem, 100 mg, 0.49 mmol) in dichloromethane (4 mL) at 0 °C was added 4-dimethylaminopyridine (6 mg, 0.05 mmol), triethylamine (140 μL, 0.98 mmol) and di-*tert*-butyl dicarbonate (214 mg, 0.980 mmol). The reaction mixture was stirred at 0 °C for 1 h, before warming to RT and stirring for a further 21 h. The reaction mixture was washed with water (10 mL), the layers separated and the organic extract concentrated *in vacuo* to give the title compound (167 mg, 93%). The material was used in crude form in the next reaction.

4,5,6,7-Tetrahydro-1*H*-pyrazolo[4,3-*c*]pyridin-3-amine hydrochloride **374**



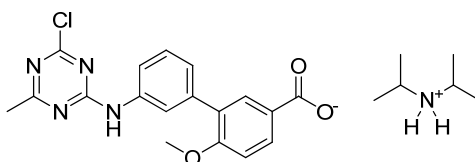
1,5-Bis(*tert*-butoxycarbonyl)-4,5,6,7-tetrahydro-1*H*-pyrazolo[4,3-*c*]pyridine-3-carboxylic acid **373** (640 mg, 1.74 mmol) was suspended in *tert*-butanol (16 mL). Diphenylphosphorazidate (375 μL, 1.74 mmol) and triethylamine (243 μL, 1.74 mmol) were added and the reaction mixture heated to 70 °C for 18 h. The solvent was removed *in vacuo* and the residue re-dissolved in 4 M hydrochloric acid in 1,4-dioxane and stirred at RT for 1 h. The solvent was removed *in vacuo* to give an orange solid containing the title compound (1.18 g, 28%). The material was used in crude form in the next reaction.

3'-((4-(3-Amino-6,7-dihydro-1H-pyrazolo[4,3-c]pyridin-5(4H)-yl)-6-methyl-1,3,5-triazin-2-yl)amino)-[1,1'-biphenyl]-3-carboxylic acid 375



Diisopropylammonium 3'-((4-chloro-6-methyl-1,3,5-triazin-2-yl)amino)-[1,1'-biphenyl]-3-carboxylic acid **337** (180 mg, 0.41 mmol), 4,5,6,7-tetrahydro-1H-pyrazolo[4,3-c]pyridin-3-amine hydrochloride **374** (308 mg, assuming 100% yield for previous steps, this equates to 0.410 mmol) and *N,N*-diisopropylethylamine (249 μ L, 1.43 mmol) were dissolved in isopropanol (4 mL) and the reaction mixture heated to 70 °C for 3 h. The reaction mixture was diluted with ethyl acetate (40 mL) and acidified with 2 M aqueous hydrochloric acid to ~pH 2. The layers were separated and the organic was washed with water (2 x 10 mL), dried over anhydrous magnesium sulfate, filtered and concentrated *in vacuo* to give a colourless gum (250 mg). Some of this material (100 mg) was dissolved in DMSO (1 mL) and purified by reverse phase HPLC on an Xbridge column using acetonitrile/water with an ammonium bicarbonate modifier. The appropriate fractions were combined and concentrated *in vacuo* to give the title compound (18 mg, 45% based on the portion of crude material purified) as an orange solid; ^1H NMR (400 MHz, DMSO- d_6) δ ppm 2.26 (s, 3 H), 2.55-2.65 (m, 2 H), 3.99-4.09 (m, 2 H), 4.56-4.73 (m, 2 H), 7.27 (d, $J=7.6$ Hz, 1 H), 7.35-7.45 (m, 2 H), 7.57-7.65 (m, 2 H), 7.83-7.91 (m, 1 H), 8.16-8.22 (m, 1 H), 8.24-8.33 (m, 1 H), 9.64 (br. s, 1 H) nb. some exchangeable protons not seen; LCMS (Method A): MH^+ 443, R_t 0.68 min, 100% by UV.

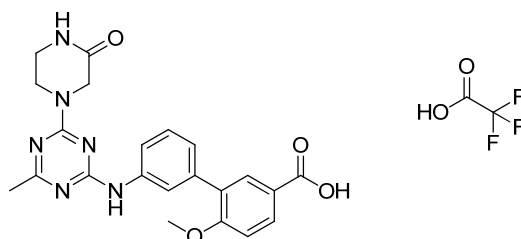
Diisopropylammonium 3'-((4-chloro-6-methyl-1,3,5-triazin-2-yl)amino)-6-methoxy-[1,1'-biphenyl]-3-carboxylate 399



3-Amino-6-methoxy-[1,1'-biphenyl]-3-carboxylic acid **398** (600 mg, 2.47 mmol) and 2,4-dichloro-6-methyl-1,3,5-triazine (Chembridge, 404 mg, 2.47 mmol) were suspended

in isopropanol (20 mL). Diisopropylethylamine (1.1 mL, 7.7 mmol) was added and the reaction mixture stirred at RT for 2 h. The filtrate formed was filtered and dried in a vacuum oven at 40 °C for 1 h to give the title compound (966 mg, 82%) as a light brown solid; ¹H NMR (DMSO-*d*₆) δ ppm 1.13 (d, *J*=6.3 Hz, 12 H), 2.42 (s, 3 H), 3.12 (dt, *J*=12.4, 6.3 Hz, 2 H), 3.83 (s, 3 H), 7.12 (d, *J*=8.6 Hz, 1 H), 7.24 (d, *J*=7.3 Hz, 1 H), 7.41 (t, *J*=7.8 Hz, 1 H), 7.68 (br. s, 1 H), 7.77 (m, 1 H), 7.85 (br. s, 1 H), 7.91 (d, *J*=8.3 Hz, 1 H), nb. three exchangeable protons not seen; LCMS (Method A): MH⁺ 371, Rt 0.95 min, 92% by UV.

6-Methoxy-3'-((4-methyl-6-(3-oxopiperazin-1-yl)-1,3,5-triazin-2-yl)amino)-[1,1'-biphenyl]-3-carboxylic acid 2,2,2-trifluoroacetate 400a

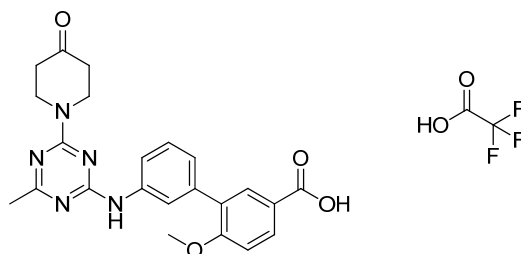


Typical Procedure U:

Diisopropylammonium 3'-((4-chloro-6-methyl-1,3,5-triazin-2-yl)amino)-6-methoxy-[1,1'-biphenyl]-3-carboxylate **399** (54 mg, 0.14 mmol), piperazin-2-one **341** (ABCR, 15 mg, 0.15 mmol) and *N,N*-diisopropylethylamine (100 μL, 0.14 mmol) were combined in isopropanol (2 mL) and the reaction mixture heated under microwave irradiation to 120 °C for 30 min. The solvent was removed *in vacuo* and the residue dissolved in tetrahydrofuran (500 μL) and methanol (150 μL). Aqueous sodium hydroxide solution (10 M, 130 μL) was added and the reaction mixture stirred at RT for 2 h, before the solvent was removed, the residue dissolved in DMSO (1 mL) and purified by Mass Directed AutoPrep on a Sunfire C₁₈ column using acetonitrile/water with a trifluoroacetic acid modifier. The appropriate fractions were combined and concentrated *in vacuo* to give the title compound (30 mg, 36 %). ¹H NMR (400 MHz, DMSO-*d*₆) δ ppm 2.07 (s, 3 H), 2.26 (s, 3 H), 3.22-3.30 (m, 2 H), 3.83 (s, 2 H), 3.91 (t, *J*=4.9 Hz, 2 H), 4.22 (br. s, 1 H), 7.10-7.13 (m, 1 H), 7.15 (d, *J*=8.6 Hz, 1 H), 7.33 (t, *J*=7.8 Hz, 1 H), 7.85 (br. s, 1 H), 7.92 (dd, *J*=8.6, 2.0 Hz, 1 H), 8.10 (br. s, 1 H), 8.42 (s, 1 H), 9.71 (br. s, 1 H), nb. one exchangeable proton not observed; LCMS (Method A): MH⁺ 435, Rt 0.71 min, 99% by UV.

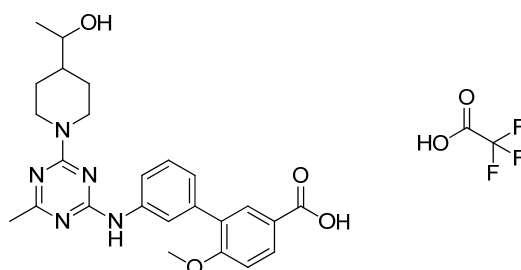
The following experiments were performed using Typical Procedure U, the data are reported as (a) amine (supplier, g, mmol); (b) product (mg, % yield).

6-Methoxy-3'-((4-methyl-6-(4-oxopiperidin-1-yl)-1,3,5-triazin-2-yl)amino)-[1,1'-biphenyl]-3-carboxylic acid 2,2,2-trifluoroacetate 400b



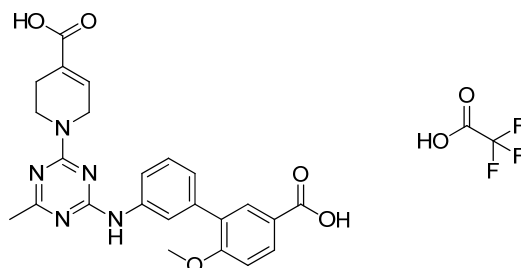
(a) Piperidin-4-one **344**, Apollo Scientific, 21 mg, 0.15 mmol; (b) 17 mg, 20%; ^1H NMR (400 MHz, DMSO- d_6) δ ppm 2.34 (s, 3 H), 2.50 (t, $J=6.2$ Hz, 4 H), 3.91 (s, 3 H), 4.11 (t, $J=6.3$ Hz, 4 H), 5.10 (br. s, 1 H), 7.19-7.26 (m, 2 H), 7.37 (t, $J=7.9$ Hz, 1 H), 7.66-7.70 (m, 1 H), 7.94 (d, $J=2.3$ Hz, 1 H), 7.97-8.01 (m, 2 H), 9.20 (br. s, 1 H); LCMS (Method A): MH^+ 473, Rt 0.79 min, 100% by UV.

(1RS)-3'-((4-(4-(1-Hydroxyethyl)piperidin-1-yl)-6-methyl-1,3,5-triazin-2-yl)amino)-6-methoxy-[1,1'-biphenyl]-3-carboxylic acid 2,2,2-trifluoroacetate 400c



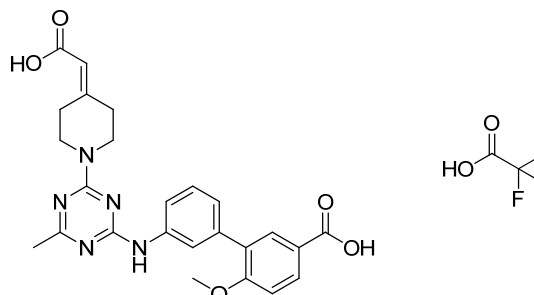
(a) (1RS)-1-(Piperidin-4-yl)ethanol **363**, Maybridge Chemicals, 20 mg, 0.15 mmol; (b) 33 mg, 36%; ^1H NMR (400 MHz, DMSO- d_6) δ ppm 1.02 (d, $J=6.0$ Hz, 3 H), 1.05-1.23 (m, 2 H), 1.40-1.52 (m, 1 H), 1.53-1.67 (m, 1 H), 1.74-1.92 (m, 1 H), 2.28 (s, 3 H), 2.87 (d, $J=3.5$ Hz, 2 H), 3.34-3.41 (m, 1 H), 3.85 (s, 3 H), 4.67-4.72 (m, 2 H), 7.18 (d, $J=7.8$ Hz, 1 H), 7.22 (d, $J=8.6$ Hz, 1 H), 7.37 (t, $J=7.9$ Hz, 1 H), 7.59 (d, $J=7.8$ Hz, 1 H), 7.85 (d, $J=2.3$ Hz, 1 H), 7.92-7.95 (m, 2 H), 7.97 (d, $J=2.0$ Hz, 1 H), 10.00 (br. s, 1 H), nb. one exchangeable proton not observed; LCMS (Method A): MH^+ 464, Rt 0.76 min, 9% by UV.

1-(4-((5'-Carboxy-2'-methoxy-[1,1'-biphenyl]-3-yl)amino)-6-methyl-1,3,5-triazin-2-yl)-1,2,3,6-tetrahydropyridine-4-carboxylic acid 2,2,2-trifluoroacetate 400d



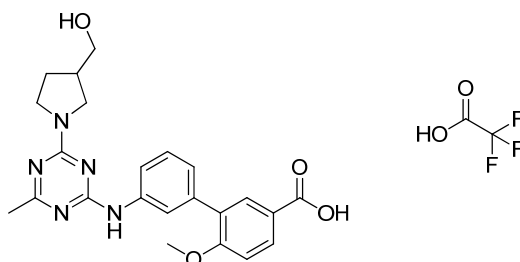
(a) 1,2,3,6-Tetrahydropyridine-4-carboxylic acid hydrochloride **366**, Sigma-Aldrich, 20 mg, 0.15 mmol; (b) 11 mg, 12%; ^1H NMR (400 MHz, $\text{DMSO-}d_6$) δ ppm 2.26 (s, 3 H), 2.29-2.34 (m, 2 H), 3.47 (br. s, 2 H), 3.85 (s, 3 H), 3.87-3.91 (m, 2 H), 4.38 (br. s, 1 H), 6.89 (br. s, 1 H), 7.14 (d, $J=7.8$ Hz, 1 H), 7.22 (d, $J=8.8$ Hz, 1 H), 7.34 (t, $J=7.9$ Hz, 1 H), 7.88 (d, $J=2.3$ Hz, 1 H), 7.95 (d, $J=2.3$ Hz, 1 H), 7.97 (d, $J=2.3$ Hz, 1 H), 9.69 (s, 1 H), 12.56 (br. s, 1 H), nb. one exchangeable proton not observed; LCMS (Method A): MH^+ 462, Rt 0.78 min, 94% by UV.

3'-((4-(4-(Carboxymethylene)piperidin-1-yl)-6-methyl-1,3,5-triazin-2-yl)amino)-6-methoxy-[1,1'-biphenyl]-3-carboxylic acid 2,2,2-trifluoroacetate 400e



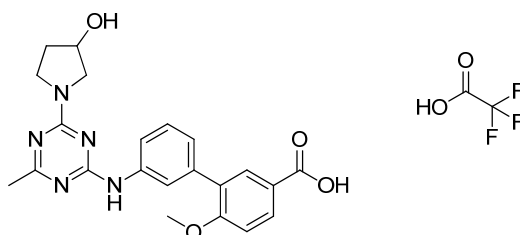
(a) 2-(Piperidin-4-ylidene)acetic acid **367**, Aurora Building Blocks, 22 mg, 0.15 mmol; (b) 25 mg, 27%; ^1H NMR (400 MHz, $\text{DMSO-}d_6$) δ ppm 2.29 (s, 3 H), 2.32-2.38 (m, 2 H), 2.86-2.95 (m, 2 H), 3.75-3.96 (m, 4 H), 3.85 (s, 3 H), 5.73 (s, 1 H), 7.18 (d, $J=7.3$ Hz, 1 H), 7.22 (d, $J=8.6$ Hz, 1 H), 7.32-7.41 (m, 1 H), 7.55-7.64 (m, 1 H), 7.64-7.74 (m, 1 H), 7.85 (d, $J=2.0$ Hz, 1 H), 7.95 (dd, $J=8.6, 2.0$ Hz, 1 H), 10.05 (br. s, 1 H); LCMS (Method A): MH^+ 476, Rt 0.79 min, 98% by UV.

(3RS)-3'-((4-(3-(Hydroxymethyl)pyrrolidin-1-yl)-6-methyl-1,3,5-triazin-2-yl)amino)-6-methoxy-[1,1'-biphenyl]-3-carboxylic acid 2,2,2-trifluoroacetate 400f



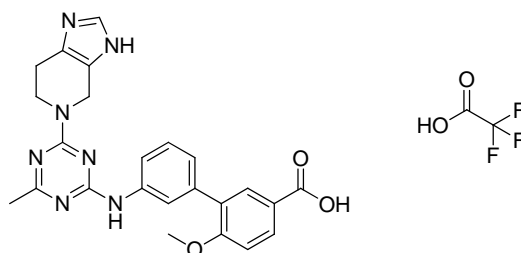
(a) (3RS)-Pyrrolidin-3-yl methanol **342**, ABCR, 16 mg, 0.15 mmol; (b) 32 mg, 37%; ¹H NMR (400 MHz, DMSO-*d*₆) δ ppm 1.77 (d, *J*=7.6 Hz, 1 H), 2.02 (d, *J*=7.3 Hz, 1 H), 2.26 (s, 3 H), 2.37-2.45 (m, 1 H), 3.34 (dd, *J*=11.6, 6.8 Hz, 1 H), 3.40-3.58 (m, 3 H), 3.61-3.72 (m, 2 H), 3.87 (s, 3 H), 4.30 (br. s, 1 H), 7.14-7.21 (m, 2 H), 7.32 (t, *J*=7.9 Hz, 1 H), 7.70 (d, *J*=8.1 Hz, 1 H), 7.89-8.01 (m, 3 H), 9.10 (br. s, 1 H), nb. one exchangeable proton not observed; LCMS (Method A): MH⁺ 436, Rt 0.69 min, 97% by UV.

(3RS)-3'-((4-(3-Hydroxypyrrolidin-1-yl)-6-methyl-1,3,5-triazin-2-yl)amino)-6-methoxy-[1,1'-biphenyl]-3-carboxylic acid 2,2,2-trifluoroacetate 400g



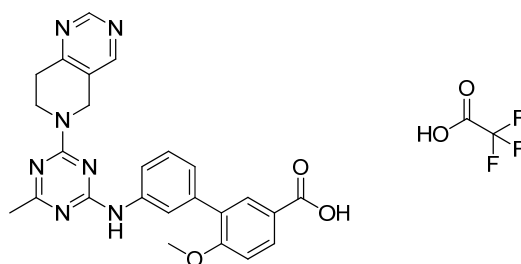
(a) (3RS)-Pyrrolidin-3-ol **343**, Anichem, 13 mg, 0.15 mmol; (b) 25 mg, 30%; ¹H NMR (400 MHz, DMSO-*d*₆) δ ppm 1.85 - 1.94 (m, 1 H), 2.02 (s, 1 H), 2.27 (s, 3 H), 3.48-3.53 (m, 1 H), 3.60-3.67 (m, 4 H), 3.87 (s, 3 H), 4.36-4.42 (m, 1 H), 5.49 (br. s, 1 H), 7.15-7.21 (m, 2 H), 7.33 (t, *J*=7.9 Hz, 1 H), 7.68-7.73 (m, 1 H), 7.92 (d, *J*=2.3 Hz, 1 H), 7.95 (dd, *J*=8.6, 2.3 Hz, 1 H), 7.98 (s, 1 H), 9.14 (br. s, 1 H); LCMS (Method A): MH⁺ 422, Rt 0.67 min, 100% by UV.

3'-((4-(6,7-Dihydro-3H-imidazo[4,5-c]pyridin-5(4H)-yl)-6-methyl-1,3,5-triazin-2-yl)amino)-6-methoxy-[1,1'-biphenyl]-3-carboxylic acid 2,2,2-trifluoroacetate 400h



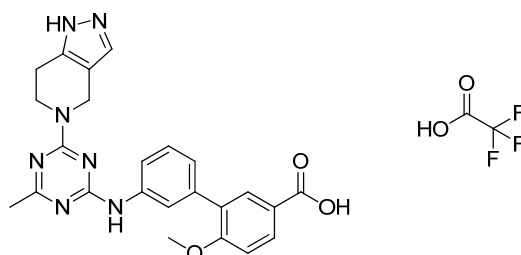
(a) 4,5,6,7-Tetrahydro-3*H*-imidazo[4,5-*c*]pyridine hydrochloride **358**, Apin Chemicals Ltd, 30 mg, 0.15 mmol; (b) 43 mg, 48%; ¹H NMR (600MHz, DMSO-*d*₆): δ ppm 2.29 (br. s, 3 H), 2.75 (br. s, 2 H), 3.86 (s, 3 H), 4.14 (br. s, 2 H), 4.93 (br. s, 2 H), 7.18 (br. s, 1 H), 7.22 (d, *J*=8.6 Hz, 1 H), 7.32-7.42 (m, 1 H), 7.64 (br. s, 1 H), 7.84-7.97 (m, 1 H), 7.88 (d, *J*=2.4 Hz, 1 H), 7.93-7.99 (m, 1 H), 8.93 (br. s, 1 H), 9.88 (br. s, 1 H); LCMS (Method A): MH⁺ 458, Rt 0.67 min, 94% by UV.

3'-((4-(7,8-Dihydropyrido[4,3-*d*]pyrimidin-6(5*H*)-yl)-6-methyl-1,3,5-triazin-2-yl)amino)-6-methoxy-[1,1'-biphenyl]-3-carboxylic acid) 2,2,2-trifluoroacetate 400i



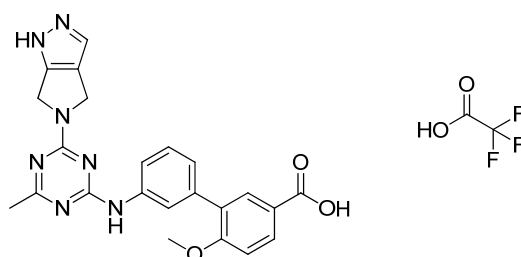
(a) 5,6,7,8-Tetrahydropyrido[4,3-*d*]pyrimidine hydrochloride **359**, Active Scientific, 26 mg, 0.15 mmol; (b) 26 mg, 28%; ¹H NMR (400 MHz, DMSO-*d*₆) δ ppm 2.31 (s, 3 H), 2.96 (t, *J*=6.0 Hz, 2 H), 3.87 (s, 3 H), 4.14 (t, *J*=6.0 Hz, 2 H), 4.95 (s, 2 H), 6.44 (br. s, 1 H), 7.17-7.20 (m, 1 H), 7.22 (d, *J*=8.6 Hz, 1 H), 7.36 (t, *J*=7.8 Hz, 1 H), 7.67 (d, *J*=8.3 Hz, 1 H), 7.94 (d, *J*=2.0 Hz, 1 H), 7.97 (dd, *J*=5.2, 3.1 Hz, 2 H), 8.52 (s, 1 H), 8.93 (s, 1 H), 9.20 (br. s, 1 H); LCMS (Method A): MH⁺ 470, Rt 0.79 min, 100% by UV.

3'-((4-(6,7-Dihydro-1H-pyrazolo[4,3-c]pyridin-5(4H)-yl)-6-methyl-1,3,5-triazin-2-yl)amino)-6-methoxy-[1,1'-biphenyl]-3-carboxylic acid 2,2,2-trifluoroacetate 400j

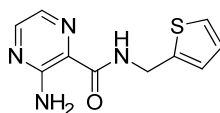


(a) 4,5,6,7-Tetrahydro-1H-pyrazolo[4,3-c]pyridine **368**, Chembridge, 19 mg, 0.15 mmol; (b) 29 mg, 33%; ^1H NMR (600MHz, $\text{DMSO-}d_6$): δ ppm 2.30 (br. s, H), 2.64-2.79 (m, 2 H), 3.86 (s, 3 H), 4.09 (br. s, 2 H), 4.67-4.91 (m, 2 H), 7.19 (d, $J=7.5$ Hz, 1 H), 7.24 (d, $J=7.7$ Hz, 1 H), 7.24-7.53 (m, 1 H), 7.38 (t, $J=7.9$ Hz, 1 H), 7.61 (d, $J=5.9$ Hz, 1 H), 7.89 (d, $J=2.0$ Hz, 1 H), 7.99 (br. s, 2 H), 10.05 (br. s, 1 H); nb. exchangeable protons not observed; LCMS (Method A): MH^+ 458, Rt 0.74 min, 98% by UV.

6-Methoxy-3'-((4-methyl-6-(pyrrolo[3,4-c]pyrazol-5(1H,4H,6H)-yl)-1,3,5-triazin-2-yl)amino)-[1,1'-biphenyl]-3-carboxylic acid 2,2,2-trifluoroacetate 400k

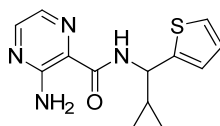


(a) 1,3,5,6-Tetrahydropyrrolo[4,3-c]pyrazole hydrochloride **369**, D-L Chiral Chemicals LLC, 28 mg, 0.15 mmol; (b) 20 mg, 23%; ^1H NMR (600 MHz, $\text{DMSO-}d_6$): δ ppm 2.31-2.35 (m, 3 H), 3.84-3.90 (m, 3 H), 4.60-4.67 (m, 4 H), 7.14-7.26 (m, 2 H), 7.33-7.44 (m, 1 H), 7.55-7.60 (m, 1 H), 7.65-7.84 (m, 1 H), 7.87-7.95 (m, 1 H), 7.95-7.99 (m, 1 H), 8.00-8.19 (m, 1 H), 10.07 (br. s, 1 H) nb. two exchangeable protons not observed; LCMS (Method A): MH^+ 444, Rt 0.74 min, 100% by UV.

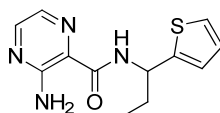
3-Amino-*N*-(thiophen-2-ylmethyl)pyrazine-2-carboxamide

3-Aminopyrazine-2-carboxylic acid (21 mg, 0.15 mmol), Pybop (78 mg, 0.15 mmol), thiophen-2-ylmethanamine **404** (Acros, 17 mg, 0.15 mmol) and DIPEA (52 μ L, 0.30 mmol) were combined in *N,N*-dimethylformamide (0.5 mL) and stirred at RT for 22 h. The solvent was removed *in vacuo* and the residue dissolved in DMSO (0.5 mL) and purified by reverse phase HPLC on an Xbridge column using acetonitrile/water with an ammonium bicarbonate modifier. The appropriate fractions were combined and concentrated *in vacuo* to give the title compound (17 mg, 32%); ^1H NMR (400 MHz, DMSO- d_6) δ ppm 4.60 (d, $J=6.3$ Hz, 2 H), 6.93-6.96 (m, 1 H), 7.00-7.02 (m, 1 H), 7.35 (dd, $J=5.0, 1.3$ Hz, 1 H), 7.52 (br. s, 2 H), 7.82 (d, $J=2.5$ Hz, 1 H), 8.20 (d, $J=2.3$ Hz, 1 H), 9.27 (t, $J=6.2$ Hz, 1 H); LCMS (Method A): MH^+ 235, Rt 0.80 min, 100% by UV.

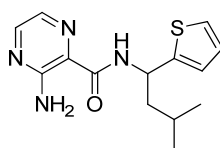
The following experiments were performed using Typical Procedure T, the data are reported as (a) amine (supplier, g, mmol); (b) product (mg, % yield).

(*RS*)-3-Amino-*N*-(cyclopropyl(thiophen-2-yl)methyl)pyrazine-2-carboxamide

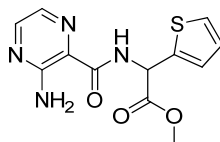
(a) (*RS*)-Cyclopropyl(thiophen-2-yl)methanamine **405**, Combi-Blocks, 28 mg, 0.15 mmol; (b) 25 mg, 54%; ^1H NMR (400 MHz, DMSO- d_6) δ ppm 0.33-0.48 (m, 2 H), 0.50-0.58 (m, 1 H), 0.60-0.69 (m, 1 H), 1.53-1.65 (m, 1 H), 4.54 (t, $J=9.3$ Hz, 1 H), 6.96 (dd, $J=5.0, 3.5$ Hz, 1 H), 7.07 (d, $J=3.3$ Hz, 1 H), 7.36 (dd, $J=5.0, 1.0$ Hz, 1 H), 7.51 (br. s, 2 H), 7.85 (d, $J=2.3$ Hz, 1 H), 8.22 (d, $J=2.3$ Hz, 1 H), 9.11 (d, $J=8.8$ Hz, 1 H); LCMS (Method A): MH^+ 275, Rt 1.00 min, 90% by UV.

(RS)-3-Amino-N-(1-(thiophen-2-yl)propyl)pyrazine-2-carboxamide 423

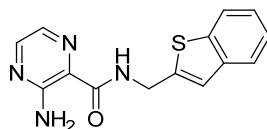
(a) *(RS)*-1-(Thiophen-2-yl)propan-1-amine **406**, Chembridge, 27 mg, 0.15 mmol; (b) 23 mg, 52%; ^1H NMR (400 MHz, $\text{DMSO-}d_6$) δ ppm 0.90 (t, $J=7.3$ Hz, 3 H), 1.90-2.08 (m, 2 H), 5.12-5.19 (m, 1 H), 6.96 (dd, $J=5.0, 3.5$ Hz, 1 H), 7.05 (d, $J=3.5$ Hz, 1 H), 7.36 (d, $J=5.0$ Hz, 1 H), 7.51 (br. s, 2 H), 7.83 (d, $J=2.3$ Hz, 1 H), 8.21 (d, $J=2.3$ Hz, 1 H), 8.87 (d, $J=9.6$ Hz, 1 H); LCMS (Method A): MH^+ 263, Rt 0.99 min, 100% by UV.

(RS)-3-Amino-N-(3-methyl-1-(thiophen-2-yl)butyl)pyrazine-2-carboxamide 424

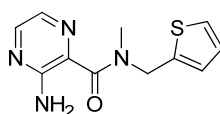
(a) *(RS)*-3-Methyl-1-(thiophen-2-yl)butan-1-amine **407**, UkrOrgSynthesis, 31 mg, 0.15 mmol; (b) 26 mg, 54%; ^1H NMR (400 MHz, $\text{DMSO-}d_6$) δ ppm 0.90 (t, $J=6.0$ Hz, 6 H), 1.53-1.64 (m, 1 H), 1.66-1.74 (m, 1 H), 1.99-2.07 (m, 1 H), 5.31-5.39 (m, 1 H), 6.95 (dd, $J=5.0, 3.5$ Hz, 1 H), 7.05 (d, $J=3.3$ Hz, 1 H), 7.35 (dd, $J=5.0, 1.3$ Hz, 1 H), 7.51 (br. s, 2 H), 7.83 (d, $J=2.5$ Hz, 1 H), 8.21 (d, $J=2.3$ Hz, 1 H), 8.91 (d, $J=9.1$ Hz, 1 H); LCMS (Method A): MH^+ 291, Rt 1.16 min, 100% by UV.

(RS)-Methyl 2-(3-aminopyrazine-2-carboxamido)-2-(thiophen-2-yl)acetate

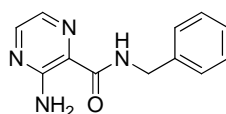
(a) *(RS)*-3-Methyl-1-(thiophen-2-yl)butan-1-amine **408**, ABCR, 31 mg, 0.15 mmol; (b) 36 mg, 55%; ^1H NMR (400 MHz, $\text{DMSO-}d_6$) δ ppm 3.72 (s, 3 H), 5.90 (d, $J=7.6$ Hz, 1 H), 7.01 (dd, $J=5.3, 3.8$ Hz, 1 H), 7.17-7.19 (m, 1 H), 7.48 (br. s, 2 H), 7.51 (dd, $J=5.0, 1.3$ Hz, 1 H), 7.86 (d, $J=2.3$ Hz, 1 H), 8.26 (d, $J=2.3$ Hz, 1 H), 9.04 (d, $J=7.6$ Hz, 1 H); LCMS (Method A): MH^+ 293, Rt 0.87 min, 95% by UV.

3-Amino-*N*-(benzo[*b*]thiophen-2-ylmethyl)pyrazine-2-carboxamide

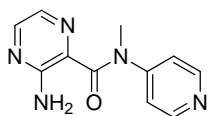
(a) Benzo[*b*]thiophen-2-ylmethanamine **409**, ABCR, 24 mg, 0.15 mmol; (b) 18 mg, 37%; ^1H NMR (600 MHz, DMSO- d_6) δ ppm 4.70 (d, $J=6.4$ Hz, 2 H), 7.27-7.31 (m, 2 H), 7.31-7.35 (m, 1 H), 7.77 (d, $J=7.9$ Hz, 1 H), 7.84-7.85 (m, 1 H), 7.87 (d, $J=7.9$ Hz, 1 H), 8.22-8.23 (m, 1 H), 9.46 (t, $J=6.0$ Hz, 1 H) (nb. NH_2 not seen); LCMS (Method A): MH^+ 285, Rt 1.01 min, 100% by UV.

3-Amino-*N*-methyl-*N*-(thiophen-2-ylmethyl)pyrazine-2-carboxamide **425**

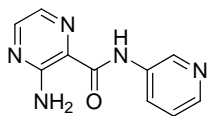
(a) *N*-Methyl-1-(thiophen-2-yl)methanamine **410**, ABCR, 19 mg, 0.15 mmol; (b) 22 mg, 53%; m.p. 77-79 °C; $\nu_{\text{max}}/\text{cm}^{-1}$ (solid) 3425 and 3316 (NH_2), 1603 (C=O); Mixture of rotamers observed in proton and carbon spectra ^1H NMR (400 MHz, DMSO- d_6) δ 2.935 and 2.942 (s, 3 H), 4.77 and 4.81 (s, 3 H), 6.49 and 6.59 (br. s, 1 H), 6.97 and 7.01 (m, 1 H), 7.02 and 7.13 (d, $J=2.8$ Hz, 1 H), 7.45 and 7.47 (d, $J=5.0$ Hz, 1 H), 7.78 and 7.81 (d, $J=2.5$ Hz, 1 H), 8.05 and 8.08 (d, $J=2.3$ Hz, 1 H); ^{13}C NMR (100 MHz, DMSO- d_6) δ ppm 32.7, 35.7, 45.2, 48.6, 126.1, 126.3, 126.6, 126.6, 126.9, 127.1, 130.2, 130.6, 131.5, 132.3, 139.1, 139.6, 143.7, 144.0, 153.5, 153.9, 166.3, 166.6; LCMS (Method A): MH^+ 249, Rt 0.71 min, 100% by UV.

3-Amino-*N*-benzylpyrazine-2-carboxamide

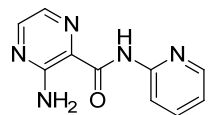
(a) Benzylamine **411**, Sigma-Aldrich, 16 mg, 0.15 mmol; (b) 17 mg, 45%; ^1H NMR (600 MHz, DMSO- d_6) δ ppm 4.45 (d, $J=6.4$ Hz, 2 H), 7.21-7.24 (m, 1 H), 7.31 (d, $J=4.2$ Hz, 4 H), 7.83 (d, $J=1.9$ Hz, 1 H), 8.21 (d, $J=1.9$ Hz, 1 H), 9.28 (t, $J=6.0$ Hz, 1 H) (nb. NH_2 not seen); LCMS (Method A): MH^+ 229, Rt 0.87 min, 100% by UV.

3-Amino-N-methyl-N-(pyridin-4-yl)pyrazine-2-carboxamide

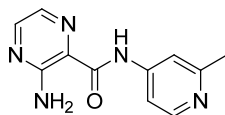
(a) *N*-methylpyridin-4-amine **412**, Sigma-Aldrich, 15 mg, 0.15 mmol; (b) 16 mg, 26%; ¹H NMR (600 MHz, DMSO-*d*₆) δ ppm 3.40 (s, 3 H), 6.70 (s, 2 H), 7.14 (d, *J*=6.0 Hz, 2 H), 7.50-7.51 (m, 1 H), 7.93-7.95 (m, 1 H), 8.42 (d, *J*=6.0 Hz, 2 H); LCMS (Method A): MH⁺ 230, Rt 0.34 min, 100% by UV.

3-Amino-N-(pyridin-3-yl)pyrazine-2-carboxamide

(a) Pyridin-3-amine **413**, Sigma-Aldrich, 14 mg, 0.15 mmol; (b) 15 mg, 40%; ¹H NMR (600 MHz, DMSO-*d*₆) δ ppm 7.35-7.42 (m, 1 H), 7.61 (br. s, 2 H), 7.92-7.96 (m, 1 H), 8.23 (d, *J*=7.6 Hz, 1 H), 8.29-8.33 (m, 2 H), 8.98-9.02 (m, 1 H), 10.75-10.79 (m, 1 H); LCMS (Method A): MH⁺ 216, Rt 0.38 min, 100% by UV.

3-Amino-N-(pyridin-2-yl)pyrazine-2-carboxamide

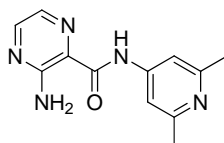
(a) Pyridin-2-amine **414**, Sigma-Aldrich, 14 mg, 0.15 mmol; (b) 8 mg, 19%; ¹H NMR (400 MHz, DMSO-*d*₆) δ ppm 7.16 - 7.20 (m, 1 H), 7.61 (br. s, 2 H), 7.85-7.90 (m, 1 H), 7.93 (d, *J*=2.3 Hz, 1 H), 8.19 (d, *J*=8.3 Hz, 1 H), 8.34 (d, *J*=2.0 Hz, 1 H), 8.37 (d, *J*=4.5 Hz, 1 H), 10.23 (s, 1 H); LCMS (Method A): MH⁺ 216, Rt 0.62 min, 100% by UV.

3-Amino-N-(2-methylpyridin-4-yl)pyrazine-2-carboxamide

(a) 2-Methylpyridin-4-amine **415**, Sigma-Aldrich, 17 mg, 0.15 mmol; (b) 12 mg, 26%; ¹H NMR (600 MHz, DMSO-*d*₆) δ ppm 2.43 (s, 3 H), 7.60 (br. s, 2 H), 7.65 (dd, *J*=5.7, 1.9 Hz, 1 H), 7.76-7.77 (m, 1 H), 7.94 (d, *J*=2.3 Hz, 1 H), 8.31 (d, *J*=2.3 Hz, 1 H), 8.33

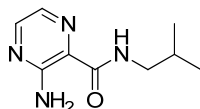
(d, $J=5.7$ Hz, 1 H), 10.72 (s, 1 H); LCMS (Method A): MH^+ 230, Rt 0.41 min, 100% by UV.

3-Amino-*N*-(2,6-dimethylpyridin-4-yl)pyrazine-2-carboxamide



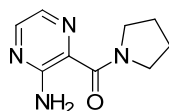
(a) 2,6-Dimethylpyridin-4-amine **416**, Anichem, 18 mg, 0.15 mmol; (b) 14 mg, 28%; 1H NMR (600 MHz, $DMSO-d_6$) δ ppm 2.38 (s, 6 H), 7.54 (s, 2 H), 7.60 (br. s, 2 H), 7.93 (d, $J=1.9$ Hz, 1 H), 8.31 (d, $J=1.9$ Hz, 1 H), 10.60 (s, 1 H); LCMS (Method A): MH^+ 244, Rt 0.44 min, 97% by UV.

3-Amino-*N*-isobutylpyrazine-2-carboxamide

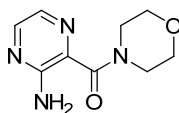


(a) 2-Methylpropan-1-amine **417**, Sigma-Aldrich, 11 mg, 0.15 mmol; (b) 5 mg, 17%; 1H NMR (400 MHz, $DMSO-d_6$) δ ppm 0.86 (d, $J=6.8$ Hz, 6 H), 1.79-1.94 (m, 1 H), 3.09 (t, $J=6.8$ Hz, 2 H), 7.51 (br. s, 2 H), 7.81 (d, $J=2.3$ Hz, 1 H), 8.19 (d, $J=2.5$ Hz, 1 H), 8.66 (t, $J=5.4$ Hz, 1 H); LCMS (Method A): MH^+ 195, Rt 0.80 min, 100% by UV.

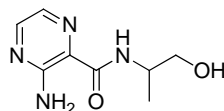
(3-Aminopyrazin-2-yl)(pyrrolidin-1-yl)methanone **426**



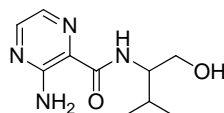
Pyrrolidine **418**, Sigma-Aldrich, 11 mg, 0.15 mmol; (b) 13 mg, 41%; 1H NMR (600 MHz, $DMSO-d_6$) δ ppm 1.83 (br. s, 4 H), 3.46-3.51 (m, 2 H), 3.58-3.62 (m, 2 H), 6.88 (br. s, 2 H), 7.79 (d, $J=2.6$ Hz, 1 H), 8.05 (d, $J=2.6$ Hz, 1 H); LCMS (Method A): MH^+ 193, Rt 0.55 min, 100% by UV.

(3-Aminopyrazin-2-yl)(morpholino)methanone

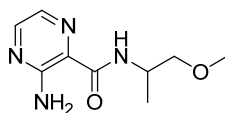
(a) Morpholine **419**, Sigma-Aldrich, 13 mg, 0.15 mmol; (b) 12 mg, 35%; ^1H NMR (600 MHz, $\text{DMSO-}d_6$) δ ppm 3.51-3.57 (m, 4 H), 3.61-3.65 (m, 2 H), 3.66-3.69 (m, 2 H), 6.52 (br. s, 2 H), 7.76 (d, $J=2.3$ Hz, 1 H), 8.03 (d, $J=2.3$ Hz, 1 H); LCMS (Method A): MH^+ 209, Rt 0.41 min, 100% by UV.

(*RS*)-3-Amino-*N*-(1-hydroxypropan-2-yl)pyrazine-2-carboxamide 427

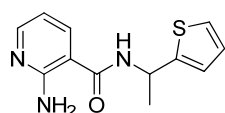
(a) (*RS*)-2-Aminopropan-1-ol **420**, Acros, 11 mg, 0.15 mmol; (b) 13 mg, 39%; ^1H NMR (600 MHz, $\text{DMSO-}d_6$) δ ppm 1.13 (d, $J=6.8$ Hz, 3 H), 3.40-3.47 (m, 2 H), 3.95-4.01 (m, 1 H), 4.86 (t, $J=5.3$ Hz, 1 H), 7.51 (br. s, 2 H), 7.81 (d, $J=2.3$ Hz, 1 H), 8.20 (d, $J=2.3$ Hz, 1 H), 8.33 (d, $J=8.7$ Hz, 1 H); LCMS (Method A): MH^+ 197, Rt 0.48 min, 100% by UV.

(*RS*)-3-Amino-*N*-(1-hydroxy-3-methylbutan-2-yl)pyrazine-2-carboxamide

(a) (*RS*)-2-Amino-3-methylbutan-1-ol **421**, Sigma-Aldrich, 15 mg, 0.15 mmol; (b) 18 mg, 48%; ^1H NMR (600 MHz, $\text{DMSO-}d_6$) δ ppm 0.85 (d, $J=6.8$ Hz, 3 H), 0.91 (d, $J=6.8$ Hz, 3 H), 1.87-1.95 (m, 1 H), 3.45-3.51 (m, 1 H), 3.53-3.59 (m, 1 H), 3.69-3.76 (m, 1 H), 4.76 (t, $J=4.9$ Hz, 1 H), 7.83 (d, $J=2.3$ Hz, 1 H), 8.19-8.20 (m, 1 H), 8.21 (d, $J=1.9$ Hz, 1 H) (nb. NH_2 not seen); LCMS (Method A): MH^+ 225, Rt 0.64 min, 100% by UV.

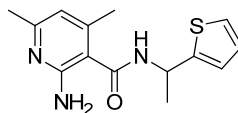
(RS)-3-Amino-N-(1-methoxypropan-2-yl)pyrazine-2-carboxamide

(a) (RS)-1-Methoxypropan-2-amine **422**, Sigma-Aldrich, 13 mg, 0.15 mmol; (b) 15 mg, 41%; ¹H NMR (600 MHz, DMSO-*d*₆) δ ppm 1.13 (d, *J*=6.8 Hz, 3 H), 3.26 (s, 3 H), 3.30-3.35 (m, 1 H), 3.41-3.45 (m, 1 H), 4.13-4.19 (m, 1 H), 7.81 (d, *J*=2.3 Hz, 1 H), 8.20 (d, *J*=2.3 Hz, 1 H), 8.40 (d, *J*=8.7 Hz, 1 H) (nb. NH₂ not seen); LCMS (Method A): MH⁺ 211, Rt 0.65 min, 100% by UV.

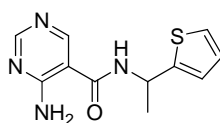
(RS)-2-Amino-N-(1-(thiophen-2-yl)ethyl)nicotinamide 433*Typical Procedure U:*

(RS)-1-(Thiophen-2-yl)ethanamine (Acros, 25 mg, 0.20 mmol), Pybop (104 mg, 0.20 mmol), 2-aminonicotinic acid **429** (Sigma-Aldrich, 28 mg, 0.20 mmol), and DIPEA (70 μL, 0.40 mmol) were combined in *N,N*-dimethylformamide (0.8 mL) and stirred at RT for 22 h. The solvent was removed *in vacuo* and the residue dissolved in DMSO (0.5 mL) and purified by reverse phase HPLC on a Sunfire C₁₈ column using acetonitrile/water with a formic acid modifier. The appropriate fractions were combined and concentrated *in vacuo* to give the title compound (22 mg, 34%); ¹H NMR (400 MHz, DMSO-*d*₆) δ ppm 1.56 (d, *J*=7.1 Hz, 3 H), 5.36-5.45 (m, 1 H), 6.59 (dd, *J*=7.8, 4.8 Hz, 1 H), 6.94-6.98 (m, 1 H), 6.98-7.03 (m, 2 H), 7.36 (d, *J*=5.0 Hz, 1 H), 7.94 (dd, *J*=7.6, 1.5 Hz, 1 H), 8.07 (d, *J*=3.3 Hz, 1 H), 8.25 (br. s, 1 H), 8.82 (d, *J*=8.1 Hz, 1 H); LCMS (Method A): MH⁺ 248, Rt 0.51 min, 100% by UV.

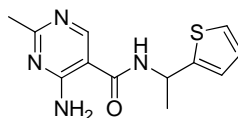
The following experiments were performed using Typical Procedure U, the data are reported as (a) acid (supplier, g, mmol); (b) product (mg, % yield).

(RS)-2-Amino-4,6-dimethyl-N-(1-(thiophen-2-yl)ethyl)nicotinamide 434

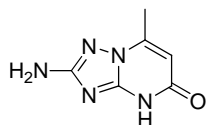
(a) 2-Amino-4,6-dimethylnicotinic acid **430**, ABCR, 33 mg, 0.20 mmol; (b) 10 mg, 15%; ^1H NMR (400 MHz, DMSO- d_6) δ ppm 1.53 (d, $J=7.1$ Hz, 3 H), 2.11 (s, 3 H), 2.20 (s, 3 H), 5.34-5.44 (m, 1 H), 5.54 (br. s, 2 H), 6.95-6.99 (m, 1 H), 7.01 (d, $J=3.5$ Hz, 1 H), 7.37 (dd, $J=5.0, 1.0$ Hz, 1 H), 8.14-8.17 (m, 1 H), 8.78 (d, $J=8.1$ Hz, 1 H); LCMS (Method A): MH^+ 276, Rt 0.54 min, 100% by UV.

(RS)-4-Amino-N-(1-(thiophen-2-yl)ethyl)pyrimidine-5-carboxamide 435

(a) 4-Aminopyrimidine-5-carboxylic acid **431**, Fluorochem, 28 mg, 0.20 mmol; (b) 20 mg, 36%; ^1H NMR (400 MHz, DMSO- d_6) δ ppm 1.57 (d, $J=7.1$ Hz, 3 H), 5.34-5.45 (m, 1 H), 6.95-6.99 (m, 1 H), 7.01-7.03 (m, 1 H), 7.37 (dd, $J=5.0, 1.0$ Hz, 1 H), 7.74 (br. s, 2 H), 8.43 (s, 1 H), 8.65 (s, 1 H), 8.99 (d, $J=8.1$ Hz, 1 H); LCMS (Method A): MH^+ 249, Rt 0.51 min, 100% by UV.

(RS)-4-Amino-2-methyl-N-(1-(thiophen-2-yl)ethyl)pyrimidine-5-carboxamide 436

(a) 4-Amino-2-methylpyrimidine-5-carboxylic acid **432**, Frontier Scientific, 31 mg, 0.20 mmol; (b) 8 mg, 14%; ^1H NMR (400 MHz, DMSO- d_6) δ ppm 1.56 (d, $J=7.1$ Hz, 3 H), 2.35 (s, 3 H), 5.35-5.44 (m, 1 H), 6.93-6.99 (m, 1 H), 7.00-7.02 (m, 1 H), 7.35-7.39 (m, 1 H), 7.67 (br. s, 2 H), 8.60 (s, 1 H), 8.90 (d, $J=8.1$ Hz, 1 H); LCMS (Method A): MH^+ 263, Rt 0.50 min, 100% by UV.

2-Amino-7-methyl-[1,2,4]triazolo[1,5-a]pyrimidin-5(4H)-one 448

1*H*-1,2,4-Triazole-3,5-diamine **446** (Sigma-Aldrich, 250 mg, 2.52 mmol), (*Z*)-ethyl 3-ethoxybut-2-enoate **447** (Apollo, 580 mg, 3.66 mmol) and sodium ethoxide (21 % in ethanol) (2.5 ml, 7.57 mmol) were refluxed in ethanol (2 ml) at 90 °C overnight. The reaction was allowed to cool then diluted with water (2 mL) and partially evaporated *in vacuo*. The aqueous volume was increased to 25 mL, washed with ethyl acetate (2 x 25 mL), then concentrated *in vacuo*. Half the resultant solid was pre-absorbed onto Florisil and purified by column chromatography (aminopropyl cartridge) eluting with 0-50 % methanol in tert-butyl methyl ether. The appropriate fractions were combined and concentrated *in vacuo* to give the title compound (200 mg, 96% based on 50% of material purified); ¹H NMR (600 MHz, DMSO-*d*₆) δ ppm 2.35 (s, 3 H), 5.77 (s, 1 H), 5.95 (s, 2 H), 12.43 (br. s, 1 H); ¹³C NMR (151 MHz, DMSO-*d*₆) δ ppm 16.2, 101.1, 140.3, 147.1, 160.7, 164.3; ¹⁵N HMBC (61 MHz, DMSO-*d*₆) δ ppm 53, 193, 197, 220 nb. one nitrogen not seen, due to correlation with broad proton signal (Figure 91). (LCMS (Method D): MH⁺ 166, Rt 0.33 min, 23% by UV).

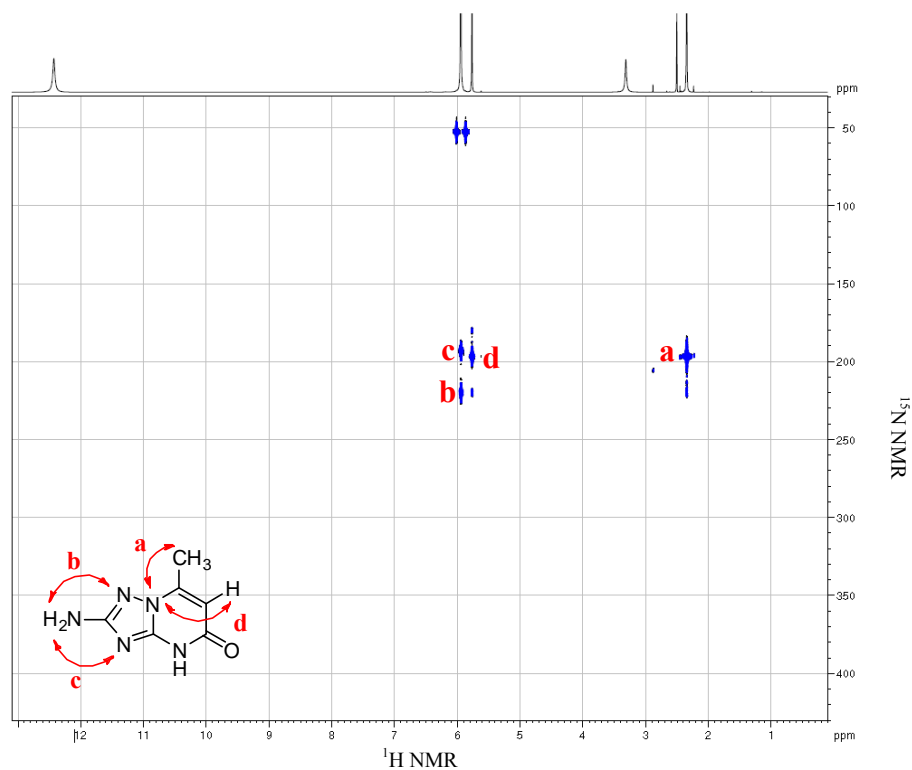
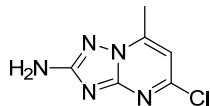
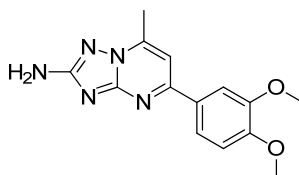


Figure 91: ¹⁵N HMBC of compound **448**

5-Chloro-7-methyl-[1,2,4]triazolo[1,5-*a*]pyrimidin-2-amine 449

2-Amino-7-methyl-[1,2,4]triazolo[1,5-*a*]pyrimidin-5(4*H*)-one **448** (2.0 g, 12 mmol) was suspended in phosphorous oxychloride (50 mL) and the reaction mixture heated to 130 °C for 4 h. The reaction mixture was concentrated *in vacuo* and the residue azeotroped with toluene (3 x 50 mL), then isopropanol to give the title compound (2.1 g, 94%). Material was used crude in the next reaction. LCMS (Method D): No clear ionisation, Rt 0.46 min, 28% by UV.

5-(3,4-Dimethoxyphenyl)-7-methyl-[1,2,4]triazolo[1,5-*a*]pyrimidin-2-amine 450

5-Chloro-7-methyl-[1,2,4]triazolo[1,5-*a*]pyrimidin-2-amine **449** (120 mg, 0.650 mmol), (3,4-dimethoxyphenyl)boronic acid **135** (120 mg, 0.65 mmol), (di(bicyclo[2.2.1]heptan-2-yl)phosphino)(2'-(dimethylamino)-[1,1'-biphenyl]-2-yl)palladium(III) chloride (37 mg, 0.065 mmol) and tripotassium phosphate (416 mg, 1.96 mmol) was suspended in 1,4-dioxane (2 mL) and water (2 mL). The reaction mixture was heated under microwave irradiation at 150 °C for 2 h. The crude reaction mixture was filtered through Celite and the filtrate concentrated *in vacuo*. The resultant residue was dissolved in dichloromethane (50 mL) and washed with water (3 x 10 mL). The layers were separated and the aqueous phase extracted with further dichloromethane (25 mL). The combined organic extracts were passed through a hydrophobic frit and concentrated *in vacuo* to give a brown gum (120 mg), which was dissolved in DMSO:methanol (1:1, 2 mL) and purified by reverse phase HPLC on an Xbridge column using acetonitrile/water with a ammonium bicarbonate modifier. The appropriate fractions were combined and concentrated *in vacuo* to give the title compound (14 mg, 7%); ¹H NMR (400 MHz, chloroform-*d*) δ ppm 2.75 (s, 3 H), 3.97 (s, 3 H), 4.02 (s, 3 H), 4.62 (br. s, 2 H), 6.96 (d, *J*=9.1 Hz, 1 H), 7.17 (s, 1 H), 7.63 (dd, *J*=8.4, 1.9 Hz, 1 H), 7.91 (d, *J*=2.0 Hz, 1 H); LCMS (Method A): MH⁺ 286, Rt 0.63 min, 77% by UV.

6.0 REFERENCES

1. Chung, F.; Barnes, N.; Allen, M.; Angus, R.; Corris, P.; Knox, A.; Miles, J.; Morice, A.; O'Reilly, J.; Richardson, M. *Respir. Med.* **2002**, *96*, 963-975.
2. British Lung Foundation, www.lunguk.org, 26-2-2011
3. Holgate, S. T. *Am. J. Respir. Crit. Care Med.* **2005**, *172*, 941-943.
4. LeRoy, G. M. *Chest (Supplementary)* **2006**, *130*, 13S-20S.
5. Global Initiative for Asthma, www.ginaasthma.org, 2-4-2014
6. Adcock, I. M.; Ford, P. A.; Bhavsar, P.; Ahmad, T.; Chung, K. F. *Curr. Allergy Asthma Rep.* **2008**, *8*, 171-178.
7. National Health Service, www.nhs.uk/Conditions/Asthma/Pages/Treatment, 22-2-2011
8. Chung, K. F.; Caramori, G.; Adcock, I. M. *Eur. J. Clin. Pharmacol.* **2009**, *65*, 853-871.
9. Sampson, A.; Holgate, S. *BMJ* **1998**, *316*, 1257-1258.
10. Currie, G. P.; Devereux, G. S.; Lee, D. K. C.; Ayres, J. G. *BMJ* **2005**, *330*, 585-589.
11. Lipworth, B. J. *BMJ* **1999**, *318*, 380-384.
12. Barnes, P. J. *Trends Pharmacol. Sci.* **2010**, *31*, 335-343.
13. Wikipedia, <http://en.wikipedia.org/wiki/COPD>, 22-6-2012
14. Patient UK, www.patient.co.uk/health/Chronic-Obstructive-Pulmonary-Disease, 13-6-2012
15. GOLD, www.goldcopd.org/, 1-6-2012
16. Rabe, K. F.; Hurd, S.; Anzueto, A.; Barnes, P. J.; Buist, S. A.; Calverley, P.; Fukuchi, Y.; Jenkins, C.; Rodriguez-Roisin, R.; van Weel, C.; Zielinski, J. *Am. J. Respir. Crit. Care Med.* **2007**, *176*, 532-555.
17. Barnes, P. J.; Adcock, I. M. *Lancet* **2009**, *373*, 1905-1917.
18. Pharmacology of Inhaled COPD Medication, www.COPDexchange.co.uk, 1-1-2013
19. Rubenfeld, G. D.; Herridge, M. S. *Chest* **2007**, *131*, 554-562.
20. Yamashita, C. M.; Lewis, J. F. *Expert Opin. Emerging Drugs* **2012**, *17*, 1-4.

21. King, F. D. *Medicinal Chemistry Principles and Practice*; 2nd ed.; RSC: Cambridge, 2002.
22. Walker, C.; Thomas, M.; Edwards, M. J. *Drug Discovery Today: Disease Mechanisms* **2006**, *3*, 63-69.
23. Cantley, L. C. *Science* **2002**, *296*, 1655-1657.
24. Marwick, J. A.; Chung, K. F.; Adcock, I. M. *Ther. Adv. Respir. Dis.* **2010**, *4*, 19-34.
25. Rommel, C.; Camps, M.; Ji, H. *Nat. Rev. Immunol.* **2007**, *7*, 191-201.
26. Wymann, M. P.; Marone, R. *Curr. Opin. Cell Biol.* **2005**, *17*, 141-149.
27. Balla, T. *Sci. Signal.* **2009**, *2*, e35.
28. Bohnacker, T.; Marone, R.; Collmann, E.; Calvez, R.; Hirsch, E.; Wymann, M. P. *Sci. Signal.* **2009**, *2*, ra27.
29. Vanhaesebroeck, B.; Ali, K.; Bilancio, A.; Geering, B.; Foukas, L. C. *Trends Biochem. Sci.* **2005**, *30*, 194-204.
30. Bi, L.; Okabe, I.; Bernard, D. J.; Nussbaum, R. L. *Mamm. Genome* **2002**, *13*, 169-172.
31. Bi, L.; Okabe, I.; Bernard, D. J.; Wynshaw-Boris, A.; Nussbaum, R. L. *J. Biol. Chem.* **1999**, *274*, 10963-10968.
32. Carson, J. D.; Van Aller, G.; Lehr, R.; Sinnamon, R. H.; Kirkpatrick, R. B.; Auger, K. R.; Dhanak, D.; Copeland, R. A.; Gontarek, R. R.; Tummino, P. J.; Luo, L. *Biochem. J.* **2008**, *409*, 519-524.
33. Bader, A. G.; Kang, S.; Zhao, L.; Vogt, P. K. *Nat. Rev. Cancer* **2005**, *5*, 921-929.
34. Okkenhaug, K.; Bilancio, A.; Farjot, G.; Priddle, H.; Sancho, S.; Peskett, E.; Pearce, W.; Meek, S. E.; Salpekar, A.; Waterfield, M. D.; Smith, A. J. H.; Vanhaesebroeck, B. *Science* **2002**, *297*, 1031-1034.
35. Hirsch, E.; Katanaev, V. L.; Garlanda, C.; Azzolino, O.; Pirola, L.; Silengo, L.; Sozzani, S.; Mantovani, A.; Altruda, F.; Wymann, M. P. *Science* **2000**, *287*, 1049-1053.
36. Clayton, E.; Bardi, G.; Bell, S. E.; Chantry, D.; Downes, C. P.; Gray, A.; Humphries, L. A.; Rawlings, D.; Reynolds, H.; Vigorito, E.; Turner, M. *J. Exp. Med.* **2002**, *196*, 753-763.
37. Jou, S. T.; Carpino, N.; Takahashi, Y.; Piekorz, R.; Chao, J. R.; Carpino, N.; Wang, D.; Ihle, J. N. *Mol. Cell. Biol.* **2002**, *22*, 8580-8591.

38. Ali, K.; Bilancio, A.; Thomas, M.; Pearce, W.; Gilfillan, A. M.; Tkaczyk, C.; Kuehn, N.; Gray, A.; Giddings, J.; Peskett, E.; Fox, R.; Bruce, I.; Walker, C.; Sawyer, C.; Okkenhaug, K.; Finan, P.; Vanhaesebroeck, B. *Nature* **2004**, *431*, 1007-1011.
39. Li, Z.; Jiang, H.; Xie, W.; Zhang, Z.; Smrcka, A. V.; Wu, D. *Science* **2000**, *287*, 1046-1049.
40. Sasaki, T.; Irie-Sasaki, J.; Jones, R. G.; Oliveira-dos-Santos, A. J.; Stanford, W. L.; Bolon, B.; Wakeham, A.; Itie, A.; Bouchard, D.; Kozieradzki, I.; Joza, N.; Mak, T. W.; Ohashi, P. S.; Suzuki, A.; Penninger, J. M. *Science* **2000**, *287*, 1040-1046.
41. Del Prete, A.; Vermi, W.; Dander, E.; Otero, K.; Barberis, L.; Luini, W.; Bernasconi, S.; Sironi, M.; Santoro, A.; Garlanda, C.; Facchetti, F.; Wymann, M. P.; Vecchi, A.; Hirsch, E.; Mantovani, A.; Sozzani, S. *EMBO J.* **2004**, *23*, 3505-3515.
42. Laffargue, M.; Calvez, R.; Finan, P.; Trifilieff, A.; Barbier, M.; Altruda, F.; Hirsch, E.; Wymann, M. P. *Immunity* **2002**, *16*, 441-451.
43. Marone, R.; Cmiljanovic, V.; Giese, B.; Wymann, M. P. *Biochim. Biophys. Acta, Proteins Proteomics* **2008**, *1784*, 159-185.
44. Barnes, P. J.; Chung, K. F.; Page, C. P. *Pharmacol. Rev.* **1998**, *50*, 515-596.
45. Lim, D. H.; Cho, J. Y.; Song, D. J.; Lee, S. Y.; Miller, M.; Broide, D. H. *Am. J. Physiol.* **2009**, *296*, L210-L219.
46. Thomas, M. J.; Smith, A.; Head, D. H.; Milne, L.; Nicholls, A.; Pearce, W.; Vanhaesebroeck, B.; Wymann, M. P.; Hirsch, E.; Trifilieff, A.; Walker, C.; Finan, P.; Westwick, J. *Eur. J. Immunol.* **2005**, *35*, 1283-1291.
47. Takeda, M.; Ito, W.; Tanabe, M.; Ueki, S.; Kihara, J.; Kato, H.; Tanigai, T.; Kayaba, H.; Sasaki, T.; Chihara, J. *Int. Arch. Allergy Immunol.* **2010**, *152*, 90-95.
48. Takeda, M.; Ito, W.; Tanabe, M.; Ueki, S.; Kato, H.; Kihara, J.; Tanigai, T.; Chiba, T.; Yamaguchi, K.; Kayaba, H.; Imai, Y.; Okuyama, K.; Ohno, I.; Sasaki, T.; Chihara, J. *J. Allergy Clin. Immunol.* **2009**, *123*, 805-812.
49. Endo, D.; Gon, Y.; Nunomura, S.; Yamashita, K.; Hashimoto, S.; Ra, C. *Int. Arch. Allergy Immunol.* **2009**, *149*, 66-72.
50. Vignola, A. M.; Chanez, P.; Chiappara, G.; Siena, L.; Merendino, A.; Reina, C.; Gagliardo, R.; Profita, M.; Bousquet, J.; Bonsignore, G. *J. Allergy Clin. Immunol.* **1999**, *103*, 563-573.
51. Xue, L.; Barrow, A.; Pettipher, R. *J. Immunol.* **2009**, *182*, 7580-7586.

52. Barnes, P. J. *Chest* **2000**, *117*, 10S-14S.
53. Ferreira, A. M.; Isaacs, H.; Hayflick, J. S.; Rogers, K. A.; Sandig, M. *Microcirculation* **2006**, *13*, 439-456.
54. Reif, K.; Okkenhaug, K.; Sasaki, T.; Penninger, J. M.; Vanhaesebroeck, B.; Cyster, J. G. *J. Immunol.* **2004**, *173*, 2236-2240.
55. Critical Care Medicine Tutorials, <http://www.ccmtutorials.com/rs/ali>, 20-6-2012
56. Abraham, E. *Crit. Care Med.* **2003**, *31*, S195-S199.
57. Kim, D. I.; Kim, S. R.; Kim, H. J.; Lee, S. J.; Lee, H. B.; Park, S. J.; Im, M. J.; Lee, Y. C. *J. Clin. Immunol.* **2012**, *32*, 340-351.
58. Yum, H. K.; Arcaroli, J.; Kupfner, J.; Shenkar, R.; Penninger, J. M.; Sasaki, T.; Yang, K. Y.; Park, J. S.; Abraham, E. *J. Immunol.* **2001**, *167*, 6601-6608.
59. Yang, K.; Arcaroli, J. J.; Abraham, E. *Am. J. Respir. Crit. Care Med.* **2003**, *167*, 1567-1574.
60. Sousa, L. P.; Lopes, F.; Silva, D. M.; Tavares, L. P.; Vieira, A. T.; Rezende, B. M.; Carmo, A. F.; Russo, R. C.; Garcia, C. C.; Bonjardim, C. A.; Alessandri, A. L.; Rossi, A. G.; Pinho, V.; Teixeira, M. M. *J. Leukocyte Biol.* **2010**, *87*, 895-904.
61. Ruckle, T.; Schwarz, M. K.; Rommel, C. *Nat. Rev. Drug Discov.* **2006**, *5*, 903-918.
62. Walker, E. H.; Perisic, O.; Ried, C.; Stephens, L.; Williams, R. L. *Nature* **1999**, *402*, 313-320.
63. Walker, E. H.; Pacold, M. E.; Perisic, O.; Stephens, L.; Hawkins, P. T.; Wymann, M. P.; Williams, R. L. *Mol. Cell* **2000**, *6*, 909-919.
64. Williams, R.; Berndt, A.; Miller, S.; Hon, W. C.; Zhang, X. *Biochem. Soc. Trans.* **2009**, *37*, 615-626.
65. Davis, A. M.; St-Gallay, S. A.; Kleywegt, G. J. *Drug Discovery Today* **2008**, *13*, 831-841.
66. Harris, S. J.; Foster, J. G.; Ward, S. G. *Curr. Opin. Invest. Drugs* **2009**, *10*, 1151-1162.
67. Pipeline Informa Healthcare, <http://gsk-pipeline.citeline.com/>, 20-6-2012
68. Pomel, V.; Klicic, J.; Covini, D.; Church, D. D.; Shaw, J. P.; Roulin, K.; Burgat-Charvillon, F.; Valognes, D.; Camps, M.; Chabert, C.; Gillieron, C.; Francon, B.; Perrin, D.; Leroy, D.; Gretener, D.; Nichols, A.; Vitte, P. A.;

- Carboni, S.; Rommel, C.; Schwarz, M. K.; Rueckle, T. *J. Med. Chem.* **2006**, *49*, 3857-3871.
69. Shugg, R. P. P.; Thomson, A.; Tanabe, N.; Kashishian, A.; Steiner, B. H.; Puri, K. D.; Pereverzev, A.; Lannutti, B. J.; Jirik, F. R.; Dixon, S. J.; Sims, S. M. *J. Biol. Chem.* **2013**, *288*, 35346-35357.
70. Sportelli, P., Rodriguez, R., Miskin, H., Vakkalanka, S., Viswanadha, S., and O'Conner, O. A. Abstract, 54th ASH Annual Meeting and Exposition, 8-12-2012
71. Broeckx, R. L. M.; Filliers, W. F. M.; Nieste, P. H. WO 2013136076, Mar 13, 2013.
72. Rueckle, T.; Shaw, J.; Church, D.; Covini, D. WO 2005011686, 20050210.
73. Barvian, N. C.; Kolz, C. N.; Para, K. S.; Patt, W. C.; Visnick, M. WO 2004052373, 20040624.
74. Rueckle, T.; Quattropiani, A.; Pomel, V.; Dorbais, J.; Covini, D.; Bischoff, A. WO 2006024666, 20060309.
75. Rueckle, T.; Jiang, X.; Gaillard, P.; Church, D.; Vallotton, T. WO 2004007491, 20040122.
76. Camps, M.; Rueckle, T.; Ji, H.; Ardisson, V.; Rintelen, F.; Shaw, J.; Ferrandi, C.; Chabert, C.; Gillieron, C.; Francon, B.; Martin, T.; Gretener, D.; Perrin, D.; Leroy, D.; Vitte, P. A.; Hirsch, E.; Wymann, M. P.; Cirillo, R.; Schwarz, M. K.; Rommel, C. *Nat. Med.* **2005**, *11*, 936-943.
77. UniProt Protein Knowledgebase, <http://www.uniprot.org/uniprot/O00329>, 6-9-2012
78. Bruce, I.; Finan, P.; Leblanc, C.; McCarthy, C.; Whitehead, L.; Blair, N. E.; Bloomfield, G. C.; Hayler, J.; Kirman, L.; Oza, M. S.; Shukla, L. WO 2003072557, 20030904.
79. Wang, T.; Green, J.; Cornebise, M.; Ledford, B.; Parsons, J.; Tanner, A.; Westcott, J. WO 2008027584, 20080306.
80. Quattropiani, A.; Rueckle, T.; Schwarz, M.; Dorbais, J.; Sauer, W.; Cleva, C.; Desforges, G. WO 2005068444, 20050728.
81. Quattropiani, A.; Pomel, V.; Rueckle, T.; Grippi-Vallotton, T. WO 2007082956, 20070726.
82. Quattropiani, A.; Dorbais, J.; Covini, D.; Desforges, G.; Rueckle, T. WO 2006125805, 20061130.

83. Budd, E.; Hatto, J. D. I.; Hayler, J. F.; Legrand, D. M.; Valade, B. WO 2007068473, 20070621.
84. Budd, E.; Fox Hayler, J.; Ian, B.; Legrand, D. M.; Cox, B. WO 2007134827, 20071129.
85. Bloomfield, G. C.; Bruce, I.; Leblanc, C.; Oza, M. S.; Whitehead, L. WO 2004078754, 20040916.
86. Bloomfield, G. C.; Bruce, I.; Hayler, J. F.; Leblanc, C.; Le Grand, D. M.; McCarthy, C. WO 2005021519, 20050310.
87. Knight, Z. A.; Gonzalez, B.; Feldman, M. E.; Zunder, E. R.; Goldenberg, D. D.; Williams, O.; Loewith, R.; Stokoe, D.; Balla, A.; Toth, B.; Balla, T.; Weiss, W. A.; Williams, R. L.; Shokat, K. M. *Cell* **2006**, *125*, 733-747.
88. Moffat, D. C. F.; Davies, S.; Alesso, S. M.; Launay, D. F. M. WO 2007129048, 20071115.
89. Moffat, D. F. C.; Davies, S.; Alesso, S. M.; Launay, D. F. M. WO 2007129005, 20071115.
90. Swinnen, D.; Jorand-Lebrun, C.; Grippi-Vallotton, T.; Gerber, P.; Gonzalez, J.; Shaw, J. WO 2009133127, 20091105.
91. Swinnen, D.; Jorand-Lebrun, C.; Grippi-Vallotton, T.; Gerber, P.; Gonzalez, J.; Shaw, J.; Jeyaprakashnarayanan, S. WO 2010100144, 20100910.
92. Wang, T.; Aronov, A.; Cornebise, M.; Maltais, F.; Ledoboer, M.; Le Tiran, A.; Marone, V.; Messersmith, D.; Cottrell, K. WO 2009129211, 20091022.
93. Booker, S.; D'Angelo, N.; D'Amico, D. WO 2009017822, 20090205.
94. Taniyama, D.; Mitsuoka, Y.; Hata, K. WO 2010125799, 20101104.
95. Mitsuoka, Y.; Masuda, M.; Taniyama, D. WO 2010024258, 20100304.
96. Aronov, A.; Bandarage, U. K.; Cottrell, K.; Davies, R.; Krueger, E.; Ledboer, M.; Ledford, B.; Le Tiran, A.; Liao, Y.; Messersmith, D.; Wang, T.; Xu, J. WO 2010096389, 20100826.
97. Convery, M.; Neu, M. PTS, GlaxoSmithKline, Stevenage, UK, Unpublished Work, 2011.
98. Ramsden, N.; Bell, K.; Cansfield, A.; Taylor, J.; Sunose, M.; Middlemiss, D. WO 2010007099, 20100121.
99. Ramsden, N.; Bell, K.; Cansfield, A.; Taylor, J.; Sunose, M.; Middlemiss, D.; Neubauer, G. WO 2009068482, 20090604.

100. Ramsden, N.; Bell, K.; Cansfield, A.; Taylor, J.; Sunose, M.; Middlemiss, D.; Ellard, K. WO 2010007100, 20100121.
101. Ramsden, N.; Bell, K.; Taylor, J.; Sunose, M.; Middlemiss, D.; Ellard, K. WO 2010092015, 20100819.
102. Wilson, F.; Ramsden, N.; Bell, K.; Cansfield, A.; Burckhardt, S.; Taylor, J.; Sunose, M.; Middlemiss, D. WO 2008025821, 20080306.
103. Bergamini, G.; Bell, K.; Shimamura, S.; Werner, T.; Cansfield, A.; Mueller, K.; Perrin, J.; Rau, C.; Ellard, K.; Hopf, C.; Doce, C.; Leggate, D.; Mangano, R.; Mathieson, T.; O'Mahony, A.; Plavec, I.; Rharbaoui, F.; Reinhard, F.; Savitski, M. M.; Ramsden, N.; Hirsch, E.; Drewes, G.; Rausch, O.; Bantscheff, M.; Neubauer, G. *Nat. Chem. Biol.* **2012**, 8, 576-582.
104. Bruce, I.; Dale, J.; Hunt, T. A. WO 2009010530, 20090122.
105. Aronov, A. WO 2011087776, 20110721.
106. Taniyama, D.; Kano, K.; Ishibashi, K.; Endoh, T. WO 2010061903, 20100603.
107. Shimada, M.; Murata, T.; Fuchikami, K.; Tsujishita, H.; Omori, N.; Kato, I.; Miura, M.; Urbahns, K.; Gantner, F.; Bacon, K. WO 2004029055, 20040408.
108. Messersmith, D.; Aronov, A.; Lauffer, D. WO 2011041634, 20110407.
109. Maier, U.; Grauert, M.; Hoffmann, M.; Hoenke, C.; Joergensen, A. WO 2007115930, 20071018.
110. Leahy, J. W.; Buhr, C. A.; Johnson, H. W. B.; Kim, B. G.; Baik, T.; Cannoy, J.; Forsyth, T. P.; Jeong, J. W.; Lee, M. S.; Ma, S.; Noson, K.; Wang, L.; Williams, M.; Nuss, J. M.; Brooks, E.; Foster, P.; Goon, L.; Heald, N.; Holst, C.; Jaeger, C.; Lam, S.; Loughheed, J.; Nguyen, L.; Plonowski, A.; Song, J.; Stout, T.; Wu, X.; Yakes, M. F.; Yu, P.; Zhang, W.; Lamb, P.; Raeber, O. *J. Med. Chem.* **2012**, 55, 5467-5482.
111. Grauert, M.; Maier, U.; Hoffmann, M.; Scheuerer, S.; Joergensen, A. US 20070238718, 20071011.
112. Gogliotti, R. D.; Lee, H. T.; Sexton, K. E.; Visnick, M. WO 2004108709, 20041216.
113. Giovannini, R.; Frattini, S.; Brandl, T.; Breitfelder, S.; Cereda, E.; Grauert, M.; Hoffmann, M.; Joergensen, A. WO 2008092831, 20080807.
114. Connolly, M.; Gogliotti, R. D.; Lee, H. T.; Plummer, M. S.; Sexton, K. E.; Visnick, M. WO 2004108713, 20041216.

115. Connolly, M. K.; Gogliotti, R. D.; Plummer, M. S.; Visnick, M. WO 2005042519, 20050512.
116. Connolly, M. K.; Cogliotti, R. D.; Hurt, C. R.; Reichard, G. A.; Visnick, M. WO 2005023800, 20050317.
117. Bruendl, M. M.; Connolly, M. K.; Goodman, A. P.; Gogliotti, R. D.; Lee, H. T.; Plummer, M. S.; Sexton, K. E.; Reichard, G. A.; Visnick, M.; Wilson, M. W. WO 2004108715, 20041216.
118. Bruendl, M. M. WO 2005105801, 20051110.
119. Bruce, I.; Dunstan, A.; Hunt, T. A.; Howsham, C. WO 2009013348, 20090129.
120. Bruce, I.; Budd, E.; Edwards, L.; Howsham, C. WO 2009115517, 20090924.
121. Breitfelder, S.; Maier, U.; Hoenke, C.; Joergensen, A. WO 2007115931, 20071018.
122. Brandl, T.; Maier, U.; Hoenke, C.; Joergensen, A. US 20070238746, 20071011.
123. Stavenger, R.; Philp, J.; Xu, W. W.; Ivy, R.; Hong, S.; Gu, M.; Ye, G.; Gotchev, D.; Yu, F.; Cui, H. CVU CEDD, GlaxoSmithKline, Philadelphia, USA, Unpublished Work, 2011.
124. Bonser, S. Screening & Compound Profiling, Platform Technology & Science, GlaxoSmithKline, Stevenage, UK, Unpublished Work, 2012.
125. Lehy, R.; Smallwood, A.; Elkins, T.; Raha, K. Structural Biology, GlaxoSmithKline, Philadelphia, USA, Unpublished Work, 2011.
126. Xie, P.; Williams, D. S.; Atilla-Gokcumen, G. E.; Milk, L.; Xiao, M.; Smalley, K. S. M.; Herlyn, M.; Meggers, E.; Marmorstein, R. *ACS Chem. Biol.* **2008**, *3*, 305-316.
127. Free, S. M., Jr.; Wilson, J. W. *J. Med. Chem.* **1964**, *7*, 395-399.
128. Bissantz, C.; Kuhn, B.; Stahl, M. *J. Med. Chem.* **2010**, *53*, 5061-5084.
129. Lipinski, C. A.; Lombardo, F.; Dominy, B. W.; Feeney, P. J. *Adv. Drug Delivery Rev.* **1997**, *23*, 3-25.
130. Lipinski, C. A. *Drug Discovery Today: Technol.* **2004**, *1*, 337-341.
131. Keseru, G. M.; Makara, G. M. *Nat. Rev. Drug Discov.* **2009**, *8*, 203-212.
132. Hopkins, A. L.; Groom, C. R.; Alex, A. *Drug Discov. Today* **2004**, *9*, 430-431.

133. Abad-Zapatero, C.; Metz, J. T. *Drug Discov. Today* **2005**, *10*, 464-469.
134. Leeson, P. D.; Springthorpe, B. *Nat. Rev. Drug Discovery* **2007**, *6*, 881-890.
135. Hughes, J. D.; Blagg, J.; Price, D. A.; Bailey, S.; DeCrescenzo, G. A.; Devraj, R. V.; Ellsworth, E.; Fobian, Y. M.; Gibbs, M. E.; Gilles, R. W.; Greene, N.; Huang, E.; Krieger-Burke, T.; Loesel, J.; Wager, T.; Whiteley, L.; Zhang, Y. *Bioorg. Med. Chem. Lett.* **2008**, *18*, 4872-4875.
136. Price, D. A.; Blagg, J.; Jones, L.; Greene, N.; Wager, T. *Expert Opin. Drug Metab. Toxicol.* **2009**, *5*, 921-931.
137. Bardoni, S. Physical Chemistry Group, GlaxoSmithKline, Stevenage, UK, Unpublished Work, 2011.
138. Physical Chemistry Group GlaxoSmithKline, Stevenage, UK, Unpublished Work, 2011.
139. Ritchie, T. J.; MacDonald, S. J. F. *Drug Discovery Today* **2009**, *14*, 1011-1020.
140. Lovering, F.; Bikker, J.; Humblet, C. *J. Med. Chem.* **2009**, *52*, 6752-6756.
141. Miyaura, N.; Suzuki, A. *Chem. Rev.* **1995**, *95*, 2457-2483.
142. Suzuki, A. *J. Organomet. Chem.* **1999**, *576*, 147-168.
143. Carrow, B. P.; Hartwig, J. F. *J. Am. Chem. Soc.* **2011**, *133*, 2116-2119.
144. Meana, A.; Rodriguez, J. F.; Sanz-Tejedor, M. A.; Garcia-Ruano, J. L. *Synlett* **2003**, 1678-1682.
145. Conreux, D.; Bossharth, E.; Monteiro, N.; Desbordes, P.; Vors, J. P.; Balme, G. *Org. Lett.* **2007**, *9*, 271-274.
146. Bertani, B.; Fabrizio, M.; Pasquarello, A.; Terreni, S. WO 2007113258, 20071011.
147. Kranenburg, M.; Kamer, P. C. J.; Van Leeuwen, P. W. N. M. *Eur. J. Inorg. Chem.* **1998**, 155-157.
148. O'Brien, C. J.; Kantchev, E. A.; Valente, C.; Hadej, N.; Chass, G. A.; Lough, A.; Hopkinson, A. C.; Organ, M. G. *Chem. Eur. J.* **2006**, *12*, 4743-4748.
149. Schnyder, A.; Indolese, A. F.; Studer, M.; Blaser, H. U. *Angew. Chem. Int. Ed.* **2002**, *41*, 3668-3671.
150. Alessi, M.; Larkin, A. L.; Ogilvie, K. A.; Green, L. A.; Lai, S.; Lopez, S.; Snieckus, V. *J. Org. Chem.* **2007**, *72*, 1588-1594.

151. Knapp, D. M.; Gillis, E. P.; Burke, M. D. *J. Am. Chem. Soc.* **2009**, *131*, 6961-6963.
152. Campbell, I. Respiratory Therapy Area, GlaxoSmithKline, Stevenage, UK, Unpublished Work, 2011.
153. Follmann, M.; Rosch, A.; Klegraf, E.; Kunz, H. *Synlett* **2001**, 1569-1570.
154. Ishiyama, T.; Murata, M.; Miyaura, N. *J. Org. Chem.* **1995**, *60*, 7508-7510.
155. Takagi, J.; Takahashi, K.; Ishiyama, T.; Miyaura, N. *J. Am. Chem. Soc.* **2002**, *124*, 8001-8006.
156. Bostroem, J.; Hogner, A.; Llinas, A.; Wellner, E.; Plowright, A. T. *J. Med. Chem.* **2012**, *55*, 1817-1830.
157. Charnwood Molecular Ltd, 7 Beaumont Court, Prince William Road, Loughborough, Leicester, LE11 5GA, UK, Unpublished Work, 2011.
158. Taibi, P.; Mobashery, S. *e-EROS Encycl. Reagents Org. Synth.* **2001**, 20-9-2012
159. Burckhardt, S. *Synlett* **2000**, 559.
160. Bethel, P. A.; Gerhardt, S.; Jones, E. V.; Kenny, P. W.; Karoutchi, G. I.; Morley, A. D.; Oldham, K.; Rankine, N.; Augustin, M.; Krapp, S.; Simader, H.; Steinbacher, S. *Bioorg. Med. Chem. Lett.* **2009**, *19*, 4622-4625.
161. Mitchell, C. J.; Ballantine, S. P.; Coe, D. M.; Cook, C. M.; Delves, C. J.; Dowle, M. D.; Edlin, C. D.; Hamblin, J. N.; Holman, S.; Johnson, M. R.; Jones, P. S.; Keeling, S. E.; Kranz, M.; Lindvall, M.; Lucas, F. S.; Neu, M.; Solanke, Y. E.; Somers, D. O.; Trivedi, N. A.; Wiseman, J. O. *Bioorg. Med. Chem. Lett.* **2010**, *20*, 5803-5806.
162. Peakdale Molecular Ltd, Peakdale Science Park, Sheffield Rd, Chapel-en-le-Frith, High Peak, SK23 0PG, UK, Unpublished Work, 2011.
163. Hardy, C. Energy minimisations carried out using Molecular Operating Environment, Unpublished Work, 2011.
164. Kranz, M. Computational Chemistry, GlaxoSmithKline, Stevenage, UK. Torsional scans carried out using Jaguar V7.9, at the B3LYP/6-31G** level of theory in Maestro V9.2.109., Unpublished Work, 2012.
165. Brameld, K. A.; Kuhn, B.; Reuter, D. C.; Stahl, M. *J. Chem. Inf. Model.* **2008**, *48*, 1-24.
166. Tame, C.; McAlpine, N. Refractory Respiratory DPU, Respiratory Therapy Area, GlaxoSmithKline, Stevenage, UK, Unpublished Work, 2011.

167. Lauwagie, S.; Millet, R.; Pommery, J.; Depreux, P.; Henichart, J. P. *Heterocycles* **2006**, *68*, 1149-1162.
168. Sabot, C.; Kumar, K. A.; Meunier, S.; Mioskowski, C. *Tetrahedron Lett.* **2007**, *48*, 3863-3866.
169. GVK Biosciences Private Ltd, Hyderabad, India, Unpublished Work, 2011.
170. Li, K. L.; Du, Z. B.; Guo, C. C.; Chen, Q. Y. *J. Org. Chem.* **2009**, *74*, 3286-3292.
171. Tame, C.; Wellaway, N. Refractory Respiratory Inflammation DPU, Respiratory Therapy Area, GlaxoSmithKline, Stevenage, UK, Unpublished Work, 2011.
172. Wabuyele, M. Physical Chemistry Group, GlaxoSmithKline, Upper Merion, USA, Unpublished Work, 2012.
173. Evans pKa Table, http://www2.lsddiv.harvard.edu/labs/evans/pdf/evans_pKa_table.pdf, 20-3-2012
174. Gleeson, M. P. *J. Med. Chem.* **2008**, *51*, 817-834.
175. Burton, P. S.; Conradi, R. A.; Ho, N. F. H.; Hilgers, A. R.; Borchardt, R. T. *J. Pharm. Sci.* **1996**, *85*, 1336-1340.
176. Luscombe, C. Computational Chemistry, GlaxoSmithKline, Stevenage, UK. Computational model built on database of ChromLogD values measured at GlaxoSmithKline, Unpublished Work, 2011.
177. Cooper, T. Respiratory TA, GlaxoSmithKline, Stevenage, UK, Unpublished Work, 2012.
178. Ishiyama, T.; Takagi, J.; Ishida, K.; Miyaura, N.; Anastasi, N. R.; Hartwig, J. F. *J. Am. Chem. Soc.* **2002**, *124*, 390-391.
179. Taylor, J.; Down, K. Refractory Respiratory DPU, Respiratory Therapy Area, GlaxoSmithKline, Stevenage, UK, Unpublished Work, 2011.
180. Seijas, J. A.; Vazquez-Tato, M. P.; Martinez, M. M.; Nunez-Corredoira, G. *J. Chem. Res. Synop.* **1999**, 420-421.
181. Rautio, J.; Kumpulainen, H.; Heimbach, T.; Oliyai, R.; Oh, D.; Jaervinen, T.; Savolainen, J. *Nat. Rev. Drug Discovery* **2008**, *7*, 255-270.
182. Bai, J. P. F.; Barash, E. H.; Chakraborty, U.; Crooks, P. A.; Dhooper, H. K.; Erhardt, P. W.; Gaudana, R.; Guarino, C. R.; Hedley, D.; Huttunen, K.; Kwatra, D. L. K.; Lesko, L.; Lockman, P. R.; Majumdar, S.; Mitra, A. K.; Moridani M.Y.; Negoita-Giras, G.; Niculescu-Duvaz, D.; O'Donnell, J. P.;

- Pacanowski, M.; Rahmen, A.; Rautio, J.; Reese, M. D.; Sloan, K.; Smith, Q. R.; Springer, C.; Vaishya, R.; Wasdo, S. C.; Warren, M. S. *Prodrugs and Targeted Delivery*; Wiley-VCH: Weinheim, 2012; Vol. 47.
183. Saklatvala, P. Exploratory Development Sciences, GlaxoSmithKline, Ware, UK, Unpublished Work, 2012.
 184. Teague, S.; Sherrif, E. Respiratory DMPK, GlaxoSmithKline, Stevenage, UK, Unpublished Work, 2012.
 185. Teague, S.; Sherrif, E. Respiratory DMPK, GlaxoSmithKline, Stevenage, UK. All animal studies were ethically reviewed and carried out in accordance with Animals (Scientific Procedures) Act 1986 and the GSK Policy on the Care, Welfare and Treatment of Animals. Unpublished Work, 2013.
 186. Silverman, R. B. Drug Metabolism. In *The Organic Chemistry of Drug Design and Drug Action*, Academic Press: San Diego, 1992.
 187. Lacroix, Y. Refractory Respiratory Inflammation DPU, Respiratory Therapy Area, GlaxoSmithKline, Stevenage, UK, Unpublished Work, 2013.
 188. Young, R. J.; Green, D. V. S.; Luscombe, C. N.; Hill, A. P. *Drug Discovery Today* **2011**, *16*, 822-830.
 189. Kumar, A.; Voet, A.; Zhang, K. Y. J. *Curr. Med. Chem.* **2012**, *19*, 5128-5147.
 190. Erlanson, D. A., <http://practicalfragments.blogspot.co.uk/>, 1-2-2014
 191. Joseph-McCarthy, D.; Campbell, A. J.; Kern, G.; Moustakas, D. *J. Chem. Inf. Model.* **2014**, *54*, 693-704.
 192. Rees, D. C.; Congreve, M.; Murray, C. W.; Carr, R. *Nat. Rev. Drug Discovery* **2004**, *3*, 660-672.
 193. Leach, A. PTS, GlaxoSmithKline, Stevenage, UK, Unpublished Work, 2011.
 194. Chung, C.; Spitzfden, C. Structural Biology and Biophysics, Platform Technology and Science, GlaxoSmithKline, Stevenage, UK, Unpublished Work, 2012.
 195. Bruce, I.; Budd, E.; Edwards, L.; Howsham, C. WO 2009115517, 20090924.
 196. Hamadi, A. Respiratory Therapy Area, GlaxoSmithKline, Stevenage, UK, Unpublished Work, 2011.
 197. Williams, L. A. *J. Chem. Soc.* **1961**, 3046-3052.

198. Pickett, S. Computational Chemistry, GlaxoSmithKline, Stevenage, UK, Unpublished Work, 2013.
199. Convery, M. PTS, GlaxoSmithKline, Stevenage, UK, Unpublished Work, 2013.
200. Maxwell, A.; Convery, M. GlaxoSmithKline, Stevenage, UK, Unpublished Work, 2014.
201. Baldwin, I.; Sloan, L.; Hardy, C.; Convery, M.; Bertrand, S.; Cansfield, A.; Barton, N.; Kranz, M. GlaxoSmithKline, Stevenage, UK, Unpublished Work, 2013.

7.0 GLOSSARY

cLogP	A calculated measure of lipophilicity. P is the partition coefficient of the compound between octanol and water.
CHI LogD	An HPLC measure of lipophilicity which is pH dependent.
ChromLogD	A GSK high throughput HPLC measure of LogD (Appendix 4); absolute values are usually higher than the equivalent CHI LogD measurement (see Figure 92).

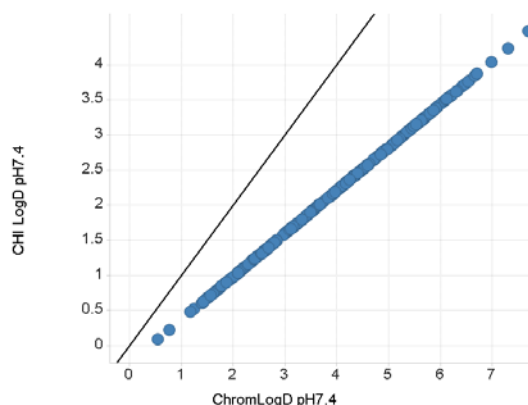


Figure 92: CHI LogD and ChromLog D correlation for representative set of GSK compounds; black line represents line of unity

CLND	A high throughput measure of solubility using chemiluminescent nitrogen detection (Appendix 3).
Free Wilson	A statistical analysis of data to ascertain if SAR is additive.
HAC	Heavy atom count. The number of non hydrogen atoms in a molecule.
pIC₅₀	-LogIC ₅₀ , where IC ₅₀ is the concentration which gives 50% inhibition.
PSA	Polar surface area; a calculated measure which gives an indication of how polar a molecule is.
SFI	Solubility forecast indicator; SFI= ChromLogD _{7.4} + number of aromatic rings.
SMARTS	A language used to describe chemical substructures

8.0 APPENDICES

Appendix 1: Sequence Alignments of Human PI3K Isoforms

Alignment of the catalytic domains of all four PI3K isoforms using Universal Protein Resource. Single letter amino acid codes used.

1	MELENYKQPVVLRDNCRRRRRMRKPSA-----AASLSSMELIPIEFVLPFSQRKCK	52	P48736	PK3CG_HUMAN
1	-----MPPRP-SSGELWGIHL-----MPPRILVECLLPNGMIV--	32	P42336	PK3CA_HUMAN
1	-----MPPGVDCPMEFWTKEE-----NQSVMVDFLLPTGVYL--	32	O00329	PK3CD_HUMAN
1	-----MCF-SFIMPPAMADILDIAWAVDSQIASDGSIPVDFLLPTGIYI--	42	P42338	PK3CB_HUMAN
	* * * * * : : : * * * .			
53	SPETALLHVAGHGNVEQMKAOVWLRALETSVAADFVHRLGPHHFLLYQK-KGQWYEIYD	111	P48736	PK3CG_HUMAN
33	----TLECLREATLITIKHELFKKARKYPLH---QLLQDESSYIFVSVTQEAEREFFD	84	P42336	PK3CA_HUMAN
33	----NFPVSRNANLSTIKQLLWHRAQYEPLF---HMLSGPEAYVFTCINQTAEQELED	84	O00329	PK3CD_HUMAN
43	----QLEVPREATISYIKQMLWKQVHNYPMF---NLLMDIDSYMFACVNTAVYEELED	94	P42338	PK3CB_HUMAN
	: * * * * * : * * * * * : * * * * * : * * * * * : * * * * *			
112	KYQVVQTLDCRLRYWKATHRSPGQIHLVQRHPPSEESQAQFQRQLTALIGYDVTDSNVHDD	171	P48736	PK3CG_HUMAN
85	ETRRLL---CDLRLFQ-----PFLKVIIEP-VGNREEKILNREIGFAIGMPVCEFDMPKDP	134	P42336	PK3CA_HUMAN
85	EQRRL---CDVQPFLL-----PVLRLVAR-EGDRVKKLINSQISLLIGKGLHEFDSLCDP	134	O00329	PK3CD_HUMAN
95	ETRRLL---CDVRRPFL-----PVLKLVTR-SCDPGEK-LDSKIGVLIGKGLHEFDSLKDP	143	P42338	PK3CB_HUMAN
	: : : : * * * * * : * * * * * : * * * * * : * * * * *			
172	ELEFTRRGLVTPRMAEVAASRDPKLYAMHPVVT-----SKPLPEYLWKKIANNCIFI	222	P48736	PK3CG_HUMAN
135	EVQDFRRNILNWCKEAVDLRDL--NSPHSRAMYVYPPNVESSPELPHIYNKLDKRGQIIV	192	P42336	PK3CA_HUMAN
135	EVNDFRAKMCQFCEEAARRRQ--LGWEAWLQYSFPLQLEPSAQTWGPGLRPLRNRALLV	192	O00329	PK3CD_HUMAN
144	EVNEFRRRKMRKFSEKILSLVG--LSWMDWLKQTYYPEHEPSIPENLE--DKLYGGKLIIV	199	P42338	PK3CB_HUMAN
	* : * : * * * * * : * * * * * : * * * * * : * * * * *			
223	V-----IHRSTTSQTIKVSPPDTPGAILQSFFTKMAKK---KSLMDIPESQSEQDFVL	272	P48736	PK3CG_HUMAN
193	VIWVIVSPMNDKQKYYTLKINHDCVPEQVIAEAIRKKTRSMLLSSEQLKLCVLEYQGKYIL	252	P42336	PK3CA_HUMAN
193	N----VKFEGSEESFTFQVSTKDVPLALMACALRKKATVFR-----OPLVEQPEDYTL	241	O00329	PK3CD_HUMAN
200	A----VHFENCQDVFSFQVSPNMNPKVWVNELAIQKRLTIHG-----KEDEVSPYDYVL	248	P42338	PK3CB_HUMAN
	. : : : . * : : * : * * * * * : * * * * * : * * * * *			
273	RVCGRDEYLVGETPIKNFQWVRHCLKNGEEIHVVLDTPPDPALDEVKREEWPLVDDCTGV	332	P48736	PK3CG_HUMAN
253	KVCGCDEYFLEKYPLSQYKIRSCIMLGRPNLMLMAKESL--YS-----QLPMDCFPTM	304	P42336	PK3CA_HUMAN
242	QVNGRHELYYGSYPLCQFYICSLHSGLTPHLTMVHSSSI--LA-----MRDEQSNPA	293	O00329	PK3CD_HUMAN
249	QVSGRVEYVFGDHPLIQFYIRNCVMNRALPHFILLVECKKI--KK-----MYEQEMIAI	300	P42338	PK3CB_HUMAN
	: * * * * * . * : : : : * * : : : . : : : .			
333	TGYHEQLT----IHGKDHEVFTVSLWDCDRKFRVKIRGIDIPVLPRTDITVVFVEANIQ	388	P48736	PK3CG_HUMAN
305	PSYSRRRISTATPY---MNGETSTKSLWVINSALRIKILCATYVNVNIRDIDKIYVRTGIY	361	P42336	PK3CA_HUMAN
294	PQ--VQKPRAKPPPAPAK--PSSVSLWSLEQPFRIELIQGSKV--NADERMKLIVVQAGLF	348	O00329	PK3CD_HUMAN
301	EAAINRNSSNLPLPLPPKTRIISHVWENMNPQIVLVKGNKL--NTEETVKVHVRAGLF	358	P42338	PK3CB_HUMAN
	. : * * * * * : * * * * * : * * * * * : * * * * *			
389	HGQQVLCQRRTSPKP-FTEEVLWVWLEFSIKIKDLPKGLLNLIQIYCGKAPALSSKASA	447	P48736	PK3CG_HUMAN
362	HGGEPLCDNVNTQRV-PCSNPRWNEWLNVDIYIPDLPRARLCLISICSVKGR-----	412	P42336	PK3CA_HUMAN
349	HGNEMLCKTVSSSEVSVCEPVWQKRFLEFDINICDLPRMARLFCALYAVIEKAKKARSTK	408	O00329	PK3CD_HUMAN
359	HGTELLCKTIVSSEVSGKNDHIWNEPLEFDINICDLPRMARLFCALYAVYAVLKDVKRTKSTK	418	P42338	PK3CB_HUMAN
	* * : * * . : . : * : * * : * * * * * : * * : : .			
448	ESP-----SSESKGVQLLYVNVNLLIDHRFLLRRGEYVLMWQISGKGEDQGSFNADK	501	P48736	PK3CG_HUMAN
413	-----KGAKEEHCPLAWGNINLFDYDTLVSGKMLNLWP-VPHGLED--LLNPI	459	P42336	PK3CA_HUMAN
409	-----KSKKADCPIDANLMLFDYKDLKGTGERCLYMWPSVPDEKGE--LLNPT	456	O00329	PK3CD_HUMAN
419	TINPSKYQTIKAGRVHYVPAWVNTHVDFKGGQLRTGDIILHSWSSFPDELEE--MLNPM	476	P42338	PK3CB_HUMAN
	. : : * * * * * : * * * * * : * * * * * : * * * * *			
502	LTSATNPDKENSMSISILLD-NYCHPIALPKHOPTDPEGD-----	541	P48736	PK3CG_HUMAN
460	GVTGSMNPKETPCLEL-EFDW--FSSVVKFPDMSVIEEHANWSVSREAGFSYSHAGLSNRL	517	P42336	PK3CA_HUMAN
457	GTVRSNPNTDSAAALLICLPEVAPHPVYYPALAKILELGRHSECVH-----	502	O00329	PK3CD_HUMAN
477	GTVQINPYTENATALHVKFPENKKQPYYPFPDKIIEKAAEIASSDS-----AN-----	525	P42338	PK3CB_HUMAN
	* * * * * . : * * * * * : * * * * * : * * * * *			

542	RVRAEMPQLRQLEAIIATDPLNPLTAEDKELLWHFRYESLK-HPKAYPKLFSSVKGQ	600	P48736	PK3CG_HUMAN
518	ARDNELRENDKEQLKAISTRDPLSEITEQEKFDFLWHRHYCVT-IPEILPKLLSVKWN	576	P42336	PK3CA_HUMAN
503	-VT----EEEQLQREILERRGSGELYEHKDLVWKLREHEVQEHFPEALARLLLVTKWN	557	O00329	PK3CD_HUMAN
526	-VSRGGKFLPVLKEILDRDPLSQLCENEMDLIWTLRQDCREIFPQSLPKLLSIKWNK	584	P42338	PK3CB_HUMAN
	: : * . * : . : : * * * : : * : * .			
601	QEIVAKTYQLLARREVWDQSALDVGLTMQLLDCNFSDENVRAIAVQKLES-LEDDVVLHY	659	P48736	PK3CG_HUMAN
577	RDEVAQMYCLVK---DWP--PIKPEQAMELLDCNYPDPMVRGFAVRCKEYLTDDKLSQY	631	P42336	PK3CA_HUMAN
558	HEDVAQMLYLLC---SWP--ELPVLSALELLDFSPDCHVGSFAIKSLRK-LTDELQY	611	O00329	PK3CD_HUMAN
585	LEDVAQLQALLQ---IWP--KLPPREALLELDFNYPDQVREYAVGCLRQ-MSDEELSQY	638	P42338	PK3CB_HUMAN
	: * * : * : * : : * * * : * * * : * . : * : : *			
660	LLQLVQAVKFEFYPHDSALARFLLKRLNRKIRIGHFLWFRLRSEIAQSRHYQORFAVILEA	719	P48736	PK3CG_HUMAN
632	LIQLVQVLKYEQYLDMLLVRFLKALTNQRIGHFFFVHLKSEMHNK-TVSQRFGLLES	690	P42336	PK3CA_HUMAN
612	LLQLVQVLKYESYLDCELTKFLDRALANRKGHFLFVHLRSEMHPV-SVALRFGLILEA	670	O00329	PK3CD_HUMAN
639	LLQLVQVLKYEFPFLDCALSRFLLEALGNRRIGQFLFVHLRSEVHIP-AVSVQFVILEA	697	P42338	PK3CB_HUMAN
	* : * * * : * : * * : * * * : * * * : * : * * * : * : * * * :			
720	YLRGCGTAMLHDFTOQVQVIEMLQKVTLDIKSLSAEKYDVSSQVVISQLKQKLENLQNSQL	779	P48736	PK3CG_HUMAN
691	YCRACGMYLKHLNR-QVEAMEKLINLTDILK-QEKKDETQK-VQMKFLVEQMRPDMFA	747	P42336	PK3CA_HUMAN
671	YCRGSLPHMKVLMK-QGEALSCLKALNDFVK-LSSQKTPKP-QTELMLHLCMRQEAYLEA	727	O00329	PK3CD_HUMAN
698	YCRGSLVGHMKVLSK-QVEALNKLKTLNLSLIK-LNAVKLNRA-KGKAMHTCLKQSAYREA	754	P42338	PK3CB_HUMAN
	* * . : * : * : * : * : * : * : * : * : * : * : * : * : * : * : * :			
780	PESFRVPYDPLKAGALAIKCKVMASKKKPLWLEFKCADPT-ALSNETIGIIFKHGDDL	838	P48736	PK3CG_HUMAN
748	LQGFSLPLNPAHQGNLRLLEECRIMSSAKRPLWLNWENPDIMSELLFQNNIIFKNGDDL	807	P42336	PK3CA_HUMAN
728	LSHLQSPDPSTLLAEVCVEQCTFMDSKMKPLWIMYSNEEAGSG---GSVGIIFKNGDDL	784	O00329	PK3CD_HUMAN
755	LSDLQSPNLPVILSELVYEKCKYMDSKMKPLWLVYMNKVFGE----DSVGVIFKNGDDL	810	P42338	PK3CB_HUMAN
	: * : * : * : * : * : * : * : * : * : * : * : * : * : * : * : * : * :			
839	RQDMLILQILRIMESIWETESLDLCLLPYGCISTGDKIGMIEIVKDATTIAKIQQST--V	896	P48736	PK3CG_HUMAN
808	RQDMLTLQIIRIMENIWQNGQLDRMLPYGCLSIGDCVGLIEVVRNSHTIMQIQCKG-GL	866	P42336	PK3CA_HUMAN
785	RQDMLTLQMIQMLMDVLWKQEGLDLRMTPYGCLPTGDRTLGIEVVLRSDTIANIQLNKSNM	844	O00329	PK3CD_HUMAN
811	RQDMLTLQMLRLMDLLWKEAGLDRMLPYGCLATGDRSLGIEVVSSETIADIQLNSSNV	870	P42338	PK3CB_HUMAN
	* * * * * : * : * : * : * : * : * : * : * : * : * : * : * : * : * : * :			
897	GNTGAFKDEVLNHWLKEKSPTEEFQAVERFVYSCAGYCVATFVLGIGDRHNDNIMITE	956	P48736	PK3CG_HUMAN
867	KGALQFNSTLHQWLKDKNKG-EIYDAAIDLFRSCAGYCVATFVLGIGDRHNSNIMVKD	925	P42336	PK3CA_HUMAN
845	AATAAFNKDALNLWLSKKNPG-EALDRAIEEFTLSCAGYCVATFVLGIGDRHSDNIMIRE	903	O00329	PK3CD_HUMAN
871	AAAAAFNKDALNLWLSKEYNSG-DDLDRAIEEFTLSCAGYCVASYVLGIGDRHSDNIMVKK	929	P42338	PK3CB_HUMAN
	: * : * . * . * * . : : * : * . * * * * * : : * * * * * . * * * . :			
957	TGNLFHIDFGHILGNYSFLGINKERVFPVLTDPDFLVMGTSGK--KTSPHFQKFDICV	1014	P48736	PK3CG_HUMAN
926	DGQLFHIDFGHFLDHKKKFGYKRERVPVLTQDFLIVISKGAQECTKTREFFERFQEMCY	985	P42336	PK3CA_HUMAN
904	SGQLFHIDFGHFLGNFKTKFGINRERVPVILTYDFVHVVIQQGKTN--NSEKFERFRGYCE	961	O00329	PK3CD_HUMAN
930	TGQLFHIDFGHILGNFKSFGIKRERVPVILTYDFIHVIQQGKTG--NTEKFGFRFQCCCE	987	P42338	PK3CB_HUMAN
	* : * * * * * : * . * . : * : * * * * * : * * * : * : * : * : * :			
1015	KAYLALRHHTNLLIILFSMMLMTGMPQLTSKEDIYIRDALTVGKNEEDAKKYFLDQIEV	1074	P48736	PK3CG_HUMAN
986	KAYLAIRQHANLFINLFSMMLGSGMPELQSFDDIAYIRKTLALDKTEQEALEYFMKQMN	1045	P42336	PK3CA_HUMAN
962	RAYTILRRHGLLFLHLFALMRAAGLPELSCSKDIQYLKDSLALGKTEEEALKHFRVRFNE	1021	O00329	PK3CD_HUMAN
988	DAYLILRRHGNLFIITLFLALMLTAGLPELTSVKDIQYLKDSLALGKSEEEALKQFKQKQFDE	1047	P42338	PK3CB_HUMAN
	** : * : * * : * * : * * : * * . * * * : * : * : * : * : * : * : * : * :			
1075	CRDKGWTVOFNWFLHLVLGKIQGKHS	1102	P48736	PK3CG_HUMAN
1046	AHGGWTTKMDWIFHTIKQHALN----	1068	P42336	PK3CA_HUMAN
1022	ALRESWTKVNWLAHNVSKDNRQ----	1044	O00329	PK3CD_HUMAN
1048	ALRESWTTKVNMAHTVRKDYRS----	1070	P42338	PK3CB_HUMAN
	. * . : * : * : * : * : * : * : * : * : * : * : * : * : * : * : * :			

Appendix 2: PI3K Alpha, Beta, Delta and Gamma Assays

The assay readout exploits the specific and high affinity binding of PIP₃ to an isolated pleckstrin homology (PH) domain in the generation of a signal. Briefly, the PIP₃ product is detected by displacement of biotinylated PIP₃ from an energy transfer complex consisting of Europium (Eu)-labelled anti-GST monoclonal antibody, a GST-tagged PH domain, biotin-PIP₃ and Streptavidin-APC. Excitation of Eu leads to a transfer of energy to APC and a sensitised fluorescence emission at 665 nm. PIP₃ formed by PI3kinase

activity competes for the binding site on the PH domain, resulting in a loss of energy transfer and a decrease in signal.

Assay protocols:

Solid compounds are typically plated with 0.1 μ L of 100% DMSO in all wells (except column 6 and 18) of a 384-well, v bottom, low volume Greiner plate. The compounds are serially diluted (4-fold in 100% DMSO) across the plate from column 1 to column 12 and column 13 to column 24, leaving columns 6 and 18 containing only DMSO to yield 11 different concentrations for each test compounds.

The assays are run using specific PI3kinase kits from Millipore (Cat# 33-001).

The assay kits consist of the following:

- 4 x PI3K reaction buffer (contains 200 mM hepes pH7, 600 mM NaCl, 40 mM $MgCl_2$, <1% cholate (w/v), <1% chaps (w/v), 0.05% sodium azide (w/v))
- PIP2 (1 mM)
- 3x Biotin PIP₃ (50 μ M)
- Detection Mix C (contains 267 mM KF)
- Detection Mix A (contains 60 μ g/mL Steptavadin-APC)
- Detection Mix B (contains 36 μ g/mL Europium-anti-GST (anti-GST-K) and 90 μ g/mL GST-SRP1-PH-domain and 1 mM DTT)
- Stop solution (contains 150 mM EDTA)

Manually add 3 μ L of reaction buffer (contains 1 mM DTT) to column 18 only for 100% inhibition control (no activity).

Manually add 3 μ L of 2 x enzyme solution to all wells except column 18. Pre-incubate with compound for 15 min.

Manually add 3 μ L of 2 x substrate solution to all wells (column 6 represents 0% inhibition control).

Leave plate for 1 h (cover from light). In case of the gamma assay only a 50 min incubation is required.

Manually add 3 μ L of the stop/detection solution to all wells.

Leave plate for 1 h (cover from light).

The assay is read upon the BMG Rubystar and the ration data is utilised to calculate 11 point curves.

NB. The substrate solution (concentrations) differ with each isoform:

Alpha: 2 x substrate solution containing 500 μM ATP, 16 μM PIP₂ and 0.03 μM 3x biotin-PIP₃

Beta: 2 x substrate solution containing 800 μM ATP, 16 μM PIP₂ and 0.03 μM 3x biotin-PIP₃

Delta: 2 x substrate solution containing 160 μM ATP, 10 μM PIP₂ and 0.03 μM 3x biotin-PIP₃

Gamma: 2 x substrate solution containing 30 μM ATP, 16 μM PIP₂ and 0.03 μM 3x biotin-PIP₃

Analysis Method:

Data processed through the XC₅₀ 4-parameter logistic curve fit algorithm in Activity Base.

Normalise to % inhibition between the high and low controls (0% and 100% inhibition respectively).

Primary Module fits: Slope, Min and Max asymptotes varies

Secondary Module fits: (i) Fix Min asymptote, (ii) Fix Max asymptote, (iii) Fix Min and Max asymptotes

Curve Fit AC: pXC₅₀ 95% CL ratio > 10

-20 < Min asymptote < 20

80 < Max asymptote < 120

Appendix 3: CLND Solubility Assay

5 μL of 10 mM DMSO stock solution diluted to 100 μL with pH 7.4 phosphate buffered saline, equilibrated for 1 h at room temperature, filtered through Millipore Multiscreen HTS-PCF filter plates (MSSL BPC). The filtrate is quantified by suitably calibrated flow injection Chemi-Luminescent Nitrogen Detection. The standard error of the CLND solubility determination is 30 μM , the upper limit of the solubility is 500 μM when working from 10 mM DMSO stock solution. This is a very rapid method of assessing approximate solubility but is likely to overestimate a compound's true solubility, particularly if that compound is highly crystalline and/or has a high melting point; it also takes no account of the compound's thermodynamic solubility or dissolution rate. This technique can detect solubilities in the range 1 μM -500 μM .

Appendix 4: ChromLogD Assay

ChromLogD is a high-throughput measure of lipophilicity, derived from the gradient retention time of the compound in reversed phase HPLC using pH 7.4 starting mobile phase with acetonitrile gradient.

Appendix 5: PI3K Gamma Dependent CD63 Up-regulation in Activated Basophils Assay

CD63 is a lysosomal protein and a cell surface marker of basophil and mast cell activation. Upon stimulation by fMLP, CD63 is upregulated, moves to the cell membrane prior to degranulation, releasing pro-inflammatory mediators such as histamine and IL-4. This assay detects the up-regulation of CD63 to the cell surface membrane through the use of an antibody cocktail which firstly distinguishes basophils from other cell populations and then identifies CD63 upregulation through increased antibody staining.

Compound preparation: Solid compounds are typically plated with 1 µl of 100% DMSO in all wells (except column 11 and 12) of a 96-well, v-bottom Greiner plate. The compounds are serially diluted (2-fold in 100% DMSO) across the plate from column 1 to 10 to yield a 10 point concentration response curve for each test compound. Columns 11 and 12 contain DMSO only. All wells are then diluted 100-fold in RPMI 1640 (containing 10 mM HEPES) and a 2.5 µl transfer is made into an empty 96-well, v-bottom Greiner plate.

PBMC preparation: Human whole blood is collected on the morning of the assay with 1ml Sodium Heparin per 100 mL blood. The blood is diluted 2-fold in PBS (containing Ca^{2+} and Mg^{2+}) and layered onto the porous barrier of Leucocept tubes (Greiner) containing 15 mL Lymphoprep (pre-spun). Sample is spun for 20 minutes at 2500 RPM and PBMC layer extracted, washed in PBS (containing Ca^{2+} and Mg^{2+}) and re-suspended to 1×10^7 cells per mL in RPMI 1640 (containing 10 mM HEPES).

Assay solutions:

- RPMI 1640 containing 10 mM HEPES

- PBS + Ca²⁺ and Mg²⁺
- PBS + Ca²⁺ and Mg²⁺ containing 0.1% DMSO
- PBS - Ca²⁺ and Mg²⁺
- 1 µM N-Formyl-Met-Leu-Phe (fMLP) in RPMI 1640 containing 10 mM HEPES (0.1 µM FAC)
- 20 mM EDTA in PBS (-Ca²⁺ and Mg²⁺)
- BD FastImmune™ Antibody Cocktail containing FITC labelled CD63/PE labelled CD123/Per-CP labelled Anti-HLA-DR diluted 2-fold in PBS (-Ca²⁺ and Mg²⁺)
- 1% Paraformaldehyde

Assay protocol:

1. Manually add 22.5 µL of cells to all wells and incubate at 37 °C for 30 minutes.
2. Add 2.5 µL of PBS containing 0.1% DMSO to column 12, mix gently and incubate at 37°C for 20 minutes.
3. Add 2.5 µL of fMLP to columns 1 to 11, mix gently and incubate at 37 °C for 20 minutes.
4. Add 2.5 µL of EDTA to all wells, mix thoroughly using an orbital shaker and incubate for 15 minutes at room temperature.
5. Add 5.0 µL Antibody cocktail to all wells, mix thoroughly using an orbital shaker and incubate for 45 minutes at room temperature in the dark.
6. Add 200.0 µL PFA to all wells and incubate for 20 minutes at room temperature in the dark.
7. Spin plates for 5 minutes at 1500 RPM.
8. Manually remove supernatant and re-suspend pellet using orbital shaker.
9. Add 200.0 µL PBS (- Ca²⁺ and Mg²⁺) to all wells.
10. Repeat steps 7-9.
11. Read plates on Flow Cytometer (BD Biosciences LSRII).

Data Analysis: Threshold PE-CD123 counts at 800 fluorescent units. Gate on the PE-CD123-positive population. From this population, gate on the PerCP-HLA-DR negative population to identify Basophils. From this population, gate on the FITC-CD63 positive

population. CD63 counts as percentage of the parent population is used to calculate % inhibition.

Normalise to % inhibition between the high and low controls (0% and 100% inhibition, respectively).

$$\%I = 100 - (100 * (\text{compound} - \text{control 2}) / (\text{Control 1} - \text{control 2}))$$

Data is processed through the 4-parameter logistic curve fit algorithm in ABase XE

$$y = a + (b - a) / (1 + (10^x / 10^c)^d)$$

Where $a = \text{min}$, $b = \text{max}$, $c = \text{inflection point}$, $d = \text{slope}$, $x = \text{compound concentration}$

Primary Module fits: Slope, Min and Max asymptotes varies.

Secondary Module fits: (i) Fix Min asymptote, (ii) Fix Max asymptote, (iii) Fix Min and Max asymptotes.

Curve Fit QC: pXC_{50} 95% CL ratio > 10.

$-20 < \text{Min asymptote} < 20$.

$80 < \text{Max asymptote} < 120$.

The human biological samples were sourced ethically and their research use was in accord with the terms of the informed consents.

Appendix 6: Artificial Membrane Permeability Assay

The donor cell contains 2.5 μL of 10 mM sample solution in pH 7.4 phosphate buffer. To enhance solubility, 0.5% hydroxypropylcyclodextrin (encapsin) is added to the buffer. The artificial membrane is prepared from 1.8% phosphatidylcholine and 1% cholesterol in decane solution. The sample concentration in both the donor and acceptor compartments is determined by LC-MS after 3 h incubation at room temperature. The permeability (logPapp) measuring how fast molecules pass through the black lipid membrane is expressed in nm/s. The average standard error of the assay is around 30 nm/s but can be higher in the low permeability range. This assay is different from the commercially available PAMPA assay offered regarding the thickness of the membrane, which in the case of the GSK assay is much thinner and can be considered as phospholipid bi-layer formed in the pores of the filter.